THE SIMULATION OF SOLAR ENERGY SYSTEMS

Donald John McLean, BSc

A Thesis submitted for the
Degree of Doctor of Philosophy

Department of Architecture and Building Science
University of Strathclyde, Glasgow
September, 1982

S Y N O P S I S

This thesis considers the long term energy problem and the role which active solar collector systems for building application might play in alleviating this problem. The major part of this thesis describes the derivation and solution of the mathematical model to simulate the principal components in a solar energy collector system. The model is based on an implicit numerical technique which allows the investigation of the simultaneous interaction between system components in liquid and photovoltaic collectors. A simulation program called FLARE, based on the aforementioned model, has been developed for use as a research and design model. This program forms the central core of a suite of interrelating computer programs which provide sophisticated user participation by means of a high level interactive graphics facility.

ACKNOWLEDGEMENTS

I wish to thank all members of the ABACUS 'team' (staff and postgraduate students) for their friendship and their direct or indirect help during the past three years.

There are, however, several people to whom I am particularly indebted:

Joe Clarke for his willingness and ability to convey his considerable knowledge on the technical aspects of this work. I also wish to thank him for his general supervision, advice and encouragement.

Professor Tom Maver (Director of ABACUS) for the use of the ABACUS facilities and for all supervision, guidance and encouragement.

Harvey Sussock for the frequent use of his brain for mathematical and computing problems.

Particular thanks to Ellenor Dunbar for the time, skill and patience with which she typed this thesis and I also wish to express my gratitude to the postgraduate students who have aided the final production of this thesis in one way or another.

Finally I wish to thank my beloved wife Morag for her love, continual support, care and encouragement throughout this work.

C O N T E N T S

INTRODUCTION

Nature regulates herself by balancing those variables which interact within a particular environment. As an example consider the balance between two species, one predator the other prey. Although many variables are involved in the predator-prey equilibrium equation, in general, the growth or decline of the prey population is normally followed by a growth or decline in the predator population. Mankind's interaction with the earth's resources is slightly different because these resources (e.g. land, water and food) are finite and there will be a different man-resource equilibrium point for each resource. In other words, each resource will support a finite maximum number of people, each individual having access to an adequate supply of the resource. The maximum size of the human population is the smallest number of people that can be supported by any one of the earth's resources. Having attained this optimum population, it would have to be maintained by a zero population growth to ensure man-resource stability. Unfortunately, many of the world's population die each year from starvation and diseases associated with malnutrition. Some experts conclude that we have passed the optimum level of human population because present food production techniques cannot support the existing population, the man-resource equilibrium point is exceeded.

Man has access to another earth resource which is becoming increasingly vital, energy. The sun generates a massive quantity of energy of which the earth intercepts only a small proportion, nevertheless, the quantity intercepted is far greater than the annual global energy consumption. However, modern man tends to rely on 'stored energy' forms, for example, fossil fuels and radioactive isotopes to meet his energy demands. The advantage of this energy form is that it can be controlled and subsequently released when required, unlike the sun which is both a fickle and periodic source which cannot be readily controlled.

The problem Man faces is that stored energy sources are being used at a rate in excess of one million times their rate of production. The man-resource equilibrium point has been passed and at the present rate of consumption, these stored energy sources will be completely depleted. This problem is more commonly known as the 'Energy Crisis'.

In order to establish whether an energy crisis exists or if it is an over-reaction, it is necessary to estimate the practical life expectancy of the stored energy resources. Projections are based on information such as: the proven and potential reserves of coal, natural gas, crude oil and uranium; the world's population growth; the rate of change of energy demand; the rate of increase in energy supply from nuclear power and other sources; and the cost of extracting rapidly diminishing resources. This is a highly complex issue, nevertheless, estimates of existing energy resources range from 20-25 years of natural gas, over 30 years of uranium (assuming fast-breeder reactors are not available), 30-50 years of crude oil, and 200-500 years of coal (1). Do these values imply a crisis? The answer depends upon a subjective assessment of the time scales involved which is difficult to achieve with some objectivity and without bias. Clearly though energy shortages may occur in the early part of next century.

At present the principal sources of energy used in the world are coal, crude oil, natural gas, nuclear power and hydroelectric power. Table 0.1 identifies the basic imbalance in the rates at which oil and gas are being consumed compared to coal and uranium. This is primarily because they are not only extremely convenient to use but oil in particular is the only practical fuel in some cases, e.g. long-haul airflights. Ironically these two energy forms are liable to be depleted soonest, when in fact there should be strict limitations on their use to preserve stocks. If any one fossil fuel were to be depleted, or the world's nuclear energy program abandoned, then the global implications would be a more rapid depletion of the remaining energy sources if the existing quality of goods and services were to be maintained. Hydroelectricity is a relatively limited source of energy because there are only a few sites worldwide where the production of hydroelectricity is practical. Therefore, if in 30-40 years both oil and gas supplies are diminished, the energy shortfall will have to be met by nuclear and coal sources.

Superimposed upon the quantity of the main energy sources available is the pollution aspects of fossil fuels and nuclear energy. Both cause

	Column (1) proven resource (EJ)	Column (2) potential resource (EJ)	Column (3) ratio of proven resources relative to total known resources (2) (%)	Column (4) 1979 relative consumption of resources (2) (%)	Column (5) ratio column (3) to column (4) (ideal units)
Coal	20,500	299,000	69.4	28.4	0.41
Crude Oil	4,120	9,790	13.9	46.1	3.42
Natural Gas	2,980	7,710	10.1	18.6	1.84
Uranium	1,940	2,630	6.7	2.4	0.36
Hydroelectricity	-	-	-	4.5	∞
Total	29,540	319,130	100.0	100.0	1.0

TABLE 0.1 Statistics on non-renewable energy sources. Information based on data given by Debs (2)

thermal pollution due to the release of waste heat in converting the stored energy into the required form, for example, coal to electricity. The effect of thermal pollution will most probably increase the average global ambient temperature. Fossil fuels when burned release carbon dioxide into the atmosphere. Experts disagree whether this will increase or decrease the average global temperatures, however, they do agree that the earth's climate will be affected. With nuclear energy the most significant problem is the disposal of toxic radioactive waste materials which will be potentially dangerous for over 20,000 years. The disposal of this waste is a highly emotive subject causing worldwide concern.

Developed countries have built their national economies on an abundant supply of inexpensive energy to ensure both technical development and a rising material standard of living for its population. Governments throughout the world came to realise the precarious position of their economies when oil prices quadrupled in 1973. The world recession of the early 1980's cannot be attributed to any single factor, but a significant reason has been the stress put on the economies of nations which require large quantities of imported energy, i.e. crude oil. In such situations developed countries may undertake one or both of the following courses of action:

(i) reduce energy wastage by conservation techniques,
(ii) utilise alternative energy sources.

Energy conservation methods can significantly reduce the primary energy demand in industrialised countries, however, these techniques may not preserve fossil fuel supplies due to the increasing demand for energy, particularly from developing countries. Nevertheless, most energy conservation techniques are easier to apply and generally offer a quicker return on capital investment than alternative or renewable energy sources.

Governments tend to take either a long-term or a short-term view of renewable energy sources. Sweden, for example, has no significant indigenous energy supply and the nation rejected a full scale nuclear

power programme in a referendum. Over many years Government supported programmes have succeeded in drastically reducing energy wastage by promoting energy conservation techniques. As a result, more attention is being paid to the commercial exploitation of alternative energy sources, three times as much is now spent on funding alternative energy research than on conservation (3). The UK, in comparison, with a well developed nuclear programme and its own indigenous energy supply has not had the same motivation to conserve energy. Massive energy savings could be made using conservation techniques, especially in buildings, consequently, three times more is spent on conservation than on alternative energy sources (4). This ratio is becoming larger due to the recently reduced funding for alternative energy projects.

At present there are many alternative energy sources under investigation worldwide, of these the source with the largest global potential is the utilisation of the sun's radiant energy. Solar energy is not only the principal long-term source of energy but it is vital to life on earth. Its commercial use offers a promise of an environmentally clean energy source causing no pollution, although slight micro climatic changes might occur if exceedingly large areas are used to collect solar energy. However, several adverse features of solar energy collection must be considered:

- the low concentration of solar flux warrants the use of large solar collection arrays.

- the maximum energy is usually available where and when it is least required. It is normally the case that deserts and equatorial regions receive more energy than the northern developed countries where a greater proportion of the energy could be utilised.

- there are seasonal and daily variations in the quantity of energy received, therefore, it is necessary that some form of storage is used to smooth out the energy supply and load demand mis-match.

One of the reasons it has taken so long to implement the widespread use of solar energy is that, while the solar fuel is free, a considerable capital investment is required to use this energy properly. Due to the availability of cheap oil, electricity and natural gas, there has been no need to utilise solar energy and only with the recent escalation of primary fuel costs (especially crude oil), over the last decade, has solar energy become more competitive with conventional energy forms. This trend should continue with solar devices becoming cheaper due to mass production.

Solar collectors are devices which intercept and transform radiant energy into another form, be it low, medium or high grade thermal energy or electricity. The principal forms of engineered solar collectors are:

(a) Flat plate solar collector. This type of collector will collect diffuse as well as direct radiation normally transforming it into low grade thermal energy. It is particularly suited to climates where there is a large quantity of diffuse radiation, for example, the UK.

(b) Concentrating collector. This collector operates by focussing the direct solar beam radiation onto a small receiving absorper area, using mirrors or lenses. Much higher temperatures can be obtained; the actual temperature depends upon the concentration ratio. These collectors operate best in strong solar beam conditions.

(c) Photovoltaic collector. This collector converts solar radiation into electrical energy by means of solar cells. It can utilise both direct and diffuse solar radiation.

It is possible to build a solar energy system capable of supplying the total annual load of a particular application, however, a system sized to meet the maximum load could be grossly oversized during periods when partial load conditions exist. As solar energy systems are capital intensive, oversizing can result in a severe economic

penalty. Consequently, most solar energy systems are smaller than would be necessary to meet the maximum load and they have to operate in parallel with a conventional (auxiliary) energy source which can be designed to meet the maximum demand.

In order to assess the best design for a solar energy system a physical model could be built and used to assess the thermal performance of the system. Physical models are both expensive and time consuming to construct, consequently, mathematical models have been developed as an alternative to physical modelling. There are two types of mathematical models for solar energy systems considered in this thesis: simple models which analyse the long term dynamics of the system and detailed models which are suitable to analyse long term and the short term system dynamics. The precise prediction of the performance of solar energy systems is complicated due to random variations in climatic conditions and the mathematically complex relationships between system components. Detailed system simulation models tend to be more suited to analysing these variations than simple system models.

Presently there is a debate on the relative merits of simple system models compared to more detailed simulation models, however, both have quite distinct area in which they operate best, all things considered. Consequently, comparisons between these models in terms of the cost to develop and operate are invalid. Simple system models are more suited to predicting the long-term performance, usually annual. Only a few variables are considered therefore little information concerning the dynamics of the system will be obtained, but that information which is generated will be available quickly and at little expense. On the other hand, detailed simulation models are generally too expensive with which to conduct long-term performance analyses, however, the detail available from simulation models allows the short term dynamic performance of the system to be investigated. A secondary function of detailed system simulation models is to develop simple system models for use in subsequent designs (see Chapter 4).

This thesis will describe in depth the mathematical formulation and

solution of a detailed dynamic system simulation model based on implicit finite difference techniques for a flat plate solar energy collector and its associated system. The techniques employed to derive and solve the resulting finite difference equations for the system are similar to those employed in a dynamic building energy model called ESP (5).

The information available from the solar energy collection system simulation model facilitates the design of each component in a system, particularly the flat plate solar collector. The advantage of this information is that the designer can make rational decisions regarding the appropriate collector and system design trade-offs necessary to promote convergence towards a more economic and efficient design.

Due to the flexibility of the model the designer can analyse the performance of straightforward or 'conceptual' designs, for example, using photoelectric solar cells to drive a fan or a pump to collect solar energy so that the system runs independently of the national grid unless auxiliary energy is required. The solar collector model can analyse air, liquid and photovoltaic collectors individually or combined with each other (i.e. hybrid solar collectors). In addition, collectors may be analysed individually or in array form; collectors can be static or fully or partially tracking; they can be free-standing or associated with some object (such as a building); they can have any physical arrangement and any number of plane transparent covers -including thin anti-reflection films; and can have associated external non-concentrating reflectors or shading devices. System components normally associated with a solar energy system are also modelled. In particular, the energy storage unit can analyse direct or indirect liquid tanks and rock bed storage units for thermal stratification; and change of phase storage units.

The solar energy system collection appraisal model consists of a suite of interrelating computer programs known collectively as FLARE. Essentially the FLARE package is concerned with the rigorous appraisal of any proposed design hypothesis in terms of the thermal performance of the solar energy collection system. At the time of writing (July 1982) the FLARE solar energy system program has been developed primarily for the design of flat plate solar collectors and is undergoing extensive testing.

CHAPTER 1 Potential of Solar Energy Systems

INTRODUCTION

In order to assess the potential contribution of any alternative energy source it is necessary to identify both the energy demand to be satisfied and the quantity of available energy from the alternative source. The justification of an alternative resource is normally made in terms of global or national energy demands, therefore, the world energy demand and the UK national consumption of energy will be analysed so that the contribution of solar energy collection can be predicted.

The World Energy Demand

The total world primary energy consumption in 1980 was 300×10^{18} J (6). This represents an average growth worldwide of 13.75% during the period 1973 to 1980. The average rate of growth or decline in energy consumption varies from country to country and year to year. This can be attributed to a number of reasons:

(a) The world economic recession has resulted in a reduced industrial output throughout the world's industrial nations, lowering energy requirements,

(b) Many countries have implemented energy conservation projects to reduce their national energy consumption,

(c) Climatic influences may have an effect on the figures, e.g. Northern Europe has 11% more degree days in 1980 than in 1973 (7).

(d) Increasing material standards of living may result in a number of effects: increased industrialisation in developing countries; greater use of energy intensive transportation; general improvement in quality of goods and services, etc.

Table 1.1 contains values of primary energy consumed during both 1973 and 1980, for 14 individual nations and the remainder of the world.

The 14 nations detailed in Table 1.1 consumed an estimated 48% of the total world primary energy consumption in 1973 falling to 44% of the total consumption in 1980. The average growth for these nations, during the period 1973-80 was 4.1% compared with the rest of the world which had a 22.7% increase. A more comprehensive list of nations may have given a clearer insight into any trend in the increase in global energy consumption, nevertheless, the increase in consumption of the 14 nations was greatest in the less industrialised countries of Turkey and South Africa and to a lesser extent Ireland and Norway. By comparison, both Sweden and the UK consumed considerably less energy in 1980 attributed in particular to a sharp fall in industrial consumption.

	YEAR		
	1973 (PJ)	1980 (PJ)	Change (%)
United States	78,700	80,400	2.2
West Germany	12,573	13,717	9.1
Canada	8,535	9,431	10.5
United Kingdom	9,236	8,579	-6.9
France	7,700	8,300	7.8
5 nations total	116,744	120,427	3.15
Belgium	2,778	2,992	7.7
South Africa	1,901	2,496	31.3
Turkey	1,060	1,466	38.3
Sweden	1,461	1,367	-6.4
Norway	935	1,125	20.3
Finland	913	1,002	9.7
Denmark	768	772	0.5
Ireland	294	347	18.0
New Zealand	302	344	13.9
14 nations total	127,156	132,358	4.1
Rest of the world	136,584	167,642	22.7
Global primary energy consumption	263,740	300,000	13.75

TABLE 1.1 World primary energy consumption, 1980 values compared to 1973 values

The importance of the USA as an energy consumer cannot be over-emphasised. The USA consumed 29.8% of the world's total primary energy in 1973 and 26.8% in 1980, but has only 5.4% of the world's population. It is no longer self-sufficient in terms of energy and depends heavily on imported energy to meet the demand. Federal financing of alternative energy R&D projects is currently running at over five hundred million dollars per annum. This is slowly having an affect e.g. solar water heating and space heating systems in an estimated 300,000 US residences are saving about one million barrels of oil (8) per annum, representing 0.008% of the US primary energy consumption. Considerable savings have also been achieved in building energy consumption due to various conservation techniques. The annual rate of growth in energy consumption for the period 1973 to 1980 was only 0.27% compared with an annual rate of 4.1% from 1960 to 1973 (9). Significantly, the growth in each of the three main sectors; transport, industry and domestic was 3.1%, 2.3% and 1.4% respectively for 1973-1980, compared to a growth of 2.2% in the national energy consumption. Unlike other industrialised countries, industrial recession was not the prime cause for reduced demand as a low rate of growth occurred in each economic sector, however, the figures reflect the savings due to conservation and alternative energy sources.

Similar to the USA those countries which rely on imported energy are actively persuing reductions in their annual energy consumption. One of the more immediate tasks of these countries has been the reduction of energy used in buildings. Promotion of building energy conservation falls into two categories viz. 'Regulations' and 'Encouragement' which normally apply to new and existing buildings respectively.

It is unusual for building regulation to be applied retrospectively to existing building stock due to the difficulty of enforcing the legislation. Regulations normally apply only to new buildings and vary from country to country. The traditional method of specifying maximum 'U' values for individual building construction elements (as used in the UK) is being replaced throughout the world by new standards. These are based on the whole building heat loss, allowing

factors such as building shape or aspect ratio to be considered. In Ireland and Belgium, new standards have been proposed which regulate the overall building heat loss according to a volume to surface area ratio.

Much of the emphasis in conservation efforts has been to control the building fabric heat loss. The Swedish energy policy is simply to insulate to a level at which the fabric loss is acceptable for their climate. Having reached this maximum practical level of insulation, the Swedes are currently putting more effort into the control and reduction of ventilation and infiltration heat losses. This policy will undoubtedly be followed in more countries as their building regulations become stricter and no further saving can be achieved from insulation.

The rate of replacing building stock in most countries is very slow, therefore, any changes in the building regulation which apply only to new houses will not have an immediate effect on the national energy consumption. Consequently, governments encourage conservation in the existing building stock by offering incentives (loans, grants, tax relief, etc) to building owners and occupiers. Several countries including Denmark, Ireland and the UK offer cheap loans and tax relief on certain insulation measures, others such as Finland and the Netherlands award grants for multiple glazing projects. Several countries, other than the USA, including New Zealand and the Netherlands aid alternative energy projects.

Carroll (7) suggests that the potential saving in most countries with a reasonable housing stock could be between 20-35% of the building energy requirements if simple energy conservation techniques are employed, excluding any alternative energy supplement. It is difficult however, to assess the quantity of energy associated with this figure. In order to assess the potential of an alternative source in any one country a detailed breakdown of the energy demands in that country is required. The UK energy demand will now be considered so that the potential of solar energy collection can be assessed.

The UK Energy Demand

During 1980 the UK produced and imported a total of 11,900 PJ of energy. About 28% of this supply was either stored or exported, the remainder - 8,599 PJ - was the national primary energy requirement (10). This constituted a fall of 7% in the UK primary energy consumption between 1973 and 1980, however, the fall has not been steady because consumption fell from 1973 to 1975, rose from 1975 to 1979 (almost to the 1973 value) and fell from 1979 to the present level of consumption. On the two occasions when energy consumption fell, it did so by about (7.8%) and was accompanied by a small (2-3%) fall in economic output. In both recessions the fall in economic output was more evident in the energy intensive industrial sector (e.g. iron and steel) than in other sectors. These fluctuations in energy consumption make it difficult to forecast consumption trends, consequently, any long term prediction of these trends will probably be inaccurate.

Considerable losses occur in converting the primary energy into a more suitable form, for example, coal to electricity. Some 30% of the energy contained in these primary fuels is lost before the energy is converted to its secondary fuel form - solid fuel, natural gas, electricity or petroleum. The analysis of the secondary fuel form in four standard sectors of end use (industry, transport, domestic and other users, the last comprising agriculture, public administration and miscellaneous) is given in Table 1.2 for 1980, it is also shown by pie charts in Figure 1.1. The Department of Energy (DEn) estimates that energy losses which occur after energy is supplied to final consumers, resulting principally from inefficiencies in the multitude of energy using appliances (e.g. domestic fires and boilers, cars, aircraft, central heating plant etc), could amount in total to almost 50% of the 5,966 PJ of energy supplied (10).

The Government has taken several steps to reduce building energy consumption. Pezzey (4) estimates that 46% of the energy consumed by final users can be attributed to buildings, however, by employing

	INDUSTRY	TRANSPORT	DOMESTIC	OTHERS	TOTAL
Natural Gas	644(31.8)	0(0.0)	886(53.5)	222(28.0)	1752(29.4)
Solid Fuel	286(14.1)	0(0.0)	306(18.5)	63 (8.0)	655(11.0)
Electricity	379(18.7)	11 (0.7)	348(21.0)	200(25.3)	938(15.7)
Petroleum	717(35.4)	1477(99.3)	116 (7.0)	306(38.7)	2616(43.9)
	2026(100.0)	1488(100.0)	1656(100.0)	791(100.0)	5961(100.0)

TABLE 1.2 Final uses by sector V Secondary fuels (1980). Values PJ (%) by sector

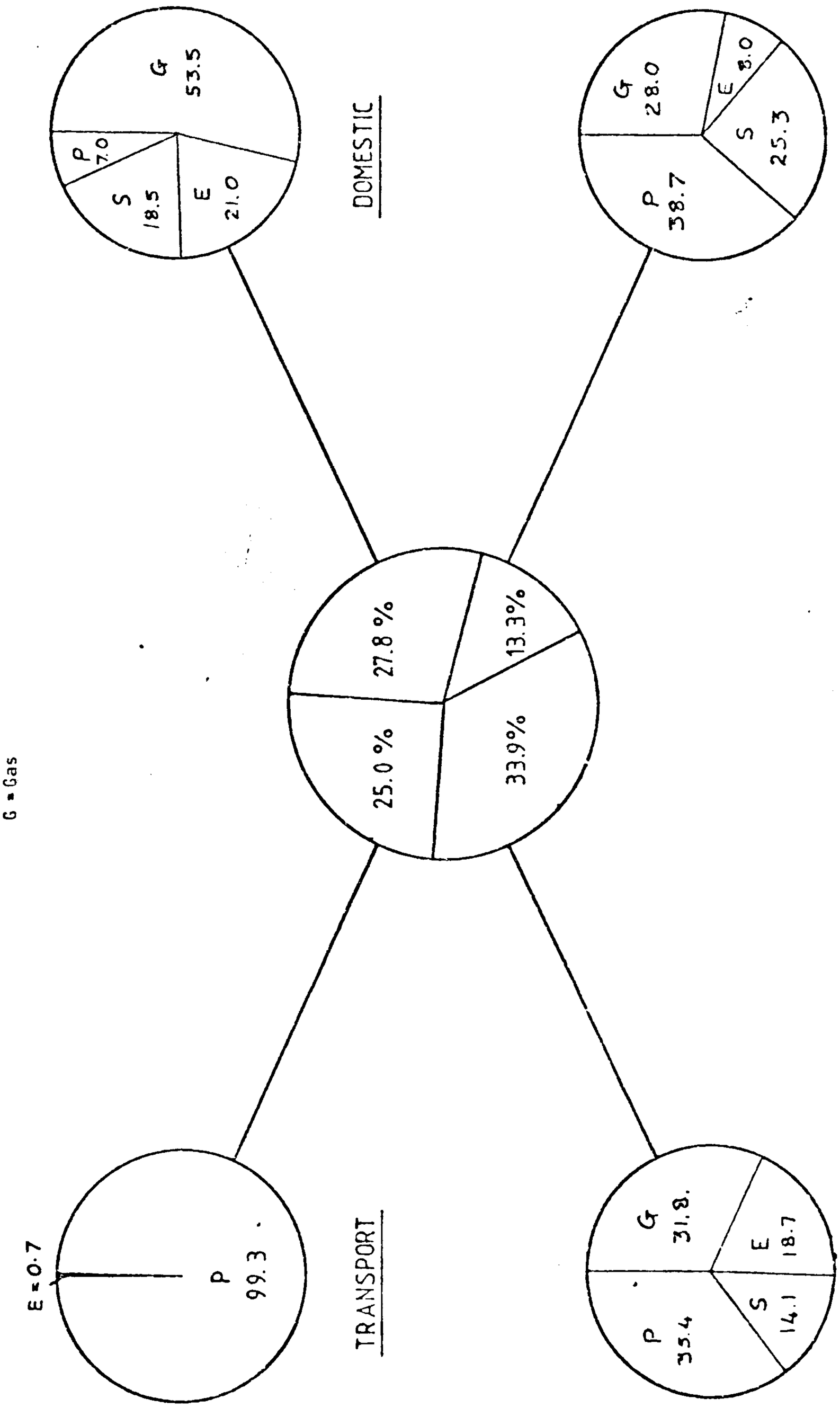

Figure 1.1 Breakdown of secondary fuel consumed in each economic sector.

simple energy conservation techniques to existing buildings could achieve a 15% reduction in the primary energy demand (11). New building regulations were introduced in the late 1970's to improve the standard of building insulation, these will not have an immediate effect because Britain has a large building stock that is being replaced very slowly (2% per annum - DEn (12)). Consequently, since 1973 the Government have been promoting several measures aimed at encouraging energy conservation in existing buildings. A summary of these governmental actions for both domestic and non-domestic buildings is given in Table 1.3.

Self-sufficiency in terms of energy is only achieved when the quantity of energy exported or stored exceeds the quantity of energy imported. In 1980 Britain had almost achieved self-sufficiency with a net balance of 5% of the primary energy consumed needing to be imported. This is in stark contrast to 1973 when this figure was over 50%. This increasing energy independency is vitally important to the stability of the British economy. There have been two principal reasons behind the reducing dependency on imported energy: the first is due to the reduction in energy consumption between 1973 and 1980, the second is the increasing quantities of energy produced by the nuclear industry and much more importantly by the North Sea oil industry. Since 1977, UK energy production has increased by 10% (13). For the UK to maintain this near self-sufficiency status into the next century its energy consumption cannot be allowed to grow at more than one or two per cent annually.

The significance of the UK's reliance on fossil fuels cannot be overstressed as fossil fuels constitute over 95% of our primary fuels, Table 1.4. The total recoverable reserve of fossil fuels around the UK is unknown although it appears that natural gas may be the first of the fossil fuels to become scarce. Each year the UK consumes more natural gas and significantly, in 1980, imports accounted for about 22% of the total natural gas used. The prime consideration should be how to replace the natural gas supply by another source other than by oil, whose 'lifetime' would be drastically reduced if required as a substitute for natural gas. Imports could solve the problem - but what would be the cost on the economy? In order to maintain energy

(i) Energy Pricing:- There has been a considerable gulf between natural gas prices and electricity prices for some time. Steps are being taken to make the costs of these two fuels comparable, therefore, over a three-year period commencing in 1980/81 gas prices will increase at 10% per annum above the rate of inflation and electricity prices will increase at about 5% per year above increases in generating costs.

(ii) Publicity Campaign:- After the oil crises of 1973, a media campaign, organised by the DEn under the "save it" banner was introduced to raise public awareness of the need for energy conservation.

(iii) Homes Insulation Programme:- This was started in 1978 to provide a government grant via local authorities to go towards the provision, in existing dwellings, of loft and hot water cylinder insulation and lagging of tanks and pipes in the loft. To mid-1981 about one million grants had been issued.

(iv) Energy Conservation Act, 1981:- This act enables the government to set mandatory standards of efficiency and safety for all new space and water heating appliances.

(v) Energy Quick Advice Service (EQAS):- Provides a free telephone service for non-domestic users organised by the DEn.

(vi) Energy Survey Scheme (Started by DEn in 1976):- Grants of up to £75 for a one day survey and up to 50% of a more comprehensive survey of non-domestic premises, 48,000 and 1,600 applications respectively to date.

(vii) Insulation Tax Allowance:- 100% first year capital allowance given for capital expenditure, by any business, on new heating and energy saving equipment and also for the addition of insulation to existing industrial buildings.

(viii) Mandatory Heating Limit:- This limit was set at 20°C in 1974 for all non-domestic buildings. A new limit of 19°C was imposed in 1980.

Table 1.3 U.K. government actions to support energy conservation in existing buildings 1973 - 1981 (4)

	1973	1980	Imported 1980
Petroleum	46.4%	37.0%	41.0%
Coal	37.6%	36.9%	6.0%
Natural Gas	12.5%	21.4%	22.7%
Nuclear	2.9%	4.1%	0.0.%
Hydro	0.6%	0.6%	0.0%

TABLE 1.4 Quantity of the primary energy supplied by various sources, 1973 and 1980, plus the quantity of the 1980 figure which is imported

self-sufficiency the energy shortfall induced by the depletion of gas or oil reserves can only be met by one or a combination of three options:

(i) Increased use of coal reserves. In some situations coal can replace gas or oil directly. Also gas or oil can be processed from coal, however, this process is less efficient than using coal directly. Furthermore, coal is becoming more difficult and more costly to mine.

(ii) Increased use or primary electrical supply. The primary electrical supply comes from three sources: coal, hydroelectric and nuclear power. Hydroelectricity is almost operating at its maximum capacity in Britain, but theoretically the nuclear industry should be able to ensure self-sufficiency. However, this is neither a cheap nor quick solution. Furthermore, at the present annual rate of growth in nuclear energy supply, averaged over the last eight years was only 4.4%. If this annual rate of growth were maintained, it would be 2000 AD before nuclear energy could supply 15% of our present energy consumption, therefore, if gas or oil were to be in short supply in 20 years, to avoid imports a rapid nuclear energy programme should be started as soon as possible to meet the expected demand.

(iii) The third option is the utilisation of alternative energy sources, e.g. wind, wave, solar, tidal, etc. The BRE (11) investigated the potential of various alternative energy sources in the UK. One of the more favorable was active solar collection. Hardacre (14) suggests that a credible potential contribution of solar heating in the UK over the next 20 years could be 26 to 105PJ for water heating and 158 to 316PJ for space heating. Based on the lower figures, 2% of the present UK primary energy requirements could be met by solar heating. There are a number of problems related to implementing a large solar heating programme:

- legal rights of unobstructed accesss to solar radiation
- local authority planning permission
- local authority rates (i.e. solar heating - is it a house improvement?)

As with other alternative energy sources, solar heating must be economically competitive with existing energy sources.

1.1 Energy Sources

There are numerous alternative energy sources to fossil fuels, nuclear fission and hydroelectric power which could, by the end of the century be supplying a small but appreciable quantity of the world's primary energy requirements. Different countries will utilise various forms of alternative energy sources to varying degrees. For example, the torrid zone nations will prefer straight-forward solar collection devices, whereas in New Zealand and Iceland geothermal will be very important and maritime nations such as the UK will be interested in wave power. These are examples and do not exclude the use of all other sources of alternative energy in these countries, however, some nations may not have access to geothermal or wave energy sources etc.

Most countries worldwide are examining their alternative energy potential and financing those schemes which are most suitable to their needs. From the experience gained due to work being conducted throughout the world individual nations will be able to make objective decisions on which alternative energy sources offers them most reward.

At present there are many alternative energy sources under consideration for exploitation throughout the world. The advantages and disadvantages of these sources with their potential will now be briefly discussed:

(a) BIOMASS

Biomass is the term given to any organic material produced by the photosynthesis process, whether or not they are suitable for food. The process has a very low efficiency and requires a large land mass for cultivation. As the world's population increases then there will be more biomass required for food and less for use in the manufacture of fuels, oils, gases and alcohol. Nevertheless there is a vast quantity of energy available, for example, in the UK the total biomass produced each year has an energy content equivalent to 12% of the UK primary energy demand. The majority of this biomass

went into producing human and animal food but with higher yield crops and more efficient use of animal wastes there clearly is a potential for biomass. It has the further advantages that the photosynthesis process consumes carbon dioxide and that it does not cause thermal pollution unless burned. This energy source may be very important in some countries but its global significance will be small by the end of the century.

(b) GEOTHERMAL

The process of retrieving energy from thermally active underground or surface areas is in limited use throughout the world. Unfortunately there are few sites where these thermally active areas exist. As with other forms of stored energy it is a thermal pollutant because it is increasing the rate of energy supply to the earth's atmosphere. Geothermal energy also has several other environmental hazards:

(i) it is occasionally found as steam, in such cases problems exist in its extraction because of toxic gases which are mixed with the steam

(ii) geothermal water is exceedingly salty, e.g. it contains as much as six times the quantity of dissolved salts compared to ocean water. This creates an additional problem because the water cannot be passed into a stream or river and if it is re-introduced into the ground then this can only be accomplished by using energy, reducing the net geothermal energy gain.

(iii) the extraction of vast quantities of water has caused sub-sidence in some areas.

Upon solving the extraction problems geothermal energy should be a source of a relatively constant supply of energy for certain countries. It will never be a major energy source, but by the year 2000 several countries will be utilising significant quantities of geothermal energy, especially New Zealand and Iceland. In Britain, there are no thermally active areas at depths less than four miles below the earth's surface.

(c) NUCLEAR FUSION

Although scientifically feasible, it has not yet been demonstrated, although by the end of the 21st century it is conceivable, that all the energy requirements of Man could be generated by this source. Nuclear fusion has two distinct advantages over nuclear fission, the first is an unlimited supply of fuel which is hydrogen and secondly it does not have the same radioactivity problems. The process will however produce vast quantities of waste heat causing thermal pollution.

(d) OTEC : Ocean Thermal Energy Conversion

This process involved extracting power from a turbine driven by the small temperature gradients present in the ocean between the surface and the water at depths of hundreds of metres. This has a low efficiency between one and three per cent (1) but as techniques improve it may eventually produce significant quantities of electrical power. There is no thermal pollution problem and OTEC has the further advantage of operating at the same capacity day and night because the ocean serves as a massive energy storage system. There is still more development required and the implications on marine life in the surrounding areas must be considered. Small quantities of energy might be available from this source next century.

(e) SOLAR : Extraterrestrial

Projects are being conceived where photovoltaic cell arrays are built in space and used to collect solar energy. The collected energy is sent to earth in the form of a concentrated beam of microwave energy. This has numerous advantages, no land required except for the receiver, ideal operating conditions for photvoltaic cells and a constant solar flux unaffected by the earth's atmosphere. Unfortunately the beamed energy will cause thermal pollution due to the extra heat load on the earth but a more serious hazard is the concentrated beam of energy. Some people believe it may damage certain layers of the atmosphere, furthermore, aeroplanes could not fly in the vicinity of the beam and it would be necessary to ensure there were safeguards against

the possibility of the beam not coming in contact with the receiver. Glaser (15) discusses the potential of solar power satellites and explains how some of the problems are being overcome. It will probably be well into the 21st century before significant energy supplies will be obtained from satellites.

(f) SOLAR : Terrestrial

Terrestrial solar collection is in limited use throughout the world. It requires further technical development and it is dependent on site, climate, etc. A storage system is normally required and there may be environmental problems associated with solar energy collection by large arrays of solar collectors. These problems will be discussed more fully later in this chapter. Despite the problems, solar energy collection appears to be one possible alternative energy source which could be a major contributor to the world's primary energy supplies in the early 21st century.

(g) TIDAL

Energy can be collected from the bi-diurnal tidal movements caused by the moon's gravitational forces. There are unfortunately only a limited number of suitable sites in the world. The French have a small pilot project on the Rance estuary near St Malo. The Canadians are studying a project for the Bay of Fundy. In Britain the Bristol Channel appears to be a favorable site as it is a large estuary which enjoys one of the highest tides in the world. Although there are a number of different schemes, the principle is that the energy contained in the flooding and ebbing of the tide in the estuary is used to operate turbines which generate electricity. Tidal energy has no pollution problems and can generate large quantities of power, the Bristol Channel alone could produce over 80 PJ per annum ($\approx$ 1% of the UK primary energy demand). However tidal energy is unlikely to be a major global source of energy.

(h) WAVE POWER

Wave power is really another form of wind power since waves are produced due to the wind and the sea acts as a very large collecting area. It is possible to generate electricity from the energy contained within individual waves. One of its advantages is that the more inclement the weather the more energy is obtained tending to match energy demands. However, a back-up device or some storage facility must be available for calm periods. Experimental models are being built for use in the UK coastal waters. As yet, most of the technical problems in large scale projects have not been overcome. Although wave power may eventually be an important alternative energy source, it will not contribute any significant quantities of energy by the 21st century.

(i) WIND POWER

A vast secondary source of energy derived from solar energy is the wind. Wind power has been used for thousands of years to power seacraft, and for hundreds of years to power mills for grinding flour and cereals. At present many sites in Britain have been designated potential wind electricity generating sites. The conversion efficiency from wind energy to electrical energy is approximately 34%. The extractable energy has been shown by Rayment (16) to be,

$$E_e = 0.0148\ A_s V_{50}^3 \quad \text{GJ per annum}$$

$$(\text{i.e. } E_e \simeq 4\ A_s V_{50}^3 \text{ kwh per annum})$$

where

E_e = the extractable energy

A_s = the swept cross sectional area of the aerogenerator rotor arm(s)

V_{50} = the wind speed exceeded 50% of the year. This is usually quite close to the mean annual wind speed.

Although an aerogenerator will theoretically operate anywhere, it is more practical to operate it under high wind conditions, for example,

if V_{50} is doubled the extractable energy increases eightfold. The value of E_e obtained from the equation given above should be considered an upper limit because there are occasions when the wind speed is either too high or too low to operate the aerogenerator. These limits of wind speed are known as the rated speed and the starting speed respectively. Wind power causes no thermal pollution but a moderately large land area is required for significant quantities of electricity to be generated. Wind power is potentially one of the most important alternative energy sources. However, its main function by 2000 AD will probably be supplying electrical power to remote isolated communities. For example, the Western Isles of Scotland has a value of V_{50} , twice that of the mainland, the potential for wind power in this site is already under investigation.

The potential contribution of each of these alternative energy sources if fully implemented, either per annum or in its lifetime, is given in Table 1.5.

Every country has the potential to exploit wind and solar energy. This does not involve drilling or advanced technology. Of the two, solar energy collection possesses the greater potential energy supply, although solar energy potential diminishes the further the site is from the equator.

Alternative Energy Source	Practical Limit
Biomass	$3 * 10^{21}$ J/year
Geothermal	10^{18} J/year
Nuclear Fusion	10^{28} J/year
OTEC	$6 * 10^{18}$ J/year
Extraterrestial Solar Radiation	∞
Terrestial Solar Radiation	$3.2 * 10^{22}$ J/year *
Tidal	10^{18} J/year
Wave	no estimate
Wind	$6 * 10^{21}$ J/year
Nuclear Fission	$6.7 * 10^{22}$ J
Fossil Fuels	$3 * 10^{22}$ J
1980 Global Consumption	$3 * 10^{20}$ J/year

TABLE 1.5 Practical Limit of Alternative Energy Sources and existing sources (17) assuming technology available

* this figure is based on the collection of 1% of the mean annual solar flux rate falling on the earth.

1.2 Available Solar Energy

The total energy intensity of extraterrestrial solar radiation measured just outside the earth's atmosphere and integrated over the entire solar spectrum is called the 'Solar Constant', denoted by G_{sc}. The term Solar Constant is a misnomer since the intensity of the extraterrestrial radiation varies throughout the year because of the eliptical orbit of the earth around the sun. The solar constant intensity is evaluated at the mean sun-earth distance, the maximum and minimum discrepancy occurring at the Perihelion and Aphelion respectively (Figure 1.2). Adjustments to the solar constant for the distance variation can be made using the empirical formula (18):

$$G_{sc}^{1} = G_{sc}\,[1 + 0.033\mathrm{Cos}\,(\frac{360-N}{370})] \qquad (1.1)$$

where G_{sc}^{1} is the corrected solar constant and N represents the year day number.

Several different values of solar constant existed before a standard value of 1.353 kwM^{-2} was proposed by Thekaekara (19). This value was used by NASA and it appeared to be universally accepted until recently when it was suggested that in light of current research the value should be 1.373 kwM^{-2} (20). Based upon Thekaekara's value, the earth intercepts 172.5 PW of extraterrestrial solar radiation.

The sun is often considered to be a blackbody. The effective black-body temperature of the sun was estimated by Thekaekara to be 5762K by using the Stefan-Boltzmann equation:

$$T\ sun = [\frac{Gsc}{\sigma} * \frac{R^2}{r^2}]^{\frac{1}{4}} \qquad (1.2)$$

where σ = Stefan-Boltzmann constant, $5.6697*10^{-8} WM^{-2}K^{-1}$

r = radius of the solar disc, $6.9598*10^{8}M$

R = the mean sun-earth distance, $1.4959*10^{11}M$

For a solar constant of 1.373 kwm^{-2} the effective blackbody tempera-ture of the sun would be 5783K.

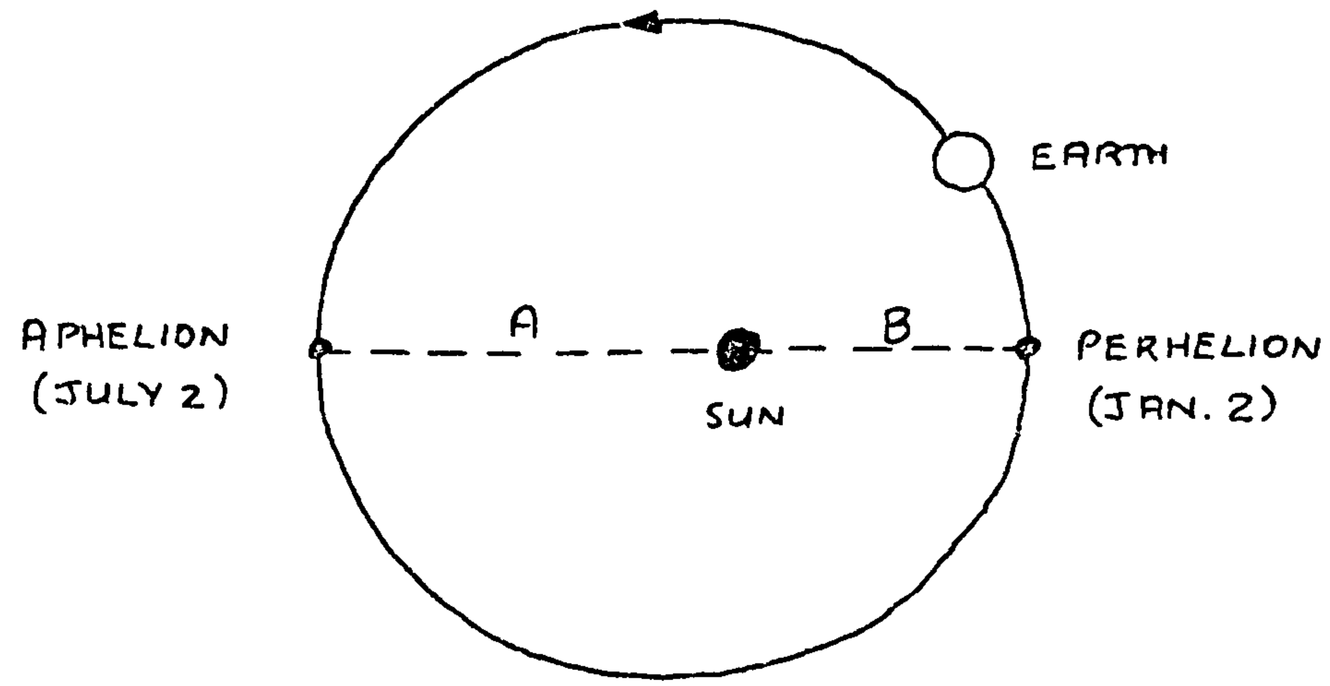

$A = 1.522 \times 10^8$ KM

$B = 1.472 \times 10^8$ KM

Figure 1.2 The earth's eliptical orbit

The curve of the extraterrestrial solar spectral irradiance, at the solar constant value as a function of wavelength, is closely approximated by the spectrum emitted by a blackbody at the effective sun temperature, however, peaks and troughs occur in the solar spectrum due to the radiative properties of the sun's incandescent gases. Thekaekara measured the extraterrestrial solar spectrum as a function of wavelength, for the solar constant (Figure 1.3), the energy associated with this curve is the same as that associated with a blackbody at a temperature of5762K. Although the solar spectrum extends from X-rays (wavelength $< 0.01\mu m$) to radio waves (wavelength $> 100m$) for most engineering applications a limited range of the spectrum can be considered: 99.9% of solar energy is in the range 0.217-10.94 μm (14) and 99% lies in the range 0.276-4.96 μm. Thekaekara's solar spectrum is used by NASA as a standard for their space programme as they require a detailed description of the solar spectral irradiance to ensure that the delicate temperature equilibrium of their space probes and satellites is maintained.

For purposes of calculating properties of materials (absorptance, reflectance and transmittance) which depend upon the spectral distribution of solar radiation, the terrestrial solar spectrum is required. Wiebelt and Henderson (21) have modified Thekaekara's extraterrestrial solar spectrum as a function of:

(a) the site - rural or urban
(b) sky conditions - cloudy or clear
(c) zenith angle or the sun - 0°-75°

Consequently the effects of the terrestrial solar spectrum may be assessed for any surface if the spectral properties of the surface are known.

Due to the earth's rotation about its own axis and its orbit around the sun, a set of geometrical relationships can be established which identify the position of the sun relative to any terrestrial site, (Appendix 1). The extraterrestrial irradiance on any horizontal surface at the outermost region of the earth's atmosphere can be

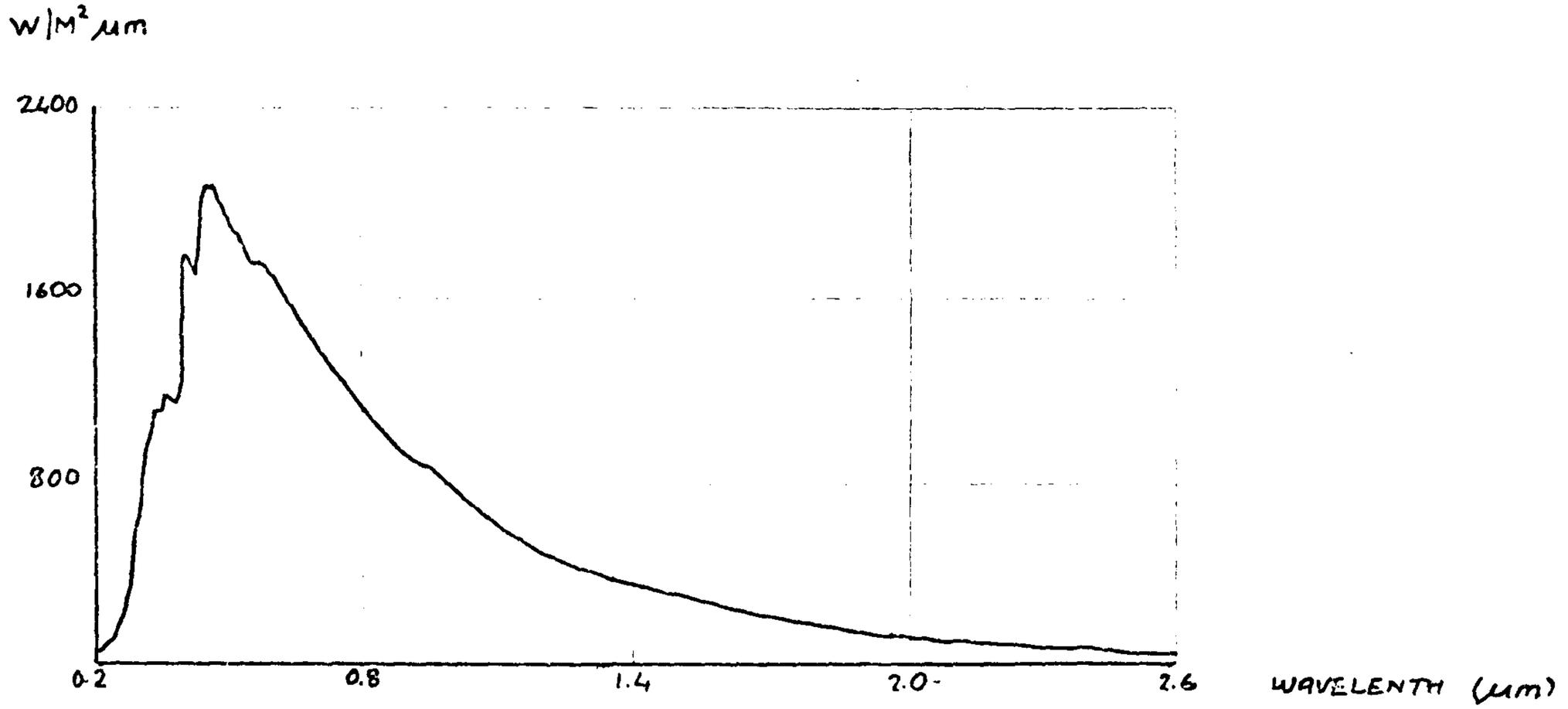

Figure 1.3 The NASA/ASTM standard spectral irradiance at the mean sun-earth distance and a solar constant of 1353 W/m (19)

calculated if the incident angle of the sun's beam is known:

$$G_0 = G_{sc}^{1} [\text{Cos } \emptyset \text{Cos} \delta \text{ CosW} + \text{Sin } \emptyset \text{ Sin} \delta] \qquad (1.3)$$

where G_0 = the extraterrestrial horizontal irradiance (WM^{-2})

$\emptyset$ = latitude of the site (degrees)

δ = declination of site (degrees)

W = hour angle (degrees)

The total daily extraterrestrial irradiation can be determined by integrating equation (1.3) over the solar day, thus

$$H_0 = 2G_{sc}^{1} [\frac{Ws}{15} \text{ Sin } \emptyset \text{ Sin} \delta + \frac{12}{\pi} \text{Cos} \emptyset \text{ Cos} \delta \text{ Sin Ws}] \qquad (1.4)$$

where H_0 is the average daily total extraterrestrial irradiation measured in JM^{-2}, Ws is the hour angle between either sunrise or sunset and the solar noon.

In the presence of the earth's atmosphere the incoming extraterrestrial radiation is reflected or scattered by various gases (CO_2, ozone etc) in the atmosphere. As a result, after a single vertical transit (at the zenith angle) through the atmospheric layer about 1000 WM^{-2} reach the earth's surface under clear sky conditions. The density of the atmosphere at the zenith angle has been selected as the standard optical thickness of the atmosphere, it is often described as air mass one, or AM1. Consequently, the lower the sun position in the sky is above the horizon, the smaller the quantity of solar radiation will be because the air mass will be greater.

The approximate mean annual solar flux rate over the entire globe is approximately 200 WM^{-2} (22) on a 24 hour basis, this corresponds to $3.2 * 10^{24}$J of energy or over 10,000 times the rate of energy consumed worldwide in 1980. Although the UK has a much lower ratio of total solar input to primary energy demand and a small ratio of solar input per head of population (12), as discussed earlier, the potential contribution of solar energy could be considerable, even although the UK receives a mean annual daily total irradiance of

only 90 wm^{-2} (12). Consider Britain's total surface area of 227,000 km^2, the total grassland and cropped area on the mainland is 113,000 km^2 and the total urban area is 23,000 km^2, the remaining area is made up of arable land, forest and inland water. If 1% of the grassland area and 2% of the urban area were covered with active solar collectors which collect 10% of all incident radiation, then over 5% of Britain's primary energy consumption could be met from these solar collectors, covering 0.7% of the UK land area.

The main drawback in full scale utilisation of solar energy collection in the UK is that despite a large annual total solar input, the radiant energy has a low flux density and tends to be of an intermittent and disperse nature, this makes its recovery difficult and expensive. As well as diurnal variation there is a wide variation in summer and winter solar input in the UK and because of frequent periods of overcast conditions some form of energy storage or other energy source is necessary to meet the demand when the solar input is low. Either of these will substantially increase both the complexity and cost of a solar collector system.

The size of the storage capacity required depends upon the length of variations in solar input:

- between day and night; storage of a few hours
- between sunny and cloudy days; storage of a few days
- between summer and winter; storage of a few months

This problem is compounded due to the high population density in the UK which limits the area of land which can be devoted to some method of solar collection.

There are also many practical and economic problems which have delayed solar energy utilisation in the past:

- very costly, not economically viable
- few credible manufacturers
- poor design and workmanship
- maintenance problems

Although these problems have not been fully resolved, significant steps have been taken and solar collection is viable at present in some countries. Within two decades solar energy may be making a small but useful contribution worldwide.

Before a large worldwide implementation of solar collection devices is undertaken, an assessment of their environmental implications must be made. All effects on the environment will be due directly or indirectly to the large surface area required to collect and store the solar energy. There are three environmental effects:

(i) The land required is vast particularly in developed countries because the land required for a significant solar contribution is greater due to a larger energy consumption. There are a number of solutions, duel use of the land may be effective, for example, in urban situation tops of roofs, roads etc may be used and in rural cases where possible collectors may be well spaced to allow surrounding land to be farmed, however, there are only limited places where this could be achieved. Alternatively, collectors may be placed in relatively desolate areas, i.e. deserts. Anywhere large groups of collectors are positioned there may be micro or meso-climatic changes due to the altered reflectivity of the surrounds, this could seriously affect the ecological system in the surrounding area (23). Collectors may be placed on the ocean but problems may occur due to the right of a country to operate such a system on international waters. One other major drawback of placing large collector arrays in remote sites or on the ocean is the energy loss due to distribution losses.

(ii) Thermal pollution will occur because the earth's albedo has been changed; this will occur particularly if collectors are sited in areas where there is a large ground albedo.

(iii) The visual impact on the environment of large collector arrays may prove unacceptable in certain circumstances, i.e. national parks, nature reserves, suburban areas, etc.

Fortunately these environmental problems will only occur if there was a massive global requirement for solar energy collectors; this will not occur in the foreseeable future. Nevertheless, solar collector devices could play a significant role, along with other alternative energy sources, in reducing the global requirement for fossil fuels.

1.3 Passive and Active Solar Systems

The distinction between passive and active solar techniques is that passive is solar-related architectural design and construction, whereas active solar energy systems are designed as part of the mechanical heating and cooling equipment in buildings, however, this does not exclude the use of devices such as small fans or motorised insulation panels in passive solar designs. Normally both passive and active systems require thermal storage but they differ in that passive solar can be considered as an energy conservation technique and active solar can be considered as an energy source.

Like all building energy conservation techniques the function of a passive solar design is to reduce auxilary energy requirements for comfort heating. The expression 'passive solar' covers a wide range of applications where a more comprehensive and considered approach to various climatic influences on the building design is undertaken. The fundamental principles of a passive solar design are to minimise heat loss from the building interior to exterior during the heating season while promoting solar heat gains through south-facing windows, subsequently reducing auxilary heating requirements. These objectives are reversed during the cooling season reducing auxilary cooling requirements. A summary of the objectives of a passive climate based design are set forth in Table 1.6, these cover all building heat exchange processes. The relative importance of these passive design principles depend upon the climatic severity and the duration of the heating and cooling seasons of the locality in which the design will abide. Therefore, due to microclimatic variations a similar design may prove unsuitable in the same locale. This implies the importance of balancing the design with the sites climatic and microclimatic variations.

A south facing window is the most common example of a passive means of utilising solar energy, but it is only one component of a passive solar 'system'. Elements in the building (floors, walls) may be constructed to have a high heat capacity to store thermal energy and reducing temperature variations. Lebens (24) has classified passive

	Heating Season		Cooling Season	
	Promote gain	Resist Loss	Resist gain	Promote loss
Conduction	-	minimise conductive heat flow	minimise conductive heat flow	Delay periodic heat flow
Convection	-	minimise external heat flow and infiltration	-	Promote ventilation
Radiation	Maximise solar gain	-	Minimise solar gain	Promote radiant cooling
Evaporation	-	-	-	Promote evaporative cooling

Table 1.6 Principles of Passive Solar Design.

solar heating into two categories, indirect and direct gain systems. The following subsets are included in the indirect heat gain category:

(a) Trombe-Michel wall
(b) Water wall
(c) Roof pond
(d) Attached/isolated sunspace (or greenhouse)
(e) Thermosyphoning collectors (air or water)

In contrast there are only two types of direct heat gain systems:

(a) Diffusing direct gain
(b) Non-diffusing direct gain

There are a wide range of devices which aid a passive solar design, for example:

- Motorised or manual blinds and/or insulation
- Internal or external shading devices
- Heat absorbing, heat reflecting or anti-reflecting double or triple window configurations using glass, plastics and thin films
- Small fans to redistribute stored energy.

Passive solar designs have several advantages compared to active solar systems:

- cost of a passive design may be less than supplying an active system if proper soil conditions exist to support the storage elements
- no new building technology required
- operation normally maintenance free
- normally independent of utilities to operate passive system, unless fans and motors are used.

However, passive solar has limitations:

- direct sunlight cannot penetrate all parts of a traditional house unless a fan is used to redistribute the energy or else thermo-

syphoning is employed.

- problems may occur due to inadvertent errors in design, e.g. passive solar used for winter heating may increase summer cooling load requirements especially if simple sunshading precautions are ignored.

- an energy supply will be required for lighting, appliances etc and some auxilary heating or cooling may still be necessary.

Passive solar techniques have already been successfully applied to domestic dwellings. In commercial office buildings, lighting and cooling, rather than winter heating, are the predominant energy demands. Lighting consumes 16% of the energy supplied to the commercial sector (25). The more artificial lighting required then the greater the cooling load requirements in a typical building. Consequently, daylighting and cooling load reduction techniques, such as shading devices, are especially important passive design elements in non-residential buildings.

One important aspect of passive solar designs is whether or not these buildings are comfortable to live and work in. With no evidence to the contrary, it is believed these buildings are comfortable, furthermore, people will probably respond to living in houses with large south facing windows and different structural design.

The active solar energy system is applied to many different solar energy processes in agricultural, commercial, domestic and industrial applications. Unlike passive solar which is an energy conservation technique, active solar requires a device to capture solar energy and a distribution system to transport this energy to where it is required either for use or storage to use at some future time. The types of solar energy system range from trickle water collectors (to heat outdoor swimming pools) to solar thermal power stations supplying several megawatts of power. Not only is there a vast range in technology required for active solar systems, but the diversity of applications and system configurations are too numerous to be adequately dealt with in this work. Therefore two types of active

systems will be considered, low-temperature thermal systems and photovoltaic systems. These systems are particularly suitable to building heating and cooling applications but they also apply to many agricultural and industrial processes.

There are two basic types of solar collector used in active solar energy systems for buildings: the concentrating solar collector and the flat plate collector. The concentrating collector uses a curved surface, usually parabolic in shape, to concentrate the sun's rays at a centre or focal point. At the focal point a blackened pipe filled with a liquid is heated, the liquid may then be distributed to where energy is required. The concentrating collector produces what is called high grade energy, i.e. the liquid can be heated to temperatures in excess of 100°C. The main advantage of this type of collector is its ability to generate high temperatures, but there are several drawbacks:

(1) it is expensive to manufacture
(2) expensive sun tracking systems may be required if the concentrator is a parabola or truncated cone type
(3) it operates poorly in climates where a large proportion of the total irradiance is diffuse in nature,
(4) there are few building energy demands which require temperatures in excess of 100°C

This means that in the UK where the diffuse component of the annual total irradiation is high , the expense of producing high grade energy for most applications may not be feasible except for a few isolated industrial applications.

Solar energy should be collected at a temperature appropriate to the application, as most buildings require low temperature energy, energy collected at temperature in excess of 100°C would have to be 'converted' to low temperature energy, undergoing thermodynamic losses in the process. The most suitable collector for building applications, is the flat plate collector. It has several advantages compared to concentrating collectors:

- low-temperature collector (i.e. $< 100°C$)
- it does not require a tracking mechanism
- it can collect diffuse radiation
- it is inexpensive to manufacture (relative to a concentrator)
- suitable for south-facing sloping roofs

Although the flat plate collectors discussed are thermal energy collectors (i.e. photothermal conversion), flat plate photvoltaic collectors will also be considered as these offer a source of electricity which would be particularly applicable in remote sites. These two types of solar collection, photothermal and photovoltaic, will be described in more detail in Chapter 2.

1.3.1 Passive and Active Solar System Modelling

There are two principal techniques of assessing the performance of a passive or active solar energy design: these are physical or mathematical modelling. Physical modelling is the more expensive and less flexible method as it involves constructing then operating a prototype model over a considerable period of time and collecting and analysing the resulting data. More economically a reduced scale model (passive or active) or a full size model (active) can be tested indoors but indoor test facilities are expensive to build and maintain. Although physical models are necessary to identify problems which cannot be anticipated, the more flexible mathematical models offer a much quicker solution to the problem at less expense. Simple mathematical models using steady or pseudo-steady state techniques can be employed to rapidly assess the long-term performance of a particular design. They require considerable care in use because many assumptions have been made in their development, however, their principal disadvantage is the lack of detailed information concerning the design, therefore, more detailed models are required. Properly formulated simulation models can provide the same quality and greater quantity of detailed information as can be obtained from a physical model. The advantage of a simulation model is that once developed it can achieve considerable savings in both time and resources to analyse a passive or active system, compared to a physical experiment. Simulation models can

provide a means of analysing the dynamic performance of a specific system in response to selected meteorological data, therefore, simulation models can be used as research or design tools.

A review of available simulation models for passive systems was conducted by Littler (26) in order to identify those which were applicable for use as passive simulators. In conclusion several models offered the necessary framework within which most passive design problems could be solved, these are ESP, DEROB and BLAST and details of the passive characteristics addressed by the models are given in Table 1.7. Also included on Table 1.7 are details of the SUNCODE program because it fits on medium sized machines making it attractive for small design offices. Work is presently being carried out at ABACUS, in the University of Strathclyde, to mount ESP onto a mini computer so that the cost of the hardware required to operate the model is reduced, thereby making it affordable for small practices.

As part of the European Community Passive Solar Programme a modelling subgroup was formed and one of their functions was to select a set of passive solar models and design procedures for mini-micro computers. programmable calculators and for manual calculation. ESP was selected by the subgroup to compare and calibrate these techniques (27).

ESP (Environmental Systems Performance) is a building energy model which can examine most passive solar designs. The model was developed by Clarke (5) and is based on a variable time-increment implicit finite difference technique. ESP is actually a suite of inter-relating interactive computer programs (Figure 1.4) of which ESPSIM conducts the simulation and the remaining programs are used to calculate data necessary for a particular design proposal. Not only are the various programs easy to operate but they offer the user a wide range of output facilities to assess the simulation results, aiding the design process.

Unlike passive solar, there are few rigorous simulation models of active solar systems available. The most well known is called

	Topic handled	ESP*	BLAST	DEROB	SUNCODE
Designs	Direct gain	✓	✓	✓	✓
	Attached sun space	✓	✓	✓	✓
	Thermosiphon	✓	✓	✓	✓
	Roof space collector	✓	✓	✓	✓
	Double envelope	difficult	×	difficult	×
	Mass walls vented	✓	✓	✓	✓
	Mass walls unvented	✓	✓	✓	✓
	Under floor rock beds	✓	✓	✓	✓
Physical problems	Air/heat movement by convection/by fans	✓	✓	✓	✓
	Infiltration	shedule	schedule	schedule	schedule
	Solar radiation mapping round spaces	✓	✓	✓	×
	Variable glass emissivity	×	×	✓	✓
	Variable room colour	✓	✓	✓	✓
	Effect of furnishings	difficult	difficult	difficult	×
	Air/temperature/stratification	×	×	✓	×
	Movable window insulation	schedule	schedule	schedule	schedule
	Isothermal and non-isothermal storage	✓	✓	✓	✓
	Phase change walls	×	✓	×	✓
	Isolated storage	✓	×†	✓	✓
	Adequate handling of beam radiation	✓	✓	✓	✓
	Adequate treatment of sky temperature	×	×	×	×
Weather Input	Complete 'set'	✓	✓	✓	✓
Daylighting		✓	✓	✓	×
Surface temperature for providing comfort temperatures		✓	difficult	✓	✓
Validation		†	†	†	†
Documentation		Very good	Poor	Good	Very good
Graphics output		Excellent	×	Excellent	×
Building input via digitising tablet		✓	×	In principle	×
Building input format		Cartesian	Cartesian	Assemble standard shapes	†
Internal tables of construction parameters such as insulation values		✓	✓	×	✓
Is it continuing to be improved		✓	✓	✓	✓

† See reference given below
* ESP entries updated by author to relate to latest version

Table 1.7

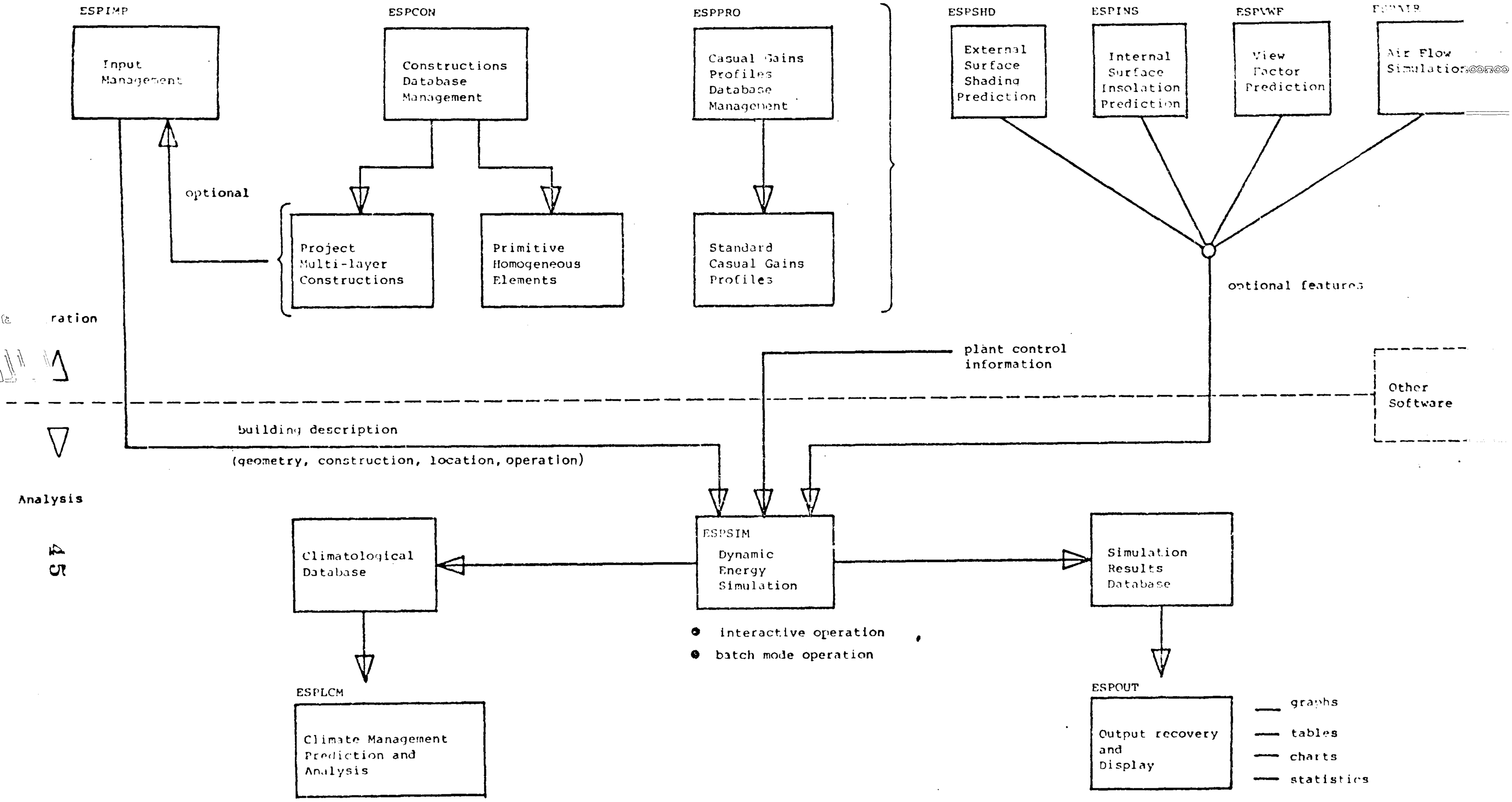

Figure 1.4 The ESP System

TRNSYS (28) which was developed at the University of Wisconsin (USA). This program is very flexible, with a comprehensive library of system components which can be readily simulated. TRNSYS is freely available and it is used worldwide by a number of institutions. In Europe the programme of the EC Modelling Group for Thermal Solar Systems is developing computer models for space heating and domestic hot water systems (29). A detailed program called EMGP1, for the simulation of solar space heating and domestic hot water systems is being developed and validated. Similar to the Passive Solar Modelling Sub-Group, which will use ESP to test simplified passive solar models, EMGP1 will be used for programs to model validation tests of simplified active solar system models. Each participating country in this programme is developing additional subroutines of system components for integration into EMGP1, which has eleven components at present. The UK participant is Fabers Computer Operations who have a program available which is similar to EMGP1 (30).

Although individual components may be modelled to differing degrees of complexity in these programs, the complete system is modelled using a modular or sequential approach. In a sequential model each system component is replaced by a black box model which has appropriate inputs and outputs representing the flow processes into and out of the component. The black box model can be simple for example an on-off feature for a pump, or complex as with a stratified liquid storage tank requiring iterative solution of the governing differential equations within the component. The complete system is formed by combining the components (or black box models) and modelling the interactions between them sequentially in some predetermined order at each time-increment (Figure 1.5), therefore, component A is modelled and output information is used as input to component B which is then modelled, the appropriate output from component B becomes the input for component C, etc. Once each system component has been modelled the simulation is incremented. This technique has many advantages since its general modular structure allows a high degree of flexibility with respect to the extension of the model, consequently, component models can be developed or updated separately and the subsequent integration with the system is easy to implement.

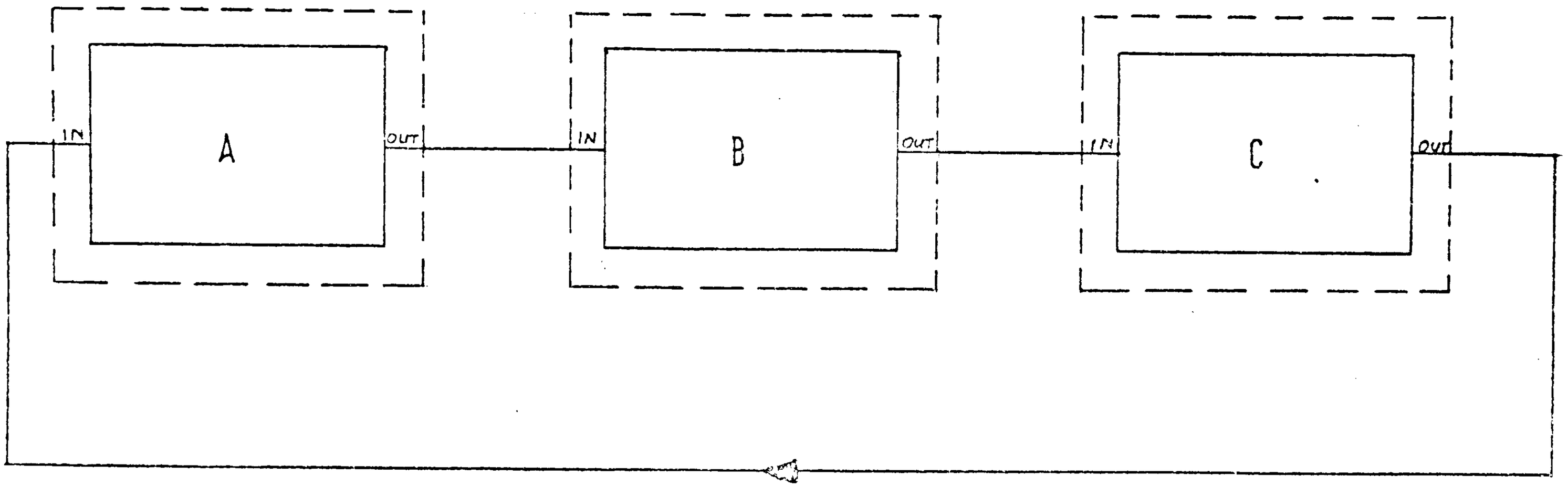

Figure 1.5 Simple representation of the modular approach to system simulation modelling

The principal disadvantage with sequential models is that the instantaneous effect of the control system and the interactions between components are not modelled adequately.

An alternative approach to modular systems modelling involves the simultaneous solution of the interactions between system components at each time-increment, offering a more realistic and accurate analysis of component interactions and control strategy. This method is called the simultaneous approach (Figure 1.6), with it the input to and the output from one component to another becomes a single process which normally requires matrix solution techniques to effect the simulation process.

This thesis is concerned with the development of an implicit finite difference model of active solar energy collection systems employing the simultaneous approach of modelling component interactions. The mathematical model will be described in Chapter 5 and the method of modelling a system will be given in Chapter 6. A prototype computer program has been developed called FLARE which is based on part of the mathematical model (Chapter 7).

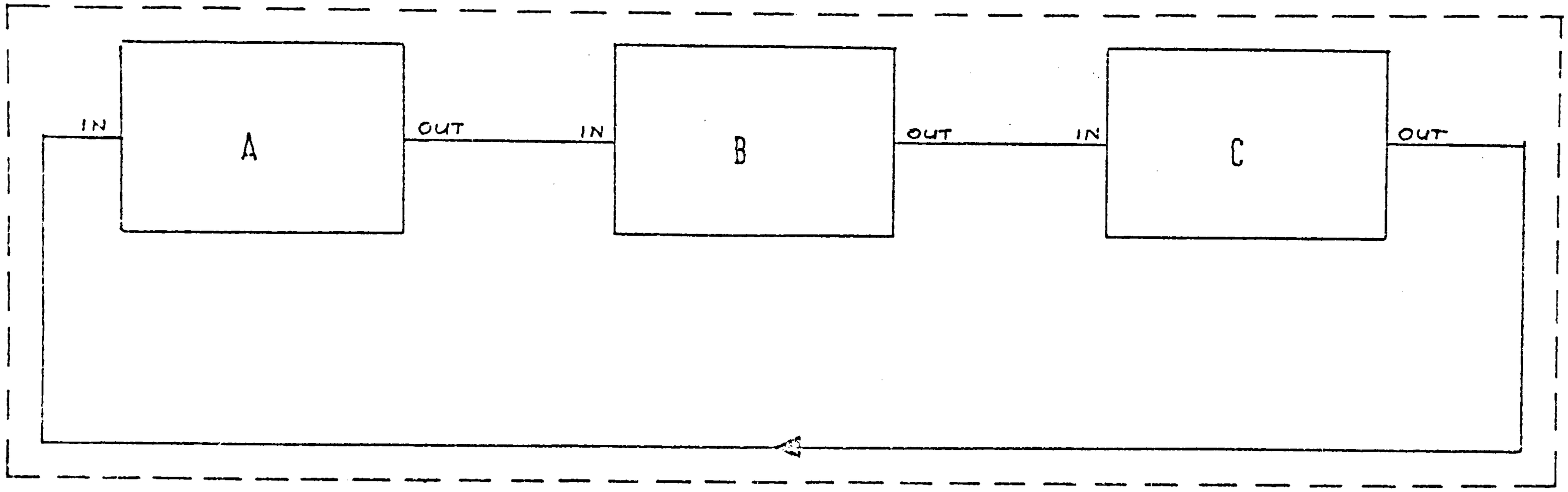

Figure 1.6 Simple representation of simultaneous approach to system simulation modelling

CHAPTER 2 Active Solar Energy Installations in Buildings

The size of active solar heating systems in buildings ranges from domestic applications using a small collector area (several sq.m.) to large installations (> 1000 sq.m.) for community or commercial applications, nevertheless, the basic components in low-temperature solar applications remain remarkably similar. In its most general form, a photothermal system can be considered as five subsystems (Figure 2.1):

- the collectors, converting solar radiation into thermal energy,
- the storage device, serving to synchronise the energy supply with demand,
- the auxiliary source, supplying additional energy to meet any solar energy supply shortfall,
- the distribution system, carrying the energy to points of use, and
- the control system, which coordinates the operation of the whole system.

A photovoltaic system is similar in principle to a photothermal system and it can be described in terms of the aforementioned subsystem.

This chapter is concerned with identifying the type of system to be modelled and establish those parts of the system which may require more detailed analysis

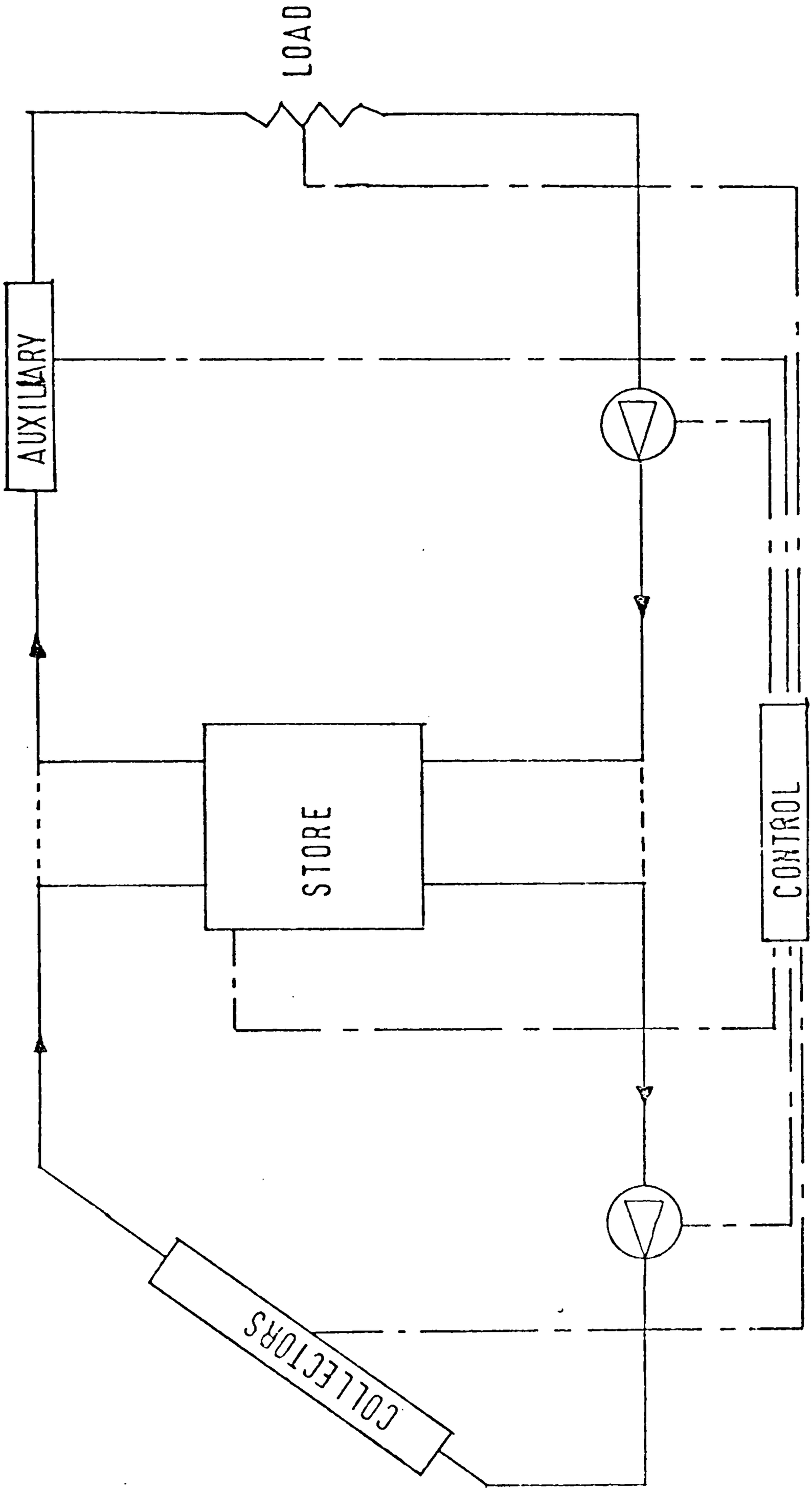

Figure 2.1 Schematic diagram of basic solar energy system

2.1 Principles Behind Solar Energy Systems

Before a mathematical model of a solar energy system is derived it is necessary to identify the basic operational principles behind photo-thermal and photovoltaic flat plate collectors and their associated system components. This will lead to a clearer understanding of the requirements of the model and aid in establishing which are the crutial components to the solar energy design.

Each of the five solar energy subsystems will be discussed.

2.1.1 Principles of a flat plate solar collector

(a) Photothermal

The type of solar collector most widely used in building active solar heating applications is the so-called flat plate collector, named after its main component a blackened flat plate (usually metal) which absorbs incident solar radiation. If this absorbed energy is not removed the absorber plate will undergo a temperature rise until a thermal balance is reached with the environment, i.e. energy losses from the absorber plate to the surrounds equals the solar input. This equilibrium point is more commonly known as the Stagnation Temperature of the collector. It is very important to ensure that the maximum stagnation temperature obtained will not cause serious damage to the absorber plate. Energy is removed from the absorber plate by circulating a fluid at a bulk temperature below the absorber plate temperature, upon contact energy will be transferred to the fluid, heating the fluid and cooling the absorber plate. The most efficient removal of the collected energy occurs when the absorber plate is maintained at the lowest possible temperature, close to that of the incoming fluid temperature. If energy removal is inefficient, an unacceptably high absorber plate equilibrium temperature may be obtained resulting in large ambient energy losses. Normally the absorber plate operates at temperatures well above ambient. In low operating temperatures applications, e.g. swimming pool heating,

a bare collector is acceptable, but in most applications to restrict the absorber plate losses a thermally insulating envelope is mounted around the absorber plate. The materials used in the absorber insulating envelope are discussed in a subsequent section.

The flow rate and heat transfer properties of the energy transporting fluid are critical to the design and performance of the collector. If the collector is performing a function where high outlet temperatures are required, the fluid flow rate will be limited to ensure elevated outlet temperatures the effect of which is increased losses, and a lower collector efficiency. When high outlet temperatures are unnecessary a large fluid rate can be used to maximise efficiency. The rate of fluid flow determines whether the flow is laminar or turbulent. Laminar flow is smoothe and gentle and associated with slow moving fluids, turbulent flow on the other hand has a chaotic flow pattern which promotes heat exchange. Although both a high flow rate and a turbulent flow pattern are suitable for maximum collector efficiency, there is a practical limit to the fluid flow rate due to the parasitic power consumed by a fan or pump in over-coming fluid resistances which increase at a faster rate than the flow rate. Consequently, an optimum flow rate exists between the collector efficiency and the parasitic power consumption. In general, turbulent flow can be maintained with aqueous liquids but with air and non-aqueous liquids there are larger power requirements and the collector may have to operate in or near the laminar flow range.

Flat plate collectors are normally classified according to the type of heat transporting fluid medium used, there are two forms - liquid and gas. Liquid collectors use a wide range of different media, e.g. water, water/antifreeze, silicon oil etc. The gas used in a gas type solar collector is exclusively air, therefore, this collector is more commonly known as an air collector.

There are many different absorber plate designs. In liquid collectors round, oval or rectangular shaped conduits are bonded above or below or passed through the absorber plate. The conduits can be arranged

with several connections between the inlet and outlet headers, or alternatively, a single pass serpentine conduit can be used. In an air collector the enclosed space above or below the absorber plate can be used as an air duct. Low heat transfer rates are evident in air collectors particularly when the flow is laminar. The heat exchange can be promoted by increasing both the contact area and the heat transfer coefficient between the absorber plate and air. This can be achieved by using special absorber plates e.g. V-corrugated, finned plate etc. Recent work has shown that matrix-type air collectors, where air is passed through a black gauze, are extremely effective (31). Nevertheless, the increase in pressure-drop due to increasing the heat transfer rate must be considered in any air collector design.

(b) Photovoltaic

Incident solar radiation can be converted directly into electricity by photovoltaic (PV) conversion using a device called a solar cell which utilises the photoelectric properties of a semiconductor. A semi-conductor, such as silicon or germanium, is a material that is classified somewhere between being a good conductor and a good insulator. Silicon is one of the most commonly used semiconductors, as about 25% of the earth's crust is made up of silicon compounds (e.g. sand) it is unlikely that shortages will occur. Since the principles that govern the operation of all photovoltaic devices are the same, the present discussion will centre upon the characteristics of the silicon solar cell. To make pure silicon more useful, minute quantities of certain impurities are deliberately added to the silicon giving rise to excess negative or positive charges which can carry electric current in the silicon. For example, phosphorous atoms give up electrons to the silicon to form N-type silicon (excess negative charges) and Boron atoms soak up electrons from the silicon leaving holes (missing electrons) which behave like excess positive charges (P-type silicon). This process is called 'doping' of the silicon.

To understand how light interacts with a semiconductor both quantum and electromagnetic wave theories of light must be used. In 1905, physicist Max Planck showed that light should be thought of, not only

a wave as described by Maxwell, but also as discrete bundles of energy called photons. The energy of each photon varies accordingly to frequency of wavelength as given by the expression:

$$E = hf$$

where h = Planck's constant (6.626196×10^{-34} J.s)

f = the frequency of the wave = c/λ

c = the speed of light ($2.997925 \times 10^{8} MS^{-1}$)

λ = the wavelength of light (m)

Since the frequency of the wave varies inversely with the wavelength then the shorter the wavelength the greater will be the energy content of the photon. This can be found from the above expression. It is convenient to describe the photon energy in terms of a unit called the electron volt (eV), one electron volt corresponds to 1.6×10^{-19} J. (An electron volt is defined as the energy gain by an electron when it is accelerated by a voltage difference of one volt). In these units the energy of a photon at 0.3 μm is 4.15 eV, at 0.6 μm it is 2 eV and at 1.2μm it is 1 eV.

When a photon penetrates a semiconductor it will force an electron out of its place in the crystal structure, forming an electron-hole pair. The electron has a negative charge, therefore, the hole it leaves will have a positive charge. Without interference the electron will be drawn back into the hole from which it came, this process is called recombination. In a solar cell a P-N junction is formed near one surface when part of the semiconductor is doped N-type and the adjacent part P-type, at the P-N junction holes and electrons will diffuse with each other, eventually this diffusion will be counteracted by a build-up of positive or negative electric charges on either side of the junction. This state causes an electrostatic field which will separate any electron-hole pairs caused by solar radiation penetration of the P-N junction, inhibiting recombination. Consequently, holes will build up in the P-type material and electrons in the N-type material. By connecting wires to the N and P-type regions those excess charges generated by solar radiation can be

made to flow through an external circuit to provide power to an external load, see Figure 2.2 (17). The use of a P-N junction is not an absolute requirement since potential barriers can be obtained by other means. A suitable metal layer on the surface of the semiconductor will generate a potential barrier at its interface with the semiconductor, this is called a 'Schottky barrier'. Similarly, a boundary layer between two different semiconductors can form a potential barrier, in this case called a 'heterojunction'.

There is a limit to the wavelength of solar radiation absorbed by a semiconductor. This limit is called the band or energy-gap, only photons with an energy content greater than the limit have the power to release electrons. In silicon the band-gap value is 1.08 eV, therefore only radiation with a wavelength less than 1.15 μm can release electrons. The energy contained in the solar spectrum above 1.15 μm accounts for 22% of the total incident solar energy, and this is entirely lost. Consequently a mathematical model of the photovoltaic process should analyse the solar cell spectrally.

The current-voltage characteristics of a silicon solar cell operating under standard test conditions (irradiance 1000 wm^{-2}, cell temperature 25°C) are shown in Figure 2.3a. This curve is obtained by connecting the solar cell to a circuit shown in Figure 2.3b, varying the load resistance and noting the values of voltage and current indicated on the meters in the circuit (32). Setting a very high load resistance will cause an open-circuit to exist as there will be no current flow. The open-circuit voltage (Voc) (point A in Figure 2.3a) can then be measured. By reducing the load resistance the voltage drops slowly but the current increases rapidly. A position is eventually reached - point B - which is known as the knee of the curve and it is normal for the maximum power output of the cell to occur at this point. As the load is reduced past the knee, the voltage will drop rapidly but the current will remain fairly constant. When the load reaches zero, the voltage will be zero and the cell is short circuited. The current at this point is labelled Isc.

At irradiance levels below 1000 wm^{-2}, the short-circuit current will

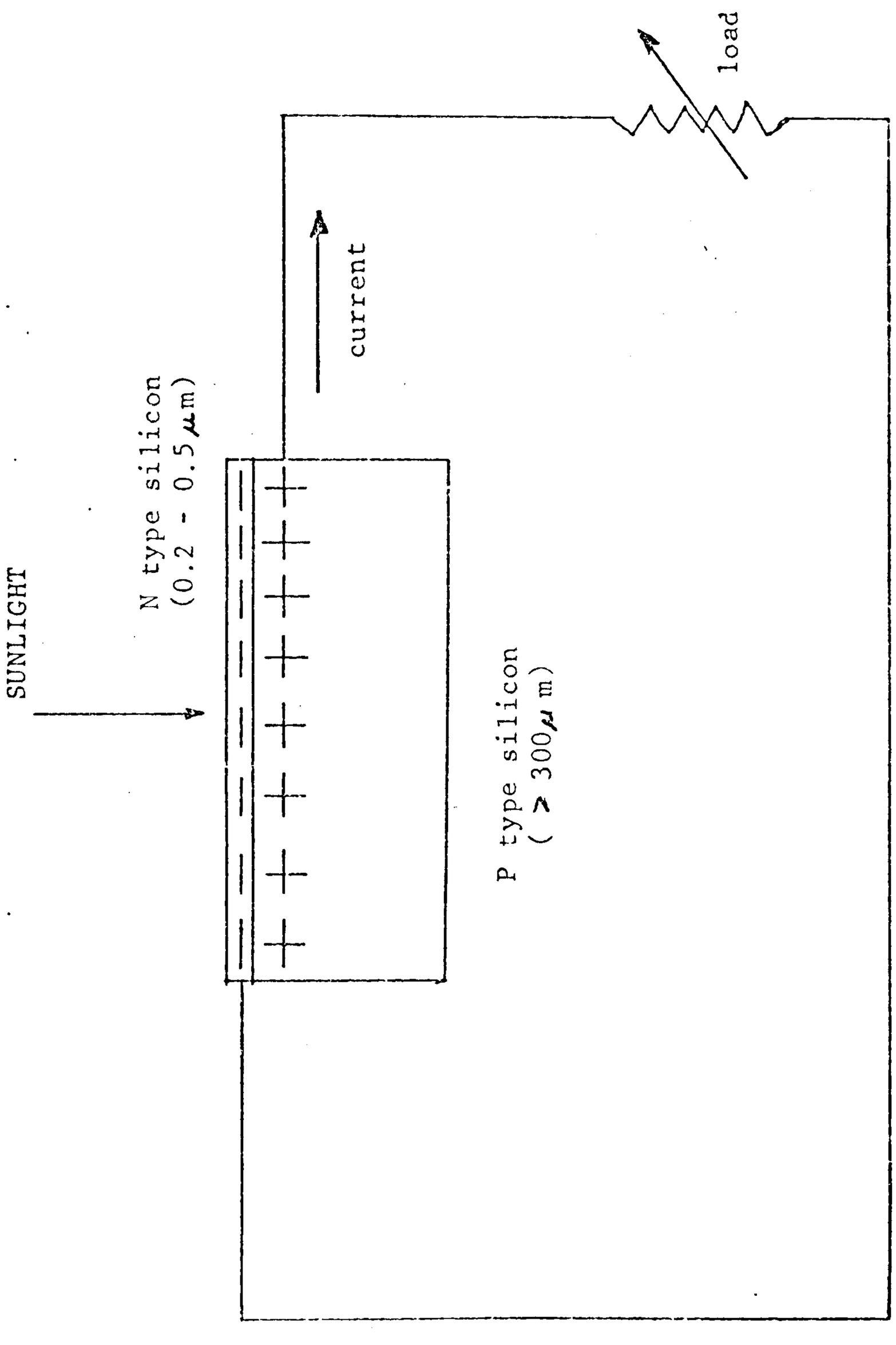
SUNLIGHT
N type silicon
(0.2 - 0.5 μm)
P type silicon
(> 300 μ m)
current
load
Silicon solar cell connected to a load

Figure 2.2

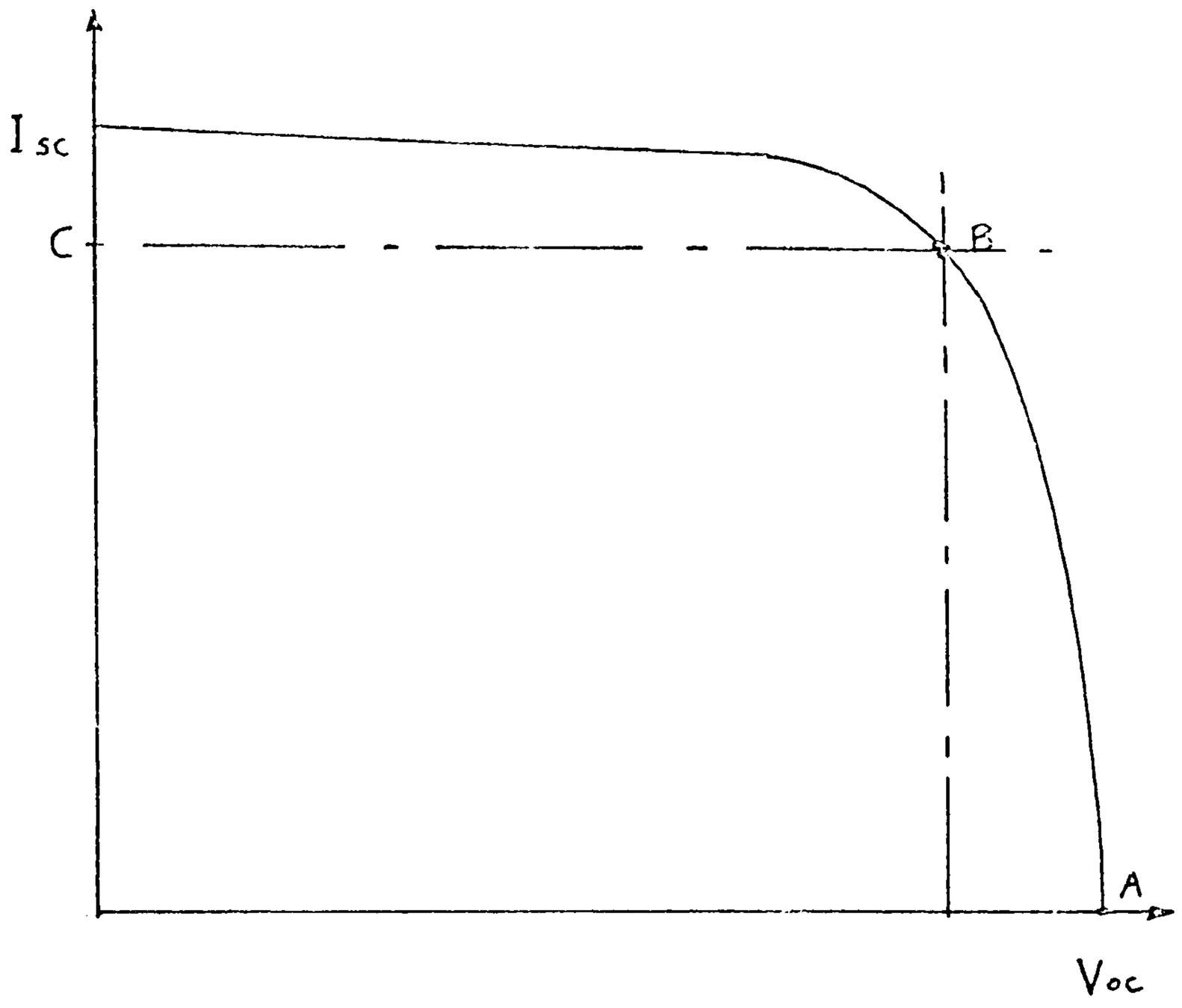

Figure 2.3a Voltage-current curve for a solar cell

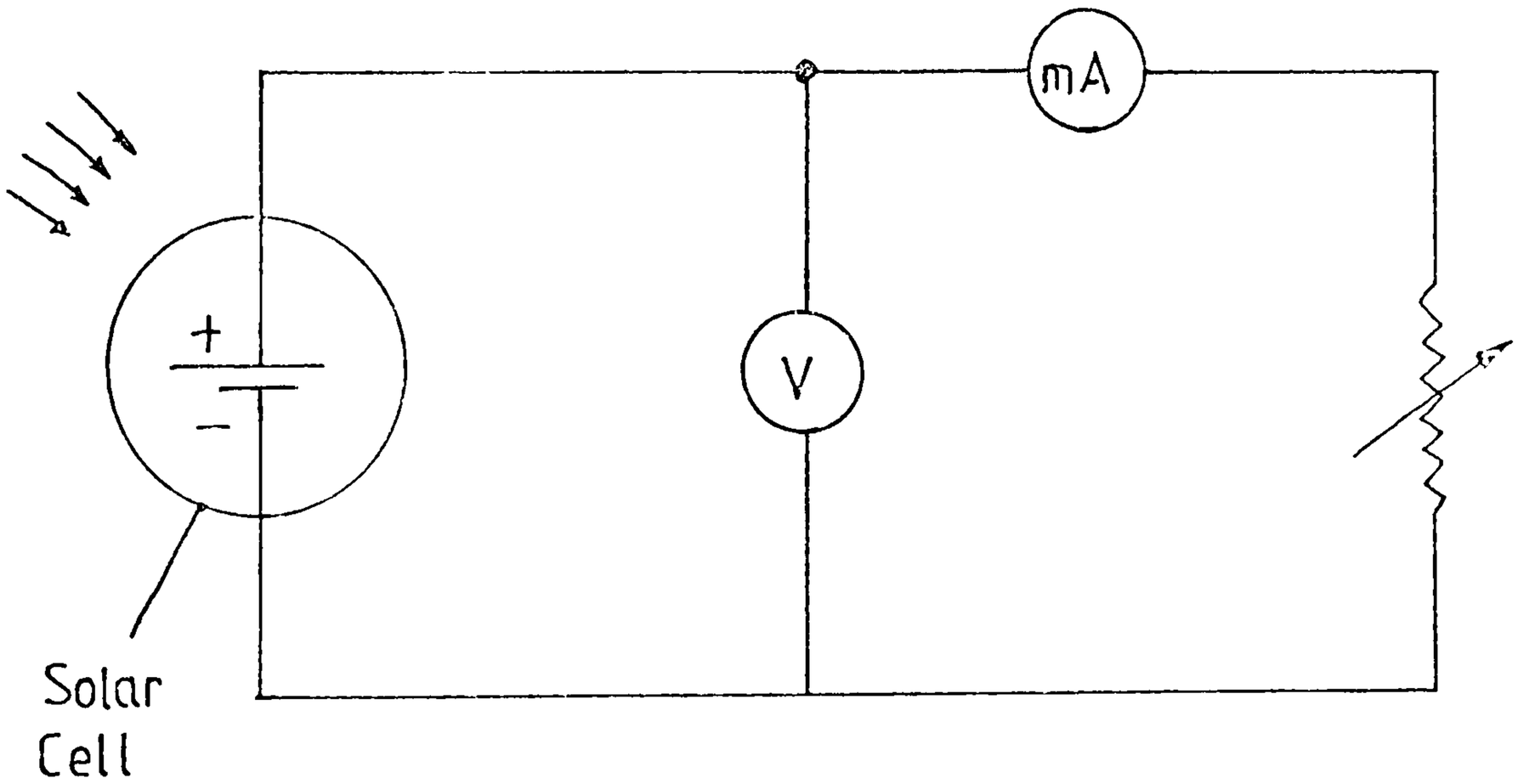

Figure 2.3b Circuit for plotting voltage-current curves

decrease linearly with the irradiance level but there is little effect on the open-circuit voltage until very low levels are reached ($< 80\ wm^{-2}$) because it is logarithmically related to the irradiance. The fact that voltage-current curves have the same shape, except at very low irradiances, has implications on many practical applications of solar cells, because the voltage at which the knee of the curve occurs does not alter significantly. Therefore, operating at the knee ensures nearly the maximum power output from the cell at all but the lowest irradiances. Thus, in many applications there is no need to change the load as the irradiance level varies.

An increase in cell temperature causes a slight rise in short-circuit current but a sharp fall in open-circuit voltage and maximum power output. Typically, the power output falls about 0.5% for every °C rise in temperature (33), so it is important to ensure that the cells run as coolly as possible under operational conditions.

With extraterrestrial photovoltaic systems the area and weight of the solar cell array are both critical, consequently, the optimum packing density is necessary (i.e. fully packed). On earth, the most economic packing density should be obtained, because rectangular cells are generally cut from round silicon crystal ingots, a good deal of waste is obtained, even using hexagonally cut cells produces waste, however, no waste occurs when using a round cell. Unfortunately round cells result in a poorer packing density and some compromise is required.

The voltage produced by a silicon solar cell is approximately 0.47 ± 0.2 volts irrespective of cell area because the voltage from the cell does not change significantly with the solar irradiance. On the other hand, because the current is strongly dependent upon irradiance it is also strongly dependent upon cell area, therefore, the larger the cell area, the greater the current produced. Nevertheless, the maximum power delivered to an external load is typically 10% to 15% of the total solar energy incident upon the cell. To obtain higher voltages cells are connected in series; higher currents are obtained by connecting cells in parallel. Such connections are made when cells

are packaged in modules. The modules then become the building blocks for arrays designed to meet specific demands.

The reasons behind an enclosure for a photothermal and a photovoltaic flat plate solar collector are different. In a photothermal collector the enclosure is used primarily as a thermal insulation envelope, improving the collection efficiency by reducing the thermal losses from the absorber plate. Although the envelope protects the absorber from the elements, it is not its principal function, unlike a photovoltaic collector. In a photovoltaic collector the solar cells are more efficient at low temperatures, consequently, there is no need to insulate against heat loss, the enclosure is employed to protect the cells from the elements and in doing so increases the temperature of the solar cells. If a photothermal collector is fitted with solar cells, then a higher collection efficiency is possible because thermal and photovoltaic collection are complementary in this hybrid system. The envelope for these collectors should be thermally insulating.

Due to its importance to the solar energy system, the absorber plate and solar cells will both be modelled in detail. In order to ensure accuracy the collector envelope will have to be modelled in some detail. There are a number of elements to consider in a collector envelope.

Absorber Plate: Although any material can be used to absorb solar radiation only a few are suitable for flat plate collectors. Metals are limited by cost to copper, aluminium and steel. Corrosion is a problem with steel and especially with aluminium when an aqueous heat transfer liquid is used. Corrosion of steel can be overcome with proper inhibitors provided the system is sealed and kept free of air. Potentially the same will be true for aluminium but, for present, aluminium is a poor choice for collectors where the maximum life is desired unless nonaqueous heat transfer fluids are used. Plastic absorber plates are seldom used because of stagnation temperature problems.

The absorber plate is usually coated with a black paint to promote solar absorption, increasing collector efficiency. Absorbers can

also be plated with black nickel or black chrome to reduce the infra-red reradiation from the absorber plate by reducing the emissivity of the surface. Although expensive, these selective absorbers improve collector efficiency, particularly if the collector operating temperature is in excess of 325K (~50°C).

If a metal is used as an absorber then it may be necessary to model the three-dimensional heat conduction effects in the material. Also if the surface is selective then a spectral analysis of incident solar radiation and long-wave radiation will be required.

Heat transporting fluids: Water and air both have the advantages of cost but there are many factors to be considered before selecting the appropriate fluid. Table 2.1 details the performance of several fluids with respect to a number of different parameters. Any mathematical model of a solar collector will require a detailed fluid-flow model.

Transparent Covers: Any number of transparent covers may be used above the absorber plate, but typically only one or two are used. The maximum quantity of solar radiation should be transmitted through these covers. In order to promote solar transmission thin anti-reflection films (e.g. magnesium fluoride) are evaporated onto the covers, this increases efficiency. Although expensive in the past, new processes have considerably reduced production costs.

The main purpose of these covers is to reduce the convective losses from the absorber plate, this is possible because the cover is generally at a lower temperature and consequently reduces ambient temperature losses. Glass is the most commonly used transparent cover because it has good transmittance properties and is durable. Plastics are also used, but their lifetime depends upon their rate of solar degradation. Plastics such as TEDLAR PVF (polyvinyl fluoride) have been developed specifically for solar glazing application and they offer a much longer life compared to normal plastic covers. One major advantage of glass compared to most plastics is that it is opaque to the infra-red reradiation of the absorber plate, whereas plastics tend to transmit some of this energy. Therefore, depending upon the application, glass covers may be necessary.

	Toxic	Environmental Hazard	cost	freezing temp	support corrosion	boiling temp.	thermal stability	spill damage
Water	-	-	-	$0^{o}C$	Y	$100^{o}C$	H	-
Water/Glycol	S	S	L	$-35^{o}C$	Y	$> 100^{o}C$	L	-
Hydrocarbons	S	-	L	-	M	-	L	S
Silicon Fluids	VS	-	H	-	-	-	H	-
Air	-	-	-	-	-	-	-	-

Table 2.1 Comparison between several heat transporting fluids.

Nb. S = slight; L = Low; H = High; M = Moderate; Y = Yes

To model a transparent material accurately the optical properties of the material in the solar and infra-red spectrum should be known.

Insulation: It is necessary to reduce back and side losses from a photothermal collector. The best type of insulation is fiberglass board as others can degrade at temperatures well below the collector stagnation point. Other insulating materials like ceramic fiber are too expensive for solar applications.

The thermal conductivity in insulation is low therefore three-dimensional heat conduction need not be considered, only the conduction in the direction of heat flow is assumed to be important.

Gaskets and Seals: The most troublesome part of the collector is the interface between the transparent cover(s) and the collector enclosure box. If the seals fail, moisture will enter the collector, the transparent cover may fog and the insulation may slump. These effects can drastically reduce the thermal performance of the collector. Therefore, gaskets and seals must resist the elements and UV light for the life of the collector while retaining excellent adhesion to all surfaces and withstanding temperature cycling. However some mathematical consideration of leaks must be made.

Although losses from the absorber plate in a photothermal collector are reduced when using an insulated enclosure, care must be taken to ensure that the transparent elements and the size of the opaque sizes of the envelope do not seriously limit the quantity of solar radiation incident upon the absorber plate.

The solar collector is the most important component in a solar energy system, therefore, the proposed mathematical model will consist of a very detailed solar collector model which will be discussed later.

2.1.2 Storage

There are four basic modes of non-biological energy storage: thermal, electrical , mechanical and chemical (e.g. molecular hydrogen).

Thermal energy can be stored as sensible heat, latent heat of phase change or in reversible chemical reactions. Electrical energy is usually stored electrochemically in batteries. Mechanical energy can be stored inertially as kinetic energy in flywheels or as potential energy in compressed air or elevated liquids (e.g. pumped water for subsequent electricity generation). Hydrogen may be stored in a number of ways (20). At present, most forms of mechanical and chemical energy storage are neither suitable for building applications nor compatible with flat plate solar collector systems. In this work, thermal and electrical energy storage will be considered for photo-thermal and photovoltaic systems respectively.

Excess energy from photothermal collectors is best stored for subsequent use in thermal storage devices. In building applications the most suitable storage forms are sensible, latent or a combination of sensible and latent energy storage. Sensible energy is stored when the temperature of the store increases, this is a function of the heat capacity of the material. Water and pebble beds are the most commonly used materials for sensible heat storage for liquid and air collectors respectively. Both of these materials are low in cost and readily available but any thermally and chemically stable solid or liquid could be used. One of the main problems of using water or pebbles is that at 66°C they have a heat capacity of 4.103MJ/K and 1.34MJ/K per unit volume respectively. This low heat capacity imposes several secondary problems: large volumes are required; high quantity insulation must surround storage units due to high heat losses at elevated storage temperatures; and they are unsuitable for more than a few days storage. Water storage itself is much better storage media than pebbles because the pebble bed would be three times larger to store the same quantity of energy. One advantage of pebble bed storage, however, is the degree of thermal stratification which can be achieved, ensuring that when withdrawing energy from the store it leaves at the maximum possible temperature. Water storage tanks can be fitted with devices to promote stratification but this adds to their manufacturing cost.

There are materials which can gain or lose heat by isothermal phase

change at temperatures compatible for use with flat plate collectors. The phase change can occur between solid and liquid (heat of fusion, Δhf), liquid and vapour (heat of vaporisation, Δhv), and solid crystalline phases (heat of solid-solid transition, Δhs). These materials are classed as latent or sensible/latent heat stores. In buildings the most common latent-heat storage materials used are the heat of fusion materials such as Calcium Chloride Hexahydrate ($CaCl_2 \cdot 6H_2O$), Magnesium Oxide Hexahydrate ($MgO_2 \cdot 6H_2O$) and Sodium Sulphate Decahydrate ($Na_2SO_4 \cdot 10H_2O$) which is more commonly known as Glauber's Salt (20). Glauber's Salt undergoes its phase change at 31°C and can store 328.5MJ per unit volume representing an energy equivalent of an 80K temperature rise in a unit volume of water. Obviously, the volume of latent storage units are smaller and tend to have lower storage temperatures compared to sensible storage units, therefore, heat losses can be considerably lower. The main disadvantages are that these materials are much more expensive than water or pebble bed storage, also the materials have a relatively short life ($<$ 1000 cycles) of only a few years before replacing the storage material.

Electrochemical storage is used exclusively for photovoltaic collector systems, it is a particularly compatible storage form because it accepts the direct current generated by the photovoltaic system. The most commonly used electrochemical storage unit is the rechargeable lead-acid battery which operates at room temperature and requires no insulation. The advantages of lead-acid batteries are that they are currently available, have a proven reliability and have a moderately high efficiency, (70%). Although they last about 10 years, their lifetime can be impared by constant daily cycling particularly if the battery is frequently charged to too high, or discharged to too low a voltage. Due to their weight vertical stacking of batteries, or use in upper floors, is not recommended. Provision must also be made to vent possible hydrogen accumulation due to water decomposition in the charging process.

Advanced non-aqueous and aqueous batteries have been developed which are demonstrably superior to lead-acid batteries. They are generally

longer lasting, more efficient and have a higher energy density for a reduced weight although there are still a number of problems to be resolved before full scale production can proceed. Consequently, their cost is still high and as yet do not offer a feasible alternative to lead-acid batteries.

It is recommended that wherever possible the storage unit should be housed within the building envelope to protect it from the elements, consequently, a finite amount of space must be reserved for the unit. This can pose a problem when space is a a premium, e.g. commercial buildings. Basements are the most suitable situation for a storage unit, particularly for sensible storage units. Unfortunately in Britain the tendency has been not to build basements, therefore, there may be a size restriction on the type of storage system suitable for existing buildings. Thermal storage with a building can prove to be both advantageous and disadvantageous. During the heating season the heat loss from the unit may reduce the building heating demand but in the cooling season the building cooling load requirement may well be increased.

The storage unit is the next most important component in a solar collector system model and as such should be modelled in some detail.

2.1.3 Auxiliary Source

There are few occasions where a particular solar energy design can economically meet the full annual energy demand, therefore, an auxiliary source of energy will normally be required to ensure system reliability and avoid gross oversizing of the solar collector system. In a photothermal system the auxiliary heater should be sized to meet the maximum demand, in preparation for solar system breakdown or depletion of the solar stored energy due to a prolonged cloudy period. A photovoltaic system is normally backed up with a connection to the electricity grid, or in some situations a small generator can be used.

An investigation on the best location for an auxiliary heater in a photothermal system was conducted by Duffie and Beckman (34). They analysed the annual solar contribution obtained from a liquid collector system with the auxiliary heater in three different positions (Figure 2.4). It was found that the maximum solar contribution was obtained with the auxiliary energy in position B, where the auxiliary heater is used to maintain the desired outlet temperature by heating the liquid from the top and warmest part of the tank. A simple in-line heater is best, but performance can be impared if the auxiliary heater has some storage capacity as this will increase system heat losses. There is no reason to believe that the auxiliary heater in an air collector system would not operate best as an in-line heater.

The mathematical model of an auxiliary energy source for photothermal systems will operate as an energy injection into the fluid passing through the component.

2.1.4 Distribution

This section is directly related to photothermal systems because the photovoltaic distribution system is an electrical circuit which is assumed to have negligible power losses.

There are two parts to the distribution system: the equipment to promote fluid distribution, and the conduits connecting the various system components. There are can any number of fans or pumps or both in the system depending upon the number of fluid circuits plus the associated valves and dampers. The resistance of the distribution network should be small to ensure that the fan or pump parasitic power consumption is low. Furthermore, the conduits must be well insulated to maximise the potential solar contribution.

There are two forms of conduits: pipe and ducts which are normally used for liquids and air respectively. A ducted system has several disadvantages compared with a piped system because the ducts will take up more space also if a ducted system were to be insulated to the same level has a piped system, insulation costs are considerably higher.

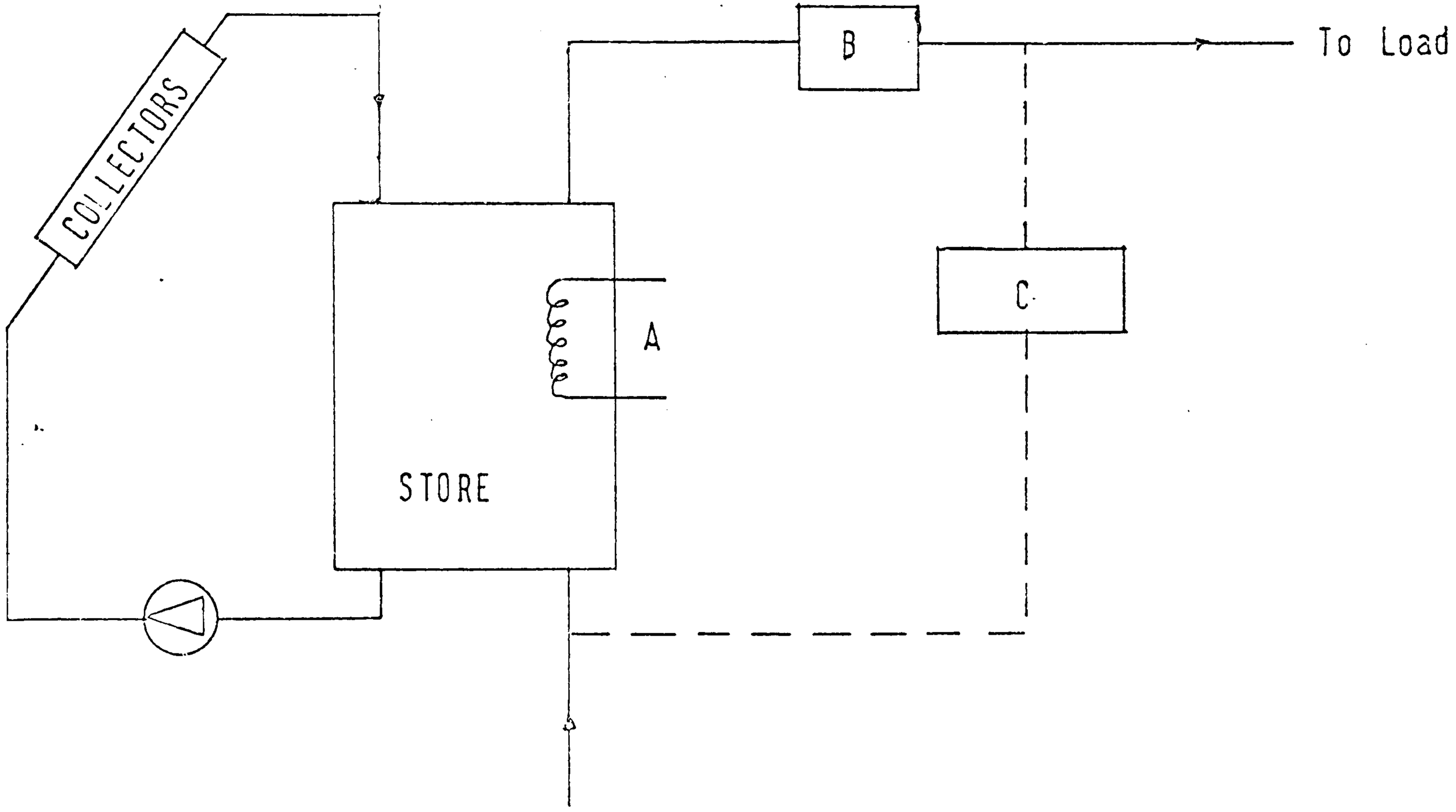

Figure 2.4 Possible positions of auxiliary in solar energy system

A simple mathematical model will be adequate for any fitting in the distribution system. Depending upon the level of accuracy required the model could assume no distribution losses reducing the computational requirement of the model

2.1.5 Control

The basic function of the controller in a solar collector system is to operate the system in such a way that the maximum quantity of solar energy is collected and subsequently delivered to meet the appropriate demands. The control system should be as simple as possible for a reliability and maintenance standpoint, however, it should not be so primitive that the thermal performance,which is strongly influenced by the controller, is seriously impaired. There are two types of control used in solar collector systems: the most common is differential control, the other is proportional control.

A manual switch or simple timer may be adequate in certain applications. However, a differential thermostat can provide a more precise and efficient means of automatic control. A typical differential controller consists of one sensor measuring collector temperature, a second measuring storage temperature, an electronic circuit which compares the two temperatures, and logic circuits which provide appropriate signals to pumps, fans, valves and dampers. The fan or pump is switched on whenever the temperature difference (ΔT on) between the collector and storage temperatures exceeds a pre-set valve, likewise the fan or pump is switched off if the temperature difference (ΔT off) falls below a pre-set valve. Care must be taken when setting ΔT on and ΔT off. If the setting is too low, then excessive fan or pump cycling occurs causing premature wear and possible fan or pump failure. If the temperature differentials are set too high, the system will be switched on and off after the most suitable times, reducing the solar energy pick-up.

The collector cycling may be reduced by throttling the fluid flowrate. This can be accomplished by a proportional controller using the temperature sensors to regulate the speed of a variable pitch or multi-

speed fan or pump. These controllers can be used to maintain either the collector outlet temperature or the temperature rise through the collector at or near a predetermined valve. Although more expensive than differential control, proportional control has the advantage that the reduced flowrates may be used to improve the control system stability without seriously compromising thermal performance (20).

In any system care must be taken to position the temperature sensors properly, as bad positioning can result in a significant reduction in the solar energy collected, e.g. a water tank sensor close to the cold water inlet can cause the controller to be 'tricked' by a small quantity of entering cold water into operating the pump such that the system could operate in a net energy loss condition.

A major problem in a fluid collector is that the collector circuit may be switched off if the set upper limit in the storage tank is reached preventing boiling or overheating in the storage medium. However, problems may occur in the collector circuit if either the boiling point of the fluid or the collector's stagnation temperature is reached. Either of these situations can occur during periods of power outage, fan or pump failure, or during installation. Consequantly the system should be designed to avoid critically high collector temperatures. In liquid collectors, liquid draindown or a blind cover system could be employed to alleviate a boiling liquid situation.

Electrical signals are sent instantaneously throughout the control subsystem between different control elements. The subsequent interactions between the controller and the system are best modelled simultaneously. The various controller and system lags do not allow immediate response to a signal, therefore, using a variable time-increment in the model the effects of each event may be analysed e.g. pump switch on or off. These control subsystem influences on the mathematical model will be discussed in subsequent chapters.

2.2 Active Solar Energy Systems

In principle, the type of solar collector system used should be compatible with its application, allowing the collector to supply direct to the source of the demand - wherever possible. Frequently, however, the system and application are incompatible because of climate, cost and the proposed (or existing) building type or the installed plant. There are four main solar collector system applications for buildings in the UK:

1. Domestic hot water heating
2. Space heating
3. Electricity generation
4. Solar cooling

The heating of water for domestic or industrial applications is one of the oldest and most practical forms of solar collection used worldwide. The system can be classified as a direct or indirect, natural or forced circulation system. Natural circulation systems are unsuitable in climates where freezing may occur, forced circulation being more common. If the system is a direct, forced circulation one, then mains water is used as the energy transporting fluid allowing direct supply from the collector, however, this system requires a liquid draindown facility primarily to ensure that freezing will not occur in the solar collector. A draindown facility can be used in an indirect system, its function is normally to avoid liquid boiling rather than freezing because the liquid is usually a non-freezing liquid e.g. water/antifreeze mixture, silicon oil. In this system a heat exchanger or an indirect water tank is required to transfer the solar energy to the water, Figure 2.5. Heated water can be used for either domestic hot water supply or space heating. There is a British Standard code of practice for solar heating systems for domestic hot water, BS 5918:1980, which is highly informative in describing these systems and their problems (35).

Due to the pioneering work by Löf (20), air collectors have begun to make an impact on the solar market. Air systems tend to be simpler

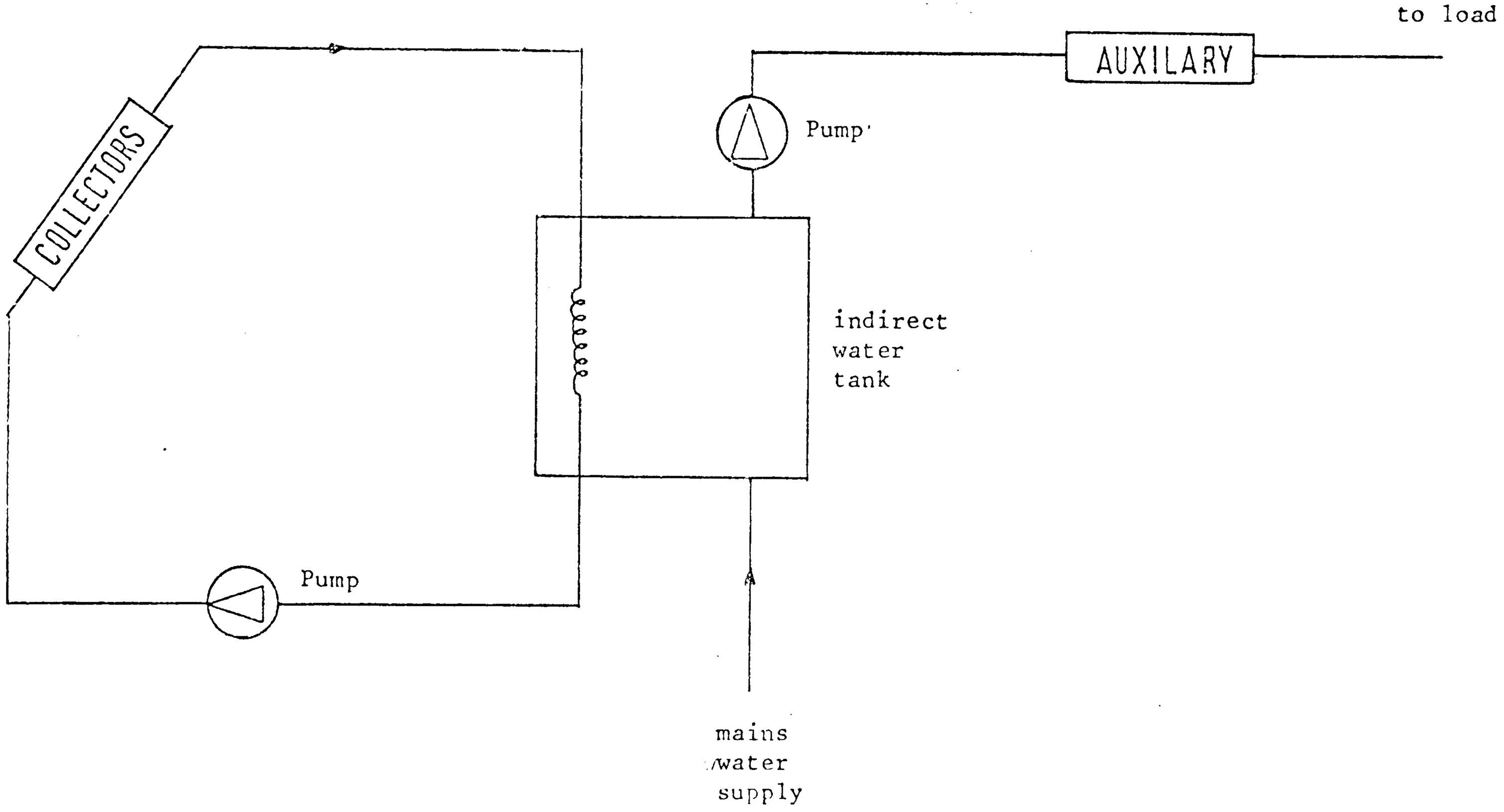

Figure 2.5 Schematic diagram of a simple liquid collector system for DHWS supply using an indirect system

and easier to maintain than water systems and do not have boiling or freezing problems associated with their use. The principal application for air collectors is in space heating where the heated air can be supplied directly to the living space. Unfortunately, air has a much lower heat capacity than a liquid, consequently, a much greater mass of air is distributed for a comparable energy content, this results in a 'bulky' system. Although air collectors can be used for water heating it is not a practical design, however, the air collector system is sometimes used to preheat water, Figure 2.6.

The average daily demand for domestic hot water is reasonably constant throughout the year, whereas space heating demand is much larger in winter than in summer. It can be concluded that domestic hot water heating can offer a better annual performance compared to a space heating application, however, in houses with a relatively constant space heating demand, solar space heating may be more suitable, particularly if a cheap form of interseasonal storage was available.

In new buildings architects can design to accommodate active solar designs, e.g. basements for sensible rock bed storage. With existing buildings the choice of solar collector system is constrained by the type of system the building can accommodate. When retrofitting a solar scheme, it should be compatible with the existing plant, for example, if space heating is being supplied via ducted warm air, then an air system should be considered. If however, space is a premium in the building, then a ducted system may be overlooked in preference to a liquid collector system. The problem of space is even more acute in terms of thermal storage. Water and pebble beds are suitable storage media but there may not be adequate space for the storage volume required, therefore, a latent heat store would have to be employed, at much greater expense. There are no general rules for the type of thermal solar collector system to use in a particular application, each must be selected on its own merits. Table 2.2 explains some design options.

Most buildings require electrical energy which can be supplied from the electrical grid, a generator or by a photovoltaic solar collector

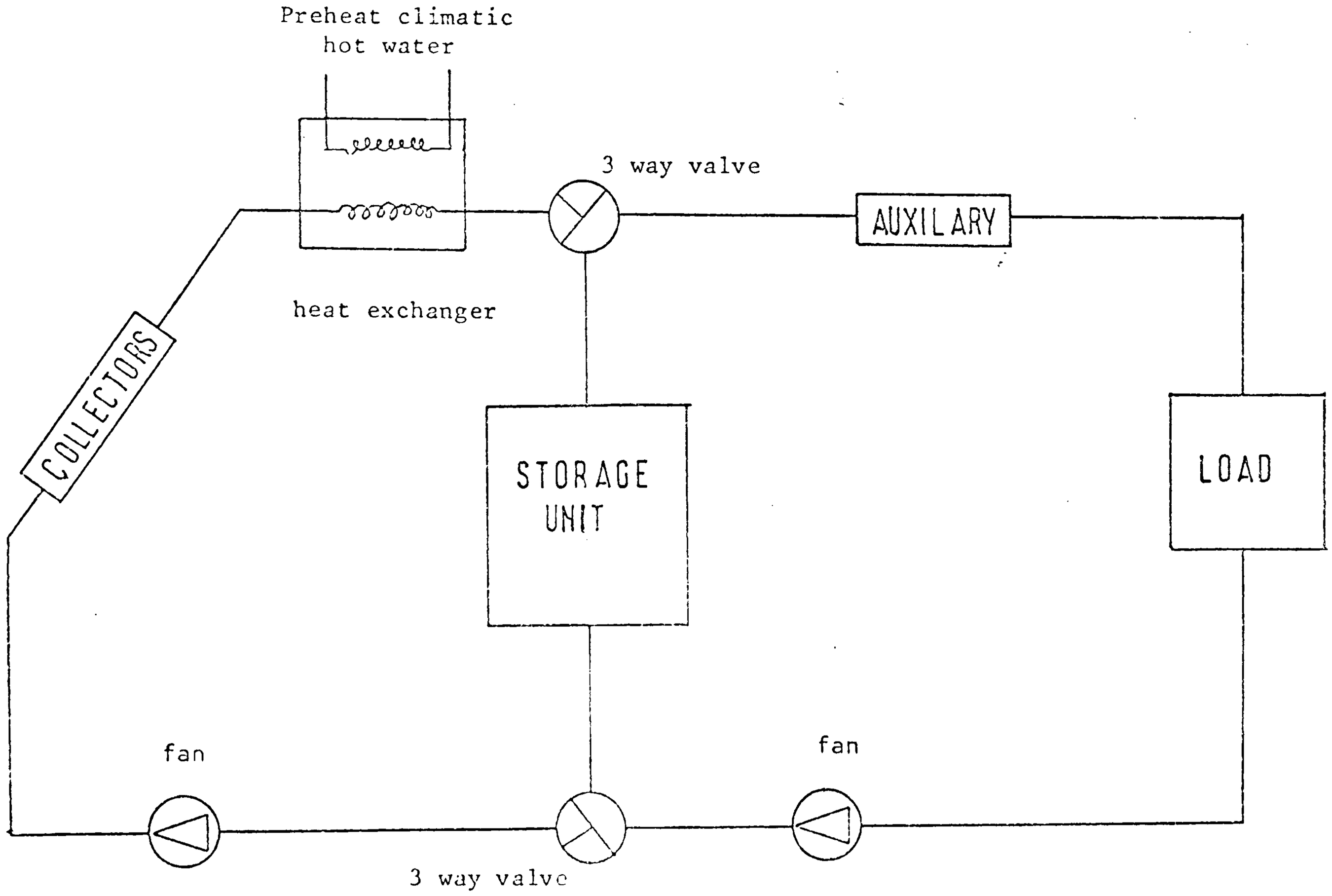

Figure 2.6 Schematic diagram of a simple air collector system for space heating and preheating DWHS supply

Climate	Application	Heat transporting Medium	direct or indirect	Storage medium	Practical use?
Non-freezing	Water heating	water	direct	water	Y
		air	indirect	water	N
	Space heating	water	direct	water	Y
			indirect	sensible and/or latent	Y
		air	direct	rock bed	Y
			indirect	sensible and/or latent	Y
	Photovoltaic	Electricity	direct	lead acid batteries	Y
Freezing	Water Heating	Fluid	indirect	sensible and/or latent	Y
		Air	indirect	sensible and/or latent	N
	Space heating	Fluid	indirect	sensible and/or latent	Y
		Air	direct	rock bed	Y

Table 2.2 Practical Design options depending upon climate, application etc.

system. In addition to a properly sized solar cell array and storage battery, the complete photovoltaic system may include:

(i) a blocking diode to prevent battery current drain through the solar cell array at night,

(ii) a voltage regulator is used to avoid overcharging the storage battery, resulting in a loss of electrolyte. This will occur when the battery is fully charged but the array is still capable of supplying more energy than the load demands, under these conditions the voltage regulator will shunt the excess current through a dummy load. It should only be used if the system is capable of producing over 20% excess energy annually.

(iii) an invertor converts DC power to AC and sends it to the load or feeds it back to the grid.

The ability to feed electrical power into the electricity grid is uncommon in Britain but in the USA the utility must pay the user at premium rates for the electricity received whether or not it requires the energy (36), as set out by the Public Utilities Regulatory Policy Act (PURPA) of 1982.

Photovoltaic systems are easily installed into existing building and have no moving parts, however, the cost of a system is being rapidly reduced due to mass production techniques, but as yet the cost of a generated watt of power by solar energy is still more expensive than that produced by nuclear fission, nevertheless, in the near future the cost should be compatible. It should be noted that cells made with present techniques have to operate about 12 years to regain the energy expended on their manufacture. Therefore, a photovoltaic system should be designed to operate for at least 15 years. A diagram of a typical photovoltaic system is shown in Figure 2.7.

There is considerable interest into the investigation and development of hybrid or combined thermal/electric flat plate collectors. In these collectors the absorber consists of an array of solar

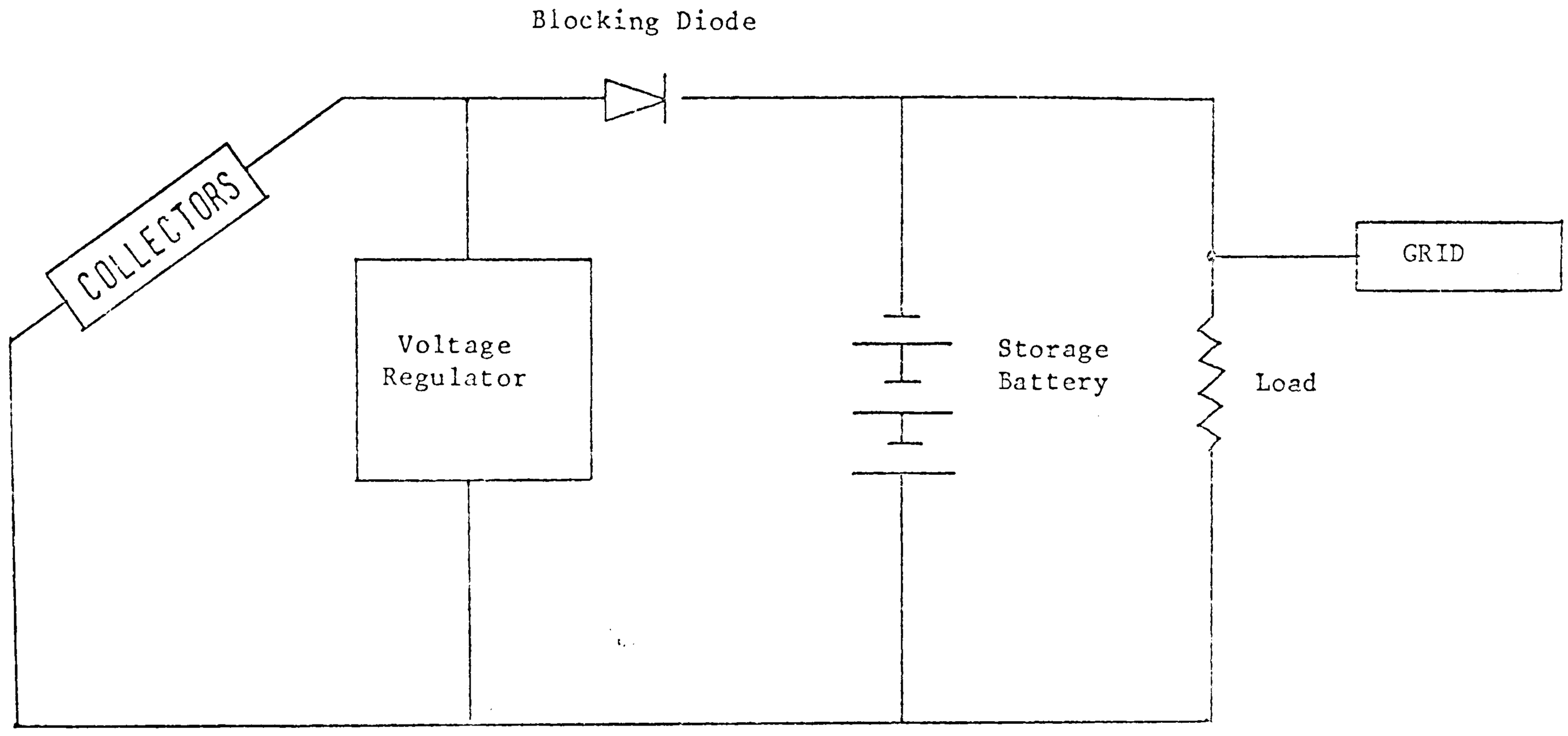

Figure 2.7 Typical photovoltaic system

cells for electricity generation while collector fluid circulating past the absorber provides thermal energy as in a conventional flat plate collector. Although some of the efficiency of solar cell array is traded off for thermal energy collection, and vice versa, the combined system has advantages (20):

(1) Up to about 60% of the available solar energy utilised
(2) Duel use of collector area, reducing total area requirements
(3) As the components fulfill several functions, they yield a most cost-effective system.

The last of the building applications of solar collector systems in the UK is solar cooling. Solar cooling has potential for large commercial buildings requiring air conditioning. It is particularly attractive because cooling loads and solar radiation availability are approximately in phase. There are various solar airconditioning systems available but solar absorption cooling is the process most suitable for commercialisation (Figure 2.8).

Solar cooling and heating systems or photovoltaic systems can be combined to increase solar utilisation, however, as solar cooling is applicable only to a few situations in the UK, it will not be considered further in this work. Details of solar cooling can be found elsewhere (20,34).

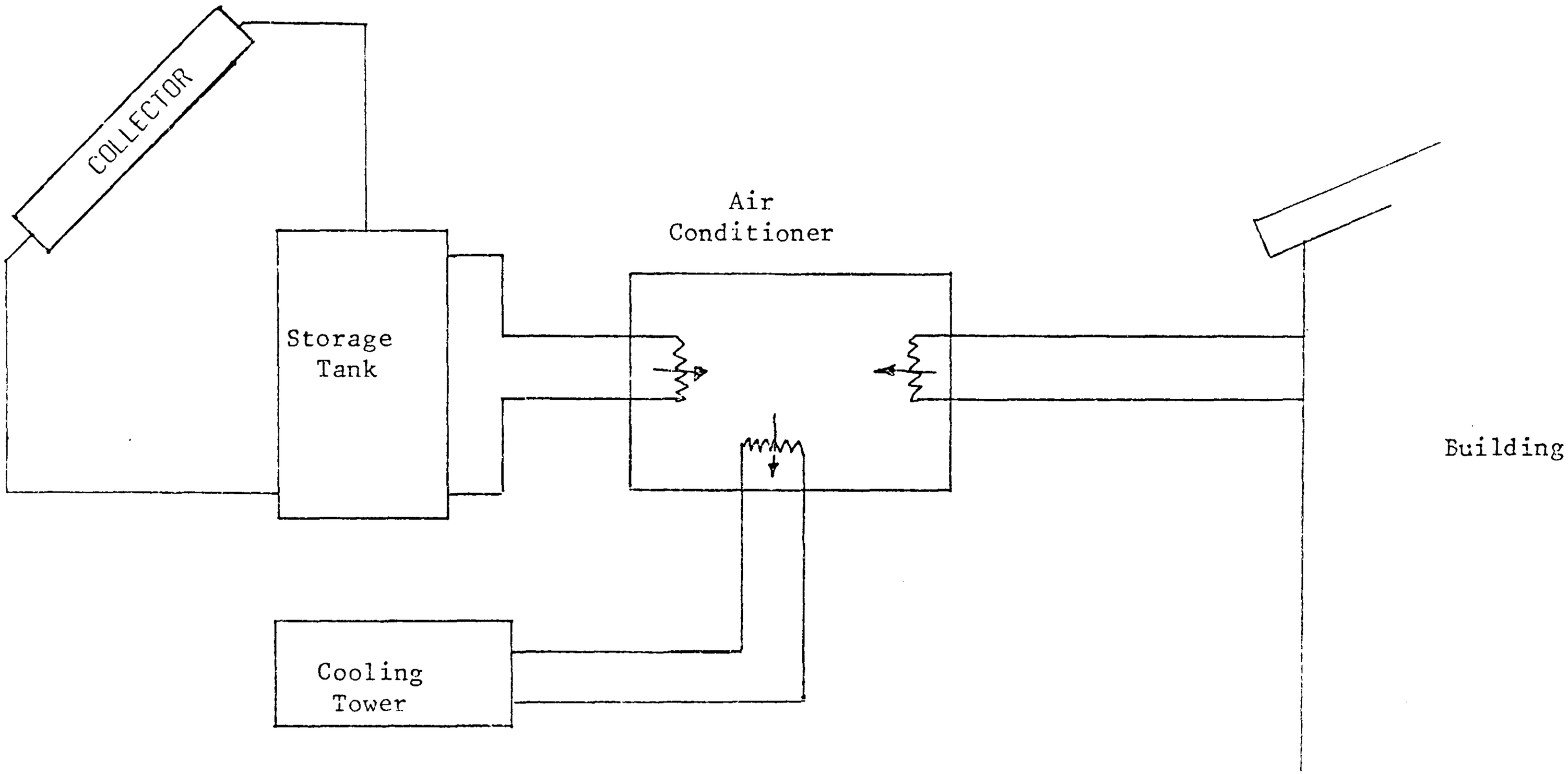

Figure 2.8 Simplified schematic of a solar absorption air conditioning system

CHAPTER 3 CLIMATOLOGICAL INFORMATION

In any energy analysis, where the boundary conditions of the system are subject to climatological influences, it is necessary to obtain representative climatological information similar to that which influences the system. Ideally, the climatic data required for an energy analysis should satisfy two main requirements (5):

(1) the climatic data should be representative of the conditions at the design locale. If representative climatic data are not available for the design site, two distinct alternatives exist, either climatic data from a site with a similar topography (to the design site), or predicted or synthesised data, is employed.

(2) the climatic data should have some quantifiable degree of acceptability, or design severity, which makes its selection meaningful in terms of the application to which it will be put. Thus, for any particular locality different climatic data sets would be required in order to subject a proposed design feature to those climatic characteristics that best examine its performance (e.g. warmest period, coldest period, highest solar radiation period, etc).

There are extensive climatological records available from the UK Meteorological Office for several sites (Section 3.1) on tape. Recorded data in this form has the advantage of a wide range of climatic data from which to select test data to analyse the appropriateness of a particular design. To facilitate comparative analysis various techniques are available to select one year's data from a number of years of data. This standard year is known as the Test Reference Year or TRY. There are sites where no - or a limited amount of - climatic data is available, various techniques are discussed in Section 3.3. to predict or synthesise climatic data in this situation.

Whatever set of hourly values of climatological information is selected

if the surface is selective then a spectral analysis of incident solar radiation and long-wave radiation will be required.

3.1 Availability of Climatological Information

There are many weather observation centres throughout the world, as they have been set up independently for meteorology study purposes and not for use in energy simulation models, the more appropriate climatic variables necessary to drive simulation models are not always available, e.g. hourly values of solar radiation, ambient temperature, etc. However, combined meteorological data tapes linking recorded hourly solar radiation measurements with other variables such as wind, temperature and humidity, are currently available for a number of sites in the UK, USA and in the European Communities.

Recently in the USA, a programme was undertaken by the US National Weather Bureau to upgrade the number and quality of meteorological centres measuring solar radiation, to rehabilitate past data in accord with new measuring technqiues, and to make these data available (with related meteorological data) on magnetic tapes for energy analyses (18). As a result, from 1978, corrected data tapes were available of hourly climatological data for 26 centres over a 23 year period. These tapes are referred to as the SOLMET tapes. The programme has now been extended to several more sites and the process of transferring to SOLMET tape format of new climatological data continues.

A number of tapes have been prepared by European Community member countries, some of which have been assembled onto EC data tapes as part of the EC solar energy programme (37). Several issues have yet to be resolved before these tapes are made available, e.g. copyright.

In the UK, the Meteorological Office have a number of centres throughout the country which take comprehensive measurements of many climatic parameters, there are also a number of smaller centres which measure a few parameters. The climatic data obtained from these stations have been collected over a number of years and are held either in manuscript form or on magnetic tape. There are tapes available covering a ten-year period from 1959-1968 inclusive for four centres Aberporth, Eskdalemuir, Kew and Lerwick. Action is being taken to extend these tapes up to 1980, providing a 22 year data tape for each observatory.

(The Kew record will be slightly shorter because the Kew Station has been closed). In addition, new tapes are being prepared for four other centres - the Aldergrove and the Aberdeen tapes will cover the period January 1968 to December 1980, the Cardington tapes will cover the period January 1972 to December 1980. A tape for the London Weather Centre is also under preparation.

Hourly values of 18 climatic variables are stored on the Meteorological Office tapes (Table 3.1). Most of the variables are measured but some are derived, for example, dry and wet bulb temperatures are used to generate other humidity parameters. Three different types of readings are presented:

(I) Spot readings, the value of the parameter is measured exactly on the hour, i.e. at 0.00, 1.00, . . .; 23.00 GMT

(II) Mean readings, correspond to the average reading over an hour period, i.e. 23.30-00.30, 00.30-01.00, . . ., 22.30:23.30 GMT

(III) Total readings, are the total value for the parameter over the hour period defined in (II) above.

Each record on the magnetic tape contains 25 values of each climatic parameter; 24 hourly values plus a mean hourly or a daily total value. Miscellaneous information such as the month number, century day, maximum and minimum values of hourly dry and wet bulb temperature, etc, are also given.

As solar radiation data are archived as hourly mean values with respect to solar or local apparent time (LAT), the Meteorological Office has converted this data to Greenwich Mean Time (GMT) using linear interpolation. At Kew the maximum effect of the Equation of Time and longitudinal differences is 16 minutes, consequently the Meteorological Office did not modify the solar radiation data for this site.

The Meteorological Office tapes were originally available for a nominal fee. It is anticipated that a charge up to 0.1p per unit of information be levied on magnetic data tapes to meet data collection and archiving costs, however, reduced rates will probably be available for

TABLE 3.1

CLIMATIC PARAMETERS ISSUED ON TAPES

ITEM	ELEMENT	UNIT	TYPE	ENTRY 25
1	Global Solar Radiation	W m^{-2}	Mean	Total
2	Diffuse Solar Radiation	W m^{-2}	Mean	Total
3	Sunshine Duration	0.1 hr	Total	Total
4	Dry Bulb Temperature	0.1 ^{o}C	Spot	Mean
5	Wet Bulb Temperature	0.1 ^{o}C	Spot	Mean
6	Specifice Enthalpy	0.1 kJ kg^{-1}	Spot	Mean
7	Atmospheric Pressure	0.1 mb	Spot	Mean
8	Wind Speed	0.1 m s^{-1}	Mean	Mean
9	Wind Direction	Degrees	Mean	Mean
10	Rainfall Amount	0.1 mm	Total	Total
11	Rainfall Duration	0.1 hr	Total	Total
12	Dew Point	0.1 ^{o}C	Spot	Mean
13	Vapour Pressure	0.1 mb	Spot	Mean
14	Relative Humidity	%	Spot	Mean
15	Direct Solar Radiation	W m^{-2}	Mean	Total
16	Net Radiation	W m^{-2}	Mean	Total
17	Global Illumination	0.1 kilolux	Mean	Total
18	Diffuse Illumination	0.1 kilolux	Mean	Total

data used for research purposes only.

In real time simulation of a climatic dependent model the larger the quantity of data available the more likely it is to obtain an appropriate period for testing a design. The Test Reference Year of any climatic data-set is normally based on the mean or extreme of one or more climatic parameters, as such it is representative of the site but it is difficult to represent the variances of many years data in one year. Predicted or synthesised climatic data, however, should not be used in simulation models unless absolutely necessary because the interrelationships between climatic parameters cannot be accurately assessed.

The methods available to obtain a Test Reference Year and to synthesise and predict climatic data will now be discussed.

3.1.1 The Test Reference Year

Ideally the performance of a building or system should be simulated against several years of climatic data, however, computational costs prohibit such a simulation. If a year is considered the longest practical simulation period and several years of climatic data are available, then a single year will have to be selected which is representative of the measured data. The 'sample' year selected is more commonly known as the Test Reference Year or TRY. The TRY is a climatic database consisting of 8760 hourly sets of both mandatory and optional climatic parameters.

The full climatic data set offers the user many more variations in climate for testing the success or failure of a design under particular conditions, nevertheless, a year of data should be sufficient to handle most designs. The main advantage of the TRY is that it offers a standard for comparing either simulation models or designs simulated by such models.

There are a number of countries which have developed TRY data. To avoid confusion and simultaneously create some commonality between each TRY data set an international format for the TRY has been proposed (Table 3.2). The format relates only to the position on the tape of data such as the month, day and hour of the record, this

tape position	element
01-05	station number
06-73	weather data (depending on country of origin *)
74-75	month
76-77	day
78-79	hour
80	continuation

* for the United States T.R.Y. data:

06-08	dry bulb temperature
09-11	wet bulb temperature
12-14	dew point temperature
15-17	wind direction
18-20	wind speed
21-24	station pressure
25	weather
26-27	total sky cover
28-29	amount of lowest cloud layer
30	type of lowest cloud or obscuring phenomena
31-33	height of base of lowest cloud layer
34-35	amount of second cloud layer
36	type of cloud - second layer
37-39	height of base of second cloud layer
40-41	summation amount of first two layers
42-43	amount of third cloud layer
44	type of cloud - third layer
45-47	height of base of third cloud layer
48-49	summation amount of first three layers
50-51	amount of fourth cloud layer
52	type of cloud - fourth layer
53-55	height of base of fourth cloud layer
56-59	solar radiation (not yet available)
60-69	blank
70-73	year

TABLE 3.2 The T.R.Y. Format

allows each country to collect and format measured results in whatever way they desire.

The 'CIBS Example Year' has been produced from many years of climatic data for Kew. The technique employed to select the TRY was based on work by Holmes and Hitchen (38). Their technique involved using several climatic parameters: dry bulb temperature, degree days, windspeed, and global and diffuse solar radiation, and for these parameters the monthly mean values were evaluated for every available year and compared to the long term monthly mean. If a significant difference occurred in the monthly value of any parameter then this year was rejected. To avoid a discontinuity in the middle of the heating season, an October to September year was chosen rather than a calendar year. The conclusion of this analysis was that the year October 1964 to September 1965 should be selected as the CIBS Example Year. (Using this technqiue, 1967 was the most suitable calendar year). This TRY data should be used exclusively for sites at or in the vicinity of Kew, but it can be applied to any site with a similar topography.

There are several other nations who have selected and made available TRY data notably the USA, Denmark and Japan. The techniques used in these countries are exclusive to that country and differ considerably.

The USA method (39) consists of eliminating from the data set the year with the highest mean monthly temperature in July. Next the year with the lowest mean monthly temperature in January is eliminated. The years associated with the hottest August and the coldest February are then eliminated. Table 3.3 indicates the rank ordering employed. This process continues by eliminating those years with the next most extreme months until only one calendar year remains which is declared the TRY. ASHRAE have applied this technique to data from over 60 cities throughout the United States. This is an extremely simple technqiue to apply, however, it is not considered suitable for estimating long-term energy requirements. Applying this technique to Kew data, Hutchin (37) established that 1971 would be the selected TRY.

hottest	July
coldest	January
hottest	August
coldest	February
hottest	June
coldest	December
hottest	September
coldest	March
warmest	May
coolest	November
warmest	October
coolest	April

coolest	July
mildest	January
coolest	August
mildest	February
coolest	June
mildest	December
coolest	September
mildest	March
coolest	May
warmest	November
coolest	October
warmest	April

TABLE 3.3 U.S.A. T.R.Y. Selection Procedure

The Danish procedure (40,41) is based on a rigorous synoptic statistical appraisal of 11 years of climatic data. The TRY selection is based on the mean daily dry bulb temperature, the daily maximum dry bulb temperature and the daily total of solar radiation, the selection is decided according to three criteria:

(1) months with abnormal conditions are excluded
(2) months with typical mean values are selected by comparing monthly mean values for each month with the average value (of the same month) over the 11 year period
(3) months with typical variations from the mean are selected, by comparing the deviation of the (daily) parameters from the above monthly mean values with the corresponding mean deviation over the complete period of record.

Each month in the period of record can be ranked according to criteria 1 and 2 and the most suitable month of the 11 year period is selected as the TRY. Although this technique is much more rigorous than the US method, the Danish TRY may contain 13 discontinuities, because each month may have been selected from a different year from the month which precedes or succeeds it.

In Japan, the TRY selection procedure is based upon the actual computed values of room heating and cooling loads, hour by hour through 10 years of data, for eight situations (two different rooms at four orientations) (42). The annual profile nearest to the 10 year average profile is declared the TRY data. This technique differs considerably from the others, which are based upon climatological data only, unrelated to any building. The advantage of the Japanese method is that it attempts to diverge from the simple statistical analysis used in other technqiues to discriminate between different sets of climatic data.

Ultimately any TRY data should be used with caution as it may contain anomalies with respect to a particular design. For example, a US reference year, because it is based upon temperature only, may have the most extreme annual total solar radiation on record, therefore,

any simulation of a passive or active solar energy design may be misleading.

3.1.2 Prediction of Hourly Climatic Values

Frequently there may be no climatic data relevant to a site, or the climatic data measured may not be appropriate. In such circumstances hourly values of those climatic parameters required by the simulation model that are not measured will have to be predicted or synthesised from available information. The resulting climatic data set must be used with care as such data may be as inappropriate for a simulation as data from another site, however, this climatic data bears some relationship to the site and several methods are available to calculate climatic data.

Solar Radiation Parameters

The UK Meteorological Office records several values of solar radiation at its main climate observation centres. They are:

(1) hourly mean values of global irradiance Gh, falling on a horizontal plane (wm^{-2})

(2) hourly mean values of diffuse irradiance, Gdh, falling on a horizontal plane (wm^{-2})

(3) hourly mean values of beam irradiance, Gbn, normal to the beam (wm^{-2})

However there are many centres where these values have not been recorded. Table 3.4 lists the Meteorological Office centres.

If the solar altitude, α , is known (see Appendix 1), then only two of the measured solar radiation terms are required to calculate the third,

$$Gh = Gdh + Gbn * \cos\alpha \qquad (3.1)$$

Although equation (3.1) gives a reasonable assessment of the relationship between Gh, Gdh and Gbn, the Meteorological Office are currently

TABLE 3.4

STATION	LATITUDE	LONGITUDE	ELEVATION (m)	ELEMENT MEASURED
LERWICK	60 08 N	01 11 W	82	T,D,L,B,SS
ESKDALEMUIR	55 19 N	03 12 W	242	T,D,L,B,SS
ALDERGROVE	54 39 N	06 13 W	68	T,D,L,B,SS
ABERPORTH	52 08 N	04 34 W	133	T,D,SS
CARDINGTON	52 06 N	00 25 W	29	T,D,SS
LONDON	51 31 N	00 07 W	77	T,D,L,SS
KEW	51 28 N	00 19 W	5	T,D,L,B,SS,I,F
BRACKNELL	51 23 N	00 47 W	73	T,D,L,SS,I,F,N,S,E,W
JERSEY	49 13 N	02 12 W	83	T,D,L,B,SS
ABERDEEN	57 10 N	02 05 W	35	T
DUNSTALLNAGE	56 28 N	05 26 W	3	T
DUNDEE	56 27 N	03 04 W	30	T,B
HURLEY	51 32 N	00 49 W	43	T

T - total solar radiation on horizontal

D - diffuse solar radiation on horizontal

L - total illumination on horizontal

B - radiation balance

SS - sunshine hours

I - direct normal solar radiation

F - diffuse illumination on horizontal

N,S,E,W - total solar radiation on vertical surfaces facing north, south, east and west respectively

Solar Radiation Stations - Elements Measured

investigating techniques to improve the accuracy of this expression.

There are a number of less sophisticated observation centres which issue for example monthly mean daily global values, daily global values and some measure only sunshine duration data. Sufficient information may be unavailable to obtain hourly global, diffuse and direct normal irradiance values. For these circumstances a number of techniques have been developed to synthesise the required irradiance values from the most informative data available. Synthesised hourly average irradiance values are suitable for testing the long term performance of a system at a particular site but when performing short term site dependent tests the data may be less informative.

Many different models exist to synthesise particular solar radiation measurements into more suitable forms. Several of the most commonly used techniques are described in Appendix 3.

Reasonably accurate models are available to compute the intensity of solar radiation under various sky conditions (i.e. clear, average and overcast). Project F of the EEC's programme dealing with solar radiation data for solar energy applications, involves the development of solar radiation prediction models for inclined surfaces (43). The University of Sheffield has developed algorithms for the prediction of solar radiation on horizontal surfaces under clear sky (Appendix 3), average cloud and overcast conditions (44). These models have been modified to predict radiation on sloping surfaces and compared with similar programs developed at the University of Berlin. It was found that Sheffield had the better clear sky model while Berlin had the better overcast sky model. Combined efforts into the development of an improved average sky model is being conducted at present (43). These models are to become the basic models for the EEC.

These climate models required knowledge of such parameters as the total atmospheric precipitable water content and the atmospheric turbidity (45). Measurements of these parameters are not readily available. Using climatological summaries of observed data, for global and diffuse radiation, at each of four principal UK weather

centres, Souster (46) has attempted to establish atmospheric turbidity and precipitable water content values. Mean daily and hourly turbidity values for high global radiation days in the UK have been estimated plus clear day precipitable water content values. For average and overcast skies, modified turbidity values called 'pseudo-turbidity' values were derived and a set of mean 'pseudo-turbidity' maps have been produced for the UK.

Irrespective of the accuracy of measured or predicted solar radiation values, if hourly time steps are used then the variability of solar radiation is damped. Solar radiation values can vary considerably within one hour but the mean hourly value is usually the only available value. Therefore, raw solar radiation values indicate mean hourly values whereas predicted data usually represents mean daily values and may be less likely to show the random variations between hourly values unless some randomness factor is applied to the model.

Non-Solar Radiation Values

Except for dry bulb temperature and wind velocity there are no prediction techniques available for the principal non-solar radiation climatic parameters. Unfortunately, there are times when only the monthly daily mean or daily mean of a climatic parameter is known. In these circumstances the parameter is assigned hourly values equal to the mean value for the period of application, e.g. day, week, month, year. Occasionally the daily maximum and minimum values of a parameter are known as well as time of occurence, in such cases linear interpolation could be employed in order to model the trend of the parameter's variation. However, if the parameter is either dry bulb temperature or relative humidity then a sinusoidal wave could be fitted to the data to represent the diurnal variations (47). This technique is suitable during spring and autumn when the solar day is about 12 hours but for summer or winter use the sinusoid will have to be modified depending upon the solar day length.

An approximation of the mean daily dry bulb temperature, T_{db}, can

be obtained from a measure of the degree of climate severity of a locality called the Degree Day (DD). The Degree Day is defined by

$$DD = \left[\int^{1\ day} (Tb - Tdb)\ dt\right]^{+} \qquad (3.2)$$

where Tb is the base temperature (15.5°C in the UK). The term within the brackets is accumulated over a one day period only when the result is positive, i.e. when the dry bulb temperature is less than the base temperature. Therefore, if the Degree Days are known then an equivalent mean daily temperature can be established. There is no guarantee that this value would be equal to the mean daily temperature as it will underestimate the temperature if the ambient temperature was greater than the base temperature at any time.

In order to produce hourly temperature and wind speed values which would be compatible with the University of Sheffield solar radiation algorithms, Page (48) (using climatic data from the four main observation centres in the UK) has analysed the variations in the hourly dry bulb temperature and wind speed values for three classes of day:

i) Days of high relative irradiaiton
ii) Mean of all days
iii) Days of low relative irradiation

These classes of day correspond to clear, average and overcast sky conditions. Both the mean hourly dry bulb temperature and wind speed for each class of day in every month were reduced to a Fourier Series. The solution of the Fourier Series depends upon the user knowing the latitude, longitude and height of the site plus the mean monthly daily temperature, mean monthly wind speed and the mean monthly sunshine hours. Although this technique is based on data from only four sites, it is assumed to be application for the whole UK. Unfortunately it cannot be used where any of the variables mentioned above are unknown.

3.2 Climatic Data Required for Energy Models

Simulation models generally operate using one-hour time-steps, this being the minimum interval over which climatic data are available. Ideally every appropriate climatic parameter should be measured preferably at smaller time-increments than one hour. There are, however, a number of limitations:

- some climatic parameters are very difficult to measure accurately, or require subjective assessment, e.g. cloud cover
- the costs of measuring every possible climatic parameter is prohibitive
- some climatic parameters are easily derived from others, therefore, there is no need to measure them
- there are parameters which exhibit minimal changes in an hour, therefore, measuring and recording these parameters for periods less than one hour is wasteful of resources
- the storage requirements for climatic data on a computer file or in manuscript form is directly proportional to the number of records stored per hour.

As discussed in the previous section, the hourly values of climatic parameters may be recorded as spot,mean or total hourly readings. Also a 'prime' set of climatic parameters must be available from which all other climatic parameters can be derived. The Science and Engineering Research Council are currently funding a project to provide a prime climatic data set combined with a list of standard algorithms for the derivation of other climatic parameters (49).

The prime climatic parameters required by an energy model varies depending upon the type and rigour of the model. A proposed list of prime climatic parameters is given in Table 3.5, a number of sub-groups can be identified wherein some similarity exists:

Solar Radiation - measured values of direct normal and diffuse horizontal radiation are required by most energy models. These radiation values are important to assess the quantity of global,

1. Direct normal radiation
2. Diffuse horizontal radiation
3. Atmospheric pressure
4. Dry bulb temperature
5. Wet bulb temperature
6. Wind speed
7. Wind direction
8. Precipitation amount
9. Precipitation duration
10. Net horizontal radiation
11. Global illumination
12. Diffuse illumination

TABLE 3.5 Proposed list of "prime" climatic parameters to be measured and stored on a meteorological tape as hourly values

diffuse and ground reflected solar radiation incident upon the external exposed surfaces of the object being modelled, e.g. a building or a solar collector. The global radiation falling on a horizontal surface can be established using equation (3.1). If the global and diffuse values of horizontal radiations are subtracted from the net radiation value the radiation exchange rate between the earth and the sky can be estimated, from this an equivalent sky temperature can be calculated. Once the sky temperature is known then the long-wave radiative exchange between any exposed surface and its surroundings can be estimated.

Air Properties - if atmospheric pressure, dry bulb temperature and wet bulb temperature are measured they can be used to derive all psychrometric properties of air, for example, relative humidity, vapour pressure, etc. Atmospheric air properties are required to analyse infiltration and exfiltration effects in buildings, or leaks in air collector solar systems. Ambient air can also be drawn into a building for cooling, heating or ventilation purposes and in a solar system it can be used as the heat transporting medium. The dry bulb temperature is used as the known boundary to an exposed external surface with which convective heat exchange occurs.

Wind - wind velocity and direction require to be measured to evaluate the effects of wind on an exposed surface. The wind velocity and its incident angle on a surface will influence the convective heat exchange between the ambient air and the surface temperature.

Precipitation - the quantity of precipitation is a measure of the rain, snow, sleet, hail, etc, which fell, if its duration is also measured then it is possible to investigate the effects of precipitation on an exposed surface, particularly if the surface is porous. Whether the surface is porous or not, there will be a heat exchange between the incident precipitation and the surface.

Illumination - global and diffuse illumination are measured for

lighting energy models in order to assess the quality and quantity of natural lighting.

If one year of hourly values of these climatic parameters are stored on tape, then there would be 105,120 hourly values corresponding to 210 kbytes storage, without including miscellaneous data such as year day number, hour number etc. At present 18 climatic parameters are held on Meteorological Office tapes.

Although 12 prime climatic parameters have been identified they will seldom be used by a single model, for example, a solar energy systems model would not require illumination data. Assumptions can be made with other parameters for example, the atmospheric pressure can be regarded as being constant and the net horizontal radiation which is used to calculate sky temperature is not required if the sky temperature can be evaluated from the derived psychrometric properties of air.

At ABACUS a computer program is available to interrogate a climatic data set. The program allows synoptic or graphical output of the data facilitating the selection of an appropriate period to conduct a test. For example, to test a design over several days during which the temperature frequently exceeds 24°C the program can be operated to detail those days in which the temperature is greater than 24°C (Figure 3.1a), graphical output of the dry bulb temperature over any period can be selected to assess its suitability (Figure 3.1b).

The ESP program uses a climate file consisting of six prime parameters: direct normal and diffuse solar irradiance, wind velocity and direction, dry bulb temperature and relative humidity. These parameters are then processed by the ESP model to obtain derived parameters. At present the FLARE model accesses the same six parameters as the ESP model, however, at some future time this climate file will be replaced by another which includes atmospheric pressure and precipitation amount and duration to the six parameters mentioned above with the wet bulb temperature replacing relative humidity.

SYNOPTIC ANALYSIS OF CLIMATIC DATA (SEQUENCES)

PERIOD CONSIDERED FROM DAY 1 OF MONTH 1 AT HOUR 1 TO DAY 31 OF MONTH 12
AT HOUR 24

ANALYSIS OF DRY BULB TEMPERATURE DEG C
SPECIFIED RANGE : 24.00 TO 40.00

DAYS (WITHIN PERIOD) DURING WHICH THE ABOVE
PARAMETER FALLS WITHIN SPECIFIED RANGE

DAY 11 OF MONTH 5
DAY 30 OF MONTH 6
DAY 7 OF MONTH 7
DAY 10 OF MONTH 7
DAY 11 OF MONTH 7
DAY 12 OF MONTH 7
DAY 13 OF MONTH 7
DAY 16 OF MONTH 7
DAY 17 OF MONTH 7
DAY 18 OF MONTH 7
DAY 26 OF MONTH 7
DAY 31 OF MONTH 7
DAY 1 OF MONTH 8
DAY 23 OF MONTH 8
DAY 27 OF MONTH 8
DAY 28 OF MONTH 8

Figure 3.1a sample of synoptic output from climatic data analysis program.

CLIMATE ANALYSIS: KEW,SOUTH ENGLAND : 51.7N 0.2W : 1957
PERIOD: 16. 7. 1 TO 18. 7.24

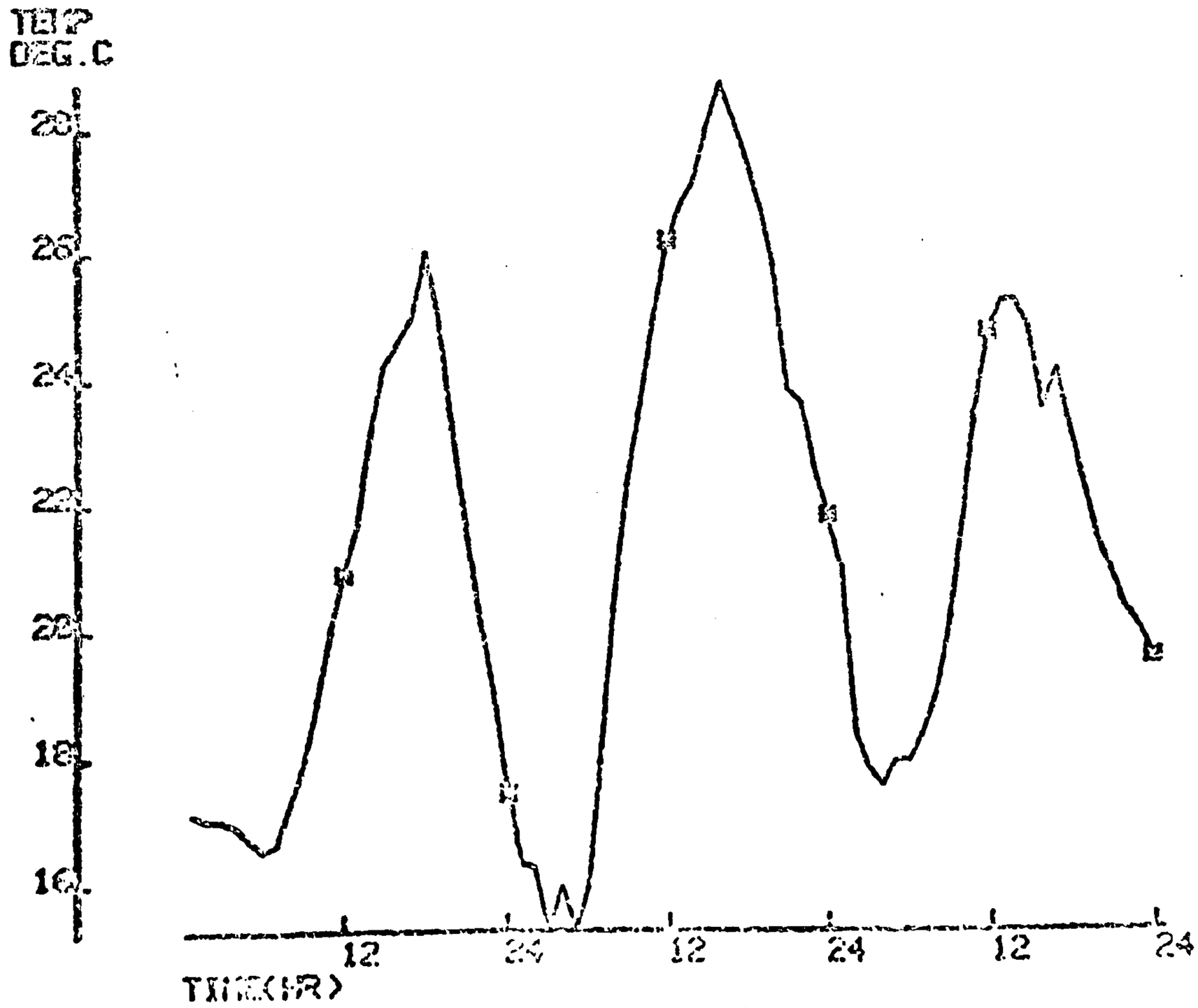

Figure 3.1.b sample of graphical output.

The use of prime parameters causes a storage versus computation confrontation. If a model has to continually recalculate derived data from the same data set then it may be computationally advantageous to calculate all the derived data initially and record it on the climate file, in that way computational time can be drastically reduced but computer storage requirements can be large. In most models, however, climate data sets are used infrequently therefore it would be uneconomical to store anything but prime climate parameters.

CHAPTER 4 Solar Energy System Modelling Techniques

Three classifications of mathematical model for solar energy systems were identified in Chapter 1:

a) steady or quasi-steady state models of the complete system

b) simulation models which employ the modular approach using quasi-steady state models for some components and iterative solutions of the partial difference equations in others

c) simulation models employing the simultaneous approach using implicit finite difference approximations for the components and the system.

In this chapter an example of each classification will be given and its ability to model the various collector subsystems, as described in Chapter 2, will be discussed.

4.1 Simple System Model

The F-Chart Method is an extensively used simple solar energy systems model which is extremely useful for the rapid design of solar space-heating and domestic hot water system. It was developed by Beckman et al (5) specifically as a design tool for predicting the performance of standard solar systems by hand or by programmable calculators. Three standard configurations were considered: liquid and air systems for space and hot water heating and systems for domestic hot water. The F-Chart method for each of these configurations was obtained by conducting hourly simulations using TRNSYS (see Section 4.2) for a wide range of parameters at several geographical locations in the US, the results of which are the basis of generalised correlations for the long term performance of a system. Therefore, this model will be unsuitable for analysing the short-term dynamic performance of the system and its components.

The F-Chart correlations or graphs were established for f, the fraction of monthly heat load supplied by solar energy, as a function of two dimensionless parameters. The first parameter, X, is related to the ratio of the collector energy loss at a reference temperature to the total heating load during the month:

$$X = F_R U_L (F_R'/F_R)(T_{REF} - \overline{T}a).\Delta\tau.Ac/L$$

The second parameter, Y, is related to the ratio of the total energy absorbed by the collector plate to the total heating load during the month

$$Y = F_R(\tau\alpha)_n(F_R'/F_R)[(\overline{\tau\alpha})/(\tau\alpha)_n]\overline{H}_T.N.Ac/L$$

where, F_R = heat removal factor associated with the collector
U_L = the collector overall heat transfer coefficient ($wm^{-2}k^{-1}$)
F_R' = the collector-heat exchanger efficiency factor
Tref = an empirically derived reference temperature (100°C)
$\overline{Ta}$ = monthly average ambient temperature (°C)
$\Delta\tau$ = number of seconds in the month (sec)
Ac = area of collector (m^2)
L = monthly total heating load for space heating and hot water(J)

$\overline{H_T}$ = monthly average daily radiation incident on the collector surface per unit area (JMc^{-2})

N = number of days in month

The ratio (F'_R/F_R) can be considered as the fractional increase in collector area required for the system with a heat exchanger to give the same energy output as one without a heat exchanger. The ratio $(\overline{\tau\alpha})/(\tau\alpha)n$ is the ratio of the monthly average transmittance-absorptance produce to the transmittance-absorptance product at normal incidence. $(\tau\alpha)n$ is calculated as a function of a weighted average for the beam, diffuse, and reflected components of the normal incident radiation.

To determine f, the fraction of the heating load supplied by solar energy for a month, values of X and Y are calculated for the collector and heating load in question. The value of f is determined from the intersection of X and Y or either an f-chart graph or from an equivalent correlated equation. This is conducted for each month in the year. The monthly solar contribution is found from the product of f and the total monthly heating load, L. Finally, the fraction of the annual heating load supplied by solar energy, F, is the sum of the monthly solar energy contributions divided by the annual loads:

$$F = \frac{\sum fL}{\sum L}$$

The F-chart correlation equations for each of the three standard systems are now defined.

a) Liquid Systems

A schematic diagram of the standard solar space and water heating system using liquid heat transfer fluids is given in Figure 4.1 (51). The fraction f of the monthly total load supplied by this system is expressed in correlated equation form by the relationship:

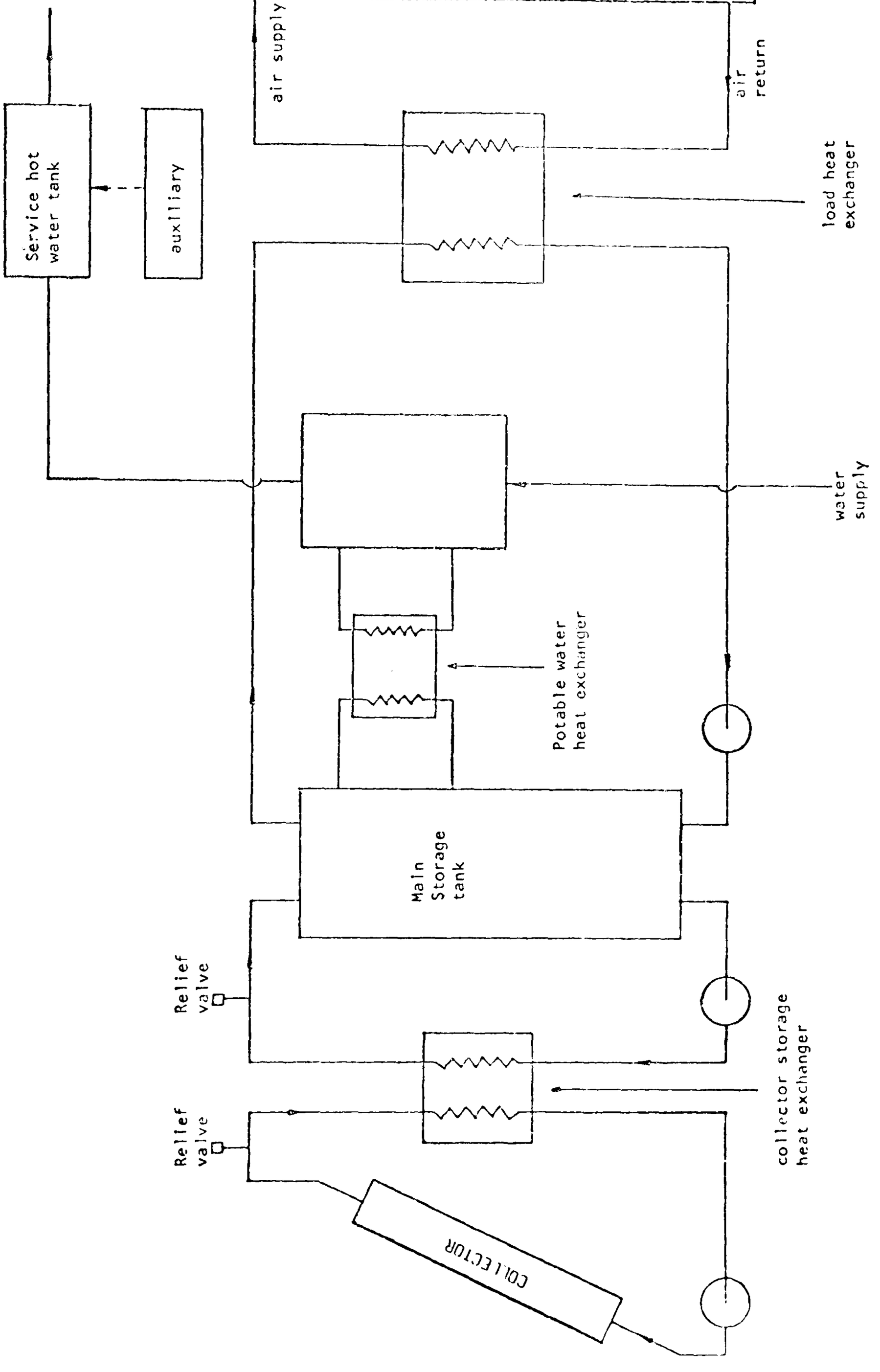

Figure 4.1 Schematic of the standard system configuration using liquid heat transfer and storage media (56)

$$f = 1.029Y - 0.065X - 0.245Y^2 + 0.0018X^2 + 0.0215Y^3 \qquad (4.1)$$

this equation is valid for the ranges : $0 \leqslant Y \leqslant 3.5$, $0 \leqslant X \leqslant 18$, and $0 \leqslant f \leqslant 1.0$.

Two correction factors are required for liquid systems to account for variations in storage size and heat exchanger size. Equation (4.1) was generated for a liquid storage capacity of 75 l/Mc², the performance of systems with different storage capacities are estimated by modifying the dimensionless group, X, by a storage size correction factor X_L given by:

$$\text{Storage size corection factor} = \frac{X_L}{X} = \left(\frac{M_L}{75}\right)^{-0.25}$$

where M_L is the actual liquid storage capacity in l/Mc². This correction factor is valid for the range $37.5 < M_L < 300$.

The second correction factor is applied by modifying Y, if the load heat exchanger is a different size from that which was used to generate equation (4.1). A measure of the size of heat exchanger required for a specific building is provided by the dimensionless parameter, E, where

$$E = \frac{\varepsilon_L \; Cmin}{UA}$$

ε_L = the effectiveness of the water-air load heat exchanger, i.e. the ratio of the actual to the maximum heat transfer rates

Cmin = the minimum fluid capacitance rate (mass flow rate times the specific heat of the fluid) in the load heat exchanger and is generally that of air

UA = the building overall energy loss coefficient-area product used to predict the building load.

From thermal considerations the optimum value of E is infinity, however, system performance is asymptotic for a value of E greater than 10. The reduction in performance due to an undersized heat exchanger will be significant for values of E less than one. Practical values of E are generally between one and three when the cost of the heat exchanger is considered.

The F-Chart was developed for E = 2, the correction factor Yc/Y for different values of E is given by

$$\frac{Yc}{Y} = 0.39 + 0.65e^{(-0.139*E)}$$

for the range $0.5 < E < 50$.

b) Domestic Water-Heating Systems

The standard configuration for a solar domestic water heating system is shown in Figure 4.2, either liquid or air collectors can be used (50). The mains water supply temperature Tm and the minimum acceptable hot water temperature (i.e. the desired delivery temperature) Tw, both affect the performance of the solar water heating system because they influence the average system operating temperature level and as a result the collector energy losses. The dimensionless group X which is related to collector energy losses can be redefined to take account of these effects by using a water heating correction factor Xw/X:

$$\frac{Xw}{X} = \frac{1.16 + 1.8Tw + 3.86Tm - 2.32\overline{Ta}}{(100 - \overline{Ta})}$$

This equation may be applied to equation (4.1) for solar space and water heating systems to estimate monthly values of f for water heating systems only.

This method for estimating water heater performance is based on a

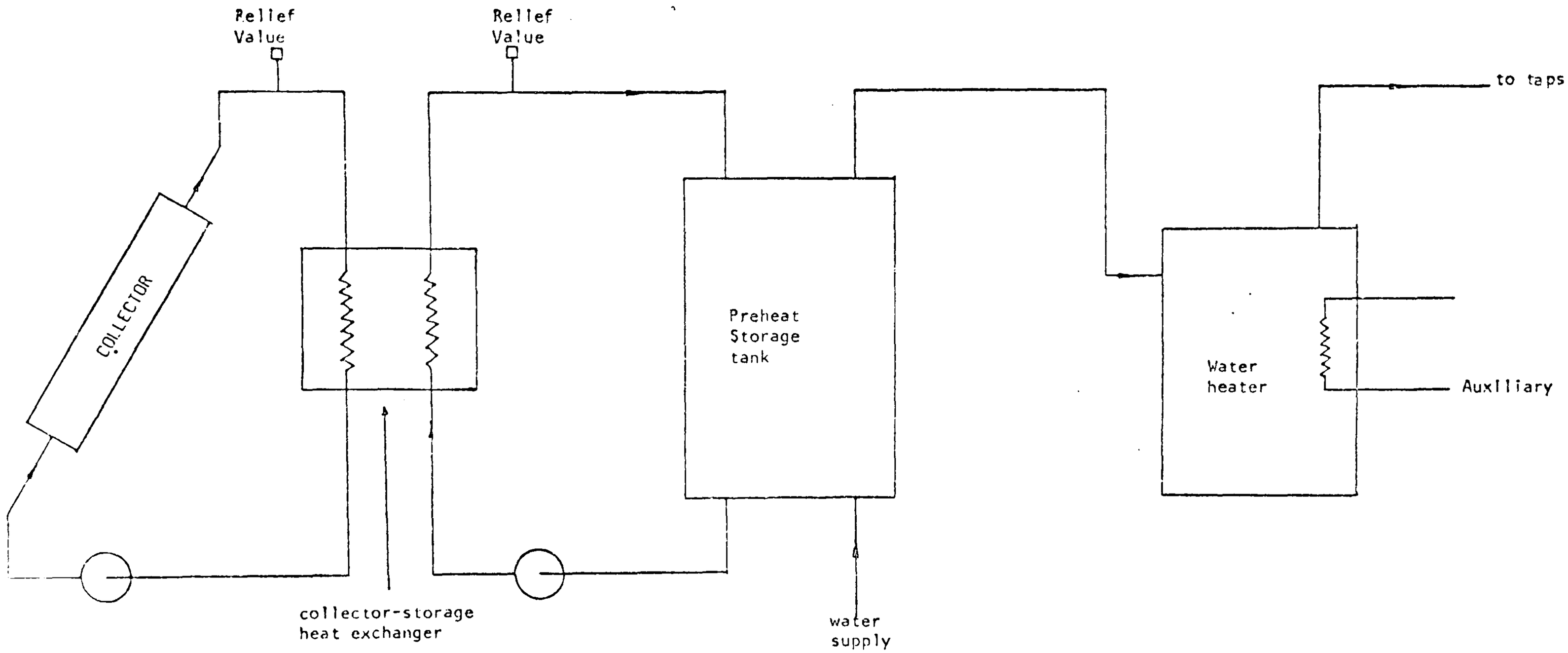

Fig 4.2 The standard system configuration for water heating only. Collector may heat air or water. (55)

storage capacity of 75 litres/Mc^2 and on the hot water demand for a 'typical' day. Considerable errors may be involved when using different storage capacities or demand profiles.

c) Air Systems

A schematic diagram of the standard configuration of a solar air heating system with a pebble bed storage unit is given in Figure 4.3, other equipment arrangements of fans and dampers can be used to provide the same mode of operation (52). The monthly fraction of the total heating load supplied by this system can be found from the expression:

$$f = 1.040Y - 0.065X - 0.159Y^2 + 0.00187X^2 - 0.0095Y^3 \quad (4.2)$$

which is valid forthe ranges $0 \leq Y \leq 3.5$, $0 \leq X \leq 18$ and $0 \leq f \leq 1.0$.

Air systems require two correction factors, one to account for storage size, the other to account for air flow rate which affects stratification in the pebble bed storage unit. The f-chart correlation for air systems is based on a storage capacity of $0.25M^3$ of pebbles per square metre of collector area. The performance of systems with different storage capacities are determined by modifying the dimensionless parameter, X

$$\text{Storage size correction factor} = \frac{Xs}{X} = \left(\frac{Ms}{0.25}\right)^{-0.30}$$

where Ms is the actual pebble bed storage capacity in M^3/Mc^2, this equation is valid for the range $0.125 < Ms < 8.0$. The collector air flow rate for equation (4.2) is 10.1 litres/second per square metre of collector area. The performance of systems having different collector air flow rates can be estimated by modifying the X value to account for the subsequent change in the pebble bed stratification:

$$\text{Collector air flowrate correction factor} = \frac{X_A}{X} = \left(\frac{M_A}{10.1}\right)^{0.28}$$

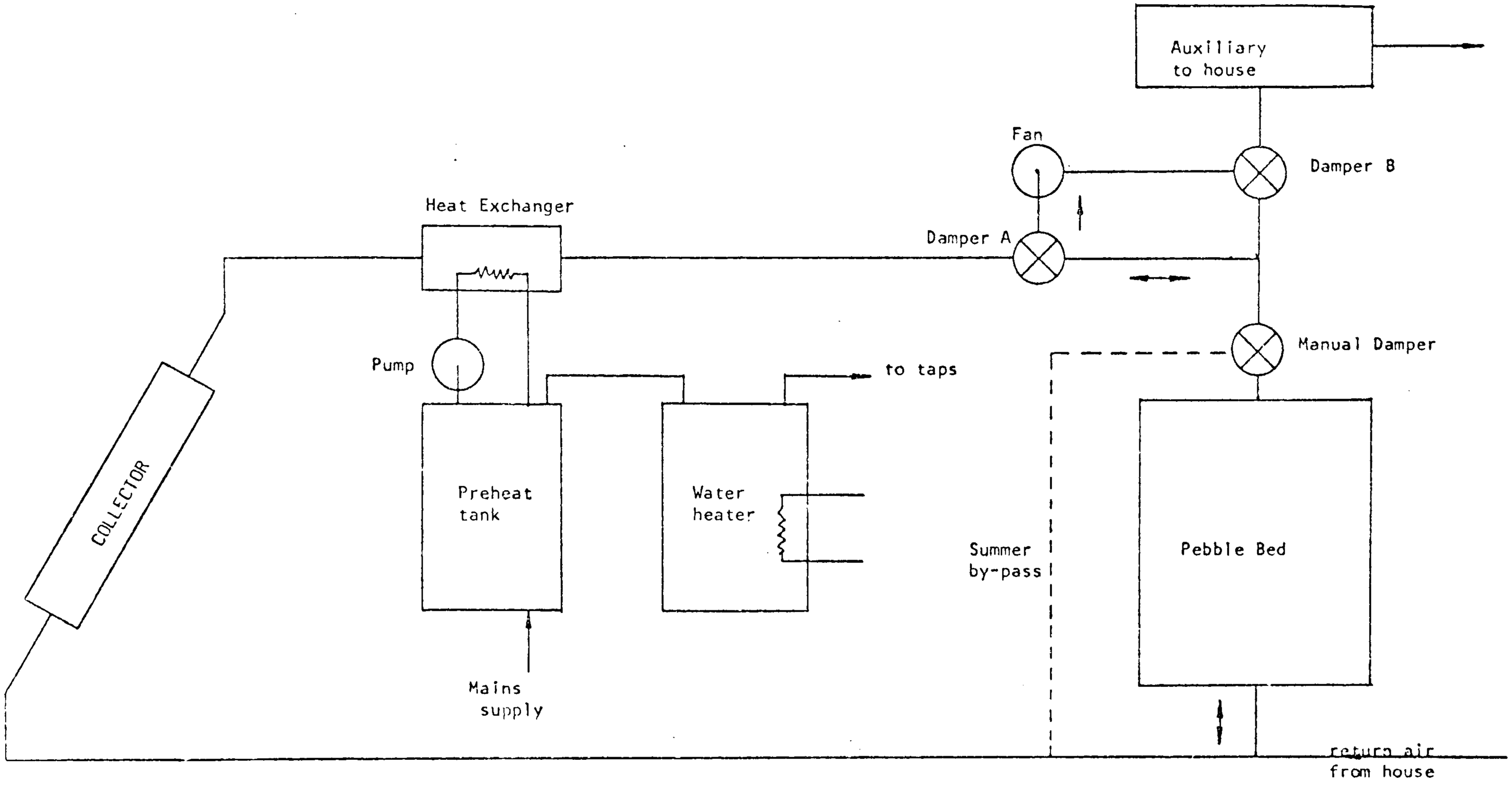

Figure 4.3 The standard air system configuration (57)

where M_A is the actual air flow rate (l/sMc^2) and is valid for the range $5 < Ma < 20$.

Although simple to operate the f-chart has a number of disadvantages:

- the only information available from each calculation is the solar fraction supplied
- as it is based on the results from a series of computer simulations it will have each assumption and inaccuracy of the simulation program inherent in its correlations
- because the method has been developed for long-term analysis based on average monthly data the short-term dynamics of the system cannot be assessed
- only three standard systems are considered and photovoltaic systems cannot be analysed
- only some parameters of the solar collector, heat exchanger and storage unit can be varied
- significant errors may result from applying f-chart to slightly modified standard systems
- there is difficulty in accurately predicting building heating loads, particularly occupant effects
- system must be carefully engineered and constructed

These disadvantages apply in one form or another in all simple models, the principal disadvantages are:

- lack of information obtained
- unsuitable for short term analysis
- not flexible

4.2 Simulation Model - Modular Approach

The modular approach used in simulation models as outlined in Section 1.3.1 is typified by the TRNSYS computer program (28). TRNSYS, an acronym for 'a transient system simulation program', is the most widely used system simulation model throughout the world. The most significant reason why TRNSYS is so widely used is that the cost of the program is kept artificially low due to funding from the US Government. Nevertheless, TRNSYS is a well documented computer program which is flexible and has several years of development behind it.

TRNSYS was developed by the Solar Energy Laboratory at the University of Wisconsin, Madison as part of a joint project with the Colorado State University (CSU) who were building a solar house. The objective of the project was to use the results from each test to compare with the results of the other. Comparative studies between measured data from the CSU house and other projects indicate that TRNSYS provides a reasonably accurate estimate of selected solar heating and cooling systems. The mean error between the simulated and measured results being less than 10% for all state variables considered (34). These state variables include storage temperature, collector outlet and inlet temperatures, collector mass flow rate, enclosure temperature, solar radiation on tilted surfaces, and the temperature in and out of various heat exchangers.

The TRNSYS program consists of a number of component subroutines and an execution program that enables the user to simulate the performance of a complete system by simulating the performance of the interconnected components. Each component may be modelled mathematically by sets of differential or algebraic equations, or both. The resulting mathematical models for the components are represented by the component subroutines in the TRNSYS program.

The initial version of TRNSYS was released in March 1975, and it has been continually updated. A list of the library of system components and ancillary subroutines for Version 10.1 is given in Table 4.1.

Component Type	Description
1	Flat-plate solar collector
2	On/Off differential controller with hysteresis
3	Pump or fan
4	Stratified fluid storage tank
5	Heat Exchanger
6	On/off auxiliary heater
7	Absorption air conditioner
8	Three-stage room thermostat
9	Data reader (for input of meteorological and other date)
10	Rock bed thermal storage
11	Tee piece, flow diverter, and flow mixer
12	Energy /(degree-hour) space heating
13	Relief valve
14	Cyclic time-dependent forcing function
15	Algebraic operator
16	Solar radiation data processor
17	Wall
18	Roof and attic
19	Room and basement
20	Heat pump
21	Liquid collector-storage subsystem
22	Air collector-storage subsystem
23	Domestic hot water subsystem
24	Quantity integrator
25	Printer
26	Plotter
27	Histogram plotter
28	Pipe and duct
29	Simulation summarizer
30	CPC collector
31	Cooling coil
32	Psychrometric data processor
33	Shading overhand and wingwalls
34	Window
35	Collector-storage wall

Table 4.1 Components in the library of the TRNSYS solar process simulation program (28).

Subsequent developments of TRNSYS have been implemented and Version 11.1 is currently available in which several component subroutines have been extended and several new components have been introduced: an economic processor, a microprocessor based controller, an electrochemical storage battery model, a regulator-invertor model, a combined thermal-PV collector model, and a combined thermal-PV subsystem model.

Consider, for the moment, a typical TRNSYS component - a flat plate solar collector. Similar to several components there are a number of different modes of operation, each dependent upon the available information. The more information that is available concerning the component then a more detailed analysis will be conducted. Figure 4.4 shows the collector component as a box with a series of INPUTS passing information to the component from other components, a series of OUTPUTS which pass information to other components and a set of PARAMETERS which are constants for the duration of the simulation. The mathematical model for this component is based on the Hottle-Whillier-Bliss equation (20).

$$Qu = Ac\ F_R\ [G_T(\overline{\tau\alpha}) - U_L(Tf,i - Ta)]$$

where Qu = useful energy output from a solar collector, (U)

Ac = the area of the collector (M^2)

F_R = collector heat removal factor

G_T = global irradiance (wm^{-2})

$(\overline{\tau\alpha})$ = ratio of the transmitted irradiance absorbed by the solar collector to the incident irradiance normal to the outermost collector cover

U_L = the overall thermal loss coefficient of the solar collector, representing the sum of the thermal losses to the surroundings by conduction, convection and re-radiation ($wm^{-2}k^{-1}$)

$T_{f,i}$ = temperature of the inlet fluid to the collector (k)

Ta = the ambient air temperature (k)

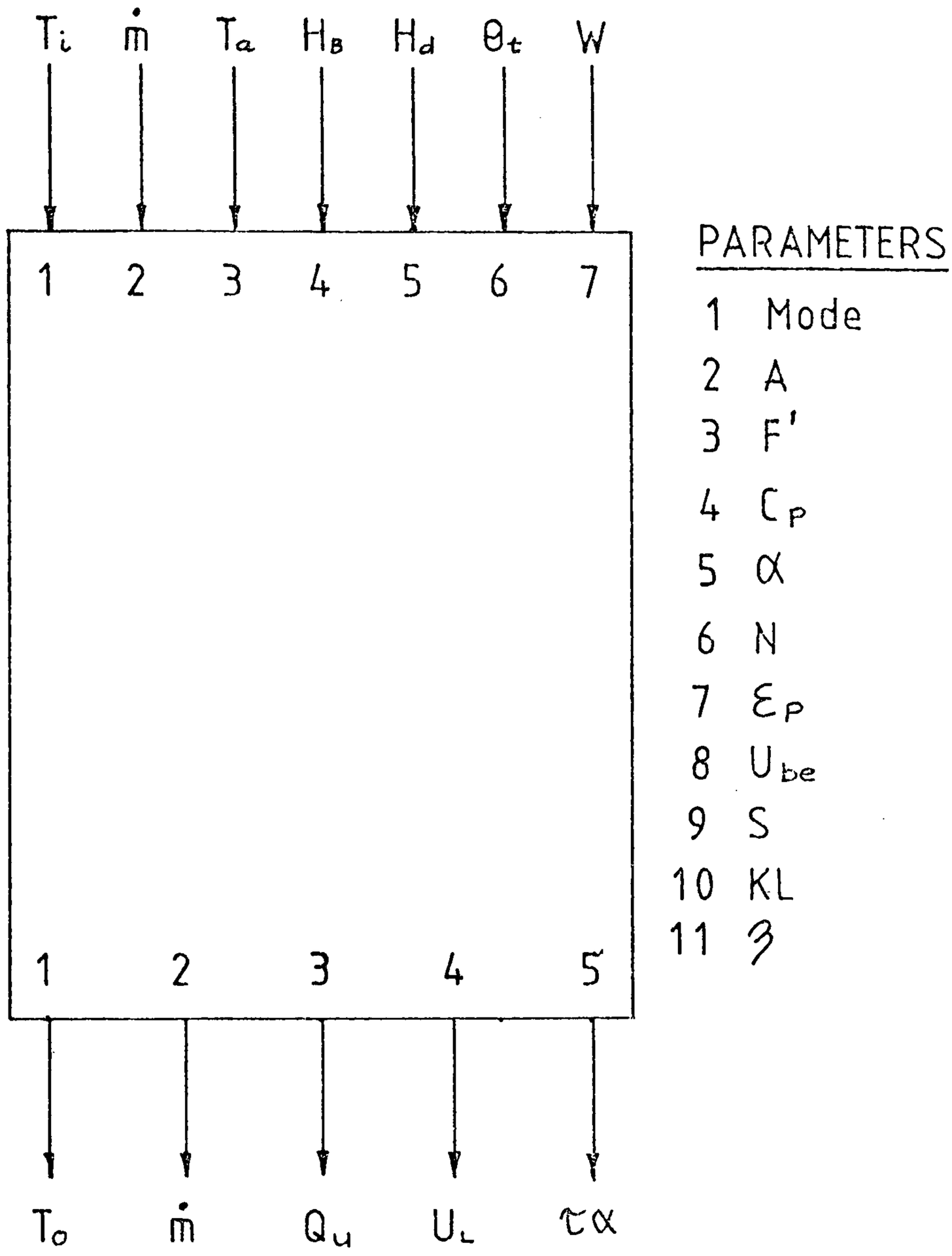

Figure 4.4 Information block diagram for a TRNSYS flat plate solar collector (for notation see Table 4.2)

Parameter No.		Description
1	MODE :	Specify 4
2	A -	Collector area (M^2)
3	F' -	Collector efficiency factor
4	C_p -	fluid thermal capacitance ($kJ\,kg^{-1}\,K^{-1}$)
5	α -	Collector plate absorptance
6	N -	Number of glass covers
7	ε_p -	Collector plate emittance
8	U_{be} -	Bottom and edge loss coefficient
9	S -	Collector tilt (deg.)
10	KL -	Extinction coefficient x thickness of covers
11	n -	Refractive index of cover

Input No.		Description
1	T_i -	Inlet fluid temperature
2	$\dot{m}$ -	collector fluid flowrate
3	T_a -	Ambient temperature
4	H_B -	Beam irradiation on collector surface
5	H_D -	diffuse irradiation on collector surface
6	θ -	angle of incidence of solar beam (deg)
7	W -	Windspeed (MS^{-1})

Output No.		Description
1	T_o -	Outlet fluid temperature
2	$\dot{m}$ -	collector fluid flowrate
3	Q_u -	rate of energy gain
4	U_L -	collector loss coefficient
5	$\tau\alpha$ -	transmittance - absorptance product

Table 4.2 Data required for a TRNSYS flat plate solar collector.

Although this model was developed for steady state analyses it is used by TRNSYS as a transient model. This is accomplished by re-calculating the collector variables F_R, $(\overline{\tau\alpha})$ and U_L at each iteration within every time-increment while allowing the other variables G_T, Tf,i and Ta to vary with respect to time.

Other mathematical models for TRNSYS components range from simple models (e.g. pump or fan) to more complex models, for example, several sections of a hot water storage tank need to be analysed when modelling the effects of thermal stratification in the tank, iterative techniques are employed to solve the differential equations between each fluid section.

To apply TRNSYS to simulate a particular system a number of steps must be followed. This procedure is best explained by applying TRNSYS to a specific problem. Consider a solar water heating system shown in Figure 4.5. The procedure is as follows:

(1) Identify all system components whose collective performance describes the performance of the system. There are five components to be modelled plus a number of ancillary components (Table 4.3).

(2) Construct an information flow diagram of the system out of the component flow diagrams (for example Figure 4.5). This facilitates the identification of the components comprising the type of direction of flow of information between them. Figure 4.6 is the information flow diagram for the system described in Figure 4.5.

(3) The next step is to assign UNIT numbers to the system components. Each component has a TYPE number associated with it, however, there may be two or more components of the same TYPE number in the system, therefore, the UNIT number refers to a particular component and it is unique to that component.

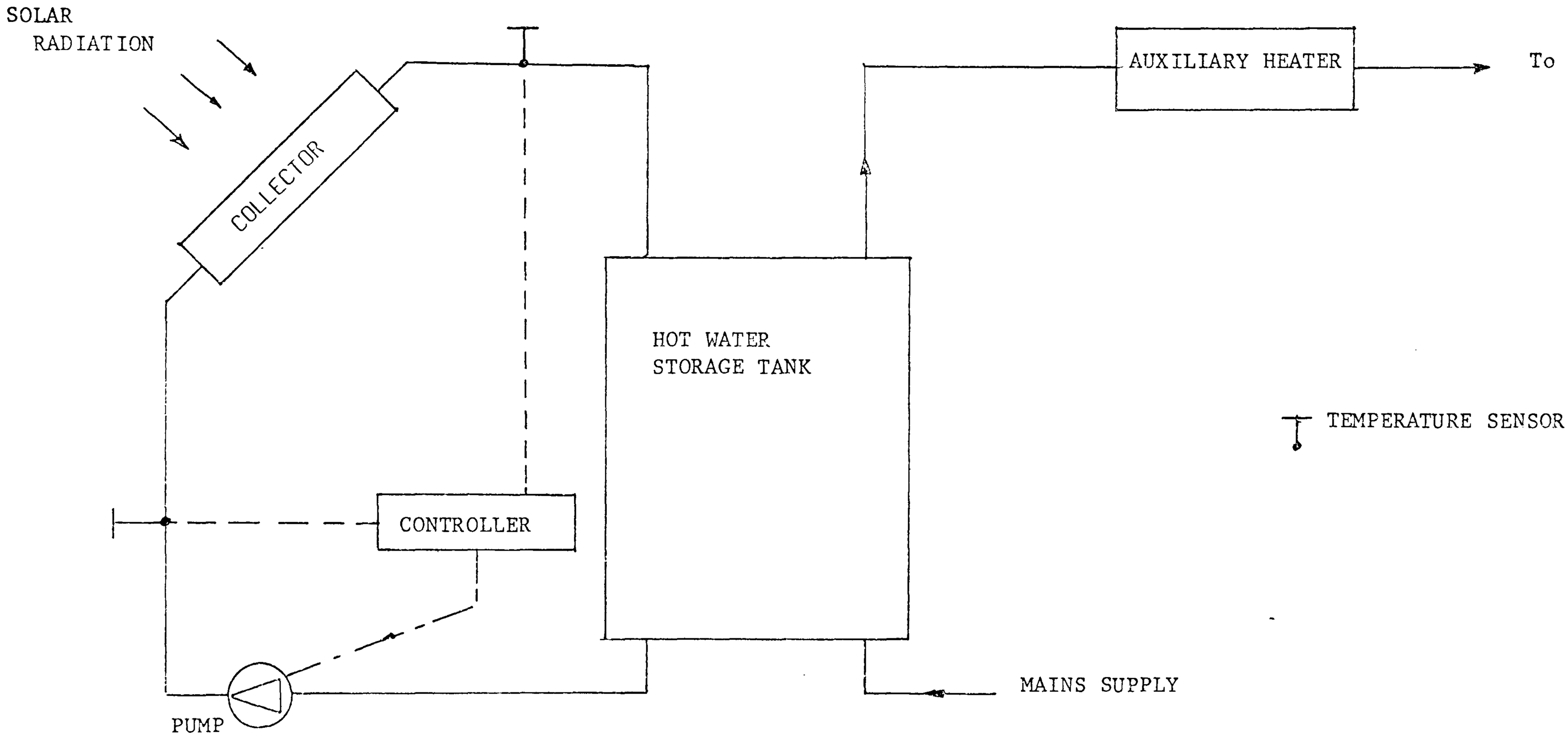

Figure 4.5 A Solar Water Heating System

UNIT	TYPE	COMPONENTS
49	9	Card reader
50	16	Solar radiation processor
1	14	Forcing function
2	1	Solar collector
3	2	On/off controller
4	3	Pump
5	4	Storage tank
6	6	Auxiliary heater
7	24	Integrator
8	25	Printer 1
9	25	Printer 2
10	26	Plotter

TABLE 4.3 List of components to be used to simulate the system under analysis

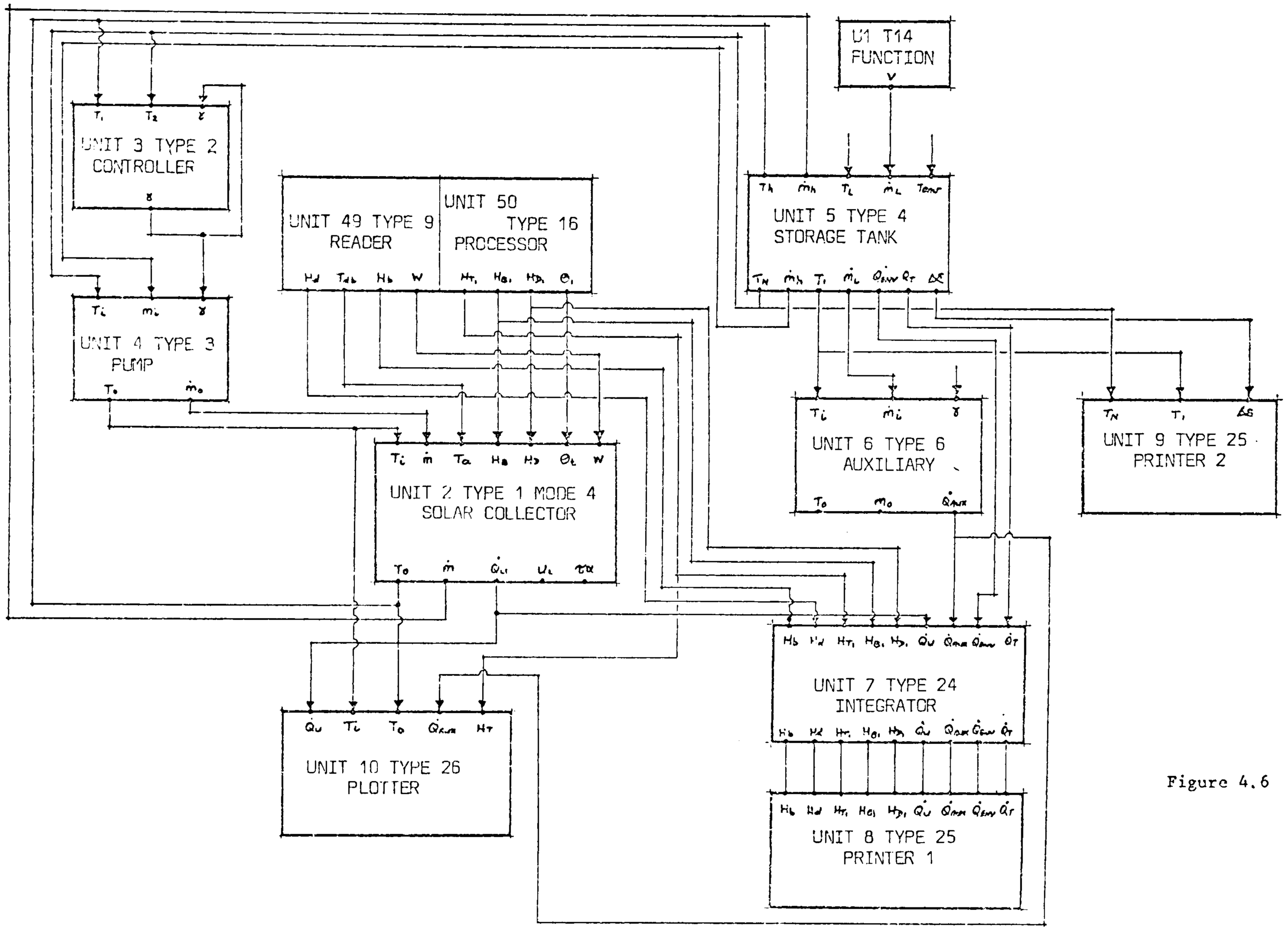

Figure 4.6 The block information flow diagram of the system under analysis

(4) The numerical values of the PARAMETERS of each component must be established. Also from the information flow diagram, component INPUTS are numbered according to the convention established by the component subroutine. If a component model involves differential equations, the TRNSYS program must be provided with the number of differential equations and the initial value for each of the state variables. These are called DERIVATIVES.

(5) Data corresponding to the system is formulated in the required form to be read by the TRNSYS program for the simulation to be performed.

TRNSYS is an extremely versatile model which can analyse numerous different systems to a reasonable degree of accuracy. The computational time required is small despite the need to iterate between time-increments. However, there are a number of problems associated with TRNSYS:

- the control of components and more importantly the interactions between each component are poorly modelled

- the solution to algebraic and differential equations may not converge causing instability. TRNSYS allows the user to define a limit for the maximum number of iterations per time-step for convergence to occur, if it does not converge before this limit, the solution at the final iteration is used. There is a second limit for the number of time-steps in which convergence has not occurred within the alloted number of iterations, if this second limit is exceeded the simulation is terminated.

- individual component models seldom analyse to give the quantity and quality of information necessary to allow a detailed component analysis, this is particularly restrictive when investigating the performance of the more important components, for example the solar collector.

- information flow diagrams are a necessary aid to identifying component interconnections, these diagrams can be exceedingly complex especially for large systems. This problem is compounded because ancillary components have also to be identified in the information flow diagram, these include data sources and all output retrieval components.

- there is also a considerable problem in formulating the data file for the TRNSYS program before conducting the simulation.

The latter problem has been solved by ABACUS because a program has been written which by means of a user controlled question/answer procedure automatically creates a properly formulated TRNSYS data file. This program is called the TRNSYS Input Management Program, or TIMP (58). The operational procedure required to conduct a TRNSYS simulation using TIMP is shown in Figure 4.7.

In TIMP, by specifying a particular component TYPE, a series of questions will be asked relating to the values of the PARAMETERS, INPUTS and DERIVATIVES of the component. This is repeated for every component necessary for a TRNSYS simulation. Once the complete system has been specified, TIMP automatically creates a properly formulated data file which can then be used by TRNSYS to conduct a system simulation.

Although more rigorous models compared to TRNSYS can be developed using the modular approach, which could be more detailed in their component analysis with improved information retrieval facility. However, with the modular approach of system simulation the control of components and system interactions is inadequate and using iterative techniques for solution of differential equations can cause instability, therefore, the principal differences between the modular and simultaneous approaches to systems modelling is that the simultaneous approach models system interactions as they happen, that is, instantaneously and because implicit finite difference approximations are used for the differential equations the solution is stable.

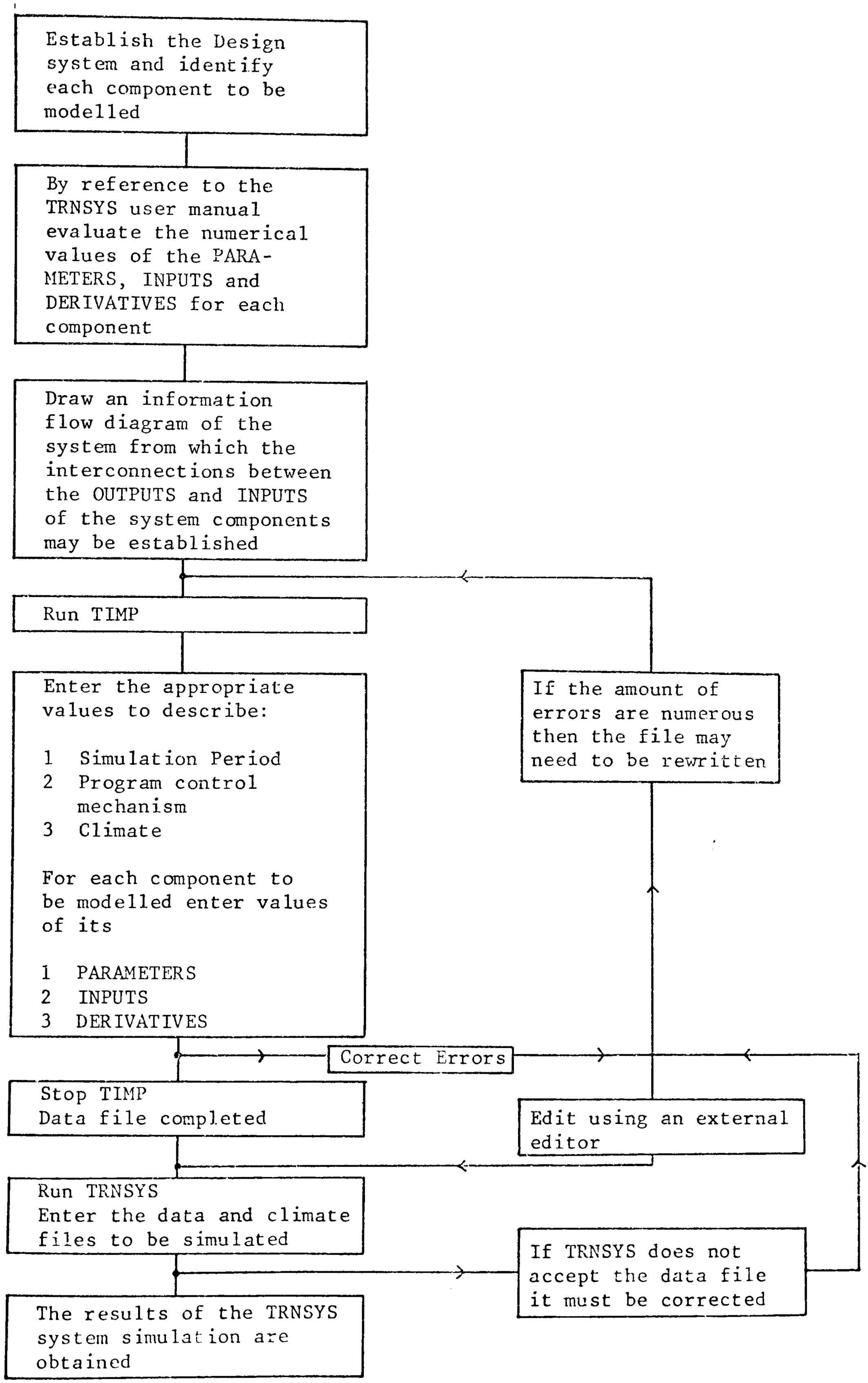

Figure 4.7 Operation of TRNSYS and the TRNSYS Input Management Program - TIMP (66)

4.3 The Simultaneous Approach to Systems Modelling

Although the concept of simultaneous systems modelling is not new, it is infrequently applied. When using implicit finite difference approximations to model system components the modelling of component interconnections are best conducted simultaneously. Implicit finite difference techniques have been applied to building energy models, for example ESP and DEROB, the rigour andflexibility available with these models as well as their accuracy indicates the suitability of this technique for modelling system components.

A three stage process is involved in applying an implicit finite difference numerical approximation to any system component:

i) the system component is made discrete by the placement of nodes at preselected points of interest throughout the system

2) for each node in turn and in terms of all surrounding nodes which are in thermal contact, the governing differential equation is replaced by an implicit numerical approximation. An equation is formed for each node.

3) the resulting set of nodal equations are solved simultaneously at each time-increment throughout some period of interest.

The numerical approximation used to establish the nodal equation is called the heat balance method and it is a variation of the direct application of finite difference equations. The heat balance method yields a similar solution for a transient heat conduction problem, however, if offers better physical insight into heat transfer problems and it can be applied with ease to system boundary conditions. The derivation of the general heat balance equation for energy exchange about any node is detailed in Section 4.3.1. The method of solving the resulting equation set for each component and modelling the component interactions simultaneously is given in Section 4.3.2.

4.3.1 Derivation of the General Heat Balance Equation

The First Law of Thermodynamics states that energy can be neither created nor destroyed only transferred from one form to another. This is more commonly known as the Conservation of Energy. If a real or imaginary boundary is drawn around a process where energy transformation is taking place (Figure 4.8) then from the First Law of Thermodynamics:

$$\left|\begin{matrix}\text{Change in}\\ \text{internal energy}\end{matrix}\right| = \left|\begin{matrix}\text{Net energy flow}\\ \text{across system boundary}\end{matrix}\right| + \left|\begin{matrix}\text{net generated}\\ \text{energy in system}\end{matrix}\right| \qquad (4.3)$$

This can be re-expressed mathematically by,

$$E = Ei - Eo + Eg \qquad (4.4)$$

where E = change in internal energy

Ei = energy into system

Eo = energy out of system

Eg = energy generated within system

If a boundary is drawn around any subvolume within the system (Figure 4.9) then it is possible to describe all the energy processes acting upon the subvolume in a similar way to the energy processes acting upon the complete system, thus,

$$\left|\begin{matrix}\text{Rate of change of}\\ \text{stored energy in}\\ \text{the system subvolume}\end{matrix}\right| = \left|\begin{matrix}\text{Net heat exchange in}\\ \text{and out of the surfaces}\\ \text{of the subvolume}\end{matrix}\right| + \left|\begin{matrix}\text{Net heat generation}\\ \text{within the sub-}\\ \text{volume}\end{matrix}\right| \qquad (4.5)$$

Although expressed slightly differently equation (4.5) is exactly the same as either equation (4.3) or (4.4) in terms of the First Law of Thermodynamics. Each of these three terms can be expressed mathematically but to do so the time increment must be considered. If a finite time interval $\Delta\tau$, starts at a particular time, τ, then at the end of the time increment the time will equal $\tau + \Delta\tau$. The stored energy in the subvolume at the start of the time step is

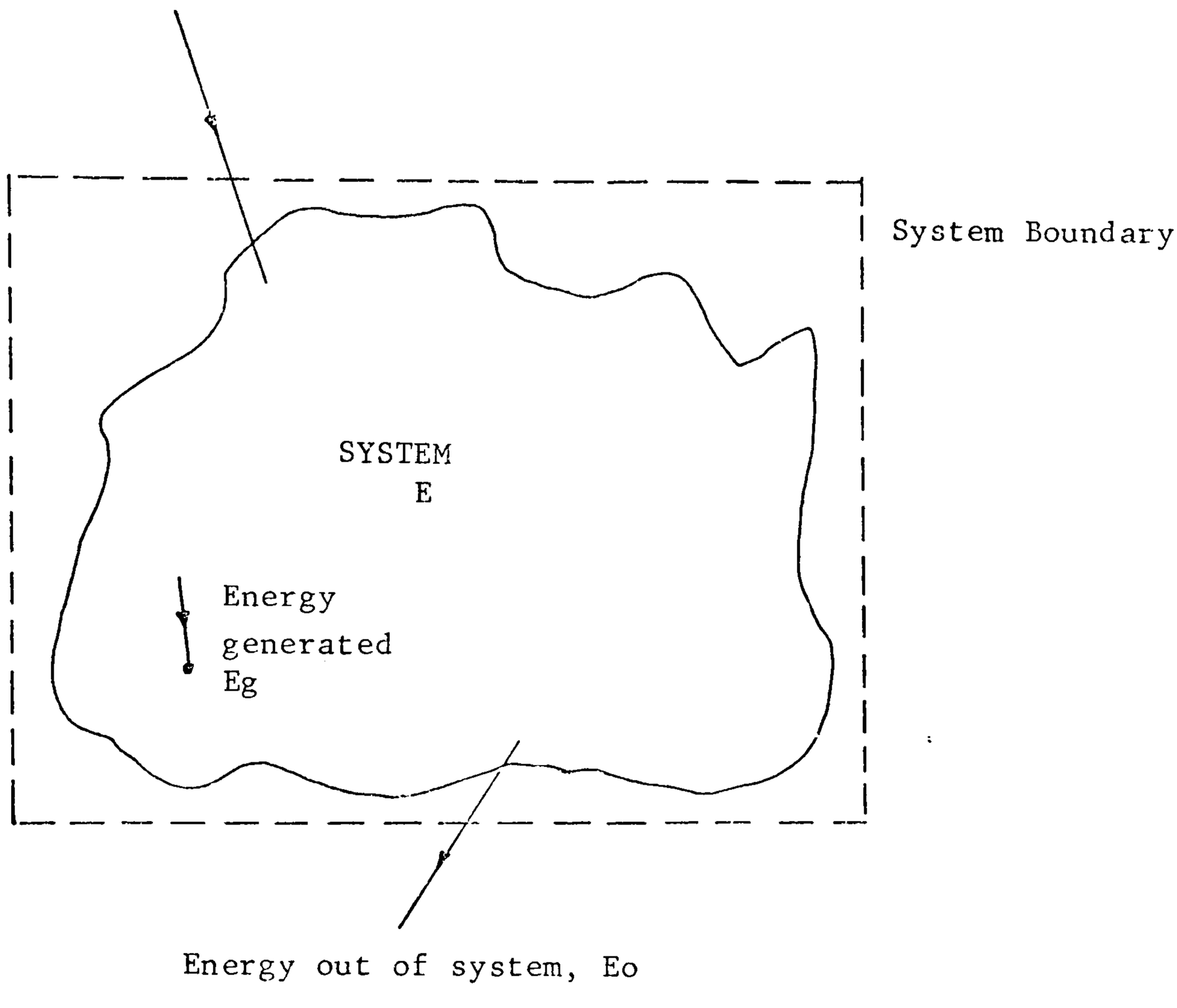

Figure 4.8 First Law of Thermodynamics

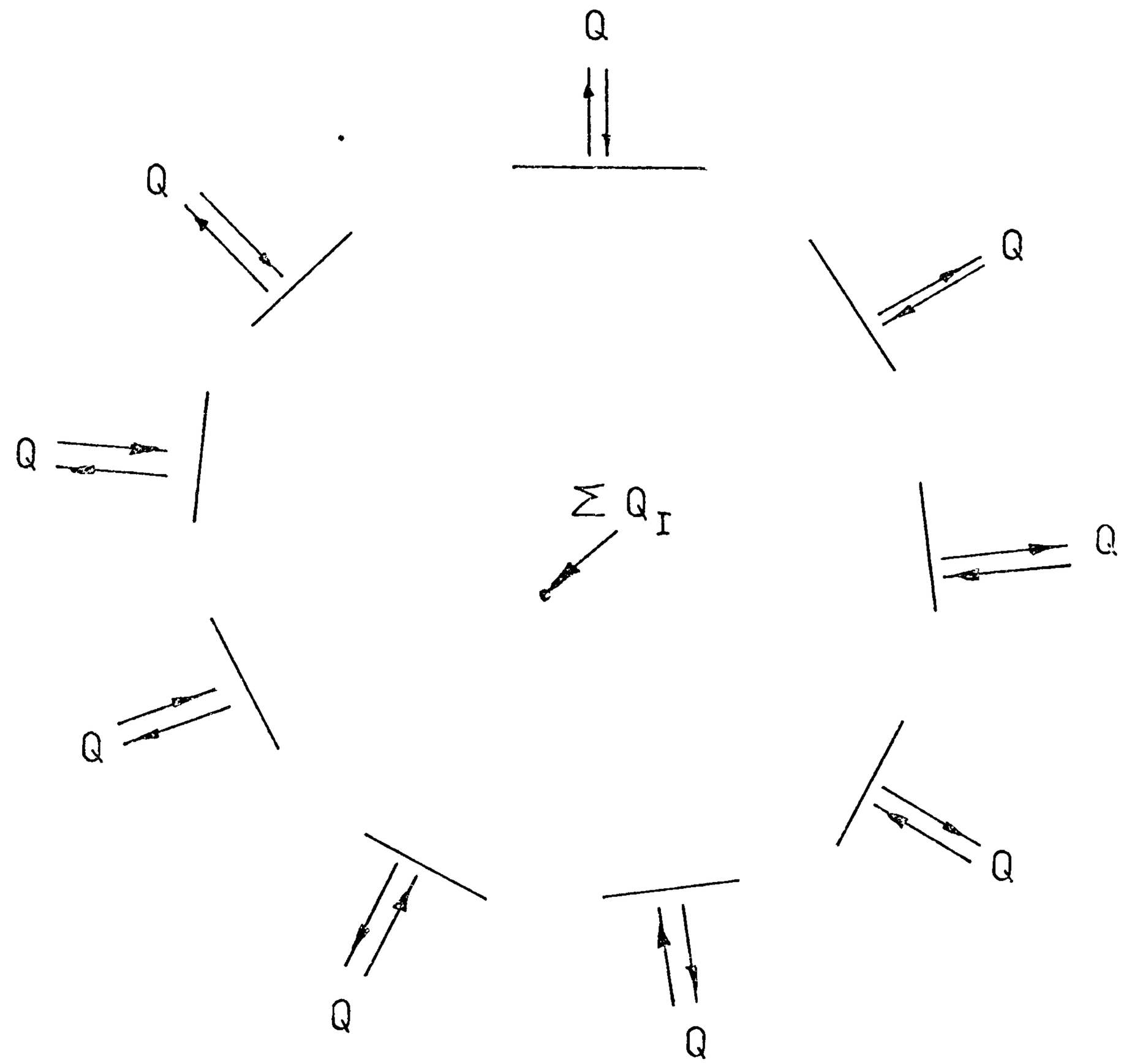

Figure 4.9 Nodal replacements of a subsystem and the heat transfer processes effecting the stored energy within the subsystem

$$Q_S(\tau) = \rho(\tau)\, C(\tau)\, V\, \theta_I(\tau) \tag{4.6}$$

where, $Q_S(\tau)$ = the stored energy in the subvolume at time τ, (w),

$\rho(\tau)$ = density of subvolume at time τ, (kgM^{-3}),

$C(\tau)$ = specific heat capacity of subvolume at time τ, ($Jkg^{-1}K^{-1}$),

V = volume of subvolume (M^3)

$\theta_I(\tau)$ = temperature of the subvolume at time, τ, the subvolume is assumed to be isothermal, (K).

A similar expression can be established for the stored energy at the end of the time step, that is, $\tau+\Delta\tau$:

$$Q_S(\tau+\Delta\tau) = \rho(\tau+\Delta\tau)\, C(\tau+\Delta\tau)\, V\, \theta_I(\tau+\Delta\tau) \tag{4.7}$$

The rate of change of stored energy in the system subvolume with respect to time for the limit as $\Delta\tau \to 0$ is

$$\frac{\partial Q_S}{\partial \tau} = \frac{\left(\rho(\tau+\Delta\tau)\, C(\tau+\Delta\tau)\, \theta_{I(\tau+\Delta\tau)} - \rho(\tau)\, C(\tau)\, \theta_{I(\tau)}\right) V}{\Delta\tau} \tag{4.8}$$

As previously described equation (4.5) equals the net heat exchange in and out of the subvolume boundaries plus the net heat generation within the subvolume. The net effect of the various heat transfer processes which occur across the surface boundaries of the subvolume are represented by

$$\sum_{j=1}^{M} Q_{j,I(\xi)} \tag{4.9}$$

where M = number of boundary surfaces to be considered

j = surface number

$Q_{j,I}$ = the net energy flow into or out of surface j

ξ = either beginning of time step, τ, or end of time step $\tau+\Delta\tau$

The sum of the different heat generation terms occurring in the subvolume are considered by the term

$$\sum Q_{I(\xi)} \tag{4.10}$$

Substituting equations (4.8) to (4.10) for the expression stated in equation (4.5), then

$$\frac{(\rho_{(\tau+\Delta\tau)} C_{(\tau+\Delta\tau)} \theta_{I(\tau+\Delta\tau)} - \rho_{(\tau)} C_{(\tau)} \theta_{I(\tau)}) V}{\Delta\tau} = \sum_{j=1}^{M} Q_{j,I(\xi)} + \sum Q_{I(\xi)} \quad (4.11)$$

where, ξ is a particular time

The process of making the system discrete results in each subvolume being replaced by a node, equation (4.11) can be applied to both subvolume and node.

In order to solve equation (4.11) it is necessary to decide at which time increment the right-hand side is calculated. It can be calculated at the start or finish of the time increment or it can be calculated from the arithmetic mean value of the values calculated at the start and finish. Each of these three methods are quite distinct and are known as the explicit, implicit and the implicit mixed technique.

The fully explicit solution of equation (4.11) involves the replacement of ξ by the present (known) time row value designated n, therefore, the future nodal temperature is evaluated in terms of known values.

The unknown nodal temperature $Q_{I(n+1)}$, by the explicit method, is

$$\theta_{I(n+1)} = \theta_{I(n)} + \frac{\sum_{j=1}^{M} Q_{j,I(n)}}{S} + \frac{\sum Q_{I(n)}}{S} \quad (4.12)$$

where $S = \frac{\rho C V}{\Delta\tau}$

The thermophysical properties of density, ρ, and specific heat, C, are the time-weighted averages of the property over the time-increment, $\Delta\tau$.

Equations arising from the explicit method are uncoupled and simple to solve, unfortunately they are only stable under very restrictive conditions, for one-dimensional heat conduction

$$F_o = \frac{\alpha \Delta\tau}{\Delta X^2} = \frac{k \Delta\tau}{\rho C \Delta X^2} \leqslant 0.5 \quad (4.13)$$

but this limitation becomes more restrictive as the space increment Δx is reduced and as the number of dimensions considered is increased, for 2-D conduction - $Fo \leqslant \frac{1}{4}$ and for 3-D conduction - $Fo \leqslant 1/6$,(54). In equation (4.13), α is the thermal diffusivity of the material (M^2S^{-1}) which has been evolved to partially quantify the rate of response of the material and Fo is the Fourier Number. The Fourier Number gives an indication of the speed at which a body will respond to a temperature change:

$$Fo = \frac{\text{Rate of conduction of heat}}{\text{Rate of storage of heat}} \qquad (4.14)$$

Low values of Fo imply that a long period of time is required to heat or cool the body or vice versa.

It is a necessary requirement of the explicit solution that the time increment is not too large and the space increment is not too small, consequently, while satisfying the stability criteria for the solution the time increment may become so small that the computation time is prohibitive even for simple problems. This is highlighted by consideration of a surface node with convection at the boundary which normally requires much smaller time increments than an intra-constructional node. A dimensionless parameter called the Biot Number (Bi) plays a fundamental role in conduction problems that involve surface convection effects.

$$Bi = \frac{h\,\Delta x}{k} = \frac{\text{thermal conductance at the surface}}{\text{thermal conductivity of the solid}} \qquad (4.15)$$

where h is the convective heat transfer coefficient ($WM^{-2}K^{-1}$). The stability criteria for a one-dimensional transient problem is (54):

$$Fo \leqslant 1/[2(1 + Bi)] \qquad (4.16)$$

This implies that for a surface node the time-step $\Delta\tau$ is restricted by

$$\Delta\tau = \frac{\Delta x^2}{\alpha} Fo \leqslant \frac{\Delta x^2}{2\alpha(1 + Bi)} \qquad (4.17)$$

Thus when Bi is very large $\Delta\tau$ may have to be very small for stability reasons, resulting in a substantial increase in computation time without specifically increasing the accuracy of the construction nodes. The surface node is therefore the controlling factor for the maximum permissable time-step.

The implicit method of solution will always be stable for any time or space increment, therefore, no restriction is set upon $\Delta\tau$ or Δx. However implicit solutions are coupled and more difficult to solve than explicit solutions. The fully implicit solution is obtained by replacing ϕ in equation (4.11) by the future (unknown) time row designated n+1, therefore

$$\Theta_{I(n+1)} = \Theta_{I(n)} + \frac{\sum_{j=1}^{M} Q_{j,I(n+1)}}{S} + \frac{\Sigma Q_{I(n+1)}}{S} \qquad (4.18)$$

The unknown nodal temperature cannot be solved directly from equation (4.18), therefore, the technique is implicit. The solution of the resulting equation-set - one for each node in the system - is conducted simultaneously.

To reduce the discretisation errors and improve the accuracy of the implicit method $\Delta\tau$ and Δx should be small, however, the penalty involved in improving accuracy is a greater computational time - some balance between these two features must be achieved. The computational time required for implicit solutions, however, is frequently less than that employed by an explicit solution because the time-increment for an implicit solution is usually longer than that required to ensure stability in explicit solutions.

A more accurate technique than either the fully explicit or fully implicit methods is the weighted average technique as proposed above. This method involves the averaging of the right-hand terms of equation (4.11) which are calculated at the present and future time increments. This equates to the addition of the fully explicit and fully implicit solution techniques, therefore, adding equations (4.12) and (4.18) yields,

$$2\Theta_{I(n+1)} = 2\Theta_{I(n)} + \frac{\sum_{j=1}^{M} Q_{j,I(n+1)}}{S} + \frac{\sum_{j=1}^{M} Q_{j,I(n)}}{S} + \frac{\Sigma Q_{I(n+1)}}{S} + \frac{\Sigma Q_{I(n)}}{S} \quad (4.19)$$

This arithmetic averaging technique across a time-increment is more commonly known as the Crank-Nicolson technique. This solution is implicit and inherently has the best features of the fully explicit and fully implicit solutions as it has a lower truncation error than the fully implicit solution while being stable, therefore, it gives more accurate answers for less computational time compared to the fully implicit scheme. There are other methods of operating between fully explicit and fully implicit solutions such as the Hopscotch Method, however the Crank-Nicolson formulation is the preferred technique for this work. Rearranging equation (4.19) yields the General Heat Balance Equation,

$$2\Delta S_I = \sum_{j=1}^{M} Q_{j,I(n+1)} + \sum_{j=1}^{M} Q_{j,I(n)} + \Sigma Q_{I(n+1)} + \Sigma Q_{I(n)} \quad (4.20)$$

where,

$$\Delta S_I = \frac{\rho C V (\Theta_{I(n+1)} - \Theta_{I(n)})}{\Delta \tau}$$

One of the principal advantages of this expression is that it can be used to model any system boundary, for example, convective heat transfer and long-wave radiative exchange at a surface. Furthermore either a cartesian or polar coordinate system can be used, however, in this work a cartesian or cartesian equivalent polar coordinate system will be used.

4.3.2 Solution of Systems Model

The general heat balance equation is applied to each node in the system. The resulting equation set for the system is solved simultaneously. This is compatible with the component interactions, which are also solved simultaneously at each discrete time-increment throughout the simulation period. There are two principal categories of solution techniques (54,55):

a) direct matrix elimination methods such as matrix inversion and Gaussian elimination

b) iterative methods such as the Gauss-Siedel iteration technique and the technique of successive over-relaxation

Direct methods obtain the solution in a finite number of operations, for linear problems the solution is complete; but for quasi-linear problems, for example, the conductivity is temperature dependent, the process must be repeated with updated coefficients evaluated based on the newly-computed temperature field. Iterative methods are normally used for non-linear problems such as thermophysical properties and long-wave radiation exchange, however, these problems can be assumed to be linear particularly for small time increment simulations. Consequently, a non-linear solar energy system simulation model can be reduced to a linear problem for which direct methods of solution can be applied. These normally require more storage space than iterative techniques and they carry a residual error due to rounding errors, however, modern computational facilities have greatly nullified such disadvantages and direct methods are widely used.

Matrix inversion is a direct method but it is extremely inefficient and should never be used in practice, except on fewer than 5 equations (54). Gaussian elimination and variants of it are generally preferred to effect the direct solution effectively. A set of N fully populated linear equations solved by Gaussian elimination require [N(N-1)(N+1)/3] multiplications and divisions for the forward reduction stage and [N^2] for the backward substitution stage, therefore, when N=50 a total of 44,150 calculations would be required at each time increment. In a heat transfer problem the resulting matrix is normally sparse and only a small fraction of these calculations would be required. This can be achieved more efficiently by using a variant of the Gaussian elimination method which will be described in Chapter 6.

The proposed operational procedure for conducting a simulation model based on the simultaneous method is as follows (see Figure 4.10):

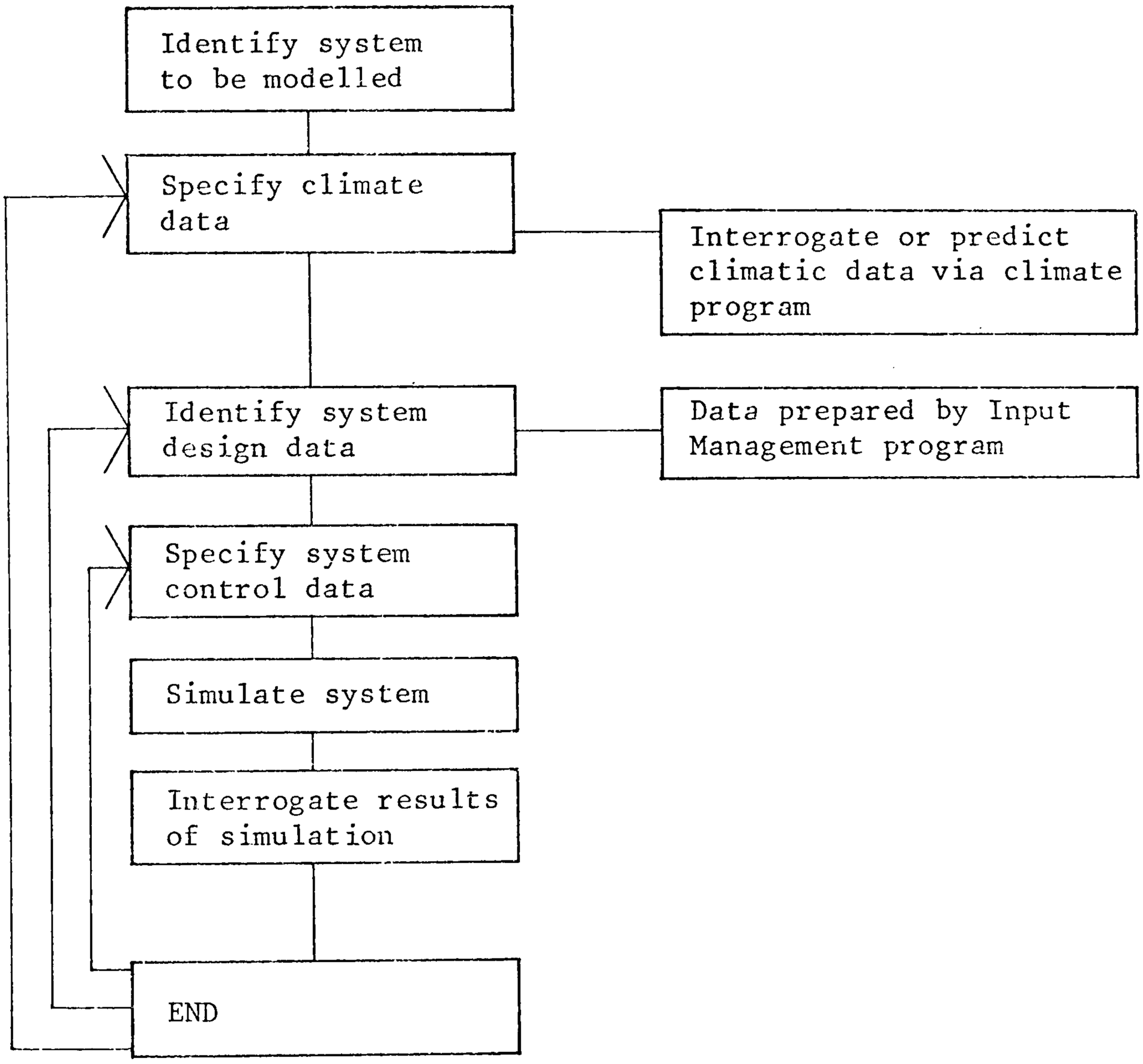

Figure 4.10 General procedure for simulating a particular design

1. Identify the system to be modelled and numerically label every system component. For example, a liquid solar energy system is labelled in Figure 4.11 (a).

2. Select or predict the climatic data necessary for simulation of the proposed system. The climate interrogation program described in Chapter 3 can be used to aid this process.

3. The user prepares the data associated with each system component by means of an input management program which will correctly structure the data into files for subsequent simulation. This program will use an interactive question/answer procedure. If a component can have more than one node then the user is asked to identify the approximate number of nodes. Figure 4.11 (b) shows an equivalent nodal representation of the liquid solar energy system identified in Figure 4.11 (a).

4. Specify the control strategy of the system. Each node in the system can be considered as a control point where a thermocouple has been sited, therefore, complex control philosophy can be analysed.

5. The simulation model in computer program form is operated using the data previously assembled. Energy balances are conducted between nodes for the start of the time-increment for which all data is known and the finish of the time-increment where the nodal temperatures are unknown. The simultaneous solution of the complete set of unknown or implicit nodal equations results in the evaluation of the unknown nodal temperatures. These become the known conditions at the present time row and the process is repeated for every time-increment within the simulation. Figure 4.12 is a matrix of the inter- and intra-nodal connections for the solar energy system shown in Figure 4.11, each X represents the node under analysis whereas a Y represents each physical contact point of node X. The matrix representing the nodal equation-set will be slightly different because a fluid node will not be in

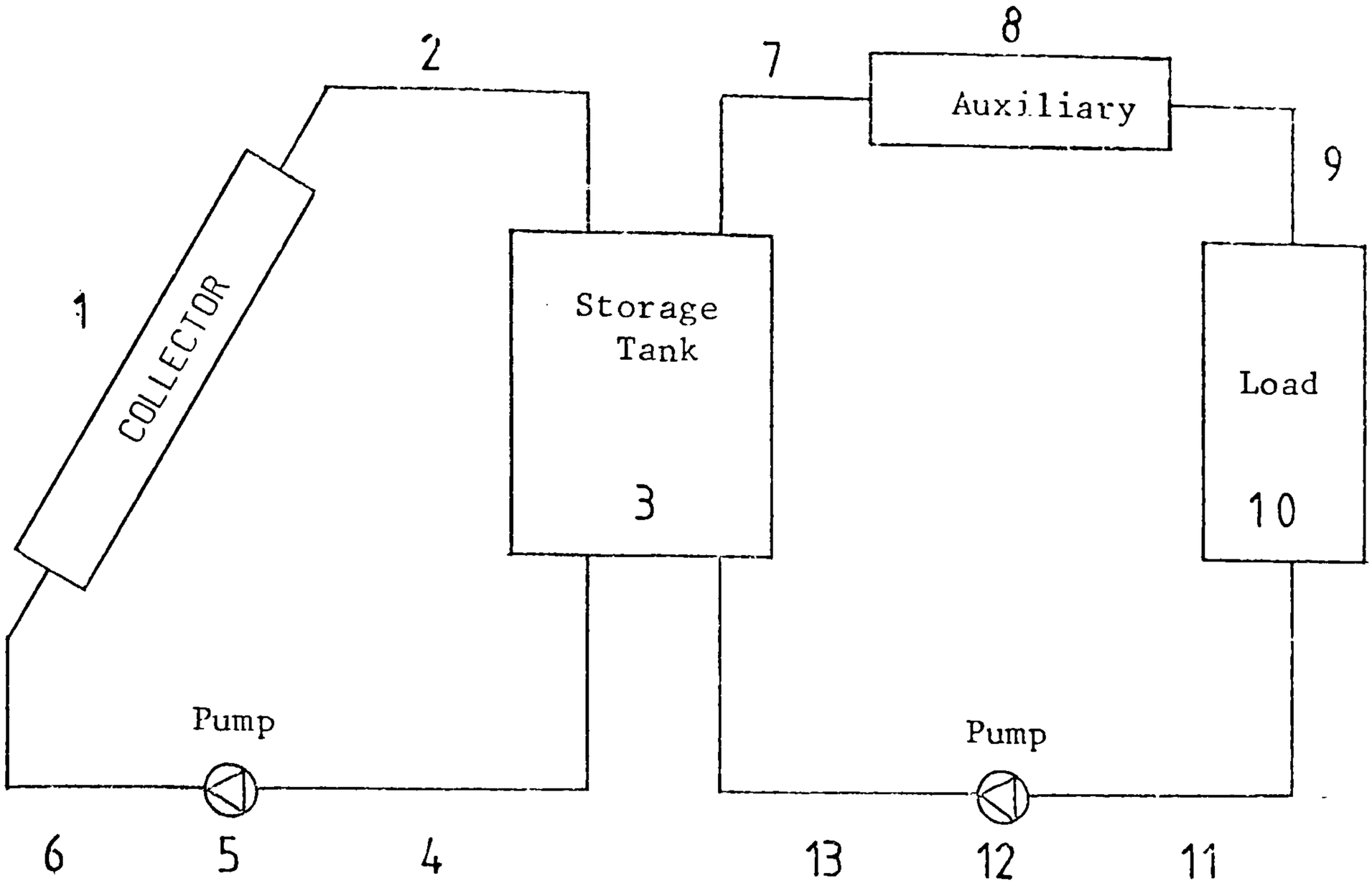

Figure 4.11(a) Simple liquid solar energy system

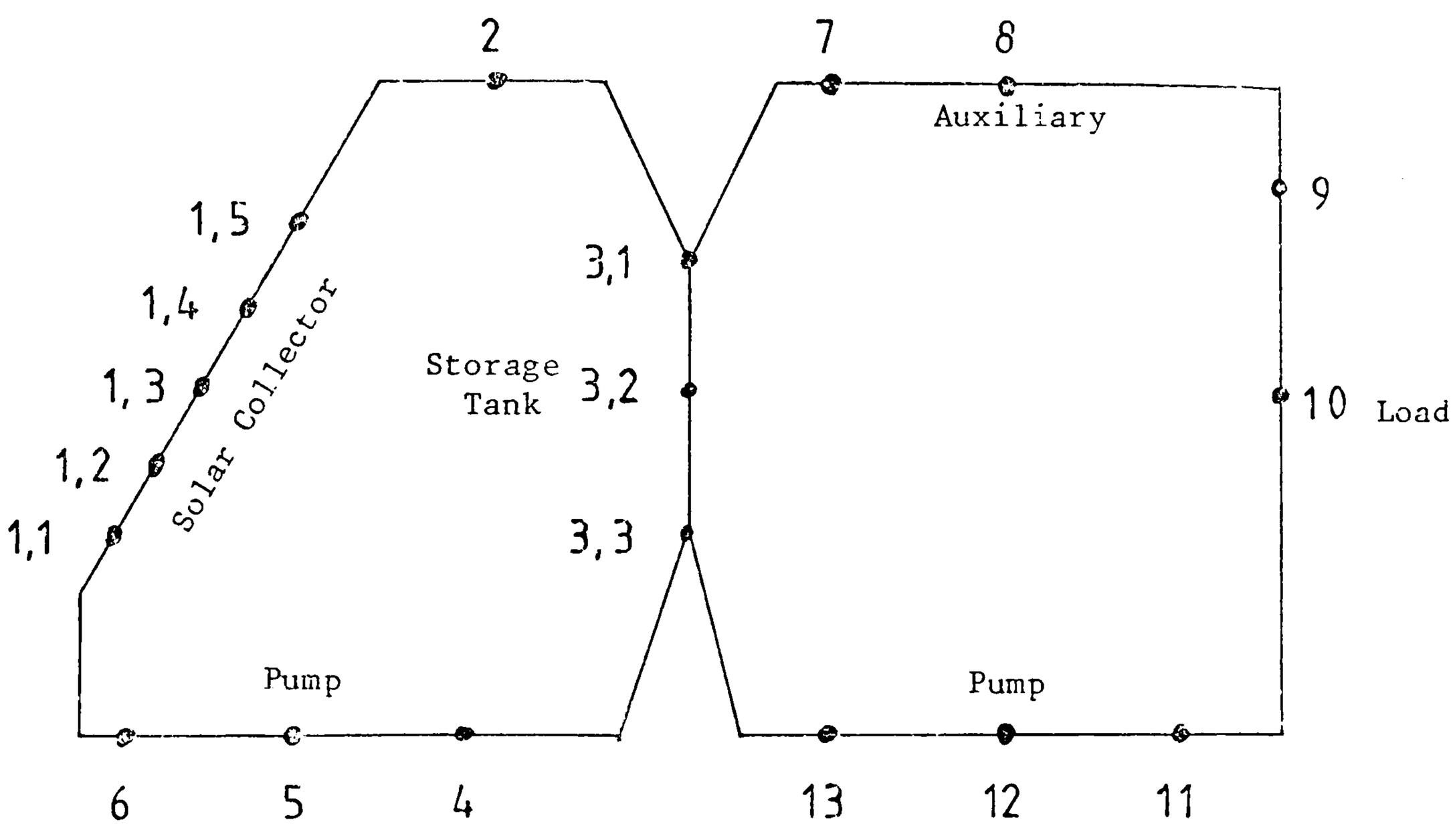

Figure 4.11(b) Equivalent nodal representation of Figure 4.8(a)

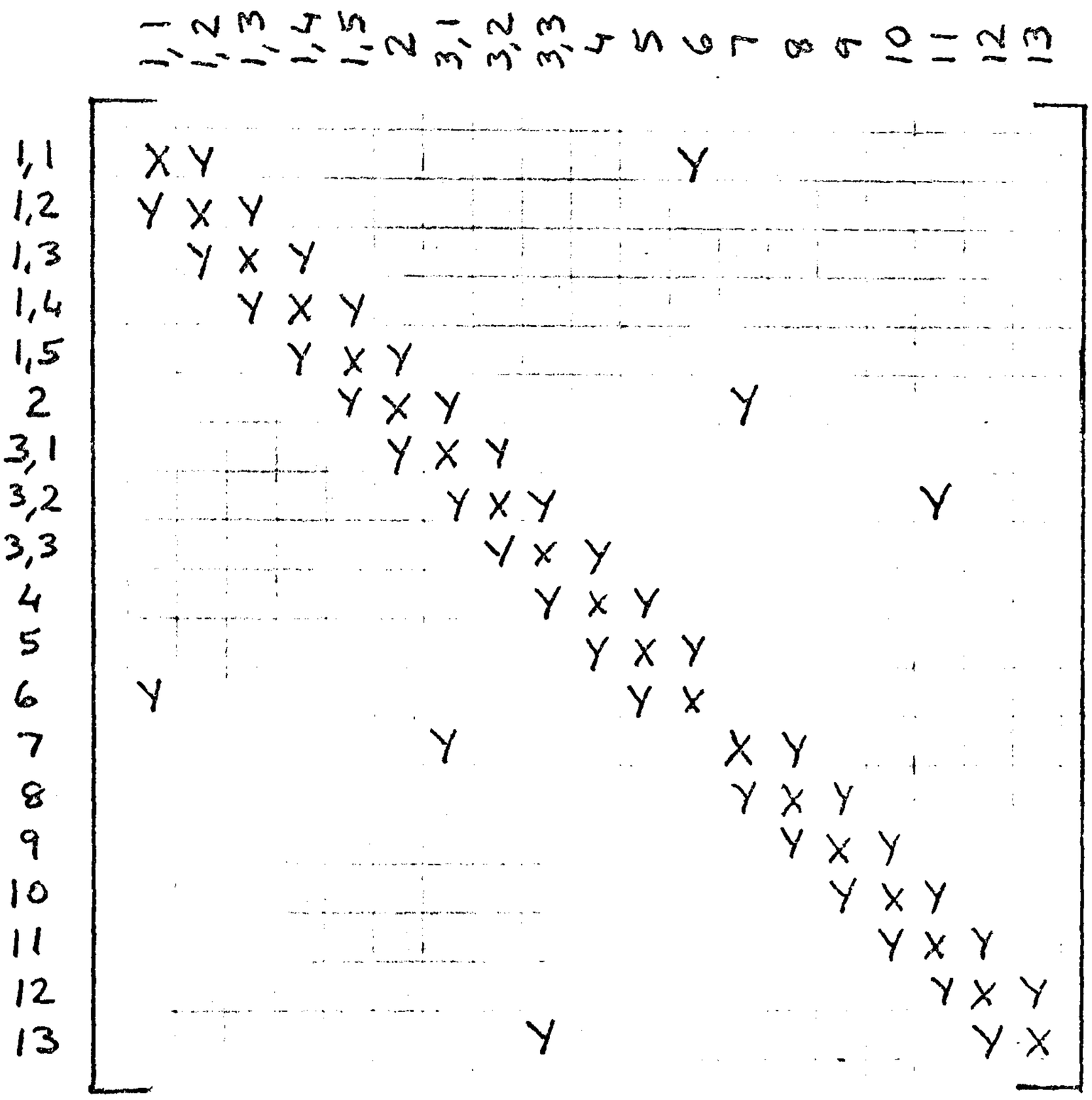

Figure 4.12 The (A) matrix associated with nodes in physical contact for figure 4.10

contact with the node it flows into. This will be explained more fully in Chapters 5 and 6.

6. Upon completion of the simulation it is possible to interrogate a file containing output information for the system. This data will include each nodal temperature and selected miscellaneous pieces of information. The data may be viewed graphically or in tabular form.

7. The user can re-specify climate data, design data or control strategy data in order to re-simulate.

This procedure will be described more fully in subsequent chapters.

Compared to the modular approach the simultaneous approach conducts a more detailed analysis of inter- and intra-connections between system and component nodes respectively. Any number of nodes may be treated as control points allowing complex control strategies to be specified, and furthermore, compared to TRNSYS this model does not rely on complex information flow diagrams and generates more data upon which design decisions may be based.

Simple models like the F-Chart can be generated from this model, however considerable research would be required to determine the form and nature of the resulting correlated equation.

The following chapter describes the mathematical model of a solar energy system based on the preferred simultaneous approach as described in this section.

CHAPTER 5 Solar Energy Systems Model

With the increasing use of solar energy systems, and the potential of hybrid photothermal/photovoltaic solar collectors, it is becoming more important to the designer of such systems to obtain a detailed analysis of their performance. As a result the need has arisen for a comprehensive design model to investigate the performance of these systems without imposing any apparent limitations on the designer as well as offering accuracy and flexibility. The FLARE solar energy systems model is the outcome of an attempt to meet these objectives. It is based on the theory of finite differencing, using an implicit numerical technique operating in conjunction with hourly values of climatological parameters. The model incorporates considerations of:

a) The effects of short-wave radiation impinging on external (opaque and transparent) and internal solar collector surfaces. The method of modelling solar radiation ultimately determines the accuracy of the computed results. In the simulation model the absorbed component of monochromatic solar radiation incident on external opaque surfaces acts as an energy injection at these surfaces, depending upon subsequent temperature and energy variations both external and internal to the solar collection, this energy may be transmitted to the collector enclosure by transient conduction. The spectral (or monochromatic transmission, absorption and reflection of incident solar radiation impinging upon external transparent materials, e.g. glass, plastics, thin films, etc, is considered for both the beam and diffuse components of solar radiation. The spectral direct solar radiation transmitted is injected at those internal surfaces upon which it would actually fall and the spectral diffuse radiant energy is injected at all internal surfaces which can be seen by the transparent surface. The magnitude of solar radiation impinging upon external surfaces is a function of the angle of incidence and, in addition, the magnitude of that falling on internal surfaces is a function of the optical properties of transparent elements and enclosure geometry. Shading may have a significant effect on both the external and internal surfaces because only diffuse solar

radiation falls on shaded surfaces.

b) the shading of external opaque and transparent surfaces and the insolation of internal surfaces. The shading of external opaque and transparent surfaces can greatly influence the magnitude of the impinging solar radiaiton. There are two algorithms available, the first is a shading algorithm the second evaluates insolation through transparent elements. The shading algorithm computes for any site, collector geometry and time the effects of shading on external surfaces due to surrounding buildings and self shading. The insolation algorithm computes for any site, internal geometry and site which surfaces are insolated by direct radiation on transmission through a transparent material.

c) internal long-wave radiation exchange between enclosure surfaces. This exchange is considered as a function of the respective surface temperatures, absorptivities, reflectivities, and emissivities and geometric configurations. If there are any surfaces which are transparent to thermal energy re-radiated from internal surfaces this energy is regarded as being lost from the system. Re-radiation is associated with the internal surfaces of the collector enclosure or, alternatively a system component within an enclosure, for example, a conduit, heat exchanger or auxiliary heater in a buidling.

d) net external long-wave radiative exchange. This exchange occurs between an exposed plane surface and its surrounding hemispherical envelope, where the envelope is a function of the view factors of the surface to the sky, ground and surrounding buildings. The surface will either have an energy injection or extraction to account for the radiative exchange.

e) natural, mixed and forced convection effects in the laminar, transitional and turbulent regions, convective heat exchanges between solid surface boundaries and a fluid for each system component will be considered. This will cause an energy transfer to the fluid from the surface or vice versa. The effects of fluid flow throughout the

system will also be analysed.

f) the effects of leaks into or out of the system. These are assumed to act directly at a fluid node with zero time lag.

g) the prevailing wind speed and direction. These parameters influence the heat exchange by convection between exposed external surfaces and the outside air. The surface convection coefficient for this heat exchange can be computed on the basis of wind conditions. This value will become more significant as the exposed component's surface temperature increases.

h) the strategy of system operation. Consideration of the control strategy for system operation is perhaps the single most important factor in a solar energy collection system because it attempts to maximise the solar contribution to a particular load. Fans, pumps, dampers, values, etc are controlled on the basis of either temperature or time and the system may be controlled at any number of points throughout the system.

i) the effects of fan or pump heat losses to the passing fluid. These are assumed to act directly at the fluid node.

j) the effects of energy exchange between a conduit or fitting with its surrounds. If there is a high degree of insulation used then this effect may be very small.

k) the deliberate energy injection into a fluid within components such as an auxiliary heater, indirect or direct hot water storage unit. The quantity of energy involved in this process can be very large and requires careful consideration.

l) the effects of thermal stratification in a liquid or rock bed storage unit. Stratification in storage units can have a significant effect on system performance, consequently, where stratification exists the storage model must allow any number of stratification levels to be considered.

m) thermal considerations of the photovoltaic effect. Impinging solar radiation will be converted to electricity and removed from the system by means of an energy loss at the appropriate node.

The simulation model allows the designer to assess and appraise alternative solar energy collection designs and operational strategies by permitting the imposition of selected conditions and restrictions on the system, with respect to time.

As described in the previous chapter the method employed in using a numerical analysis technique to solve for any system component is a three stage process. The first stage which involves the placement of nodes at discrete points throughout the system is described for a solar collector system in section 5.1. Once each node has been identified the second stage involves using the General Heat Balance Equation, as derived in Chapter 4, to establish a difference equation for each node in the system. A set of general difference equations for various nodal categories are derived in Section 5.2, these equations are then written in a complete form (Section 5.4) after they have been modified by various heat generation terms which are described in Section 5.3. The third and final stage of the process involves the solution of the equation-set simultaneously. This is described in Chapter 6, in which the complete difference equations are applied to a simple solar collector system and the solution technique employed is detailed.

5.1 Nodal Replacement of a Solar Energy Collection System

Six of the most common components of a solar energy system are to be modelled, these are:

1. solar collector capable of operating as an air, liquid or photovoltaic flat plate collector or in any combination of these three collector types.

2. conduits - these include pipes, ducts, valves, three port valves, tees, etc

3. fans or pumps

4. auxiliary energy units

5. heat exchangers

6. sensible and latent energy storage units. The sensible storage units are a hot water storage unit and a rockbed storage unit.

With the probable exception of the solar collector, each component will be contained within a building and the system may be designed to meet the space heating requirements of its host. Although the building is not modelled in this work, connections with the ESP building energy model will be shown in Chapter 7.

The General Heat Balance Equation derived in Section 4.3.1 can be applied to any node and is used after each component has been made discrete. The resulting equation for each node is stable and results in physically realistic solutions(54). However, truncation errors occur as a result of the replacement of derivatives by finite difference approximations (the finite difference solution of the derivative in Appendix 5 gives some indication of the error involved for one-dimensional problems). This type of error is unavoidable, nevertheless, it can be minimised by reducing the space and time increments used. Whilst accuracy considerations dictate that both the space and time increments be small,

the alternative considerations of speed and computational costs require that increments are large.

In buildings, energy is normally transferred from the inside to the outside (or vice versa) through the thinnest part of the wall, roof or floor constructions, which may be single or multi-element constructions. It can be assumed that the temperature of the construction at any plane normal to the heat flow is uniform, there will be no heat flow in the directions normal to the heat flow direction, consequently, one-dimensional conduction exists through a multielement construction in a building. However, variation in temperature can occur in the plane normal to heat flow. These variations are dependent upon the position of the plane relative to localised hot-spots, for example, if a radiator is fixed to a wall, then the temperature immediately behind the radiator will be greater than the average wall temperature. The same effect will result from an external surface being partially shaded or internal surfaces being insolated. A flat plate solar collector can also be modelled in terms of one dimensional heat flow, however, it is more likely that temperature variations will occur in the plane normal to the heat flow because of: external and internal shading and absorber plate temperature variations due to the mode of energy collection in both air and liquid collectors. As a result a solar collector should ideally be considered as a three dimensional problem, and ideally all other system components should also be modelled in three dimensions.

The consequence of a three dimensional or lattice structure of nodes to model a solar energy system will be a vast quantity of nodes, many of which do not significantly affect the accuracy of the model. For example, nodes positioned in some materials will have negligible heat flow in one or two dimensions, therefore, the nodes in these directions are of little significance but their solution increases computation time. The method of making a component discrete using as few nodes as possible to reduce computation time whilst ensuring a low truncation error requires an understanding of the thermal processes involved in the component.

To assess the number of nodes required to model an element of a multilayered wall construction in the dominant direction of heat flow, assumed to be in the X dimension, Clarke (5) conducted two tests, the first involved varying the space increment whilst holding the time increment constant, the second involved varying the time increment for a constant space increment. For one dimensional heat flow it was concluded that a three node per element scheme - one node placed at each element boundary and one at the centre plane is most suitable in terms of accuracy, speed and cost of computation. For multilayered constructions, internal boundary nodes would be shared by the two adjacent elements so that each multilayered construction can be represented by (2E+1) nodes, where E is the number of elements. Considering a three element construction (Figure 5.1), it will be represented by seven nodes. The time increment should have a maximum interval of one hour which is the sampling frequency of the available climatological data. There is no restriction on how small the time increment can be, however, the smaller the time increment becomes, the greater will be the computation time. Climatic data for time increments less than one hour can be obtained by linear interpolation between the appropriate hourly values.

In most solar system components the energy emitted is uniform over its surface, therefore, one dimensional heat flow can be assumed to exist. In a solar collector a three node/element scheme is suitable and accuracy is maintained without using a lattice nodal structure. However, elements such as the absorber plate will required a three-dimensional nodal scheme because of variations in surface temperature.

Forced fluid flow is essential to the operation of air and liquid flat plate solar collectors (except for those that employ thermo-siphoning), therefore, a three dimensional nodal network of the fluid flow is desirable. Patankar (56) developed a general model for fluid flow in three dimensions by applying numerical methods, however, there are many variables within the model which are extremely difficult to evaluate, for example, pressure and density differences and diffusion conductances between nodes. In air collectors the problem is compounded because fully developed flow seldom occurs and the fluid flow field at entry and exit points is very difficult

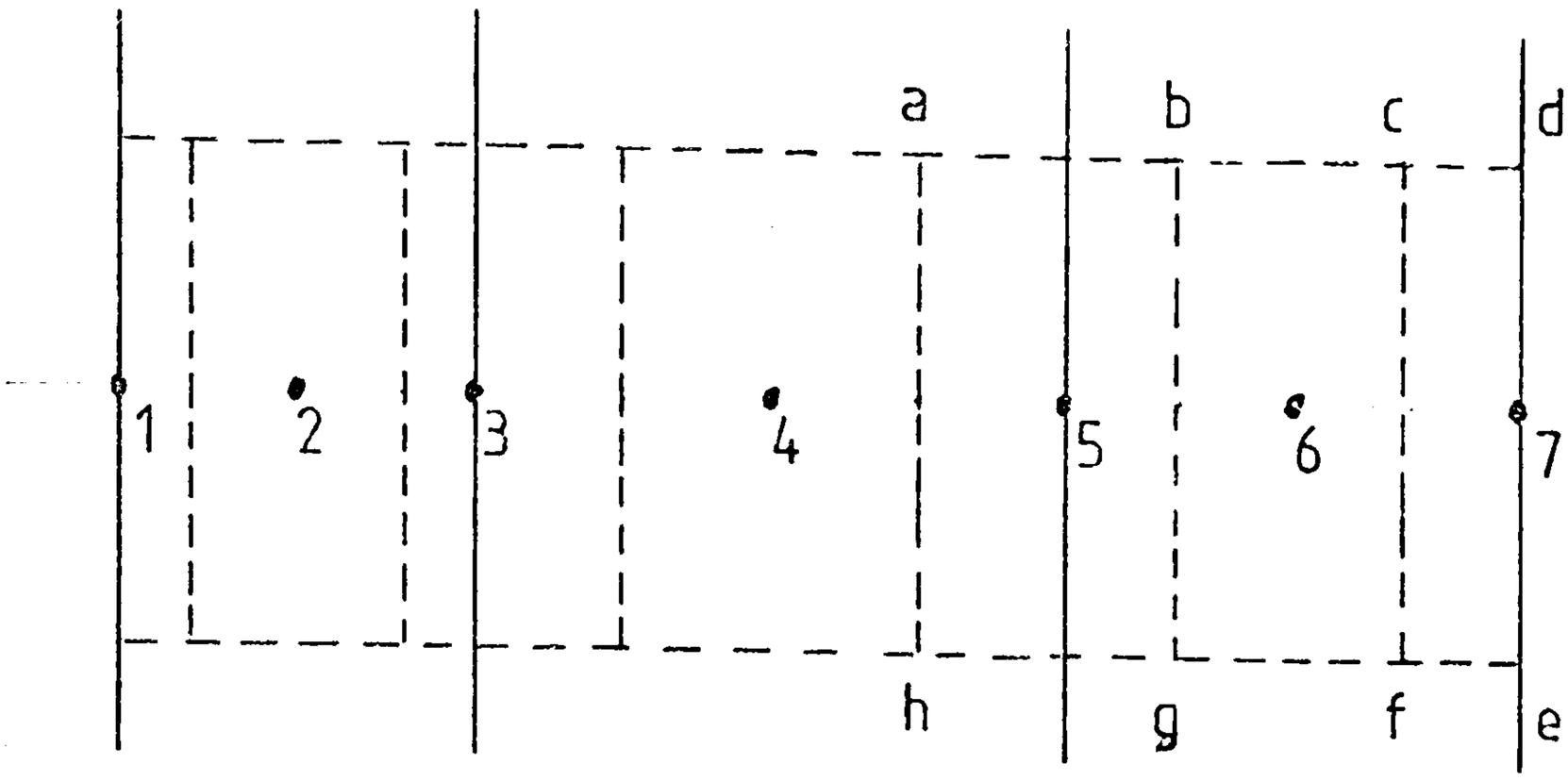

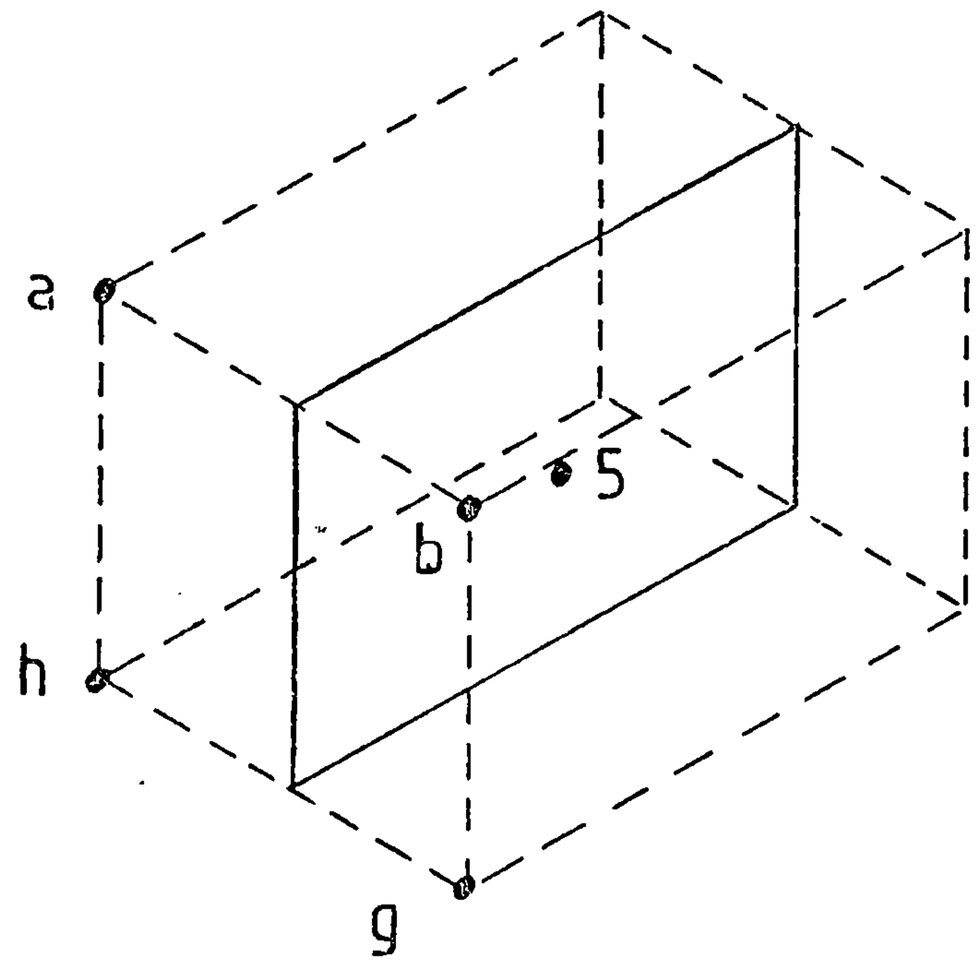

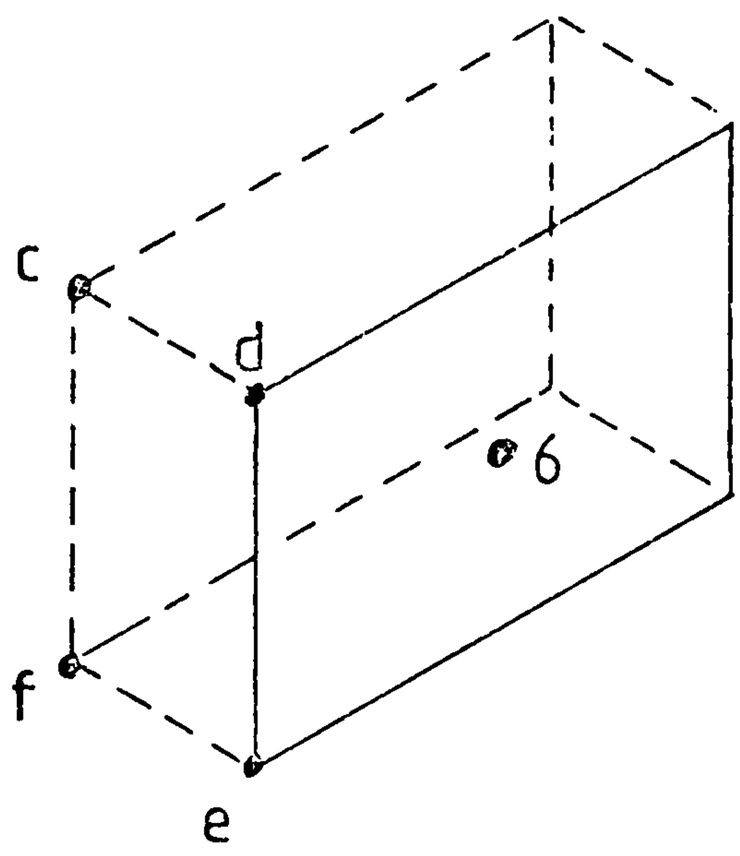

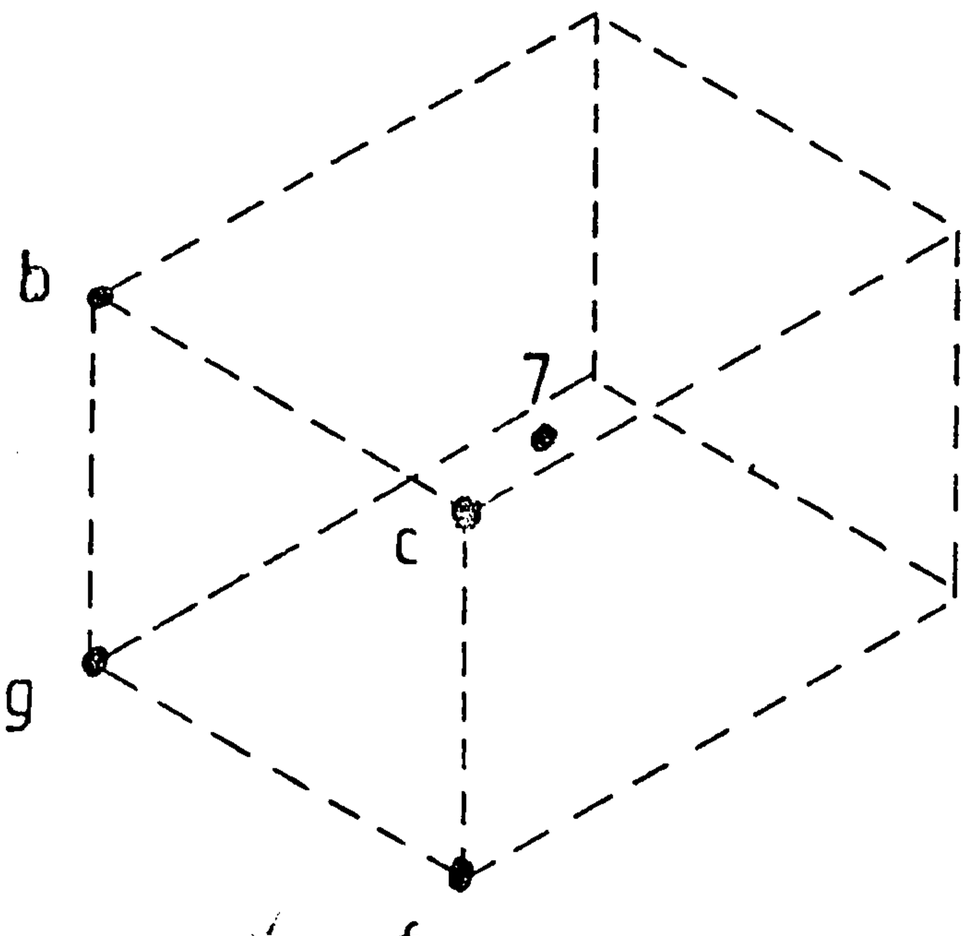

Figure 5.1 Nodal representation of a multielement construction in which heat conduction in one-dimension is dominant.

to predict. Although these problems are not insurmountable, the computation time necessary to conduct a three dimensional fluid flow analysis would be prohibitive due to iteration. Furthermore a detailed fluid flow field model would have to be available for different collector geometric configurations, resulting in an expensive storage overhead reducing the model flexibility.

It is proposed that fluid flow is modelled in one dimension, that of the flow direction. This model can be used to investigate natural and forced convection simultaneously. In a forced fluid flow convection problem nodes will be positioned at discrete intervals in the direction of fluid flow. Each node represents a stationary subvolume of component through which a fluid flows. The principal advantage of this one dimensional flow model is that it can use available analytical and empirical equations to estimate the convective heat transfer coefficients between the fluid and its surface boundaries. In addition a very simple two dimensional flow model could be constructed from this model using a series of non-participating boundaries in the flow direction and assuming some thermal connections between them, this would allow stratified fluid flow in a duct to be considered.

5.1.1 Discretisation of System Components

Each system component will now be made discrete. The thermal processes to be modelled in each component will be identified and the replacement nodal scheme established.

a) Solar Collector

Figure 5.2 shows the thermal processes involved in a solar collector. Irrespective of the collector type (unless it is a ductless collector) it can be regarded as a group of multielement constructions surrounding an enclosure, therefore, depending upon which enclosure surface is under consideration there can be a one , two or three dimensional nodal structure. Figure 5.3 shows the placement of nodes corresponding to Figure 5.2. It is assumed that the internal surfaces of the collector enclosure are more liable to temperature variations than the external surface, therefore, the number of nodes per element may decrease from the inside surface to the outside but not vice versa. This means that if each internal surface of the collector is modelled by a single node, then one dimensional conduction will prevail throughout the collector.

Consider a three dimensional nodal network in a multielement construction of a flat plate solar collector enclosure. Although a three node/element scheme is invoked for each element in the dominant direction of heat flow, it is assumed that any number of nodes can be considered in either dimension perpendicular to heat flow. A regularly shaped plane element can be replaced by a number of nodes, each representing a subvolume of the element. In a multielement construction where several of these elements are positioned with plane faces adjoining only conductive heat transfer is considered. This gives rise to a family or category of nodes which represent the transient conduction through and storage within multielement constructions. This nodal category applies not only to solar collectors but to the multilayered construction surrounding water storage tanks, rock bed storage units, conduits, etc. There are a number of nodal types within this category, for example, nodes situated at the centre of a homogeneous element

Condensation & convection

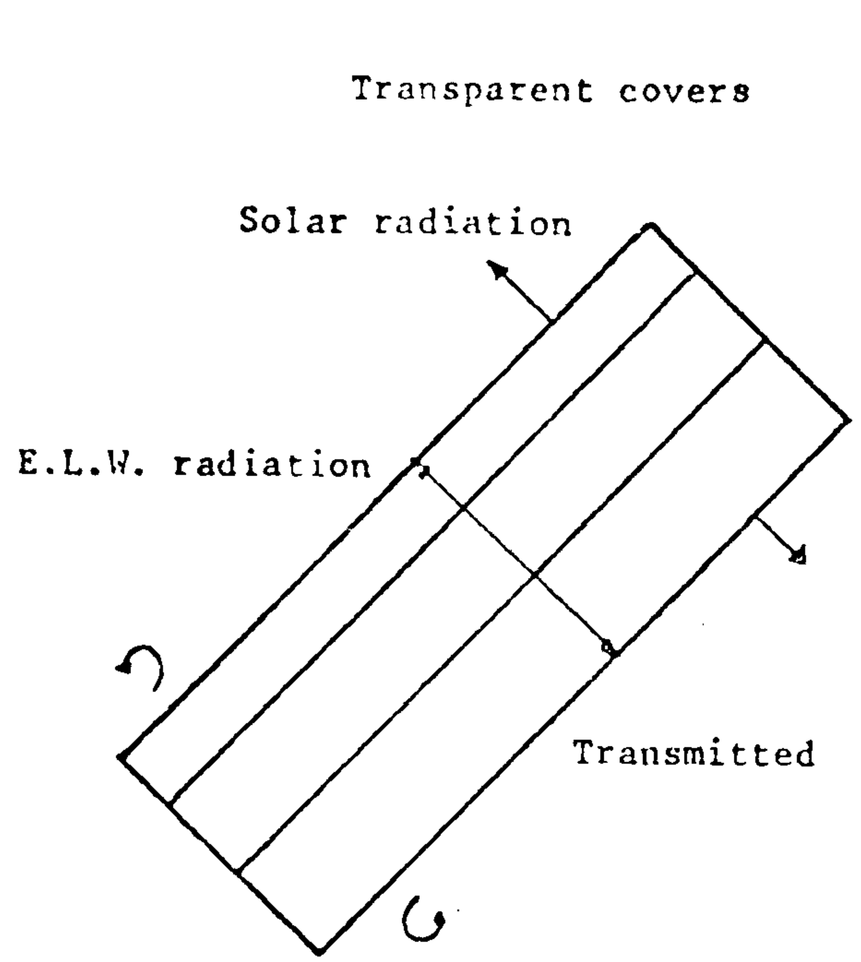

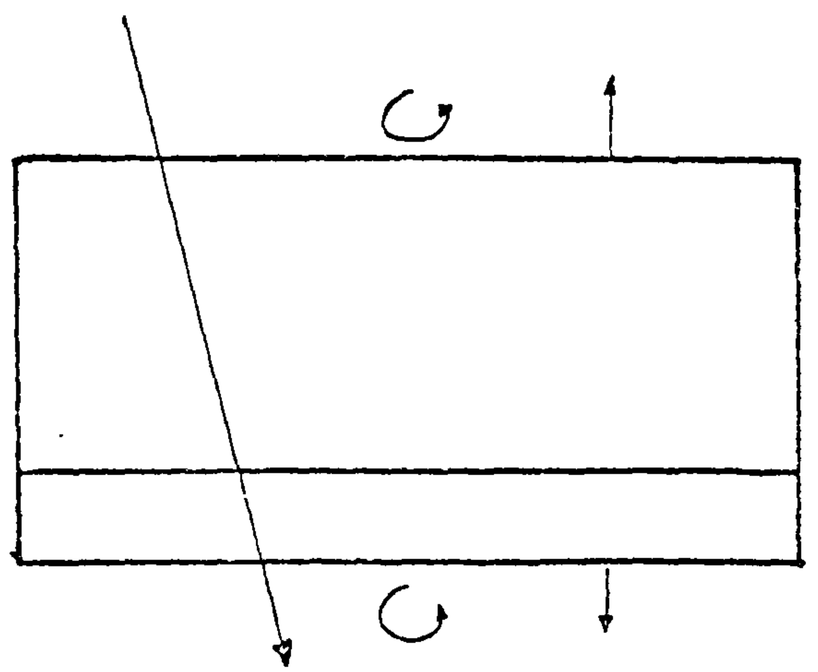

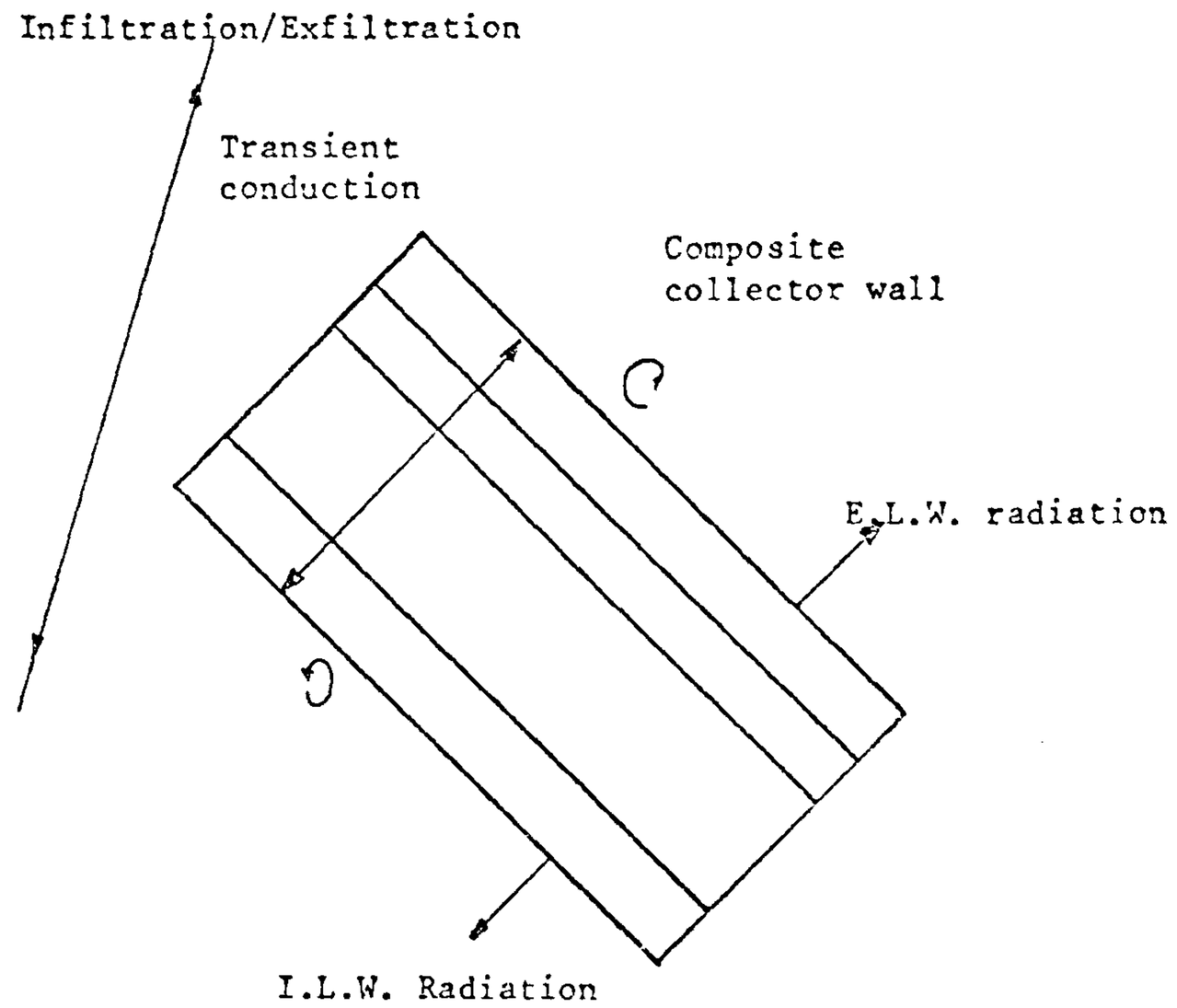

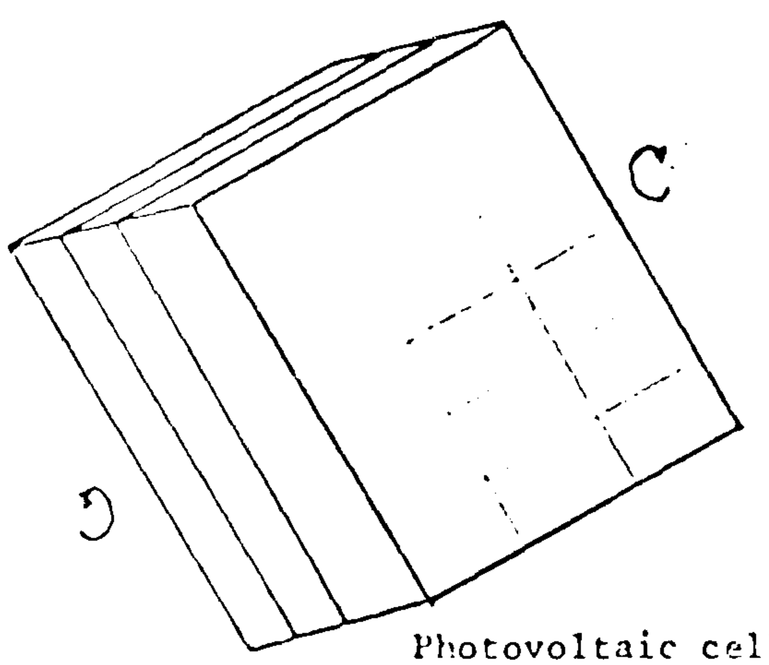

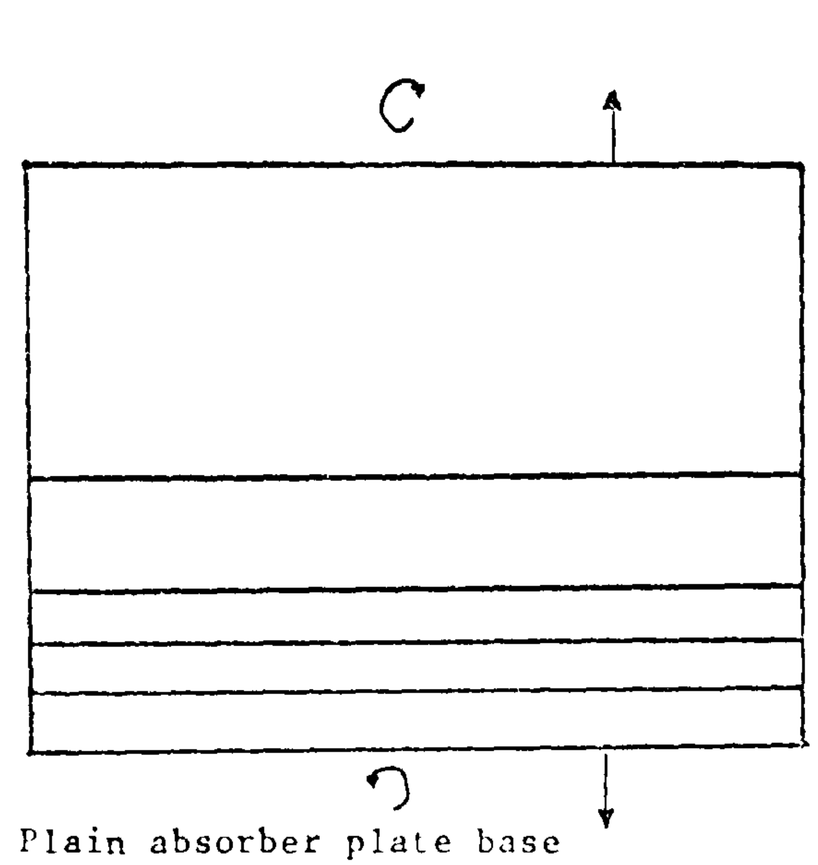

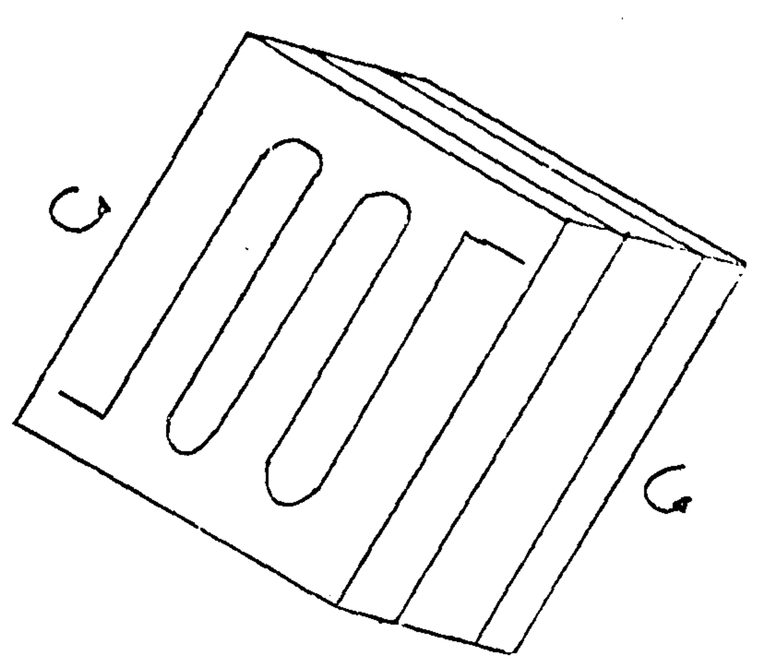

Figure 5.2 Heat transfer processes associated with flat plate solar collectors.

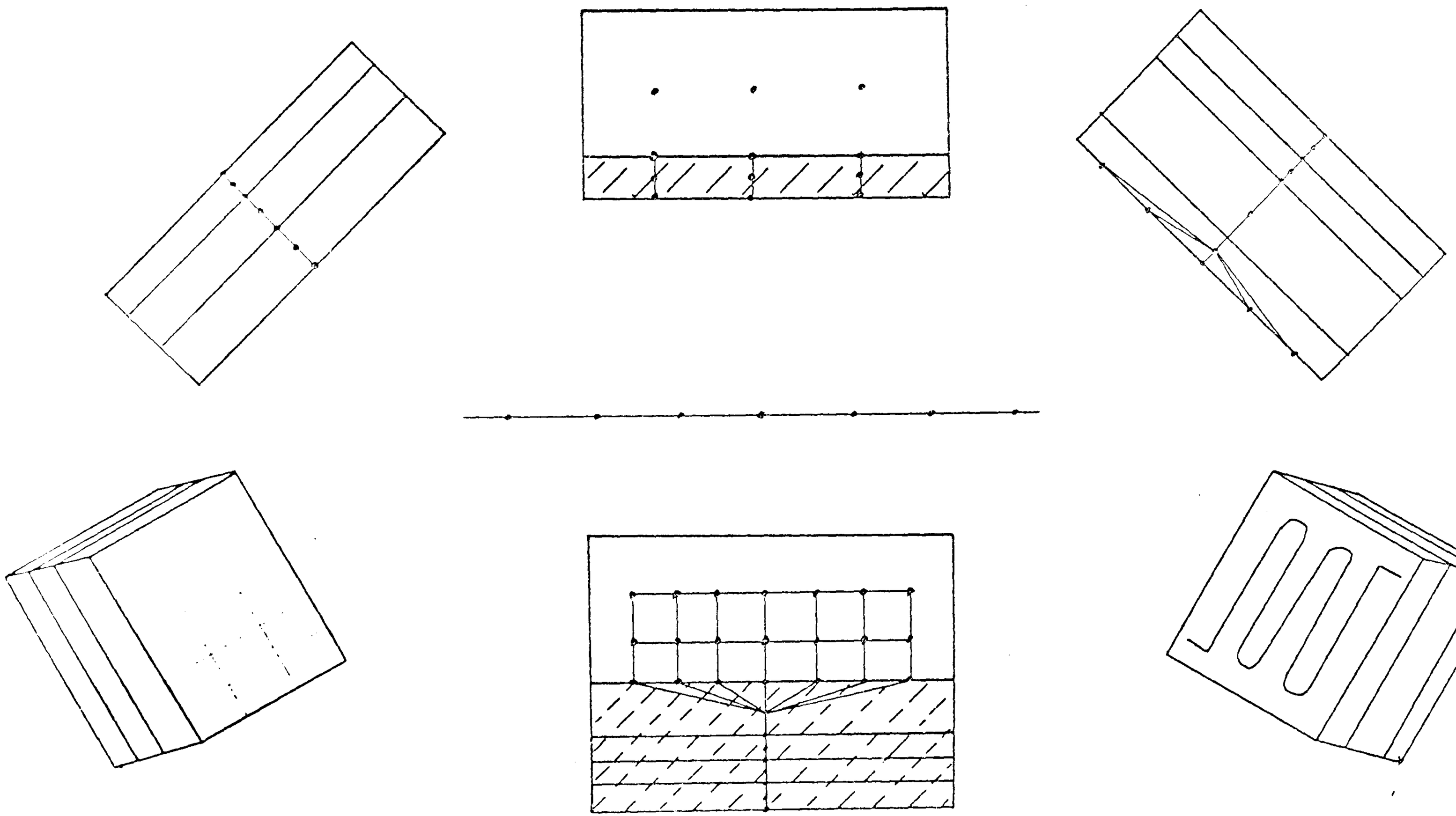

Figure 5.3 Placement of nodes at points of interest throughout flat plate solar collector (conduction contact paths and fluid flow paths shown)

which can be modelled in one, two or three dimensions.

The consequences of one dimension fluid flow is that each node can be connected to more than one surface node, for example, an air fluid node in a solar collector enclosure is connected to at least four different surface nodes (Figure 5.4) whereas, if a lattice structure of nodes had been used to model the fluid (i.e. three dimensional fluid flow) then each fluid node would have been connected to a single surface node. The one dimensional fluid flow node in a solar collector represents a second distinct nodal category.

One restriction put on the solar collector model is that the number of fluid nodes, P, controls the number of nodes on any surface parallel to fluid flow P^1, because the division of P by P^1 or P^1 by P must be an integer number. This ensures that a particular surface node will be in thermal contact with one or more complete fluid boundaries and vice versa. This restriction does not relate to the amount of nodes perpendicular to the fluid flow on these surfaces, see Figure 5.5.

There is a third and final category associated with a solar collector which represents all surfaces nodes, that is, nodes at the exposed surfaces of each multielement construction.

In the solar collector model the objective is to minimise the number of nodal points without reducing accuracy. This is achieved by omitting nodes in the Y or Z dimensions of any category 1 element in which the heat flow is negligible in Y or Z dimensions. Therefore, any insulation element will automatically reduce the nodal network to a one dimensional heat flow problem from that point. Figure 5.6 shows the sectional plan and elevation of such a nodal scheme applied to a single duct flat plate solar collector.

Three nodal categories have been identified which are used to define a solar collector:

Category 1 node: these represent the transient conduction through and storage within multielement constructions. Nodes

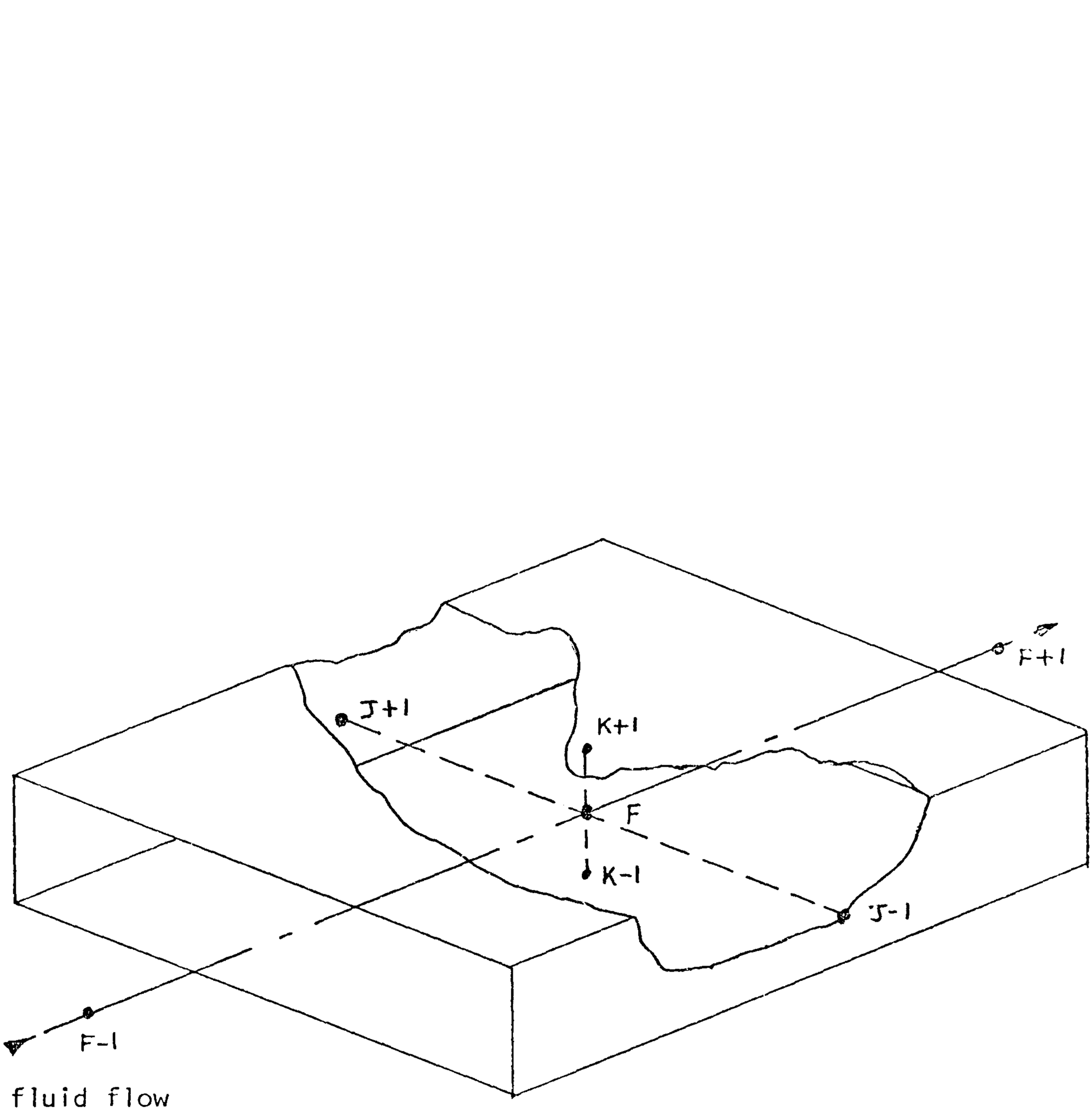

Figure 5.4 One-dimensional fluid flow through a duct

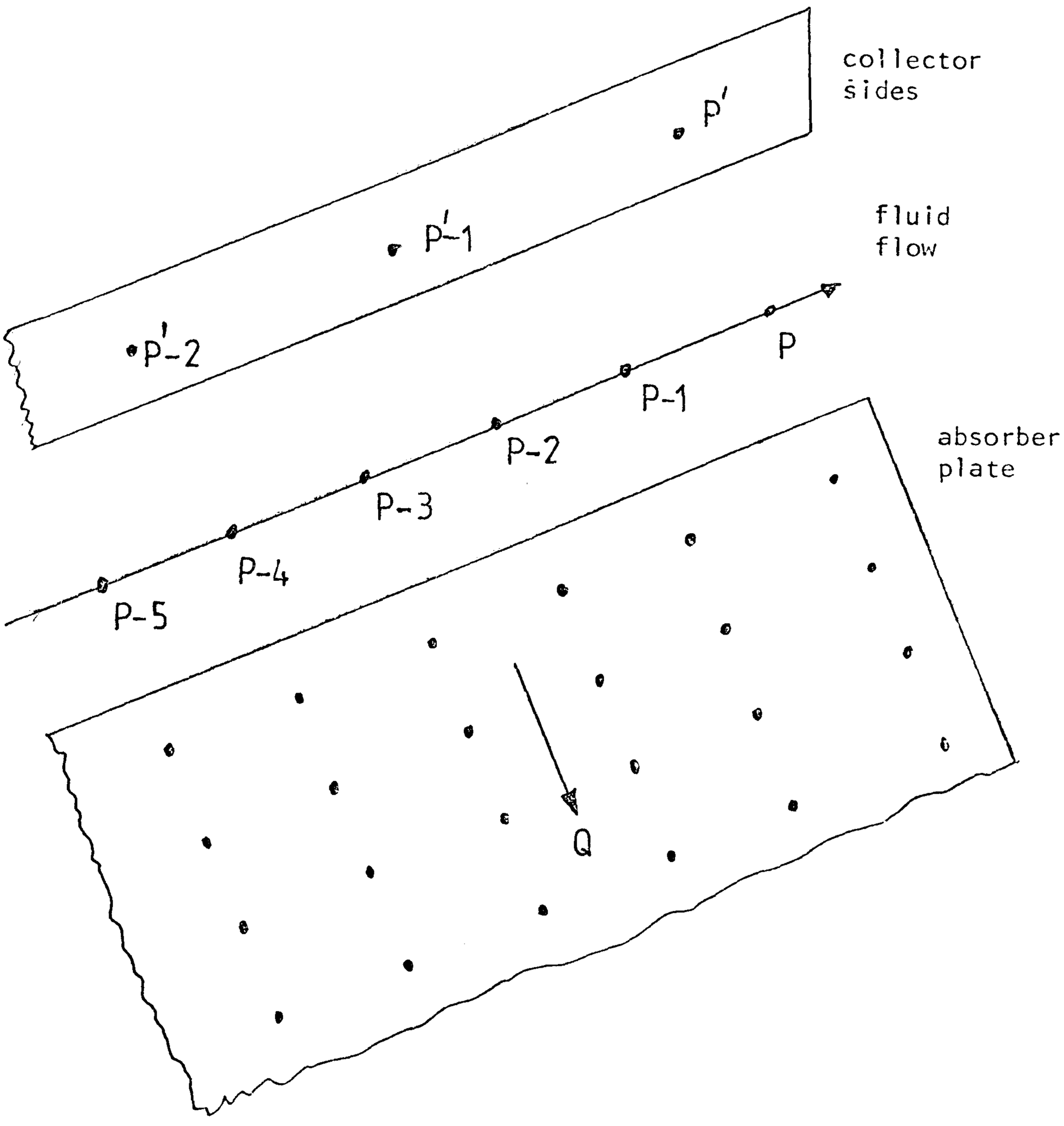

Figure 5.5 P node fluid flow: absorber plate P*Q nodes.

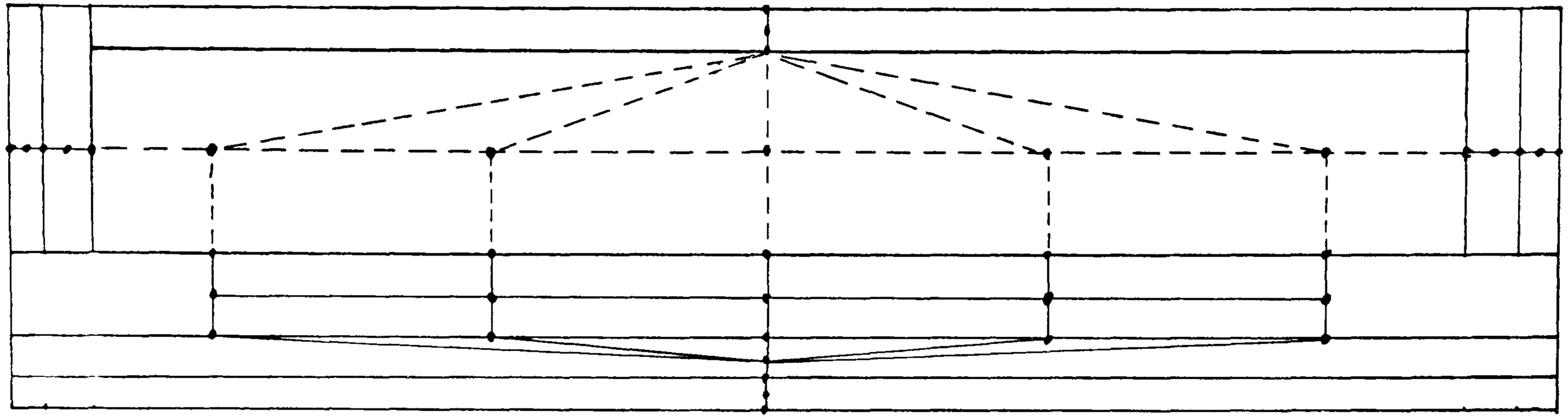

Figure 5.6a Section on XX. Connections: Convective - - -, Conductive ———

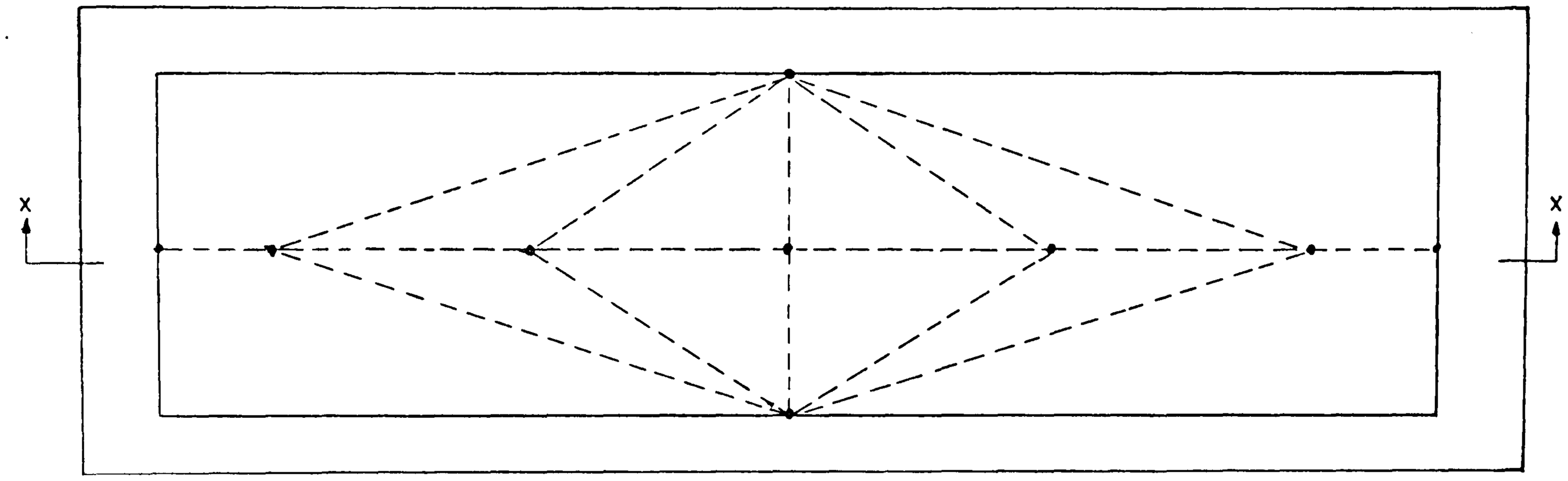

Figure 5.6b Plan of solar collector with surface and fluid nodes shown.

in this category include:

- nodes at the centre plane of homogeneous elements, nodes at the plain boundary between different homogeneous elements (mixed region nodes).

Category 2 node: represents a fluid node. This node can be used to analyse forced or free convection associated with an asymmetrically heating or cooling boundary.

Category 3 node: these represent convection, conduction and radiation exchanges at surface node. Nodes in this category include:

- nodes at the external surface of the component exposed to external climatic influences
- nodes at the external surface of the component not exposed to external climatic influences
- nodes at the internal surface of the collector enclosure.

It has been assumed in this model that corner effects are negligible in the collector because it would have required several nodes to model small effects thereby increasing computation time for no significant increase in accuracy. It is also assumed that air in the collector does not absorb solar radiation.

b) Conduit or Fitting

Nodes can be positioned in a solar energy collector system to analyse the interconnections between different components, for example, conduits, tees, three-way val es etc. Figure (5.7) shows a conduit and a mixing or separating point with the appropriate heat exchanges identified. This node type is classed as a Category 4 node and it is similar to a Category 2 fluid node in a solar collector. The Category 2 node applies to an asymmetric fluid boundary temperature, however, in a

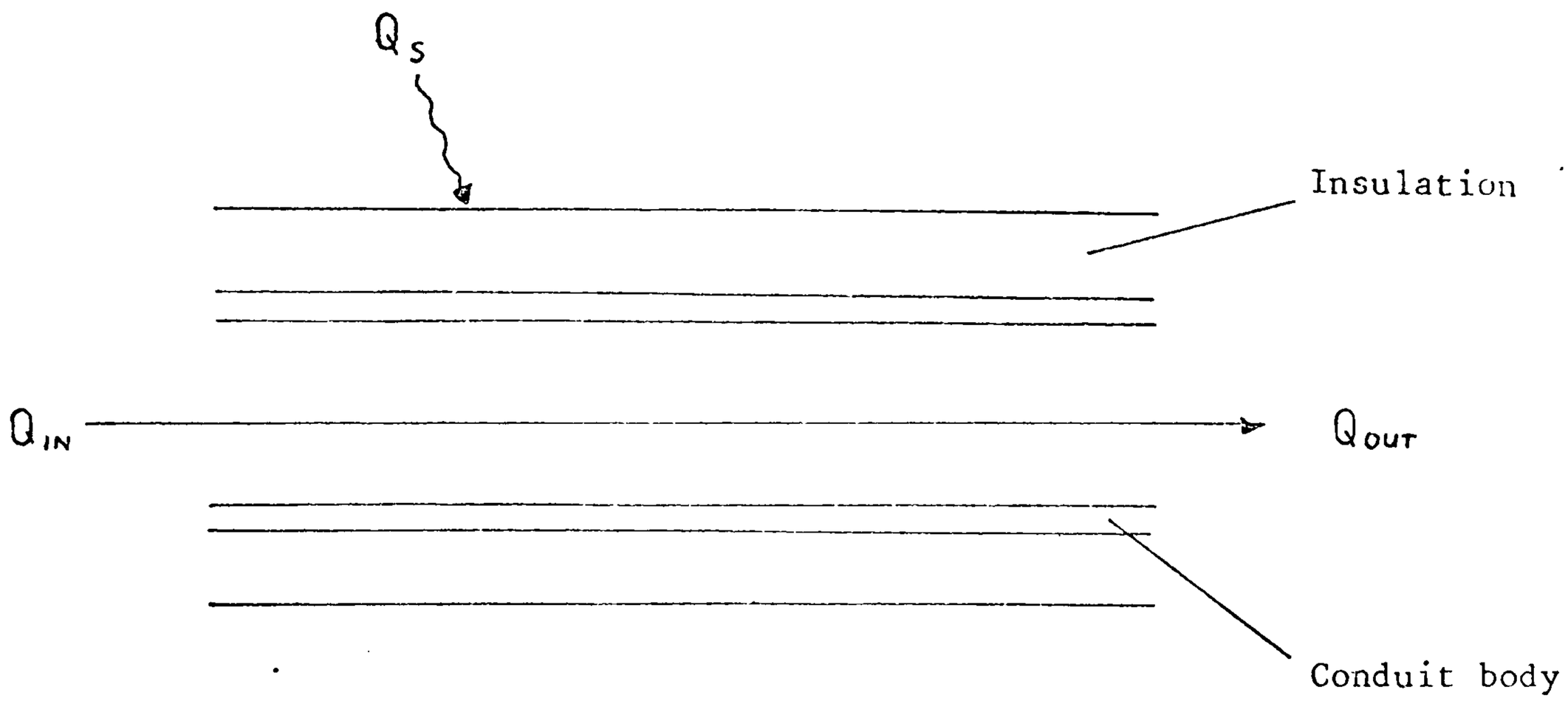

Figure 5.7(a) Conduit

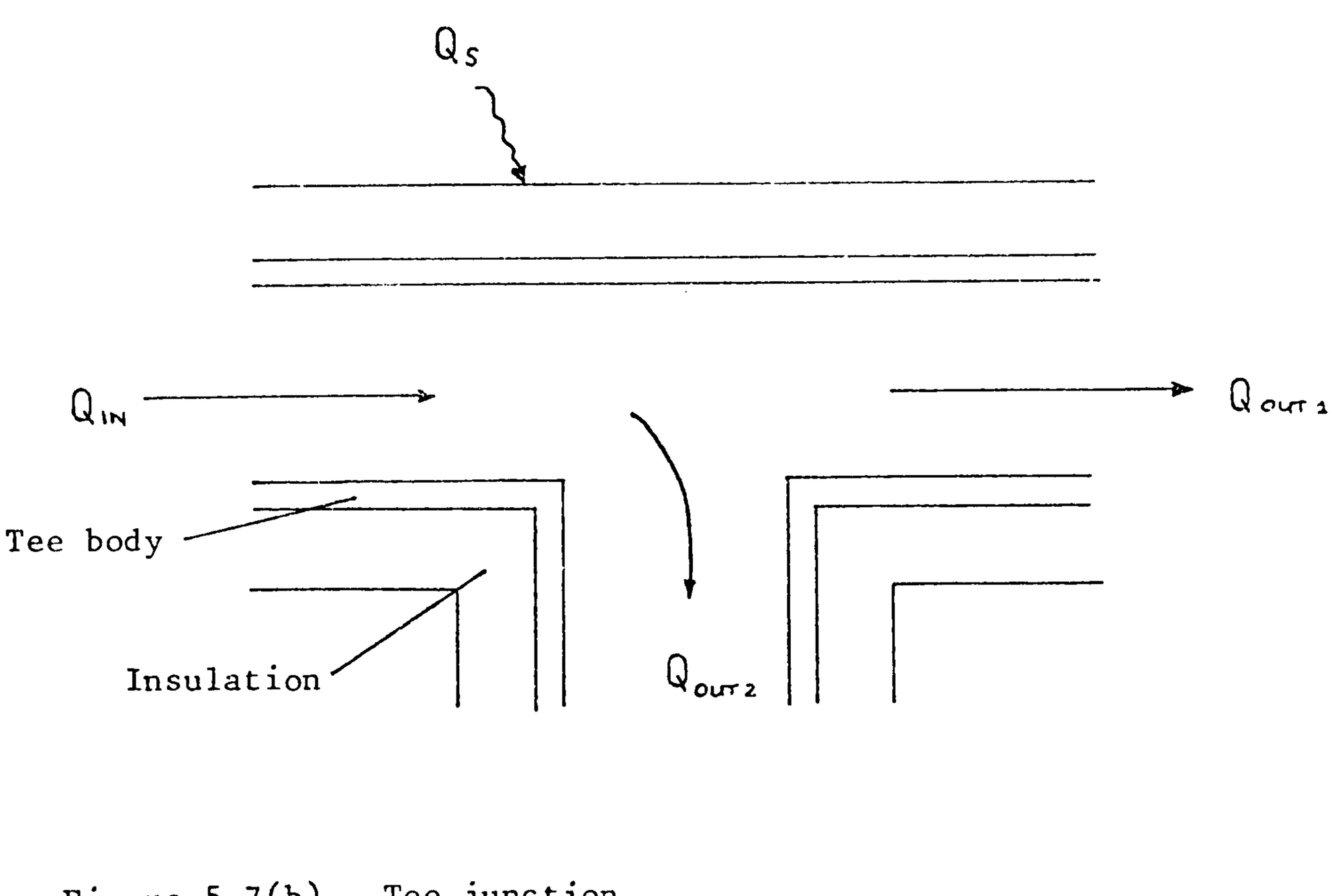

Figure 5.7(b) Tee junction

conduit or fitting the internal surface temperature can be assumed to be at the same temperature.

The term Qs in Figure (5.7) represents the energy into or out of the subvolume due to conductive heat transfer with the surrounds. There are two methods of analysing this process (Figure 5.8):

a) The nodal representation of the conductive processes using Category 1 and Category 3 nodes
b) A simple lumped capacitance/resistance network of the elements in the conduit or fitting

The former method is very accurate and generates much data concerning the conduit or fitting. However, several nodes are required for each conduit or fitting, in a large system this represents considerable computation time. Using the latter method a single node can be used to represent the component. This is the preferred method.

c) Pump or Fan

Figure (5.9a) shows the thermal processes associated with this component and Figure (5.9b) gives the equivalent nodal representation of a pump or fan. This component is classified as a Category 5 node. It is assumed that a single node can be used to represent the component.

d) Auxiliary Heater

Although this component can be a very important item in a solar energy system, using a simple non-specific model allows many types of energy source to be considered, for example a boiler, heater battery, etc. Consequently Figure (5.10a) shows the thermal processes involved and Figure (5.10b) represent the nodal equivalent of the component. The auxiliary heater nodes are classified as Category 6 node.

If required, the homogeneous elements surrounding this component may be modelled using Category 1 and 3 nodes at the expense of computation

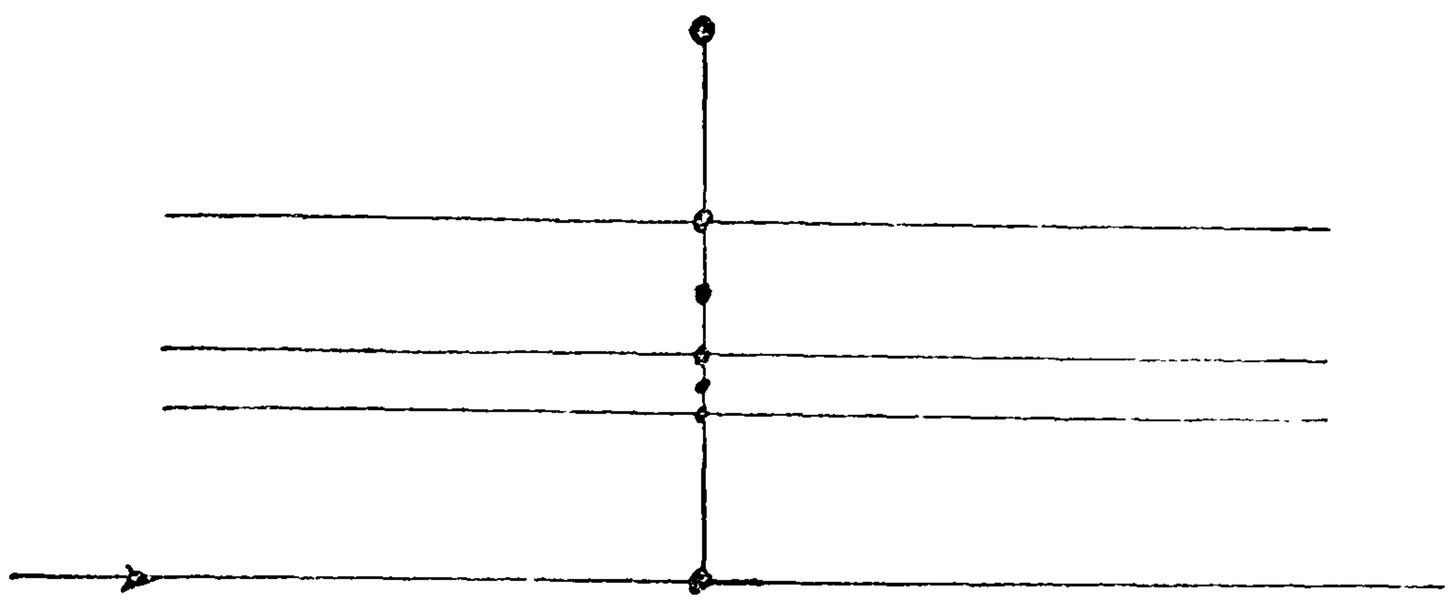

Figure 5.8a: Nodal Representation of Conduit

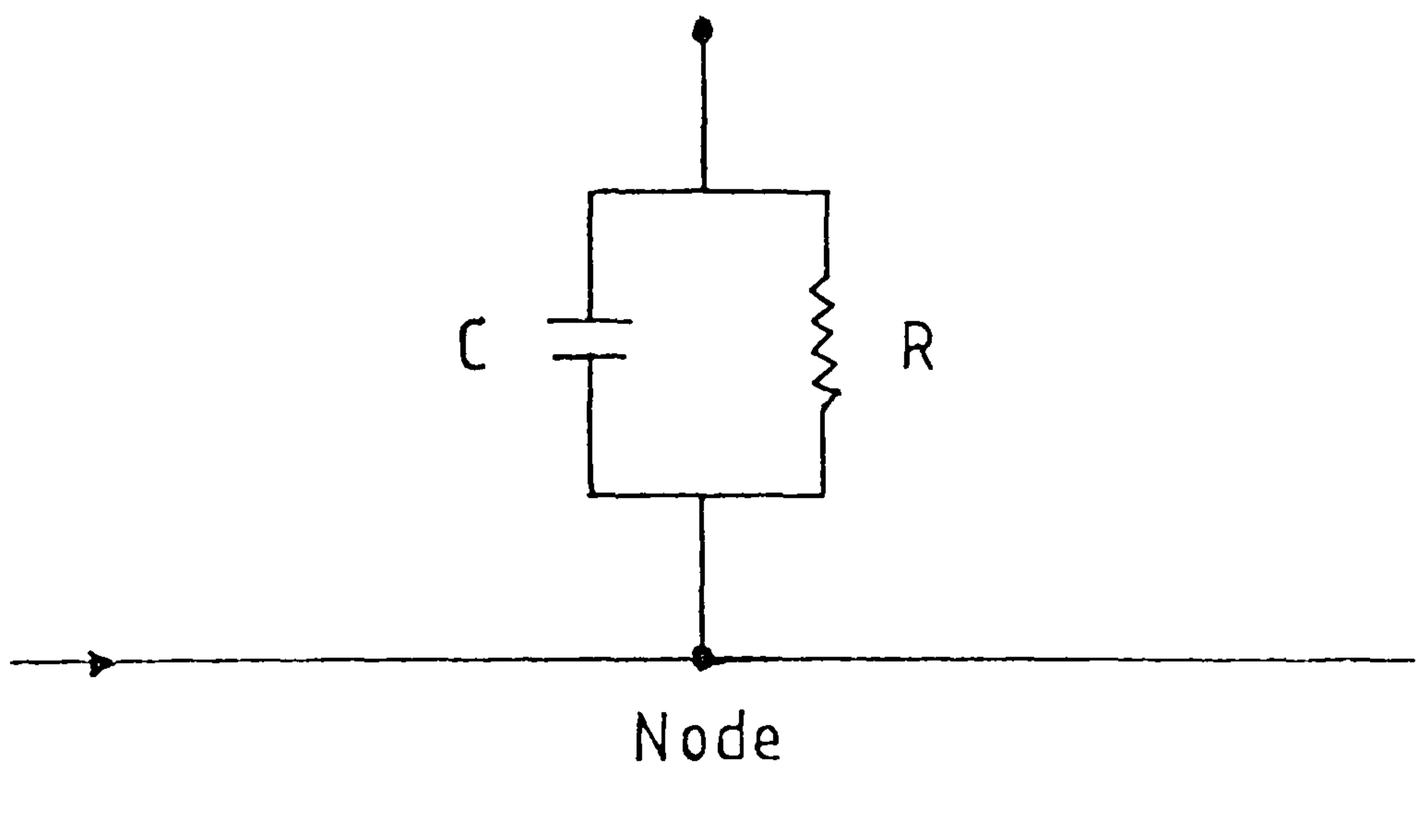

Figure 5.8b: Simple lumped resistance/capacitance network for conduit

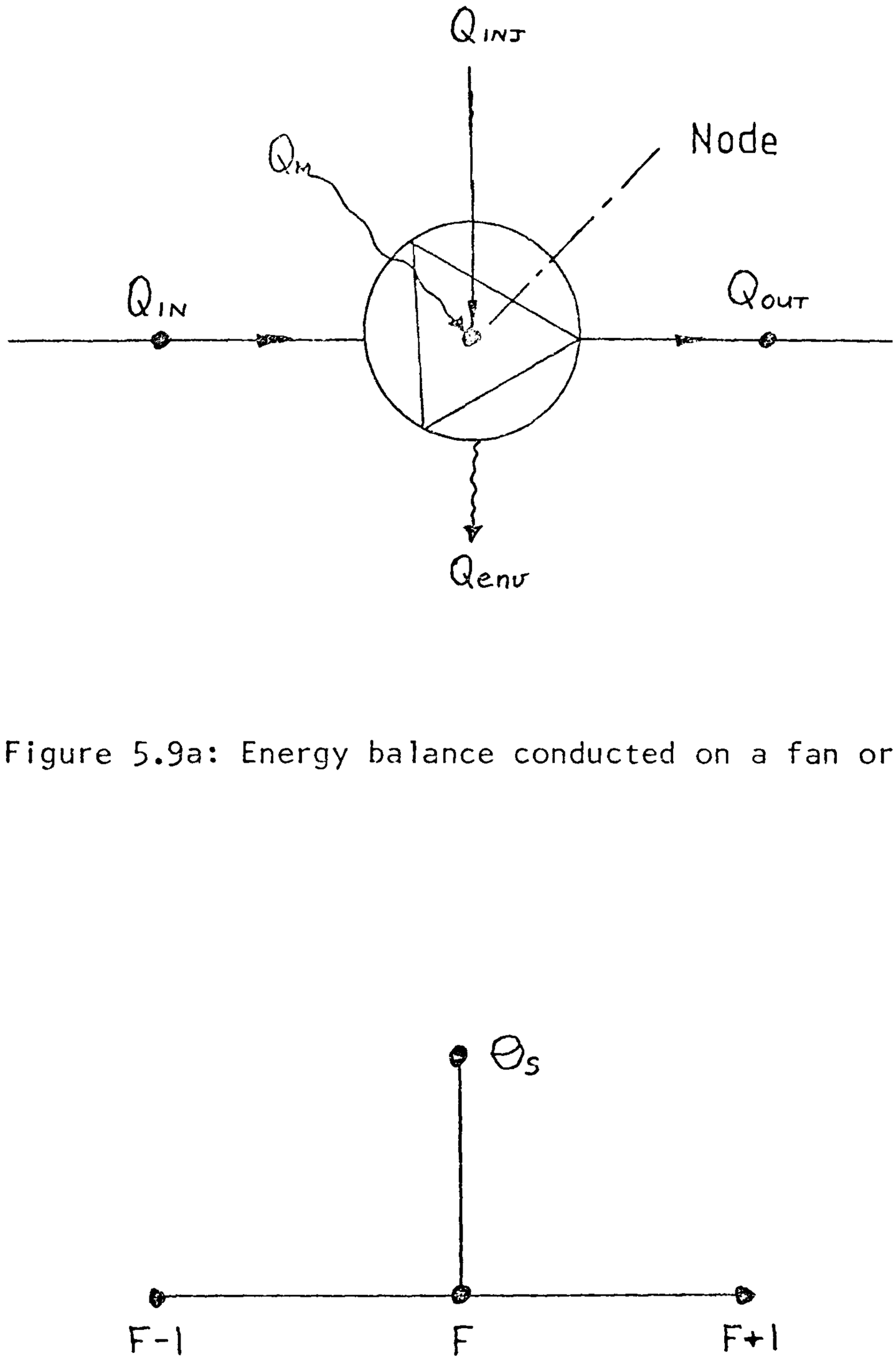

Figure 5.9a: Energy balance conducted on a fan or pump

Figure 5.9b: Nodal representation

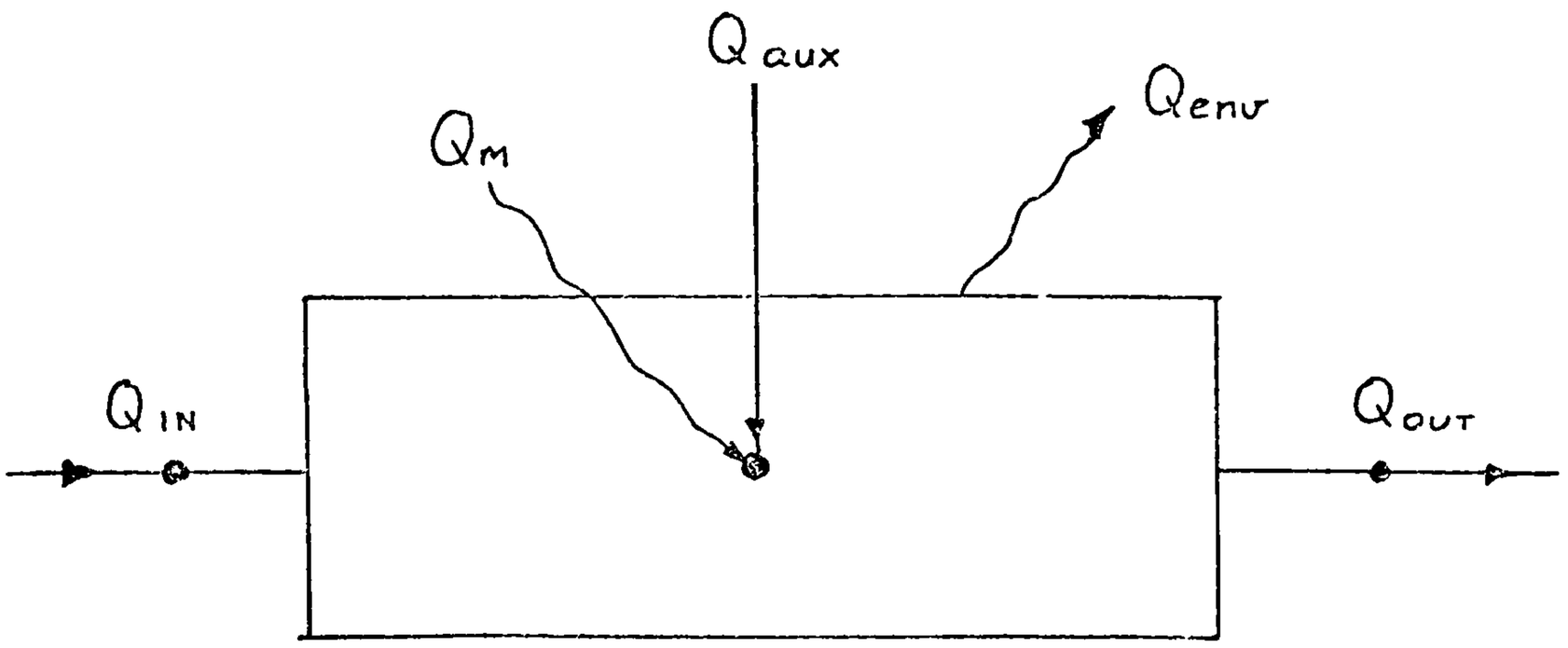

Figure 5.10a: Schematic diagram of heat transfer processes associated with an auxiliary heater

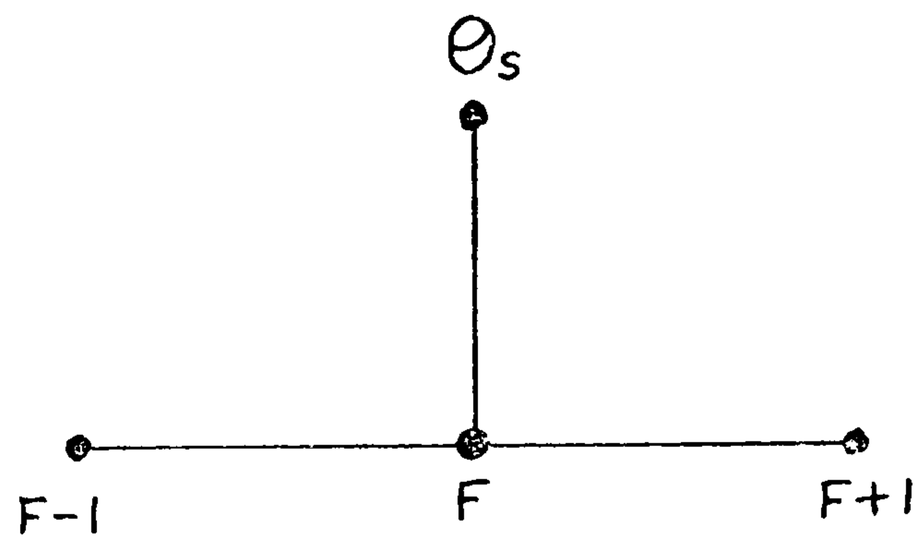

Figure 5.10b: Nodal representation of node F

time.

The Category 6 node representation of an auxiliary heater can be used to represent either a finite or an infinite energy source.

e) Heat Exchanger

Conventional heat exchangers are devices in which two fluid streams separated from each other by a solid wall, exchange thermal energy: one stream is heated while the other is cooled. There are a number of arrangements used to transfer the energy from one fluid to another, e.g. double pipe, crossflow and shell and tube heat exchangers. Figure 5.11 identifies the principal energy exchanges in a heat exchanger. There are three possibilities to make a heat exchanger discrete:

1. many nodes can be used to 'discretise' the heat exchanger to produce a detailed model.
2. the heat exchanger can be treated as two fluid conduits, i.e. two Category 4 nodes.
3. a single node can be used to represent both fluid streams and the heat transfer between them.

The first method although attractive is highly complex because of the difficulty in assessing dynamically the energy transfer processes between discrete sections of the heat exchanger. Furthermore the computational effort required could seriously impede the speed of computation due to the number of extra nodes required. The second method offers the advantage of using two Category 4 nodes and treating the problem as two separate conduits, one receiving a quantity of energy from the other, see Figure 5.12. A third method is available where a single node is used to represent all the heat transfer processes involved in the heat exchanger. Figure 5.13 shows the nodal representation of this node.

The nodes derived to model a heat exchanger are classified under Category 7 nodes.

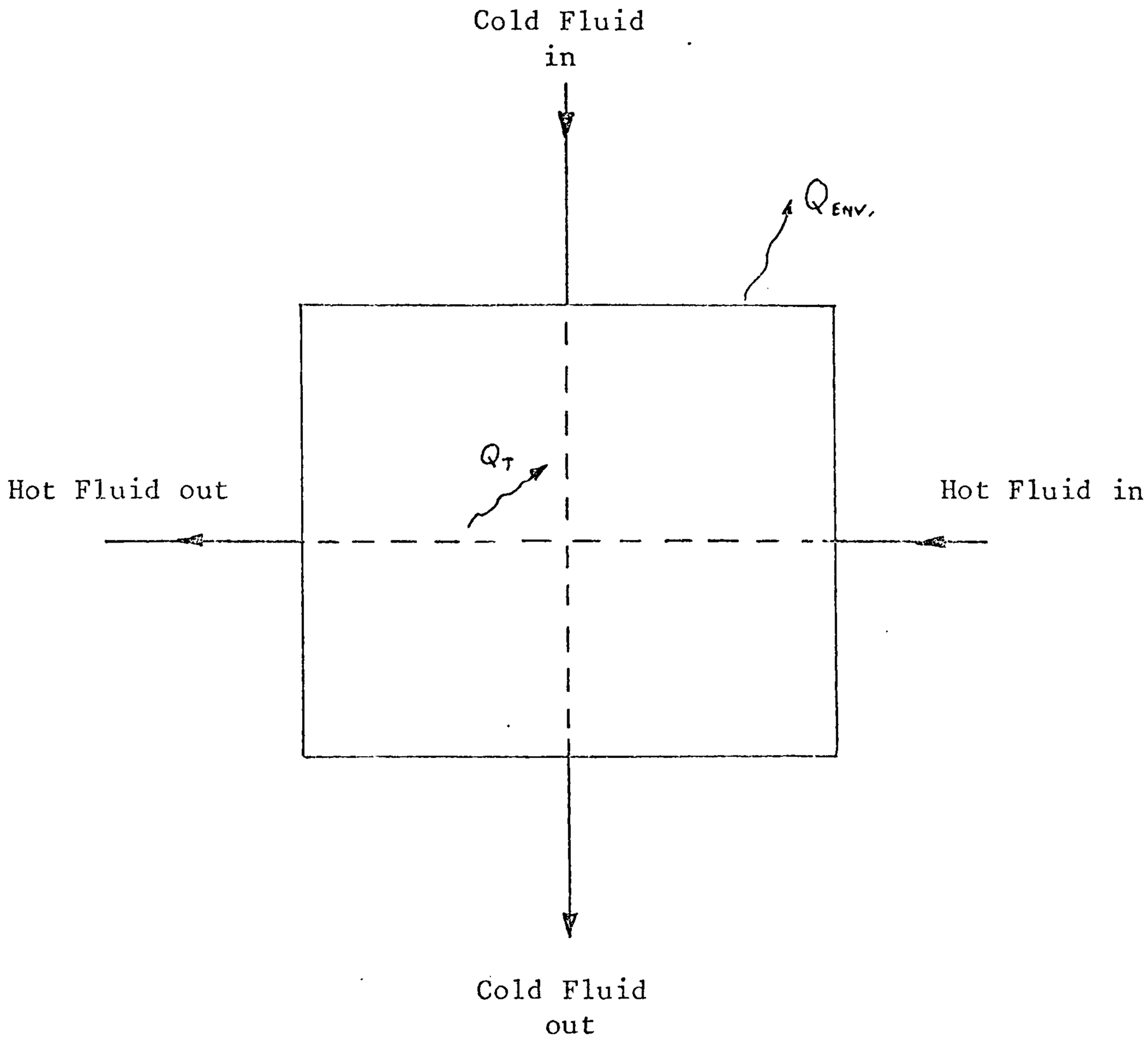

Figure 5.11 Energy processes to be analysed by a simple heat exchanger model

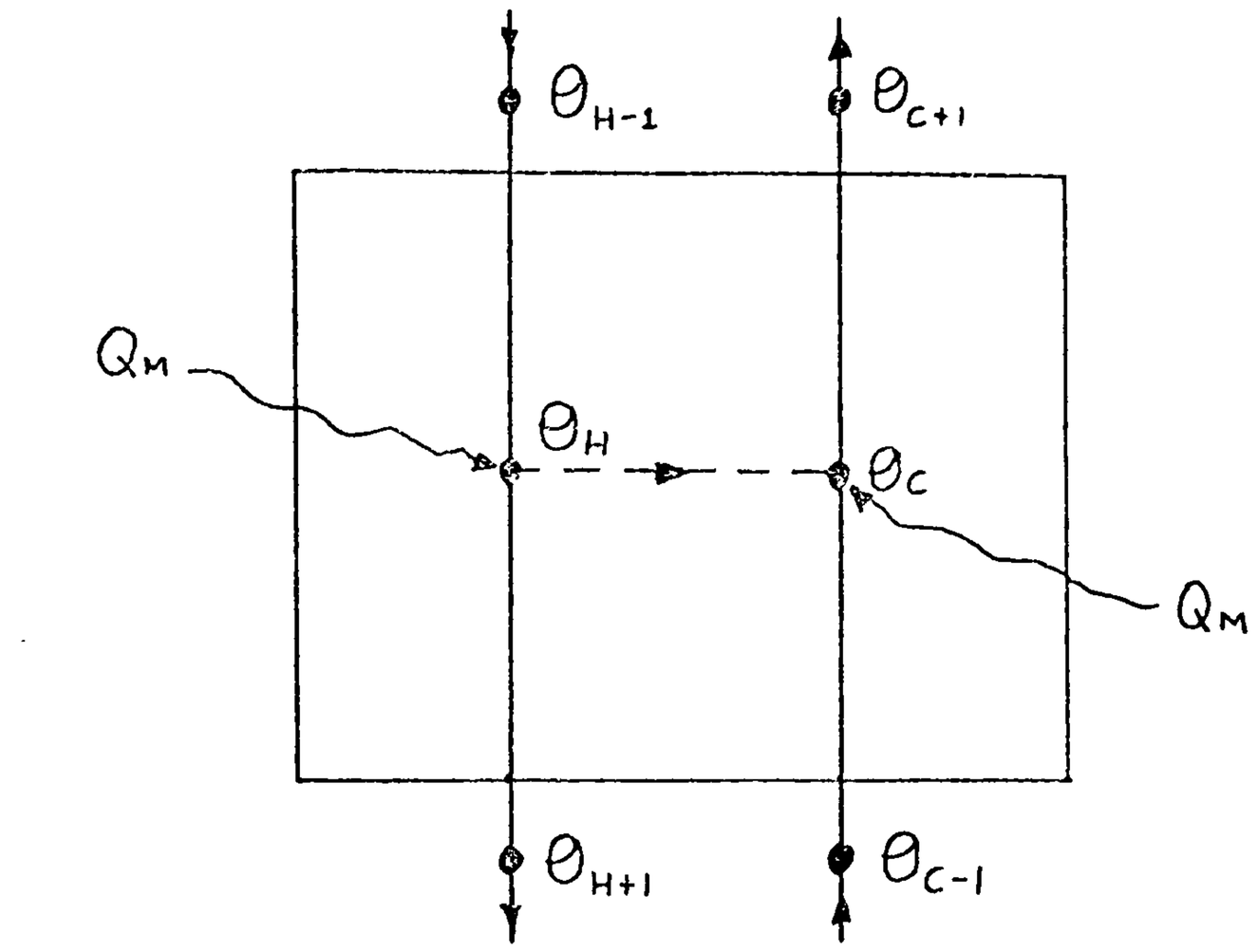

Figure 5.12: Nodal representation of two node crossflow heat exchanger

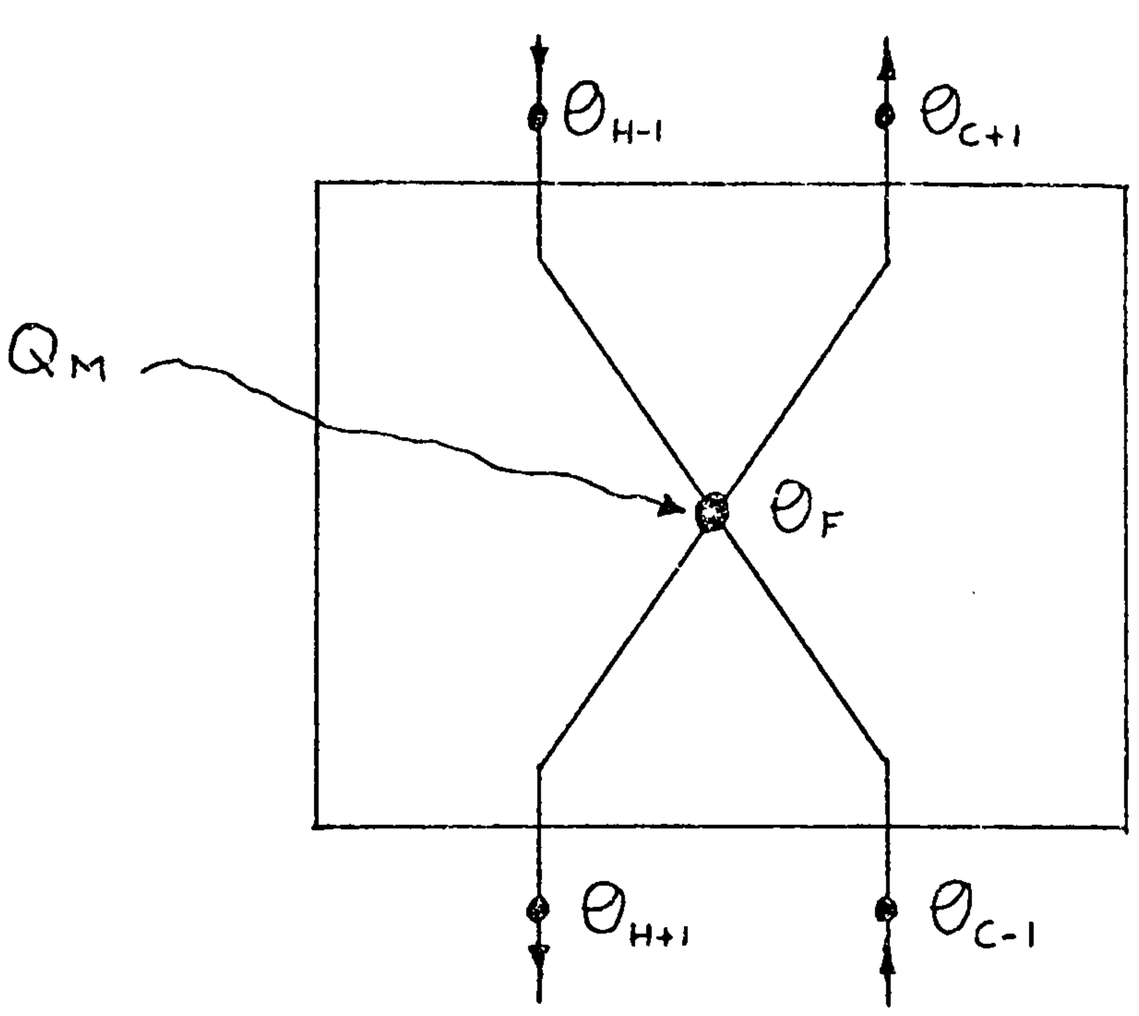

Figure 5.13: Nodal representation of one node crossflow heat exchanger

f) Sensible and Latent Energy Storage

A category of nodes is available, Category 8, which represents nodes in an energy storage unit such as rock bed storage units, an indirect or direct liquid storage tank or a latent heat storage unit. The sensible energy storage units require slightly different models because of thermal stratifications. Figures (5.14) and (5.15) show the thermal processes associated with the rock bed and liquid storage units respectively.

The container of a rock bed storage unit can be made discrete using Category 1 and 3 nodes (Figure 5.16a) or by an equivalent capacitance/ resistance network (Figure 5.16b) as described for the Category 4 nodes. As the detailed storage model can be easily established using Category 1 and Category 3 nodes to model the elements surrounding the thermal storage material, the General Heat Balance equation will only be applied to the simple capacitive/resistance network. The nodal representation of a liquid storage tank can be represented by Figure (5.16b).

Figure 5.17 represents the processes involved in a latent energy storage unit, however, this component is assumed to be a two-node model because it is assumed to be isothermal and no stratification occurs within the latent energy storage material.

Each of the eight nodal categories can have any number of nodal types associated with them. The following section involves identifying these nodal types and applying the General Heat Balance Equation to obtain a difference equation which represents the node.

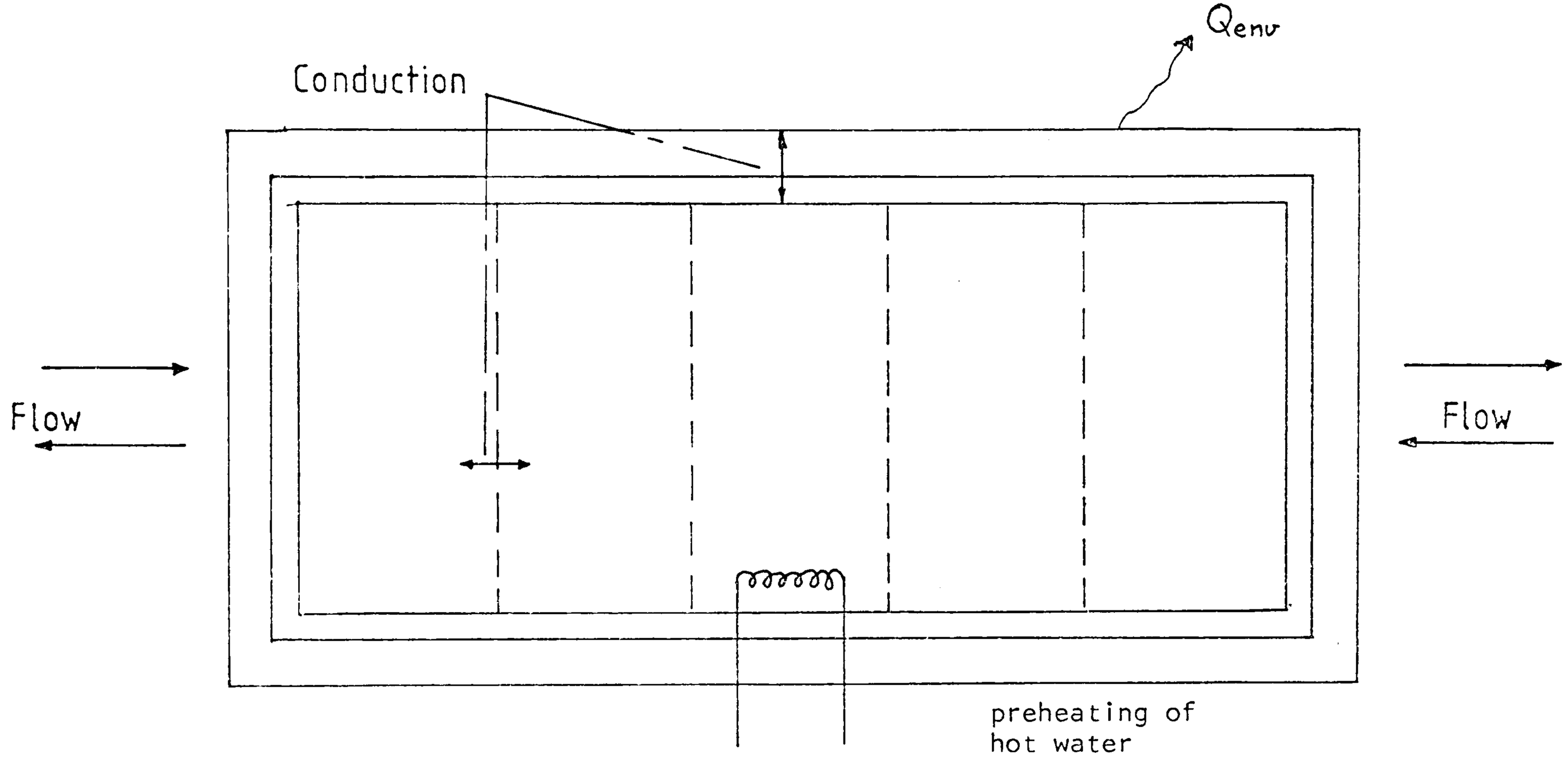

Figure 5.14 Energy processes in rock bed thermal energy store.

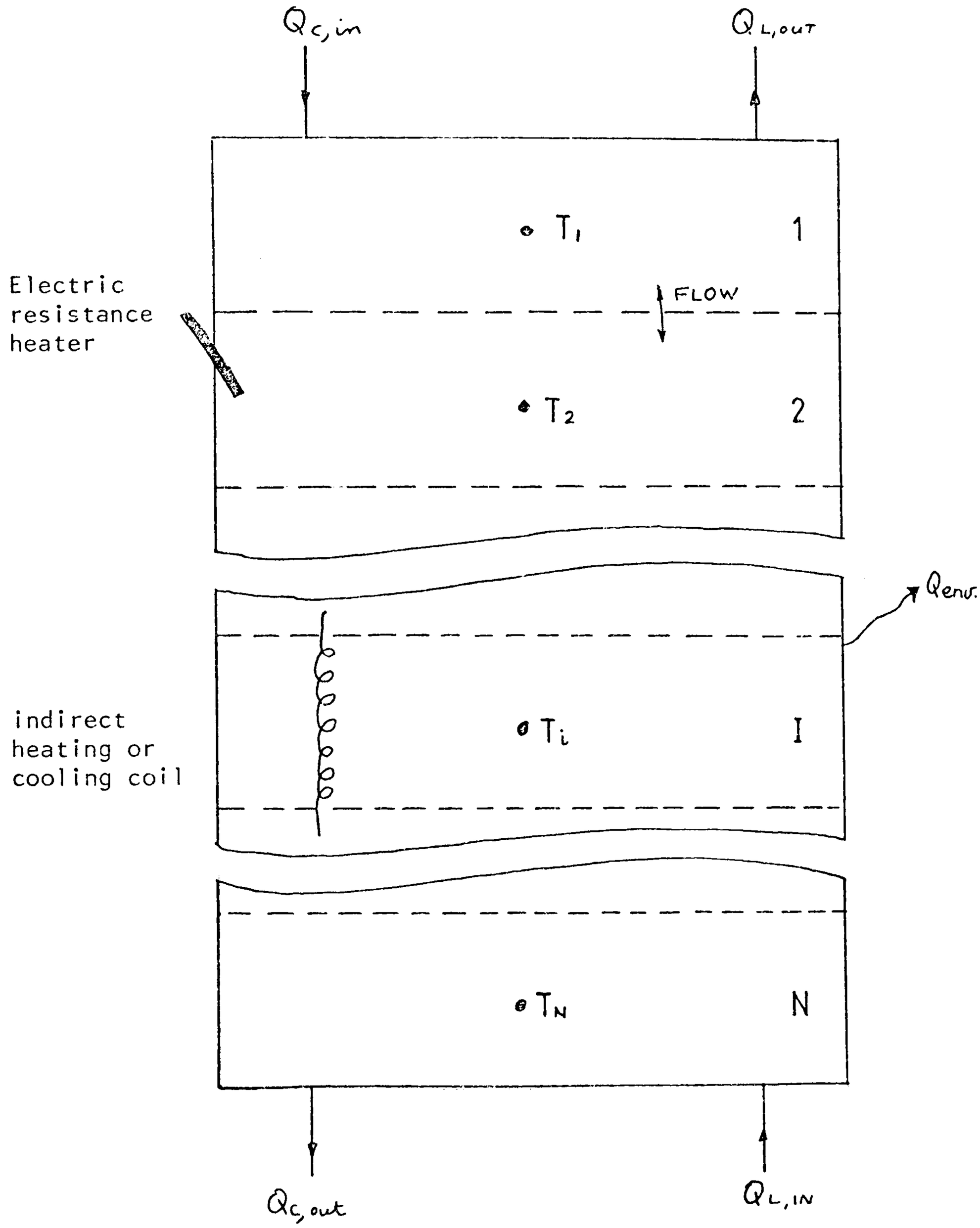

Figure 5.15 Liquid storage tank with N thermal stratifications.

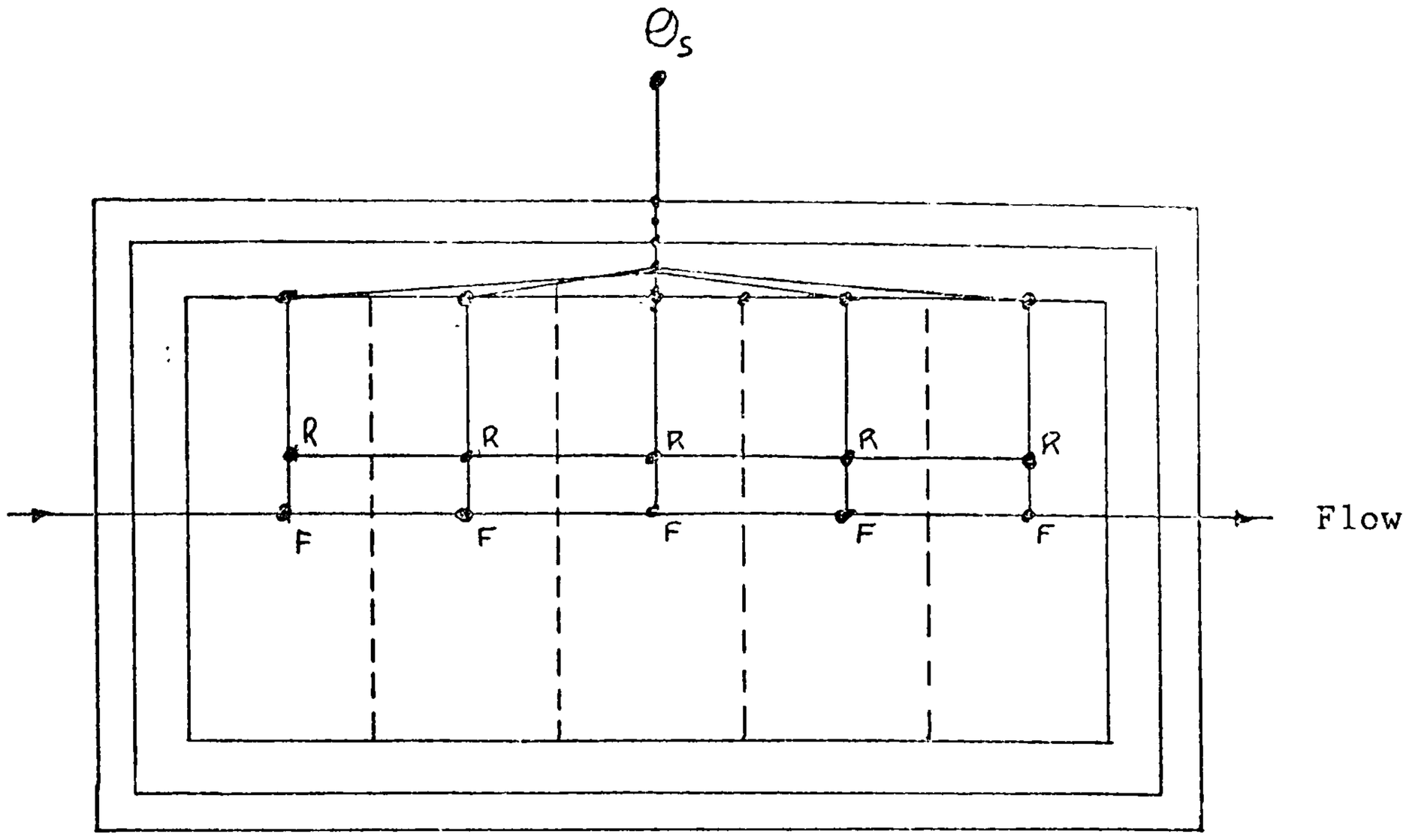

Figure 5.16(a) Rock bed storage unit modelled using category 1 and 3 nodes

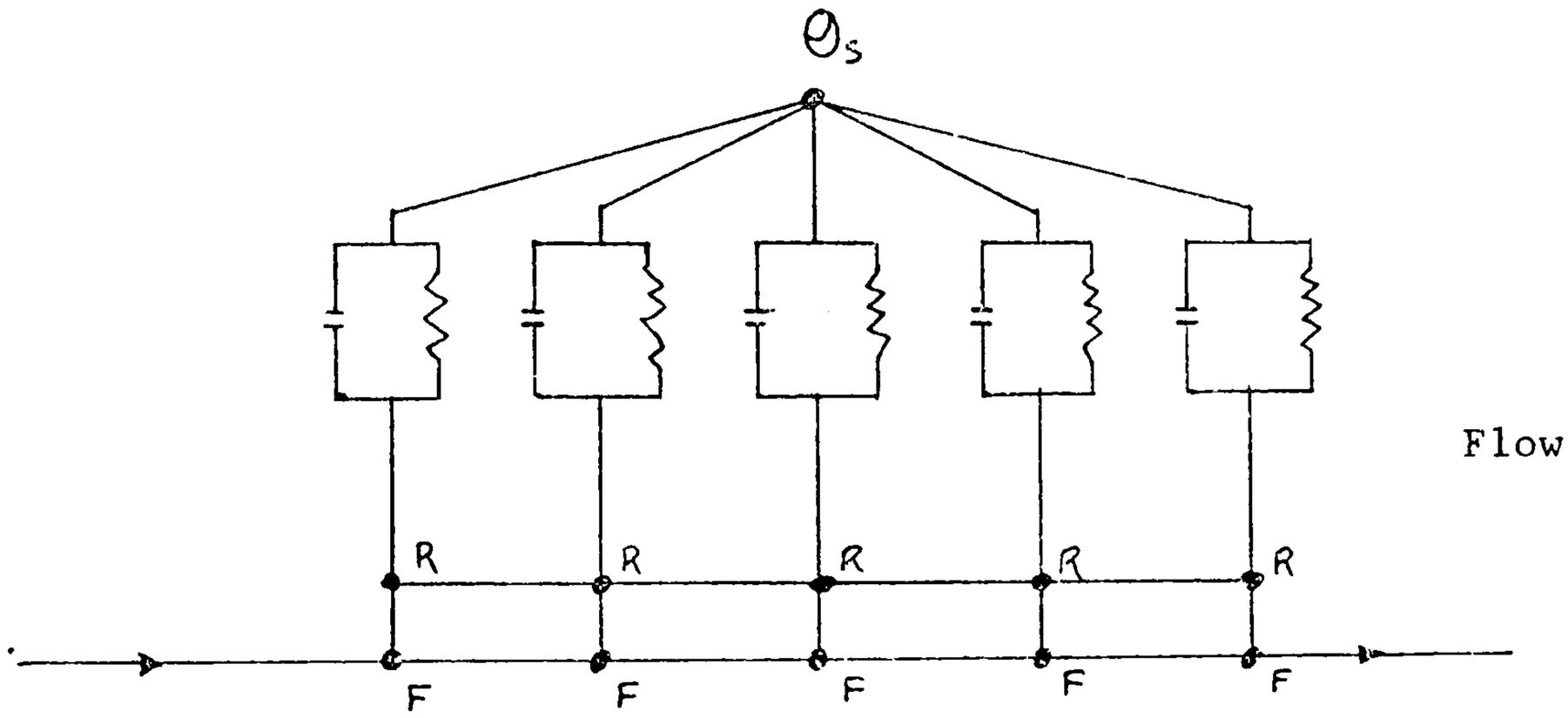

Figure 5.16(b) The capacitance/resistance network equivalent for the rock bed storage unit

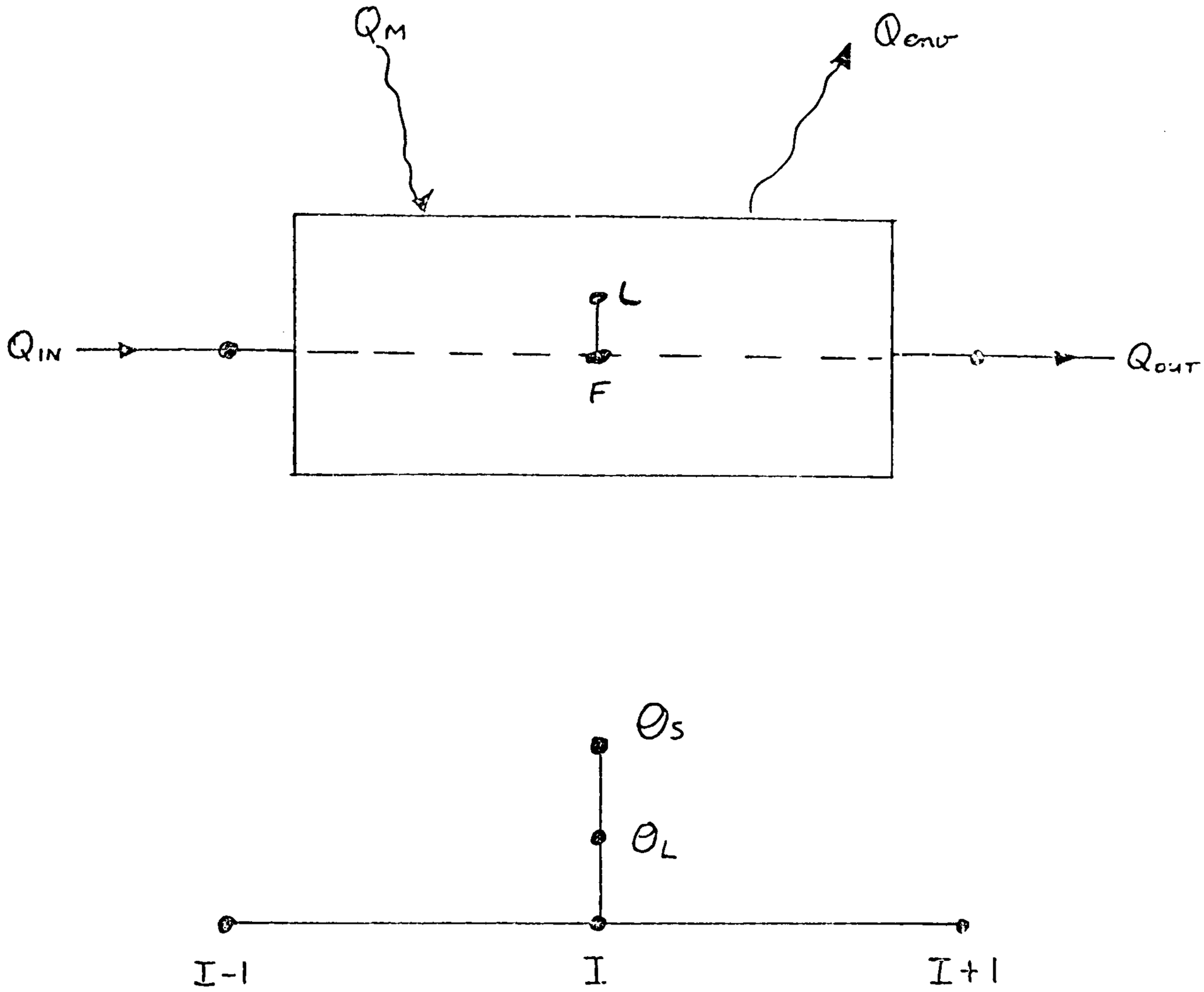

Figure 5.17 Energy balance conducted on a latent heat storage unit

5.2 Derivation of Difference Equation for a Solar Energy System

Although there can be any number of nodes in the solar energy system, these can be grouped together into a number of categories (as shown in the previous section) representing a particular family of nodes to which the General Heat Balance Equation is applied. In this model eight different categories have been identified for nodes which:

1. represent transient conduction and storage within multielement constructions
2. represent a fluid flow
3. represent a surface boundary
4. represent a conduit, tees, valve, etc
5. represent pumps and fans
6. represent auxiliary energy sources
7. represent heat exchangers
8. represent energy storage units

There can be any number of different types of nodes in these categories.

In this section a general difference equation will be generated for each node within the eight different nodal categories by applying the General Heat Balance Equation to each node. The General Heat Balance Equation was derived in Section 4.3.1 and is given by:

$$2\Delta S_I = \sum_{j=1}^{M} Q_{j,I(n+1)} + \sum_{j=1}^{M} Q_{j,I(n)} + \sum Q_{I(n+1)} + \sum Q_{I(n)} \qquad (5.1)$$

where,

M = the number of boundary surfaces relating to a subvolume which is represented by node I.

j = surface number

$Q_{j,I(k)}$ = the net energy flow into or out of the subvolume through surface j, at time k , (w)

$Q_{I(k)}$ = the sum of the heat generation sources associated with node I, at time k, (w)

ϕ = time increment counter n or n+1 for present and future time rows respectively

ΔS_I = rate of change of energy storage in node I,

$$\Delta S_I = \frac{\rho C V (\theta_{I(n+1)} - \theta_{I(n)})}{\Delta \tau}$$

C = time-averaged value of specific heat during time increment $\Delta\tau$, (J/KgK)

ρ = time-averaged value of density during time increment $\Delta\tau$, (Kg/M^3)

V = volume of node I (M^3)

$\theta_{I(\phi)}$= temperature of node I at time ϕ , (degC)

$\Delta\tau$ = length of time increment,(s)

Equation (5.1) will sometimes be referred to as the GHBE which stands for the General Heat Balance Equation. In words this equation states that the rate of change of stored energy is a function of the energy flow across both space and time increments.

5.2.1 Derivation of General Difference Equations for Each Nodal Category

Category 1 Nodes

a) Type 1 : node positioned at the centre of a homogeneous element with energy flow in three dimensions

If a very detailed analysis of a solar collector is required then a three dimensional heat conduction analysis could be performed for certain nodes, for example, nodes in the centre plane of the absorber plate. This nodal type is particuarly suited to modelling liquid collectors which can have serpentined tubes passing through the absorber plate causing a wide variation in temperature in the YZ plane.

If a node is positioned within a homogeneous anisotropic element then it will be in conductive thermal contact with six nodes in a three dimensional network, as shown in Figure 5.18. Each conductive flowpath is described by

$$Q_{j,I} = A_{j,I} \frac{k_{j,I(\xi)}}{\Delta T_I} \left(\theta_{j(\xi)} - \theta_{I(\xi)} \right) \qquad (5.2)$$

where $Q_{j,I}$ = heat conduction between nodes j and I (watts)

$A_{j,I}$ = area of thermal contact between j and I (M^2)

$k_{j,I}$ = thermal conductivity between nodes j and I ($WM^{-1}K^{-1}$)

ξ = present (n) or future (n+1)

θ_j = temperature of connecting node j, (K)

θ_I = temperature of node I, (K)

j = thermal contact flowpath identifier

$\Delta T_{j,I}$ = thickness of subvolume depending upon dimension (m)

$$\Delta T_I = \Delta x_I = \Delta y_I = \Delta z_I = \delta_{j,I} + \delta_{I,j}$$

$\delta_{j,I}$ = semi-thickness of subvolume (m)

The thermal conductivity, $k_{j,I(\xi)}$, in each directionis found by taking the time-weighted average value over the appropriate time interval $\Delta\tau$, similar to the values of density and specific heat

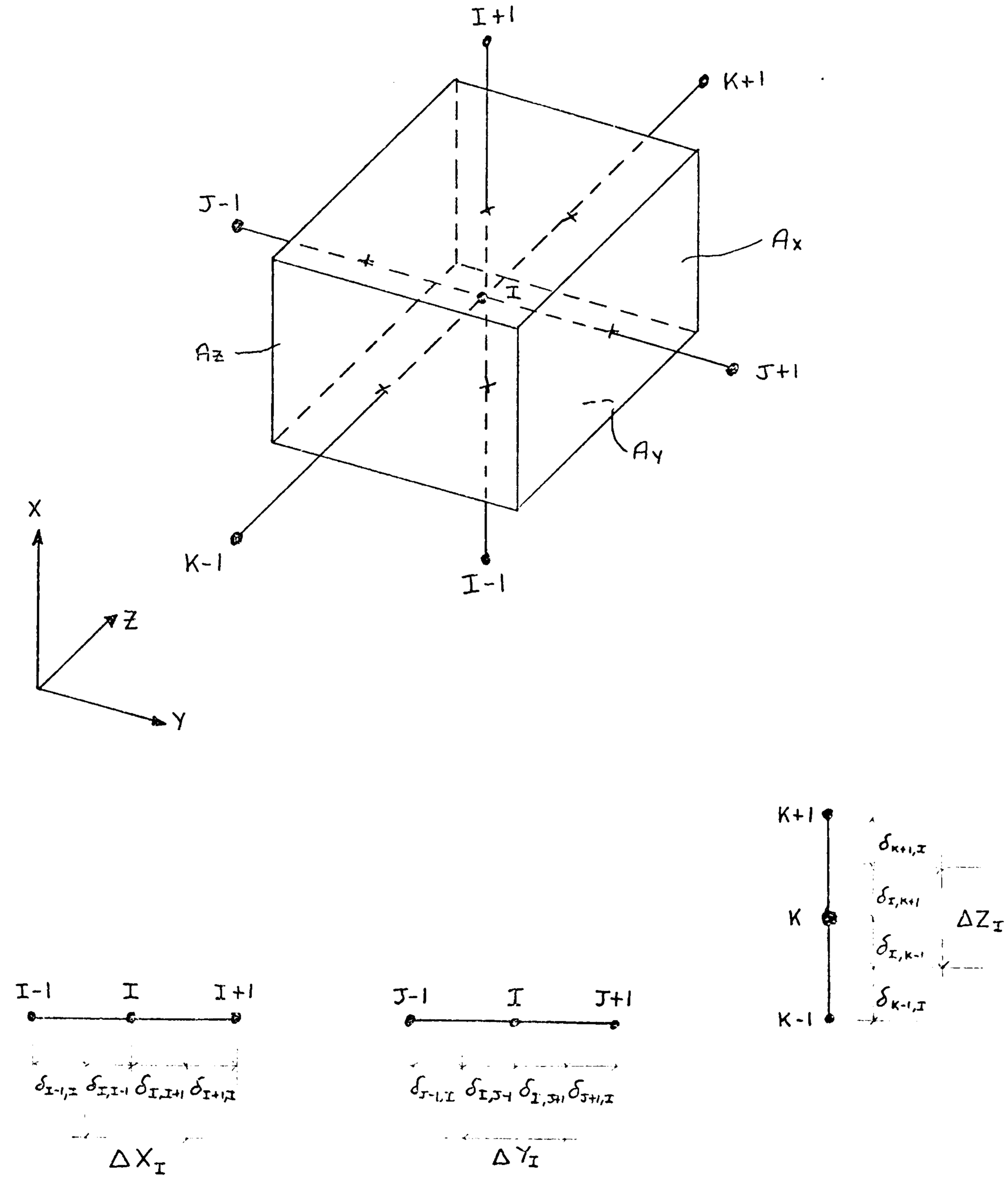

Figure 5.18 Node positioned at the centre of a homogeneous anisotropic element

PAGE NUMBERING AS ORIGINAL

Separating the terms of equation (5.4) such that all unknown temperature terms (n+1) are taken to the left hand side of the equation and rearranging:

$$\left[2+\frac{A_x}{S}\left(\frac{k_{I-1,I}}{\Delta X_I}+\frac{k_{I+1,I}}{\Delta X_I}\right)+\frac{A_y}{S}\left(\frac{k_{J-1,I}}{\Delta Y_I}+\frac{k_{J+1,I}}{\Delta Y_I}\right)+\frac{A_z}{S}\left(\frac{k_{K-1,I}}{\Delta Z_I}+\frac{k_{K+1,I}}{\Delta Z_I}\right)\right]\theta_{I(n+1)}$$

$$-\frac{A_x}{S}\left(\frac{k_{I-1,I}}{\Delta X_I}\theta_{I-1(n+1)}+\frac{k_{I+1,I}}{\Delta X_I}\theta_{I+1(n+1)}\right)-\frac{A_y}{S}\left(\frac{k_{J-1,I}}{\Delta Y_I}\theta_{J-1(n+1)}+\frac{k_{J+1,I}}{\Delta Y_I}\theta_{J+1(n+1)}\right)$$

$$-\frac{A_z}{S}\left(\frac{k_{K-1,I}}{\Delta Z_I}\theta_{K-1(n+1)}+\frac{k_{K+1,I}}{\Delta Z_I}\theta_{K+1(n+1)}\right)=\left(\sum Q_{I(n+1)}+\sum Q_{I(n)}\right)/S$$

$$+\left[2-\frac{A_x}{S}\left(\frac{k_{I-1,I}}{\Delta X_I}+\frac{k_{I+1,I}}{\Delta X_I}\right)+\frac{A_y}{S}\left(\frac{k_{J-1,I}}{\Delta Y_I}+\frac{k_{J+1,I}}{\Delta Y_I}\right)+\frac{A_z}{S}\left(\frac{k_{K-1,I}}{\Delta Z_I}+\frac{k_{K+1,I}}{\Delta Z_I}\right)\right]\theta_{I(n)}$$

$$+\frac{A_x}{S}\left(\frac{k_{I-1,I}}{\Delta X_I}\theta_{I-1(n)}+\frac{k_{I+1,I}}{\Delta X_I}\theta_{I+1(n)}\right)+\frac{A_y}{S}\left(\frac{k_{J-1,I}}{\Delta Y_I}\theta_{J-1(n)}+\frac{k_{J+1,I}}{\Delta Y_I}\theta_{J+1(n)}\right)$$

$$+\frac{A_z}{S}\left(\frac{k_{K-1,I}}{\Delta Z_I}\theta_{K-1(n)}+\frac{k_{K+1,I}}{\Delta Z_I}\theta_{K+1(n)}\right) \qquad (5.5)$$

where,

$$S=\rho C V/\Delta\tau$$

Equation (5.5) is the general solution of a category 1 node. This equation may be written in an alternative form:

$$(2+\alpha_7)\theta_{I(n+1)}-\alpha_1\theta_{I-1(n+1)}-\alpha_2\theta_{I+1(n+1)}-\alpha_3\theta_{J-1(n+1)}-\alpha_4\theta_{J+1(n+1)}$$

$$-\alpha_5\theta_{K-1(n+1)}-\alpha_6\theta_{K+1(n+1)}=(2-\alpha_7)\theta_{I(n)}+\alpha_1\theta_{I-1(n)}+\alpha_2\theta_{I+1(n)}+\alpha_3\theta_{J-1(n)}$$

$$+\alpha_4\theta_{J+1(n)}+\alpha_5\theta_{K-1(n)}+\alpha_6\theta_{K+1(n)}+\alpha_8\sum Q_{I(n+1)}+\alpha_8\sum Q_{I(n)} \qquad (5.6)$$

where,

$$\alpha_1=\frac{A_x k_{I-1,I}}{S\Delta X_I} \quad ; \quad \alpha_2=\frac{A_x k_{I+1,I}}{S\Delta X_I}$$

$$\alpha_3=\frac{A_y k_{J-1,I}}{S\Delta Y_I} \quad ; \quad \alpha_4=\frac{A_y k_{J+1,I}}{S\Delta Y_I}$$

$$\alpha_5=\frac{A_z k_{K-1,I}}{S\Delta Z_I} \quad ; \quad \alpha_6=\frac{A_z k_{K+1,I}}{S\Delta Z_I}$$

$$\alpha_7=\alpha_1+\alpha_2+\alpha_3+\alpha_4+\alpha_5+\alpha_6 \quad ; \quad \alpha_8=\frac{1}{S}=\frac{\Delta\tau}{\rho C V}$$

Separating the terms of equation (5.4) such that all unknown temperature terms (n+1) are taken to the left hand side of the equation and rearranging:

$$\left[2+\frac{A_x}{S}\left(\frac{k_{I-1,I}}{\Delta X_I}+\frac{k_{I+1,I}}{\Delta X_I}\right)+\frac{A_y}{S}\left(\frac{k_{J-1,I}}{\Delta Y_I}+\frac{k_{J+1,I}}{\Delta Y_I}\right)+\frac{A_z}{S}\left(\frac{k_{K-1,I}}{\Delta Z_I}+\frac{k_{K+1,I}}{\Delta Z_I}\right)\right]\theta_{I(n+1)}$$

$$-\frac{A_x}{S}\left(\frac{k_{I-1,I}}{\Delta X_I}\theta_{I-1(n+1)}+\frac{k_{I+1,I}}{\Delta X_I}\theta_{I+1(n+1)}\right)-\frac{A_y}{S}\left(\frac{k_{J-1,I}}{\Delta Y_I}\theta_{J-1(n+1)}+\frac{k_{J+1,I}}{\Delta Y_I}\theta_{J+1(n+1)}\right)$$

$$-\frac{A_z}{S}\left(\frac{k_{K-1,I}}{\Delta Z_I}\theta_{K-1(n+1)}+\frac{k_{K+1,I}}{\Delta Z_I}\theta_{K+1(n+1)}\right)=\left(\sum Q_{I(n+1)}+\sum Q_{I(n)}\right)/S$$

$$+\left[2-\frac{A_x}{S}\left(\frac{k_{I-1,I}}{\Delta X_I}+\frac{k_{I+1,I}}{\Delta X_I}\right)+\frac{A_y}{S}\left(\frac{k_{J-1,I}}{\Delta Y_I}+\frac{k_{J+1,I}}{\Delta Y_I}\right)+\frac{A_z}{S}\left(\frac{k_{K-1,I}}{\Delta Z_I}+\frac{k_{K+1,I}}{\Delta Z_I}\right)\right]\theta_{I(n)}$$

$$+\frac{A_x}{S}\left(\frac{k_{I-1,I}}{\Delta X_I}\theta_{I-1(n)}+\frac{k_{I+1,I}}{\Delta X_I}\theta_{I+1(n)}\right)+\frac{A_y}{S}\left(\frac{k_{J-1,I}}{\Delta Y_I}\theta_{J-1(n)}+\frac{k_{J+1,I}}{\Delta Y_I}\theta_{J+1(n)}\right)$$

$$+\frac{A_z}{S}\left(\frac{k_{K-1,I}}{\Delta Z_I}\theta_{K-1(n)}+\frac{k_{K+1,I}}{\Delta Z_I}\theta_{K+1(n)}\right) \qquad (5.5)$$

where,

$$S=\rho C V/\Delta\tau$$

Equation (5.5) is the general solution of a category 1 node. This equation may be written in an alternative form:

$$(2+\alpha_7)\theta_{I(n+1)}-\alpha_1\theta_{I-1(n+1)}-\alpha_2\theta_{I+1(n+1)}-\alpha_3\theta_{J-1(n+1)}-\alpha_4\theta_{J+1(n+1)}$$

$$-\alpha_5\theta_{K-1(n+1)}-\alpha_6\theta_{K+1(n+1)}=(2-\alpha_7)\theta_{I(n)}+\alpha_1\theta_{I-1(n)}+\alpha_2\theta_{I+1(n)}+\alpha_3\theta_{J-1(n)}$$

$$+\alpha_4\theta_{K+1(n)}+\alpha_5\theta_{K-1(n)}+\alpha_6\theta_{K+1(n)}+\alpha_8\sum Q_{I(n+1)}+\alpha_8\sum Q_{I(n)} \qquad (5.6)$$

where,

$$\alpha_1=\frac{A_x k_{I-1,I}}{S\Delta X_I}\quad;\quad \alpha_2=\frac{A_x k_{I+1,I}}{S\Delta X_I}$$

$$\alpha_3=\frac{A_y k_{J-1,I}}{S\Delta Y_I}\quad;\quad \alpha_4=\frac{A_y k_{J+1,I}}{S\Delta Y_I}$$

$$\alpha_5=\frac{A_z k_{K-1,I}}{S\Delta Z_I}\quad;\quad \alpha_6=\frac{A_z k_{K+1,I}}{S\Delta Z_I}$$

$$\alpha_7=\alpha_1+\alpha_2+\alpha_3+\alpha_4+\alpha_5+\alpha_6\quad;\quad \alpha_8=\frac{1}{S}=\frac{\Delta\tau}{\rho CV}$$

It is important to note that the dimensionless coefficient that corresponds to each node in thermal contact with node I equates to the Fourier number, i.e,

$$Fo = \frac{A_{j,I}\, k_{j,I}\, \Delta\tau}{\Delta T_I\, \rho C V}$$

If the element under analysis is isotropic and not anisotropic then,

$$k = k_{I-1,I} = k_{I+1,I} = k_{J-1,I} = k_{J+1,I} = k_{K-1,I} = k_{K+1,I}$$

As most materials are isotropic the conductivity will be denoted as such. This will result in more succinct expressions. If anisotropic materials are considered then the appropriate equations can be easily re-arranged to suit. Re-expressing equation (5.5) in the form required by an isotropic material yields,

$$(2+a_7)\,\theta_{I(n+1)} - a_1\theta_{I-1(n+1)} - a_2\theta_{I+1(n+1)} - a_3\theta_{J-1(n+1)} - a_4\theta_{J+1(n+1)}$$

$$-a_5\theta_{K-1(n+1)} - a_6\theta_{K+1(n+1)} = (2-a_7)\theta_{I(n)} + a_1\theta_{I-1(n)} + a_2\theta_{I+1(n)}$$

$$+a_3\theta_{J-1(n)} + a_4\theta_{J+1(n)} + a_5\theta_{K-1(n)} + a_6\theta_{K+1(n)} + a_8\left(\Sigma Q_{I(n+1)} + \Sigma Q_{I(n)}\right) \qquad (5.7)$$

where,

$$a_1 = a_2 = \frac{Ax\,k}{S\Delta X} \quad ; \quad a_3 = a_4 = \frac{Ay\,k}{S\Delta Y}$$

$$a_5 = a_6 = \frac{Az\,k}{S\Delta Z} \quad ; \quad a_7 = a_1 + a_2 + a_3 + a_4 + a_5 + a_6$$

$$a_8 = \frac{1}{S} = \frac{\Delta\tau}{\rho C V}$$

$$\Delta X = \Delta X_I$$
$$\Delta Y = \Delta Y_I$$
$$\Delta Z = \Delta Z_I$$

The term $\Sigma Q_{I(\phi)}$ in GHBE represents the summation of heat generation sources which are not considered by the general equation, thus for N heat generation sources

$$\Sigma Q_{I(\phi)} = Q_{1(\phi)} + Q_{2(\phi)} + Q_{3(\phi)} + \ldots\ldots + Q_{N(\phi)} + Q_{M(\phi)} \qquad (5.8)$$

where the $Q_{m(\ell)}$ term is an extra term giving the user flexibility to consider any problem. For the Category 1 nodes three heat generation terms are considered therefore, equation (5.8) becomes

$$\sum Q_{I(\ell)} = Q_{s,\alpha(\ell)} + Q_{P(\ell)} + Q_{liq(\ell)} + Q_{M(\ell)} \qquad (5.9)$$

where $Q_{s,\alpha(\ell)}$ = the quantity of solar radiation absorbed by the transparent element at time ℓ

$Q_{P(\ell)}$ = the quantity of radiative energy converted to electricity by solar cells at time ℓ

$Q_{liq(\ell)}$ = the energy exchange if node is associated with liquid flow in absorber plate conduits at time ℓ

The method of solving these terms and the reasons why they apply to a particular nodal category are discussed in Section 5.3. Applying equation (5.9) to equation (5.7) yields the full solution of the Cateogry 1, Type 1 node.

Figure 5.19 shows the nodal arrangement when equation (5.7) is applicable, it is apparent that edge and corner nodes are not in thermal contact with six nodes but with five and four nodes respectively. Nodes in the X-dimension are unaffected but one node may be missing in the Y-dimension or the Z dimension, or both.

Equation (5.7) can account for edge and corner nodes by setting the temperature and the temperature coefficient of the missing node(s) to zero. This procedure is necessary in all multi-dimensional node equations.

b. Type 2 - Two Dimensional Heat Conduction

In an air collector the air passed over the absorber plate will normally pick up energy uniformly perpendicular to the air flow direction. In this case, the number of nodes (Q - Figure 5.19) in the Z dimension are set to one because if more than one existed they would have approximately the same temperature, therefore, the conductive heat transfer

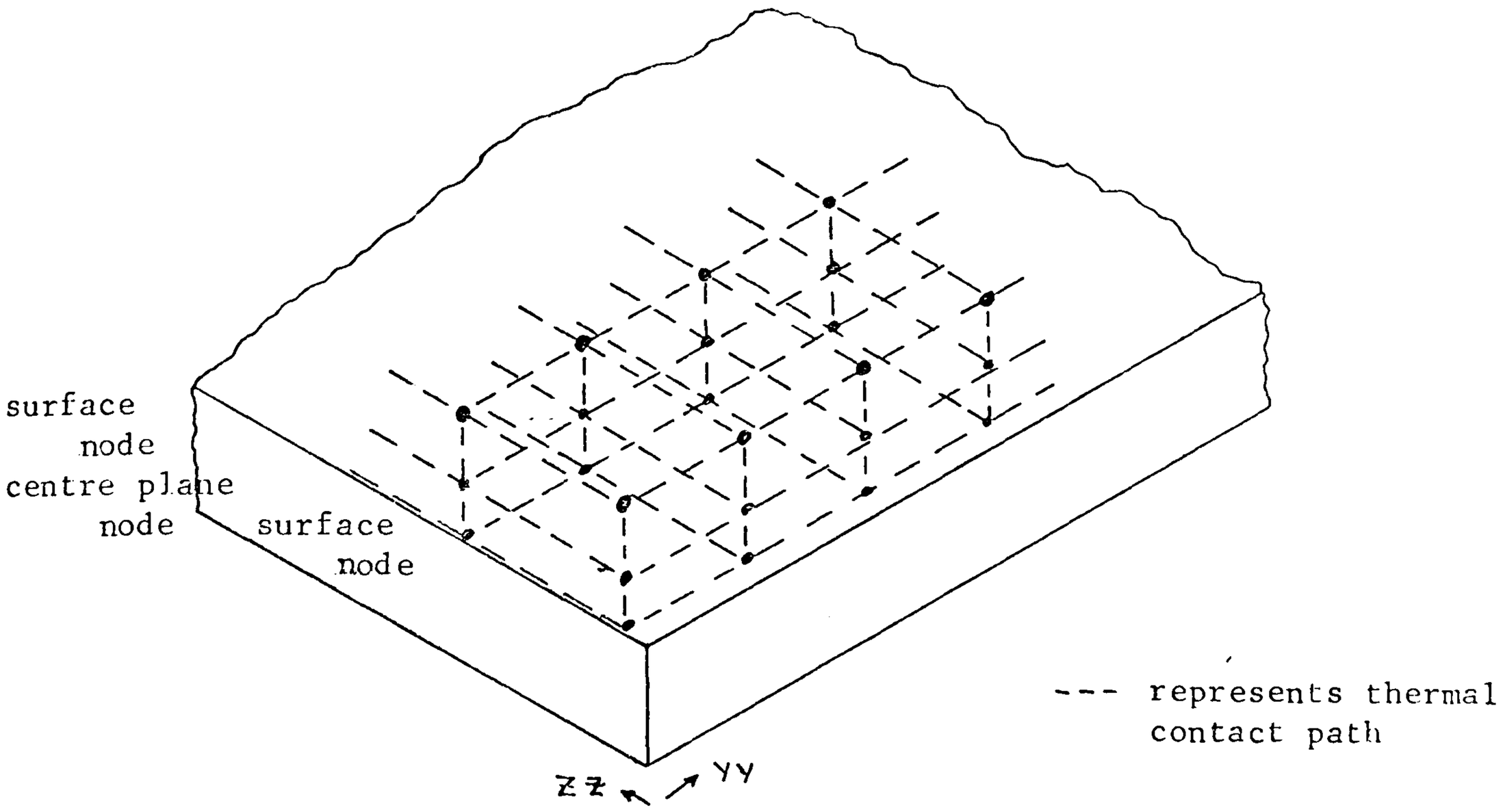

Figure 5.19(a) Nodal network for 3-dimensional conduction in a homogeneous isotropic element, for example, a solar collector absorber plate

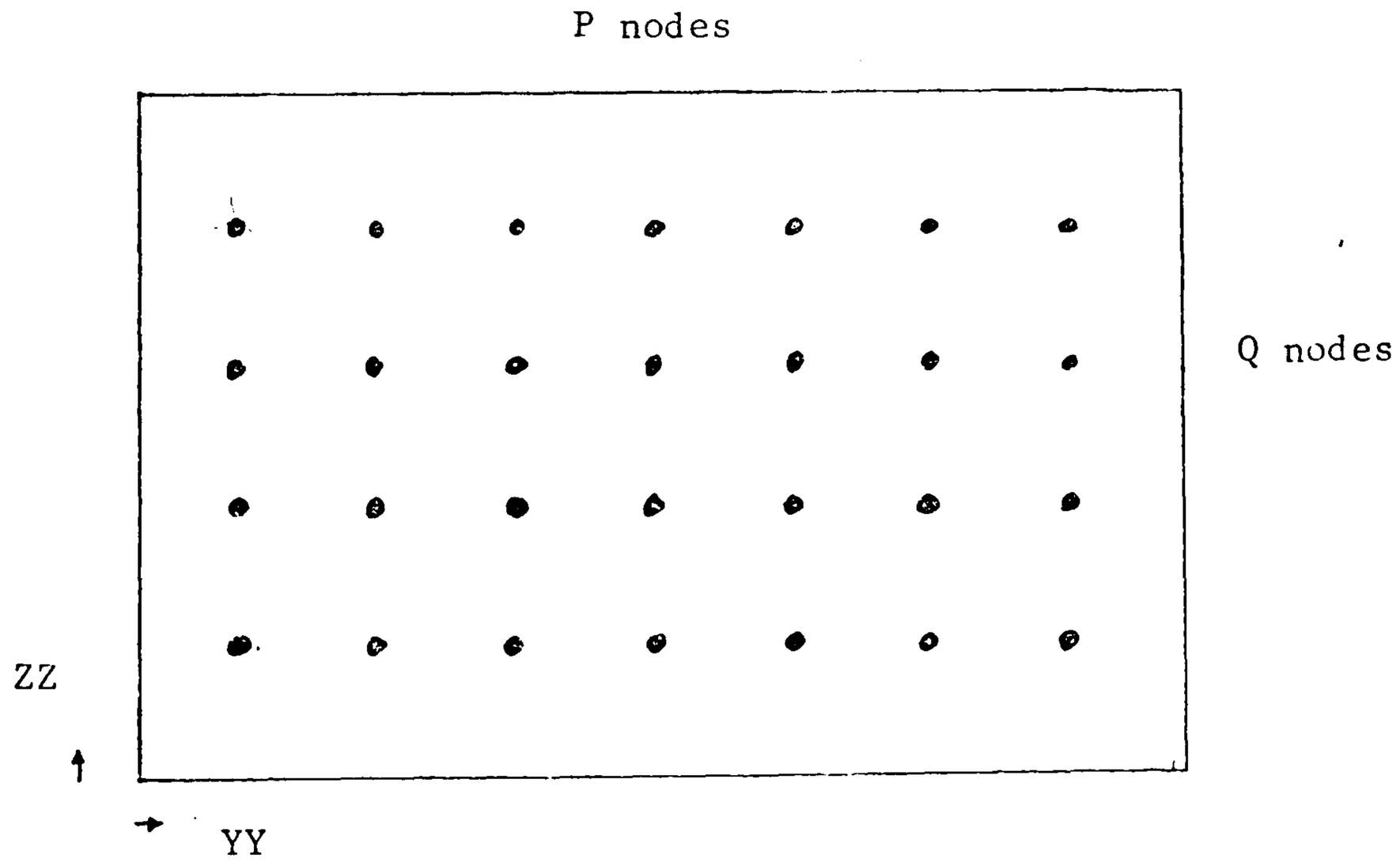

Figure 5.19(b) Plan of absorber plate

in this dimension would be negligible. Consequently two dimensional heat conduction exists where the X dimension corresponds to the absorber plate thickness and the Y dimension corresponds to the nodes positioned in the direction of fluid flow. Equation (5.7) can be used to establish the general solution for this nodal type by setting every term in the Z direction to zero. Re-arranging yields,

$$(2+b_5)\,\theta_{I(n+1)} - b_1\,\theta_{I-1(n+1)} - b_2\,\theta_{I+1(n+1)} - b_3\,\theta_{J-1(n+1)} - b_4\,\theta_{J+1(n+1)}$$

$$=(2-b_5)\theta_{I(n)} + b_1\,\theta_{I-1(n)} + b_2\,\theta_{I+1(n)} + b_3\,\theta_{J-1(n)} + b_4\,\theta_{J+1(n)}$$

$$+ b_6\left(\Sigma Q_{I(n+1)} + \Sigma Q_{I(n)}\right) \qquad (5.10)$$

where,

$$b_1 = b_2 = \frac{A_X k}{s\Delta X} \quad ; \quad b_3 = b_4 = \frac{A_Y k}{s\Delta Y}$$

$$b_5 = b_1 + b_2 + b_3 + b_4 \quad ; \quad b_6 = \frac{1}{s} = \frac{\Delta\tau}{\rho C V}$$

and equation (5.9) applies for the $\Sigma Q_{I(\ell)}$ term. The nodes at each end of the absorber plate will have only one conductive connection in the Y dimension. Depending on whether the node under analysis is first or last in the absorber plate, then the values of b_3 and θ_{J-1} or b_4 and θ_{J+1} respectively are set to zero.

c. Type 3 - One Dimensional Heat Conduction

It has been assumed that elements such as insulation rapidly attenuate temperature variations in the prominent direction of heat flow, then the temperature at any point in the YZ plane at the centre of an element will be closely approximated by the temperature of node I, where the element is positioned after the insulation in the direction away from the collector enclosure. Consequently the heat flow in both the Y and Z dimensions is negligible, therefore, dropping the temperature, $\theta_{j,I}$ and its associated temperature coefficient for the Y and Z dimension terms for equation (5.7), after re-arranging the following expression is obtained:

$$2(1+C_1)\theta_{I(n+1)} - C_1\theta_{I-1(n+1)} - C_1\theta_{I+1(n+1)}$$
$$= 2(1-C_1)\theta_{I(n)} + C_1\theta_{I-1(n)} + C_1\theta_{I+1(n)} + C_2\left(\Sigma Q_{I(n+1)} + \Sigma Q_{I(n)}\right) \quad (5.11)$$

where,

$$C_1 = \frac{A_x k}{S\Delta X} \quad ; \quad C_2 = \frac{1}{S} = \frac{\Delta\tau}{\rho C V}$$

The $\Sigma Q_{I(f)}$ term is described by equation (5.9).

d. Type 4 - One Dimensional Conduction with Node 1 Connected to more than Two Different Conduction Flowpaths

This node is required if, for example, a two or three dimensional analysis on the absorber plate was performed and the material adjacent to the absorber plate was insulation, see Figure (5.20). Each of the boundary temperatures may differ from the others, but it is assumed that after conducting through a half thickness of the adjoining element (e.g. insulation) the temperature of node I represents the temperature in the YZ plane as described for the previous nodal type. To analyse this node it is assumed that there are R different (I+1) terms corresponding to P*Q nodes and one (I-1) term. Using both the GHBE and equation (5.11) it can be shown that:

$$\left(2 + \sum_{j=1}^{R} d_j + d_{R+1}\right)\theta_{I(n+1)} - \sum_{j=1}^{R} d_j\,\theta_{I+1,j(n+1)} - d_{R+1}\,\theta_{I-1(n+1)}$$
$$= \left(2 - \sum_{j=1}^{R} d_j - d_{R+1}\right)\theta_{I(n)} + \sum_{j=1}^{R} d_j\,\theta_{I+1,j(n)} + d_{R+1}\,\theta_{I-1(n)}$$
$$+ d_{R+2}\left(\Sigma Q_{I(n+1)} + \Sigma Q_{I(n)}\right) \quad (5.12)$$

where,

$$d_j = \frac{A_{I+1,j}\,k}{S\Delta X} \quad ; \quad d_{R+1} = \frac{A_x k}{S\Delta X}$$

$$d_{R+2} = \frac{1}{S} = \frac{\Delta\tau}{(\rho C V/2) + \sum_{j=1}^{R}(\rho_j C_j V_j/2)}$$

Equation (5.9) applies for the $\Sigma Q_{I(f)}$ terms.

As declared in Section 5.1, the element in which one dimensional

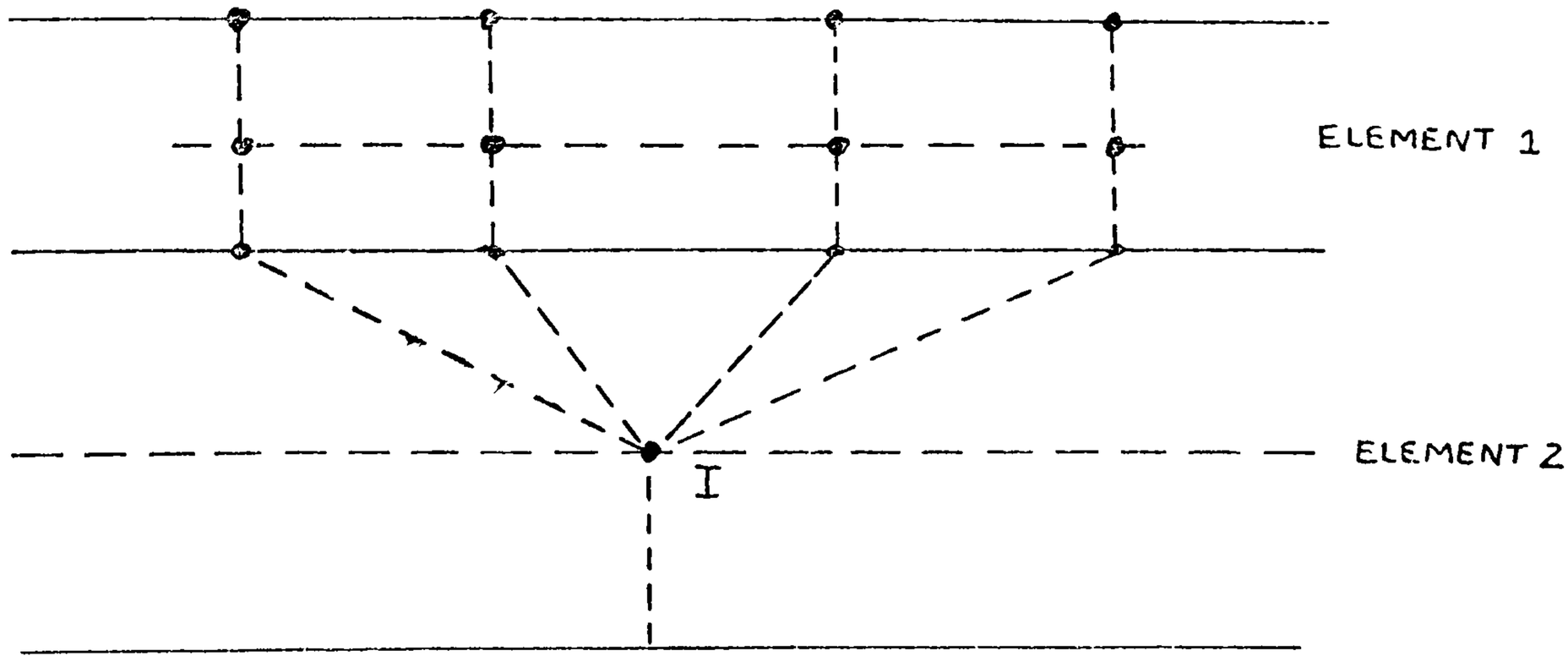

Figure 5.20 Node I connected to more than two conduction flowpaths

conduction prevails must be further from the enclosure than the element modelled by two or three dimensional conduction.

A subclassification of the Category 1 nodes are those nodes positioned at the boundary between two homogeneous elements which are assumed to be of different composition.

e) Type 5 - Node Positioned between Two Homogeneous Elements which have a Three Dimensional nodal Structure

This category of node differs from the type 1 node because two different materials make up the nodal subvolume. If both materials are considered to be anisotropic then for three dimensional conductive heat transfer the six nodes in thermal contact with the node in question are as shown in Figure 5.21. In this analysis it is assumed that the main conductive heat flow occurs in the X dimension, perpendicular to the plane adjoining both elements. The conductive flow in the X dimension can be described by a similar expression to equation (5.2),

$$Q_{j,I(\xi)} = A_{j,I} \frac{k_{j,I}}{\Delta X_{j,I}} \left(\theta_{j(\xi)} - \theta_{I(\xi)}\right) \qquad (5.13)$$

where j represents nodes I-1 and I+1.

The conduction heat flow paths in both the Y and Z dimensions are affected by the ratio of the areas of both elements in the appropriate dimension, therefore, equation (5.13) is re-expressed to take account of this effect, thus

$$Q_{j,I(\xi)} = \left(\frac{A_{(j,I)_1} k_{(j,I)_1}}{\Delta T_{j,I}} + \frac{A_{(j,I)_2} k_{(j,I)_2}}{\Delta T_{j,I}}\right)\left(\theta_{j(\xi)} - \theta_{I(\xi)}\right) \qquad (5.14)$$

where j represents nodes J-1, J+1, K-1 and K+1. From Figure 5.9 suffix 1 and 2 identify the two adjoining elements.

Substituting equations (5.13) and (5.14) into the GHBE results in,

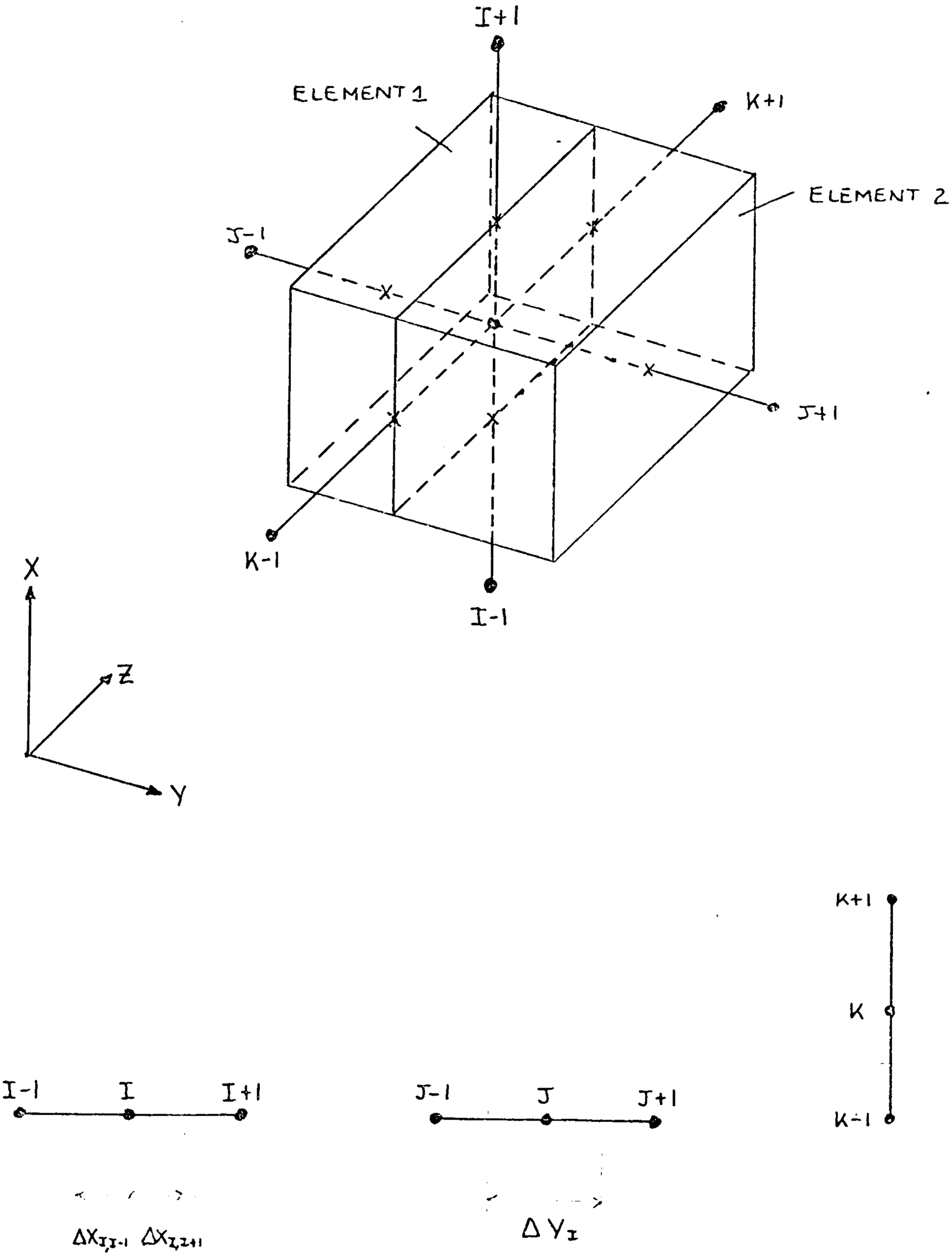

Figure 5.21 Node positioned on the boundary between two homogeneous anisotropic elements

$$\frac{2(\rho_1 C_1 V_1 + \rho_2 C_2 V_2)}{\Delta\tau}\left(\theta_{I(n+1)} - \theta_{I(n)}\right) = \frac{A_x\, k_{I-1,I}}{\Delta X_{I-1,I}}\left(\theta_{I-1(n+1)} - \theta_{I(n+1)}\right)$$

$$+ \frac{A_x\, k_{I+1,I}}{\Delta X_{I+1,I}}\left(\theta_{I+1(n+1)} - \theta_{I(n+1)}\right) + \left(\frac{A_{(J-1,I)_1}\, k_{(J-1,I)_1}}{\Delta Y_I} + \frac{A_{(J-1,I)_2}\, k_{(J-1,I)_2}}{\Delta Y_I}\right)\left(\theta_{J-1(n+1)} - \theta_{I(n+1)}\right)$$

$$+ \left(\frac{A_{(J+1,I)_1}\, k_{(J+1,I)_1}}{\Delta Y_I} + \frac{A_{(J+1,I)_2}\, k_{(J+2,I)_2}}{\Delta Y_I}\right)\left(\theta_{J+1(n+1)} - \theta_{I(n+1)}\right)$$

$$+ \left(\frac{A_{(K-1,I)_1}\, k_{(K-1,I)_1}}{\Delta Z_I} + \frac{A_{(K-1,I)_2}\, k_{(K-1,I)_2}}{\Delta Z_I}\right)\left(\theta_{K-1(n+1)} - \theta_{I(n+1)}\right)$$

$$+ \left(\frac{A_{(K+1,I)_1}\, k_{(K+1,I)_1}}{\Delta Z_I} + \frac{A_{(K+1,I)_2}\, k_{(K+1,I)_2}}{\Delta Z_I}\right)\left(\theta_{K+1(n+1)} - \theta_{I(n)}\right)$$

$$+ \frac{A_x\, k_{I-1,I}}{\Delta X_{I-1,I}}\left(\theta_{I-1(n)} - \theta_{I(n)}\right) + \frac{A_x\, k_{I+1,I}}{\Delta X_{I+1,I}}\left(\theta_{I+1(n)} - \theta_{I(n)}\right)$$

$$+ \left(\frac{A_{(J-1,I)_1}\, k_{(J-1,I)_1}}{\Delta Y_I} + \frac{A_{(J-1,I)_2}\, k_{(J-1,I)_2}}{\Delta Y_I}\right)\left(\theta_{J-1(n)} - \theta_{I(n)}\right)$$

$$+ \left(\frac{A_{(J+1,I)_1}\, k_{(J+1,I)_1}}{\Delta Y_I} + \frac{A_{(J+1,I)_2}\, k_{(J+1,I)_2}}{\Delta Y_I}\right)\left(\theta_{J+1(n)} - \theta_{I(n)}\right)$$

$$+ \left(\frac{A_{(K-1,I)_1}\, k_{(K-1,I)_1}}{\Delta Z_I} + \frac{A_{(K-1,I)_2}\, k_{(K-1,I)_2}}{\Delta Z_I}\right)\left(\theta_{K-1(n)} - \theta_{I(n)}\right)$$

$$+ \left(\frac{A_{(K+1,I)_1}\, k_{(K+1,I)_1}}{\Delta Z_I} + \frac{A_{(K+1,I)_2}\, k_{(K+1,I)_2}}{\Delta Z_I}\right)\left(\theta_{K+1(n)} - \theta_{I(n)}\right) + \sum Q_{I(n+1)} + \sum Q_{I(n)}$$

where, V_N = volume of element N (where N is 1 or 2)

Equation (5.15) is similar in format to equation (5.5), if it were to undergo the same procedure for re-arrangement (i.e. all unknown temperature values to the left-hand side of the equation), then it is possible to express equation (5.15) in exactly the same form of equation as equation (5.6), however, the coefficients of the equation are different

$$(2+\beta_7)\theta_{I(n+1)} - \beta_1\theta_{I-1(n+1)} - \beta_2\theta_{I+1(n+1)} - \beta_3\theta_{J-1(n+1)} - \beta_4\theta_{J+1(n+1)}$$

$$- \beta_5\theta_{K-1(n+1)} - \beta_6\theta_{K+1(n+1)} = (2-\beta_7)\theta_{I(n)} + \beta_1\theta_{I-1(n)} + \beta_2\theta_{I+1(n)} + \beta_3\theta_{J-1(n)}$$

$$+ \beta_4\theta_{J+1(n)} + \beta_5\theta_{K-1(n)} + \beta_6\theta_{K+1(n)} + \beta_8\sum Q_{I(n+1)} + \beta_8\sum Q_{I(n)} \qquad (5.16)$$

where,

$$\beta_1 = \frac{Ax\ k_{I-1,I}}{S\Delta X_{I-1,I}} \quad ; \quad \beta_2 = \frac{Ax\ k_{I+1,I}}{S\Delta X_{I+1,I}}$$

$$\beta_3 = \frac{A_{(J-1,I),1}\ k_{(J-1,I),1} + A_{(J-1,I)2}\ k_{(J-1,I)2}}{S\Delta Y_I} \quad ; \quad \beta_4 = \frac{A_{(J+1,I),1}\ k_{(J+1,I),1} + A_{(J+1,I)2}\ k_{(J+1,I)2}}{S\Delta Y_I}$$

$$\beta_5 = \frac{A_{(K-1,I),1}\ k_{(K-1,I),1} + A_{(K-1,I)2}\ k_{(J-1,I)2}}{S\Delta Z_I} \quad ; \quad \beta_6 = \frac{A_{(K+1,I),1}\ k_{(K+1,I),1} + A_{(K+1,I)2}\ k_{(K+1,I)2}}{S\Delta Z_I}$$

$$\beta_7 = \beta_1 + \beta_2 + \beta_3 + \beta_4 + \beta_5 + \beta_6 \quad ; \quad \beta_8 = \frac{1}{S} = \frac{\Delta\tau}{\rho_1 C_1 V_1 + \rho_2 C_2 V_2}$$

For an isotropic material equation (5.15) can be re-expressed to give:

$$(2+e_7)\theta_{I(n+1)} - e_1\theta_{I-1(n+1)} - e_2\theta_{I+1(n+1)} - e_3\theta_{J-1(n+1)} - e_4\theta_{J+1(n+1)}$$

$$- e_5\theta_{K-1(n+1)} - e_6\theta_{K+1(n+1)} = (2-e_7)\theta_{I(n)} + e_1\theta_{I-1(n)} + e_2\theta_{I+1(n)} + e_3\theta_{J-1(n)}$$

$$+ e_4\theta_{J+1(n)} + e_5\theta_{K-1(n)} + e_6\theta_{K+1(n)} + e_8\left(\Sigma Q_{I(n+1)} + \Sigma Q_{I(n)}\right) \qquad (5.17)$$

where,

$$e_1 = \frac{Ax\ k_1}{S\Delta X_{I-1,I}} \quad ; \quad e_2 = \frac{Ax\ k_2}{S\Delta X_{I-1,I}}$$

$$e_3 = \frac{A_{(I-1,I),1}\ k_1 + A_{(I-1,I)2}\ k_2}{S\Delta Y} \quad ; \quad e_4 = \frac{A_{(J+1,I),1}\ k_1 + A_{(J+1,I)2}\ k_2}{S\Delta Y}$$

$$e_5 = \frac{A_{(K-1,I),1}\ k_1 + A_{(K-1,I)2}\ k_2}{S\Delta Z} \quad ; \quad e_6 = \frac{A_{(K+1,I),1}\ k_1 + A_{(K+1,I)2}\ k_2}{S\Delta Z}$$

$$e_7 = e_1 + e_2 + e_3 + e_4 + e_5 + e_6 \quad ; \quad e_8 = \frac{1}{S} = \frac{\Delta\tau}{(\rho_1 C_1 V_1 + \rho_2 C_2 V_2)}$$

The postscripts 1 and 2 relate to the two different elements where 1 represents that element pertaining to node (I-1) and 2 represents node (I+1). The volumes V_1 and V_2 represent that part of the subvolume which is element 1 and 2 respectively.

Equation (5.9) could be used to represent this nodal type, however, it is known that $Q_{s\alpha(k)}$ and $Q_{p(k)}$ do not apply consequently equation (5.9) can be re-written as,

$$\Sigma Q_I(\phi) = Q_{liq}(\phi) + Q_M(\phi) \qquad (5.18)$$

Corner and edge nodes can be dealt with as described in subsection (a) above.

f) Type 6 - node positioned between two homogeneous elements which have negligible heat flow in the Z dimension

This node type occurs due to the use of Category 1, Type 2 nodes in an air collector. Heat conduction in the Z direction is negligible, therefore, Z dimension terms can be omitted. Using equation (5.17), it is possible to establish the following expression,

$$(2+f_5)\theta_{I(n+1)} - f_1\theta_{I-1(n+1)} - f_2\theta_{I+1(n+1)} - f_3\theta_{J-1(n+1)} - f_4\theta_{J+1(n+1)}$$

$$=(2-f_5)\theta_{I(n)} + f_1\theta_{I-1(n)} + f_2\theta_{I+1(n)} + f_3\theta_{J-1(n)} - f_4\theta_{J+1(n)}$$

$$+ f_6\left(\Sigma Q_{I(n+1)} + \Sigma Q_{I(n)}\right) \qquad (5.19)$$

where,

$$f_1 = \frac{A_x k_1}{S\Delta X_{I-1,I}} \quad ; \quad f_2 = \frac{A_x k_2}{S\Delta X_{I+1,I}}$$

$$f_3 = \frac{A_{(J-1,I)1}\,k_1 + A_{(J-1,I)2}\,k_2}{S\Delta Y} \quad ; \quad f_4 = \frac{A_{(J+1,I)1}\,k_1 + A_{(J+1,I)2}\,k_2}{S\Delta Y}$$

$$f_5 = f_1 + f_2 + f_3 + f_4 \quad ; \quad f_6 = \frac{1}{S} = \frac{\Delta\tau}{\rho_1 C_1 V_1 + \rho_2 C_2 V_2}$$

and the $\Sigma Q_{I(\phi)}$ term is as given by equation (5.18). Missing nodes are dealt with as Category 1, Type 2 nodes.

It is important to note that both node Types 5 and 6 can be used as the basis for the equation for nodes on the boundary between a multi-nodal element and a single nodal element, for example, the node situated between the absorber plate in a solar collector and insulation, see cases (h) and (i).

g) Type 7 - Node on the Boundary between Two Homogeneous Elements with One Dimensional Heat Conduction.

If the heat flow in the Y and Z dimensions is negligible in adjacent elements then this nodal type can be established using equation (5.17) and setting all Y and Z dimension terms to zero, therefore,

$$(2+g_1+g_2)\theta_{I(n+1)} - g_1\theta_{I-1(n+1)} - g_2\theta_{I+1(n+1)}$$

$$=(2-g_1-g_2)\theta_{I(n)} + g_1\theta_{I-1(n)} + g_2\theta_{I+1(n)} + g_3(\Sigma Q_{I(n+1)} + \Sigma Q_{I(n)}) \quad (5.20)$$

where,

$$g_1 = \frac{A_x k_1}{S\Delta X_{I-1,I}} \quad ; \quad g_2 = \frac{A_x k_2}{S\Delta X_{I+1,I}}$$

$$g_3 = \frac{1}{S} = \frac{\Delta\tau}{\rho_1 C_1 V_1 + \rho_2 C_2 V_2}$$

and equation (5.18) applies for $\Sigma Q_{I(t)}$

h) Type 8 - Node on the Boundary between an Element with a Three Dimensional Nodal Structure and One with No Y or Z Dimensional Conduction

This nodal type has the same equation form as node Type 5 described in (e) above, i.e. equation (5.17). However, the coefficients are different because it is assumed that there is no I-1 node. Based on this assumption, the following equation is obtained,

$$(2+h_7)\theta_{I(n+1)} - h_1\theta_{I-1(n+1)} - h_2\theta_{I+1(n+1)} - h_3\theta_{J-1(n+1)} - h_4\theta_{J+1(n+1)} - h_5\theta_{K-1(n+1)}$$

$$-h_6\theta_{K+1(n+1)} = (2-h_7)\theta_{I(n)} + h_1\theta_{I-1(n)} + h_2\theta_{I+1(n)} + h_3\theta_{J-1(n)} + h_4\theta_{J+1(n)}$$

$$+h_5\theta_{K-1(n)} + h_6\theta_{K+1(n)} + h_8(\Sigma Q_{I(n+1)} + \Sigma Q_{I(n)}) \quad (5.21)$$

where,

$$h_1 = \frac{A_x k_1}{S\Delta X_{I-1,I}} \quad ; \quad h_2 = \frac{A_x k_2}{S\Delta X_{I+1,I}}$$

$$h_3 = \frac{A(J-1,I)_2\, k_2}{S\Delta Y} \quad ; \quad h_4 = \frac{A(J+1,I)_2\, k_2}{S\Delta Y}$$

$$h_5 = \frac{A(K-1,I)_2\, k_2}{S\Delta Z} \quad ; \quad h_6 = \frac{A(K+1,I)_2\, k_2}{S\Delta Z}$$

$$h_7 = h_1 + h_2 + h_3 + h_4 + h_5 + h_6 \quad ; \quad h_8 = \frac{1}{S} = \frac{\Delta\tau}{\rho_1 C_1 V_1 + \rho_2 C_2 V_2}$$

The $\Sigma Q_{I(t)}$ in equation (5.21) is given by equation (5.18). Refer to the Type 5 node in this category for notation.

i) <u>Type 9 - Node on the Boundary between Two Elements, One with No Conduction in the Z Dimension, the Other with No Y or Z Dimension Conduction</u>

The equation of the Type 9 node can be obtained from Node Type 6 (Section (f) above) by the same procedure as the Type 8 node was obtained from the Category 1, Type 5 node. Element 2 has no Z dimension conduction and Element 1 has no Y or Z dimension conduction. Thus,

$$(2 + \ell_5)\,\theta_{I(n+1)} - \ell_1\,\theta_{I-1(n+1)} - \ell_2\,\theta_{I+1(n+1)} - \ell_3\,\theta_{J-1(n+1)} - \ell_4\,\theta_{J+1(n+1)}$$

$$= (2 - \ell_5)\,\theta_{I(n)} + \ell_1\,\theta_{I-1(n)} + \ell_2\,\theta_{I+1(n)} + \ell_3\,\theta_{J-1(n)} + \ell_4\,\theta_{J+1(n)}$$

$$+ \ell_6\,(\Sigma Q_{I(n+1)} + \Sigma Q_{I(n)}) \qquad (5.22)$$

where,

$$\ell_1 = \frac{A_X\, k_1}{S\Delta X_{I-1,I}} \quad ; \quad \ell_2 = \frac{A_X k_2}{S\Delta X_{I+1,I}}$$

$$\ell_3 = \frac{A(J-1,I)_2\, k_2}{S\Delta Y} \quad ; \quad \ell_4 = \frac{A(J+1,I)_2\, k_2}{S\Delta Y}$$

$$\ell_5 = \ell_1 + \ell_2 + \ell_3 + \ell_4 \quad ; \quad \ell_6 = \frac{1}{S} = \frac{\Delta\tau}{(\rho_1 C_1 V_1 + \rho_2 C_2 V_2)}$$

Equation (5.18) applies to equation (5.22) for the $\Sigma Q_{I(t)}$ term.

Category 2 Node

Although the General Heat Balance Equation can be used to analyse a node through which a fluid flows, it is more convenient to have a General Heat Balance Equation for fluid flow because it will allow a clearer understanding of the process taking place. Consider the fluid momentum process with a fluid subvolume as an addition to the GHBE,

$$2\Delta S_F = \sum_{j=1}^{M} Q_{j,F(\phi)} + \sum_{k=1}^{N} Q_{k,F(\phi)} + \sum Q_{F(\phi)} \qquad (5.23)$$

where this expression is similar in form to equation (5.1) except that node I is replaced by node F (to denote a fluid node) and an extra term has been added to the equation

$$\sum_{k=1}^{N} Q_{k,F(\phi)} \qquad (5.24)$$

where, N = the number of different fluid streams either entering or leaving the subvolume

k = a particular fluid stream

If a fluid stream enters the nodal subvolume it will be added to the subvolume and it can heat or cool the fluid node, whereas fluid simultaneously leaving the subvolume will be lost from the subvolume and regarded as a heat loss from the fluid node.

Equation (5.24) can be re-expressed in the form:

$$\sum_{k=1}^{N} \dot{m}_{k(\phi)} H_{k(\phi)} \qquad (5.35)$$

where, $\dot{m}_{k(\phi)}$ is the mass flow rate of the fluid stream k entering or leaving the subvolume at time (ϕ) and it is a vector quantity. $H_{k(\phi)}$ is the enthalpy ($J.Kg^{-1}$) of fluid stream k at time ϕ .

The General Heat Balance Equation for forced convective fluid flow in one dimension can be expressed as,

$$2\Delta S_F = \sum_{j=1}^{M} Q_{j,F(n+1)} + \sum_{j=1}^{M} Q_{j,F(n)} + \sum_{k=1}^{N} \dot{m}_{k(n+1)} H_{k(n+1)}$$

$$+ \sum_{k=1}^{N} \dot{m}_{k(n)} H_{k(n)} + \Sigma Q_{F(n+1)} + \Sigma Q_{F(n)} \qquad (5.36)$$

where,

$$\Delta S_F = \frac{\rho_F C_F V (\theta_{F(n+1)} - \theta_{F(n)})}{\Delta \tau}$$

and M represents the number of subvolume boundary surfaces with which the fluid is in thermal contact. It is assumed that no conductive or radiative exchange occurs between the fluid and any part of the subvolume boundary that is also fluid.

It is important to note that if no forced convection occurs then each value of $\dot{m}_k$ is zero and the natural convection case occurs. In such cases equation (5.26) reduces to the GHBE - equation (5.1).

If heat exchange within the fluid subvolume occurs at constant pressure then the enthalpy, H, may be defined as,

$$H = U + W$$

where U is the internal energy of the fluid due to molecular activity and W is the energy resulting from the pressure within the fluid subvolume. The enthalpy of a fluid can also be equated to the temperature of the fluid:

$$H = Cp\,\theta$$

where Cp is the specific heat capacity of the fluid at constant pressure (J/Kg.degC) and θ is the fluid temperature relative to the Celsius temperature scale.

If a number of constituent fluids are in the fluid then the enthalpy, H, is found from

$$\sum_{c=1}^{C} \dot{m}_c H_c = \left(\sum_{c=1}^{C} \dot{m}_c C_{P_c} \theta_c \right)$$

$$\Rightarrow \quad \bar{H} = \left[\left(\sum_{c=1}^{C} \dot{m}_c C_{pc} \theta_c\right) / \left(\sum_{c=1}^{C} \dot{m}_c\right)\right] \theta$$

$$\Rightarrow \quad \bar{H} = \overline{C_p}\, \theta \qquad (5.27)$$

where C = number of constituent fluids in fluid subvolume

$\bar{H} = \sum_{c=1}^{C} H_c$ = enthalpy of fluid subvolume ($KJ.Kg^{-1}$)

$\overline{C_p} = \left(\sum_{c=1}^{C} \dot{m}_c C_{pc}\right) / \left(\sum_{c=1}^{C} \dot{m}_c\right)$

i.e. the specific heat capacity of the mixed fluid subvolume ($J.Kg^{-1}.K^{-1}$)

Consider the convective heat transfer process occurring at each solid surface in the fluid subvolume boundary. At each surface the convective heat exchange can be described mathematically by the expression:

$$Q_{j,F(\ell)} = hc_{j,F(\ell)}\, A_{j,F} \left(\theta_{j(\ell)} - \theta_{F(\ell)}\right) \qquad (5.28)$$

where j = fluid subvolume solid boundary surface under consideration

$Q_{j,F}$ = convective heat exchange between the fluid and surface j in its solid boundary (watts)

$A_{j,F}$ = area of contact between surface j and the fluid (m^2)

θ_j = temperature of surface j (K)

θ_F = fluid temperature (K)

$hc_{j,F}$ = convective heat transfer coefficient ($WM^{-2}K^{-1}$)

ℓ = the evaluation time row n or n+1 representing present and future time rows respectively.

The convective heat transfer coefficient ($hc_{j,F}$) between surface j and the fluid represents any convective process. Analytical and empirical relationships can be used to estimate the value of hc in a one dimensional fluid model, enabling equation (5.28) to be used to analyse natural, mixed and forced convection as well as considering condensation effects at a fluid/solid interface. The appropriate analytical and empirical expressions for convective and condensation processes for solar collector systems will be discussed in Appendix 6.

Substituting equation (5.28) into the GHBE for fluid flow and replacing the enthalpy term with equation (5.27) yields

$$2\Delta S_F = \sum_{j=1}^{M} hc_{j,F(n+1)} A_{j,F} \left(\theta_{j(n+1)} - \theta_{F(n+1)}\right)$$
$$+ \sum_{j=1}^{M} hc_{j,F(n)} A_{j,F} \left(\theta_{j(n)} - \theta_{F(n)}\right) + \sum_{k=1}^{N} \dot{m}_{k(n+1)} \overline{Cp}_{k(n+1)} \theta_{k(n+1)}$$
$$+ \sum_{k=1}^{N} \dot{m}_{k(n)} \overline{Cp}_{k(n)} \theta_{k(n)} + \Sigma Q_{F(n+1)} + \Sigma Q_{F(n)} \qquad (5.29)$$

This expression can now be used to derive the general difference equation for fluid flow in a solar collector.

Consider Figure (5.22) where there is a fluid flowpath into and out of the subvolume in a forced convective case or where buoyancy causes fluid movement between subvolumes. A fluid flows into the subvolume from node F-1 at temperature θ_{F-1}, simultaneously fluid leaves the subvolume to enter node F+1, the leaving fluid temperature is that of the subvolume under analysis, i.e. θ_F.

In solar collectors leaks may occur due to cracked cover plates, burst liquid tubes, etc. These leaks may cause fluid to enter or leave the subvolume. If a single leak is considered then for leakage into the subvolume the enthalpy of the leak may be known or unknown, however, if the leak is from the subvolume then fluid leaves at temperature θ_F.

As there are three fluid flowpaths then the value of N in equation (5.29) is set to three, thus

$$2\Delta S_F = \sum_{j=1}^{M} hc_{j,F(n+1)} A_{j,F} \left(\theta_{j(n+1)} - \theta_{F(n)}\right) + \sum_{j=1}^{M} hc_{j,F(n)} A_{j,F} \left(\theta_{j(n)} - \theta_{F(n)}\right)$$
$$+ \left[\dot{m}_{i(n+1)} \overline{Cp}_{F-1(n+1)} \theta_{F-1(n+1)} - \dot{m}_{o(n+1)} \overline{Cp}_{F(n+1)} \theta_{F(n+1)}\right.$$
$$\left. \pm \dot{m}_{\ell(n+1)} \overline{Cp}_{\ell(n+1)} \theta_{\ell(n+1)}\right] + \left[\dot{m}_{i(n)} \overline{Cp}_{F-1(n)} \theta_{F-1(n)} - \dot{m}_{o(n)} \overline{Cp}_{F(n)} \theta_{F(n)}\right.$$
$$\left. \pm \dot{m}_{\ell(n)} \overline{Cp}_{\ell(n)} \theta_{\ell(n)}\right] + \Sigma Q_{F(n+1)} + \Sigma Q_{F(n)} \qquad (5.30)$$

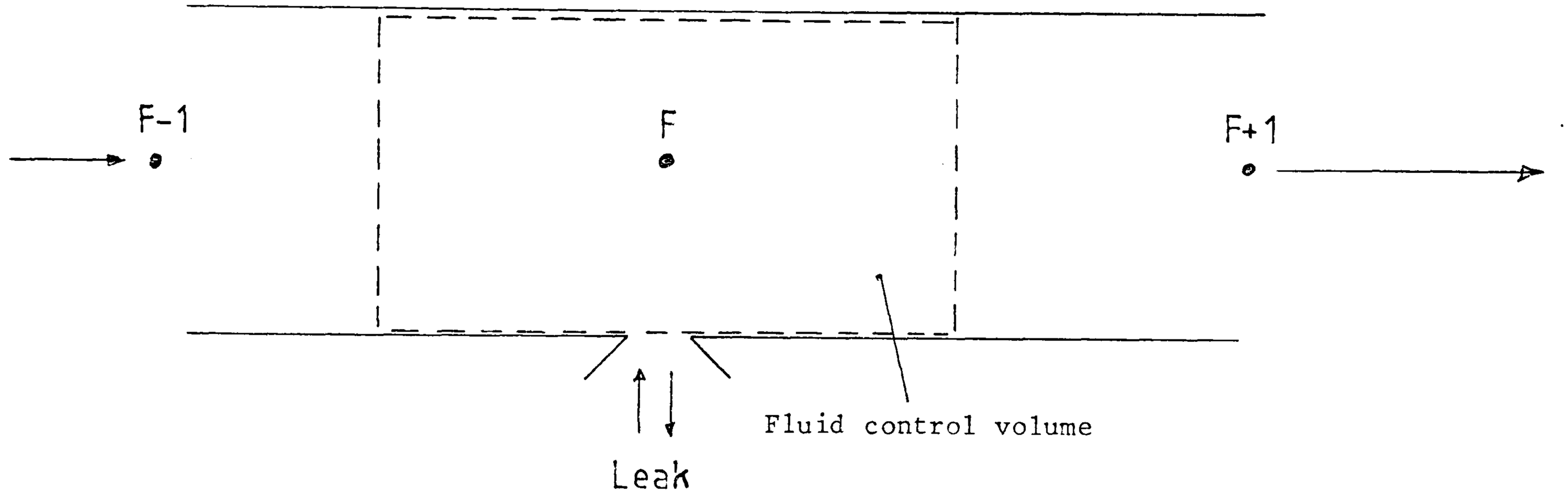

Figure 5.22 Fluid flowpaths

where, i = inlet fluid

o = outlet fluid

l = leaking fluid - into (+ve) or out of (-ve) the sub-volume.

Equation (5.34) can be rearranged with all unknown temperature values positioned on the left-hand side of the equation and all known temperature values and heat injection terms on the other side of the equation. Equation (5.30) can be re-written to give:

$$(2+m_{M+2(n+1)})\,\theta_{F(n+1)} - \sum_{j=1}^{M} m_{j(n+1)}\,\theta_{j(n+1)} - m_{M+1(n+1)}\,\theta_{F-1(n+1)}$$

$$=(2-m_{M+2(n)})\,\theta_{F(n)} + \sum_{j=1}^{M} m_{j(n)}\,\theta_{j(n)} + m_{M+1(n)}\,\theta_{F-1(n)} + m_{M+3}\,(\Sigma Q_{F(n+1)} + \Sigma Q_{F(n)}) \qquad (5.31)$$

where,

$$m_{j(t)} = \frac{h_{c\,j,F(t)}\,A_{j,F}}{S} \quad ; \quad m_{M+1(t)} = \frac{\dot{m}_{F-1(t)}\,C_{p\,F-1(t)}}{S}$$

$$m_{M+2(t)} = \left[\left(\sum_{j=1}^{M} h_{c\,j,F(t)}\,A_{j,F}\right) + \left(\dot{m}_{o(t)}\,\overline{C_{p\,F(t)}}\right) + \left(\dot{m}_{\ell(t)}\,\overline{C_{p\,\ell(t)}}\right)\right] / S$$

$$m_{M+3} \simeq \frac{1}{S} = \frac{\Delta\tau}{\rho_F\,C_F\,\theta_F}$$

m = number of solid boundaries surrounding the subvolume

As all energy terms associated with node F have been considered in equation (5.31) then the $\Sigma Q_{F(t)}$ which is identical to $\Sigma Q_{I(t)}$ is expressed as

$$\Sigma\,Q_{F(t)} = Q_{M(t)} \qquad (5.32)$$

If there is no leak in the subvolume then $\dot{m}_{\ell(t)}$ is zero.

Category 3 Node

This category of node is similar to the Category 1 nodes which model heat conduction between two adjoining isotropic homogeneous elements, however, in this case one of the elements is replaced by a fluid because

the node is situated at the outer surface of a single or multilayered construction where convection and radiation occurs. There are four node types to consider, in each assume that element 1 (i.e. the element associated with the I-1 node) is a fluid node

a) Type 1 - Surface Node Where Element 2 has a Three Dimensional Nodal Grid

This nodal type can be compared to a Category1, Type 8 node. The difference between the two nodes is that element 1 in the category 1 node is a homogeneous element whereas in this nodal category element 1 is a fluid. If the GHBE is used to derive this node then the conductive processes in element I-1 are replaced by a convective process. The heat exchange caused by a convective process is given by equation (5.28). Either by applying equation (5.28) to the GHBE and solving or using the result obtained from the Category 1, Type 8 node and substituting the effects of a convective process for a conductive process, the following equation is derived for this nodal type:

$$(2 + n_{7(n+1)})\theta_{I(n+1)} - n_{1(n+1)}\theta_{I-1(n+1)} - n_2\theta_{I+1(n+1)} - n_3\theta_{J-1(n+1)} - n_4\theta_{J+1(n+1)}$$

$$-n_5\theta_{K-1(n+1)} - n_6\theta_{K+1(n+1)} = (2 - n_{7(n)})\theta_{I(n)} + n_{1(n)}\theta_{I-1(n)} + n_2\theta_{I+1(n)}$$

$$+n_3\theta_{J-1(n)} + n_4\theta_{J+1(n)} + n_5\theta_{K-1(n)} + n_6\theta_{K+1(n)} + n_8\left(\sum Q_{I(n+1)} + \sum Q_{I(n)}\right) \qquad (5.33)$$

where

$$n_{1(t)} = \frac{Ax\ hc_{I,F(t)}}{S} \quad ; \quad n_2 = \frac{Ax\ k_2}{S\Delta X_{I+1,I}}$$

$$n_3 = \frac{A_{(J-1,I)2}\ k_2}{S\Delta Y} \quad ; \quad n_4 = \frac{A_{(J+1,I)2}\ k_2}{S\Delta Y}$$

$$n_5 = \frac{A_{(K-1,I)2}\ k_2}{S\Delta Z} \quad ; \quad n_6 = \frac{A_{(K+1,I)2}\ k_2}{S\Delta Z}$$

$$n_{7(t)} = n_{1(t)} + n_2 + n_3 + n_4 + n_5 + n_6 \quad ; \quad n_8 = \frac{1}{S} = \frac{\Delta\tau}{\rho_2 C_2 V_2 + \rho_F C_F V_F}$$

$h_{c_{I,F(t)}}$ = convective heat transfer coefficient between surface I and the fluid ($WM^{-2}.K^{-1}$)

Eight heat generation terms have been identified for a surface node, however, some of these terms are mutually exclusive depending upon the nature of the surface

$$\Sigma Q_{I(t)} = Q_{s,E(t)} + Q_{s,R(t)} + Q_{s,I(t)} + Q_{ELWR(t)} + Q_{ILWR(t)} + Q_{rain(t)} + Q_{liq(t)} + Q_{M(t)} \quad (5.34)$$

where $Q_{s,E(t)}$ = the quantity of solar radiation absorbed at an external surface node

$Q_{s,R(t)}$ = the quantity of solar radiation absorbed at an external surface node from a planar reflector

$Q_{s,I(t)}$ = the quantity of solar radiation absorbed by internal surfaces

$Q_{ELWR(t)}$ = the external longwave radiative exchange between a surface and its surrounds

$Q_{ILWR(t)}$ = the internal longwave radiative exchange between internal surfaces of an enclosure

$Q_{rain(t)}$ = the energy exchange between the surface and precipitation.

Equation (5.34) can be applied to equation (5.33) to replace the $\Sigma Q_{I(t)}$ term.

Edge and corner nodes are solved by omitting any temperature and temperature coefficient representing a node which is not in thermal contact with the edge or corner node. In detailed analysis of a liquid collector this nodal type may be required.

b) Type 2 - Surface Node with No Conduction in the Y Dimension of the Homogeneous Element

A Category 1, Type 9 node can be compared with this surface node. Proceeding in the same manner as described in the derivation of equation (5.33) or alternatively directly from equation (5.33) the expression

for this node is,

$$(2 + O_{5(n+1)})\,\theta_{I(n+1)} - O_{1(n+1)}\,\theta_{I-1(n+1)} - O_2\,\theta_{I+1(n+1)} - O_3\,\theta_{J-1(n+1)} - O_4\,\theta_{J+1(n+1)}$$
$$= (2 - O_{5(n)})\,\theta_{I(n)} + O_{1(n+1)}\,\theta_{I-1(n)} + O_2\,\theta_{I+1(n)} + O_3\,\theta_{J-1(n)} + O_4\,\theta_{J+1(n)}$$
$$+ O_6\left(\Sigma Q_{I(n+1)} + \Sigma Q_{I(n)}\right) \qquad (5.35)$$

where,

$$O_{1(k)} = \frac{A_x\, h_{C\,I,F(k)}}{S} \quad ; \quad O_2 = \frac{A_x\, k_2}{S\,\Delta X_{I+1,I}}$$

$$O_3 = \frac{A_{(J-1,I)2}\, k_2}{S\Delta Y} \quad ; \quad O_4 = \frac{A_{(J+1,I)2}\, k_2}{S\Delta Y}$$

$$O_{5(k)} = O_{1(k)} + O_2 + O_3 + O_4 \quad ; \quad O_6 = \frac{1}{S} = \frac{\Delta\tau}{\rho_2 C_2 V_2 + \rho_F C_F V_F}$$

Equation (5.34) is used for $\Sigma Q_{I(k)}$. This node type is applied, for example, to detailed analyses of air collectors.

c) Type 3 - Surface Node with No Conduction in the Y and Z Dimensions of the Homogeneous Element

There are instances where a single node is used in a solar collector to model the fluid, i.e. in a liquid collector where the air above the absorber plate is affected only by buoyancy forces. If a single node is used on the sides of the collector then there will be no conduction in the Y and Z dimensions. Therefore, from equation (5.30) neglecting the Y and Z dimension terms the following expression for this surface node is obtained:

$$(2 + p_{1(n+1)} + p_2)\,\theta_{I(n+1)} - p_{1(n+1)}\,\theta_{I-1(n+1)} - p_2\,\theta_{I+1(n+1)} = (2 - p_{1(n)} - p_2)\,\theta_{I(n)}$$
$$+ p_{1(n)}\,\theta_{I-1(n)} + p_2\,\theta_{I+1(n)} + p_3\left(\Sigma Q_{I(n+1)} + \Sigma Q_{I(n)}\right) \qquad (5.36)$$

where

$$p_{1(k)} = \frac{A_x\, h_{C\,I,F(k)}}{S} \quad ; \quad p_2 = \frac{A_x\, k_2}{S\,\Delta X_{I+1,I}}$$

$$p_3 = \frac{1}{S} = \frac{\Delta\tau}{\rho_2 C_2 V_2 + \rho_F C_F V_F}$$

and the $\Sigma Q_{I(k)}$ is expressed by equation (5.34).

d) Type 4 - Surface Node with No Conduction in the Y and Z Dimensions of the Homogeneous Element, Connected to More Than One Fluid Node

A collector side wall surface may be represented by a single node, in such circumstances the sides of the collector which run parallel to the fluid flow are connected to each node in the fluid flow. If there is only one node then case (c) above applies, however, assuming that there are P fluid nodes equation (5.37) can be employed to derive the equation for this Type 4 node, thus,

$$\left(2+\sum_{j=1}^{P} q_{j(n+1)}+q_{p+1}\right)\theta_{I(n+1)}-\sum_{j=1}^{P} q_{j(n+1)}\,\theta_{F,j(n+1)}-q_{p+1}\,\theta_{I+1(n+1)}$$

$$=\left(2-\sum_{j=1}^{P} q_{j(n)}-q_{p+1}\right)\theta_{I(n)}+\sum_{j=1}^{P} q_{j(n)}\,\theta_{F,j(n)}+q_{p+1}\,\theta_{I+1(n)}+q_{p+2}\left(\Sigma Q_{I(n+1)}+\Sigma Q_{I(n)}\right) \qquad (5.37)$$

where,

$$q_{j(k)}=\frac{A_x\, h_{c\,j,F(k)}}{S} \quad ; \quad q_{p+1}=\frac{A_x\, k_2}{S\Delta X_{I+1,I}}$$

$$q_{p+2}=\frac{1}{S}=\frac{\Delta\tau}{\left(\rho_2 C_2 V_2+\sum_{j=1}^{P}\rho_j C_j V_j\right)}$$

with equation (5.34) used to describe $\Sigma Q_{I(k)}$

Category 4 Node

Consider an energy balance on any conduit or fitting which is modelled using the resistance/capacitance network, to solve the conductive and thermal storage effects in the walls of a fitting. Figure (5.23) shows the thermal influences on the node representing this component, applying the GHBE for fluid flow - equation (5.26) - to the energy balance yields,

$$2\Delta S_F=\sum_{a=1}^{A} Q_{a,in(k)}-\sum_{b=1}^{B} Q_{b,out(k)}+Q_{S(k)}+Q_{M(k)} \qquad (5.38)$$

where, A = number of fluid flowpaths into node F

B = number of fluid flowpaths out of node F

$Q_{a,in(k)}$ = energy transported into node F by fluid flowpath a, therefore

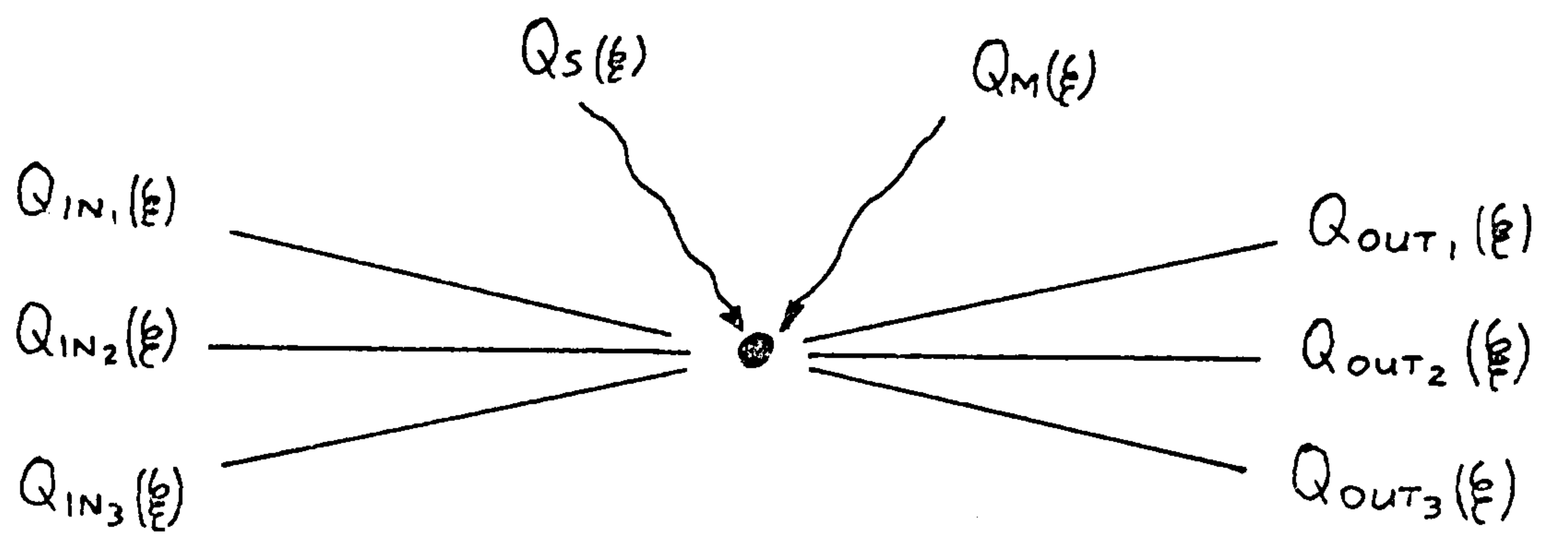

Figure 5.23 Energy balance at a category 4 node

$$Q_{a,in}(\xi) = \dot{m}_a(\xi)\,\overline{C_{pa}}(\xi)\,\theta_a(\xi) \qquad (5.39)$$

Qb,out(ξ)= energy transported from node F by fluid flowpath b, therefore

$$Q_{b,out}(\xi) = \dot{m}_b(\xi)\,\overline{C_{pa}}(\xi)\,\theta_a(\xi) \qquad (5.40)$$

It is assumed in this node that there are no leaks into or out of the subvolume, unlike the Category 2 node.

The Qs(ξ) term takes account of the thermal resistance between the fluid and the surrounds, this can be described by the expression

$$Q_{S(\xi)} = A_c\,U_c(\xi)\left(\theta_s(\xi) - \theta_F(\xi)\right) \qquad (5.41)$$

where Ac = area of contact (M^2)

$\theta_s(\xi)$ = temperature of the surrounds (degC)

Uc(ξ) = the heat transfer coefficient between the fluid node and its surrounds ($WM^{-2}K^{-1}$)

The capacitance effects are included in the storage term, thus

$$\Delta S_F = \frac{\left(\rho_F C_F V_F + \sum_{e=1}^{E} \rho_e C_e V_e\right)\left(\theta_{F(n+1)} - \theta_{F(n)}\right)}{\Delta\tau} \qquad (5.42)$$

where E is the number of elements in the conduit. Obviously this method will not be as accurate or informative as a full nodal representation, however, it will require much less computational effort to solve. The former method is straightforward; this method involves substituting equations (5.39) to (5.42) into equation (5.38), giving

$$2\frac{\left(\rho_F C_F V_F + \sum_{e=1}^{E} \rho_e C_e V_e\right)}{\Delta\tau}\left(\theta_{F(n+1)} - \theta_{F(n)}\right) = \sum_{a=1}^{A} \dot{m}_{a(n+1)}\,\overline{C_{p_{f,a}(n+1)}}\,\theta_{a(n+1)}$$

$$+ \sum_{a=1}^{A} \dot{m}_{a(n)}\,\overline{C_{p_{f,a}(n)}}\,\theta_{a(n)} - \sum_{b=1}^{B} \dot{m}_{b(n+1)}\,\overline{C_{p_{f,F(n+1)}}}\,\theta_{F(n+1)}$$

$$- \sum_{b=1}^{B} \dot{m}_{b(n)}\,\overline{C_{p_{f,F(n)}}}\,\theta_{F(n)} + A_c\,U_{c(n+1)}\left(\theta_{s(n+1)} - \theta_{F(n+1)}\right)$$

$$+ A_c\,U_{c(n)}\left(\theta_{s(n)} - \theta_{F(n)}\right) + \Sigma Q_{I(n+1)} + \Sigma Q_{I(n)}$$

Re-arranging and re-expressing this equation yields

$$\left(2+\sum_{b=1}^{B} r_{A+b(n+1)} + r_{A+B+1(n+1)}\right)\theta_{F(n+1)} - \sum_{a=1}^{A} r_{a(n+1)}\,\theta_{a(n+1)} - r_{A+a+1(n+1)}\,\theta_{s(n+1)}$$
$$= \left(2-\sum_{b=1}^{B} r_{A+b(n)} - r_{A+B+1(n)}\right)\theta_{F(n)} + \sum_{a=1}^{A} r_{a(n)}\,\theta_{a(n)} + r_{A+a+1(n)}\,\theta_{s(n)} + r_{A+B+2}\left(\Sigma Q_{I(n+1)} + \Sigma Q_{I(n)}\right) \qquad (5.43)$$

where

$$\sum_{a=1}^{A} r_{a(t)} = \sum_{a=1}^{A} \frac{m_{a(t)}\,\overline{C_{pa}}_{(t)}}{S} \quad ; \quad \sum_{b=1}^{B} r_{A+b(t)} = \sum_{b=1}^{B} \frac{\dot{m}_{b(t)}\,\overline{C_{p_F}}_{(t)}}{S}$$

$$r_{A+B+1(t)} = \frac{A_c\,U_{c(t)}}{S} \quad ; \quad r_{A+B+2} = \frac{\Delta\tau}{\left(\rho_F C_F V_F + \sum_{e=1}^{E} \rho_e C_e V_e\right)}$$

As equation (5.43) has identified all heat generation terms associated with a Cateogry 4 node, then $\Sigma Q_{F(t)}$ equates to $Q_{m(t)}$.

Category 5 Node

When generating the flow energy to transport a fluid through a particular system, the fan or pump, not being 100% efficient, will exchange energy with the surrounds and with the fluid. It is assumed, however, that the fan or pump imparts enough flow energy to overcome the pressure drop in the system due to fluid flow resistances. Figure 5.24 represents the energy balance at this component node. Assuming only one fluid flowpath into and out of the component then applying the GHBE for fluid flow results in the expression

$$2\Delta S_F = Q_{in(t)} - Q_{out(t)} + \Sigma Q_{F(t)} \qquad (5.44)$$

where Qin(t) = $\dot{m}_{(t)}\,\overline{C_{p_{F-1}}}_{(t)}\,\theta_{F-1(t)}$

Qout(t) = $\dot{m}_{(t)}\,\overline{C_{p_F}}_{(t)}\,\theta_{F(t)}$

Qinj(t) = mechanical energy losses injected into the fluid stream

$$\Delta S_F = \frac{\rho_c C_c V_c \left(\theta_{F(n+1)} - \theta_{F(n)}\right)}{\Delta\tau}$$

c = component (i.e. fan or pump)

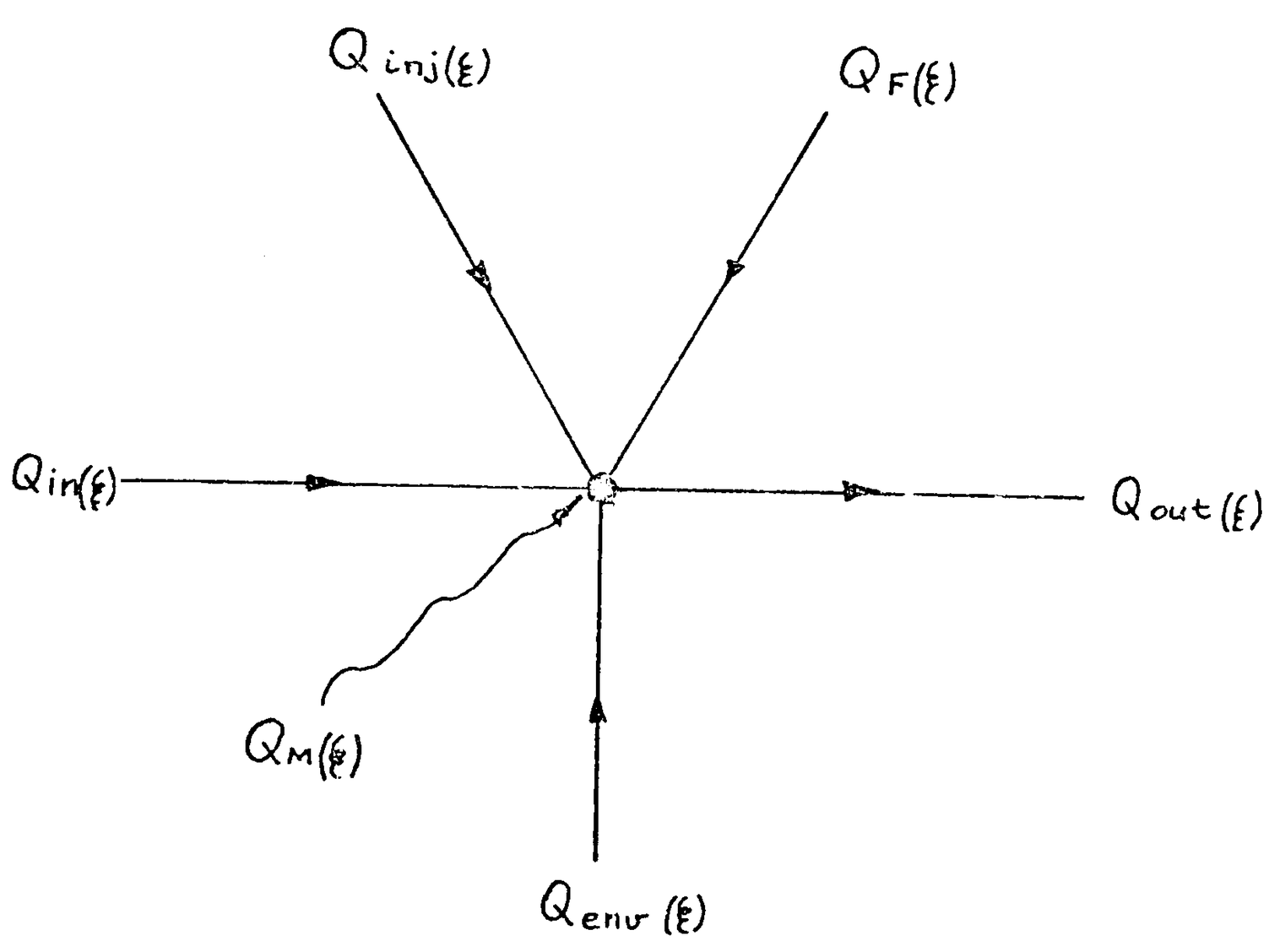

Figure 5.24 Energy balance on category 5 node

It is assumed that the fluid has negligible storage capacity within the component because of a small volume, and that the component is isothermal.

Equation (5.44) can be re-expressed and re-arranged to give

$$(2+\Delta_{1(n+1)})\,\theta_{F(n+1)} - \Delta_{2(n+1)}\,\theta_{F-1(n+1)} = (2-\Delta_{1(n)})\,\theta_{F(n)}$$

$$+\Delta_{2(n)}\,\theta_{F-1(n)} + \Delta_3\left(\Sigma Q_{F(n+1)} + \Sigma Q_{F(n)}\right) \qquad (5.45)$$

where,

$$\Delta_{1(\xi)} = \frac{\dot{m}_{(\xi)}\,\overline{C_{p_F}}_{(\xi)}}{S} \quad ; \quad \Delta_{2(\xi)} = \frac{\dot{m}_{(\xi)}\,C_{p_{F-1}(\xi)}}{S}$$

$$\Delta_3 = \frac{1}{S} = \frac{\Delta\tau}{\rho_c C_c V_c}$$

The summation of the heat generation terms are

$$\Sigma Q_{F(\xi)} = Q_{inj(\xi)} + Q_{env(\xi)} + Q_{cond(\xi)} + Q_{M(\xi)} \qquad (5.46)$$

where Qenv(ξ)= the energy exchange between the component and its surrounds

Qcond(ξ)= the energy exchange due to conduction if conduit is used in the absorber plate of liquid collectors.

Equation (5.46) can be substituted for $\Sigma Q_{F(\xi)}$ in equation (5.45).

Category 6 Node

An auxiliary heater can be treated in a similar manner to a fan or pump. Conducting an energy balance on a node representing an auxiliary heater (Figure 5.25) and substituting into the GHBE for fluid flow yields:

$$2\Delta S_F = Q_{in(\xi)} - Q_{out(\xi)} + \Sigma Q_{F(\xi)} \qquad (5.47)$$

This expression is similar to equation (5.44), however, the storage capacity of the fluid in an auxiliary heater may be significant whereas

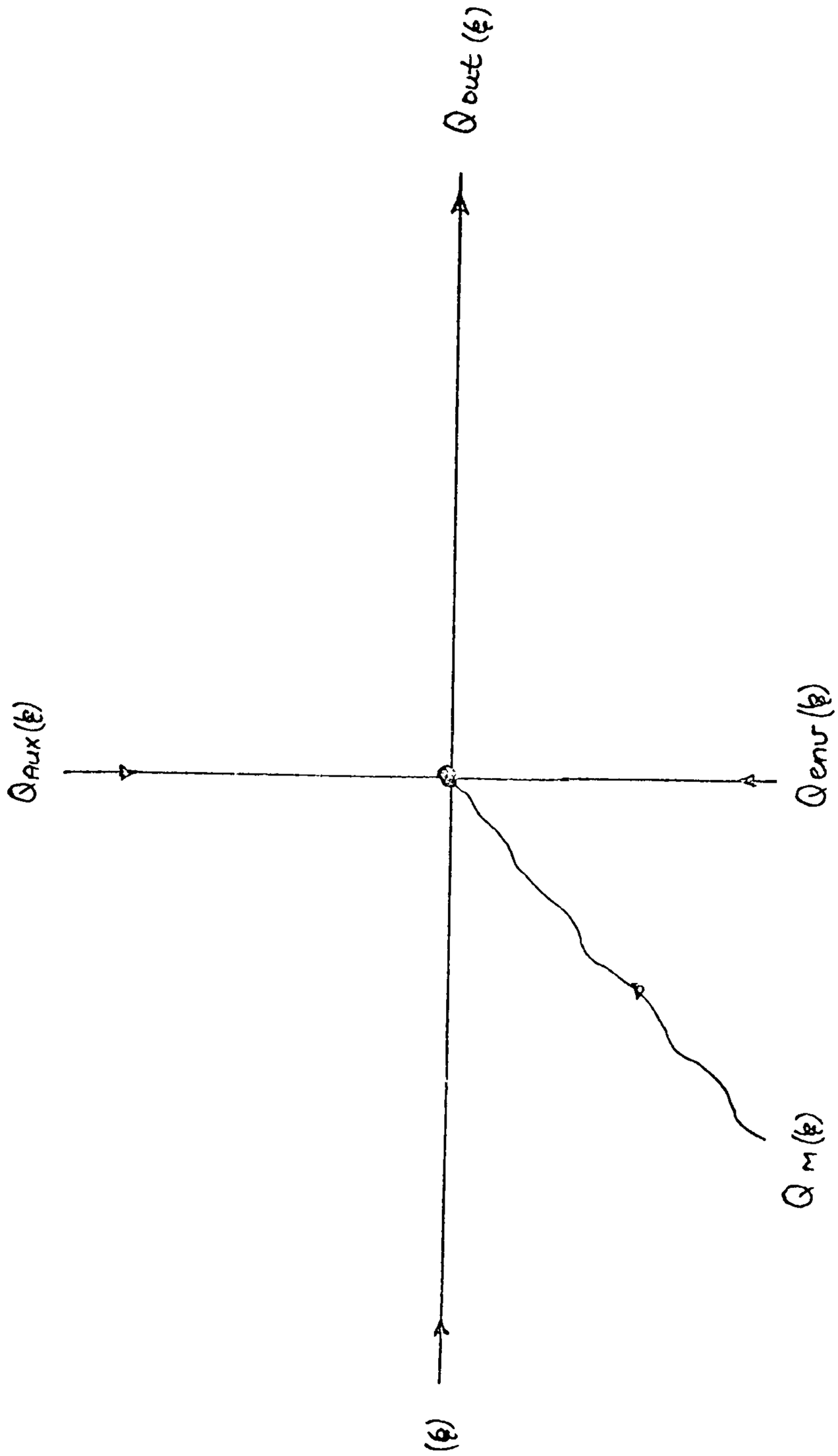

Figure 5.25 Energy balance on category 6 node

in a fan or pump it was considered to be negligible, therefore,

$$\Delta S_F = \frac{(\rho_c C_c V_c + \rho_F C_F V_F)}{\Delta \tau} (\theta_{F(n+1)} - \theta_{F(n)})$$

The solution of equation (5.47) gives an expression which has the same form as equation (5.45). Using the notation given for a Category 5 node:

$$(2 + t_{1(n+1)})\theta_{F(n+1)} - t_{2(n+1)}\theta_{F-1(n+1)} = (2 - t_{1(n)})\theta_{F(n)}$$

$$+ t_{2(n)}\theta_{F-1(n)} + t_3(\Sigma Q_{F(n+1)} + \Sigma Q_{F(n)}) \qquad (5.48)$$

where,

$$t_1(\xi) = \frac{\dot{m}(\xi)\,\overline{C_p}_{F(\xi)}}{S} \quad ; \quad t_2(\xi) = \frac{\dot{m}(\xi)\,\overline{C_p}_{F-1}(\xi)}{S}$$

$$t_3 = \frac{1}{S} = \frac{\Delta \tau}{\rho_c C_c V_c + \rho_F C_F V_F}$$

and

$$\Sigma Q_F(\xi) = Q_{aux}(\xi) + Q_{env}(\xi) + Q_M(\xi) \qquad (5.49)$$

The Qaux(ξ) term has the same effect as the energy injection term in equation (5.44), however, it is a far more controlled and deliberate heat injection used for the specific purpose of obtaining a desired outlet temperature.

Category 7 Nodes

Two types of models have been identified to analyse a heat exchanger: a two node model and a one node model, but before these nodes are derived, the energy processes within the heat exchanger in this model require clarification.

The maximum possible rate of heat transfer between the two fluids for specified inlet fluid temepratures is attained when one of the two fluids undergoes the maximum temperature difference in the exchanger. This maximum equals the difference in the entering temperatures for

the hot and the cold fluid, which of the two fluids undergoes this maximum temperature change depends on the relative value of the heat capacity, C, of either fluid where,

$$C = M_f \overline{C_{p,f}} \qquad (WK^{-1})$$

Assuming negligible heat losses in the heat exchanger then for energy balance the energy given up by the hot fluid must be received by the cold fluid, only the fluid with the small heat capacity, C, can undergo the maximum temperature change, therefore, the maximum rate of heat transfer is

$$Qmax = \dot{C}min(\theta h,_{in} - \theta c,_{in})$$

where $\dot{C}min$ is the minimum heat capacity and can be either the hot fluid - denoted h - or the cold fluid, denoted c. The actual rate of heat transfer is somewhat less than the maximum value, the ratio between these two values is called the exchanger effectiveness, ε, where:

$$\varepsilon = \frac{\text{actual rate of heat transfer}}{\text{maximum possible rate of heat transfer}}$$

Therefore, the actual rate of heat transfer Q_T is,

$$Q_T = \varepsilon\, Qmax$$
$$Q_T = \varepsilon\, \dot{C}min(\theta h,_{in} - \theta c,_{in}) \qquad (5.50)$$

Analysing only the energy transfer between the two fluids, and using the GHBE for the hot fluid then,

$$\cdot \quad Z\Delta S_h = \dot{C}_{h(\xi)}(\theta_{h,in(\xi)} - \theta_{h,out(\xi)}) - Q_{T(\xi)} \qquad (5.51a)$$

and the cold fluid:

$$Z\Delta S_c = \dot{C}_{c(\xi)}(\theta_{c,in(\xi)} - \theta_{c,out(\xi)}) + Q_{T(\xi)} \qquad (5.51b)$$

The method of treating the heat exchanger as two interconnected Category 4 nodes uses equations (5.51a) and (5.51b) as the basis of the two node heat exchanger model. The connection between the two nodes ensures that the quantity of energy received at one node equates to the energy lost from the other node. When using a single node model to represent all the heat transfer processes in the heat exchanger it is necessary to sum the effects of the two node model, suggesting the combination of equations (5.51a) and (5.51b), however, adding these equations results in the energy transfer term $Q_{T(\xi)}$ being summated to zero. It is necessary therefore to re-express equation (5.51b) for the cold fluid to the following form:

$$-2\Delta S_c = \dot{C}_c(\xi)\left(\theta_{c,out}(\xi) - \theta_{c,in}(\xi)\right) - Q_T(\xi) \qquad (5.51c)$$

Two different node types are identified for a heat exchanger - the first to model a two node heat exchanger model, the second to model a heat exchanger represented by a single node.

a) Type 1 - Node to Represent Either Node in a Two Node Heat Exchanger Model

The energy exchange for the hot or the cold fluid can be expressed mathematically by a single expression:

$$2\Delta S_F = \dot{C}_F(\xi)\left(\theta_{F,out}(\xi) - \theta_{F,in}(\xi)\right) \pm Q_T(\xi) + \Sigma Q_I(\xi) \qquad (5.52)$$

where F = hot or cold fluid

$Q_{T(\xi)}$ = heat transfer from the hot fluid (-ve) or heat transfer to the cold fluid (-ve)

Substituting equation (5.50) for $Q_{T(\xi)}$, equation (5.52) becomes:

$$2\Delta S_F = \dot{C}_F(\xi)\left(\theta_{F,out}(\xi) - \theta_{F,in}(\xi)\right) \pm \varepsilon(\xi)\dot{C}_{min}(\xi)\left(\theta_{h,in}(\xi) - \theta_{c,in}(\xi)\right) + \Sigma Q_F(\xi) \qquad (5.53)$$

where $\varepsilon(\xi)$ for various heat exchangers is given in Table 5.1, in which

FLOW GEOMETRY	RELATIONSHIP
Double Pipe	
Parallel Flow	$\varepsilon = \dfrac{1 - \exp[-N(1+C)]}{(1+C)}$
Counter Flow	$\varepsilon = \dfrac{1 - \exp[-N(1-C)]}{1 - C\exp[-N(1-C)]}$
Cross Flow	
$\dot{C}_{max,mixed}$; $\dot{C}_{min,unmixed}$	$\varepsilon = (1/C)\{1 - \exp[C(1-e^{-N})]\}$
$\dot{C}_{max,unmixed}$; $\dot{C}_{min,mixed}$	$\varepsilon = 1 - \exp\{(1/C)[1 - \exp(-NC)]\}$
Shell and Tube	
One shell pass 2,4,6 tube passes	$\varepsilon = 2\left\{1+C+(1+C^2)^{1/2}\left(\dfrac{1+\exp[-N(1+C^2)^{1/2}]}{1-\exp[-N(1+C^2)^{1/2}]}\right)\right\}^{-1}$

Table 5.1 Heat Exchanger Effectiveness Relationships (20).

Nb. $N = NTU = \dfrac{UA}{\dot{C}_{min}}$; $C = \dfrac{\dot{C}_{min}}{\dot{C}_{max}}$

$\varepsilon(\phi)$ is a function of two ratios, the Number of Thermal Units (NTU) and the ratio of the heat capacities of the two fluids, i.e.

$$NTU = \frac{UA}{\dot{C}_{min}} \quad \text{and} \quad C = \frac{\dot{C}_{min}}{\dot{C}_{max}}$$

where UA is the product of the overall heat transfer coefficient and the contact area.

The fluid in and out values correspond to nodes F-1 and F respectively see Figure (5.12). Rearranging equation (5.53) for the hot side fluid gives

$$(2 - U_{1(n+1)})\,\theta_{H(n+1)} + (U_{1(n+1)} + U_{2(n+1)})\,\theta_{H-1(n+1)} - U_{2(n+1)}\,\theta_{C-1(n+1)}$$

$$= (2 + U_{1(n)})\,\theta_{H(n)} - (U_{1(n)} + U_{2(n)})\,\theta_{H-1(n)} + U_{2(n)}\,\theta_{C-1(n)} + U_3\,(\Sigma Q_{I(n+1)} + \Sigma Q_{I(n)}) \qquad (5.54a)$$

and for the cold side fluid,

$$(2 - U_{1(n+1)})\,\theta_{C(n+1)} + (U_{1(n+1)} + U_{2(n+1)})\,\theta_{C-1(n+1)} - U_{2(n+1)}\,\theta_{H-1(n+1)}$$

$$= (2 + U_{1(n)})\,\theta_{C(n)} - (U_{1(n)} + U_{2(n)})\,\theta_{C-1(n)} + U_{2(n)}\,\theta_{H-1(n)} + U_3\,(\Sigma Q_{I(n+1)} + \Sigma Q_{I(n)}) \qquad (5.54b)$$

where

$$U_{1(\xi)} = \frac{\dot{C}_{F(\xi)}}{S} \quad ; \quad U_{2(\xi)} = \frac{\varepsilon(\xi)\,\dot{C}_{min(\xi)}}{S}$$

$$U_3 = \frac{1}{S} = \frac{\Delta\tau}{\rho_F C_F V_F}$$

F = hot fluid node, H, or cold fluid node, C

F-1 = hot fluid node, H-1, or cold fluid node, C-1

The summation of the heat generation terms unconsidered by equations (5.54a) and (5.54b) are given by equation (5.55)

$$\Sigma Q_{I(\xi)} = Q_{env(\xi)} + Q_{M(\xi)} \qquad (5.55)$$

b) Type 2 - Single Node Representation of Heat Exchanger

The equation for a single node model of a heat exchanger is established either from the GHBE for fluid flow or from the addition of equations (5.51a) and (5.51c) plus a heat generation term to account for other losses or gains to the heat exchanger - Figure 5.13 - thus

$$2\Delta S_H - 2\Delta S_c = \dot{C}_{H(\xi)}\left(\theta_{H-1(\xi)} - \theta_{H(\xi)}\right) + \dot{C}_c\left(\theta_{c(\xi)} - \theta_{c-1(\xi)}\right) - 2Q_T(\xi) + \Sigma Q_I(\xi)$$

(5.56)

This equation may be expanded to give:

$$\frac{2\left[\rho_H C_H V_H\left(\theta_{H(n+1)} - \theta_{H(n)}\right) - \rho_c C_c V_c\left(\theta_{c(n+1)} - \theta_{c(n)}\right)\right]}{\Delta\tau} =$$

$$\dot{C}_{H(n+1)}\left(\theta_{H-1(n+1)} - \theta_{H(n+1)}\right) + \dot{C}_{H(n)}\left(\theta_{H-1(n)} - \theta_{H(n)}\right) + \dot{C}_{c(n+1)}\left(\theta_{c(n+1)} - \theta_{c-1(n+1)}\right)$$

$$+ \dot{C}_{c(n)}\left(\theta_{c(n)} - \theta_{c-1(n)}\right) - 2\varepsilon_{(n+1)}\dot{C}_{min(n+1)}\left(\theta_{H-1(n+1)} - \theta_{c-1(n+1)}\right)$$

$$- 2\varepsilon_{(n)}\dot{C}_{min(n)}\left(\theta_{H-1(n)} - \theta_{c-1(n)}\right) + \Sigma Q_{I(n+1)} + \Sigma Q_{I(n)}$$

After re-arrangement this equation can be re-written in the form:

$$\left(U_1 + U_{3(n+1)}\right)\theta_{H(n+1)} - \left(U_2 + U_{4(n+1)}\right)\theta_{c(n+1)} + \left(U_{5(n+1)} - U_{3(n+1)}\right)\theta_{H-1(n+1)}$$

$$+\left(U_{4(n+1)} - U_{5(n+1)}\right)\theta_{c-1(n+1)} = \left(U_1 - U_{3(n)}\right)\theta_{H(n)} + \left(U_{4(n)} - U_2\right)\theta_{c(n)}$$

$$+\left(U_{3(n)} - U_{5(n)}\right)\theta_{H-1(n)} + \left(U_{5(n)} - U_{4(n)}\right)\theta_{c-1(n)} + \Sigma Q_{I(n+1)} + \Sigma Q_{I(n)}$$

(5.57)

where,

$$U_1 = \frac{2\rho_H C_H V_H}{\Delta\tau} \quad ; \quad U_2 = \frac{2\rho_c C_c V_c}{\Delta\tau}$$

$$U_{3(\xi)} = C_{H(\xi)} \quad ; \quad U_{4(\xi)} = C_{c(\xi)}$$

$$U_{5(\xi)} = 2\varepsilon_{(\xi)}\dot{C}_{min(\xi)}$$

and equation (5.55) is used to describe the $\sum Q_{I(\epsilon)}$ term.

Until extensive validation tests have been conducted, it is unknown whether the two-node or the single node heat exchanger model is more accurate. There is only a slight difference to the computation cost and speed of simulation due to a two node model, compared to a single node model, therefore, until the accuracy of the models are assessed either Type 1 or Type 2 nodes can be used to model the heat exchanger.

Category 8 Nodes

The philosophy behind the modelling of a latent energy storage unit is different from all previous nodes because it allows a energy to be added or withdrawn from the store at a constant temperature during its latent phase. Sensible storage can be modelled as any other node where energy added to the store results in a rise in the temperature of the storage medium. Thermal stratification is very important in sensible energy storage units, therefore, several nodes may be required to model a sensible storage unit to adequately analyse thermal stratification. It is assumed there is little stratification in a latent storage unit and a single node is sufficient to model the unit.

a) Type 1 - Liquid Sensible Energy Storage Node

Hot water is generally stored in an insulated upright cylindrical tank. This tank geometry promotes thermal stratification causing the water temperature at the top of the tank to be somewhat hotter than at the bottom. Thermal stratification is desirable because the hot water supplied to the load (drawn from the top of the tank) is hotter than it would be in a fully mixed tank. In addition, a liquid solar collector will operate more efficiently, particularly if the system is direct because the temperature of the water at the bottom of the tank is much lower compared to a fully mixed tank, thus, colder water is passed back to the solar collector.

The thermal performance of a liquid-filled sensible storage tank, subject to thermal stratificaiton, can be modelled by assuming that

the tank consist of N fully mixed equal volume segments, as shown in Figure (5.15). The degree of stratification is determined by the value of N. If N is equal to one, the storage tank is modelled as a fully mixed tank and no stratification effects are possible. It is assumed that an electric resistance heating element subject to temperature or time control is optionally included in each stratification layer, allowing the addition of electrical energy to the tank during selected periods. As the tank may be indirect a conduit is passed through the tank segment and it exchanges heat with the fluid.

Fluid flow between segments can be due to two factors:

- Natural convective flow across the segment boundary if the upper segment is at a lower temperature than the lower segment.

- External flows into or out of the storage tank set up upward and downward flows between segments, Figure 5.26.

Fluid flow between these thermally stratified segments is considered to be fully mixed and at the temperature of the segment from where it came.

Conducting an energy balance on the Xth segment, Figure 5.27, in terms of the GHBE for fluid flow it can be written that

$$2\Delta S_x = \sum_{i=1}^{I} Q_{i,in}(\xi) - \sum_{j=1}^{J} Q_{j,x\ out.}(\xi) \pm \sum_{k=0}^{K} Q_{k,s}(\xi) + \sum_{l=0}^{L} Q_{l,M}(\xi)$$

$$+ Q_{loss}(\xi) + Q_{HE}(\xi) + Q_{E}(\xi) + \Sigma Q_x(\xi) \qquad (5.58)$$

where

I = the number of external flowpaths into segment X

$Q_{i,in}(\xi)$ = the energy contained in fluid flowpath, i, entering the storage tank at segment X,

$$Q_{i,in}(\xi) = \dot{m}_{j,x}(\xi)\,\overline{C_{pf,x}}(\xi)\,\Theta_x(\xi) \qquad (5.59)$$

J = the number of external flowpaths leaving segment X

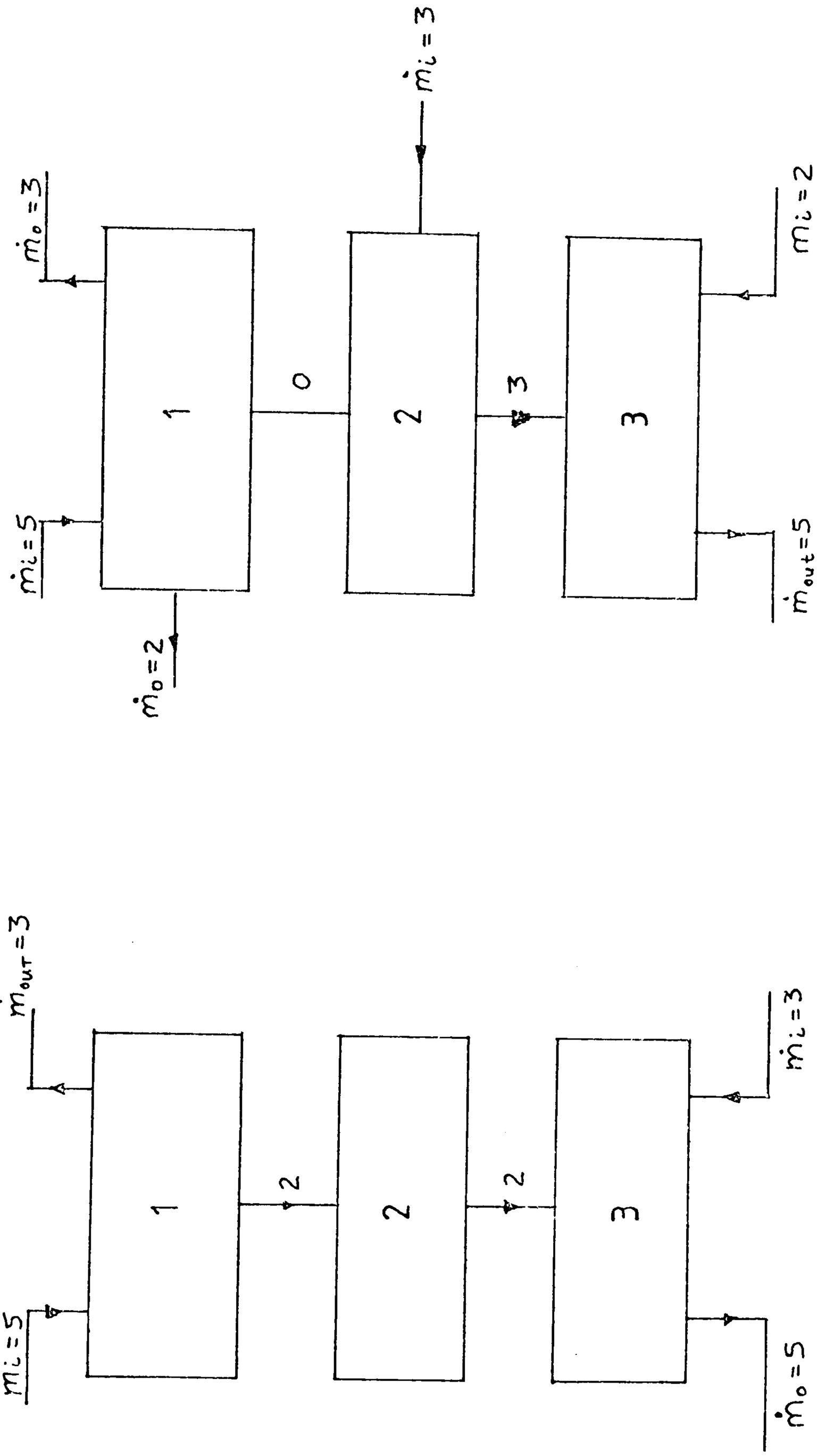

Figure 5.26 Examples of intra-segment fluid flow in a three segment liquid storage tank.

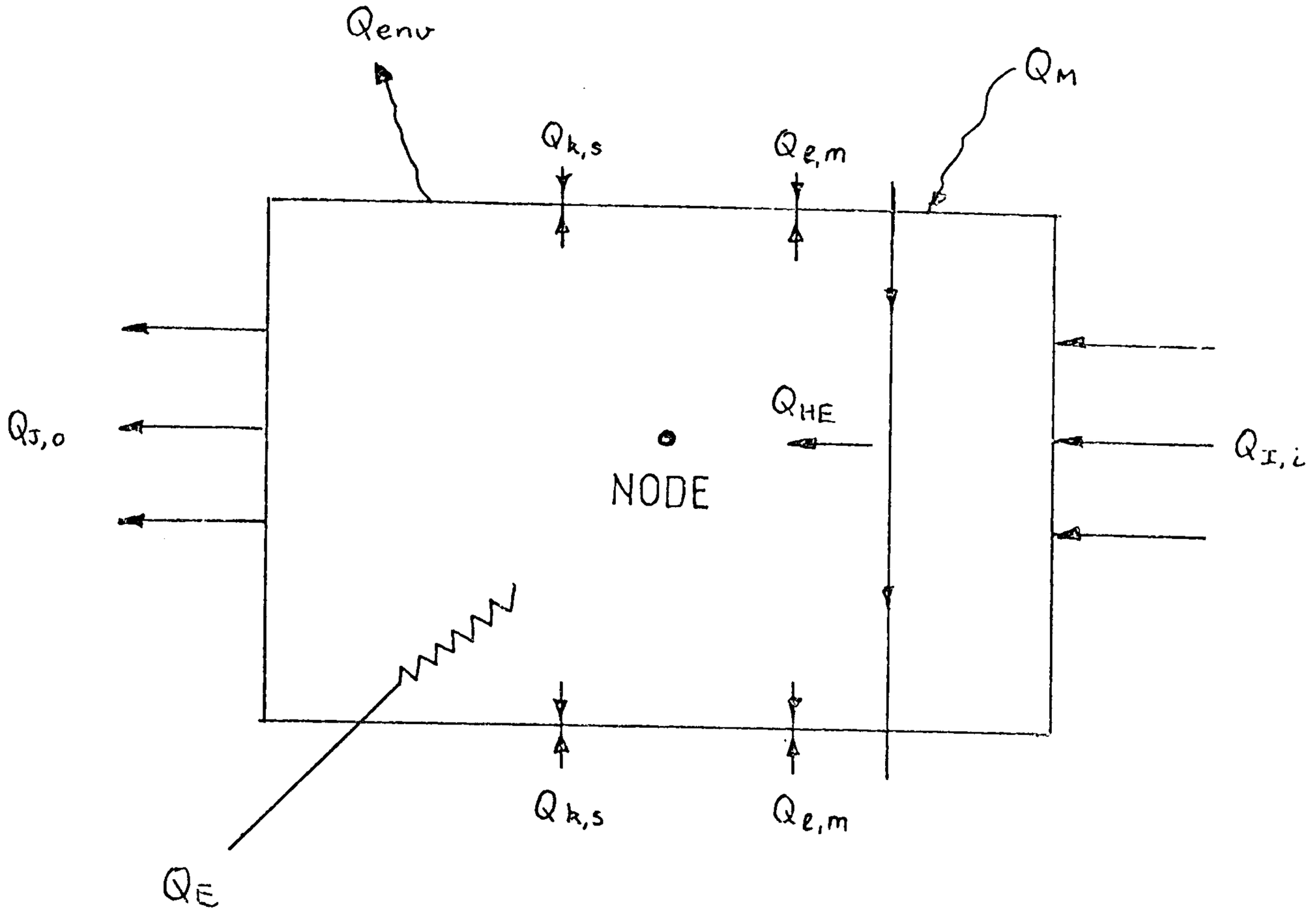

Figure 5.27 Energy flows associated with any segment of the water storage tank.

$Q_{j,x\,out(t)}$ = the energy contained in fluid flowpath, j, leaving the storage tank at segment X at the fluid properties of segment X

$$Q_{j,x\,out(t)} = \dot{m}_{j,x(t)}\,\overline{C_{p_{f,x(t)}}}\,\Theta_{x(t)} \qquad (5.60)$$

$Q_{k,s(t)}$ = the net energy flow between segment X and segments X-1 and X+1 caused by external fluid flows:
if flow is out of segment X then

$$Q_{k,s(t)} = \dot{m}_x\,\overline{C_{p_{f,x}(t)}}\,\Theta_{x(t)}$$

if flow is into segment X then

$$Q_{k,s(t)} = \dot{m}_{N(t)}\,\overline{C_{p_{f,N}(t)}}\,\Theta_{N(t)}$$

where N represents X-1 or X+1

K = number of internal flow streams into or out of the segment, the maximum is two i.e. flow to or from segment X-1 and X+1. If K=1 then only one flow either from X-1 or X+1 or node X could be at the top or bottom of the storage tank. If K=0 either no flow between segments or a one node model of a fully mixed storage tank is used.

$Q_{\ell,M(t)}$ = the energy transported into the upper segment as a result of natural convection occurring due to the upper segment being at a lower temperature compared to the lower segment. Flow from segment X to segment X-1 is

$$Q_{\ell,m(t)} = \dot{m}_{x,x-1(t)}\,C_{p_{f,x(t)}}\left(\Theta_{x-1(t)} - \Theta_{x(t)}\right)$$

flow from segment X+1 into segment X relative to segment X is

$$Q_{\ell,M(t)} = \dot{m}_{x,x+1(t)}\,\overline{C_{p_{f,x}(t)}}\left(\Theta_{x+1(t)} - \Theta_{x(t)}\right)$$

L = number of natural convection flowpaths, the maximum is two, i.e. X to X-1 and X to X+1. if in either of these cases the upper segment is hotter than the lower segment no natural convective movement wili occur between segments.

$Q_{loss(t)}$ = energy lost from segment X to the environment

$$Q_{loss(t)} = U_{(t)}A\left(\Theta_{s(t)} - \Theta_{x(t)}\right) \qquad (5.61)$$

$U(\phi)$ = thermal resistance from the inside of the tank to the ambient environment, ($WM^{-2}K^{-1}$)

A = contact area between tank segment and environment (M^2)

$\theta_{S(\phi)}$ = the ambient temperature of the environment (K)

$Q_{HE(\phi)}$ = the heat exchange between the storage liquid and the fluid flowing through the immersed conduit (Figure 5.27). This applies to indirect tanks only. If a Category 4 node is employed, analysing the conduit by a simple lumped capacitance/resistance model then the energy exchange between the conduit fluid, F, and the liquid in segment X can be found from equation 5.41, thus

$$Q_{HE(\phi)} = A_c U_{c(\phi)} (\theta_{c(\phi)} - \theta_{x(\phi)}) \qquad (5.62)$$

$\theta_{C(\phi)}$ = temperature of conduit fluid (K)

$Q_{E(\phi)}$ = the electrical resistance energy input, (W)

$$\Delta S_x = \frac{\rho_x C_x V_x + \sum_{e=1}^{E} \rho_e C_e V_e}{\Delta \tau} \left(\theta_{x(n-1)} - \theta_{x(n)}\right)$$

E= number of elements in the construction of storage tank.

Using these expressions equation (5.59) can be rewritten to give:

$$2\Delta S_x = \sum_{i=1}^{I} m_{i(n+1)} \overline{C_{pf,i(n+1)}} \theta_{i(n+1)} + \sum_{i=1}^{I} m_{i(n)} \overline{C_{pf,i(n)}} \theta_{i(n)}$$

$$- \sum_{j=1}^{J} \dot{m}_{j,x(n+1)} \overline{C_{pf,x(n+1)}} \theta_{x(n+1)} - \sum_{j=1}^{J} \dot{m}_{j,x(n)} \overline{C_{pf,x(n)}} \theta_{x(n)} + \alpha_{1(n+1)} \beta_{1(n+1)} \dot{m}_{x-1,x(n+1)} \overline{C_{pf,x(n+1)}} \theta_{x-1(n+1)}$$

$$+ \alpha_{1(n)} \beta_{1(n)} \dot{m}_{x-1,x(n)} \overline{C_{pf,x-1(n)}} \theta_{x-1(n)} - \alpha_{1(n+1)} (1 - \beta_{1(n+1)}) \dot{m}_{x,x-1(n+1)} \overline{C_{pf,x(n+1)}} \theta_{x(n+1)}$$

$$- \alpha_{1(n)} (1 - \beta_{1(n)}) \dot{m}_{x,x-1(n)} \overline{C_{pf,x(n)}} \theta_{x(n)} + \alpha_{2(n+1)} (1 - \beta_{2(n+1)}) \dot{m}_{x+1,x(n+1)} \overline{C_{pf,x+1(n+1)}} \theta_{x+1(n+1)}$$

$$+ \alpha_{2(n)} (1 - \beta_{2(n)}) \dot{m}_{x+1,x(n)} \overline{C_{pf,x+1(n)}} - \alpha_{2(n+1)} \beta_{2(n+1)} \dot{m}_{x,x+1(n+1)} \overline{C_{pf,x(n+1)}} \theta_{x(n+1)}$$

$$- \alpha_{2(n)} \beta_{2(n)} \dot{m}_{x,x+1(n)} \overline{C_{pf,x(n)}} \theta_{x(n)} + \gamma_{1(n+1)} \dot{m}_{x,x-1(n+1)} \overline{C_{pf,x(n+1)}} (\theta_{x-1(n+1)} - \theta_{x(n+1)})$$

$$+ \gamma_{1(n)} \dot{m}_{x,x-1(n)} \overline{C_{pf,x(n)}} (\theta_{x-1(n)} - \theta_{x(n)}) + \gamma_{2(n+1)} \dot{m}_{x,x+1(n+1)} \overline{C_{pf,x(n+1)}} (\theta_{x+1(n+1)} - \theta_{x(n+1)})$$

$$+ \gamma_{2(n)} \dot{m}_{x,x+1(n)} \overline{C_{pf,x(n)}} (\theta_{x+1(n)} - \theta_{x(n)}) + U_{(n+1)} A (\theta_{s(n+1)} - \theta_{x(n+1)})$$

$$+ U_{(n)} A (\theta_{s(n)} - \theta_{x(n)}) + A_c U_{c(n+1)} (\theta_{F(n+1)} - \theta_{x(n+1)}) + A_c U_{c(n)} (\theta_{F(n)} - \theta_{x(n)})$$

$$+ Q_{E(n+1)} + Q_{E(n)} + \Sigma Q_{x(n+1)} + \Sigma Q_{x(n)} \qquad (5.63)$$

where, α = 1 when there is fluid flow across the boundary between two segments due to external fluid flow; if there is no fluid flow α = 0. If α = 1 the the flow between segments may be upwards (β = 1) or downwards (β = 0). The boundary between segments X-1 and X is denoted 1, and the boundary between X+1 and X is denoted 2. Also, the value of γ represents the natural convective forces occurring due to the upper segment being at a lower temperature than the lower segment:

if $(\theta_{x-1} - \theta_x) < 0$ $\quad \gamma_1 = 1$ $\quad$ otherwise $\quad \gamma_1 = 0$

if $(\theta_x - \theta_{x+1}) < 0$ $\quad \gamma_2 = 1$ $\quad$ otherwise $\quad \gamma_2 = 0$

Re-arranging equation (5.63) and expressing the general solution for segment or node X in terms of its temperature coefficients:

$$\begin{aligned}
&(2 + W_{I+J+9(n+1)})\,\theta_{x(n+1)} - \sum_{i=1}^{I} W_{i(n+1)}\,\theta_{i(n+1)} - (W_{I+J+1(n+1)} + W_{I+J+5(n+1)})\,\theta_{x-1(n+1)} \\
&- (W_{I+J+3(n+1)} + W_{I+J+6(n+1)})\,\theta_{x+1(n+1)} - W_{I+J+7(n+1)}\,\theta_{S(n+1)} - W_{I+J+8(n+1)}\,\theta_{F(n+1)} \\
&= (2 - W_{I+J+9(n+1)})\,\theta_{x(n)} + \sum_{i=1}^{I} W_{i(n)}\,\theta_{i(n)} + (W_{I+J+1(n)} + W_{I+J+5(n)})\,\theta_{x-1(n)} \\
&+ (W_{I+J+3(n)} + W_{I+J+6(n)})\,\theta_{x+1(n)} + W_{I+J+7(n)}\,\theta_{S(n)} + W_{I+J+8(n)}\,\theta_{F(n)} \\
&+ W_{I+J+10}\,(\Sigma Q_{I(n+1)} + \Sigma Q_{I(n)}) \qquad (5.64)
\end{aligned}$$

where,

$$W_{i(t)} = \frac{\dot{m}_{i(t)}\,\overline{C_{pf,i(t)}}}{S} \quad ; \quad W_{I+j(t)} = \frac{\dot{m}_{j,x(t)}\,\overline{C_{pf,x(t)}}}{S}$$

$$W_{I+J+1(t)} = \frac{\alpha_{1(t)}\,\beta_{1(t)}\,\dot{m}_{x-i,x(t)}\,C_{pf\,x-1(t)}}{S} \quad ; \quad W_{I+J+2(t)} = \frac{\alpha_{1(t)}\,(1-\beta_{1(t)})\,\dot{m}_{x,x-1(t)}\,\overline{C_{pf,x(t)}}}{S}$$

$$W_{I+J+3(t)} = \frac{\alpha_{2(t)}\,(1-\beta_{2(t)})\,\dot{m}_{x+1,x(t)}\,\overline{C_{pf,x(t)}}}{S} \quad ; \quad W_{I+J+4(t)} = \frac{\alpha_{2(t)}\,\beta_{2(t)}\,\dot{m}_{x,x+1(t)}\,\overline{C_{pf,x(t)}}}{S}$$

$$W_{I+J+5(t)} = \frac{\gamma_{1(t)}\,\dot{m}_{x,x-1(t)}\,\overline{C_{pf,x(t)}}}{S} \quad ; \quad W_{I+J+6(t)} = \frac{\gamma_{2(t)}\,\dot{m}_{x,x+1(t)}\,\overline{C_{pf,x(t)}}}{S}$$

$$W_{I+J+9(t)} = \sum_{j=1}^{J} W_{I+j(t)} + W_{I+J+2(t)} + W_{I+J+4(t)} + W_{I+J+5(t)} + W_{I+J+6(t)} + W_{I+J+7(t)} + W_{I+J+8(t)}$$

$$W_{I+J+10(t)} = \frac{1}{S} = \frac{\Delta\tau}{(\rho_x C_x V_x + \sum_{e=1}^{E} \rho_e C_e V_e)}$$

and

$$\Sigma Q_{I(t)} = Q_{c(t)} + Q_{M(t)} \qquad (5.65)$$

Equation (5.64) applies to any segment of either a direct or an indirect liquid energy storage tank with or without thermal stratification. It should be noted that if the tank is direct then $W_{1+3+9}(\theta)$ is zero.

b) Type 2 - Sensible Energy Storage - Rock Bed

The principal difference between rock bed and liquid storage is the medium used to store energy. A greater level of thermal stratification can be achieved with rock bed storage compared to liquid storage, consequently, more segments or nodes may be required to model a rock bed storage unit than a liquid sensible energy storage unit. Similar to a liquid storage unit each of the N equal volume segments are assumed to be at the same temperature, which is θ_I, where I is the temperature of the node representing the segment. However, in a liquid storage unit entering fluid mixes with the fluid node, whereas, in a rock bed storage unit the fluid and rock must be analysed by different nodes.

There is only one entry and exit for the fluid through the rock bed storage unit; although air can flow in either direction. The air is assumed to have a uniform flow distribution through the rock bed. Unlike the liquid storage tank no electrical resistance heating element is included, occasionally however preheat liquid is obtained by passing conduits through the rock bed therefore a conduit/ rock bed heat exchange is considered. Figure 5.28 identifies the heat exchanges involved in a heat balance conducted on segment I, that is node I. The heat balance can be expressed mathematically using the General Heat Balance Equation

$$2\Delta S_I = Q_{Trans}(\theta) + \sum_{k=1}^{K} Q_{I,k\,cond}(\theta) + Q_{HE}(\theta) + Q_{Loss}(\theta) + \Sigma Q_I(\theta) \qquad (5.66)$$

where,

$$Q_{Trans}(\theta) = h_v(\theta)\, V_I \left(\theta_F(\theta) - \theta_I(\theta)\right) \qquad (5.67)$$

$h_v(\theta)$ = rock bed volumetric heat transfer, coefficient (W/M^3K), see Appendix 6 for method of calculation.

V_I = volume of segment I under consideration (M^3)

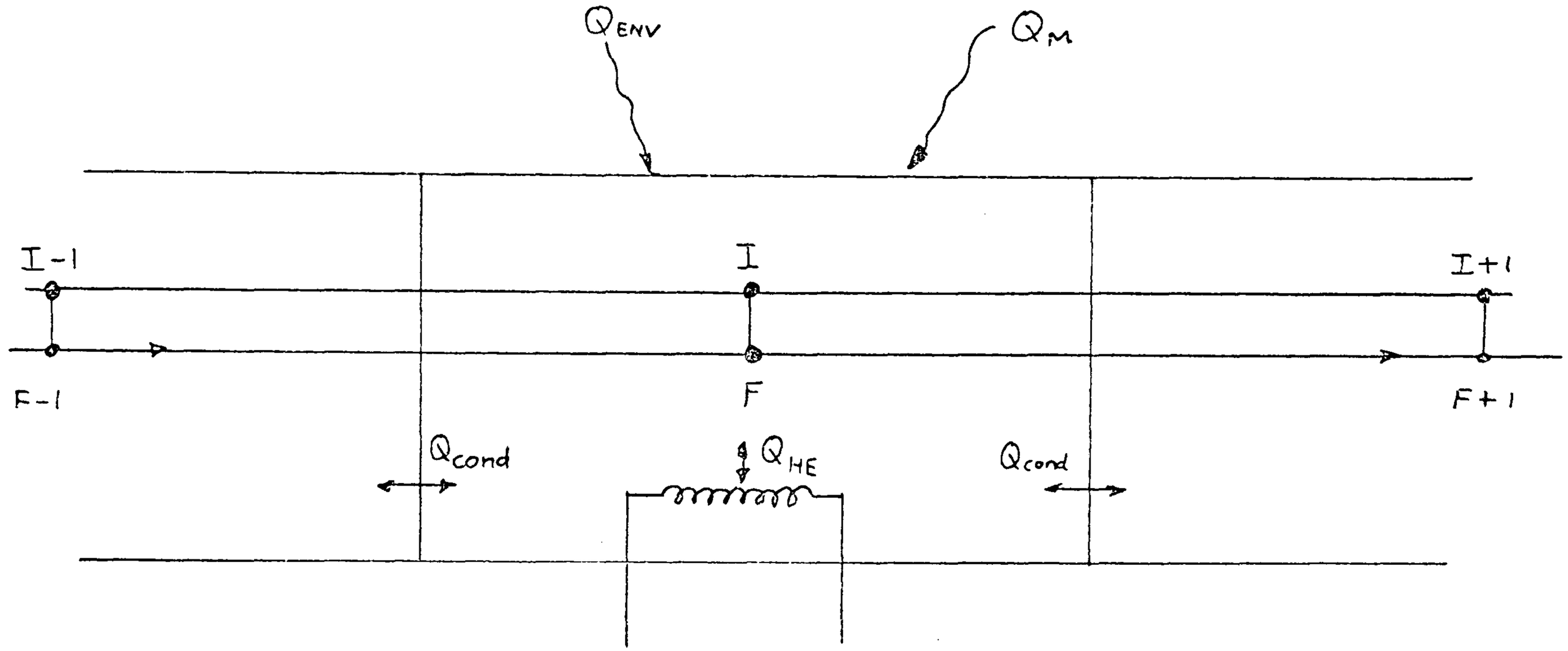

Figure 5.28 Heat exchanges involved in segment I of a rock bed storage unit

$\theta_{F(t)}$ = fluid temperature (degC)

$\theta_{I(t)}$ = temperature of segment I (degC)

$Q_{load(t)}$ = equation (5.61).

$Q_{HE(t)}$ = equation (5.62)

K = number of conduction paths, maximum is two, i.e. I-1 to I and I to I+1. K is only one for the first and last segments of the storage unit

$Q_{I,K\ cond(t)}$ = the conductive heat exchanges across the segment boundaries of node I,

$$Q_{I,K\ cond(t)} = \frac{Ak}{\Delta X}\left(\theta_{N(t)} - \theta_{I(t)}\right)$$

N = nodes I-1 or I+1

A = contact area between segments N (M^2)

k = conductivity of rock or pebble ($WM^{-1}.K^{-1}$)

ΔX = the distance measured between the two segment nodes (M)

$$\Delta S_I = \frac{\rho_R C_R V_R}{\Delta \tau}\left(\theta_{I(n+1)} - \theta_{I(n)}\right)$$

where rock is denoted R. Equation (5.66) can be re-expressed to give,

$$2\Delta S_I = h_{v(n+1)} V\left(\theta_{F(n+1)} - \theta_{I(n)}\right) + h_{v(n)} V\left(\theta_{F(n)} - \theta_{I(n)}\right)$$
$$+ \beta_{(n+1)} \frac{Ak}{\Delta X}\left(\theta_{I-1(n+1)} - \theta_{I(n+1)}\right) + \beta_{(n)} \frac{Ak}{\Delta X}\left(\theta_{I-1(n)} - \theta_{I(n)}\right)$$
$$+ \gamma_{(n+1)} \frac{Ak}{\Delta X}\left(\theta_{I+1(n+1)} - \theta_{I(n+1)}\right) + \gamma_{(n)} \frac{Ak}{\Delta X}\left(\theta_{I+1(n)} - \theta_{I(n)}\right)$$
$$+ A_c U_{c(n+1)}\left(\theta_{c(n+1)} - \theta_{I(n+1)}\right) + A_c U_{c(n)}\left(\theta_{c(n)} - \theta_{I(n)}\right) + U_{(n+1)} A\left(\theta_{s(n+1)} - \theta_{I(n+1)}\right)$$
$$+ U_{(n)} A\left(\theta_{s(n)} - \theta_{I(n)}\right) + \Sigma Q_{I(n+1)} + \Sigma Q_{I(n)} \qquad (5.68)$$

where, β = 1 unless node I is the first node in the storage unit and β =0

γ = 1 unless node I equals node N whereupon γ is set to zero

By restructuring equation (5.68) the following equation is obtained:

$$(2 + x_{6(n+1)})\theta_{I(n+1)} - x_{1(n+1)}\theta_{I-1(n+1)} - x_{2(n+1)}\theta_{I+1(n+1)} - x_{3(n+1)}\theta_{F(n+1)} - x_{4(n+1)}\theta_{C(n+1)}$$
$$- x_{5(n+1)}\theta_{S(n+1)} = (2 - x_{6(n)})\theta_{I(n)} + x_{1(n)}\theta_{I-1(n)} + x_{2(n)}\theta_{I+1(n)} + x_{3(n)}\theta_{F(n)}$$
$$+ x_{4(n)}\theta_{C(n)} + x_{5(n)}\theta_{S(n)} + x_7\left(\Sigma Q_{I(n+1)} + \Sigma Q_{I(n)}\right) \qquad (5.69)$$

where,

$$x_1(\xi) = \frac{\beta(\xi) A k}{S \Delta X} \quad ; \quad x_2(\xi) = \frac{\gamma(\xi) A k}{S \Delta X}$$

$$x_3(\xi) = \frac{h_v(\xi) V}{S} \quad ; \quad x_4(\xi) = \frac{A_c U_c(\xi)}{S}$$

$$x_5(\xi) = \frac{U(\xi) A}{S} \quad ; \quad x_6(\xi) = x_1(\xi) + x_2(\xi) + x_3(\xi) + x_4(\xi) + x_5(\xi)$$

$$x_7 = \frac{1}{S} = \frac{\Delta \tau}{P_R C_R V_R}$$

The $\Sigma Q_I(\xi)$ term equates to the miscellaneous term $Qm(\xi)$. If there is no conduit in the storage unit then set $x_4(\xi)$ to zero. The values of β and γ are dependent on flow direction.

Having established the general difference equation for the rock bed - equation (5.69) - it is now necessary to consider the fluid node in the rock bed.

Conducting an energy balance on the fluid node in a segment of a rock bed storage unit and expressing the result in terms of the GHBE for fluid flow gives,

$$2\Delta S_F = Q_{in}(\xi) - Q_{out}(\xi) + Q_{Trans}(\xi) + \Sigma Q_F(\xi) \qquad (5.70)$$

where

$$Q_{in}(\xi) = \dot{m}(\xi)\, \overline{C_{P\,F-1}}(\xi)\, \theta_{F-1}(\xi)$$

$$Q_{out}(\xi) = \dot{m}(\xi)\, \overline{C_{P\,F}}(\xi)\, \theta_F(\xi)$$

$$Q_{Trans}(\xi) = -h_v(\xi) A \left(\theta_F(\xi) - \theta_I(\xi)\right)$$

$$\Delta S_F = \frac{\rho_A C_A V_A}{\Delta \tau} \left(\theta_{F(n+1)} - \theta_{F(n)}\right)$$

Substituting these expressions into equation (5.70) results in,

$$2\Delta S_F = \dot{m}_{(n+1)}\, \overline{C_{P\,F-1(n+1)}}\, \theta_{F-1(n+1)} + \dot{m}_{(n)}\, \overline{C_{P\,F-1(n)}}\, \theta_{F-1(n)}$$

$$- \dot{m}_{(n+1)}\, \overline{C_{P\,F(n+1)}}\, \theta_{F(n+1)} - \dot{m}_{(n)}\, \overline{C_{P\,F(n)}}\, \theta_{F(n)} + h_{v(n+1)} V \left(\theta_{I(n+1)} - \theta_{F(n+1)}\right)$$

$$+ h_{v(n)} V \left(\theta_{I(n)} - \theta_{F(n)}\right) + \Sigma Q_{I(n+1)} + \Sigma Q_{I(n)}$$

Re-arranging and re-labelling yields,

$$(2+\alpha_{3(n+1)})\,\theta_{F(n+1)} - \alpha_{1(n+1)}\,\theta_{F-1(n+1)} - \alpha_{2(n+1)}\,\theta_{I(n+1)} = (2-\alpha_{3(n)})\,\theta_{F(n)}$$

$$+\alpha_{1(n)}\,\theta_{F-1(n)} + \alpha_{2(n)}\,\theta_{I(n)} + \alpha_4\,(\Sigma Q_{I(n+1)} + \Sigma Q_{I(n)}) \qquad (5.71)$$

where,

$$\alpha_{1(\xi)} = \frac{\dot{m}_{(\xi)}\,\overline{C_{p\,F-1(\xi)}}}{S} \quad ; \quad \alpha_{2(\xi)} = \frac{h_{v(\xi)}\,V}{S}$$

$$\alpha_{3(\xi)} = \alpha_{2(\xi)} + \frac{\dot{m}_{(\xi)}\,\overline{C_{p\,F(\xi)}}}{S} \quad ; \quad \alpha_4 = \frac{1}{S} = \frac{\Delta\tau}{\rho_A\,C_A\,V_A}$$

In equation (5.71) the $\Sigma Q_{I(\xi)}$ term is reduced to $Q_{m(\xi)}$.

As a consequence of the rock bed storage model two nodes will be required for each segment of unit analysed.

c) Type 3 - Node Representing a Latent Heat Energy Storage Unit

There is no thermal stratification considered in a latent energy storage unit, therefore, a single node may be used to represent the unit. The temperature of the unit is complicated because the storage medium is a phase-change material which can gain or lose heat by isothermal phase change. The most common storage media used are those which have a solid to liquid phase-change, these are referred to as the heat of fusion materials. The rate of change of heat stored with respect to time is solved normally in the solid or liquid phases because the rate of change is associated with a change in storage temperature, that is, sensible storage applies. During the isothermal phase-change there is no change in storage temperature therefore the rate of change of heat stored is zero.

Similar to a rock bed storage unit the latent heat storage unit (Figure 5.17) must be modelled using two nodes. Conducting an energy balance on the phase-change material by applying the GHBE results in the following expression

$$2\Delta S_I = Q_{ex(\xi)} + Q_{loss(\xi)} + \Sigma Q_{I(\xi)} \qquad (5.72)$$

where $Q_{ex(\xi)}$ = the energy exchange between the fluid and the storage media. This takes account of the same process as Qtrans(ξ) identified for the rock bed storage unit

$$Q_{ex(\xi)} = U_{ex(\xi)} A_{ex} (\theta_{F(\xi)} - \theta_{I(\xi)})$$

$U_{ex(\xi)}$ = heat loss coefficient between fluid and storage media ($WM^{-2}K^{-1}$)

Aex = area of contact between fluid and storage media (M^2)

and Qloss(ξ) is obtained from equation (5.61).

Equation (5.72) can be re-written in the form:

$$2\Delta S_I = U_{ex(n+1)} A_{ex} (\theta_{F(n+1)} - \theta_{I(n+1)}) + U_{ex(n)} A_{ex} (\theta_{I-1(n)} - \theta_{I(n)})$$

$$+ U_{L(n+1)} A (\theta_{S(n+1)} - \theta_{I(n+1)}) + U_{L(n)} A (\theta_{S(n)} - \theta_{I(n)}) + \Sigma Q_{I(n+1)} + \Sigma Q_{I(n)} \qquad (5.73)$$

now let

$$X = \frac{2 \rho_s C_s V_s}{\Delta \tau} \qquad (5.74)$$

where s denotes storage material. Re-arranging equation (5.73) gives

$$(X + y_{3(n+1)}) \theta_{I(n+1)} - y_{1(n+1)} \theta_{I-1(n+1)} - y_{2(n+1)} \theta_{s(n+1)} = (X - y_{3(n)}) \theta_{I(n)}$$

$$+ y_{1(n)} \theta_{I-1(n)} + y_{2(n)} \theta_{s(n)} + (\Sigma Q_{I(n+1)} + \Sigma Q_{I(n)}) \qquad (5.75)$$

where,

$$y_{1(\xi)} = U_{ex(\xi)} A_{ex} \quad ; \quad y_{2(\xi)} = U_{L(\xi)} A \quad ; \quad y_{3(\xi)} = y_{1(\xi)} + y_{2(\xi)}$$

In equation (5.75) the $\Sigma Q_{I(\xi)}$ term reduces to Qm(ξ). During the solid or liquid sensible heating or cooling phase X is given by equation (5.74), however, during the isothermal phase-change the value of X is zero. Consequently, equation (5.75) applies to both the sensible and latent phases.

The fluid node associated with the latent heat storage unit is the same

as equation (5.70) except that Qtrans(ℓ) is replaced by Qex(ℓ). As a consequence equation (5.71) can be used to describe this node, thus relabelling yields,

$$(2+\gamma_{3(n+1)})\theta_{F(n+1)} - \gamma_{1(n+1)}\theta_{F-1(n+1)} - \gamma_{2(n+1)}\theta_{I(n+1)} = (2-\gamma_{3(n)})\theta_{F(n)}$$

$$+\gamma_{1(n)}\theta_{F-1(n)} + \gamma_{2(n)}\theta_{I(n)} + \gamma_4\left[\Sigma Q_{I(n+1)} + \Sigma Q_{I(n)}\right] \qquad (5.76)$$

where,

$$\gamma_1(\ell) = \frac{\dot{m}(\ell)\,\overline{C_{PF-1}(\ell)}}{S} \quad ; \quad \gamma_2(\ell) = \frac{U_{ex}(\ell)\,A_{ex}}{S}$$

$$\gamma_3(\ell) = \gamma_2(\ell) + \frac{\dot{m}(\ell)\,\overline{C_{PF}(\ell)}}{S} \quad ; \quad \gamma_4 = \frac{1}{S} = \frac{\Delta\tau}{\rho_A C_A V_A}$$

In each of the three Category 8 nodes the energy exchange between the node and its surrounding has been expressed in terms of an overall heat transfer coefficient. If greater accuracy is desired then Cateogry 1 and Category 3 type nodes can be applied to the casing and insulation surrounding the storage unit nodes.

Electrochemical storage (i.e. batteries) is not modelled because it would require a mixed parameter difference equation in terms of temperature and volts and amps. This would require the modification of each general difference equation to suit. When electrochemical storage is required, it is treated as a 'black box' model, that is, only at the completion of each time step will the residual capacity of the battery be assessed in terms of the photovoltaic solar collector performance and the electrical demand over the time increment.

5.3 Heat Generation Sources

In section 5.2.1 each derived general difference equation contains a term denoted by $\Sigma Q_I(\tau)$ which is the summation of the mathematically unconsidered heat generation sources associated with node I at the present (n) and future (n+1) time rows. The purpose of this section is to establish the heat generation terms, associated with each node, contained in $\Sigma Q_J(\tau)$ and use them to write the complete difference equations for each node. Fifteen different heat generation terms were identified in Section 5.2.1 these are:

$Q_{s,\alpha}(\tau)$ = the quantity of solar radiation absorbed by a node at the centre of a transparent homogeneous element at time τ, if the element is opaque then $Q_{s,\alpha}(\tau)$ will be zero.

$Q_{s,\varepsilon}(\tau)$ = the quantity of solar radiation absorbed by an opaque surface or by absorbing thin transparent films deposited on the surface of a transparent element at time τ.

$Q_{s,r}(\tau)$ = the quantity of solar radiation reflected from a planar reflector fixed to a solar collector and absorbed as described above.

$Q_{s,I}(\tau)$ = the quantity of solar radiation absorbed at an internal surface or by absorbing thin films on the inner surface of a transparent cover at time τ.

$Q_{p}(\tau)$ = the quantity of radiative energy converted to electricity by solar cells at time τ. This term applies only to the centre node of the solar cells and is zero if no solar cells are present in the element.

$Q_{liq}(\tau)$ = the energy exchange between an absorber plate node and conduits containing liquid in a liquid collector at time τ.

$Q_{ELWE}(t)$ = the net external longwave radiative exchange at time t between an exposed surface and its surrounds

$Q_{ILWR}(t)$ = the net internal longwave radiative exchange at time t between an internal surface and all other internal surfaces with which it is in radiative contact.

$Q_{rain}(t)$ = the energy exchange at an exposed surface at time t due to the effects of precipitation.

$Q_{inj}(t)$ = the energy injected into a fluid passing through a fan or pump at time t due to mechanical losses.

$Q_{env}(t)$ = the energy exchange between the surface of certain components and its surrounds at time t .

$Q_{aux.}(t)$ = the auxiliary energy injected into a fluid at time t by an auxiliary heater.

$Q_E(t)$ = the energy generated by an electric resistive element in a liquid storage tank at time t .

$Q_{cond}(t)$ = the energy exchange due to conduction in a liquid collector between the fluid node and an absorber plate node at time .

$Q_M(t)$ = a miscellaneous heat injection term.

A summary of the heat generation terms associated with each node is presented in Table 5.2

Three types of surfaces have been identified for Category 3 nodes, therefore, it is possible to be more specific concerning the heat injection nodes for a surface than using equation (5.34).

1. An external surface exposed to climatological influences:

$$\sum Q_I(t) = Q_{s,\varepsilon}(t) + Q_{s,\kappa}(t) + Q_{\varepsilon LWE}(t) + Q_{rain}(t) + Q_{inj}(t) + Q_M(t) \qquad (5.77)$$

Category	Nodes	$\sum Q_I(\xi)$	Equation
1	1-4	$Q_{s,\alpha}(\xi) + Q_{p(\xi)} + Q_{liq}(\xi) + Q_M(\xi)$	5.9
1	5-9	$Q_{liq}(\xi) + Q_M(\xi)$	5.18
2	ALL	$Q_M(\xi)$	5.32
3	ALL	$Q_{s,E}(\xi) + Q_{s,R}(\xi) + Q_{s,I}(\xi) + Q_{ELWR}(\xi) + Q_{ILWR}(\xi) + Q_{rain}(\xi) + Q_{liq}(\xi) + Q_M(\xi)$	5.34
4	ALL	$Q_M(\xi)$	5.43
5	ALL	$Q_{inj}(\xi) + Q_{env}(\xi) + Q_{cond}(\xi) + Q_M(\xi)$	5.46
6	ALL	$Q_{aux}(\xi) + Q_{env}(\xi) + Q_M(\xi)$	5.49
7	ALL	$Q_{env}(\xi) + Q_M(\xi)$	5.55
8	1	$Q_E(\xi) + Q_M(\xi)$	5.65
8	2-3	$Q_M(\xi)$	5.69

TABLE 5.2 Summary of the heat injection terms associated with each nodal category

2. An internal surface of an enclosure:

$$\Sigma Q_I(t) = Q_{s,I}(t) + Q_{I,wx}(t) + Q_{liq}(t) + Q_m(t) \qquad (5.78)$$

3. An external surface not exposed to climatological influences. The sum of the heat generation sources is in the same format as equation (5.78).

Figure 5.29 shows the heat generation sources at these surfaces.

The values of the heat generation terms are known at the present time value, however, the future heat generation terms may be either known or unknown. If the values are unknown because they are dependent upon some future nodal temperature then they are transferred to the left-hand side of the difference equation to be solved. There are however several future heat generation terms which are known because they are not a function of future nodal temperatures or the sources are known at the future time row. These terms can be passed to the known or right-hand side of the difference equation.

The following section will identify the mathematical models associated with each heat generation source described above.

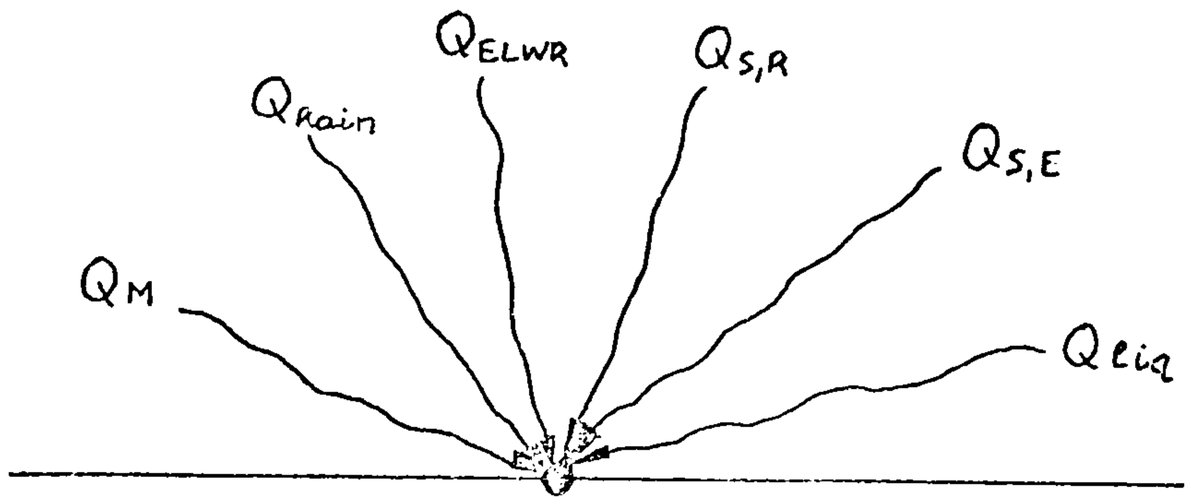

Figure 5.29(a) Node positioned on an external exposed surface

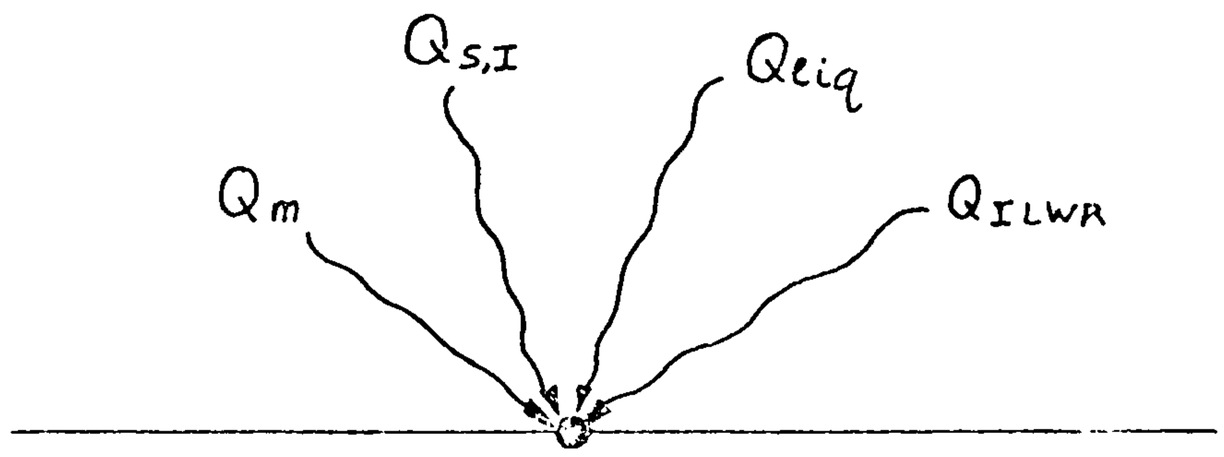

Figure 5.29(b) Node positioned on an internal surface or an external non-exposed surface

5.3.1 Solar Radiation

Consider solar radiation incident upon a flat plate solar collector, if it falls on the exposed opaque external surfaces of the collector enclosure it will be partially absorbed and partially reflected, whereas solar radiation incident upon exposed transparent surfaces is simultaneously absorbed, reflected and transmitted. The transmitted component is partially absorbed and partially reflected at that internal surface upon which it falls. In a photothermal collector the internal surface temperatures of the enclosure will rise due to the absorbed solar radiation and this energy can be transferred by convection to a fluid and transported away from the collector. A photovoltaic collector will convert some of the transmitted solar radiation incident upon its solar cells to electricity.

The model has access to a climate file (Chapter 3) containing hourly values of direct normal and horizontal diffuse solar irradiance, denoted Gbn and Gdh respectively. The derivations that follow assume the availability of this data as a starting point or boundary condition.

The spectral characteristics of solar radiation were discussed in Section 1.2. The terrestrial solar spectrum is given as a function of site, sky conditions and zenith angle of the sun (21). If, for example, the reflectivity (ρ) of an opaque transparent surface is a function of wavelength only, the total reflectance of the surface can be predicted by integrating over the whole solar spectrum, thus,

$$\rho = \frac{\int_{\lambda_1}^{\lambda_2} I_\lambda \tau_\lambda \, d\lambda}{\int_{\lambda_1}^{\lambda_2} I_\lambda \, d\lambda}$$

where I_λ = the solar intensity at wavelength λ

ρ_λ = the spectral reflectivity at wavelength λ

λ_1 = the shortest wavelength in the solar spectrum

λ_2 = the largest wavelength in the solar spectrum

Similarly values for the total absorptance (α) and total transmittance (τ) could be obtained. Frequently continuous spectral data is

unavailable, instead the average spectral value of a property is given for specific wavebands within the solar spectrum. The total solar reflectance, therefore, may be evaluated by modifying the integral expression, thus

$$\rho = \sum_{i=1}^{N} I_{\Delta\lambda i}\, \rho_{\Delta\lambda i}\, \Delta\lambda i \Big/ \sum_{i=1}^{N} I_{\Delta\lambda i}\, \Delta\lambda i$$

where N is the number of wavebands into which the solar spectrum is divided, $I_{\Delta\lambda i}$ is the solar intensity contained within waveband i (i.e. λi to $\lambda i + \Delta\lambda i$), and $\rho_{\Delta\lambda i}$ is the average reflectivity in waveband i.

It is assumed that average values of surface properties are used within each waveband, therefore, each waveband can be considered to be monochromatic in nature and the waveband can be represented by a single value which is deemed to be at the wavelength where the solar intensity equals the mean value of the solar intensities integrated over the waveband. Consequently, a spectral problem is reduced to an analysis on a series of wavelengths representing a series of monochromatic wavebands. The simplest case arises when there is only one waveband considered, in the situation solar radiation is regarded as being monochromatic.

In this work the properties of non-selective opaque surfaces are assumed to be independent of wavelength, for the analysis of these surfaces monochromatic solar radiation is suitable. The values of the properties for selective opaque or transparent surfaces may be dependent of wavelength, therefore, they can be modelled either spectrally or monochromatically.

The sum of the direct, diffuse and ground reflected solar radiation incident upon an exposed external surface at any time t is $Q_{s,\varepsilon}(t)$ and it is a function of geometry and surface properties. The total direct solar irradiance incident on an exposed transparent or opaque surface inclined at angle to the horizontal at time t is given by

$$q_{D}(t) = G_{dn}(t) \cos \theta_{i,D}(t)$$

where $q_{D}(t)$ = the incident direct radiation on an exposed surface (WM^{-2})

$\theta_{i,D}(t)$ = the angle of incidence between the sun's rays and the normal to the surface

t = n or n+1

The angle of incidence for a fixed non-tracking surface is established in Appendix 1, is written

$$\cos\theta_{i,D}(t) = \sin\alpha(t)\cos\beta(t) - \sin\beta(t)\cos\alpha(t)\cos[\gamma(t) - \chi(t)]$$

where $\alpha(t)$ = the solar altitude above the horizon

$\gamma(t)$ = the solar azimuth

$\chi(t)$ = orientation of the surface

If the solar collector is attached to a tracking device then the surface tilt and orientation will vary with time. Table 5.3 details the solution for $\cos\theta_{i,D}$ for a variety of tracking collectors.

The total diffuse radiaiton from the sky incident upon an exposed surface inclined at β at time t is given by $q_{d}(t)$, where

$$q_{d}(t) = G_{dh}(t)\left(\frac{1+\cos\beta(t)}{2}\right)$$

This assumes isotropic sky conditions and it underestimates the total irradiance on south facing surfaces by 4-5%, therefore, a different model has been proposed for anisotropic sky conditions (57)

$$q_{d}(t) = G_{dh}(t)\left(\frac{1+\cos\beta(t)}{2}\right)\left[1 + F(t)\cos^{2}\theta_{i}(t)\sin^{3}(90-\alpha(t))\right]$$

$$*\left[1 + F(t)\sin^{3}\left(\frac{\beta(t)}{2}\right)\right]$$

where

$$F(t) = \left(1 - \frac{G_{dh}(t)}{G_{h}(t)}\right)$$

DESCRIPTION	AXIS (AXES)	COSINE OF INCIDENCE ANGLE (cos i)
1. Two-axis fully tracking collector	Horizontal axis and vertical axis	1
2. Uniform rotation about a solar axis	Polar axis	$\cos\delta$
3. East-West horizontal	Horizontal, east-west axis	$(1 - \cos^2\alpha \sin^2 a_s)^{1/2}$
4. North-South horizontal	Horizontal, north-south axis	$(1 - \cos^2\alpha \cos^2 a_s)^{1/2}$
5. Rotation of a horizontal collector about a vertical axis	Vertical axis	$\sin\alpha$
6. Rotation of a vertical axis surface about a vertical axis	Vertical axis	$\cos\alpha$
7. Rotation about a vertical axis of a surface tilted upward at β^o	Vertical axis	$\sin(\alpha+\beta)$

TABLE 5.3 Tracking schemes and solar incidence angles (20)

$G_h(\xi)$ = the horizontal global irradiance (WM^{-2}) which can be found from equation (3.1) in Chapter 3.

However, the isotropic model is more accurate for north, east and west surface orientations, therefore, the isotropic model will be used for all surface orientations which are facing away from the sun's disc (i.e. self shaded) while the anisotropic model is used for surfaces facing the sun. For an isotropic sky the effective angle of incidence of the diffuse solar radiation can be calculated from the following expression derived by Brandemuchl and Beckman (58)

$$\theta_{i,d}(\xi) = 59.68 - 0.1388\,\beta(\xi) + 0.001497\,\beta^2(\xi)$$

The total diffuse radiation reflected from the ground which is incident upon an exposed surface inclined at ξ is given by

$$q_g(\xi) = \rho_g\, G_{dh}(\xi)\left(\frac{1-\cos\beta(\xi)}{2}\right)$$

where ρ_g is the effective reflectance of the surrounding ground. The ground is assumed isotropic and the effective angle of diffuse solar radiation from the ground (59) is

$$\theta_{i,g}(\xi) = 90.0 - 0.5788\,\beta(\xi) + 0.002693\,\beta^2(\xi)$$

The total solar radiation incident upon an exposed opaque surface at time ξ is a function of solar absorptivity and surface shading, therefore,

$$Q_{s,E}(\xi) = A_s\alpha_s\left[q_D(\xi)\left(1 - S_o(\xi)\right) + q_d(\xi) + q_g(\xi)\right] \qquad (5.79)$$

where $Q_{s,E}(\xi)$ = solar radiation incident on exposed opaque surfaces as identified in equation (5.77)

A_s = area of surface (M^2)

α_s = absorptivity of surface

$S_o(\xi)$ = the opaque surface shading expressed as a fraction of the total area of the surface. The value of $S_o(\xi)$ varies

between 0 and 1 indicating no shading and fully shaded respectively. The method of calculating $S_o(\phi)$ is outlined in Appendix 7.

Planar reflectors are used to redirect solar beam radiation onto exposed surfaces of a solar collector that would not otherwise be incident upon the surface. It is assumed that only one specular reflector is used, its position relative to a solar collector is shown in Figure 5.30. The total direct solar irradiance incident upon a planar reflector is

$$q_{D,R}(\phi) = G\, dn(\phi) \cos\theta_R(\phi)$$

where θ_R is the angle of incidence on the reflector. Direct solar radiation is partially reflected and partially absorbed by the reflector, the reflected component which is incident upon an exposed surface is given by

$$q_R(\phi) = \rho_R\, q_{D,R}(\phi) \cos\theta_{i,R}(\phi)$$

where ρ_R = the reflectivity of the planar reflector

$\theta_{i,R}(\phi)$ = angle of incidence of reflected direct solar radiation, from Figure 5.30

$$\theta_{i,R}(\phi) = 180.0 - \theta_R(\phi) - \theta_A(\phi)$$

$\theta_A(\phi)$ = the angle between the reflector and the collector (Figure 5.30)

The quantity of energy absorbed by an opaque surface is

$$Q_{S,R}(\phi) = A_S \alpha_S q_R(\phi) R_o(\phi) \qquad (5.80)$$

where $Q_{S,R}(\phi)$ = the direct solar radiation incident on an exposed surface after reflector from a planar reflector (from equation (5.34)), (W),

$R_o(\phi)$ = the fraction of the total opaque surface area which is insolated due to the planar reflector. The value of

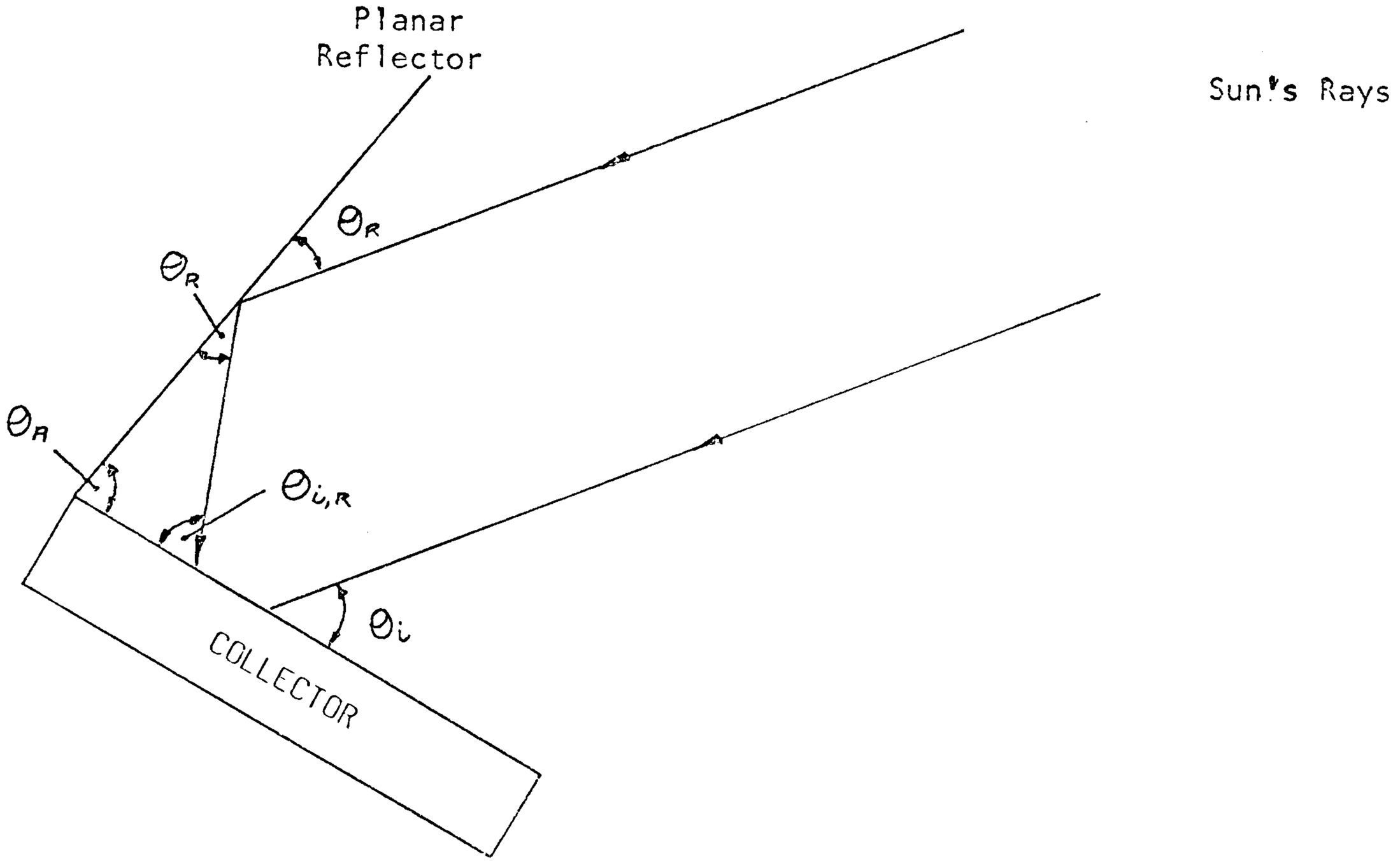

Figure 5.30 Operation of a planar reflector.

$R_o(t)$ varies between 0 and 1, indicating no reflection onto the surface and surface full covered by the reflection respectively. The method of calculating $R_o(t)$ is outlined in Appendix 7.

If an exposed transparent surface has M wavebands associated with its optical properties then for each waveband the transmissivity, absorptivity and reflectivity of the material will be predicted at four angles of incidence: $\theta_{i,D}$; $\theta_{i,d}$; $\theta_{i,g}$ and $\theta_{i,R}$. The method of calculating these values for both the parallel and perpendicular polarisation components, which are analysed separately, is described in Section 3.3.1.1. If the transparent medium has thin films on its inner and outer surfaces then

$$\hat{\alpha} = \alpha_{f1} + \alpha + \alpha_{f2}$$

where $\hat{\alpha}$ = the total absorptivity of the complete transparent system

α_{f1} & α_{f2} = the absorptivity of the outer and inner-most thin films

α = the absorptivity of the transparent substrate.

The method of predicting these values is given in 3.3.1.1.

The instantaneous total absorption of solar radiation by a transparent material plus thin films is found from summating the quantity of solar radiation absorbed by the element, in each waveband, from each of the four radiation sources and the internal surfaces reflection term, therefore:

$$\hat{Q}_{s,\hat{\alpha}(t)} = A_s \left\{ \sum_{m=1}^{M} \left[\hat{\alpha}_{D,m}(t)\, q_{D,m}(t) \left(1 - S_T(t)\right) + \hat{\alpha}_{d,m(t)}\, q_{d,m(t)} \right.\right.$$

$$\left.\left. + \hat{\alpha}_{g,m(t)}\, q_{g,m(t)} + \hat{\alpha}_{R,m(t)}\, q_{R,m(t)} R_T(t) + \hat{\alpha}_{r,m} \Sigma q_{r,m(t)} \right] \right\} \quad (5.81)$$

where q = the quantity of solar radiation in waveband m for each category (WM^{-2})

$S_T(t)$ = shading on the transparent element at time t expressed as a fraction of its total surface area

$R_T(t)$ = the fraction of the total transparent surface area which is insolated by solar radiation reflected from a planar reflector

category which has been reflected from internal surfaces and is incident upon the transparent element. Multiple instantaneous diffuse reflections are considered

$\hat{\alpha}_{r,m}$ = the absorptivity of the transparent system due to multiple diffuse internal reflections at an angle of incidence, θ_r, of $180.0/\pi$.

The term $\hat{\alpha}$ in equation (5.81) relates to the total absorptivity of the transparent system for each solar radiation component within waveband m. The total energy absorbed by this system is $\hat{Q}_{s,\hat{\alpha}}(t)$ which can be re-expressed as

$$\hat{Q}_{s,\hat{\alpha}}(t) = Q_{s,\alpha f_1}(t) + Q_{s,\alpha}(t) + Q_{s,\alpha f_2}(t)$$

where $Q_{s,\alpha}(t)$ = the total solar energy absorbed by the transparent element (W) described in equation (5.9), it can be found from

$$Q_{s,\alpha}(t) = \frac{\alpha}{\hat{\alpha}} Q_{s,\hat{\alpha}}(t)$$

$Q_{s,\alpha f_1}(t)$ = the total solar energy absorbed by the thin films on the outermost surface of the transparent element (Watts). If this surface is an exposed external surface then $Q_{s,E}(t) = Q_{s,\alpha f_1}(t)$ - see equation (5.77), if the surface is an internal surface then $Q_{s,I}(t) = Q_{s,\alpha f_1}(t)$ applies [see equation (5.78)]. $Q_{s,\alpha f_1}(t)$ is found by the same method as $Q_{s,\alpha}(t)$.

$Q_{s,\alpha f_2}(t)$ = total solar energy absorbed by the thin films on the innermost surface of the transparent element, therefore, $Q_{s,I}(t) = Q_{s,\alpha f_2}(t)$ applies for all cases. $Q_{s,\alpha f_2}(t)$ is found as $Q_{s,\alpha}(t)$

Consequently, absorbing thin films are attributed to either $Q_{s,I}(t)$ or $Q_{s,E}(t)$ so that they are surface heat injections.

The value of $\Sigma \varrho_{r,m}(t)$ can only be assessed by considering the transmitted

subsequently incident upon the internal surface of the transparent element where it will be absorbed, transmitted and re-reflected.

Consider beam solar radiation (direct and planar reflected) transmitted through a transparent element at time t,

$$\sum_{m=1}^{M} q_{BT,m(t)} = \sum_{m=1}^{M} \left[\tau_{D,m(t)}\, q_{D,m(t)} (1 - S_{T(t)}) + \tau_{R,m(t)} q_{R,m(t)} R_{T(t)} \right]$$

where $q_{BT,m(t)}$ = the quantity of beam radiation transmitted in waveband m, (WM^{-2})

τ = the transmissivity of the element for direct or planar reflected solar radiation in waveband m.

Beam radiation insolates particular surfaces despending upon the angle of incidence and the geometric position of the internal surfaces. The apportioning between internal surfaces can be predicted by using an Insolation prediction algorithm (Appendix 7). Any one node receives a beam radiation injection at time t equal to,

$$Q_{I,(t)} = A_I \alpha_I \left[\sum_{m=1}^{M} \left\{ \tau_{D,m(t)}\, q_{D,m(t)} (1 - S_{T(t)}) * I_{D(t)} + \tau_{R,m(t)}\, q_{R,m(t)}\, R_{T(t)} I_{R(t)} \right\} \right] \quad (5.82)$$

where $I_{(t)}$ = the insolation on an internal surface expressed as a function of the surface area for the direct (D) and reflected (R) beam radiation.

The directly transmitted portion of the diffuse components at any time t is given by

$$\sum_{m=1}^{M} q_{dT,m(t)} = \sum_{m=1}^{M} \left[\tau_{d,m(t)}\, q_{d,m(t)} + \tau_{g,m(t)}\, q_{g,m(t)} \right]$$

where

$q_{dT,m(t)}$ = the directly transmitted diffuse solar radiation in waveband m.

Although sky and ground diffuse solar radiation can be equated to a single angle, that is θd and θg respectively, upon transmission

in nature and it is assumed to fall at the same intensity on all internal surfaces, except the surface through which it is transmitted. The magnitude of the resulting energy injection at any internal surface node is found by an area weighting technique and is described by

$$Q_{I2}(\xi) = \left[\sum_{m=1}^{M} q_{dT,m}(\xi)\right] \frac{\alpha_I}{\Sigma A_I'} A_I \qquad (5.83)$$

where α_I = absorptivity of internal surface under consideration

$\Sigma A_I'$ = the sum of the areas of all internal surfaces exlcuding the surface containing the transparent surface (M^2)

All surfaces are general reflectors that is they are somewhere between being specular and diffuse reflectors. With general reflectors the reflected component of the total (beam plus diffuse) solar radiation from internal surfaces depends upon the angle of incidence, geometry and the reflective properties of the surface. This problem is considerably simplified by treating all internal opaque surfaces as diffuse reflectors, therefore, any radiation reflected from an internal surface is perfectly diffuse. The exception to this rule is for beam radiation transmitted through a transparent element and incident upon another transparent element, in such cases it is assumed the inter-reflections are specular in nature between two infinite parallel planes. For diffusely reflecting internal surfaces the total reflected component at time ξ is given by

$$Q_{r,I}(\xi) = \frac{\rho_I}{\alpha_I}\left(Q_{I,1}(\xi) + Q_{I2}(\xi)\right)$$

where $Q_{r,I}(\xi)$ = the total reflected energy from surface I ,(W)

ρ_I = reflectivity of surface I

This reflected energy is apportioned to all other surfaces in the enclosure using an area weighting, thus, the quantity absorbed by each surface after the first reflection at time ξ is,

$$\alpha_{r,m}\, q_{(r,m),1}(\xi) = \alpha_{r,m} \sum_{n=1}^{N} \left[\frac{Q_{r,1}(\xi)}{\Sigma A_n}\right]$$

$q_{(r,m)1}(\xi)$= the quantity of solar radiation absorbed after the first reflection at surface I (WM^{-2})

N = number of surfaces reflecting energy to surface I

ΣA_n = the sum of the enclosure surface areas exlcuding surface n.

The energy reflected from each surface for the second and subsequent reflections at time ξ is given by

$$Q_{r,j}(\xi) = \rho_I A_I q_{(r,m)J}(\xi)$$

where J is the number of the reflection.

Energy will be lost from the enclosure by transmittance through transparent elements, however, if the transparent element is a membrane between two ducts in a solar collector then the transmitted energy through the membrane will supplement $Qr,J(\xi)$ for the transparent surface at reflection J. For collectors with two or more parallel transparent covers, $Qr,J(\xi)$ for the connecting elements at time (ξ), is given by

$$Q_{r,J}(\xi) = \rho_I A_I q_{(r,m)J}(\xi) + Q_T(\xi)_J$$

where $Q_T(\xi)$ is the transmitted energy for reflection J. This value can now be used to repeat the procedure for the second and subsequent reflections until the quantity of solar radiation reflected is negligible. Thus

$$\sum q_{r,m}(\xi) = q_{(r,m)_1}(\xi) + q_{(r,m)_2}(\xi) + q_{(r,m)_3}(\xi) + \ldots.$$

and the total energy absorbed at an internal surface is given by

$$Q_{I\,3}(\xi) = A_I \alpha_{r,m} \sum_{j=1}^{J} q_{(r,m)j} \qquad (5.84)$$

The total solar radiation absorbed by an internal opaque surface at any time ξ is found from the addition of equations (5.82), (5.83) and (5.84),

where

$Q_{s,I(\xi)}$ = the quantity of solar radiation absorbed by an internal surface - see equation (5.78)

As solar radiation reflecting within a solar collector does so at the speed of light the radiative reflection process is assumed to be instantaneous.

To conduct an analysis of solar absorption by internal surfaces a detailed model of the properties of transparent materials is required, the following section describes the mathematical model to conduct such an analysis.

5.3.1.1 Properties of Transparent Materials

Transparent covers are situated above an absorber plate to reduce convective and infra-red radiation losses, however, the covers attenuate the incident solar radiation due to their reflective and absorptive properties. It is crucial to any solar collector model to accurately predict the absorption, reflection and transmission of the collectors transparent elements, these properties are a function of the incident solar spectrum and the thickness, refractive index and extinction coefficient of the diathermous material, furthermore, the refractive index and the extinction coefficient are both functions of wavelength The problem is made considerably more complex if the surfaces of the transparent element are coated with thin films to promote surface transmission, compared to untreated surfaces.

In this section a mathematical model to predict the reflection, absorption and transmission properties of any plane, parallel diathermous materials is outlined.

The refractive index, n, of any non-magnetic, isotropic dielectric material is defined as the ratio of the velocity of the incident radiation in a vacuum to the velocity of the incident radiation in the given material:

$$n = \frac{\text{velocity in a vacuum}}{\text{velocity in the medium}} = \frac{c}{\upsilon}$$

where c = the speed of light

υ = velocity within the transparent material

The refractive index, n, is the most important variable for describing the reflective and transmissive properties of a transparent window system. Table 5.4 gives some typical refractive indices. The refractive indices in this table are not based upon the velocity in a vacuum but the velocity in air, this does not affect the results because the refractive index is a ratio and therefore any substance could be used as the datum. Ordinary air has a refractive index of n = 1.0003 compared to vacuum but it is assumed that both air and vacuum have a refractive index equal to one.

Dispersion is the term used to describe the variation of the refractive index with wavelength, λ . As this infers, if several wavebands are considered within the solar spectrum then each will have a different average refractive index; the range of values may not vary significantly but the net effect upon the surface reflectance over the solar spectrum could be significant.

If the dispersion is considered to be normal then the following rules apply over the electromagnetic spectrum:

(1) the refractive index decreases as λ increases

(2) the rate of decrease, $dn/d\lambda$, is greater at shorter wavelengths.

Cauchy was first to attempt to represent the curve of normal dispersion

MATERIAL	n
Ordinary window glass	1.52
Polymethymethacrylate (plexiglass)	1.49
Teflon	1.343
Polyvinyl Fluoride (Tedlar)	1.46
Polyethylene (Mylar)	1.65
White glass	1.50
Water	1.333
Air	1.00
Magnesium Fluoride	1.38
Silicon	3.48
Germanium	3.80
Cryolete	1.35
Titonium dioxide	2.62
Thorium dioxide	2.20

TABLE 5.4 Refracture indices of various substances averaged over the solar spectrum (20,64) relative to air

$$n = A + \frac{B}{\lambda^2} + \frac{C}{\lambda^4}$$

where A, B and C are constants and characteristic of a specific material.

Cauchy's equation does not hold for all materials, subsequently other dispersion formulae have been developed to suit particular materials. The dispersion equation of a material may be obtained from the manufacturer or alternatively from the Handbook of Optics (59) which contains the dispersion equations for many materials.

The Laws of Reflection and Refraction (Figure 5.31) are important in assessing the properties of a diathermous material. The Law of Refraction, also known as Snell's Law, can be expressed mathematically, for a beam of electromagnetic energy passing through several refracting media with parallel boundaries, in the form

$$n_0 \sin\phi_0 = n_1 \sin\phi_1 = n_2 \sin\phi_2 = \text{- - - - -}$$

Therefore, the angle of refraction within any media can be established if the refractive index and the angle of incidence of the outer medium is known. In a solar collector case the boundary medium is air and the angle of incidence can be found from Section 5.3.1.

There are two distinct components of polarisation of natural solar radiation, the S component which is normal to the plane of incidence and the P component which is parallel to the plane of incidence. As solar radiation is assumed to be unpolarised, then the intensity, I, of the incident radiation consists of equal quantities of both components of polarisation, thus

$$I = 0.5(I_p + I_s)$$

As the intensity, I, at a boundary between air and the window is either reflected, R, or transmitted, T, then

$$I = 0.5\ (R_p + R_s + T_p + T_s)$$

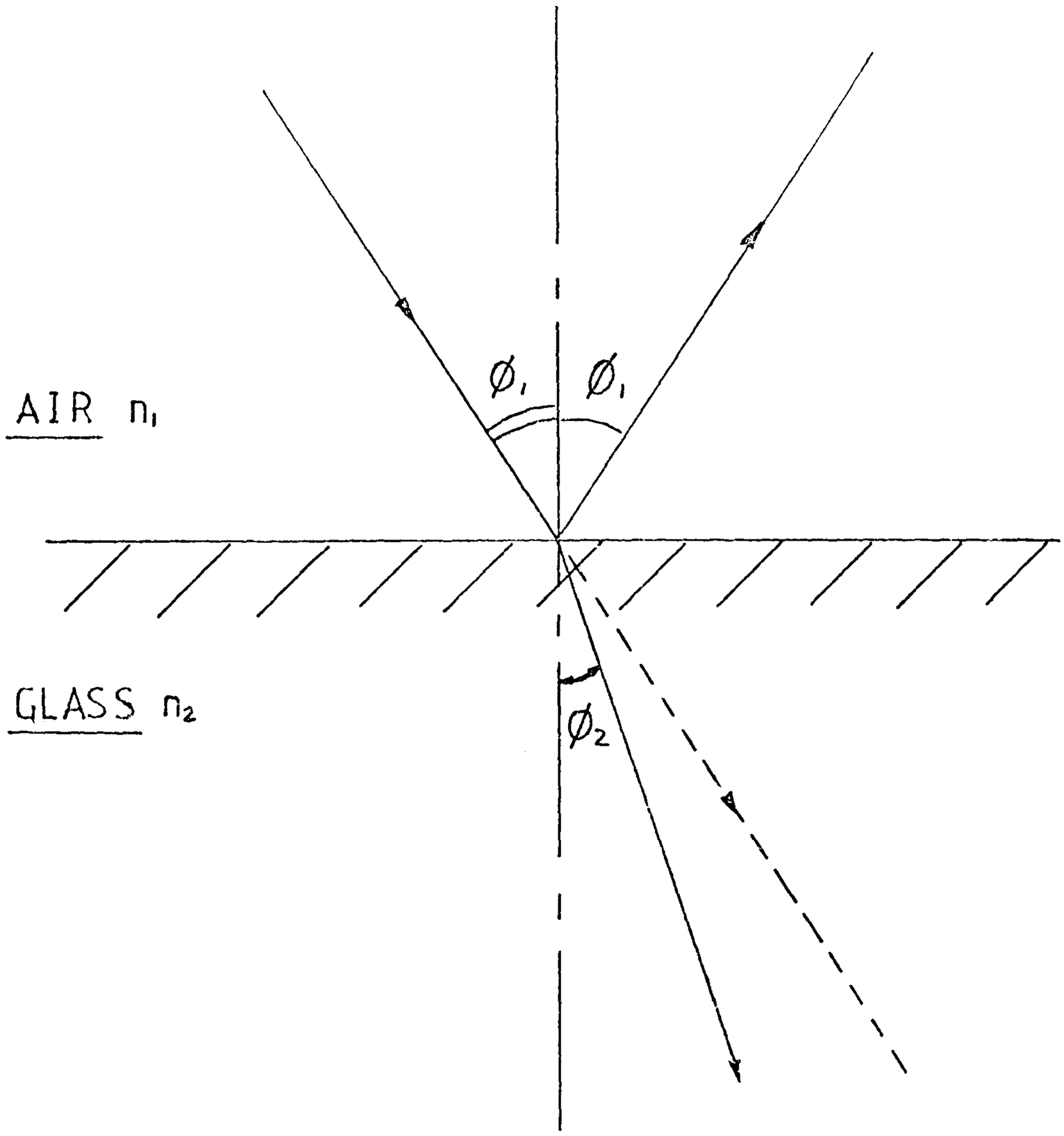

Figure 5.31 Laws of Reflection and Refraction of electromagnetic radiation at the boundary between two dielectric media of refractive indices n_1 and n_2 respectively

normal angles of incidence

$$R_p = I * \rho_p = \frac{\tan^2 (\emptyset_1 - \emptyset_2)}{\tan^2 (\emptyset_1 + \emptyset_2)} * I \qquad (5.86)$$

$$R_s = I * \rho_s = \frac{\mathrm{Sin}^2 (\emptyset_1 - \emptyset_2)}{\mathrm{Sin}^2 (\emptyset_1 + \emptyset_2)} * I \qquad (5.87)$$

$$T_p = I * \rho_p = \frac{n_2 \cos\emptyset_2}{n_1 \cos\emptyset_1} \left(\frac{2\sin\emptyset_2 \cos\emptyset_1}{\sin(\emptyset_1+\emptyset_2)\cos(\emptyset_1-\emptyset_2)} \right)^2 * I \qquad (5.88)$$

$$T_s = I * \rho_s = \frac{n_2 \cos\emptyset_2}{n_1 \cos\emptyset_1} \left(\frac{2\sin\emptyset_2 \cos\emptyset_1}{\sin(\emptyset_1+\emptyset_2)} \right)^2 * I \qquad (5.89)$$

When the angle of incidence is normal to the window then the following expressions are used

$$R_{p(s)} = I * \rho_{p(s)} = I * \left(\frac{n_2 - n_1}{n_2 + n_1} \right)^2 \qquad (5.90)$$

$$T_{p(s)} = I * \rho_{p(s)} = I * \left(\frac{n_2}{n_1} \right) * \left(\frac{2n_1}{n_1 + n_2} \right)^2 \qquad (5.91)$$

where p(s) indicates that this equation is suitable for both the P and S components of polarisation.

If the transparent material is a conductor, that is, it absorbs some of the transmitted radiation, then it can be shown from the Maxwell Equations for electromagnetic waves that the refractive index is complex (61), this can be written in the form

$$\bar{n}^2 = (n - ik)^2$$

Where k is the index of absorption and it is a measure of the attenuation of the incident wave as it passes through the medium.

Bouger's Law (54) which is based on the assumption that the absorbed radiation is proportional to the local intensity, I, within the medium and the distance the radiation travels in the medium, x:

$$dI = IKdx$$

where K is the extinction coefficient of the material; this has been shown to be equal to (60),

$$K = \frac{4\pi nk}{\lambda}$$

the extinction coefficient for several materials are given in Table 5.5.

Integrating between the limits of zero (at the surface) and L (the path length of the incident beam through the medium) the transmission coefficient, τa, for any angle of incidence is evaluated from

$$\tau a = \frac{I_L}{I_o} = e^{-KL} \qquad (5.92)$$

where I_o = intensity of energy at the surface

I_L = intensity of energy at distance L for the surface

L = the path length of the incident beam, for non-normal angles of incidence

$$L = Z \cos\emptyset'$$

Z = the physical thickness of the medium

$\emptyset'$ = the angle of refraction

The ratio of the intensity absorbed to the incident intensity is called the absorptivity this can be expressed for either component of polarisation as

$$\alpha_{p(s)} = 1 - \tau a_{p(s)} \qquad (5.93)$$

When the incident solar radiation is monochromatic, then it is assumed that the medium reduces the intensity of all wavelengths within the

MATERIAL	K (cm^{-1})
Polyvinyl Fluoride (Tedlar)	1.4
Teflon	0.59
Polyethylene (Mylar)	2.05
Polyethylene	1.65
Ordinary window glass	0.3
White glass	0.04
Heat-absorbing glass	1.3 - 2.7

TABLE 5.5 Extinction coefficients for transparent materials in the solar spectrum (20)

absorption. If the solar spectrum is considered using a number of monochromatic wavebands then general absorption is assumed to occur within each waveband.

Properties of a Transparent System

At present, there are two main techniques for predicting the properties of absorptivity, reflectivity and transmissivity for a transparent system:

(1) The Duffie and Beckman technique (34): several ordinary transparent panes can be analysed for monochromatic radiation
(2) The Mitalas and Stephenson technique (62): similar to the previous technique but the window system may be analysed by a series of ten monochromatic wavebands, preset by the authors.

Neither of these techniques can be used to model thin films, however both techniques are very accurate, therefore, the model proposed to handle plain glass and plastic materials will be similar except that it can deal with any amount of monochromatic wavebands specified by the user.

If a monochromatic solar beam or a monochromatic waveband is analysed it may be represented by a beam of electromagnetic energy between the boundaries of the solar spectrum, therefore, it is assumed to be unpolarised. If this beam is incident upon a single sheet of transparent material (e.g. plain glass) then at the first air/element boundary incident energy is partially reflected and partially transmitted. The ratio of ρ to τ can be evaluated from equations (5.86) to (5.91). The reflective component is 'lost' from the system and the transmitted component is refracted. If the element is a conductor then the absorbed quantity can be established by equations (5.92) and (5.93). This absorption continues until it meets the element/air boundary whereupon energy is reflected and transmitted, that part which is transmitted from the second boundary is lost from the element, however, the reflected part sets up a series of internal reflections within the

quantity to be reflected. The reflected, transmitted and absorbed components for the transparent element, summed to infinite result in a geometric series, which can be written

$$\rho_E = \rho_1 + \frac{\tau_1^2 \tau_a^2 \rho_2}{1 - \tau_a^2 \rho_2 \rho_1} \qquad (5.94)$$

$$\alpha_E = \frac{\tau_1 \alpha (1 + \tau_a \rho_2)}{(1 - \tau_a^2 \rho_2 \rho_1)} \qquad (5.95)$$

$$\tau_E = \frac{\tau_1 \tau_2 \tau_a}{(1 - \tau_a^2 \rho_2 \rho_1)} \qquad (5.96)$$

where E represents the transparent element and suffix 1 and 2 represent the first and second boundaries of the element respectively. The values of ρ_E, α_E and τ_E are calculated for both the p and s components of polarisation and the mean values found, however, as the values are different for the p and s components the transmitted solar radiation will be polarised, therefore

$$\overline{\rho}_E + \overline{\alpha}_E + \overline{\tau}_E = 1$$

where $\overline{\rho}_E = \rho_{E\,p(s)}$; $\overline{\alpha}_E = \alpha_{E\,p(s)}$; $\overline{\tau}_E = \tau_{E\,p(s)}$. If there are N monochromatic wavebands within the solar spectrum then the ratio of reflectivity, absorptivity and transmissivity are found from Section 5.3.1.

For a multi-element transparent cover system in a solar collector the quantity of solar energy incident upon the absorber plate depends upon the interaction between the tranparent elements and the absorber plate for each polarisation component. Due to the transmitted solar radiation being polarised the parallel and perpendicular components will be treated separately and the mean value found only for the total value of the system. Figure 5.33 represents a collector cover system with L parallel plain transparent sheets. The values of ρ_E, τ_E and α_E are calculated for each element. The transmitted component from the first element is tracked throughout the system until is is either absorbed by an element or reflected out of or transmitted through the system. Therefore, depending upon angle of incidence and solar spectrum, the energy system reflectance and transmittance can be

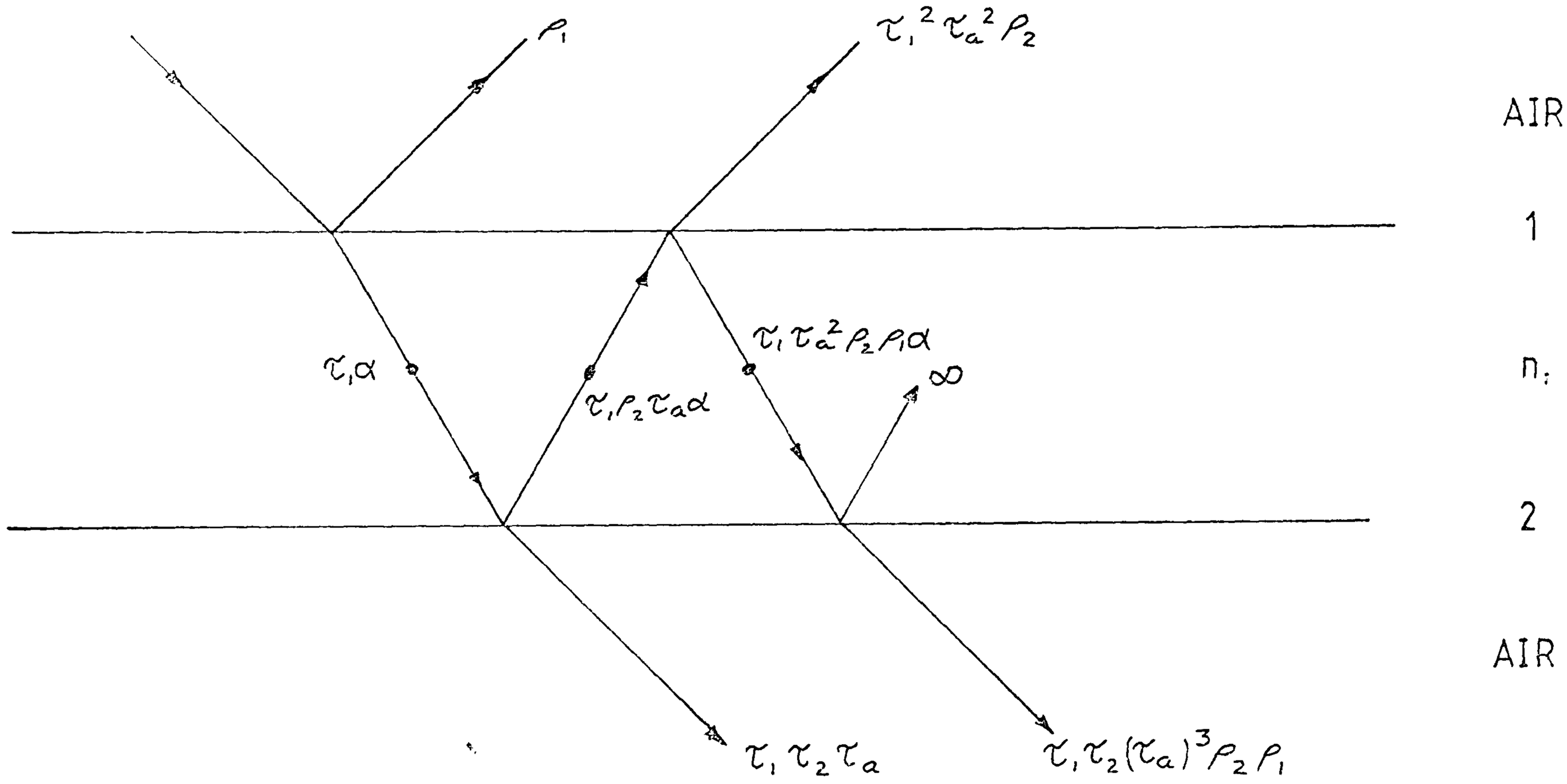

Figure 5.32 For a particular element within the glazing system, (refractive index n_1), the effects of internal reflection are shown

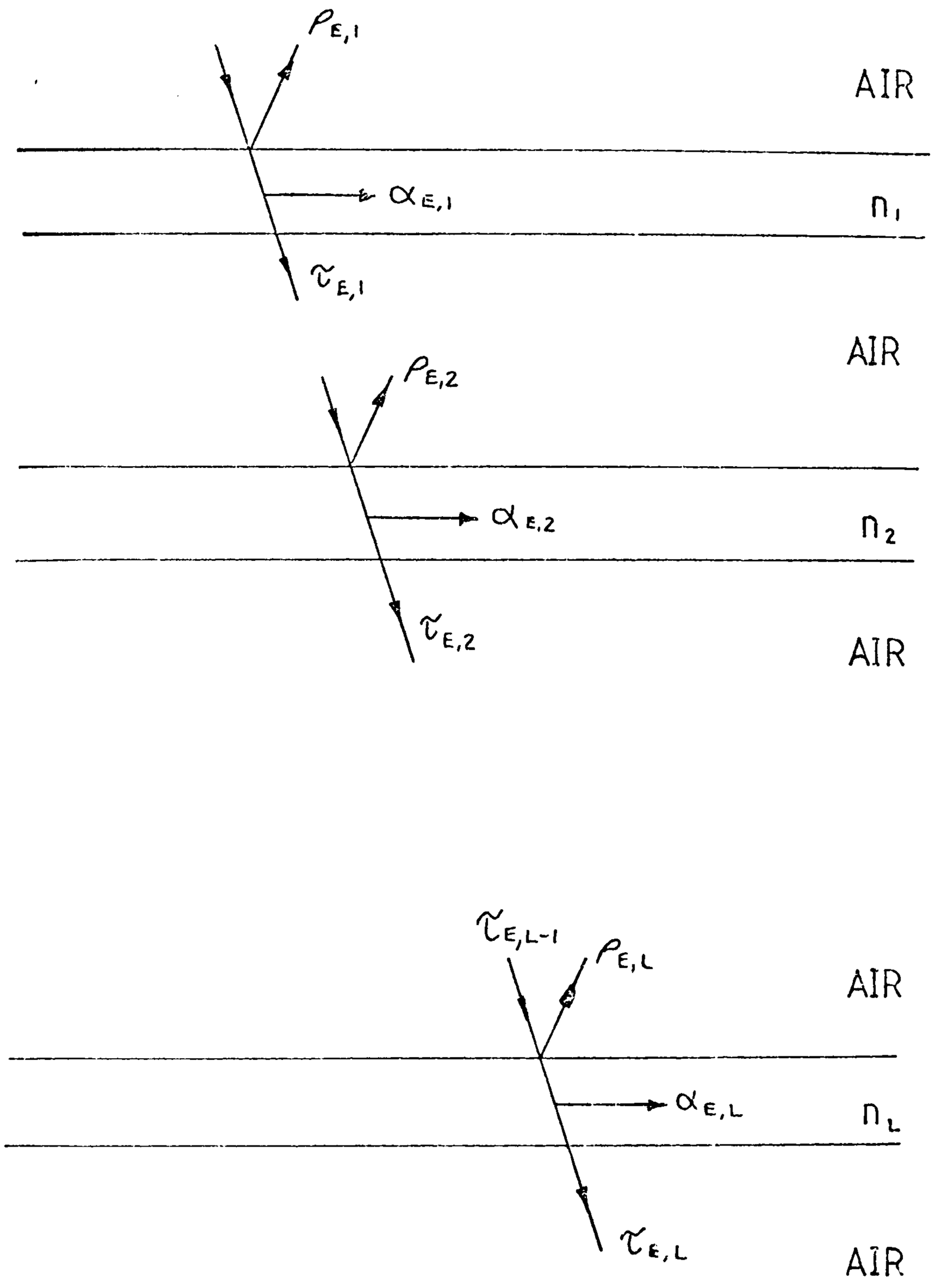

Figure 5.33 Tracking of ρ_E and τ_E for multiple reflections between substrates.

established, plus the absorptance of each transparent element.

This technique compares favourably with the results of the two techniques mentioned earlier. However, in Section 5.3.1 a slightly different technique of solving the solar radiation apportioning of the multi-element transparent cover is used. The former method outlined above is used in the WINDOW computer program described in Appendix 8.

Anti-Reflection Thin Films

All transparent materials reflect some radiation from their surfaces, any lowering of the surface reflectance of a solar collector cover system will be a direct gain to the collector. Films applied to a substrate (that is a collector cover) can decrease undesirable reflectance from the system.

Films applied to a transparent substrate may be regarded as thick or thin, depending upon their 'optical thickness' which is the product of the film's refractive index and physical thickness. It has been established by Vasicek (61) that the film may be considered to be thick if the following expression is satisfied

$$n_f t > 2.5 \lambda_d \qquad (5.97)$$

where n_f = the refractive index of the film
t = the physical thickness of the film
λ_d = the wavelength of the solar spectrum which is being designed for minimum reflection

If this condition is not satisfied, the film is considered to be thin.

The essential difference between calculations of thick and thin films is that a thick film is analysed as a glass plate, i.e. only the ratio of the intensities are taken into account, whereas with a thin film the corresponding path of phase difference of the wavelength of the incident solar radiation ray is also considered.

It is apparent from equation (5.97) that there may be some materials which will be thick in the ultra-violet and visible ranges of the solar spectrum and thin in the infra-red, however, in most cases the films will be thin with physical thicknesses less than 1 μm for which the problem of a simultaneous thick and thin film seldom occurs.

Consider a single thin film and substrate. Minimum reflectance from the surface at normal incidence for a particular design wavelength can be obtained if the single film has an optical thickness equal to a quarter of the design wavelength, thus

$$n_f t = \frac{\lambda_d}{4}$$

Zero reflectance can be achieved at normal incidence for this wavelength if the film has a refractive index which satisfies the following expression

$$n_f = \sqrt{n_o n_s}$$

where n_o and n_s are the refractive indices of the air and substrate respectively.

True zero reflectance from a surface is obtained only for normal incidence and at the design wavelength, however, there is a waveband centred at the design wavelength in which the reflectance is below that of the surface without the film, outwith this waveband the reflectance will be greater, Figure 5.34. For non-normal angles of incidence the minimum reflectance will occur at the design wavelength with a similar waveband of reduced surface reflectivity.

Although the surface reflectance of the substrate is reduced beneath the film, the radiation will still undergo absorption and reflection from the second substrate boundary. More of the reflected energy will be transmitted out of the system because the quantity of energy is greater and the reflection from the first substrate boundary is reduced.

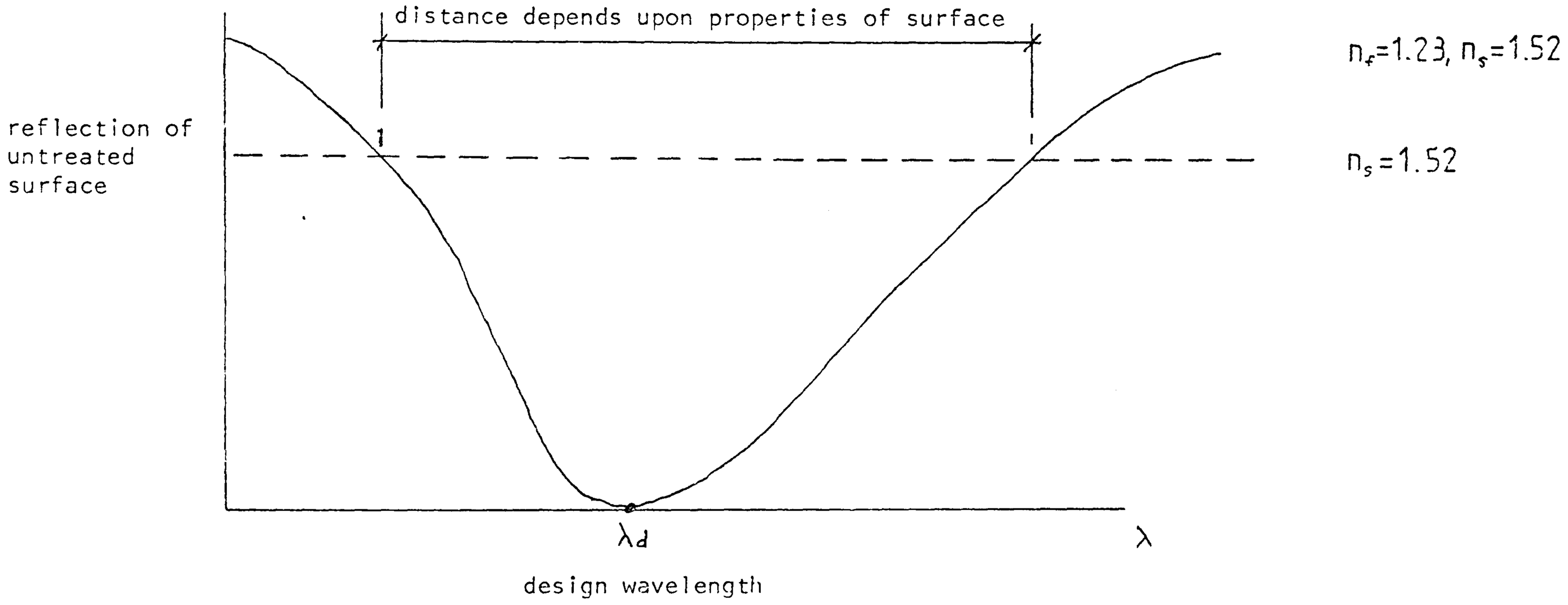

Figure 5.34 Typical reflectance from an anti-reflection surface at normal incidence compared to an untreated surface.

If more than one film is used then zero reflectivity can be satisfied simultaneously for the same number of wavelengths at normal incidence as there are thin films, in such cases the surface is said to be achromatised. Furthermore, a more complete antireflection is achieved over a wider spectral region. The conditions for multiple thin films are more easily satisfied compared to single thin films and as a result more materials are available for use as thin films.

The mathematical model for assessing the reflectivity and transmissivity of a single thin film and a series of thin films will now be described.

Reflection and Transmission by Thin Films

Consider a beam of solar energy at wavelength λ, which is at an angle of incidence, ϕ_o, with a plane homogeneous isotropic non-conducting thin film of thickness t and refractive index n_f, supported on a substrate of refractive index n_s, as shown in Figure 5.35. The first medium is assumed to be air which has a refractive index n_o=1.0.

A mathematical analysis by Heavens (63) on the effects of multiple reflections occurring within a film bounded by air and a transparent substrate for which the following expressions were derived for predicting the ratios of the reflected and transmitted energy intensity with the indicent energy intensity falling upon the film

$$R = \frac{r_1^2 + 2 r_1 r_2 \cos 2\delta_f + r_2^2}{1 + 2 r_1 r_2 \cos 2\delta_f + r_1^2 r_2^2} \qquad (5.98)$$

$$T = \frac{n_s \cos \phi_s}{n_o \cos \phi_o} \left(\frac{t_1^2 t_2^2}{1 + 2 r_1 r_2 \cos 2\delta_f + r_1^2 r_2^2} \right) \qquad (5.99)$$

where suffix 1 and 2 refer to the two boundaries shown in Figure (5.35) and r and t are dependent on the angle of incidence ϕ_o, the component of polarisation and the refractive indices n_o, n_f and n_s.

The δ_f represents the change in phase of the beam as it traverses the

film where

$$\delta_f = \frac{2\pi}{\lambda} n_f t_f \cos \phi_f \qquad (5.100)$$

Heavens (63) extended this technique to handle more than one film but with each successive film the solution becomes more complicated. A further disadvantage of this technique is that it cannot analyse conducting metal films which is a severe restriction as these films are used extensively in producing highly reflective window systems.

Vasicek (61) and others (64), (65) have anlysed thin films by applying the appropriate boundary conditions to the Maxwell equations such that the expression describing the ratio of the reflected amplitude to the incident amplitude, as given by the square root of equation (5.98), may be expressed in the form of a 2 x 2 matrix. It has been shown by the aforementioned authors that the amplitude conditions of boundary 1, (Figure 5.35) for both the electric field strength E , and the magnetic field strength, H , depend upon the boundary conditions of E and H at boundary 2. The matrix is the connection between these boundaries, thus,

$$\begin{bmatrix} E^1 \\ H^1 \end{bmatrix} = \begin{bmatrix} m_{11} & m_{12} \\ m_{21} & m_{22} \end{bmatrix} \begin{bmatrix} E^2 \\ H^2 \end{bmatrix} = [M_1] \begin{bmatrix} E^2 \\ H^2 \end{bmatrix} \qquad (5.101)$$

where m_{11}, m_{12}, m_{21} and m_{22} depend upon the system under analysis. Table 5.6 gives the expressions which describe these coefficients.

Matrix M_1 characterises any film under analysis. At normal incidence, this matrix becomes:

$$M_1 = \begin{bmatrix} \cos\delta_1 & \frac{i}{N} \sin\delta_1 \\ iN_1 \sin\delta_1 & \cos\delta_1 \end{bmatrix} \qquad (5.102)$$

where δ_1 is given by δ_f in equation (5.100).

Vasicek (61) derived an expression of describing the ratio of the reflective to the incident amplitudes which has the same net result if squared as equation (5.98)

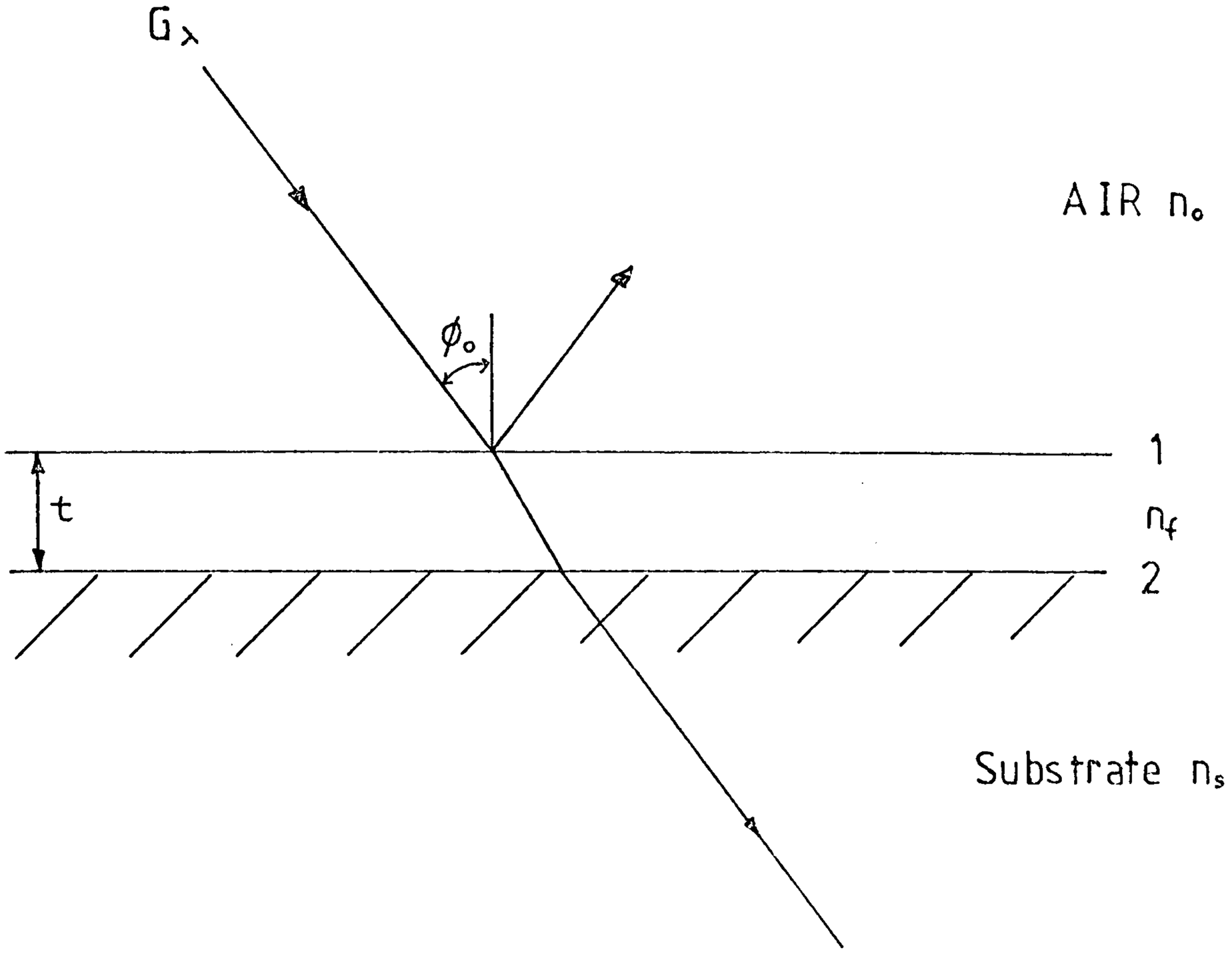

Figure 5.35 A single thin dielectric film on a transparent substrate. The ratios ρ and τ are a function of the angle of incidence ϕ_o, the wavelength, λ, of the incident radiation, the thickness, t, of the film and the refractice indices n_0, n_f and n_s.

TABLE 5.6 The coefficients of equation (5.103) may be described by the following expressions

coefficient	normal incidence of light	non normal angles of incidence	
		p component	s component
a	$\frac{n_o}{n_s}$	$\frac{n_o \cos \phi_{f\ last}}{n_s \cos \phi_o}$	$\frac{n_o \cos \phi_o}{n_s \cos \phi_{f\ last}}$
b	n_o	$\frac{n_o}{\cos \phi_o}$	$n_o \cos \phi_o$
c	$\frac{1}{n_s}$	$\frac{\cos \phi_{f\ last}}{n_s}$	$\frac{1}{n_s \cos \phi_{f\ last}}$
m_{11}	$\cos \delta_f$	$\cos \delta_f$	$\cos \delta_f$
m_{12}	$\frac{i}{n_f} \sin \delta_f$	$i \frac{\cos \phi_f}{n_f} \sin \delta_f$	$\frac{i}{n_f \cos \phi_f} \sin \delta_f$
m_{21}	$i n_f \sin \delta_f$	$i \frac{n_f}{\cos \phi_f} \sin \delta_f$	$i n_f \cos \phi_f \sin \delta_f$
m_{22}	$\cos \delta_f$	$\cos \delta_f$	$\cos \delta_f$

NOTE:

1. The refractive indices may be complex (65)
2. ϕ_f last represents the refractive angle within the film adjacent to the substrate

$$r_{P(S)} = \frac{a m_{11} + b m_{12} - c m_{21} - m_{22}}{a m_{11} + b m_{12} + c m_{21} + m_{22}} \qquad (5.103)$$

where a, b and c for normal or non-normal angles of incidence are given in Table 5.6. These coefficients depend upon the refractive indices of the first medium n_o and the last medium n_s, i.e. for normal incidence

$$a = \frac{n_o}{n_s} \quad ; \quad b = n_o \quad ; \quad c = \frac{1}{n_s} \qquad (5.104)$$

Subsequently, because the coefficients m_{11}, m_{12}, m_{21} and m_{22} are a function of the film and independent of first and last medium then these coefficients can be made to represent a series of thin films. Consider a thin film system of l layers as shown in Figure 5.36. The refraction indices n_s and the thicknesses t_j of each layer must be known, as each film can be represented by a matrix - equation (5.102) - it follows that the relationship between E^1 and H^1 and E^l and H^l can be described by

$$\begin{vmatrix} E' \\ H' \end{vmatrix} = \begin{vmatrix} m_{11}' & m_{12}' \\ m_{21}' & m_{22}' \end{vmatrix} \begin{vmatrix} m_{11}^2 & m_{12}^2 \\ m_{21}^2 & m_{22}^2 \end{vmatrix} \cdots\cdots \begin{vmatrix} m_{11}^l & m_{12}^l \\ m_{21}^l & m_{21}^l \end{vmatrix} \begin{vmatrix} E^l \\ H^l \end{vmatrix} \qquad (5.105)$$

or alternatively

$$\begin{vmatrix} E' \\ H' \end{vmatrix} = [M_1][M_2] \cdots\cdots [M_l] \begin{vmatrix} E^l \\ H^l \end{vmatrix} \qquad (5.106)$$

which can be shown to equal

$$\begin{vmatrix} E' \\ H' \end{vmatrix} = |M| \begin{vmatrix} E^l \\ H^l \end{vmatrix} \qquad (5.107)$$

where the system containing l thin films, each with a characteristic matrix (M_j) may be expressed as

$$[M] = \sum_{j=1}^{l} [M_j] \qquad (5.108)$$

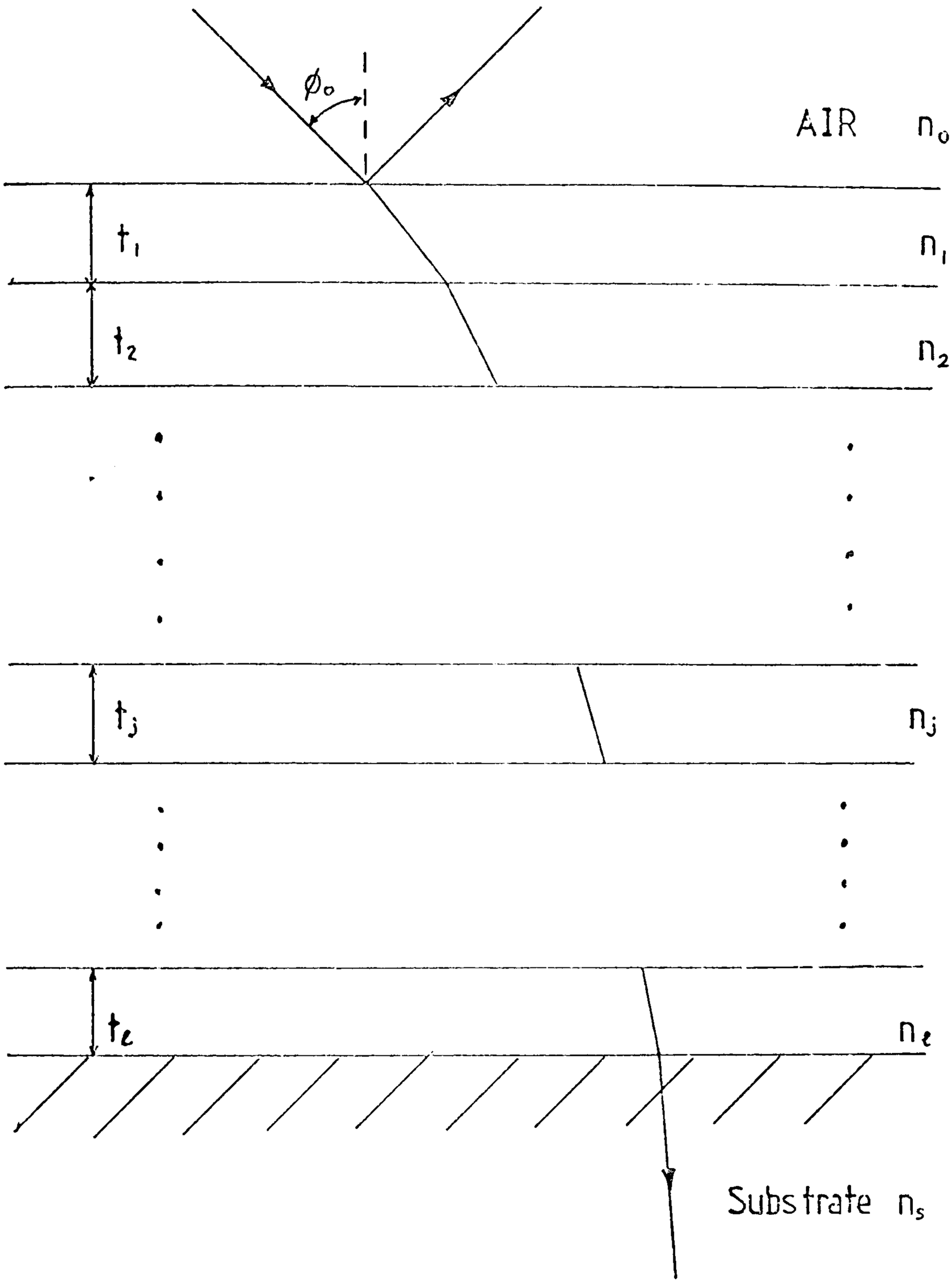

Figure 5.36 The parameters required for analysing a multi-layer thin dielectric film construction

The method by which this technqiue has been developed to include conducting films (i.e. thin metallic films) which are highly absorptive and reflective, is described elsewhere (60).

Rousseau and Mathieu (65) determined the transmittance amplitude for the set of thin films under analysis at normal incidence. The derived equation (5.109) complements equation (5.103) for the reflected amplitude

$$t_{p(s)} = \frac{2N_o}{am_{11} + bm_{12} + cm_{21} + m_{22}} \qquad (5.109)$$

The coefficients in this equation are modified depending upon the angle of incidence and the value of polarisation, in a similar way to equation (5.103).

Consequently, equations (5.103) and (5.109) can be related to the intensity of the reflected and transmitted coefficients by the following equations, which are valid for any angle of incidence

$$R_{p(s)} = |r|^2 \qquad (5.110)$$

$$T_{p(s)} = \frac{n_s \cos \phi_s}{n_o \cos \phi_o} |t|^2 \qquad (5.111)$$

From these two equations the absorption of the multilayer film may be calculated from

$$A_{p(s)} = I - R_{p(s)} - T_{p(s)} \qquad (5.112)$$

or alternatively dividing throughout by the intensity, I,

$$\alpha_{p(s)} = 1 - \rho_{p(s)} - \tau_{p(s)} \qquad (5.113)$$

Analysis of the Combined Thin Film and Substrate System

The analysis of a glazing which has its surface properties modified by thin films does not follow the internal reflections of an ordinary

transparent substrate given in Figure 5.32. The matrix method of analysing a series of thin films, takes into account the effects of the reflected component of the incident radiation from the boundary of the last thin film and the glass surface, see Figures 5.37 to 5.39.

One important feature of thin films is that they may have greatly differing ratios of reflectivity, absorptivity and transmissivity depending upon the direction of the incident beam. Therefore, the reflected component of the incident solar radiation, which is reflected from an internal surface, will not be absorbed, reflected and transmitted in the same ratios as happened when the beam was incident upon the glazing surface in the usual incident direction. This effect must be taken into account.

There are three different glazing systems configurations for analysis:

SYSTEM 1. one or more thin films on both glass surfaces (see Figure 5.37)

SYSTEM 2. one or more thin films on the inner glass surface, none on the outer (see Figure 5.38)

SYSTEM 3. one or more thin films on the outer glass surface, none on the inner (see Figure 5.39)

In Figures 5.37 to 5.39 the properties which have a negative value preceeding their label have this value associated with that of the property in the opposite direction to the incident direction. A geometric series can be obtained for the properties of the thin film and substrate system.

SYSTEM 1: see Figure 5.37 for notation.

$$r = \rho_{f_1} + \frac{\tau_{f_1}\tau_a^2\rho_{f_2}(-\tau_{f_1})}{1-\tau_a^2\rho_{f_2}(-\rho_{f_1})}$$

$$f_1 = \alpha_{f_1} + \frac{\tau_{f_1}\tau_a^2\rho_{f_2}(-\alpha_{f_1})}{1-\tau_a^2\rho_{f_2}(-\rho_{f_1})}$$

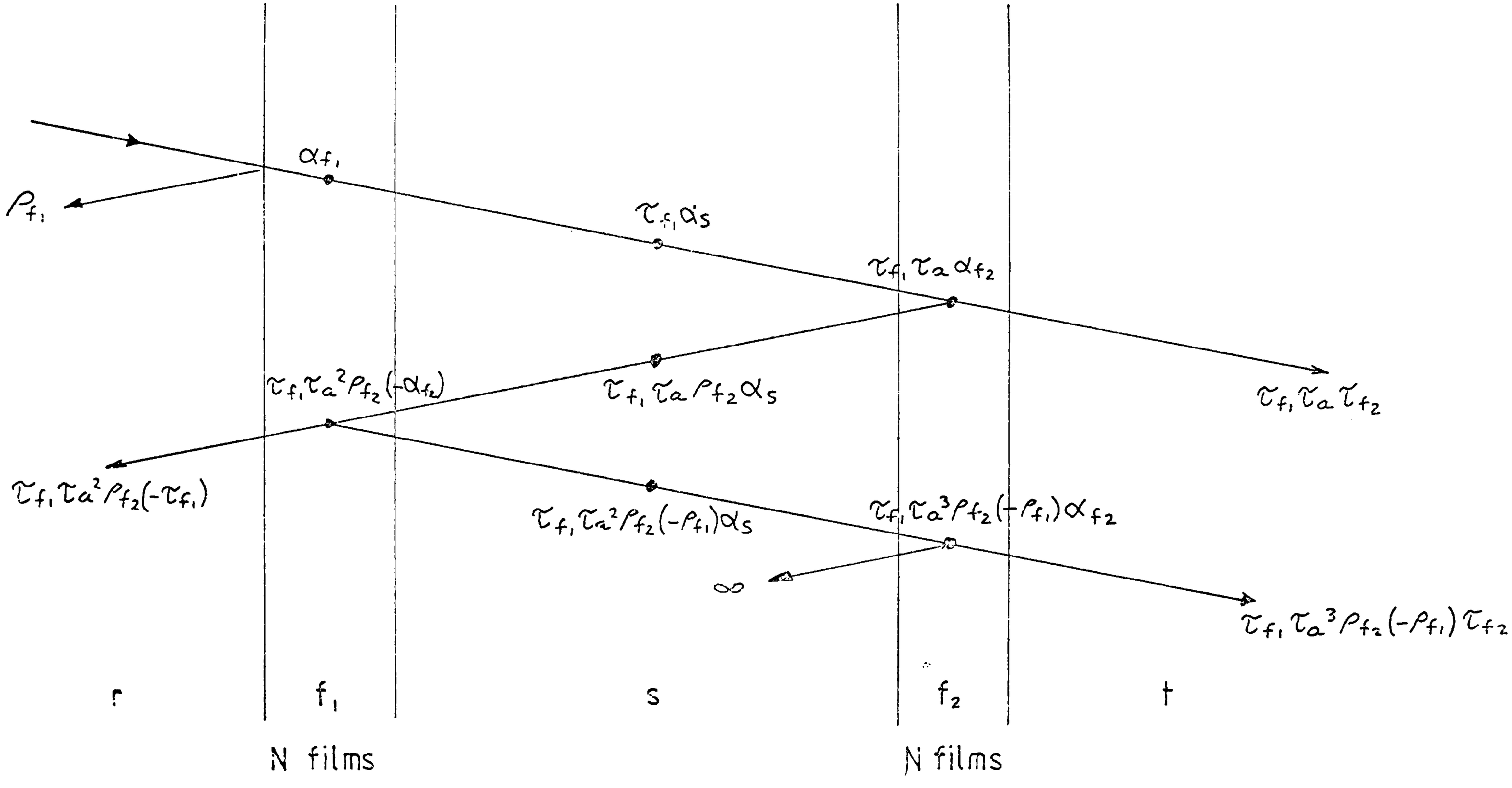

Figure 5.37 Considers an element of the glazing system which has one or more thin films on both glass surfaces

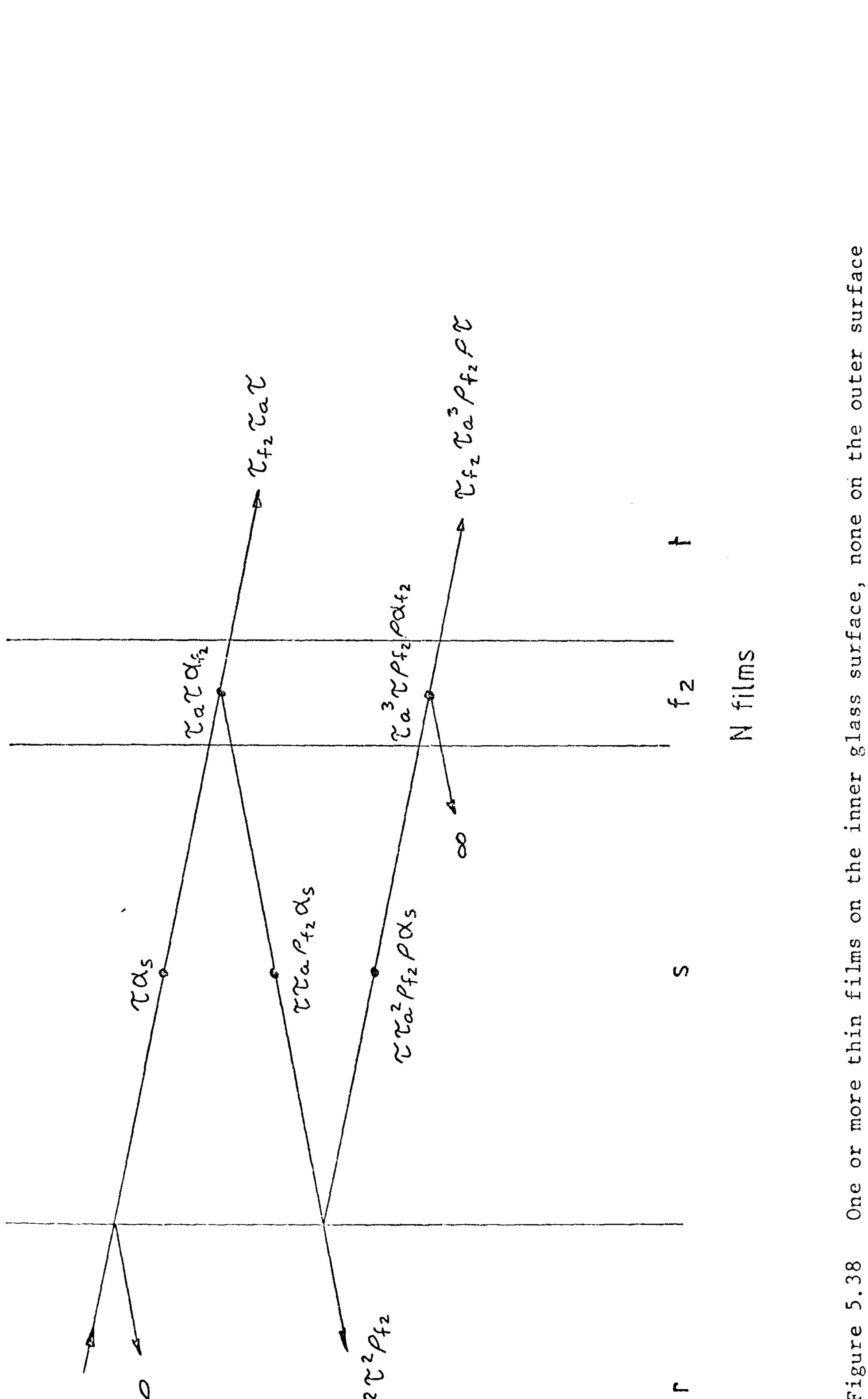

Figure 5.38 One or more thin films on the inner glass surface, none on the outer surface

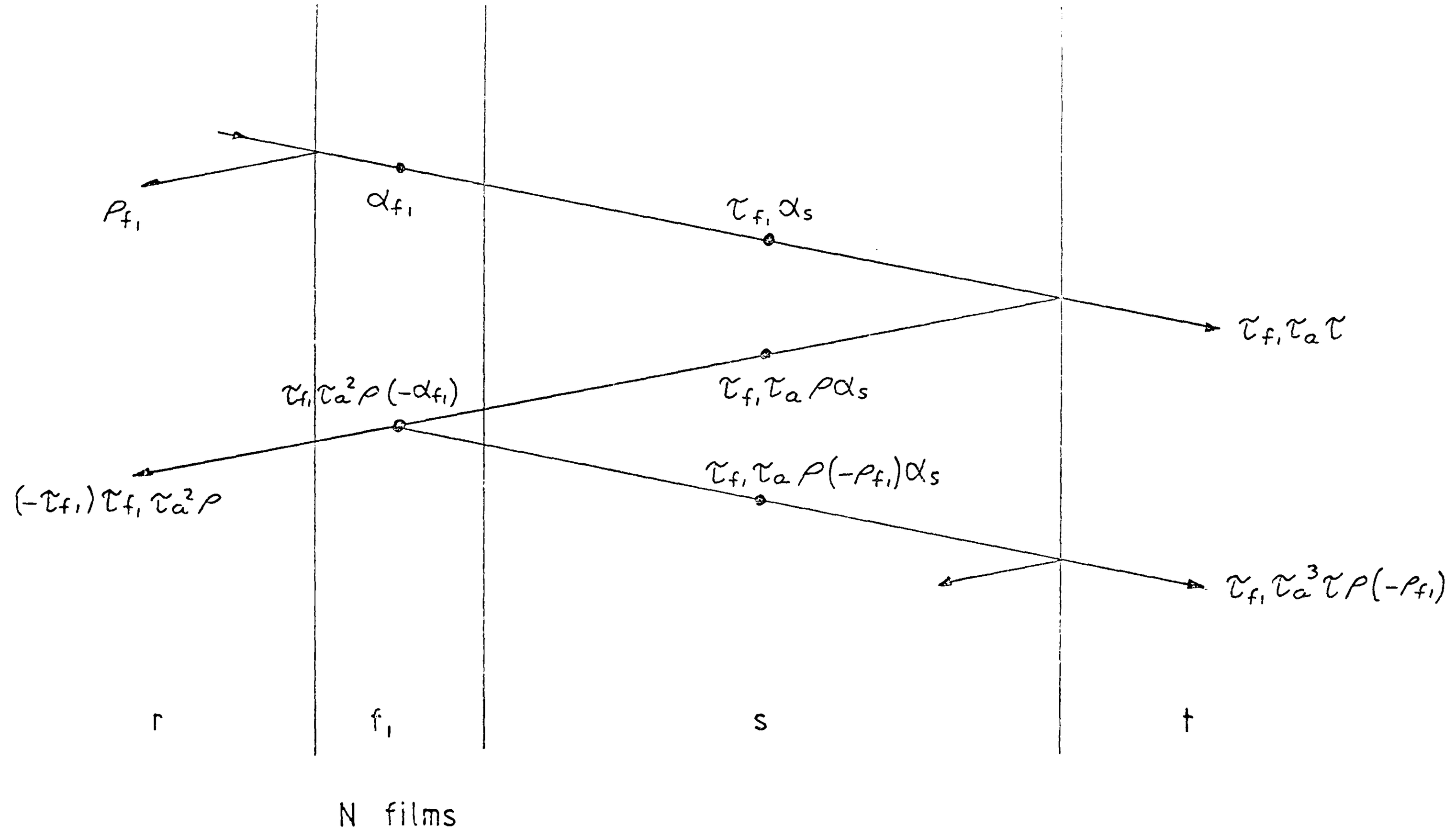

Figure 5.39 One or more thin films on the outer glass surface, none on the inner surface

$$s = \frac{\tau_{f1}\alpha_s(1-\tau_a\rho_{f2})}{(1-\tau_a^2\rho_{f2}(-\rho_{f1}))}$$

$$f_2 = \frac{\tau_{f1}\tau_a\alpha_{f2}}{(1-\tau_a^2\rho_{f2}(-\rho_{f1}))}$$

$$t = \frac{\tau_{f1}\tau_a\tau_{f2}}{(1-\tau_a^2\rho_{f2}(-\rho_{f1}))}$$

where r = reflectivity of system

f_1, f_2 = absorptivity of outer films and inner films respectively

s = absorptivity of substrate

t = transmissivity of system

SYSTEM 2: for notation see Figure 5.38.

$$r = \rho + \frac{\tau_a^2\tau^2\rho_{f2}}{1-\tau_a^2\rho_{f2}\rho}$$

$$s = \frac{\tau\alpha_s(1+\tau_a\rho_{f2})}{1-\tau_a^2\rho_{f2}\rho}$$

$$r = \frac{\tau_a\tau\alpha_{f2}}{1-\tau_a^2\rho_{f2}\rho}$$

$$t = \frac{\tau_{f1}\tau_a\tau}{1-\tau_a^2\rho_{f2}\rho}$$

SYSTEM 3: for notation see Figure 5.39.

$$r = \rho_{f1} + \frac{\rho\tau_a^2\tau_{f1}(-\tau_{f1})}{(1-\tau_a^2\rho(-\rho_{f1}))}$$

$$f_1 = \alpha_{f1} + \frac{\tau_{f1}\rho(-\alpha_{f1})\tau_a^2}{1-\tau_a^2\rho(-\rho_{f1})}$$

$$s = \frac{\tau_{f1}\alpha_s(1+\tau_a\rho)}{1-\tau_a^2\rho(-\rho_{f1})}$$

$$t = \frac{\tau_{f1}\tau_a\tau}{1-\tau_a^2\rho(-\rho_{f1})}$$

When required each of the aforementioned systems are solved for every monochromatic waveband for both components of polarisation, the ratios of the properties are equated to one and assigned to the system. The values of f_1 and f_2 are used to establish values of heat injection at the surfaces of transparent elements as described in Section 5.3.1, in which the following expression was given,

$$\hat{\alpha} = \alpha_{f,} + \alpha + \alpha_{f2}$$

which is identical to

$$\hat{\alpha} = f_1 + S + f_2$$

The operation of a computer program called WINDOW based on this mathematical model is outlined in Appendix 8.

5.3.2 Precipitation

The effects of precipitation on a solar collector must be considered because of the collectors rapid response to climatic changes. The precipitation can be rain, snow, hail, etc, but if it is not rain then its rain equivalent is recorded (Chapter 3). No mathematical models are available to analyse the energy exchange at an exposed surface due to incident precipitation, therefore, a simple model has been devised to take some account of the process. The energy exchange at a surface due to the quantity, duration and temperature of precipitation falling on an exposed surface at any time ξ is represented by the term Qrain(ξ) which is associated with equation (5.77), where

$$Qrain(\xi) = \rho(\xi)\, v(\xi)\, As\, Cp(\xi)\, (\theta rain(\xi) - \theta s(\xi)) \qquad (5.114)$$

and, $\rho(\xi)$ = density of rain (KgM^{-3})

$v(\xi)$ = velocity of rain (MS^{-1}). This is found from the quantity of precipitation and its duration

As = area of surface (M^2)

$Cp(\xi)$ = specific heat capacity of rain ($J.Kg^{-1}.K^{-1}$)

$\theta s(\xi)$ = temperature of the surface under consideration (K)

$\theta rain(\xi)$ = temperature of the rain (K)

This is a very simple model of a highly complex problem; its purpose is to take some account of precipitation. The following assumptions have been made in this model:

- all precipitation is assumed to be rain
- the temperature of the rain equals the ambient wet bulb temperature which can be evaluated from the ambient temperature and relative humidity values in the climate file, see Appendix 2
- rainfall velocity is constant during time-increment
- no account taken of material porosity
- no evaporation takes place as all the rain is assumed to run off the surface immediately, therefore, no fluid is left on the surface after the time-increment
- no modification of the heat transfer coefficient for the exposed surface

- no account of driven rain due to wind direction is made, therefore, each surface has the same rain velocity

The values of precipitation quantity and duration are obtained from the appropriate values of the meteorological tapes if this data is used for the climate files, otherwise they must be estimated in some way. It is assumed that $\theta_{rain}(t)$ is known at both the present(n) and future (n+1) time rows, therefore, equation (5.114) can be re-written in the form

$$Q_{rain}(t) = \Phi_2(t) - \Phi_1(t)\,\theta_s(t) \qquad (5.115)$$

where,

$$\Phi_1(t) = \rho(t)\,U(t)\,A_s\,C_p(t) \quad ; \quad \Phi_2(t) = \Phi_1(t)\,\theta_{rain}(t)$$

5.3.3 Longwave Radiation Exchange

The net longwave radiation exchange between two opaque surfaces at any time t, is given by

$$q_{12}(t) = \sigma\, f'_{1\to2}(t)\,(T_1^4(t) - T_2^4(t))$$

where σ = Stefan-Boltzman constant ($5.6697*10^{-8} WM^{-2}.K^{-4}$)

$f'_{1\to2}$ = non-grey body geometric view factor between two surfaces

T = the absolute temperature of the surface (K) which equals $\theta + 273.15$

Wrangham's (66) expression for the grey body (i.e. $\varepsilon=\alpha$) view factors between two surfaces allowing for multiple diffuse reflections has been modified to eliminate the Kirchoff's Law restriction

$$f'_{1\to2}(t) = \frac{\varepsilon_1 T_1^4 F_{1\to2} - \varepsilon_2 T_2^4 F_{1\to2} + \rho_1 \varepsilon_2 T_2^4 F_{1\to2} - \rho_2 \varepsilon_1 T_1^4 F_{1\to2} A_1/A_2}{(T_1^4 - T_2^4)(1 - \rho_1\rho_2 F_{1\to2}^2 A_1/A_2)} \qquad (5.116)$$

where ε = surface emissivity

ρ = surface reflectivity

A = area of surface (M^2)

$F_{1\to2}$ = black body view factor between surfaces. There are a

number of analytical methods of assessing this value (67), however, in this work the user can employ a simple algorithm to assess $F_{1\to 2}$ (68) or a detailed algorithm (69). Computer programs based upon both will be discussed in subsequent chapters.

The total net longwave radiation gain at an internal surface at time ξ is the result of the exchange between surface S and all other surfaces with which it is in radiative contact,

$$q_{Lw}(\xi) = \sum_{j=1}^{J} \sigma f_{j\to s}(\xi)\left(T_j^4(\xi) - T_s^4(\xi)\right)$$

where J is the number of surfaces in radiative contact with surface S. This expression can be rewritten to give

$$Q_{ILWR}(\xi) = A_s \sum_{j=1}^{J} h_{r_{j\to s}}(\xi)\left(T_j(\xi) - T_s(\xi)\right)$$

or,

$$Q_{ILWR}(\xi) = A_s \sum_{j=1}^{J} h_{r_{j\to s}}(\xi)\left(\theta_j(\xi) - \theta_s(\xi)\right) \qquad (5.117)$$

where

$Q_{ILWR}(\xi)$ = the net longwave radiative exchange at surface S (W), from equation (5.78)

$h_{r_{j\to s}}(\xi)$ = the radiative coefficient between surface S and surface j ($S.M^{-2}.K^{-1}$)

$$h_{r_{j\to s}}(\xi) = \sigma f_{j\to s}\left(T_j(\xi) + T_s(\xi)\right)\left(T_j^2(\xi) + T_s^2(\xi)\right)$$

Unfortunately the radiation coefficient $h_{r_{j\to s}}(\xi)$ is a function of the prevailing surface temperatures and evaluation at the future time row ($\xi = n+1$) is not possible since the surface temperatures are as yet unknown. Iterative techniques could be employed, at each time increment, to model the longwave radiation exchange with considerable accuracy, however, this could not be justified in terms of the increased computation. Therefore, it is proposed to compute the radiation coefficient one time increment in arrears for both $\xi = n$ and $\xi = n+1$, so that,

$$hr_{j\to s(n)} = \sigma F_{j\to s}\left(T_{j(n-1)} + T_{s(n-1)}\right)\left(T_{j(n-1)}^2 + T_{s(n-1)}^2\right)$$

and,

$$hr_{j\to s(n+1)} = \sigma F_{j\to s}\left(T_{j(n)} + T_{s(n)}\right)\left(T_{j(n)}^2 + T_{s(n)}^2\right)$$

This method will be most accurate when used for small time increment simulations.

Some elements are transparent to re-radiated thermal energy particularly some plastic covers, consequently energy may be lost from the enclosure in a similar manner to the shortwave solar radiation re-reflected through transparent materials. If the transmissivity of a material in a particular range of the electromagnetic spectrum is known then to account for the longwave energy transmitted the quantity of energy emitted within the waveband will have to be calculated. This calculation is also required for selective surfaces which have different emissivities in different wavebands, therefore, it is important the emitted longwave energy spectrum for any surface is known.

The quantity of energy emitted from a surface within a specific waveband identified by the boundary wavelengths λ_1 and λ_2 can be found by considering the energy emitted from a black body. If a black body is at a temperature T(K) then the fraction of black body energy emitted between zero and λ is given by the factor $f_{0-\lambda(T)}$. Polynominal approximations for $f_{0-\lambda(T)}$ are available (34), for $\gamma > 2$

$$f_{0-\lambda(T)} = \frac{15}{\pi^4} \sum_{m=1,2\ldots} \frac{e^{-m\gamma}}{m^4}\left\{\left[(m\gamma+3)m\gamma+6\right]m\gamma+6\right\}$$

and for $\gamma < 2$

$$f_{0-\lambda(T)} = 1 - \frac{15}{\pi^4}\gamma^3\left(\frac{1}{3} - \frac{\gamma}{8} + \frac{\gamma^2}{60} - \frac{\gamma^4}{5040} + \frac{\gamma^6}{272{,}160} - \frac{\gamma^8}{13{,}305{,}600}\right)$$

where,

$$\gamma = \frac{C_2}{\lambda T}$$

C_2 = Planck's second radiation constant ($1.43879 * 10^{-8}$ μmK)

If $f_{0\to\lambda(T)}$ is solved for the boundaries λ_1 and λ_2 of a waveband then

subtraction of the two values will give the ratio of the emitted black body energy between λ_1 and λ_2 to the total emitted black body energy at temperature T, therefore

$$\ell_{\lambda_1 \to \lambda_2}(T) = \ell_{0 \to \lambda_2}(T) - \ell_{0 \to \lambda_1}(T)$$

The energy emitted from a real surface in waveband λ_1 to λ_2 at time ξ is given by

$$q_{\lambda_1 - \lambda_2}(\xi) = \varepsilon_{\lambda_1 - \lambda_2}\, \ell_{\lambda_1 - \lambda_2}(\xi)(T_s)\, \sigma\, T_s^4(\xi)$$

where Ts is the absolute surface temperature (K) and $\varepsilon_{\lambda_1 - \lambda_2}$ is the emissivity in the waveband λ_1 to λ_2. This expression can be used to establish the transmitted thermal radiation between surface S and a transparent element within a particular waveband.

Wein's Law (55) can be used to determine the wavelength associated with the maximum spectral emissive power for a black body surface

$$\lambda \text{ max} = \frac{2897.8}{T}$$

It is useful to identify λ max so that it can be compared with any region of the spectrum which is transmitted by a transparent material.

The net longwave radiative exchange between an exposed external surface and its surrounds was identified in equation (5.77), it can have a significant effect on a surface particularly if the surface is in radiative exchange with the sky vault during clear sky nights.

Consider an exposed plane surface (Figure 5.40), the net external longwave radiation exchange is the difference between the simultaneous emission of longwave radiant heat from the surface and the longwave radiant heat received by the surface from its surroundings, therefore

$$Q_{ELWR} = Q_E - Q_S$$

where Q_e = energy received by a surface from its environment (watts)

Q_S = energy emitted by a surface to its surrounding environment (watts)

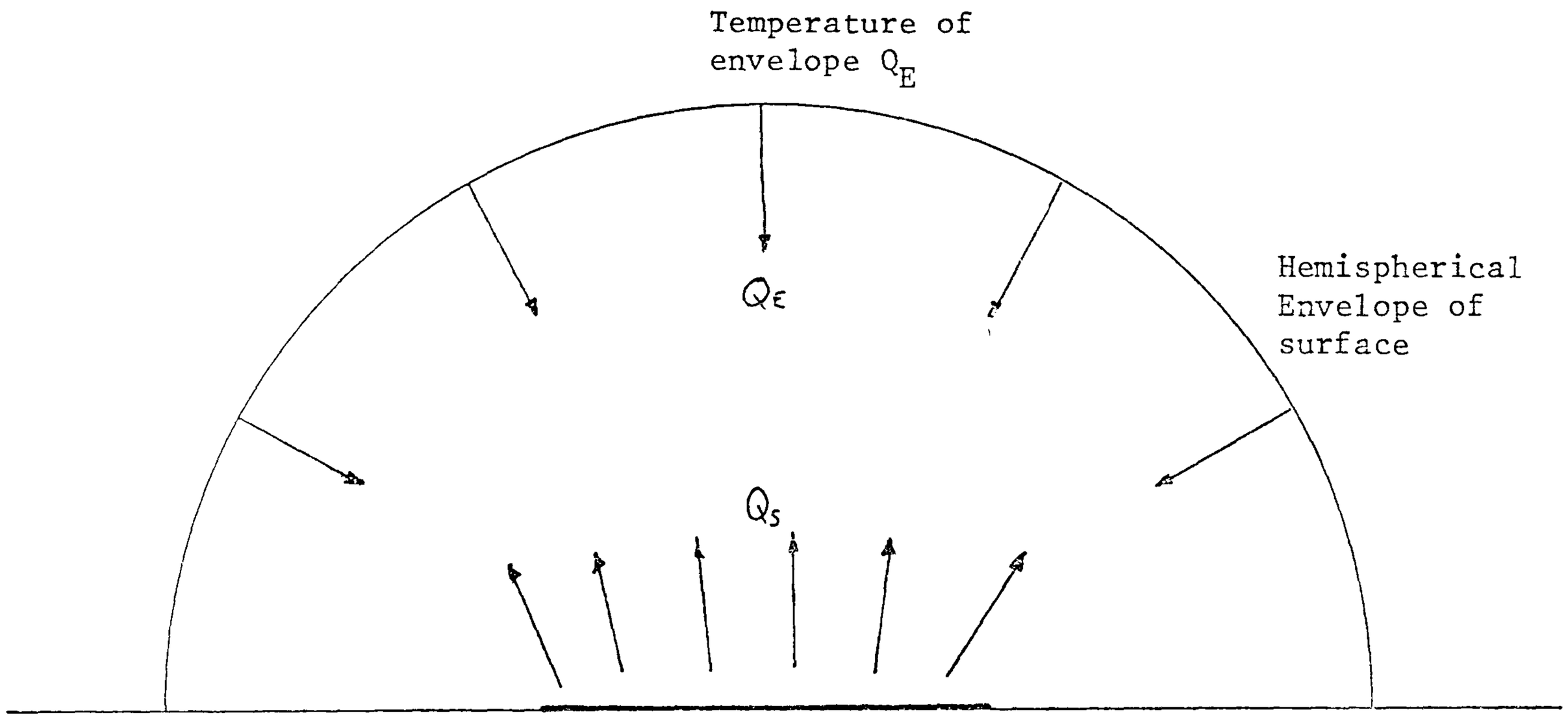

Figure 5.40 The interaction at the exposed surface of the emitted, Q_S, and the received, Q_E, longwave radiation.

The term 'longwave radiation' is used because the wavelengths of both the emitted and received radiation are predominantly in the infra-red region of the electromagnetic spectrum.

Lacy (70) suggests that in a normal British night-time climate an exposed building surface may be subjected to a radiation loss of $60WM^{-2}$, consequently, if night-time surfaces drop below the ambient temperature dew will form on the surface, this phenomena is more frequent during cloudless night sky conditions. During daytime however the incident shortwave solar radiation on the surface usually exceeds any longwave radiation imbalance.

If it is assumed that the incoming longwave radiation from the surrounding envelope of any surface can be associated with a mean black body hemispherical envelope temperature, T_E, then the quantity of energy incident upon the surface can be described by the Boltzman equation

$$Q_E = A_S \sigma T_E^4 \qquad (5.118)$$

The net longwave radiation at time ξ can be expressed as,

$$Q_{ELWR(\xi)} = A_S \varepsilon_S \sigma (T_{E(\xi)}^4 - T_{S(\xi)}^4) \qquad (5.119)$$

where ε_s = emissivity of the exposed surface
σ = Stefan-Boltzman constant $(WM^{-2}.K^{-4})$
T_S = mean surface temperature, (K) or $(\Theta s + 273.15)$

The process involved in evaluating the mean hemispherical envelope temperature is relatively simple. The quantity of energy received by a surface depends upon the nature of its surrounding envelope. The incident energy upon the surface may consist of energy emitted from three sources: the sky, the ground and the surrounding surfaces (i.e. buidlings). Thus

$$Q_E = Qsky + Qgrd + Qbld \qquad (5.120)$$

where Qsky = energy emitted from the sky portion of the envelope (watts)

Qgrd = energy emitted from the ground porition of the envelope (watts)

Qbld = energy emitted from the surrounding surfaces portion of the envelope (watts)

It was assumed that the surrounding envelope is a perfect radiator, as this assumption is applied to the sky, ground and surrounding building temperatures then substituting equation (5.120) into equation (5.118) and re-expressing yields,

$$A_S \sigma T_E^4 = A_S(A \sigma Tsky^4 + B \sigma Tgrd^4 + C \sigma Tbld^4) \qquad (5.121)$$

where Tsky = mean sky vault temperature (K)

Tgrd = mean ground temperature (K)

Tbld = mean temperature of surrounding buildings (K)

Methods of calculating Tsky, Tgrd and Tbld are given in Appendix 10. The coefficients A, B and C refer to that portion of the surface's envelope which is sky, ground and surrounding buildings respectively. This implies that A, B and C are geometric relationships which correspond to view factors; each coefficient varies between zero and one depending on the siting of the exposed surface, therefore, the summation of A, B and C equates to one

$$A + B + C = 1 \qquad (5.122)$$

Table 5.7 lists the values of A, B and C for vertical surfaces in different sites. Appendix 9 describes the method by which these geometric relationships are calculated and how they can be applied to non-vertical surfaces.

Substituting equation (5.121) into the expression for the net longwave radiation - equation (5.119) - then for any time ξ ,

$$Q_{ELWR(\xi)} = A_S \varepsilon_S \sigma (A_{(\xi)} Tsky^4_{(\xi)} + B_{(\xi)} Tgrd^4_{(\xi)} + C_{(\xi)} Tbld^4_{(\xi)} - T_{S(\xi)}^4)$$

TABLE 5.7 View factors of the sky vault (Av), ground (Bv) and surrounding buildings (Cv), that are in the surrounding envelope of a vertical surface, depending upon the nature of the site under analysis.

	Av	Bv	CV
1. City centre site : surrounding building at same height, twice as long and half the height away from the surface, i.e. normal	0.36	0.36	0.28
2. Urban site : Normal case	0.41	0.41	0.18
3. Rural site : Normal case	0.45	0.45	0.10
4. City centre site : equally weighted proportions	0.33	0.33	0.34
5. City centre site : surface well below the mean height of the surrounding buildings	0.15	0.33	0.52
6. City centre site : surface at same height as surrounding buildings, i.e. sloping roof	0.50	0.20	0.30
7. Urban site : surface at same height as surrounding buildings, i.e. sloping roof	0.50	0.30	0.20
8. Rural site : isolated	0.50	0.50	0.00
9. Total enclosed surface : i.e. if solar collector is tested indoors, surfaces will be surrounded by 'building'	0.00	0.00	1.00

This expression can be linearised to the form of equation (5.117)

$$Q_{ELWR(\xi)} = A_S hr_{E \rightarrow S(\xi)} \left(\theta_{E(\xi)} - \theta_{S(\xi)}\right) \qquad (5.123)$$

where

$hr_{E-S(\xi)}$ = the radiative coefficient between surface S and its surrounding envelope E, $(W.M^{-2}.K^{-1})$

$$= \sigma \varepsilon_S \left(T_{E(\xi)} + T_{S(\xi)}\right)\left(T_{E(\xi)}^2 + T_{S(\xi)}^2\right)$$

As described earlier the radiative coefficient is calculated one time increment in arrears and assuming the surrounding envelope to the surface is known at its future (n+1) value then equation (5.123) can be re-written as

$$Q_{ELWR(\xi)} = \exists_2(\xi) - \exists_1(\xi)\,\theta_S(\xi) \qquad (5.124)$$

where $\exists_1(\xi) = A_S hr_{E \rightarrow S(\xi)}$

$\exists_2(\xi) = \exists_1(\xi)\,\theta_E(\xi)$

There are alternative methods of calculating $Q_{ELWR(\xi)}$, Cole (71,72) assumed no surrounding buildings and considered only the effects of sky and ground radiation the values of which were estimated as a function of the screen air wet bulb temperature. This technique has been used by several authors (73,74) and some of this work is described in Appendix 10.

Non-exposed external surfaces undergo a longwave radiation exchange, it can be modelled using equation (5.123), however, in this work it will be denoted Q_{ILWR} and is assumed that the surrounding envelope temperature is known at both the present and future time rows. Consq-quently equation (5.124) can be used to model $Q_{ILWR(\xi)}$.

5.3.4 Component Energy Injection Sources

In a fan or pump the power supplied by either component is regarded as being converted to heat and causes an increase in the temperature of the fluid handled (47). The power supplied at time ξ is mathematically described by

$$P(\xi) = \frac{\dot{V}(\xi)p(\xi)}{(\zeta(\xi)/100)} \qquad (5.125)$$

where $P(\xi)$= component power supplied (W)
$V(\xi)$= volumetric flow-rate (M^3S^{-1})
$p(\xi)$= total pressure (NM^{-2})
$\zeta(\xi)$= component efficiency (%)

This equates to the energy injected into the fluid at time ξ, where

$$Q_{inj}(\xi) = \dot{V}(\xi)\rho(\xi)C(\xi)(\theta_{f,out}(\xi) - \theta_{f,in}(\xi)) \qquad (5.126)$$

and $Q_{inj}(\xi)$= energy injected, (W), as given by equation (5.46)
$\rho(\xi)$ = density of fluid (KgM^{-2})
$C(\xi)$ = specific heat of fluid ($JKg^{-1}K^{-1}$)
$\theta_{f,out}(\xi)$= temperature of fluid flowing out of component (K)
$\theta_{f,in}(\xi)$= temperature of fluid flowing into component (K)

Re-arranging equation (5.125) and subsituting into equation (5.126) yields

$$Q_{inj}(\xi) = \frac{P(\xi)\zeta(\xi)\rho(\xi)C(\xi)}{100p(\xi)}(\theta_{f,out}(\xi) - \theta_{f,in}(\xi)) \qquad (5.127)$$

This heat generation source depends on controller operation of the component based on information available at the known (present) time-step, this information will be processed by the controller to determine component operational status for the time increment to be conducted. From the General Heat Balance Equation for fluid flow $\theta_{f,out}(\xi)$, in equation (5.127), equals $\theta_{I(\xi)}$ the fluid node temperature under analysis. Equation (5.127) can be re-written in the form,

$$Q_{inj}(t) = \dot{m}_c(t)\left(\theta_{I(t)} - \theta_{f,in(t)}\right) \qquad (5.128)$$

where

$$\dot{m}_c(t) = \frac{P(t)\,\beta(t)\,\rho(t)\,C(t)}{100\,\Delta t}$$

the values of $\dot{m}_c$ are assumed to be known at n and n+1.

There are several components for which the estimation energy exchange with the surround is too complex to analyse by normal methods. This is because components such as pumps, fans, auxiliary heaters, etc, are modelled by a single node and their external surface geometry is unknown or irregular. The loss from the component to the surrounds at any time t is a function of the temperature of the surrounding air (θ_s), the component surface temperature (θ_c), the surface area of the component (Ac) and the convective/radiative exchange coefficient between the component surface and its surrounds (h), therefore at any time t

$$Qenv(t) = f(\theta_{s(t)}, \theta_{c(t)}, Ac, h_{(t)}) \qquad (5.129)$$

where $Qenv(t)$ is the energy exchange between the component and its surrounds. As this term represents an estimation of the energy exchange it is assumed that the value is known at both the present (n) and future (n+1) time rows.

The purpose of an auxiliary heater is to heat the entering fluid to a desired outlet fluid temperature, the quantity of auxiliary energy required to be injected into the fluid at any time t is denoted $Q_{AUX(t)}$ (from equation 5.49). The desired outlet temperature can be pre-set in a fixed or variable form if it is assumed that the auxiliary heater is the last component before the load to which the fluid is suppled, therefore, the fluid leaving the auxiliary heater becomes the desired inlet condition to the load. In domestic hot water service systems liquid is normally required at a particular value, this becomes the fixed desired inlet condition. A variable desired inlet fluid temperature can be calculated for a space heating system if a file containing values

of the load demand and space temperature are available at regular time intervals (maximum interval of one hour). This data can be created from actual measurements or from simulation models such as ESP. Therefore, the desired outlet temperature from the auxiliary heater is a system boundary condition and as such it is known at both the present (ℓ =n) and future (ℓ =n+1) time rows.

Assuming that there is some form of control on the quantity of energy injected by the auxiliary heater, and if there is sufficient auxiliary energy to obtain the desired outlet temperature, there will be no over or under-shoot of this value and the exact quantity of auxiliary energy will be delivered. However, there are situations where the maximum quantity of auxiliary energy injected into the fluid cannot achieve the desired outlet temperature, therefore, the outlet temperature from the auxiliary heater is unknown as $Q_{AUX(\ell)}$ is set to its maximum value. In such cases (or where no auxiliary is used) the shortfall in demand is assumed to be delivered from an auxiliary heater operating in parallel.

In a liquid energy storage tank the energy injected into any tank segment by an electric resistive element at any time ℓ is denoted $Q_{E(\ell)}$ - equation (5.65). At the start of a time increment (ℓ =n) a controller will decide whether or not the electric element should be off or on for the duration of the time increment. The controller decision is based on a thermostat measuring liquid temperature at some segment and testing if this value is above or below a desired tank segment temperature. If the electric element is switched on then energy, at a fixed rate, will be injected at the appropriate segment node without any time lag. This could result in the segment temperature overshooting the desired temperature, however, this will have little or no significance if the electric element is correctly sized and the time increments are sufficiently small.

Alternatively, the electric element may be time dependent not temperature dependent. In such cases the electric element will be switched on during specific periods and it will be controlled only by an upper liquid temperature setting which will act as a safety override.

5.3.5 Photovoltaic

Detailed mathematical models are available (20,75), however, there are several problems associated with their use:

- assume ideal diode properties
- they produce non-linear results
- it is difficult to break results into a temperature and temperature coefficients
- difficult to analyse performance except for a short-circuit, open-circuit or for maximum power output
- manufactuburers solar cell specifications do not contain the required data to conduct a detailed analysis.

Therefore, a simple empirical formulation is used which is based on data obtained from experimental data. This data is normally provided by manufacturers when specifying solar cells. The technique assumes that the solar cells operate at the maximum power output at all times, that is, at the knee of the curve (see Chapter 2).

The quantity of radiative energy which is converted to electrical power by the solar cell at any time ξ is denoted $Qp(\xi)$, identified in equation (5.72). Evans (76) represented this heat generation term by the expression

$$Q_p(\xi) = \alpha_c G_T(\xi) A_c N_c \beta_R [1 - \beta(\theta_I(\xi) - \theta_R) + \gamma \log_{10} G_T(\xi)] \qquad (5.130)$$

where
$G_{T(\xi)}$ = total incident irradiance (WM^{-2})
Ac = area of each solar cell (M^2)
Nc = number of cells in array
α_c = absorptivity of cells
θ_R = test reference temperature (deg C)
β_R = cell efficiency at θ_R
$\theta_{I(\xi)}$ = temperature of cell (deg C)
β = temperature coefficient for cell efficiency
γ = intensity coefficient for cell efficiency

This equation may be applied to single cells that can be grouped together to form arrays in which N cells connected in parallel by M, such parallel connected groups connected in series would give a current of

$$I_A = NI_C$$

and a voltage of

$$V_A = MV_C$$

where I_A and V_A represent the current and voltage of the array and I_C and V_C represent the current and voltage of each cell.

The value of $Qp(\xi)$ depends on the temperature of the solar cells and consequently it is not known at the future time row. Equation (5.130) can be re-arranged to give

$$Qp(\xi) = -\omega_1(\xi)\Theta_I(\xi) + \omega_2(\xi) \qquad (5.131)$$

where

$$\omega_1(\xi) = \alpha_c G_T(\xi) A_c N_c \beta R$$
$$\omega_2(\xi) = \alpha_c G_T(\xi) A_c N_c \beta R [1 + \beta \Theta R + \gamma \log_{10} G_T(\xi)]$$

$G_T(\xi)$ is the only variable term in both $\omega_1(\xi)$ and $\omega_2(\xi)$ as it is a known boundary condition then both $\omega_1(\xi)$ and $\omega_2(\xi)$ are known at $\xi = n$ and $\xi = n+1$.

5.3.6 Liquid Collectors

Liquid Collectors operate by passing a fluid through conduits which are connected in some way to the absorber plate, see Chapter 2. The conduits can be any shape; they can be positioned above, below or through the absorber plate or they can have any arrangement, for example, parallel or serpentined. The method of modelling this collector is to connect absorber plate nodes (Categories 1, 2 and 3) to conduit nodes (Category 4). However, by doing this there is a conductive energy exchange which has to be considered, each conduit will have a Qcond(ξ) term associated with the conductive energy exchange between it and the absorber plate node, this will have the same numerical value as the Qliq(ξ) term for the conductive energy between the absorber plate and that particular conduit. The Qliq(ξ) term may have several conduits associated with it and each must be taken into account. These two heat injection terms may be expressed mathematically by

$$Q_{cond}(\xi) = A_c \frac{k_c}{\Delta x} \left(\theta_{Ab}(\xi) - \theta_I(\xi)\right) \qquad (5.132)$$

where Ac = contact area between conduit and absorber plate (M^2)
kc = conductivity ($WM^{-1}K^{-1}$)
ΔX = effective thickness of conduit (M)
$\theta_{Ab}(\xi)$ = temperature of absorber plate (K)
$\theta_I(\xi)$ = temperature of conduit node (K)

and $$Q\,liq(\xi) = \sum_{l=0}^{L} A_l \frac{k_l}{\Delta x_l} \left(\theta_{c,l}(\xi) - \theta_I(\xi)\right) \qquad (5.133)$$

where L = number of conduits connected to node I
Ac = area of contact with node 1 (M^2)
kl = conductivity of material connected absorber plate with conduit node ($WM^{-1}K^{-1}$)
$\Delta X1$ = effective thickness of conduit (M)
$\theta_{c,l}(\xi)$ = nodal temperature of conduit 1 (K)
$\theta_I(\xi)$ = temperature of absorber plate (K)

The term Qcond(ξ) was identified by equation (5.46) and Qliq(ξ) is associated with equations (5.9), (5.18), (5.77) and (5.78).

5.4 The Difference Equations in Complete Form

In Table 5.2 and equations (5.77) and (5.78) the summation of the heat generation sources for each nodal category are identified. In order to write the complete form of the difference equations derived in Section 5.2.1, the appropriate summation of heat generation terms for each node is applied and re-defined in terms of the mathematical models described in Section 5.3. The resulting expression is re-arranged to ensure that all unknown terms are on the left-hand side of the equation and the right-hand side contains all known values. Each node type of every category will now be written in its complete form by this method. The notation for each category corresponds to the appropriate derivation in Section 5.2.1.

Category1

a. Type 1 - node positioned at the centre of a homogeneous element with three dimensional conduction

The derived differential equation for this nodal category is given by equation (5.38) which is

$$(2+a_7)\theta_{I(n+1)} - a_1\theta_{I-1(n+1)} - a_2\theta_{I+1(n+1)} - a_3\theta_{J-1(n+1)} - a_4\theta_{J+1(n+1)}$$

$$-a_5\theta_{K-1(n+1)} - a_6\theta_{K+1(n+1)} = (2-a_7)\theta_{I(n)} + a_1\theta_{I-1(n)} + a_2\theta_{I+1(n)}$$

$$+a_3\theta_{J-1(n)} + a_4\theta_{J+1(n)} + a_5\theta_{K-1(n)} + a_6\theta_{K+1(n)} + a_8\left(\Sigma Q_{I(n+1)} + \Sigma Q_{I(n)}\right) \qquad (5.7)$$

where

$$a_1 = a_2 = \frac{A_x k}{S\Delta X} \quad ; \quad a_3 = a_4 = \frac{A_y k}{S\Delta Y}$$

$$a_5 = a_6 = \frac{A_z k}{S\Delta Z} \quad ; \quad a_7 = a_1 + a_2 + a_3 + a_4 + a_5 + a_6$$

$$a_8 = \frac{1}{S} = \frac{\Delta\tau}{\rho C V}$$

$$\Delta X = \Delta X_I$$

$$\Delta Y = \Delta Y_I$$

$$\Delta Z = \Delta Z_I$$

The summation of the heat generation terms for this nodal category described by equation (5.9), can be re-written in terms of equations (5.81), (5.131) and (5.133), thus

$$\sum Q_{I(t)} = Q_{s,\alpha(t)} + \omega_{2(t)} - \omega_{1(t)}\theta_{I(t)} + \sum_{\ell=0}^{L} A\ell \frac{k\ell}{\Delta X\ell}\left(\theta_{c,\ell(t)} - \theta_{I(t)}\right) + Q_{M(t)}$$

rearranging gives

$$\sum Q_{I(t)} = Q_{s,\alpha(t)} + \omega_{2(t)} - \left(\omega_{1(t)} + \sum_{\ell=0}^{L} A\ell \frac{k\ell}{\Delta X\ell}\right)\theta_{I(t)} + \sum_{\ell=0}^{L} A\ell \frac{k\ell}{\Delta X\ell}\theta_{c,\ell(t)} + Q_{M(t)}$$

(5.134)

Substituting equation (5.134) into equation (5.7) and transferring the future unknown temperature terms ($\theta_I(n+1)$ and $\theta_C(n+1)$) to the left-hand side of the equation the following expression is established

$$\left[2 + a_7 + a_8\left(\omega_{1(n+1)} + \sum_{\ell=0}^{L} A\ell \frac{k\ell}{\Delta X\ell}\right)\right]\theta_{I(n+1)} - a_1\theta_{I-1(n+1)} - a_2\theta_{I+1(n+1)}$$

$$- a_3\theta_{J-1(n+1)} - a_4\theta_{J+1(n+1)} - a_5\theta_{K-1(n+1)} - a_6\theta_{K+1(n+1)} - a_8\sum_{\ell=0}^{L} A\ell \frac{k\ell}{\Delta X\ell}\theta_{c,\ell(n+1)}$$

$$= \left[2 - a_7 - a_8\left(\omega_{1(n)} + \sum_{\ell=0}^{L} A\ell \frac{k\ell}{\Delta X\ell}\right)\right]\theta_{I(n)} + a_1\theta_{I-1(n)} + a_2\theta_{I+1(n)}$$

$$+ a_3\theta_{J-1(n)} + a_4\theta_{J+1(n)} + a_5\theta_{K-1(n)} + a_6\theta_{K+1(n)} + a_8\sum_{\ell=0}^{L} A\ell \frac{k\ell}{\Delta X\ell}\theta_{c,\ell(n)}$$

$$+ a_8\left(Q_{s,\alpha(n+1)} + Q_{s,\alpha(n)} + \omega_{2(n+1)} + \omega_{2(n)} + Q_{M(n+1)} + Q_{M(n)}\right)$$

This equation can be re-labelled to give the differential equation in its complete form,

$$(2 + A_{4(n+1)})\theta_{I(n+1)} - A_1\theta_{I-1(n+1)} - A_1\theta_{I+1(n+1)} - A_2\theta_{J-1(n+1)} - A_2\theta_{J+1(n+1)}$$

$$- A_3\theta_{K-1(n+1)} - A_3\theta_{K+1(n+1)} - \sum_{\ell=0}^{L} A_{6+L}\theta_{c,\ell(n+1)} = (2 - A_{4(n)})\theta_{I(n)}$$

$$+ A_1\theta_{I-1(n)} + A_1\theta_{I+1(n)} + A_2\theta_{J-1(n)} + A_2\theta_{J+1(n)} + A_3\theta_{K-1(n)} + A_3\theta_{K+1(n)}$$

$$+ \sum_{\ell=0}^{L} A_{6+\ell}\theta_{c,\ell(n)} + A_5\left(Q_{s,\alpha(n+1)} + Q_{s,\alpha(n)} + \omega_{2(n+1)} + \omega_{2(n)} + Q_{M(n+1)} + Q_{M(n)}\right)$$

(5.135)

where,

$$A_1 = a_1 = a_2 = \frac{A_x k}{S\Delta X} \quad ; \quad A_2 = a_3 = a_4 = \frac{A_y k}{S\Delta Y}$$

$$A_3 = a_5 = a_6 = \frac{A_z k}{S\Delta Z} \quad ; \quad A_4 = a_7 + \frac{\omega_1(\xi)}{S} + \sum_{\ell=0}^{L} A_{6+\ell}$$

$$A_5 = a_8 = \frac{1}{S} = \frac{\Delta\tau}{\rho C V} \quad ; \quad A_{6+\ell} = \frac{A_\ell k_\ell}{S\Delta X_\ell} \qquad (\ell = 0, 1, 2, .., L)$$

$$\omega_1(\xi) = \alpha_c G_{T(\xi)} A_c N_c \beta_R \beta \quad ; \quad \omega_2(\xi) = \alpha_c G_{T(\xi)} A_c N_c \beta_R [1 + \beta\theta_R + \gamma \log G_{T(\xi)}]$$

The notation for these temperature coefficients is given in equations (5.7), (5,81), (5.131) and (5.133).

The procedure for establishing the complete form for the remaining nodes is identical to this case, therefore, the complete form of the differential equation will be explained as succinctly as possible for each node. Furthermore, all notation for the temperature coefficient will not be explained for each node as it has been fully detailed in the derived differential equations (Section 5.2.1) and the heat generation equations (Section 5.3)

b) Type 2 - Node Positioned at the Centre of a Homogeneous Element with Two Dimensional Conduction

This is solved in a similar manner to the Type 1 node, equation (5.134) is substituted into equation (5.10) and the resulting expression is re-arranged to give,

$$\left[2 + b_5 + b_6\left(\omega_{1(n+1)} + \sum_{\ell=0}^{L} A_\ell \frac{k_\ell}{\Delta X_\ell}\right)\right]\theta_{I(n+1)} - b_1\theta_{I-1(n+1)} - b_2\theta_{I+1(n+1)}$$

$$- b_3\theta_{J-1(n+1)} - b_4\theta_{J+1(n+1)} - b_6\sum_{\ell=0}^{L} A_\ell \frac{k_\ell}{\Delta X_\ell}\theta_{C,\ell(n+1)}$$

$$= \left[2 + b_5 - b_6\left(\omega_{1(n)} + \sum_{\ell=0}^{L} A_\ell \frac{k_\ell}{\Delta X_\ell}\right)\right]\theta_{I(n)} + b_1\theta_{I-1(n)} + b_2\theta_{I+1(n)} + b_3\theta_{J-1(n)}$$

$$+ b_4\theta_{J+1(n)} + b_6\sum_{\ell=0}^{L} A_\ell \frac{k_\ell}{\Delta X_\ell}\theta_{C,\ell(n)} + b_6\left(\theta_{S,\alpha(n+1)} + \theta_{S,\alpha(n)} + \omega_{2(n+1)} + \omega_{2(n)} + Q_{M(n+1)} + Q_{M(n)}\right)$$

Re-writing this expression in its complete form:

where,

$$B_1 = b_1 = b_2 = \frac{A_x k}{S\Delta X} \quad ; \quad B_2 = b_3 = b_4 = \frac{A_y k}{S\Delta Y}$$

$$B_{3(k)} = b_5 + \frac{\omega_{1(k)}}{S} + \sum_{\ell=0}^{L} B_{5+\ell} \quad ; \quad B_4 = \frac{1}{S} = \frac{\Delta\tau}{\rho c v}$$

$$B_{5+\ell} = \frac{A_\ell k_\ell}{S \Delta x_\ell} \qquad (\ell = 0, 1, 2, .., L)$$

c) Type 3 - Node Positioned at the Centre of a Homogeneous Element, One-Dimensional Heat Conduction

This nodal type is solved exactly as the previous two nodes, equation (5.134) is substituted into equation (5.11) and the following equation is formed as a result,

$$\left[2 + 2C_1 + C_2\left(\omega_{1(n+1)} + \sum_{\ell=0}^{L} A_\ell \frac{k_\ell}{\Delta x_\ell}\right)\right] \theta_{I(n+1)} - C_1 \theta_{I-1(n+1)} - C_1 \theta_{I+1(n+1)}$$

$$+ C_2 \sum_{\ell=0}^{L} A_\ell \frac{k_\ell}{\Delta x_\ell} \theta_{c,\ell(n+1)} = \left[2 - 2C_1 - C_2\left(\omega_{1\,n+1)} + \sum_{\ell=0}^{L} A_\ell \frac{k_\ell}{\Delta x_\ell}\right)\right] \theta_{I(n)} - C_1 \theta_{I-1(n)}$$

$$- C_1 \theta_{I+1(n)} - C_2 \sum_{\ell=0}^{L} A_\ell \frac{k_\ell}{\Delta x_\ell} \theta_{c,\ell(n)} + C_2\left(Q_{s,\alpha(n+1)} + Q_{s,\alpha(n)} + \omega_{2(n+1)} + \omega_{2(n)} + Q_{M(n+1)} + Q_{M(n)}\right)$$

This expression can be re-written in its completed form as,

$$(2 + C_{3(n+1)})\,\theta_{I(n+1)} - C_1 \theta_{I-1(n+1)} - C_1 \theta_{I+1(n+1)} - \sum_{\ell=0}^{L} C_{4+\ell}\,\theta_{c,\ell(n+1)}$$

$$= (2 - C_{3(n)})\,\theta_{I(n)} + C_1 \theta_{I-1(n)} + C_1\,\theta_{I+1(n)} + \sum_{\ell=0}^{L} C_{4+\ell}\,\theta_{c,\ell(n)} + C_2\left(Q_{s,\alpha(n+1)}\right.$$

$$\left. + Q_{s,\alpha(n)} + \omega_{2(n+1)} + \omega_{2(n)} + Q_{M(n+1)} + Q_{M(n)}\right) \qquad (5.137)$$

where,

$$C_1 = c_1 = \frac{A \times h}{S \Delta X} \quad ; \quad C_2 = c_2 = \frac{1}{S} = \frac{\Delta\tau}{\rho c v}$$

$$C_{3(k)} = 2C_1 + \frac{\omega_{1(k)}}{S} + \sum_{\ell=0}^{L} C_{4+\ell} \quad ; \quad C_{4+\ell} = \frac{A_\ell k_\ell}{S \Delta x_\ell} \quad (\ell = 0, 1, 2, ----, L)$$

d) Type 4 - Node Positioned at the Centre of a Homogeneous Element with One Dimensional Conduction where Node 1 is Connected to More Than Two Different Conduction Flowpaths

Similar to the previous nodes, equation (5.134) is substituted into equation (5.12), re-arranging this expression and re-labelling yields,

$$(2+D_{R+L+4(n+1)})\theta_{I(n+1)} - \sum_{j=1}^{R} D_j\,\theta_{I+1,j(n+1)} - D_{R+1}\,\theta_{I-1(n+1)} - \sum_{\ell=0}^{L} D_{R+L+3}\,\theta_{C,\ell(n+1)}$$

$$= (2-D_{R+L+4(n)})\theta_{I(n)} + \sum_{j=1}^{R} D_j\,\theta_{I+1,j(n)} + D_{R+1}\,\theta_{I-1(n)} + \sum_{\ell=0}^{L} D_{R+L+3}\,\theta_{C,\ell(n)}$$

$$+ D_{R+2}\left(Q_{S,\alpha(n+1)} + Q_{S,\alpha(n)} + \omega_{2(n+1)} + \omega_{2(n)} + Q_{M(n+1)} + Q_{M(n)}\right)$$

where, (5.138)

$$D_j = \frac{A_{I+1,j}\,k}{s\Delta x} \quad (j=1,2,\ldots,R) \quad ; \quad D_{R+1} = \frac{A_x\,k}{s\Delta x}$$

$$D_{\ell+2} = \frac{1}{s} = \frac{\Delta\tau}{(\rho c v/2) + \left(\sum_{j=1}^{R} \rho_j c_j v_j/2\right)} \; ; \; D_{R+\ell+3} = \frac{A_\ell\,k_\ell}{s\Delta x_\ell} \quad (\ell=0,1,2,\ldots L)$$

$$D_{R+L+4(6)} = \sum_{j=1}^{R} D_j + D_{R+1} + \frac{\omega_{1(6)}}{s} + \sum_{\ell=0}^{L} D_{R+\ell+2}$$

R = the number of different (I+1) terms corresponding to P*Q nodes.

e) Type 5 - Node Positioned between Two Homogeneous Elements which have a Three Dimensional Nodal Structure

The derived difference equation for this node is given by equation (5.17) Category 1 nodes described by equation (5.18) are re-written using equation (5.133)

$$\Sigma Q_{I(6)} = \sum_{\ell=0}^{L} A_\ell\,\frac{k_\ell}{\Delta x_\ell}\left(\theta_{C,\ell(6)} - \theta_{I(6)}\right) + Q_{M(6)} \qquad (5.139)$$

The following equation is obtained if equation (5.139) is substituted for the summation of the heat injection terms in equation (5.17)

$$(2+e_7)\theta_{I(n+1)} - e_1\theta_{I-1(n+1)} - e_2\theta_{I+1(n+1)} - e_3\theta_{J-1(n+1)} - e_4\theta_{J+1(n+1)} - e_5\theta_{K-1(n+1)}$$

$$-e_6\theta_{K+1(n+1)} = (2-e_7)\theta_{I(n)} + e_1\theta_{I-1(n)} + e_2\theta_{I+1(n)} + e_3\theta_{J-1(n)} + e_4\theta_{J+1(n)}$$

$$+ e_5\theta_{K-1(n)} + e_6\theta_{K+1(n)} + e_8\left(\sum_{\ell=0}^{L} A_\ell\,\frac{k_\ell}{\Delta x_\ell}\left(\theta_{C,\ell(6)} - \theta_{I(6)}\right) + Q_{M(6)}\right)$$

Re-arranging this expression into its complete form and re-labelling yields,

$$(2+E_7)\theta_{I(n+1)} - E_1\theta_{I-1(n+1)} - E_2\theta_{I+1(n+1)} - E_3\theta_{J-1(n+1)} - E_4\theta_{J+1(n+1)} - E_5\theta_{K-1(n+1)}$$

$$-E_6\theta_{K+1(n+1)} - \sum_{\ell=0}^{L} E_{8+\ell}\,\theta_{C,\ell(n+1)} = (2-E_7)\theta_{I(n)} + E_1\theta_{I-1(n)} + E_2\theta_{I+1(n)} + E_3\theta_{J-1(n)}$$

$$+ E_4\theta_{J+1(n)} + E_5\theta_{K-1(n)} + E_6\theta_{K+1(n)} + \sum_{\ell=0}^{L} E_{8+\ell}\,\theta_{C,\ell(n)} + E_8\left(Q_{M(n+1)} + Q_{M(n)}\right)$$

(5.140)

where,

$$E_1 = \frac{A_x k_1}{S \Delta X_{I-1,I}} \quad ; \quad E_2 = \frac{A_x k_2}{S \Delta X_{I+1,I}}$$

$$E_3 = \frac{A_{(J-1,I),1} k_1 + A_{(J-1,I)2} k_2}{S \Delta Y} \quad ; \quad E_4 = \frac{A_{(J+1,I),1} k_1 + A_{(J+1,I)2} k_2}{S \Delta Y}$$

$$E_5 = \frac{A_{(K-1,I),1} k_1 + A_{(K-1,I)2} k_2}{S \Delta Z} \quad ; \quad E_6 = \frac{A_{(K+1,I),1} k_1 + A_{(K+1,I)2} k_2}{S \Delta Z}$$

$$E_7 = E_1 + E_2 + E_3 + E_4 + E_5 + E_6 + \sum_{\ell=0}^{L} E_{8+\ell} \quad ; \quad E_8 = \frac{1}{S} = \frac{\Delta \tau}{\rho_1 c_1 V_1 + \rho_2 c_2 V_2}$$

$$E_{8+\ell} = \frac{A_\ell k_\ell}{S \Delta X_\ell} \qquad (\ell = 0, 1, 2, \ldots, L)$$

f) Type 6 - Node Positioned on the Boundary Between Two Homogeneous Elements which have Negligible Heat Flow in the Z-dimension

Similar to Type 5 above, equation (5.139) is substituted into equation (5.19) which is then re-arranged and re-notated resulting in the expression,

$$(2 + F_5)\,\theta_{I(n+1)} - F_1 \theta_{I-1(n+1)} - F_2 \theta_{I+1(n+1)} - F_3 \theta_{J-1(n+1)} - F_4 \theta_{J+1(n+1)}$$
$$- \sum_{\ell=0}^{L} F_{6+\ell}\, \theta_{C,\ell(n+1)} = (2 - F_5)\theta_{I(n)} + F_1 \theta_{I-1(n)} + F_2 \theta_{I+1(n)} + F_3 \theta_{J-1(n)}$$
$$+ F_4 \theta_{J+1(n)} + \sum_{\ell=0}^{L} F_{6+\ell}\, \theta_{C,\ell(n)} + F_6 \left(Q_{M(n+1)} + Q_{M(n)}\right) \qquad (5.141)$$

where,

$$F_1 = \frac{A_x k_1}{S \Delta X_{I-1,I}} \quad ; \quad F_2 = \frac{A_x k_2}{S \Delta X_{I+1,I}}$$

$$F_3 = \frac{A_{(J-1,I),1} k_1 + A_{(J-1,I)2} k_2}{S \Delta Y} \quad ; \quad F_4 = \frac{A_{(J+1,I),1} k_1 + A_{(J+1,I)2} k_2}{S \Delta Y}$$

$$F_5 = F_1 + F_2 + F_3 + F_4 + \sum_{\ell=0}^{L} F_{6+\ell} \quad ; \quad F_6 = \frac{1}{S} = \frac{\Delta \tau}{\rho_1 c_1 V_1 + \rho_2 c_2 V_2}$$

$$F_{6+\ell} = \frac{A_\ell k_\ell}{S \Delta X_\ell} \qquad (\ell = 0, 1, 2, \ldots, L)$$

g) Type 7 - Node on the Boundary Between Two Homogeneous Elements Modelled by One Dimensional Heat Conduction

As Type 5, substituting equation (5.139) into equation (5.20), re-arranging and re-labelling the following expression is established for the complete difference equation,

$$(2+G_4)\,\theta_{I(n+1)} - G_1\,\theta_{I-1(n+1)} - G_2\,\theta_{I+1(n+1)} - \sum_{\ell=0}^{L} G_{4+\ell}\,\theta_{C,\ell(n+1)} = (2-G_4)\,\theta_{I(n)}$$

$$+ G_1\,\theta_{I-1(n)} + G_2\,\theta_{I+1(n)} + \sum_{\ell=0}^{L} G_{4+\ell}\,\theta_{C,\ell(n)} + G_3\left(Q_{M(n+1)} + Q_{M(n)}\right) \qquad (5.142)$$

where

$$G_1 = \frac{A_X\,k_1}{S\,\Delta X_{I-1,I}} \quad ; \quad G_2 = \frac{A_X\,k_2}{S\,\Delta X_{I+1,I}}$$

$$G_3 = \frac{1}{S} = \frac{\Delta\tau}{\rho_1 C_1 V_1 + \rho_2 C_2 V_2} \quad ; \quad G_4 = G_1 + G_2 + \sum_{\ell=0}^{L} \frac{A_\ell\,k_\ell}{S\,\Delta X_\ell}$$

$$G_{4+\ell} = \frac{A_\ell\,k_\ell}{S\,\Delta X_\ell} \qquad (\ell = 0, 1, 2, \ldots L)$$

h) Type 8 - Node on the Boundary between an Element with a Three Dimensional Nodal Network and One with No Y or Z Dimension Conduction

The procedure is identical to that used for the Type 5 node, therefore, equation (5.139) is substituted into equation (5.21) and the resulting re-arranged and re-numbered expression is,

$$(2+H_7)\,\theta_{I(n+1)} - H_1\,\theta_{I-1(n+1)} - H_2\,\theta_{I+1(n+1)} - H_3\,\theta_{J-1(n+1)} - H_4\,\theta_{J+1(n+1)} - H_5\,\theta_{K-1(n+1)}$$

$$- H_6\,\theta_{K+1(n+1)} - \sum_{\ell=0}^{L} H_{8+\ell}\,\theta_{C,\ell(n+1)} = (2-H_7)\,\theta_{I(n)} + H_1\,\theta_{I-1(n)} + H_2\,\theta_{I+1(n)} + H_3\,\theta_{J-1(n)}$$

$$+ H_4\,\theta_{J+1(n)} + H_5\,\theta_{K-1(n)} + H_6\,\theta_{K+1(n)} + \sum_{\ell=0}^{L} H_{8+\ell}\,\theta_{C,\ell(n)} + H_8\left(Q_{M(n+1)} + Q_{M(n)}\right) \qquad (5.143)$$

where

$$H_1 = \frac{A_X\,k_1}{S\,\Delta X_{I-1,I}} \quad ; \quad H_2 = \frac{A_X\,k_2}{S\,\Delta X_{I+1,I}}$$

$$H_3 = \frac{A_{(J-1,I)2}\,k_2}{S\,\Delta Y} \quad ; \quad H_4 = \frac{A_{(J+1,I)2}\,k_2}{S\,\Delta Y}$$

$$H_5 = \frac{A_{(K-1,I)2}\,k_2}{S\,\Delta Z} \quad ; \quad H_6 = \frac{A_{(K+1,I)2}\,k_2}{S\,\Delta Z}$$

$$H_7 = H_1 + H_2 + H_3 + H_4 + H_5 + H_6 + \sum_{\ell=0}^{L} H_{8+\ell} \quad ; \quad H_8 = \frac{1}{S} = \frac{\Delta\tau}{\rho_1 C_1 V_1 + \rho_F C_F V_F}$$

$$H_{8+\ell} = \frac{A_\ell\,k_\ell}{S\,\Delta X} \qquad (\ell = 0, 1, 2, \ldots, L)$$

i) Type 9 - Node on the Boundary between Two Elements, One with No Conduction in the Z Dimension, the Other with No Y or Z Conduction

As node Type 5, substitute equation (5.139) into equation (5.22) then re-arranging the expression and re-labelling yields,

$$(2+I_5)\Theta_{I(n+1)} - I_1\Theta_{I-1(n+1)} - I_2\Theta_{I+1(n+1)} - I_3\Theta_{J-1(n+1)} - I_4\Theta_{J+1(n+1)}$$
$$-\sum_{\ell=0}^{L} I_{6+\ell}\,\Theta_{c,\ell(n+1)} = (2-I_5)\Theta_{I(n)} + I_1\Theta_{I-1(n)} + I_2\Theta_{I+1(n)} + I_3\Theta_{J-1(n)}$$
$$+I_4\Theta_{J+1(n)} + \sum_{\ell=0}^{L} I_{6+\ell}\,\Theta_{c,\ell} + I_6\left(Q_{M(n+1)}+Q_{M(n)}\right) \qquad (5.144)$$

where,

$$I_1 = \frac{Ax\,k_1}{S\Delta X_{I-1,I}} \quad ; \quad I_2 = \frac{Ax\,k_2}{S\Delta X_{I+1,I}}$$

$$I_3 = \frac{A_{(J-1,I)2}\,k_2}{S\Delta Y} \quad ; \quad I_4 = \frac{A_{(J+1,I)2}\,k_2}{S\Delta Y}$$

$$I_5 = I_1+I_2+I_3+I_4+\sum_{\ell=0}^{L} I_{6+\ell} \quad ; \quad I_6 = \frac{1}{S} = \frac{\Delta\tau}{\rho_1 c_1 V_1 + \rho_2 c_2 V_2}$$

$$I_{6+\ell} = \frac{A_\ell k_\ell}{S\Delta X_\ell} \qquad (\ell = 0, 1, 2, \ldots, L)$$

Category 2

a) Type 1 - Node Associated with Fluid Flow

The difference equation for this node type is given by equation (5.31). The summation of the heat generation terms associated with the node is given by equation (5.56) which states $\Sigma Q_{I(\ell)} = Q_{M(\ell)}$, substituting this into equation (5.31) yields,

$$(2+m_{M+2(n+1)})\Theta_{F(n+1)} - \sum_{j=1}^{M} m_{j(n+1)}\Theta_{j(n+1)} - m_{M+1(n+1)}\Theta_{F-1(n+1)}$$
$$= (2-m_{M+2(n)})\Theta_{F(n)} + \sum_{j=1}^{M} m_{j(n)}\Theta_{j(n)} + m_{M+1(n)}\Theta_{F-1(n)} + m_{M+3}\left(Q_{M(n+1)}+Q_{M(n)}\right)$$

Where F indicates that node I is a fluid node. No re-arrangement of this expression is required, re-labelling gives,

$$(2+J_{M+2(n+1)})\Theta_{I(n+1)} - \sum_{j=1}^{M} J_{j(n+1)}\,\theta_{j(n+1)} - J_{M+1(n+1)}\,\Theta_{I-1(n+1)}$$
$$= \left(2-J_{M+2(n)}\right)\Theta_{I(n)} + \sum_{j=1}^{M} J_j\,\theta_{j(n)} + J_{M+1(n)}\,\Theta_{I-1(n)} + J_{M+3}\left(Q_{M(n+1)}+Q_{M(n)}\right) \qquad (5.145)$$

where,

$$J_{j(\ell)} = m_{j(\ell)} = \frac{h c_{j,I(\ell)}\,A_{j,I}}{S} \quad ; \quad J_{M+1(\ell)} = m_{M+1(\ell)} = \frac{\dot{m}_{I-1(\ell)}\,\overline{c\rho}_{I-1(\ell)}}{S}$$

$$J_{n+2}(\xi) = m_{n+2}(\xi) = \left[\left(\sum_{j=1}^{M} h_{cj,I}(\xi) A_{j,I} + \left(\dot{m}_o(\xi)\overline{C_{pI}(\xi)}\right) + \left(\dot{m}_i(\xi)\overline{C_{pi}(\xi)}\right)\right]\right] / S$$

$$J_{n+3} = m_{n+3} = \frac{1}{S} = \frac{\Delta\tau}{\rho_I C_I V_I}$$

M = number of solid boundaries associated with the subvolume.

It is important to note that node I can be interchanged with node F to represent a fluid node.

Category 3

In Section 5.2.1 four types of surface node were identified, as there are three different types of component surface to consider, i.e. explosed external surface, non-exposed external surface and an internal surface, then twelve permutations of node type and surface are possible. However, not all the permutations are acceptable, for example, equation (5.37) is applicable only to an internal surface node. Nevertheless, more than four different types of surface node are now considered.

a) Surface Node Where the Solid Element (Element 2) Has a Three Dimensional Nodal Grid

The difference equation for this node was established by equation (5.33):

$$(2 + n_7(n+1))\theta_{I(n+1)} - n_1(n+1)\theta_{I-1(n+1)} - n_2\theta_{I+1(n+1)} - n_3\theta_{J-1(n+1)} - n_4\theta_{J+1(n+1)} - n_5\theta_{K-1(n+1)} - n_6\theta_{K+1(n+1)} = (2 - n_7(n))\theta_{I(n)} + n_1(n)\theta_{I-1(n)} + n_2\theta_{I+1(n)} + n_3\theta_{J-1(n)} + n_4\theta_{J+1(n)} + n_5\theta_{K-1(n)} + n_6\theta_{K+1(n)} + n_8\left(\Sigma Q_{I(n+1)} + \Sigma Q_{I(n)}\right) \quad (5.33)$$

where,

$$n_1(\xi) = \frac{A_x h_{c\,I,F}(\xi)}{S} \quad ; \quad n_2 = \frac{A_x k_2}{S\Delta X_{I+1,I}}$$

$$n_3 = \frac{A_{(J-1,I)2}\, k_2}{S\Delta Y} \quad ; \quad n_4 = \frac{A_{(J+1,I)2}\, k_2}{S\Delta Y}$$

$$n_5 = \frac{A_{(K-1,I)2}\, k_2}{S\Delta Z} \quad ; \quad n_6 = \frac{A_{(K+1,I)2}\, k_2}{S\Delta Z}$$

$$\Pi_7(\xi) = \Pi_1(\xi) + \Pi_2 + \Pi_3 + \Pi_4 + \Pi_5 + \Pi_6 \quad ; \Pi_8 = \frac{1}{S} = \frac{\Delta\tau}{\rho_2 C_2 V_2 + \rho_F C_F V_F}$$

$h_{c_{I,F}}$ = convective heat transfer coefficient between surface I and the fluid ($WM^{-2}K^{-1}$)

The heat generation terms of each surface type are applied to equation (5.33) and solved:

Type 1 Node - exposed external surface.

The heat generation terms for an exposed external surface are described by equation (5.77) and can be re-expressed using equations (5.79), (5.80), (5.115), (5.124) and (5.143),

$$\Sigma Q_I(\xi) = Q_{S,E}(\xi) + Q_{S,R}(\xi) + \Theta_2(\xi) - \Theta_1(\xi)\,\theta_{I(\xi)} + \Gamma_2(\xi) - \Gamma_1(\xi)\,\theta_I(\xi)$$

$$+ \sum_{l=0}^{L} A_l \frac{k_l}{\Delta x_l}\left(\theta_{c,l}(\xi) - \theta_{I(\xi)}\right) + Q_M(\xi)$$

this can be re-arranged to give:

$$\Sigma Q_I(\xi) = Q_{S,E}(\xi) + Q_{S,R}(\xi) - \left(\Theta_1(\xi) + \Gamma_1(\xi) + \sum_{l=0}^{L} A_l \frac{k_l}{\Delta x_l}\right)\theta_I(\xi)$$

$$+ \Theta_2(\xi) + \Gamma_2(\xi) + \sum_{l=0}^{L} A_l \frac{k_l}{\Delta x_l}\,\theta_{c,l}(\xi) + Q_M(\xi) \qquad (5.146)$$

For this nodal type the fluid node, I-1, is the external ambient air temperature and is known for both the present and future values because the data is held in the climate file, therefore, the temperature $\theta_{I-1(\xi)}$ equals $\theta_A(\xi)$; the external ambient air temperature. Substituting equation (5.146) into equation (5.33) the future values of θ_I and $\theta_{c,l}$ in equation (5.146) are transferred to the unknown side of the equation and the future value of θ_A is passed to the known side of the expression. The resulting equation is,

$$\left[2+n_7(n+1)+n_8\left(\Theta_{1(n+1)}+J_{1(n+1)}+\sum_{\ell=0}^{L} A\ell\ \frac{k\ell}{\Delta x\ell}\right)\right]\Theta_{I(n+1)}-n_2\Theta_{I+1(n+1)}$$

$$-n_3\Theta_{I-1(n+1)}-n_4\Theta_{I+1(n+1)}-n_5\Theta_{K-1(n+1)}-n_6\Theta_{K+1(n+1)}-n_8\sum_{\ell=0}^{L} A\ell\ \frac{k\ell}{\Delta x\ell}\Theta_{c,\ell(n+1)}$$

$$=\left[2-n_7(n)-n_8\left(\Theta_{1(n)}+J_{1(n)}+\sum_{\ell=0}^{L} A\ell\ \frac{k\ell}{\Delta x\ell}\right)\right]\Theta_{I(n)}+n_1(n+1)\Theta_{A(n+1)}+n_1(n)\Theta_{A(n)}$$

$$+n_2\Theta_{I+1(n)}+n_3\Theta_{I-1(n)}+n_4\Theta_{I+1(n)}+n_5\Theta_{K-1(n)}+n_6\Theta_{K+1(n)}+n_8\sum_{\ell=0}^{L} A\ell\ \frac{k\ell}{\Delta x\ell}\Theta_{c,\ell(n)}$$

$$+n_8\left[Q_{s,E(n+1)}+Q_{s,E(n)}+Q_{s,R(n+1)}+Q_{s,R(n)}+\Theta_{2(n+1)}+\Theta_{2(n)}+J_{2(n+1)}+J_{2(n)}+Q_{n(n+1)}+Q_{n(n)}\right]$$

Re-labelling this expression gives,

$$(2+K_7(n+1))\Theta_{I(n+1)}-K_2\Theta_{I+1(n+1)}-K_3\Theta_{I-1(n+1)}-K_4\Theta_{I+1(n+1)}-K_5\Theta_{K-1(n+1)}$$

$$-K_6\Theta_{K+1(n+1)}-\sum_{\ell=0}^{L} K_{8+\ell}\Theta_{c,\ell(n+1)}=(2-K_7(n))\Theta_{I(n)}+K_2\Theta_{I+1(n)}+K_3\Theta_{I-1(n)}$$

$$+K_4\Theta_{I+1(n)}+K_5\Theta_{K-1(n)}+K_6\Theta_{K+1(n)}+K_1(n+1)\Theta_{A(n+1)}+K_1(n)\Theta_{A(n)}+\sum_{\ell=0}^{L} K_{8+\ell}\Theta_{c,\ell(n)}$$

$$+K_8\left[Q_{s,E(n+1)}+Q_{s,E(n)}+Q_{s,R(n+1)}+Q_{s,R(n)}+\Theta_{2(n+1)}+\Theta_{2(n)}+J_{2(n+1)}+J_{2(n)}+Q_{n(n+1)}+Q_{n(n)}\right] \quad (5.147)$$

where,

$$K_1(\xi)=n_1(\xi) \quad ; K_2=n_2$$

$$K_3=n_3 \quad ; K_4=n_4$$

$$K_5=n_5 \quad ; K_6=n_6$$

$$K_7(\xi)=n_7(\xi)+\frac{a_1(\xi)}{s}+\frac{J_1(\xi)}{s}+\sum_{\ell=0}^{L} K_{8+\ell}$$

$$K_8=\frac{1}{s}=\frac{\Delta\tau}{\rho_2 c_2 V_2} \quad ; K_{8+\ell}=\frac{A\ell k\ell}{s\Delta x\ell} \quad (\ell=0,1,2,\ldots,L)$$

Type 2 Node - Internal Surface

In this work nodes are numbered from the external surface to the internal surface, therefore, for an internal surface node element 2 is the fluid node, I+1, and no node I-1 as was used for the external node. Equation (5.33) can be re-numbered to suit. The sum of the heat generation sources for an internal surface are given by equation (5.78), re-expressing using equations (5.85), (5.119) and (5.133) yields:

$$\Sigma Q_{I(\xi)}=Q_{s,I(\xi)}+A_s\sum_{j=1}^{J} h_{r_{j\to I}(\xi)}\left(\Theta_{j(\xi)}-\Theta_{I(\xi)}\right)$$

$$+\sum_{\ell=0}^{L} A\ell\ \frac{k\ell}{\Delta x\ell}\left(\Theta_{c,\ell(\xi)}-\Theta_{I(\xi)}\right)+Q_{\sim(\xi)}$$

this can be re-written in the form:

$$\sum Q_I(\xi) = Q_{s,I}(\xi) + A_s \sum_{j=1}^{J} hr_{j\to I}(\xi)\,\theta_{j(\xi)} + \sum_{\ell=0}^{L} A\ell\,\frac{k\ell}{\Delta x\ell}\,\theta_{c,\ell}(\xi)$$
$$- \left(A_s \sum_{j=1}^{J} hr_{j\to I(\xi)} + \sum_{\ell=0}^{L} A\ell\,\frac{k\ell}{\Delta x\ell}\right)\theta_{I(\xi)} + Q_{M(\xi)} \qquad (5.148)$$

Substituting this equation into the modified version of equation (5.33) and re-arranging yields:

$$\left[2 + n_7'(n+1) + n_8'\left(A_s \sum_{j=1}^{J} hr_{j\to I(n+1)} + \sum_{\ell=0}^{L} A\ell\,\frac{k\ell}{\Delta x\ell}\right)\right]\theta_{I(n+1)} - n_1'\theta_{I-1(n+1)} - n_2'\theta_{I+1(n)}$$
$$- n_3'\theta_{J-1(n+1)} - n_4'\theta_{J+1(n+1)} - n_5'\theta_{K-1(n+1)} - n_6'\theta_{K+1(n+1)} - n_8'\left(A_s \sum_{j=1}^{J} hr_{j\to I(n+1)}\theta_{j(n+1)}\right.$$
$$\left. + \sum_{\ell=0}^{L} A\ell\,\frac{k\ell}{\Delta x\ell}\theta_{c,\ell(n+1)}\right) = \left[2 - n_7'(n) - n_8\left(A_s \sum_{j=1}^{J} hr_{j\to I(n)} + \sum_{\ell=0}^{L} A\ell\,\frac{k\ell}{\Delta x\ell}\right)\right]\theta_{I(n)}$$
$$+ n_1'\theta_{I-1(n)} + n_2'\theta_{I+1(n)} + n_3'\theta_{J-1(n)} + n_4'\theta_{J+1(n)} + n_5'\theta_{K-1(n)} + n_6'\theta_{K+1(n)}$$
$$+ n_8'\left(A_s \sum_{j=1}^{J} hr_{j\to I(n)}\theta_{j(n)} + \sum_{\ell=0}^{L} A\ell\,\frac{k\ell}{\Delta x\ell}\theta_{c,\ell(n)}\right) + n_8'\left(Q_{s,I(n+1)} + Q_{s,I(n)} + Q_{M(n+1)} + Q_{M(n)}\right)$$

where,

$$n_1' = \frac{A_x k_1}{S\Delta X_{I+1,I}} \quad ; \quad n_2'(\xi) = \frac{A_x h_{c\,I,F}(\xi)}{S}$$

$$n_3' = \frac{A_{(J-1,I),1} k_1}{S\Delta Y} \quad ; \quad n_4' = \frac{A_{(J+1,I),1} k_1}{S\Delta Y}$$

$$n_5' = \frac{A_{(K-1,I),1} k_1}{S\Delta Z} \quad ; \quad n_6' = \frac{A_{(K+1),I),1} k_1}{S\Delta Z}$$

$$n_7'(\xi) = n_1' + n_2'(\xi) + n_3' + n_4' + n_5' + n_6' \quad ; \quad n_8' = \frac{1}{S} = \frac{\Delta\tau}{\rho_1 c_1 V_1 + \rho_F c_F V_F}$$

Re-labelling this expression,

$$\left[2 + L_{J+7(n+1)}\right]\theta_{I(n+1)} - L_{J+1}\theta_{I-1(n+1)} - L_{J+2(n+1)}\,\theta_{I+1(n+1)} - L_{J+3}\,\theta_{J-1(n+1)}$$
$$- L_{J+4}\theta_{J+1(n+1)} - L_{J+5}\,\theta_{K-1(n+1)} - L_{J+6}\,\theta_{K+1(n+1)} - \sum_{j=1}^{J} L_{j(n+1)}\,\theta_{j(n+1)} - \sum_{\ell=0}^{L} L_{J+8+\ell}\,\theta_{c,\ell(n+1)}$$
$$= \left[2 - L_{J+7(n)}\right]\theta_{I(n)} + L_{J+1}\theta_{I-1(n)} + L_{J+2(n)}\,\theta_{I+1(n)} + L_{J+3}\theta_{J-1(n)} + L_{J+4}\theta_{J+1(n)}$$
$$L_{J+5}\,\theta_{K-1(n)} + L_{J+6}\,\theta_{K+1(n)} + \sum_{j=1}^{J} L_{j(n)}\theta_{j(n)} + \sum_{\ell=0}^{L} L_{J+8+\ell}\,\theta_{c,\ell(n)}$$
$$+ L_{J+8}\left(Q_{s,I(n+1)} + Q_{s,I(n)} + Q_{M(n+1)} + Q_{M(n)}\right) \qquad (5.149)$$

where,

$$L_{j(\xi)} = \frac{A_s\,hr_{j\to I}(\xi)}{S} \qquad (j = 1, 2, \ldots J); \quad L_{J+1} = n_1'$$

$$L_{J+2}(t) = n_2'(t) \quad ; \quad L_{J+3} = n_3'$$
$$L_{J+4} = n_4' \quad ; \quad L_{J+5} = n_5'$$
$$L_{J+6} = n_6' \quad ; \quad L_{J+7} = n_7'$$
$$L_{J+8} = n_8' \quad ; \quad L_{J+8+\ell} = \frac{A\ell k\ell}{s\Delta x\ell} \qquad (\ell = 0, 1, 2 \ldots L)$$

Type 3 Node - non-exposed external surface.

Similar to an exposed external surface the θ_{I-1} term is assumed known and equal to θ_s, the ambient temperature of the surrounding enclosure. Equation (5.78) represents the sum of the heat generation sources for an internal non-exposed surface, which can be re-written in terms of equations (5.85), (5.124) and (5.133) thus,

$$\Sigma Q_I(t) = Q_{s,I}(t) + \Gamma_2(t) - \Gamma_1(t)\theta_I(t) + \sum_{\ell=0}^{L} A\ell \frac{k\ell}{\Delta x\ell} \left(\theta_{c,\ell}(t) = \theta_I(t)\right) + Q_m(t)$$

this can be re-arranged to give

$$\Sigma Q_I(t) = Q_{s,I}(t) + \Gamma_2(t) - \left(\Gamma_1(t) + \sum_{\ell=0}^{L} A\ell \frac{k\ell}{\Delta x\ell}\right)\theta_I(t) + \sum_{\ell=0}^{L} A\ell \frac{k\ell}{\Delta x\ell}\theta_{c,\ell}(t) + Q_m(t) \qquad (5.150)$$

Substituting this expression into equation (5.33) and re-arranging it is possible to write,

$$\left[2 + n_7(n+1) + n_8\left(\Gamma_1(n+1) + \sum_{\ell=0}^{L} A\ell \frac{k\ell}{\Delta x\ell}\right)\right]\theta_{I(n+1)} - n_2\theta_{I+1(n+1)} - n_3\theta_{J-1(n+1)}$$
$$- n_4\theta_{J+1(n+1)} - n_5\theta_{K-1(n+1)} - n_6\theta_{K+1(n+1)} - n_8\sum_{\ell=0}^{L} A\ell \frac{k\ell}{\Delta x\ell}\theta_{c,\ell(n+1)}$$
$$= \left[2 - n_7(n) - n_8\left(\Gamma_1(n) + \sum_{\ell=0}^{L} A\ell \frac{k\ell}{\Delta x\ell}\right)\right]\theta_I(n) + n_1(n+1)\theta_{s(n+1)} + n_8(n)\theta_s(n) + n_2\theta_{I+1(n)}$$
$$+ n_3\theta_{J-1(n)} + n_4\theta_{J+1(n)} + n_5\theta_{K-1(n)} + n_6\theta_{K+1(n)} + n_8\sum_{\ell=0}^{L} A\ell \frac{k\ell}{\Delta x\ell}\theta_{s,\ell(n)}$$
$$+ n_8\left[Q_{s,I(n+1)} + Q_{s,I(n)} + \Gamma_{2(n+1)} + \Gamma_{2(n)} + Q_{m(n+1)} + Q_{m(n)}\right]$$

Re-numbering this expression results in the following equation for the complete difference equation,

$$(2 + M_7(n+1))\theta_{I(n+1)} - M_2\theta_{I+1(n+1)} - M_3\theta_{J-1(n+1)} - M_4\theta_{J+1(n+1)} - M_5\theta_{K-1(n+1)}$$
$$- M_6\theta_{K+1(n+1)} - \sum_{\ell=0}^{L} M_{8+\ell}\theta_{c,\ell(n+1)} = (2 - M_7(n))\theta_{I(n)} + M_1(n+1)\theta_{s(n+1)}$$
$$M_1(n)\theta_{s(n)} + M_2\theta_{I+1(n)} + M_3\theta_{J-1(n)} + M_4\theta_{J+1(n)} + M_5\theta_{K-1(n)} + M_6\theta_{K+1(n)}$$
$$+ \sum_{\ell=0}^{L} M_{8+\ell}\theta_{c,\ell(n)} + M_8\left(Q_{s,I(n+1)} + Q_{s,I(n)} + \Gamma_{2(n+1)} + \Gamma_{2(n)} + Q_{m(n+1)} + Q_{m(n)}\right) \qquad (5.151)$$

where,

$$M_1(\xi) = n_1(\xi) \quad ; \quad M_2 = n_2$$

$$M_3 = n_3 \quad ; \quad M_4 = n_4$$

$$M_5 = n_5 \quad ; \quad M_6 = n_6$$

$$M_7(\xi) = n_7(\xi) + \frac{\Im_1(\xi)}{S} + \sum_{\ell=0}^{L} M_{8+\ell}$$

$$M_8 = \frac{1}{S} = \frac{\Delta\tau}{\rho_2 C_2 V_2} \quad ; \quad M_{8+\ell} = \frac{A_\ell k_\ell}{S\Delta x_\ell} \qquad (\ell = 0, 1, 2, \ldots L)$$

b) Surface Node with No Conduction in the Y Dimension of the Homogeneous Element

The difference equation for this node is given by (5.35),

$$(Z + O_{5(n+1)})\,\theta_{I(n+1)} - O_{1(n+1)}\,\theta_{I-1(n+1)} - O_2\,\theta_{I+1(n+1)} - O_3\,\theta_{J-1(n+1)} - O_4\,\theta_{J+1(n+1)}$$
$$= (2 - O_{5(n)})\,\theta_{I(n)} + O_{1(n)}\,\theta_{I-1(n)} + O_2\,\theta_{I+1(n)} + O_3\,\theta_{J-1(n)} + O_4\,\theta_{J+1(n)}$$
$$+ O_6\,(\Sigma Q_{I(n+1)} + \Sigma Q_{I(n)}) \qquad (5.35)$$

where,

$$O_1(\xi) = \frac{A_x\, h_{c\,I,F(\xi)}}{S} \quad ; \quad O_2 = \frac{A_x\, k}{S\Delta x_{I+1,I}}$$

$$O_3 = \frac{A_{(J-1,I)2}\, k_2}{S\Delta Y} \quad ; \quad O_4 = \frac{A_{(J+1,I)2}\, k_2}{S\Delta Y}$$

$$O_{5(\xi)} = O_1(\xi) + O_2 + O_3 + O_4 \quad ; \quad O_6 = \frac{1}{S} = \frac{\Delta\tau}{\rho_2 C_2 V_2 + \rho_F C_F V_F}$$

The complete difference equations for each surface type is solved by exactly the same procedure as outlined for each surface. The principal difference is that any temperature and temperature coefficient associated with heat conduction in the Z dimension is set to zero in the solid homogeneous element. Therefore, only a summary of the solution of the complete difference equation is described for each surface node.

Type 4 Node - exposed external surface

Substituting equation (5.146) into equation (5.35) and setting the temperature θ_{I-1} to be the known external ambient temperature θ_4, then re-arranging and re-numbering yields,

$$(2+N_{5(n+1)})\Theta_{I(n+1)} - N_2\Theta_{I+1(n+1)} - N_3\Theta_{I-1(n+1)} - N_4\Theta_{I+1(n+1)} - \sum_{\ell=0}^{L} N_{6+\ell}\Theta_{c,\ell(n+1)}$$

$$= (2-N_{5(n)})\Theta_{I(n)} + N_{1(n+1)}\Theta_{A(n+1)} + N_{1(n)}\Theta_{A(n)} + N_2\Theta_{I+1(n)} + N_3\Theta_{I-1(n)}$$

$$+ N_4\Theta_{I+1(n)} + \sum_{\ell=0}^{L} N_{6+\ell}\Theta_{c,\ell(n)} + N_6\left[Q_{S,B(n+1)} + Q_{S,B(n)} + Q_{S,R(n+1)} + Q_{S,R(n)}\right.$$

$$\left.+\Theta_{2(n+1)} + \Theta_{2(n)} + J_{2(n+1)} + J_{2(n)} + Q_{M(n+1)} + Q_{M(n)}\right) \qquad (5.152)$$

where,

$$N_{1(\ell)} = O_{1(\ell)} \quad ; \quad N_2 = O_2$$

$$N_3 = O_3 \quad ; \quad N_4 = O_4$$

$$N_{5(\ell)} = O_{5(\ell)} + \frac{\Theta_{1(\ell)}}{S} + \frac{J_{1(\ell)}}{S} + \sum_{\ell=0}^{L} N_{6+\ell}$$

$$N_6 = O_6 \quad ; \quad N_{6+\ell} = \frac{Ack_\ell}{S\Delta x_\ell} \quad (\ell = 0,1,2\ldots L)$$

Type 5 Node - internal surface

This is similar to the type 2 node. Equation (5.35) is modified to take account of element 1 being the solid homogeneous element while the fluid is element 2, substituting equation (5.148) for the summation of the heat generation terms in equation (5.35), re-arranging and re-numbering yields the following expression for the complete difference equation,

$$(2+O_{j+5(n+1)})\Theta_{I(n+1)} - O_{J+1}\Theta_{I-1(n+1)} - O_{J+2(n+1)}\Theta_{I+1(n+1)} - O_{J+3}\Theta_{J-1(n+1)}$$

$$- O_{J+4}\Theta_{J+1(n+1)} - \sum_{j=1}^{J} O_{j(n+1)}\Theta_{j(n+1)} - \sum_{\ell=0}^{L} O_{J+6+\ell}\Theta_{c,\ell(n+1)} = (2-O_{J+5(n)})\Theta_{I(n)}$$

$$+ O_{J+1}\Theta_{I-1(n)} + O_{J+2(n)}\Theta_{I+1(n)} + O_{J+3}\Theta_{J-1(n)} + O_{J+4}\Theta_{J+1(n)} + \sum_{j=1}^{J} O_{j(n)}\Theta_{j(n)}$$

$$+ \sum_{\ell=0}^{L} O_{J+6+\ell}\Theta_{c,\ell} + O_{J+8}\left(Q_{S,I(n+1)} + Q_{S,I(n)} + Q_{M(n+1)} + Q_{M(n)}\right)$$

(5.153)

where,

$$O_{j(\ell)} = \frac{A_S h_{r\,j\to I(\ell)}}{S} \quad (j = 1, 2, \ldots, J)$$

$$O_{J+1} = \frac{Ax\,k_1}{S\,\Delta x_{I-1,I}} \quad ; \quad O_{J+2(\ell)} = \frac{Ax\,h_{c\,I,F(\ell)}}{S}$$

$$O_{J+3} = \frac{A_{(J-1,I),1}\,k_1}{S\Delta Y} \quad ; \quad O_{J+4} = \frac{A_{(J+1,I),1}\,k_1}{S\Delta Y}$$

$$O_{J+5(k)} = O_{J+1} + O_{J+2(k)} + O_{J+3} + O_{J+4} + \frac{A_s}{S} \sum_{j=1}^{J} hr_{j\to I(k)} + \sum_{\ell=0}^{L} O_{J+6+\ell}$$

$$O_{J+6} = \frac{1}{S} = \frac{\Delta\tau}{\rho_1 C_1 V_1 + \rho_F C_F V_F} \quad ; \quad O_{J+6+\ell} = \frac{A\ell k\ell}{S\Delta x\ell}$$

Type 6 Node - non-exposed external surface

Substitute equation (5.150) into equation (5.35) and set the temperature θ_{I-1} to θ_s, the ambient air temperature of the surrounds which is known at both present (n) and future (n+1) time rows. The complete difference for this node can be written as follows,

$$(2+P_{5(n+1)})\theta_{I(n+1)} - P_2\theta_{I+1(n+1)} - P_3\theta_{J-1(n+1)} - P_4\theta_{J+1(n+1)} - \sum_{\ell=0}^{L} P_{6+\ell}\theta_{c,\ell(n+1)}$$

$$= (2-P_{5(n)})\theta_{I(n)} + P_{1(n+1)}\theta_{s(n+1)} + P_{1(n)}\theta_{s(n)} + P_2\theta_{I+1(n)} + P_3\theta_{J-1(n)} + P_4\theta_{J+1(n)}$$

$$+ \sum_{\ell=0}^{L} P_{6+\ell}\theta_{c,\ell(n} + P_6\left(Q_{s,I(n+1)} + Q_{sI(n)} + \exists_{2(n+1)} + \exists_{2(n)} + Q_{M(n+1)} + Q_{M(n)}\right) \quad (5.154)$$

where,

$$P_{1(k)} = O_{1(k)} \quad ; \quad P_2 = O_2$$

$$P_3 = O_3 \quad ; \quad P_4 = O_4$$

$$P_{5(k)} = O_{5(k)} + \frac{\exists_{1(k)}}{S} + \sum_{\ell=0}^{L} P_{6+\ell}$$

$$P_6 = O_6 \quad ; \quad P_{6+\ell} = \frac{A\ell k\ell}{S\Delta x\ell} \quad (\ell = 0, 1, 2, \ldots L)$$

b) Surface Node With No Conduction in the Y or Z Dimensions of the Solid Homogeneous Element

The difference equation for this node was given by equation (5.36)

$$(2 + b_{1(n+1)} + b_2)\theta_{I(n+1)} - b_{1(n+1)}\theta_{I-1(n+1)} - b_2\theta_{I+1(n+1)}$$

$$= (2 - b_{1(n)} - b_2)\theta_{I(n)} + b_{1(n)}\theta_{I-1(n)} + b_2\theta_{I+1(n)} + b_3\left(\Sigma Q_{M(n+1)} + \Sigma Q_{M(n)}\right) \quad (5.36)$$

where,

$$P_1(\xi) = \frac{A_x \, h_{c\,I,F}(\xi)}{S} \quad ; \quad P_2 = \frac{A_x \, k_2}{S \, \Delta x_{I+1,I}}$$

$$P_3 = \frac{1}{S} = \frac{\Delta\tau}{\rho_2 c_2 v_2 + \rho_F c_e v_F}$$

The complete difference equations for surface nodes modelled by X dimension conduction are solved by an identical procedure to the (a) type nodes above.

Type 7 Nodes - exposed external surface

Equation (5.146) is substituted into equation (5.36) and the temperature θ_{I-1} is replaced by the known external ambient air temperature, θ_A. The resulting expression is re-arranged and re-numbered to give,

$$(2 + Q_{3(n+1)})\,\theta_{I(n+1)} - Q_2\,\theta_{I+1(n+1)} - \sum_{\ell=0}^{L} Q_{4+\ell}\,\theta_{c,\ell(n+1)} = (2 - Q_{3(n)})\,\theta_{I(n)}$$
$$+ Q_{1(n+1)}\,\theta_{A(n+1)} + Q_{1(n)}\theta_{A(n)} + Q_2\,\theta_{I+1(n)} + \sum_{\ell=0}^{L} Q_{4+\ell}\,\theta_{c,\ell(n)} + Q_4\,(Q_{S,E(n+1)}$$
$$+ Q_{S,E(n)} + Q_{S,R(n+1)} + Q_{S,R(n)} + \Phi_{2(n+1)} + \Phi_{2(n)} + \Gamma_{2(n+1)} + \Gamma_{2(n)} + Q_{M(n+1)} + Q_{M(n)}) \qquad (5.155)$$

where,

$$Q_1(\xi) = P_1(\xi) \quad ; \quad Q_2 = P_2$$

$$Q_3(\xi) = P_1(\xi) + P_2 + \frac{\Phi_1(\xi)}{S} + \frac{\Gamma_1(\xi)}{S} + \sum_{\ell=0}^{L} Q_{4+\ell}$$

$$Q_4 = P_3 \quad ; \quad Q_{4+\ell} = \frac{A_\ell k_\ell}{S \Delta x_\ell} \qquad (\ell = 0, 1, 2, \ldots L)$$

Type 8 Node - internal surface

The heat generation sources as described by equation (5.148) are substituted into equation (5.36) which has been modified because the fluid node is I+1 and not I-1, therefore, re-labelling the re-arranged equation yields,

$$(2 + R_{J+3(n+1)})\,\theta_{I(n+1)} - R_{J+1}\,\theta_{I-1(n+1)} - R_{J+2(n+1)}\,\theta_{I+1(n+1)} - \sum_{j=1}^{J} R_{j(n+1)}\,\theta_{j(n+1)}$$
$$- \sum_{\ell=0}^{L} R_{J+4+\ell}\,\theta_{c,\ell(n+1)} = (2 - R_{J+3(n)})\,\theta_{I(n)} + R_{J+1}\,\theta_{I-1(n)} + R_{J+2(n)}\,\theta_{I+1(n)}$$
$$+ \sum_{j=1}^{J} R_{j(n)}\,\theta_{j(n)} + \sum_{\ell=0}^{L} R_{J+4+\ell}\,\theta_{c,\ell(n)} + R_{J+4}\,(Q_{S,I(n+1)} + Q_{S,I(n)} + Q_{M(n+1)} + Q_{M(n)}) \qquad (5.156)$$

where,

$$R_j = \frac{A_s h_{rj \Rightarrow I}(\xi)}{S} \qquad (j = 1, 2, 3, \ldots J)$$

$$R_{J+1} = \frac{A \times k_1}{S \Delta X_{I-1,I}} \quad ; \quad R_{J+2}(\xi) = \frac{A \times hc_{I,F}(\xi)}{S}$$

$$R_{J+3} = R_{J+1} + R_{J+2}(\xi) + \frac{A_s}{S} \sum_{j=1}^{J} h_{rj \Rightarrow I}(\xi) + \sum_{\ell=0}^{L} R_{J+L+\ell}$$

$$R_{J+L} = \frac{1}{S} = \frac{\Delta \tau}{\rho_1 C_1 V_1 + \rho_F C_F V_F} \quad ; \quad R_{J+L+\ell} = \frac{A_\ell k_\ell}{S \Delta X_\ell}$$

Type 9 Node - non-exposed external surface

Substituting equation (5.150) into equation (5.36) and setting θ_{I-1} equal to θ , the surrounding ambient air temperature within an enclosure, the complete difference equation can be written in the form,

$$(2 + S_{3(n+1)})\theta_{I(n+1)} - S_2 \theta_{I+1(n+1)} - \sum_{\ell=0}^{L} S_{4+\ell} \theta_{c,\ell(n+1)} = (2 - S_{3(n)})\theta_{I(n)}$$
$$+ S_{1(n+1)} \theta_{s(n+1)} + S_{1(n)} \theta_{s(n)} + S_2 \theta_{I+1(n)} + \sum_{\ell=0}^{L} S_{4+\ell} \theta_{c,\ell(n)} + S_4 (Q_{s,I(n+1)} + Q_{s,I(n)}$$
$$+ J_{2(n+1)} + J_{2(n)} + Q_{m(n+1)} + Q_{m(n)}) \qquad (5.157)$$

where,

$$S_1(\xi) = O_1(\xi) \quad ; \quad S_2 = O_2$$

$$S_3(\xi) = S_1(\xi) + S_2 + \frac{J_1(\xi)}{S} + \sum_{\ell=0}^{L} S_{4+\ell}$$

$$S_4 = O_4 \quad ; \quad S_{4+\ell} = \frac{A_\ell k_\ell}{S \Delta X_\ell} \qquad (\ell = 0, 1, 2, \ldots L)$$

d) Surface Node With No Conduction in the Y and Z Dimensions of the Homogeneous Element Connected to more than One Fluid Node

This node sub-classification is applicable only to internal surface nodes because the ambient air next to an exposed surface is considered to be a boundary condition and is therefore known, described by a single node temperature - θ_R or θ_S .

Type 10 Node - internal surface

The difference equation for this node type is given by equation (5.37)

Modifying this equation because the surface is internal, the fluid node is I+1 not I-1, then re-arranging the equation after equation (5.148) has been substituted for the summation of the heat generation sources yields,

$$\left[2+\sum_{i=1}^{P} q'_{i(n+1)}+q'_{p+1}+q'_{p+2}\left(A_s\sum_{j=1}^{J} hr_{j\to I(n+1)}+\sum_{\ell=0}^{L} A_\ell\,\frac{k_\ell}{\Delta x_\ell}\right)\right]\theta_{I(n+1)}$$

$$-\sum_{i=1}^{P} q_{i'(n+1)}\,\theta_{F,i(n+1)}-q'_{p+1}\,\theta_{I+1(n)}-q'_{p+2}\,A_s\sum_{j=1}^{J} hr_{j\to I(n)}\,\theta_{j(n)}+q'_{p+2}\sum_{\ell=0}^{L} A_\ell\,\frac{k_\ell}{\Delta x_\ell}\theta_{c,\ell(n+}$$

$$=\left[2-\sum_{i=1}^{P} q_{i'}-q'_{p+1}-q'_{p+2}\left(A_s\sum_{j=1}^{J} hr_{j\to I(n)}+\sum_{\ell=0}^{L} A_\ell\,\frac{k_\ell}{\Delta x_\ell}\right)\right]\theta_{I(n)}$$

$$+\sum_{i=1}^{P} q'_{i(n)}\,\theta_{F,i(n)}+q'_{p+1}\,\theta_{I+1(n)}-q_{p+2}\,A_s\sum_{j=1}^{J} hr_{j\to I(n)}\,\theta_{j(n)}$$

$$+q'_{p+2}\sum_{\ell=0}^{L} A_\ell\,\frac{k_\ell}{\Delta x_\ell}\,\theta_{c,\ell(n)}+q'_{p+2}\left(Q_{s,I(n+1)}+Q_{s,I(n)}+Q_{M(n+1)}+Q_{M(n)}\right)$$

where,

$$q'_{i(\xi)}=\frac{A_x\,hc_{i,F(\xi)}}{S}\quad(i=1,2,\ldots P)\;;\quad q'_{p+1}=\frac{A_x\,k_1}{S\,\Delta x_{I-1,I}}$$

$$q'_{p+2}=\frac{1}{S}=\frac{\Delta\tau}{\left(\rho_1 c_1 V_1+\sum_{i=1}^{P}\rho_{F,i}\,C_{F,i}\,V_{F,i}\right)}$$

P = number of fluid nodes in thermal contact with node I.

$\theta_{F,i(\xi)}$= temperature of fluid node i

This equation can be re-written to give the differential equation in its complete form:

$$\left(2+T_{J+P+3(n+1)}\right)\theta_{I(n+1)}-\sum_{i=1}^{P} T_{J+i(n+1)}\,\theta_{F,i(n+1)}-T_{J+P+1}\,\theta_{I-1(n+1)}$$

$$-\sum_{j=1}^{J} T_{j(n+1)}\theta_{j(n+1)}-\sum_{\ell=0}^{L} T_{J+P+3+\ell}\,\theta_{c,\ell(n+1)}=\left(2-T_{J+P+3(n)}\right)\theta_{I(n)}$$

$$+\sum_{i=1}^{P} T_{J+i(n)}\,\theta_{F,i(n)}+T_{J+P+1}\,\theta_{I-1(n)}+\sum_{j=1}^{J} T_{j(n)}\,\theta_{j(n)}+\sum_{\ell=0}^{L} T_{J+P+3+\ell}\,\theta_{c,\ell(n)}$$

$$+T_{J+P+2}\left(Q_{s,I(n+1)}+Q_{s,I(n)}+Q_{M(n+1)}+Q_{M(n)}\right)\qquad(5.158)$$

where,

$$T_{j(\xi)}=\frac{h'_{r\,j\to I(\xi)}\,A_s}{S}\qquad(j=1,2,\ldots,J)$$

$$T_{J+i(\xi)}=q'_{i(\xi)}\quad(i=1,2,\ldots,P)\;;\quad T_{J+P+1}=q'_{P+1}$$

$$T_{J+P+2} = Q'_{P+2}$$

$$T_{J+P+3}(t) = \sum_{j=1}^{J} T_j(t) + \sum_{i=1}^{P} T_{J+i}(t) + T_{J+P+1} + \sum_{l=0}^{L} T_{J+P+3+l}$$

$$T_{J+P+3+l} = \frac{A_l k_l}{S \Delta x_l} \qquad (l = 0, 1, 2, \ldots L)$$

Category 4

a) Type 1 - Node Representing a Conduit or Fitting

The difference equation for a conduit or a fitting (tee, three port valve, etc) is given by equation (5.43). There are no heat generation sources associated with this node except for a miscellaneous term, therefore, equation (5.32) is substituted into equation (5.43) the result of which is,

$$\left(2 + \sum_{b=1}^{B} r_{A+b(n+1)} + r_{A+B+1(n+1)}\right)\theta_{F(n+1)} - \sum_{a=1}^{A} r_{a(n+1)}\theta_{a(n+1)} - r_{A+B+1(n+1)}\theta_{S(n+1)}$$

$$= \left(2 - \sum_{b=1}^{B} r_{A+b(n)} - r_{A+B+1(n)}\right)\theta_{F(n)} + \sum_{a=1}^{A} r_{a(n)}\theta_{a(n)} + r_{A+B+1(n)}\theta_{S(n)} + r_{A+B+2}\left(Q_{M(n+1)} + \theta_{M(n)}\right.$$

where F indicates that node I is a fluid node. The surrounding ambient air temperature, θ_S, is assumed to be a known boundary condition, therefore, re-arranging and re-numbering the expression yields,

$$\left(2 + \sum_{b=1}^{B} U_{A+b(n+1)} + U_{A+B+1(n+1)}\right)\theta_{I(n+1)} - \sum_{a=1}^{A} U_{a(n+1)}\theta_{a(n+1)} = \left(2 - \sum_{b=1}^{B} U_{A+b(n)} - U_{A+B+1(n)}\right)\theta_{I(n)}$$

$$+ \sum_{a=1}^{A} U_{a(n)}\theta_{a(n)} + U_{A+B+1(n+1)}\theta_{S(n+1)} + U_{A+B+1(n)}\theta_{S(n)} + U_{A+B+2}\left(Q_{M(n+1)} + \theta_{M(n)}\right)$$

(5.159)

where

$$U_{a(t)} = r_{a(t)} = \frac{m_{a(t)}\,\overline{C_{p\,a(t)}}}{S} \qquad (a = 1, 2, \ldots, A)$$

$$U_{A+b(t)} = r_{A+b(t)} = \frac{m_{b(t)}\,\overline{C_{p\,F(t)}}}{S} \qquad (b = 1, 2, \ldots, B)$$

$$U_{A+B+1}(\xi) = r_{A+B+1}(\xi) = \frac{A_c U_c \xi)}{S}$$

$$U_{A+B+2} = r_{A+B+2} = \frac{\Delta\tau}{\left(\sum_{e=1}^{E} \rho_e C_e V_e + \rho_F C_F V_F\right)}$$

A = number of fluid flowpaths entering subvolume

B = number of fluid flowpaths leaving subvolume

E = number of elements in conduit or fitting

b) Type 2 - One Fluid Flowpath Entering Conduit or Fitting is Known At Present and Future Value

This situation will arise with fluid being drawn into the system, for example, ambient air or mains water into air and liquid collectors respectively. The fluid coming from a source external to the system is a boundary condition and is assumed known for both present and future time row values. If a=1 is the known entering fluid flowpath then equation (5.159) can be re-arranged and re-labelled giving,

$$\left(2 + \sum_{b=1}^{B} V_{A+b(n+1)} + V_{A+B+1(n+1)}\right)\Theta_{I(n+1)} - \sum_{a=1}^{A} V_{a(n+1)}\,\Theta_{a(n+1)}$$

$$= \left(2 - \sum_{b=1}^{B} V_{A+b(n)} - V_{A+B+1(n)}\right)\Theta_{I(n)} + \sum_{a=1}^{A} V_{a(n)}\,\Theta_{a(n)} + V_{1(n+1)}\,\Theta_{1(n+1)}$$

$$+ V_{1(n)}\,\Theta_{1(n)} + V_{A+B+1(n+1)}\,\Theta_{S(n+1)} + V_{A+B+1(n)}\,\Theta_{S(n)} + V_{A+B+2}\left(Q_{E1(n+1)} + Q_{M(n)}\right) \quad (5.160)$$

where,

$$V_1(\xi) = \frac{\dot{m}_1(\xi)\,\overline{C_{p_1}(\xi)}}{S} \quad ; \; V_a(\xi) = U_a(\xi) \; (a = 2, 3, 4, \ldots A)$$

$$V_{A+B}(\xi) = U_{A+b}(\xi) \quad (b = 1, 2, 3, \ldots B) \quad ; \; V_{A+B+1}(\xi) = U_{A+B+1}(\xi)$$

$$V_{A+B+2} = U_{A+B+2}$$

Category 5

a) Type 1 - Node Representing a Fan or Pump

The difference equation for a fan or pump component is given by equation (5.45). Energy is injected into the fluid due to component mechanical

energy losses and equation (5.70) can be used to formulate the sum of the heat generation terms using equations (5.128), (5.129) and (5.132), therefore,

$$\Sigma Q_I(\xi) = \gamma(\xi)\left(\theta_I(\xi) - \theta_{f,in}(\xi)\right) + Q_{env}(\xi) + A_c \frac{k_c}{\Delta x}\left(\theta_{Ab}(\xi) - \theta_I(\xi)\right) + Q_m(\xi)$$

re-arranging gives

$$\Sigma Q_I(\xi) = Q_{env}(\xi) - \gamma(\xi)\theta_{f,in}(\xi) + \left(\gamma(\xi) - \frac{A_c k_c}{\Delta x}\right)\theta_I(\xi) + \frac{A_c k_c}{\Delta x}\theta_{Ab}(\xi) + Q_m(\xi) \quad (5.161)$$

substituting equation (5.161) into equation (5.45) and re-arranging gives:

$$\left[2 + \Delta_{1(n+1)} + \Delta_3\left(\frac{A_c k_c}{\Delta x} - \gamma_{(n+1)}\right)\right]\theta_{I(n+1)} - \left(\Delta_{2(n+1)} - \Delta_3\gamma_{(n+1)}\right)\theta_{I-1(n+1)}$$

$$-\Delta_3\frac{A_c k_c}{\Delta x}\theta_{Ab(n+1)} = \left[2 - \Delta_{1(n)} - \Delta_2\left(\frac{A_c k_c}{\Delta x} - \gamma_{(n)}\right)\right]\theta_{I(n)} + \left(\Delta_{2(n)} - \Delta_3\gamma_{(n)}\right)\theta_{I-1(n)}$$

$$+\Delta_3\frac{A_c k_c}{\Delta x}\theta_{Ab(n)} + \Delta_3\left(Q_{env(n+1)} + Q_{env(n)} + Q_{m(n+1)} + Q_{m(n)}\right)$$

Expressing this equation in its complete difference form:

$$\left(2 + W_{1(n+1)}\right)\theta_{I(n+1)} - W_{2(n+1)}\theta_{I-1(n+1)} - W_3\theta_{Ab(n+1)} = \left(2 - W_{1(n)}\right)\theta_{I(n)}$$

$$+ W_{2(n)}\theta_{I-1(n)} + W_3\theta_{Ab(n)} + W_4\left(Q_{env(n+1)} + Q_{env(n)} + Q_{m(n+1)} + Q_{m(n)}\right)$$

(5.162)

where

$$W_1(\xi) = \Delta_1(\xi) + \frac{\Delta_3 A_c k_c}{\Delta x} - \Delta_3\gamma(\xi) = \frac{\dot{m}(\xi)\overline{C_{p_I}(\xi)}}{S} + \frac{A_c k_c}{S\Delta x} + \frac{\gamma(\xi)}{S}$$

$$W_2(\xi) = \Delta_2(\xi) + \Delta_3\gamma(\xi) = \frac{\dot{m}(\xi)\overline{C_{p_{I-1}(\xi)}}}{S} + \frac{\gamma(\xi)}{S}$$

$$W_3 = \frac{A_c k_c}{S\Delta x} \quad ; \quad W_4 = \Delta_3 = \frac{1}{S} = \frac{\Delta\tau}{\rho_c C_c V_c}$$

Category 6

The difference equation for an auxiliary heater is given by equation (5.48). Substituting the sum of heat generation sources - equation (5.73) into equation (5.48) gives,

$$(2 + t_{1(n+1)})\,\Theta_{I(n+1)} - t_{2(n+1)}\,\Theta_{I-1(n+1)} = (2 - t_{1(n)})\,\Theta_{I(n)} + t_{2(n)}\,\Theta_{I-1(n)}$$
$$+ t_3\left(Q_{Aux(n+1)} + Q_{Aux(n)} + Q_{env(n+1)} + Q_{env(n)} + Q_{M(n+1)} + Q_{M(n)}\right)$$

(5.48)

where,

$$t_{1(\xi)} = \frac{\dot{m}_{(\xi)}\,\overline{C_{p_I}}_{(\xi)}}{S} \quad ; \quad t_{2(\xi)} = \frac{\dot{m}_{(\xi)}\,\overline{C_{p}}_{I-1\,(\xi)}}{S}$$

$$t_3 = \frac{1}{S} = \frac{\Delta\tau}{(\rho_c C_c V_c + \rho_F c_F V_F)}$$

and I replaces suffix F.

There are two types of Category 6 nodes to consider: the first node occurs when a pre-set outlet temperature is obtained, the second applies to the auxiliary component when it supplies at its maximum rate.

a) Type 1 node - Auxiliary Heater Which Achieves a Set-Outlet Temperature

The outlet temperature from an auxiliary heater is normally at that temperature required to meet a particular load, i.e. space or water heating. In a space heating case the mass flow rate is constant, therefore, as the load is a boundary condition on the system the desired outlet temperature can be established. On the other hand, water heating systems normally operate at a fixed outlet temperature and a variable mass flow rate which is found because the load profile is known. In either case if a pre-set outlet condition is achieved then the $Q_{aux(\xi)}$ term in equation (5.48) is zero because the known outlet temperature contains the exact quantity of auxiliary energy required to boost the inlet fluid to the desired temperautre. Transferring the $\Theta_{F(n+1)}$ term in equation (5.48) to the known side and using a new notation yields,

$$2\,\Theta_{I(n+1)} - X_{2(n+1)}\,\Theta_{I-1(n+1)} = (2 - X_{1(n)})\,\Theta_{I(n)} + X_{2(n)}\,\Theta_{I-1(n)}$$
$$+ X_{1(n+1)}\,\Theta_{I(n+1)} + X_3\left(Q_{env(n+1)} + Q_{env(n)} + Q_{M(n+1)} + Q_{M(n)}\right) \qquad (5.163)$$

where,

$$X_1(\xi) = t_1(\xi) \quad ; \quad X_2(\xi) = t_2(\xi)$$
$$X_3 = t_3$$

b) Type 2 - Auxiliary Heater Operating at Maximum Output

In this case the desired outlet temperature cannot be achieved by the auxiliary heater, therefore, the outlet temperature from the auxiliary heater is unknown at the future value and Qaux supplies the maximum available energy. Equation (5.48) adequately describes the difference equation in complete form. In different notation the equation becomes:

$$(2+Y_{1(n+1)})\Theta_{I(n+1)} + Y_{2(n+1)}\Theta_{I-1(n+1)} = (2-Y_{1(n)})\Theta_{I(n)} + Y_{2(n)}\Theta_{I-1(n)}$$
$$Y_3\left(Q_{aux(n+1)} + Q_{aux(n)} + Q_{env(n+1)} + Q_{env(n)} + Q_{r(n+1)} + Q_{r(n)}\right) \qquad (5,164)$$

where,

$$Y_1(\xi) = t_1(\xi) \quad ; \quad Y_2(\xi) = t_2(\xi)$$
$$Y_3 = t_3$$

Category 7

There are two different heat exchanger models to consider: the first is a two node model the second is a one node model. The heat generation sources associated with both of these models are given by equation (5.79).

a) Type 1 - Two Node Heat Exchanger Model

In this case one node represents the hot fluid, the other represents the cold fluid, equations (5.54a) and (5.54b) are the difference equations for these nodes respectively. Applying equation (5.79) to equation (5.54a) and re-labelling results in:

$$(2-Z_{1(n+1)})\Theta_{H(n+1)} + (Z_{1(n+1)} + Z_{2(n+1)})\Theta_{H-1(n+1)} - Z_{2(n+1)}\Theta_{C-1(n+1)}$$
$$= (2+Z_{1(n)})\Theta_{H(n)} - (Z_{1(n)} + Z_{2(n)})\Theta_{H-1(n)} + Z_{2(n)}\Theta_{C-1(n)}$$
$$+ Z_3\left(Q_{env(n+1)} + Q_{env(n)} + Q_{r(n+1)} + Q_{r(n)}\right) \qquad (5.165a)$$

and equation (5.54b) becomes:

$$(2 - Z_{1(n+1)})\,\theta_{H(n+1)} + (Z_{1(n+1)} + Z_{2(n+1)})\,\theta_{C-1(n+1)} - Z_{2(n+1)}\,\theta_{H-1(n+1)}$$

$$= (2 + Z_{1(n)})\,\theta_{C(n)} - (Z_{1(n)} + Z_{2(n)})\,\theta_{C-1(n)} + Z_{2(n)}\,\theta_{H-1(n)}$$

$$+ Z_3\left(Q_{env(n+1)} + Q_{env(n)} + Q_{H(n+1)} + Q_{H(n)}\right) \qquad (5.165b)$$

from equation (5.54)

$$Z_{1(\xi)} = U_{1(\xi)} = \frac{\dot{m}_{(\xi)}\,\overline{C_{p_I}}_{(\xi)}}{S} \quad ; \quad Z_{2(\xi)} = U_{2(\xi)} = \frac{\varepsilon_{(\xi)}\,\dot{C}_{min(\xi)}}{S}$$

$$Z_3 = U_3 = \frac{1}{S} = \frac{\Delta\tau}{\rho_I C_I V_I}$$

$\varepsilon_{(\xi)}$ = effectiveness of heat exchange

$\dot{C}_{min}$ = minimum heat capacity and can be either the hot or cold fluid

H denotes hot fluid

C denotes cold fluid

b) Type 2 - One Node Heat Exchanger Model

The difference equation for this nodal type is given by equation (5.57), as equation (5.79) applies for the heat generation term then re-numbering yields:

$$(\Lambda_1 + \Lambda_{3(n+1)})\,\theta_{H(n+1)} - (\Lambda_2 + \Lambda_{4(n+1)})\,\theta_{C(n+1)} + (\Lambda_{5(n+1)} - \Lambda_{3(n+1)})\,\theta_{H-1(n+1)}$$

$$+ (\Lambda_{5(n+1)} - \Lambda_{5(n+1)})\,\theta_{C-1(n+1)} = (\Lambda_1 - \Lambda_{3(n)})\,\theta_{H(n)} + (\Lambda_{4(\xi)} - \Lambda_2)\,\theta_{C(n)}$$

$$+ (\Lambda_{3(n)} - \Lambda_{5(n)})\,\theta_{H-1(n)} + (\Lambda_{5(n)} - \Lambda_{4(n)})\,\theta_{C-1(n)} + Q_{env(n+1)} + Q_{env(n)} + Q_{H(n+1)} + Q_{H(n)}$$

(5.166)

from equation (5.81)

$$\Lambda_1 = U_1 = \frac{2\rho_H C_H V_H}{\Delta\tau} \quad ; \quad \Lambda_2 = U_2 = \frac{2\rho_C C_C V_C}{\Delta\tau}$$

$$\Lambda_{3(\xi)} = U_{3(\xi)} = \dot{m}_{H(\xi)}\,\overline{C_{pH(\xi)}} \quad ; \quad \Lambda_{4(\xi)} = U_{4(\xi)} = \dot{m}_{C(\xi)}\,\overline{C_{pC}}$$

$$\Lambda_{5(\xi)} = U_{5(\xi)} = 2\,\varepsilon_{(\xi)}\,\dot{C}_{min(\xi)}$$

Category 8

Nodes representing liquid sensible storage, rock bed sensible storage and latent energy storage are now considered.

a) Type 1 Node - Liquid Sensible Energy Storage

The difference equation for this node is given by equation (5.64). The sum of the heat generation sources are given by equation (5.89) and this replaces the $\Sigma Q_{I(\xi)}$ term in equation (5.64). The temperature of the surrounds, θ_s, is known and this term is transferred to the known side of the expression. In equation (5.64) node X is replaced by node I, therefore, the complete difference equation for this node is given by,

$$(2+\Pi_{I+J+9(n+1)})\theta_{I(n+1)} - \sum_{i=1}^{I} \Pi_{i(n+1)}\theta_{i(n+1)} - \Pi_{I+J+1(n+1)}\theta_{I-1(n+1)}$$

$$- \Pi_{I+J+3(n+1)}\theta_{I+1(n+1)} - \Pi_{I+J+8(n+1)}\theta_{F(n+1)} = (2-\Pi_{I+J+9(n)})\theta_{I(n)}$$

$$+ \sum_{i=1}^{I} \Pi_{i(n)}\theta_{i(n)} + \Pi_{I+J+1(n)}\theta_{I-1(n)} + \Pi_{I+J+3(n)}\theta_{I+1(n)}$$

$$+ \Pi_{I+J+9(n+1)}\theta_{S(n+1)} + \Pi_{I+J+9(n)}\theta_{S(n)} + \Pi_{I+J+8(n)}\theta_{F(n)}$$

$$+ \Pi_{I+J+10}\left(Q_{E(n+1)} + Q_{E(n)} + Q_{M(n+1)} + Q_{M(n)}\right) \qquad (5.167)$$

where,

$$\Pi_{i(\xi)} = \omega_{i(\xi)} = \frac{m_{i(\xi)}\,\overline{Cp_{f,i}(\xi)}}{S} \qquad (i = 1, 2, 3 \ldots I)$$

$$\Pi_{I+j(\xi)} = \omega_{I+j(\xi)} = \frac{m_{j(\xi)}\,\overline{Cp_{f,j}(\xi)}}{S} \qquad (j = 1, 2, 3 \ldots J)$$

$$\Pi_{I+J+1(\xi)} = \omega_{I+J+1(\xi)} + \omega_{I+J+5(\xi)} = \frac{\alpha_{1(\xi)}\,\beta_{1(\xi)}\,\dot{m}_{I-1,I(\xi)}\,Cp_{f,I-1(\xi)}}{S} + \Pi_{I+J+5(\xi)}$$

$$\Pi_{I+J+2(\xi)} = \omega_{I+J+2(\xi)} = \frac{\alpha_{1(\xi)}(1-\beta_{1(\xi)})\,\dot{m}_{I,I-1(\xi)}\,\overline{Cp_{f,I}(\xi)}}{S}$$

$$\Pi_{I+J+3(\xi)} = \omega_{I+J+3(\xi)} + \omega_{I+J+6(\xi)} = \frac{\alpha_{2(\xi)}(1-\beta_{2(\xi)})\,\dot{m}_{I+1,I(\xi)}\,Cp_{f,I+1}}{S} + \Pi_{I+J+6(\xi)}$$

$$\Pi_{I+J+4(\xi)} = \omega_{I+J+4(\xi)} = \frac{\alpha_{2(\xi)}\,\beta_{2(\xi)}\,\dot{m}_{I,I+1(\xi)}\,\overline{Cp_{f,I}(\xi)}}{S}$$

$$\Pi_{I+J+5(\xi)} = \omega_{I+J+5(\xi)} = \frac{\gamma_{1(\xi)}\,\dot{m}_{I,I-1(\xi)}\,\overline{Cp_{f,I}(\xi)}}{S}$$

$$\Pi_{I+J+6(\xi)} = \omega_{I+J+6(\xi)} = \frac{\gamma_{2(\xi)}\,\dot{m}_{I,I+1(\xi)}\,\overline{Cp_{f,I}(\xi)}}{S}$$

$$\Pi_{I+J+7}(\xi) = W_{I+J+7}(\xi) = \frac{U(\xi)A}{S}$$

$$\Pi_{I+J+8}(\xi) = W_{I+J+8}(\xi) = \frac{U_c A_c}{S}$$

$$\Pi_{I+J+9}(\xi) = \sum_{j=1}^{J} \Pi_{I+j}(\xi) + \Pi_{I+J+2}(\xi) + \Pi_{I+J+4}(\xi) + \Pi_{I+J+5}(\xi) + \Pi_{I+J+6}(\xi)$$

$$+ \Pi_{I+J+7}(\xi) + \Pi_{I+J+8}(\xi)$$

$$\Pi_{I+J+10} = W_{I+J+10} = \frac{1}{S} = \frac{\Delta\tau}{\rho_I C_I V_I + \sum_{e=1}^{E} \rho_e C_e V_e}$$

The notation for these terms is given in equations (5.62) and (5.63).

b) Type 2 Node - Rock Bed Sensible Energy Storage

Equation (5.69) represents the difference equation for the rock node in this unit. As there are no heat generation sources associated with this node except for the miscellaneous term, then $\Sigma Q_{I(\xi)} = Q_{M(\xi)}$. Taking the known $\theta_{S(n+1)}$ term to the knownside of the equation the following complete difference equation is obtained after re-numbering,

$$(2 + \Psi_{6(n+1)})\theta_{I(n+1)} - \Psi_{1(n+1)}\theta_{I-1(n+1)} - \Psi_{2(n+1)}\theta_{I+1(n+1)} - \Psi_{3(n+1)}\theta_{F(n+1)}$$

$$- \Psi_{4(n+1)}\theta_{C(n+1)} = (2 - \Psi_{6(n)})\theta_{I(n)} + \Psi_{1(n)}\theta_{I-1(n)} + \Psi_{2(n)}\theta_{I+1(n)}$$

$$+ \Psi_{3(n)}\theta_{F(n)} + \Psi_{4(n)}\theta_{C(n)} + \Psi_{5(n+1)}\theta_{S(n+1)} + \Psi_{5(n)}\theta_{S(n)} + \Psi_{7}(Q_{M(n+1)} + Q_{M(n)})$$

(5.168)

where,

$$\Psi_{1(\xi)} = \chi_{1(\xi)} = \frac{\beta(\xi)Ak}{S\Delta x} \quad ; \quad \Psi_{2(\xi)} = \chi_{2(\xi)} = \frac{\gamma(\xi)Ak}{S\Delta x}$$

$$\Psi_{3(\xi)} = \chi_{3(\xi)} = \frac{h_v(\xi)V}{S} \quad ; \quad \Psi_{4(\xi)} = \chi_{4(\xi)} = \frac{A_c U_c(\xi)}{S}$$

$$\Psi_{5(\xi)} = \chi_{5(\xi)} = \frac{U(\xi)A}{S} \quad ; \quad \Psi_{6(\xi)} = \Psi_{1(\xi)} + \Psi_{2(\xi)} + \Psi_{3(\xi)} + \Psi_{4(\xi)} + \Psi_{5(\xi)}$$

$$\psi_7 = \quad = \frac{1}{S} = \frac{\Delta\tau}{\rho_R C_R V_R}$$

The fluid node in a rock bed storage unit was given in equation (5.71) as the summation of the heat generation terms is Qm(ξ) then this equation can be re-labelled to give

$$(2 + \Gamma_{3(n+1)})\theta_{F(n+1)} - \Gamma_{1(n+1)}\theta_{F-1(n+1)} - \Gamma_{2(n+1)}\theta_{I(n+1)}$$
$$= (2 - \Gamma_{3(n)})\theta_{F(n)} + \Gamma_{1(n)}\theta_{F-1(n)} + \Gamma_{2(n)}\theta_{I(n)} + \Gamma_4(Q_{M(n+1)} + Q_{M(n)}) \qquad (5.169)$$

where,

$$\Gamma_1(\xi) = \alpha_1(\xi) = \frac{\dot{m}(\xi)\,\overline{C_{p\,F-1}(\xi)}}{S} \quad ; \quad \Gamma_2(\xi) = \alpha_2(\xi) = \frac{h_{ur}(\xi)V}{S}$$

$$\Gamma_3(\xi) = \alpha_3(\xi) = \Gamma_2(\xi) + \frac{\dot{m}(\xi)\,\overline{C_{p\,F}(\xi)}}{S} \quad ; \quad \Gamma_4 = \alpha_4 = \frac{1}{S} = \frac{\Delta\tau}{\rho_A C_A V_A}$$

c) Type 3 Node - Latent Energy Storage Unit

In the difference equation for the phase change material in this section - equation (5.75) - the value of $\theta_{S(n+1)}$ is known and the sum of the heat generation sources are Qm(ξ), therefore, the complete difference equation is given in the form:

$$(\omega + \Omega_{3(n+1)})\theta_{I(n+1)} - \Omega_{1(n+1)}\theta_{I-1(n+1)} = (\omega - \Omega_{3(n)})\theta_{I(n)}$$
$$+ \Omega_{1(n)}\theta_{I-1(n)} + \Omega_{2(n+1)}\theta_{S(n+1)} + \Omega_{2(n)}\theta_{S(n)} + Q_{M(n+1)} + Q_{M(n)}$$
$$(5.170)$$

from equation (5.75)

$$\omega = X = \frac{2(\rho_S C_S V_S)}{\Delta\tau} \quad ; \quad \Omega_1(\xi) = Y_1(\xi) = U_{ex}(\xi)A_{ex}$$

$$\Omega_2(\xi) = Y_2(\xi) = U_L(\xi)A \quad ; \quad \Omega_3(\xi) = \Omega_1(\xi) + \Omega_2(\xi)$$

Let W=1 during the solid or liquid sensible heating or cooling phase and W=0 during the isothermal phase-change period.

The fluid node relating to this unit is given in equation (5.76). As the $\Sigma Q_{I(t)}$ term equates to $Q_{M(t)}$ it is possible to write

$$(2+\sigma_{3(n+1)})\theta_{F(n+1)} - \sigma_{1(n+1)}\theta_{F-1(n+1)} - \sigma_{2(n+1)}\theta_{I(n+1)}$$
$$= (2-\sigma_{3(n)})\theta_{F(n)} + \sigma_{1(n)}\theta_{F-1(n)} + \sigma_{2(n)}\theta_{I(n)} + \sigma_{4}(Q_{n(n+1)} + Q_{(n)}) \quad (5.171)$$

where,

$$\sigma_{1(\xi)} = \gamma_{1(\xi)} = \frac{\dot{m}_{(\xi)}\overline{C_{p_{F-1(\xi)}}}}{S} \quad ; \quad \sigma_{2(\xi)} = \gamma_{2(\xi)} = \frac{U_{ec(\xi)}A_{ec}}{S}$$

$$\sigma_{3(\xi)} = \gamma_{3(\xi)} = \sigma_{2(\xi)} + \frac{\dot{m}_{(\xi)}\overline{C_{p_{F(\xi)}}}}{S} \quad ; \quad \sigma_{4} = \gamma_{4} = \frac{1}{S} = \frac{\Delta\tau}{\rho_A C_A V_A}$$

The procedure for selecting and using the appropriate complete differnece equations in the solution of a design is discussed in the following chapter. However, a summary of the most frequently used complete difference equations is given in Table 5.8. This list of equations represents the basic nodal equations for use in a solar energy system model. The derived equations not included in Table 5.8 are employed if a more detailed model is required. Table 5.9 gives a list of the heat generation terms associated with the complete difference equations, these terms are now designated $q_{(t)}$.

Description	Expression	Reference Equation
1. Node positioned at the centre of a homogeneous element modelled in one-dimension*	$(2+C_{3(n+1)})\theta_{I(n+1)} - C_1\theta_{I-1(n+1)} - C_1\theta_{I+1(n+1)}$ $= (2-C_3(n))\theta_{I(n)} + C_1\theta_{I-1(n)} + C_1\theta_{I+1(n)} + C_2 q(t)$	5.137
2. Node positioned on the boundary between two homogeneous elements modelled in one-dimension	$(2+G_4(n+1))\theta_{I(n+1)} - G_1\theta_{I-1(n+1)} - G_2\theta_{I+1(n+1)}$ $= (2-G_4(n))\theta_{I(n)} + G_1\theta_{I-1(n)} + G_2\theta_{I+1(n)} + G_3 q(t)$	5.142
3. Node associated with fluid flow through a solar collector	$(2+J_{M+2(n+1)})\theta_{I(n+1)} - \sum_{j=1}^{M} J_{j(n+1)}\theta_{j(n+1)} - J_{M+1(n+1)}\theta_{I-1(n+1)}$ $= (2-J_{M+2(n)})\theta_{I(n)} + \sum_{j=1}^{M} J_{j(n)}\theta_{j(n)} + J_{n+1(n)}\theta_{I-1(n)} - J_{M+3} q(t)$	5.145
4. Node positioned on the external exposed surface of a solar collector*	$(2+Q_{3(n+1)})\theta_{I(n+1)} - Q_2\theta_{I+1(n+1)} = (2-Q_3(n))\theta_{I(n)}$ $+ Q_{1(n+1)}\theta_{A(n+1)} + Q_1(n)\theta_{A(n)} + Q_2\theta_{I+1(n)} + Q_4 q(t)$	5.155
5. Node positioned on the internal surface of a solar collector*	$(2+R_{J+3(n+1)})\theta_{I(n+1)} - R_{J+1}\theta_{I-1(n+1)} - R_{J+2(n+1)}\theta_{I+1(n+1)} - \sum_{j=1}^{I} R_{j(n+1)}\theta_{j(n+1)}$ $= (2-R_{J+3(n)})\theta_{I(n)} + R_{J+1}\theta_{I-1(n)} + R_{J+2(n)}\theta_{I+1(n)} + \sum_{j=1}^{I} R_{j(n)}\theta_{j(n)} + R_{J+4} q(t)$	5.156
6. Node representing a conduit or fitting-Category 4	$(2+\sum_{b=1}^{B} U_{A+b(n+1)} + U_{A+B+1(n+1)})\theta_{I(n+1)} - \sum_{a=1}^{A} U_{a(n+1)}\theta_{a(n+1)} = (2-\sum_{b=1}^{B} U_{A+b(n)}$ $+ U_{A+B+1(n)})\theta_{I(n)} + \sum_{a=1}^{A} U_{a(n)}\theta_{a(n)} + U_{A+B+1(n+1)}\theta_{S(n+1)} + U_{A+B+1(n)}\theta_{S(n)} + U_{A+B+2} q(t)$	5.159
7. Node representing a fan or pump - Category 5	$(2+W_{1(n+1)})\theta_{I(n+1)} - W_{2(n+1)}\theta_{I-1(n+1)} - W_3\theta_{A6(n+1)}$ $= (2-W_{1(n)})\theta_{I(n)} + W_{2(n)}\theta_{I-1(n)} + W_3\theta_{A6(n)} + W_4 q(t)$	5.162
8. Node representing an auxiliary heater - Category 6	$(2+Y_{1(n+1)})\theta_{I(n+1)} + Y_{2(n+1)}\theta_{I-1(n+1)} = (2-Y_1(n))\theta_{I(n)}$ $+ Y_{2(n)}\theta_{I-1(n)} + Y_3 q(t)$	5.164
9. Node representing a heat exchanger - Category 7	$(\Lambda_1+\Lambda_{3(n+1)})\theta_{H(n+1)} - (\Lambda_2+\Lambda_{4(n+1)})\theta_{C(n+1)} + (\Lambda_{5(n+1)} - \Lambda_{5(n)})\theta_{H-1(n+1)} + (\Lambda_{4(n+1)} - \Lambda_{5(n+1)})\theta_{C-1(n+1)}$ $= (\Lambda_1-\Lambda_{3(n)})\theta_{H(n)} - (\Lambda_{4(n)}-\Lambda_2)\theta_{C(n)} + (\Lambda_{3(n)} - \Lambda_{5(n)})\theta_{H-1(n)} + (\Lambda_{5(n)} - \Lambda_{4(n)})\theta_{C-1(n)} + q_{(t)}$	5.166
10. Node representing a segment of a liquid sensible energy storage unit	$(2+\Pi_{I+J+9(n+1)})\theta_{I(n+1)} - \sum_{i=1}^{I} \Pi_{i(n+1)}\theta_{i(n+1)} - \Pi_{I+J+1(n+1)}\theta_{I+1(n+1)} - \Pi_{I+J+3(n+1)}\theta_{I+1(n+1)}$ $- \Pi_{I+J+6(n+1)}\theta_{F(n+1)} = (2-\Pi_{I+J+9(n)})\theta_{I(n)} + \sum_{i=1}^{I} \Pi_{i(n)}\theta_{i(n)} + \Pi_{I+J+1(n)}\theta_{I-1(n)}$ $+ \Pi_{I+J+3(n)}\theta_{I+1(n)} + \Pi_{I+J+4(n+1)}\theta_{S(n+1)} + \Pi_{I+J+9(n)}\theta_{S(n)} + \Pi_{I+J+6(n)}\theta_{F(n)} + \Pi_{I+J+10} q(t)$	5.167
11. Node representing a segment of a rockbed sensible energy storage unit	$(2+\Psi_{6(n+1)})\theta_{I(n+1)} - \Psi_{1(n+1)}\theta_{I-1(n+1)} - \Psi_{2(n+1)}\theta_{I+1(n+1)} - \Psi_{3(n+1)}\theta_{F(n+1)}$ $- \Psi_{4(n+1)}\theta_{C(n+1)} = (2-\Psi_{6(n)})\theta_{I(n)} + \Psi_{1(n)}\theta_{I-1(n)} + \Psi_{2(n)}\theta_{I+1(n)} + \Psi_{3(n)}\theta_{F(n)}$ $\Psi_{4(n)}\theta_{C(n)} + \Psi_{7(n+1)}\theta_{S(n+1)} + \Psi_{7(n)}\theta_{S(n)} + \Psi_9 q(t)$	5.168
12. Node representing fluid flow through a segment of a rock bed storage unit	$(2+\Gamma_{3(n+1)})\theta_{F(n+1)} - \Gamma_{1(n+1)}\theta_{F-1(n+1)} - \Gamma_{2(n+1)}\theta_{I(n+1)}$ $= (2-\Gamma_{3(n)})\theta_{F(n)} + \Gamma_{1(n)}\theta_{F-1(n)} + \Gamma_{2(n)}\theta_{I(n)} + \Gamma_4 q(t)$	5.169
13. Node representing a segment of a latent energy storage unit	$(\omega+\Omega_{3(n+1)})\theta_{I(n+1)} - \Omega_{1(n+1)}\theta_{I-1(n+1)} = (\omega-\Omega_{3(n)})\theta_{I(n)}$ $+ \Omega_{1(n)}\theta_{I-1(n)} + \Omega_{2(n+1)}\theta_{S(n+1)} + \Omega_{2(n)}\theta_{S(n)} + q_{(t)}$	5.170
14. Node representing fluid flow through a latent energy storage unit	$(2+\sigma_{3(n+1)})\theta_{F(n+1)} - \sigma_{1(n+1)}\theta_{F-1(n+1)} - \sigma_{2(n+1)}\theta_{I(n+1)}$ $= (2-\sigma_{3(n)})\theta_{F(n)} + \sigma_{1(n)}\theta_{F-1(n)} + \sigma_{2(n)}\theta_{I(n)} + \sigma_4 q(t)$	5.171

Table 5.8 Summary of the basic equation for a solar energy systems model

* If the node in question is an absorber plate node which is associated with a liquid collector then add $\sum_{i=0}^{I} \times \theta_{c,i(t)}$ for time steps n and $n+1$

Nb. $q_{(t)}$ values for each equation are given in Table 5.9

$q(t)$	Equations Reference Numbers
1. $Q_{s,\alpha}(t) + \omega_2(t) + Q_M(t)$	5.135 - 5.138
2. $Q_M(t)$	5.140 - 5.145, 5.159, 5.160 5.168 - 5.171
3. $Q_{s,E}(t) + Q_{s,R}(t) + \omega_2(t) + \exists_2(t) + Q_M(t)$	5.147, 5.152, 5.155
4. $Q_{s,I}(t) + Q_M(t)$	5 149, 5.153, 5.156, 5.158
5. $Q_{s,I}(t) + \exists_2(t) + Q_M(t)$	5.151, 5.154, 5.157
6. $Q_{env}(t) + Q_M(t)$	5.162, 5.163, 5.165, 5.166
7. $Q_{aux}(t) + Q_{env}(t) + Q_M(t)$	5.164
8. $Q_E(t) + Q_M(t)$	5.167

TABLE 5.9 Summary of $q(t)$ terms associated with equations (5.135 - 5.171) derived in Chapter 5

CHAPTER 6 The Solution of the Solar Collector Systems Model

In Chapter 4 a three stage process was specified to apply a numerical analysis technique to solve for any system component. The first two stages are fully described in Chapter 5, they were the placement of nodes at discrete points in each solar energy system component and the derivation of a difference equation for each node. This chapter deals with the third and final stage which is the simultaneous solution of the system components and system interactions using the simultaneous approach.

The purpose of this chapter is to explain the method of solving the resulting matrix of difference equations for any solar energy system with the system components described in Chapter 5. To describe this stage effectively the process of nodal placement, the application of difference equations and subsequent solution of the resulting matrix for a simple solar collector system will be explained. Section 6.2 identifies the matrices to be solved in more complex systems.

The derived difference equations from Chapter 5 can be applied to a number of different applications to those for which it was originally developed. Several of these alternative applications are mentioned in Section 6.3.

6.1 Detailed Solution Method

Consider figure 6.1 which represents a typical solar energy collection system designed to meet the requirements of a particular space heating load. To simplify the analysis fans and conduits in the system are assumed to be thermally non-participating, consequently, only six system components will be modelled. These are:

1. the solar collector
2. damper 1
3. rock bed storage unit
4. damper 2
5. damper 3
6. auxiliary heater.

In the solar collector the default nodal scheme is chosen, that is, one fluid node and one-dimensional conduction through each multi-element construction surrounding the fluid node. The default nodal scheme for a storage unit is one pair of nodes - a material and a fluid node. In this case three pairs of nodes are specified to model thermal stratification. The remaining four components are modelled using single nodes.

The solar collector is a single duct air collector with a glass transparent cover, as shown in figure 6.2. The construction of the walls and base of the collector is identified in figure 6.3. The nodal placement is also shown. The complete nodal replacement for the solar collector is given in figure 6.4 A node numbering scheme has been employed where, for example, node 1,4,3 represents node 3 in wall 4 of the solar collector which is component 1. Boundary nodes connected to the external surfaces of the collector have also been identified by setting the node value to zero. In this case the boundary node to the collector is external ambient air temperature the value of which is obtained from the climate file, (see chapter 3).

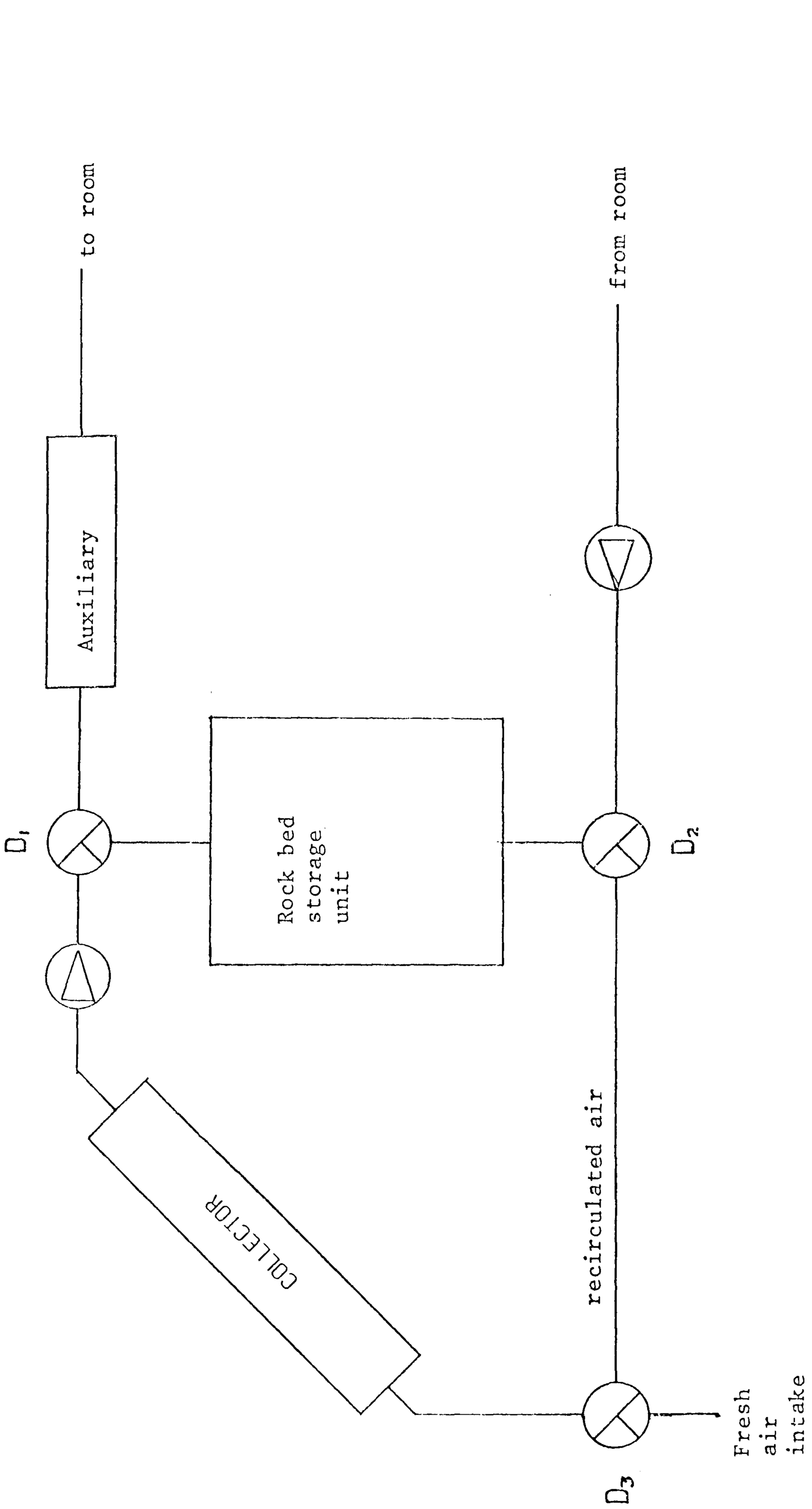

Figure 6.1 Typical air collector system to supply space heating load.

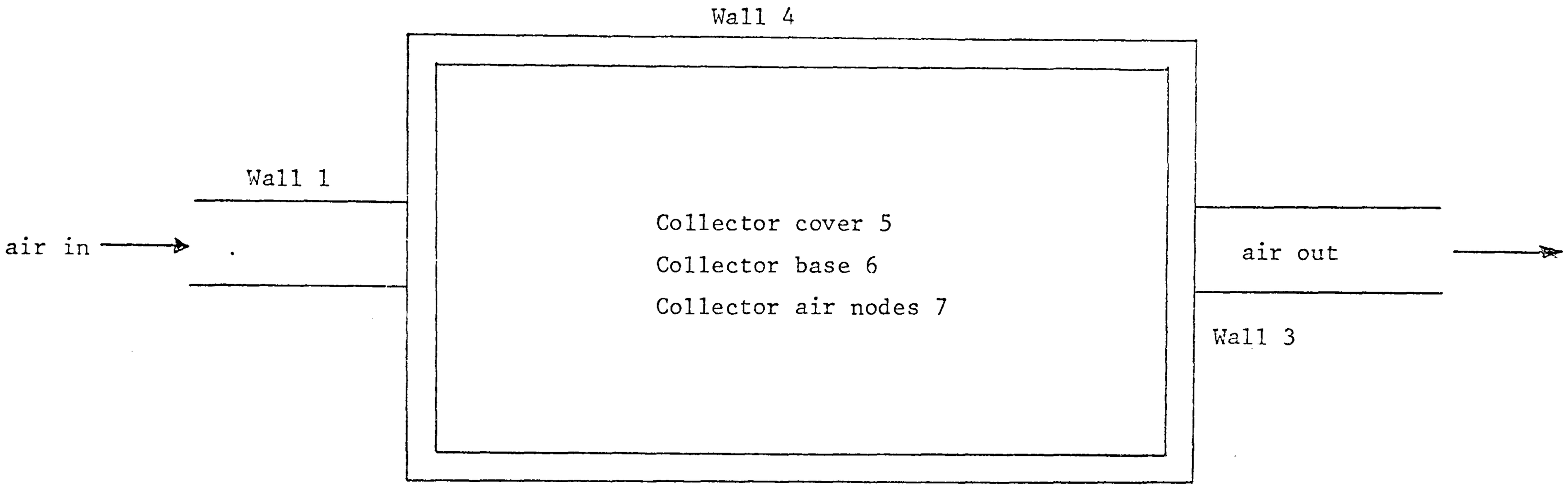

Figure 6.2 Solar collector.

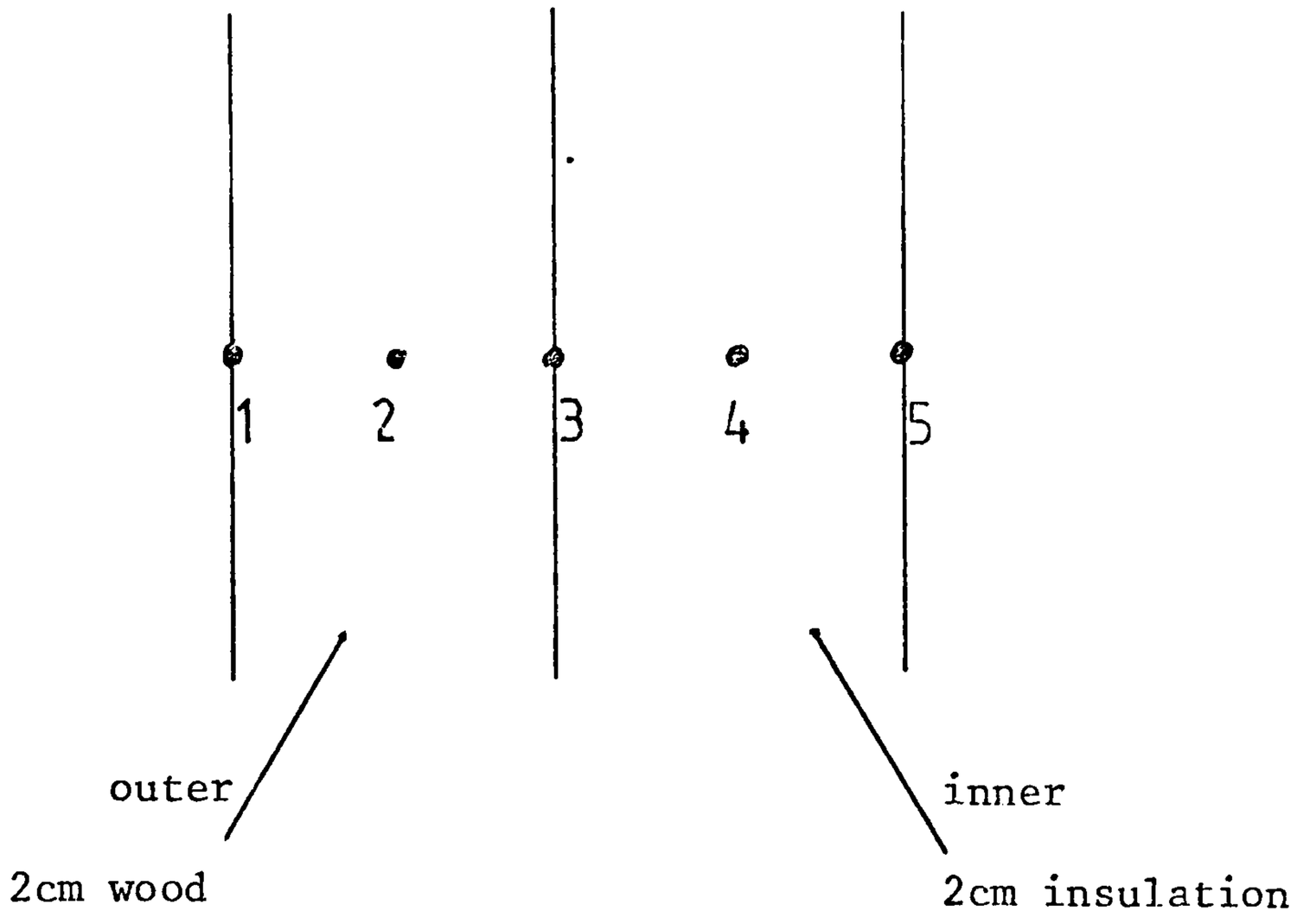

a) Used for walls 1, 2, 3 and 4

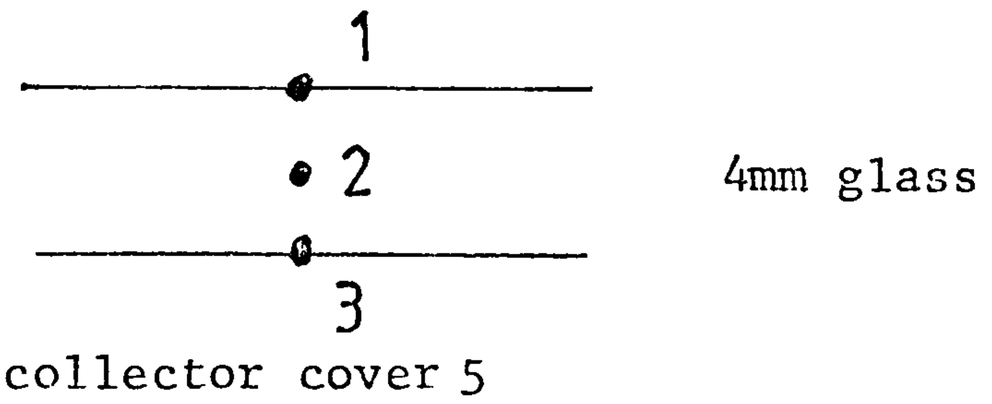

b) Used for collector cover 5

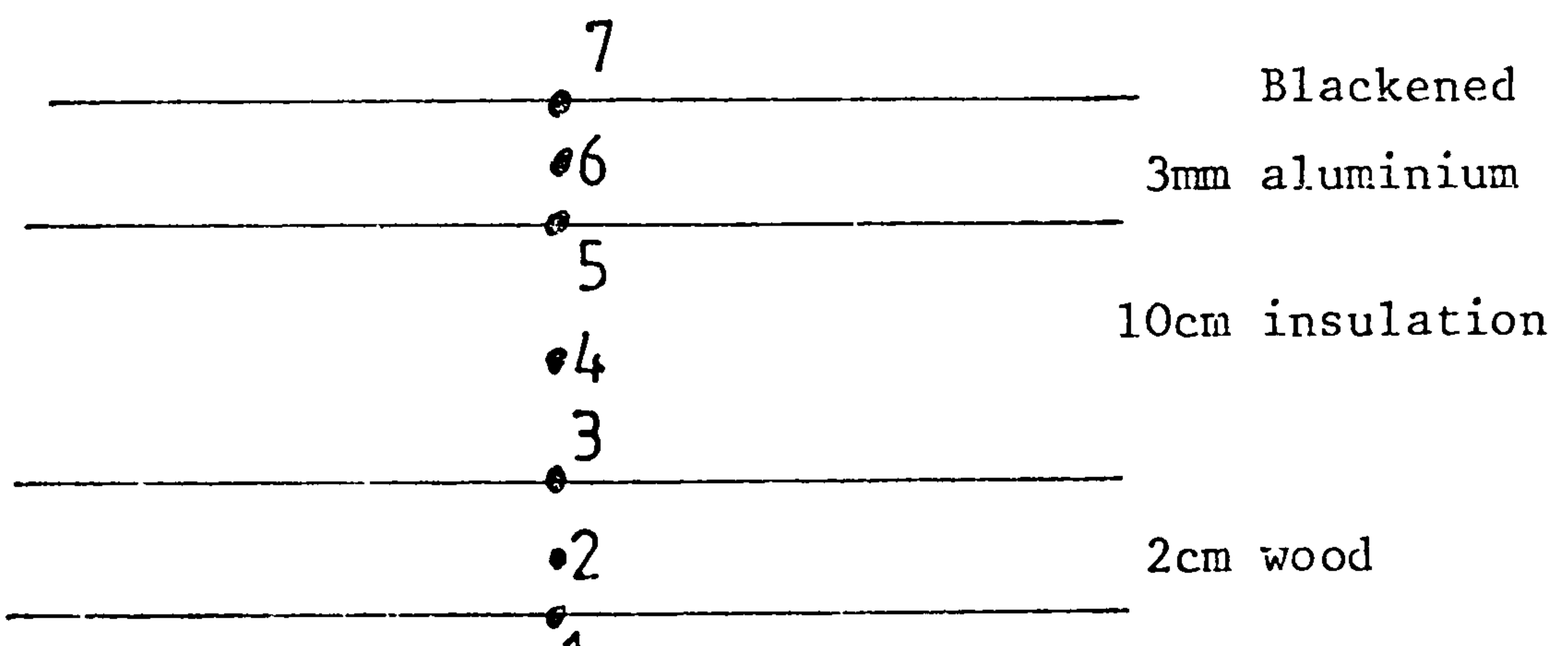

c) Used for absorber plate

Figure 6.3 Constructional details of the solar collector.

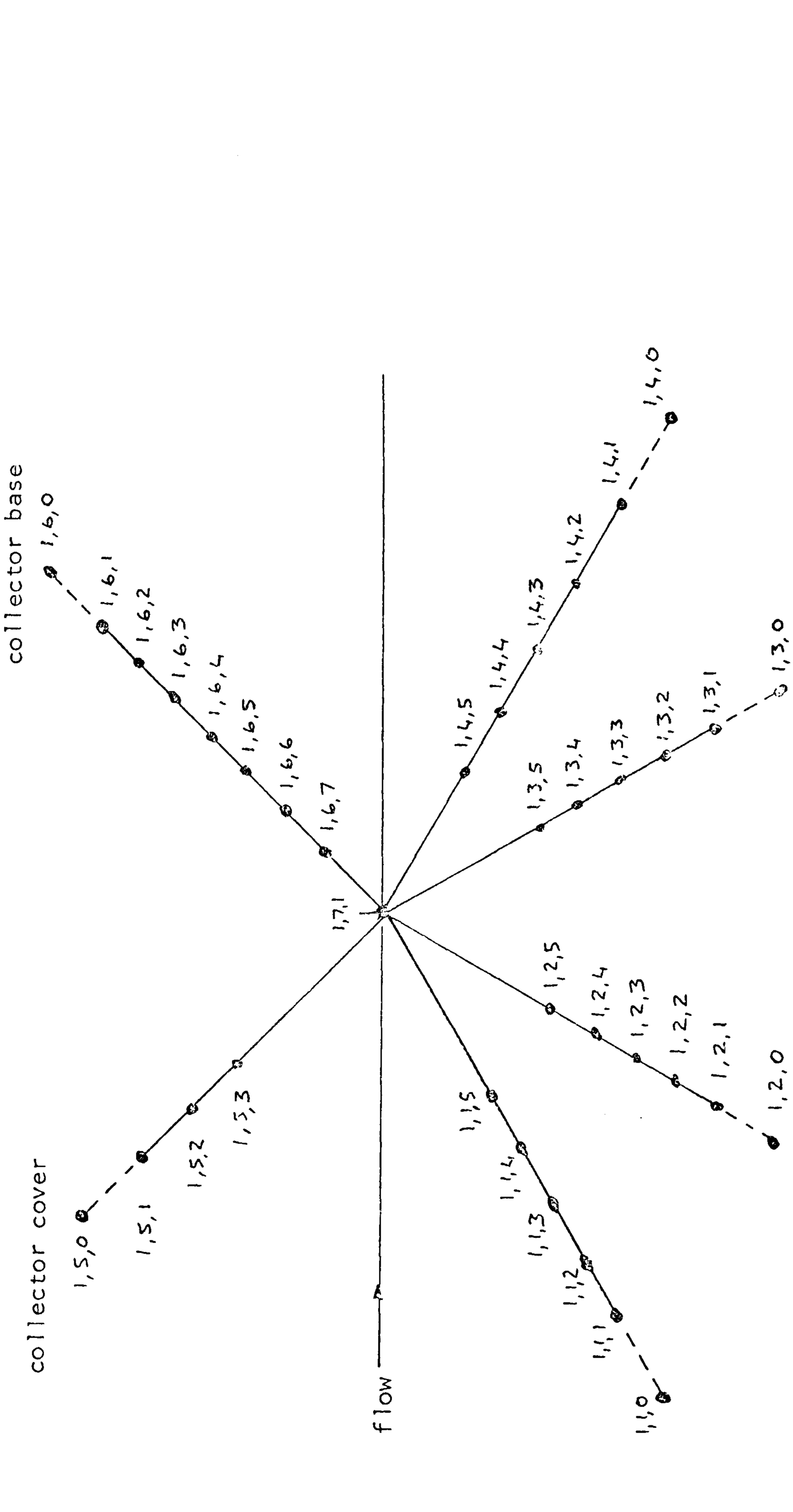

Figure 6.4: Nodal Equivalent Scheme (node numbers - component, construction, node)

The three dampers in the system are each modelled by a single Category 4 node. Figure 6.5 shows the nodal representation of a damper which may have two inlet flows A and B. The node is numbered depending upon the component number, therefore, dampers 1, 2 and 3 are represented by nodes 2, 4 and 5 respectively. Node C, Ø represents the boundary condition to the component. It is assumed that each damper is situated indoors and the temperature of the surrounding air, θs, is theboundary condition.

The rock bed storage unit has been given three stratification segments, therefore, six nodes will be required to model this component because there will be three pairs of material and fluid nodes. The nodal scheme for this component is shown in figure 6.6, where the boundary condition is θs. The numbering scheme for this component is given by component No., segment No., rock or fluid - for example, 3, 1, F or 3, 2, R, etc.

The final component to be modelled is the auxiliary heater which is modelled by a single node, figure 6.7. In this example it is called node 6.

The system specified in figure 6.1 can be replaced by its nodal equivalent which is shown in figure 6.8. Two nodes are notated by K for their nodal number, this is to indicate that these nodes are boundary conditions and have a known temperature.

Nine different types of nodes are required to model the system under consideration. A list of these nodes is given in Table 6.1. This list is a subset of the list of basic nodes required to simulate a solar energy system given in Table 5.8 of Chapter 5. There is a total of 41 nodes to be considered, therefore, there will be 41 implicit difference equations to be solved simultaneously. The implicit difference equations, representing the nodal energy balance at each point in time,can be expressed in matrix form where:

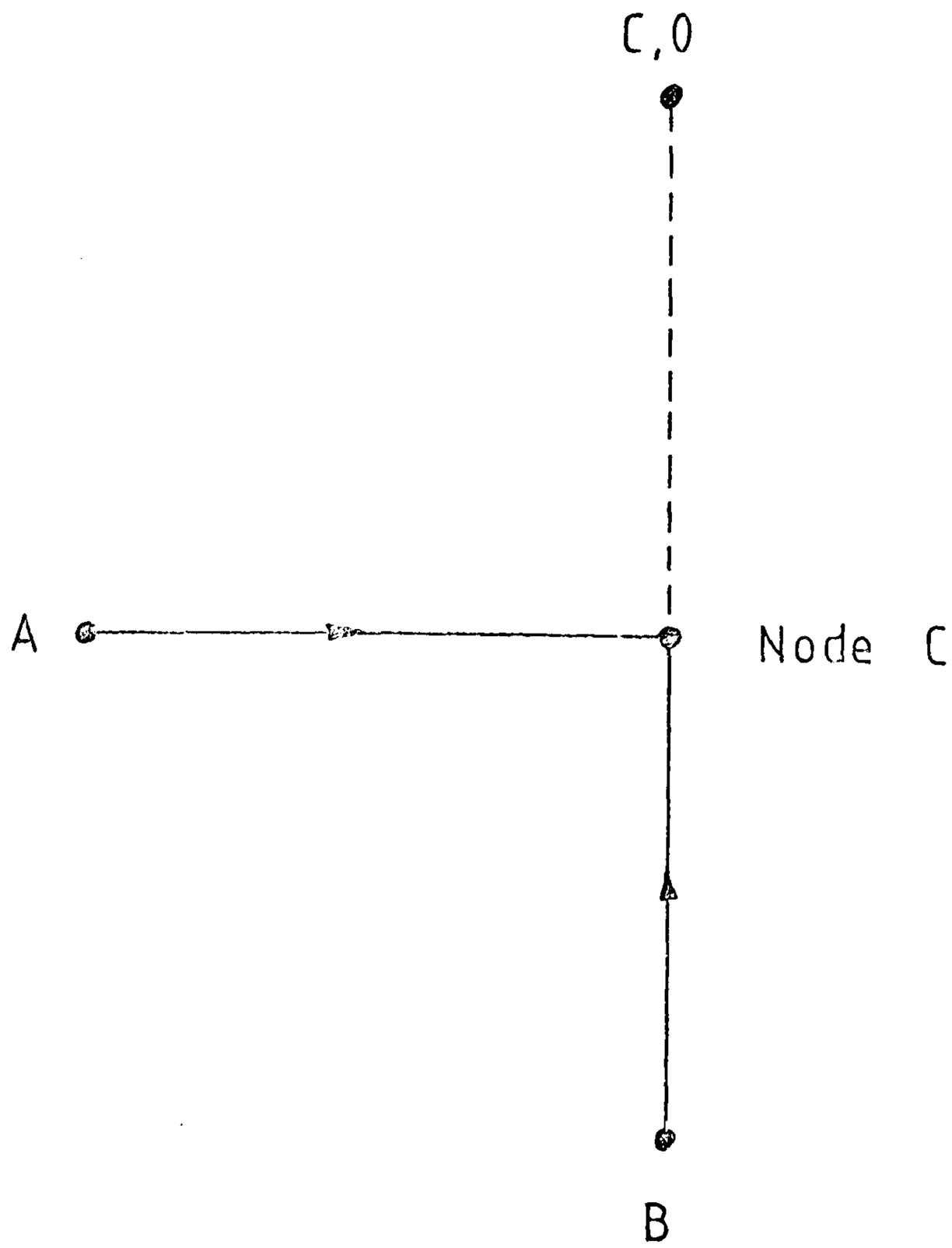

Figure 6.5: Nodal representation of Dampers 1,2 and 3
(where C is the component number)

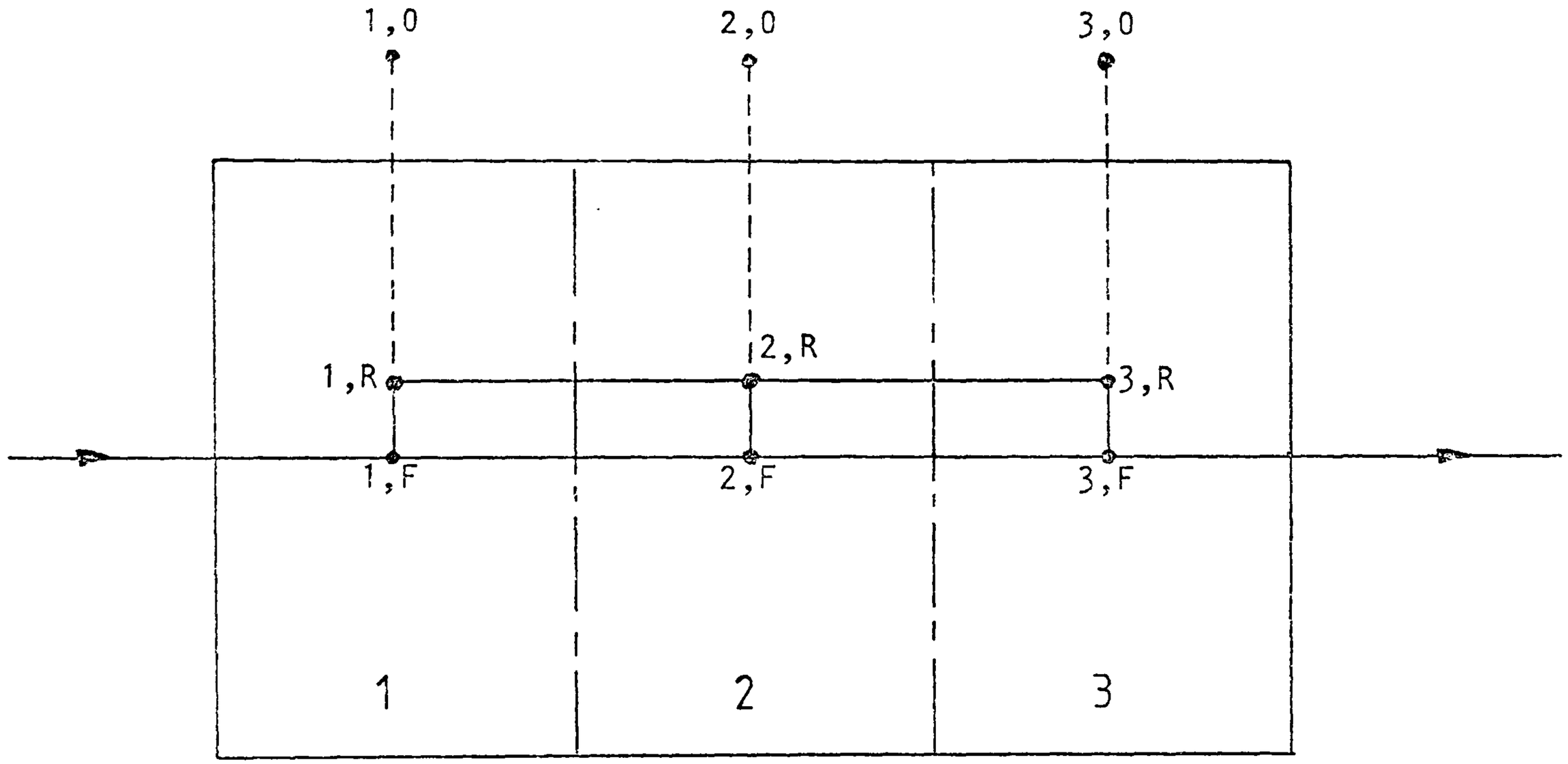

Nodes A,B & C rock nodes , 1,2 & 3 fluid nodes

Figure 6.6: Nodal representation of rock bed stages unit (component 3 from Figure 6.1)

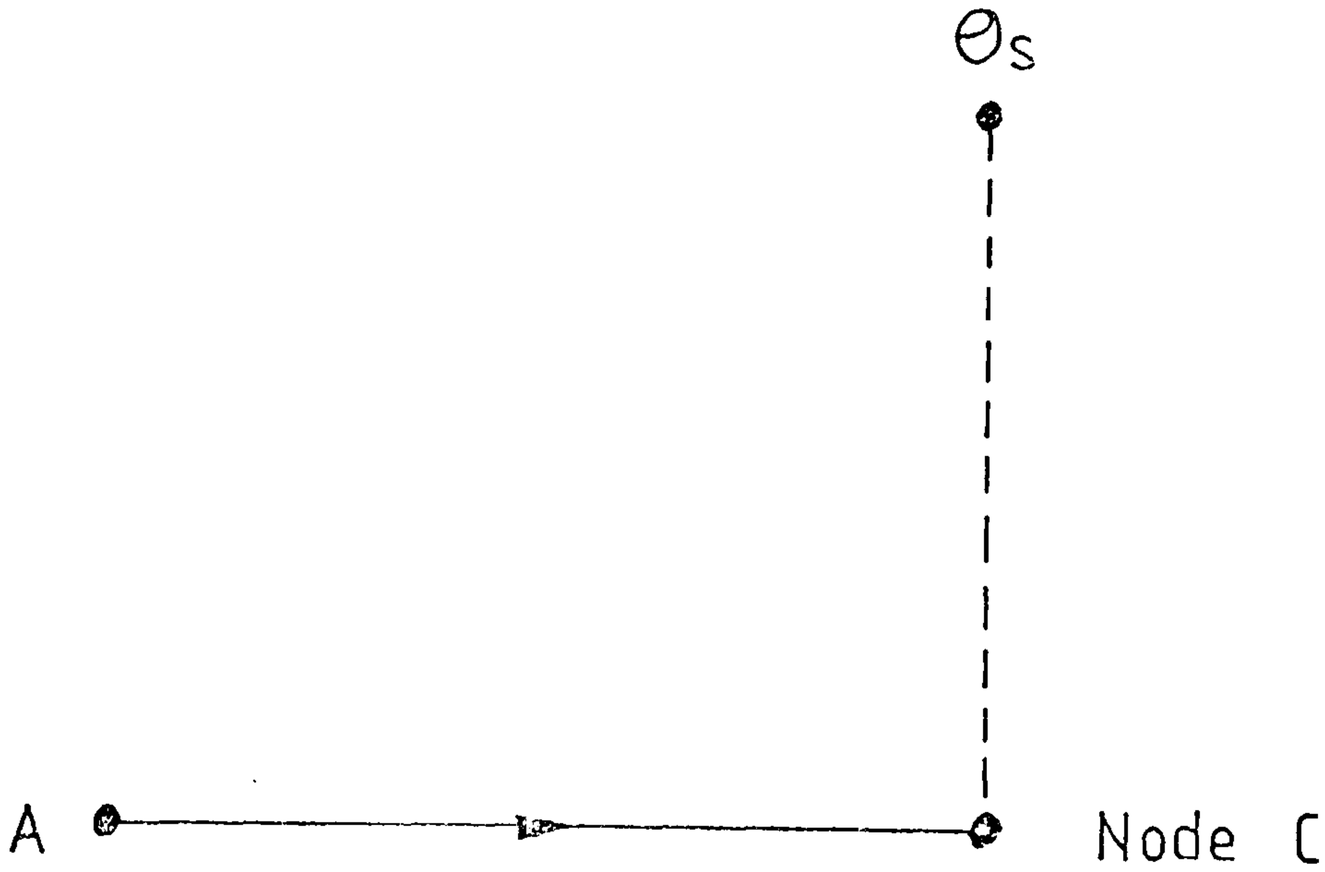

Figure 6.7: Nodal scheme for an auxiliary heater.
In this example, the auxiliary heater
is component 6, therefore, C=6

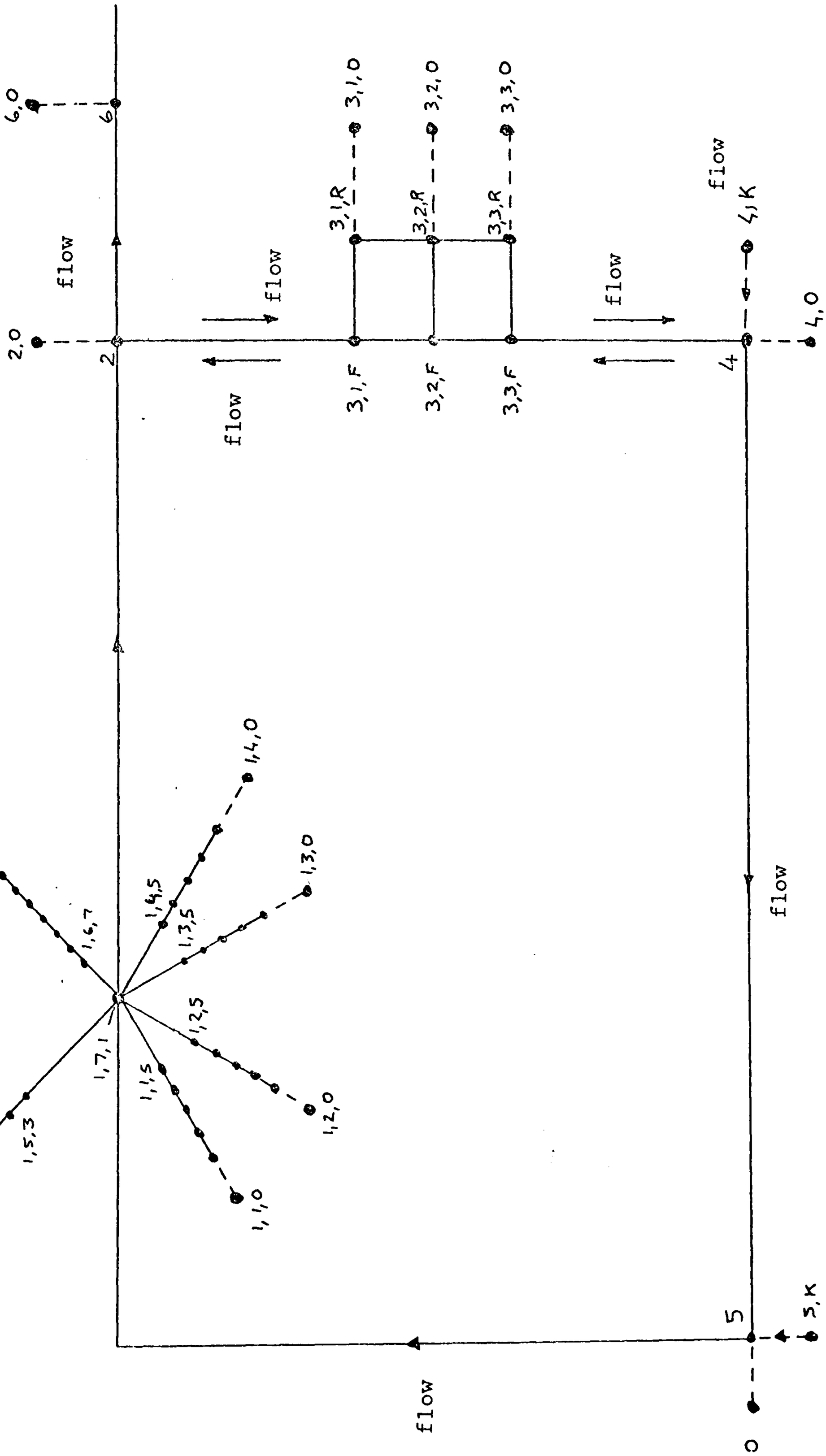

Figure 6.8 Nodal equivalent of complete system (for solar collector nodal numbering see figure 6.4)

	Description	Expression	Reference Equation
1.	Node positioned at the centre of a homogeneous element modelled in one-dimension*	$(2+C_{3(n+1)})\theta_{I(n+1)} - C_1\theta_{I-1(n+1)} - C_1\theta_{I+1(n+1)}$ $= (2-C_{3(n)})\theta_{I(n)} + C_1\theta_{I-1(n)} + C_1\theta_{I+1(n)} + C_2 q(t)$	5.137
2.	Node positioned on the boundary between two homogeneous elements modelled in one-dimension	$(2+G_{4(n+1)})\theta_{I(n+1)} - G_1\theta_{I-(n+1)} - G_2\theta_{I+1(n+1)}$ $= (2-G_{4(n)})\theta_{I(n)} + G_1\theta_{I-1(n)} + G_2\theta_{I+1(n)} + G_3 q(t)$	5.142
3.	Node associated with fluid flow through a solar collector	$(2+J_{M+2(n+1)})\theta_{I(n+1)} - \sum_{j=1}^{M} J_{j(n+1)}\theta_{j(n+1)} - J_{M+1(n+1)}\theta_{I-1(n+1)}$ $= (2-J_{M+2(n)})\theta_{I(n)} + \sum_{j=1}^{M} J_{j(n)}\theta_{j(n)} + J_{M+1(n)}\theta_{I-1(n)} - J_{M+3} q(t)$	5.145
4.	Node positioned on the external exposed surface of a solar collector*	$(2+Q_{3(n+1)})\theta_{I(n+1)} - Q_2\theta_{I+1(n+1)} = (2-Q_{3(n)})\theta_{I(n)}$ $+ Q_{1(n+1)}\theta_{A(n+1)} + Q_{1(n)}\theta_{A(n)} + Q_2\theta_{I+1(n)} + Q_4 q(t)$	5.155
5.	Node positioned on the internal surface of a solar collector*	$(2+R_{J+3(n+1)})\theta_{I(n+1)} - R_{J+1}\theta_{I-1(n+1)} - R_{J+2(n+1)}\theta_{I+1(n+1)} - \sum_{j=1}^{J} R_{j(n+1)}\theta_{j(n+1)}$ $= (2-R_{J+3(n)})\theta_{I(n)} + R_{J+1}\theta_{I-1(n)} + R_{J+2(n)}\theta_{I+1(n)} + \sum_{j=1}^{J} R_{j(n)}\theta_{j(n)} + R_{J+4} q(t)$	5.156
6.	Node representing a conduit or fitting-Category 4	$(2+\sum_{b=1}^{B} U_{A+b(n+1)} + U_{A+B+1(n+1)})\theta_{I(n+1)} - \sum_{a=1}^{B} U_{a(n+1)}\theta_{a(n+1)} = (2-\sum_{b=1}^{B} U_{A+b(n)}$ $+ U_{A+B+1(n)})\theta_{I(n)} + \sum_{a=1}^{B} U_{a(n)}\theta_{a(n)} + U_{A+B+1(n+1)}\theta_{S(n+1)} + U_{A+B+1(n)}\theta_{S(n)} + U_{A+B+2} q(t)$	5.159
7.	Node representing an auxiliary heater - Category 6	$(2+Y_{1(n+1)})\theta_{I(n+1)} + Y_{2(n+1)}\theta_{I-1(n+1)} = (2-Y_{1(n)})\theta_{I(n)}$ $+ Y_{2(n)}\theta_{I-1(n)} + Y_3 q(t)$	5.164
8.	Node representing a segment of a rockbed sensible energy storage unit	$(2+\Psi_{6(n+1)})\theta_{I(n+1)} - \Psi_{1(n+1)}\theta_{I-1(n+1)} - \Psi_{2(n+1)}\theta_{I+1(n+1)} - \Psi_{3(n+1)}\theta_{F(n+1)}$ $- \Psi_{4(n+1)}\theta_{C(n+1)} = (2-\Psi_{6(n)})\theta_{I(n)} + \Psi_{1(n)}\theta_{I-1(n)} + \Psi_{2(n)}\theta_{I+1(n)} + \Psi_{3(n)}\theta_{F(n)}$ $\Psi_{4(n)}\theta_{C(n)} + \Psi_{7(n+1)}\theta_{S(n+1)} + \Psi_{7(n)}\theta_{S(n)} + \Psi_9 q(t)$	5.168
9.	Node representing fluid flow through a segment of a rock bed storage unit	$(2+\Gamma_{3(n+1)})\theta_{F(n+1)} - \Gamma_{1(n+1)}\theta_{F-1(n+1)} - \Gamma_{2(n+1)}\theta_{I(n+1)}$ $= (2-\Gamma_{3(n)})\theta_{F(n)} + \Gamma_{1(n)}\theta_{F-1(n)} + \Gamma_{2(n)}\theta_{I(n)} + \Gamma_4 q(t)$	5.169

Table 6.1 List of nodal equations required to model the solar system given in Figure 6.1.

* If the node in question is an absorber plate node which is associated with a liquid collector then add $\sum_{\ell=0}^{L} X\theta_{c,\ell(t)}$ for time steps n and $n+1$

Nb. $q(t)$ values for each equation are given in Table 5.9

$$\underline{A} \cdot \underline{\theta}_{(n+1)} = \underline{B} \cdot \underline{\theta}_{(n)} + \underline{C} \qquad (6.1)$$

where,

$\underline{A}$ = matrix of coefficients of the unknown (future) nodal temperatures

$\underline{B}$ = matrix of coefficients of the known (present) nodal temperatures

$\underline{C}$ = matrix of heat generation terms relating to the climatic influences at the present and future time rows

$\underline{\theta}_{(n+1)}$ = column matrix of unknown nodal temperatures

$\underline{\theta}_{(n)}$ = column matrix of known nodal temperatures

In matrices $\underline{A}$ and $\underline{B}$ the equations for each node are entered into a particular row of the matrix while the matrix column represents all self - and cross- coupling terms associated with each node.

The next stage of the process is to calculate the temperature coefficients in each difference equation and transfer the result to its appropriate position in the matrix. The positioning of nodes within the system will affect the solution technique. To ensure the solution proceeds in a particular manner the solar collector will always be the first component modelled in the system, therefore,if there are N nodes for a solar collector the first N rows in the matrix will be filled with the difference equations associated with these nodes. Although the user can specify the sequence for subsequent components in the system, the model will operate more efficiently if these components are specified according to the system loops which occur,for example in Figure 6.1 components 1 to 5 from the collector loop.

As the collector is the first component considered, then starting at wall 1 the difference equation for node 1,1,1 which is an external surface node is found from Table 6.1, applying this expression to node 1 gives:

$$(2 + Q_{3(n+1)})\,\Theta_{1,1,1(n+1)} - Q_2\,\Theta_{1,1,2(n+1)} = (2 - Q_{3(n)})\,\Theta_{1,1,1(n)}$$

$$+ Q_{1(n+1)}\,\Theta_{1,1,0(n+1)} + Q_{1(n)}\,\Theta_{1,1,0(n)} + Q_2\,\Theta_{1,1,2(n)} + Q_4\,q(t) \qquad (6.2)$$

where the temperature coefficients for this expression are given in equation (5.155):

$$Q_{1(t)} = \frac{A_{1,1}\,hc_{1,1(t)}}{S} \quad ; \quad Q_{2(t)} = \frac{A_{1,1}\,k_{1,1}}{S\Delta X_{1,1}} \quad ; \quad Q_{4(t)} = \frac{1}{S} = \frac{\Delta\tau}{\rho_{1,1}\,C_{1,1}\,V_{1,1}}$$

$$Q_{3(t)} = Q_{1(t)} + Q_{2(t)} + \frac{\rho_{(t)}\,v_{(t)}\,A_{1,1}\,C_{p(t)}}{S} + \frac{A_{1,1}\,h_{r\,\varepsilon\to s(t)}}{S}$$

$hc_{1,1(t)}$ = the convective heat exchange at the external surface due to wind loss (see Appendix 6)

$h_{r\varepsilon\to s(t)}$ = the longwave radiative heat transfer coefficient between the surface and its surrounds (see equation 5.123)

$q_{(t)}$ = the summation of heat generation sources for this node (see item 3, Table 5, in Chapter 5).

the terms $A_{1,1}$, $k_{1,1}$, $\Delta X_{1,1}$, $C_{1,1}$, $P_{1,1}$, $V_{1,1}$, all relate to element 1 of wall 1 and $\rho_{(t)}$, $v_{(t)}$ and $C_{p(t)}$ are all properties of precipitation incident upon the external surface (see equation 5.114).

Each temperature coefficient in equation (6.2) is now calculated and entered into row 1 of the equation (6.1) as shown in figure 6.9. In matrices $\underline{A}$ and $\underline{B}$ the self-coupling term is entered into column 1 and the single cross-coupling term is placed in column 2. Having entered these values into row 1 of equation (6.1) the second node in wall 1 can be considered. This node is positioned at the centre of a homogeneous element and from Table 6.1 it can be expressed in the form:

$$(2 + C_{3(n+1)})\,\Theta_{1,1,2(n+1)} - C_1\,\Theta_{1,1,1(n+1)} - C_1\,\Theta_{1,1,3(n+1)}$$
$$= (2 - C_{3(n)})\,\Theta_{1,1,2(n)} + C_1\,\Theta_{1,1,1(n)} + C_1\,\Theta_{1,1,3(n)} + C_2\,q(t) \qquad (6.3)$$

where $q_{(t)}$ is given by item 1 in Table 5.9 in Chapter 5. Each temperature coefficient is calculated depending upon the terms associated with each C value. As this is the second node in the system it is entered into row 2 of the matrix as shown in figure 6.10. The self coupling for this node is in column 2 and cross

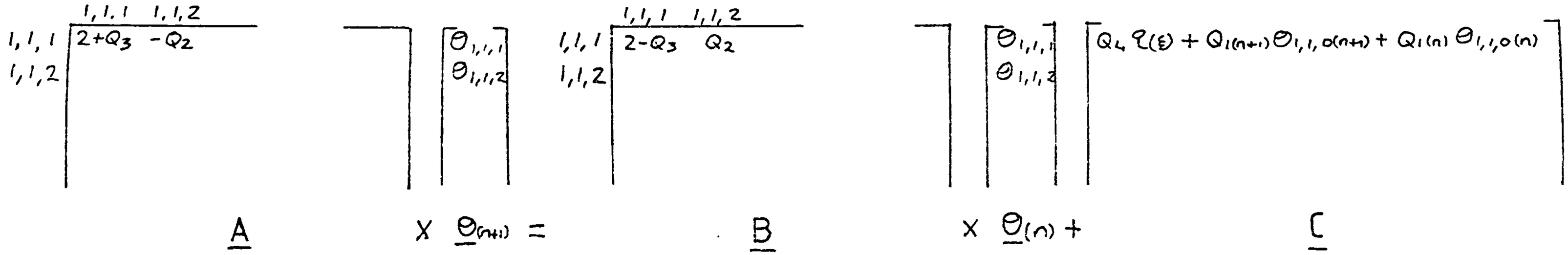

Figure 6.9: Difference equation for node 1,1,1 entered into equation (6.2).

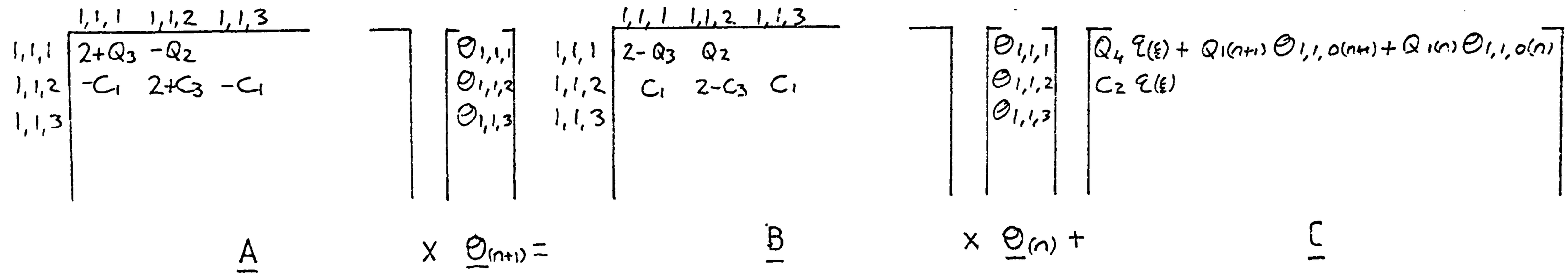

Figure 6.10: Difference equation for node 1,1,2 entered into equation (6.2)

couplings exist for the conductive heat transfer between this node and nodes 1, 1, 1 and 1, 1, 3.

Repeating this process for nodes 3 and 4 until node 5 of surface 1 is reached. This is an internal surface node and is taken from Table 6.1,

$$(2+R_{8(n+1)})\,\theta_{1,1,5(n+1)} - R_6\,\theta_{1,1,4(n+1)} - R_{7(n+1)}\,\theta_{1,7,1(n+1)} - R_{1(n+1)}\,\theta_{1,2,5(n+1)}$$
$$- R_{2(n+1)}\,\theta_{1,3,5(n+1)} - R_{3(n+1)}\,\theta_{1,4,5(n+1)} - R_{4(n+1)}\,\theta_{1,5,3(n+1)} - R_{5(n+1)}\,\theta_{1,6,7(n+1)}$$
$$= (2 - R_{8(n)})\,\theta_{1,1,5(n)} + R_6\,\theta_{1,1,4(n)} + R_{7(n)}\,\theta_{1,7,1(n)} + R_{1(n)}\,\theta_{1,2,5(n)}$$
$$+ R_{2(n)}\,\theta_{1,3,5(n)} + R_{3(n)}\,\theta_{1,4,5(n)} + R_{4(n)}\,\theta_{1,5,3(n)} + R_{5(n)}\,\theta_{1,6,7(n)} + R_9\,q(\phi) \qquad (6.4)$$

where $q(\phi)$ is given by item 4 in Table 5.9. This node models the conductive heat transfer process between the node and the air node 1, 7, 1 and the radiative heat transfer process with all other internal surface nodes. Calculating the values of each temperature coefficient, i.e. Figure 6.11 shows the results of applying these coefficients to row 5 of the matrix.

In this example rows 6 to 41 of the matrix are filled with the appropriate temperature coefficients until the difference equation for all 41 nodes have been written in matrix form. The resulting complete matrix, in the notation of equation (6.1), is shown in Figure 6.12. Inthis diagram the self-coupling term is designated by an unmarked coefficient, for example $(2+C_3)$ is represented by C $(2+G_4)$ by G and so forth.

As all the terms on the right hand side of equation (6.1) are known they can be combined into a single column matrix Z, where

$$\underline{Z} = \underline{B} \cdot \underline{\theta}_{(n)} + \underline{C}$$

therefore, equation (6.1) becomes

$$\underline{A} \cdot \underline{\theta}_{(n+1)} = \underline{Z} \qquad (6.5)$$

	1,1,1	1,1,2	1,1,3	1,1,4	1,1,5	→ 1,2,5	→ 1,3,5	→ 1,4,5	→ 1,5,3	→ 1,6,7	1,7,1
1,1,1	$(2+Q_3)$	$-Q_2$									
1,1,2	$-C_1$	$(2+C_3)$	$-C_1$								
1,1,3		$-G_1$	$(2+G_4)$	$-G_2$							
1,1,4			$-C_1$	$(2+C_3)$	$-C_1$						
1,1,5				$-R_6$	$(2+R_8)$	$-R_1$	$-R_2$	$-R_3$	$-R_4$	$-R_5$	$-R_7$

$$\underline{A} \times \underline{\theta}_{(n+1)} =$$

$\theta_{1,1,1}$
$\theta_{1,1,2}$
$\theta_{1,1,3}$
$\theta_{1,1,4}$
$\theta_{1,1,5}$
$\theta_{1,2,5}$
$\theta_{1,3,5}$
$\theta_{1,4,5}$
$\theta_{1,5,3}$
$\theta_{1,6,7}$
$\theta_{1,7,1}$

Figure 6.11: Difference equation for Node 1,1,5 entered into equation (6.2)

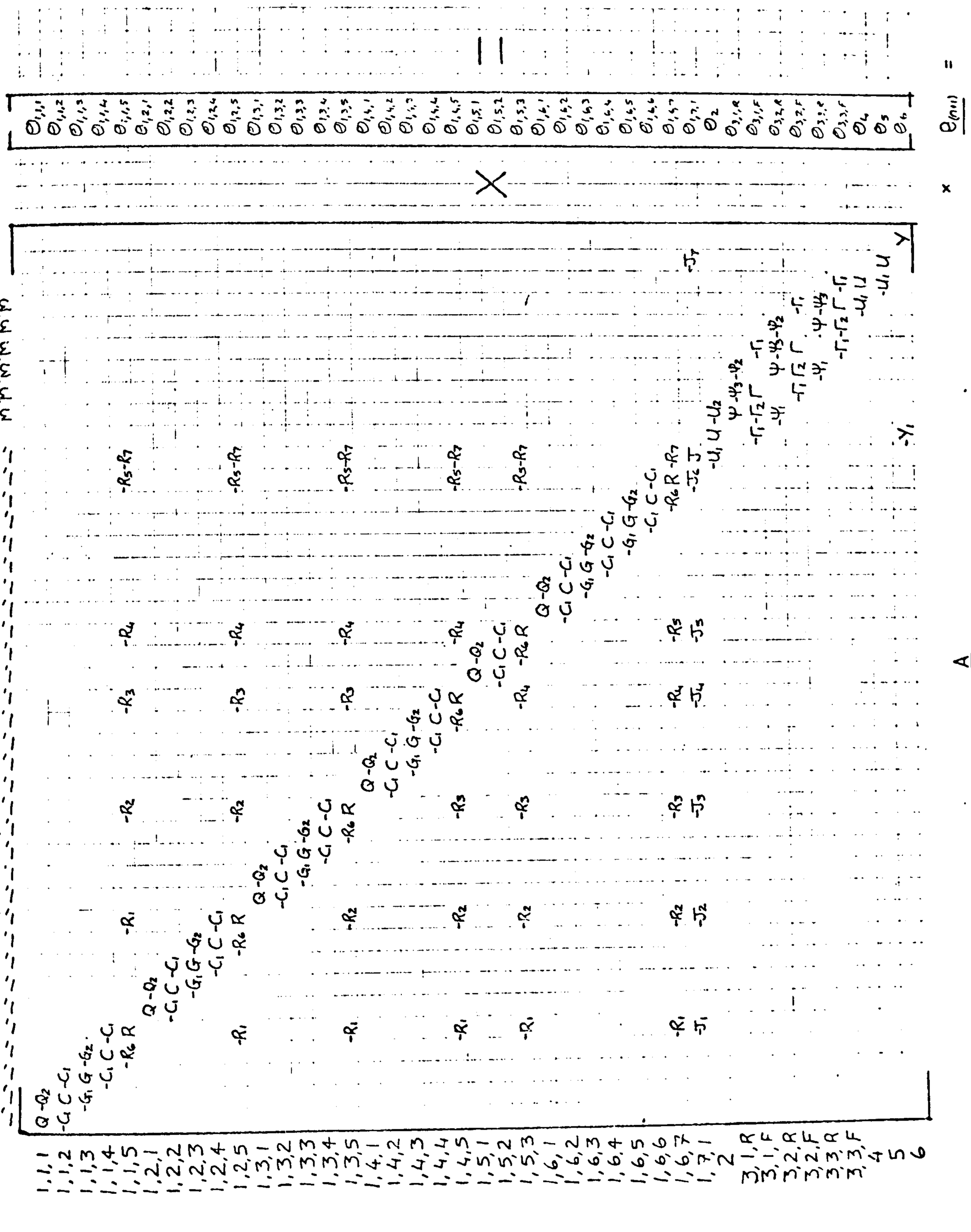

Figure 6.12 The complete matrix equation ($\underline{A}\,\underline{Q}_{(n+1)} = \underline{B}\,\underline{Q}_{(n)} + \underline{C}$) for the nodal scheme given in Figure 6.8

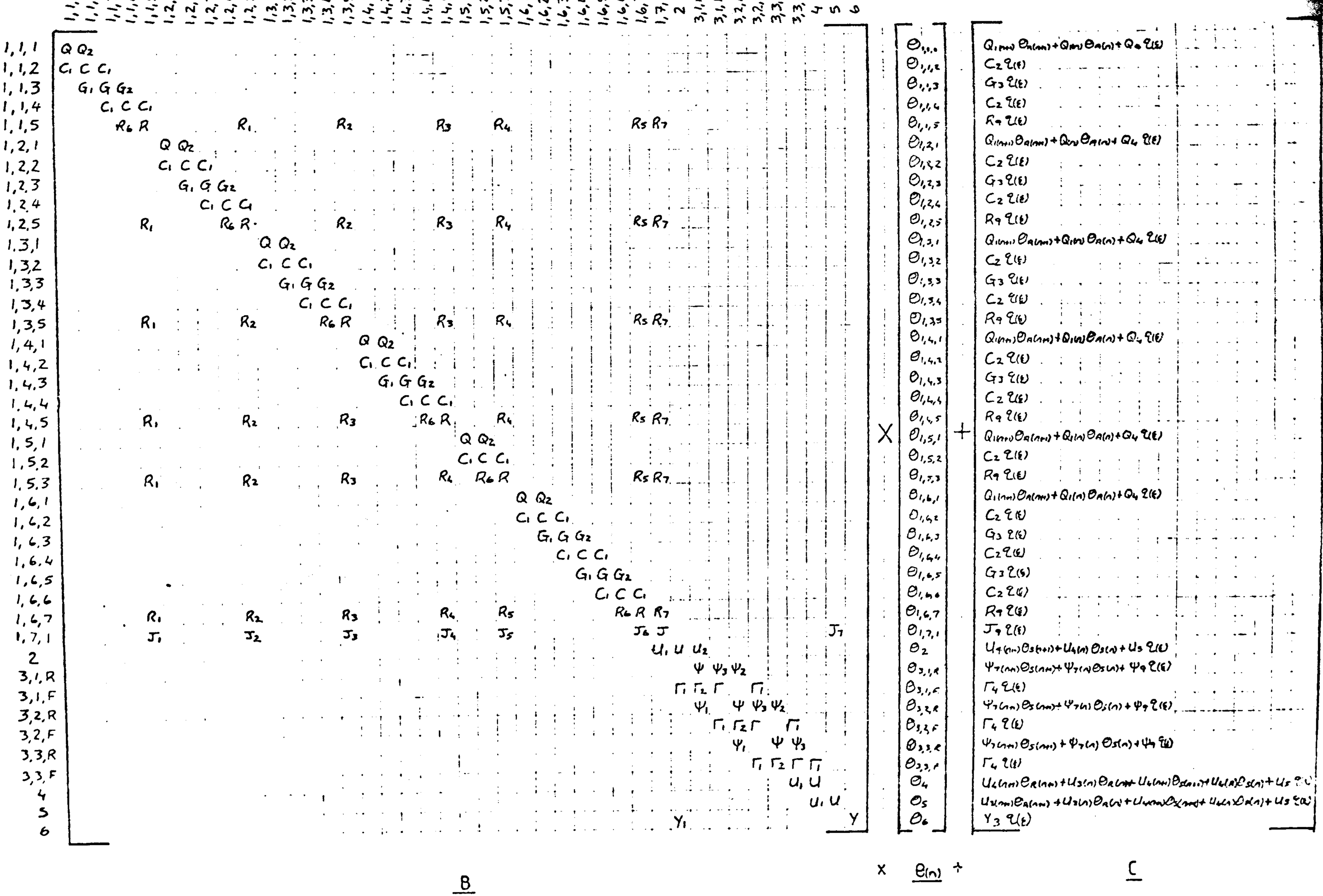

Figure 6.12 Continued.

A straight-forward Gaussian elimination technique requires more computation time than is necessary to solve equation (6.5) because the $\underline{A}$ matrix is sparse. Despite most coefficients being zero this method will check each appropriate coefficient in the forward reduction stage for a non-zero value and during the backward substitution temperatures are frequently multiplied by matrix coefficients that have a zero value. A modified Gaussian elemination technique is subsequently employed to reduce computation time compared to the full Gaussian method. This alternative method requires partitioning the matrix into two sections - one for the collection, the other for the remaining system components.

Consider the nodes associated with the solar collector in the $\underline{A}$ matrix given in Figure 6.12. The collector can be forward reduced independent of the system, furthermore, each collector enclosure boundary construction can be forward reduced, from the outside node to the next-to-inside node, independent of the rest of the collector. The six sub-matrices representing the four walls, cover and back of the collector are shown in Figure 6.13. These matrices contain the coefficients relating to the intra-constructional nodal equations addressing material conduction, heat storage and heat generation. This sub-matrix will also contain the conductive cross-coupling coefficient and the self-coupling coefficient of the internal surface node. These sub-matrices are designated by $\underline{C}$. The process of Gaussian elimination can be explained considering a $\underline{C}$ matrix of dimensions MxM, where M is the number of nodes under analysis. This matrix will consist of M^2 coefficient termed $a_{x\ y}$ where x and y are the row and column numbers, of matrix $\underline{C}$, respectively. To effect a forward reduction the first equation in the matrix is used to eliminate any non-zero terms in the first column of the matrix below the self-coupling term. This is achieved by multiplying the first equation by a_{m1}/a_{11}, where m is the row number in column 1 which contains the non-zero term, therefore, all coefficients in matrix $\underline{C}$ and $\underline{Z}$ are multiplied by a_{m1}/a_{11} and the resulting equation eliminating a_{m1}. The procedure is repeated until all matrix coefficients below the self-coupling term are zero. The second equation is used to eliminate all non-zero coefficients a_{m2} in column two below the self-coupling coefficient. The third equation is used to eliminate a_{m3} and

$$\begin{vmatrix} Q & -Q_2 & & & & \\ -C_1 & C & -C_1 & & & \\ & -G_1 & G & -G_2 & & \\ & & -C_1 & C & -C_1 & \\ & & & -R_6 & R & \end{vmatrix} \times \begin{vmatrix} \theta_{1,w,1} \\ \theta_{1,w,2} \\ \theta_{1,w,3} \\ \theta_{1,w,4} \\ \theta_{1,w,5} \end{vmatrix} = \begin{vmatrix} Z_{1,w,1} \\ Z_{1,w,2} \\ Z_{1,w,3} \\ Z_{1,w,4} \\ Z_{1,w,5} \end{vmatrix}$$

Figure 6.13a Sub-matrix for collector walls (w=1,2,3,4)

$$\begin{vmatrix} Q & -Q_2 & & \\ -C_1 & C & -C_1 & \\ & -R_6 & R & \end{vmatrix} \times \begin{vmatrix} \theta_{1,5,1} \\ \theta_{1,5,2} \\ \theta_{1,5,3} \end{vmatrix} = \begin{vmatrix} Z_{1,5,1} \\ Z_{1,5,2} \\ Z_{1,5,3} \end{vmatrix}$$

Figure 6.13b Sub-matrix for collector cover.

$$\begin{vmatrix} Q & -Q_2 & & & & & \\ -C_1 & C & -C_1 & & & & \\ & -G_1 & G & -G_2 & & & \\ & & -C_1 & C & -C_1 & & \\ & & & -G_1 & G & -G_2 & \\ & & & & -C_1 & C & -C_1 \\ & & & & & -R_6 & R \end{vmatrix} \times \begin{vmatrix} \theta_{1,6,1} \\ \theta_{1,6,2} \\ \theta_{1,6,3} \\ \theta_{1,6,4} \\ \theta_{1,6,5} \\ \theta_{1,6,6} \\ \theta_{1,6,7} \end{vmatrix} = \begin{vmatrix} Z_{1,6,1} \\ Z_{1,6,2} \\ Z_{1,6,3} \\ Z_{1,6,4} \\ Z_{1,6,5} \\ Z_{1,6,6} \\ Z_{1,6,7} \end{vmatrix}$$

Figure 6.13c Sub-matrix for collector base.

$$\begin{vmatrix} Q & -Q_2 & & & & \\ & C' & -C_1 & & & \\ & & G' & -G_2 & & \\ & & & C' & -C_1 & \\ & & & & R' & \end{vmatrix} \times \begin{vmatrix} \theta_{1,w,1} \\ \theta'_{1,w,2} \\ \theta'_{1,w,3} \\ \theta'_{1,w,4} \\ \theta'_{1,w,5} \end{vmatrix} = \begin{vmatrix} Z_{1,w,1} \\ Z'_{1,w,2} \\ Z'_{1,w,3} \\ Z'_{1,w,4} \\ Z'_{1,w,5} \end{vmatrix}$$

Figure 6.14 Result of forward reduction on collector wall sub-matrix $\underline{C}_w$ (primes denote modified coefficients). Surface node coefficients passed to the $\underline{I}$ matrix.

so forth. The process is completed when equation M is reached. The result of conducting the forward reduction process on the C matrix of the first collector wall is shown in Figure 6.14 in which primes denote modified coefficients. The modified internal surface self-coupling coefficient R^1 found after the forward reduction of each C matrix is passed to an I matrix which contains the internal surface radiative and convective coefficients for each surface and the fluid node difference equation, see Figure 6.15. Upon completing the forward reduction of matrix I the resulting equation for the fluid node i.e node 1, 7, 1 is,

$$J'_{(n+1)}\,\theta_{1,7,1(n+1)} - J_{7(n+1)}\,\theta_{5(n+1)} = Z'_{1,7,1} \qquad (6.6)$$

This expression incorporates the thermal processes in the solar collector at each simulation time increment at the collector fluid node, it also represents the thermal connection between the solar collector and its associated system. The partitioned system matrix S is shown in Figure 6.16 with equation (6.6) added. Conducting a forward reduction on matrix S until the final equation is reached then

$$\theta_{M(n+1)} = \frac{Z_M'}{a_{MM}'}$$

where M represents the last equation in a matrix. The remaining nodal temperatures in matrix S are found by back-substitution via

$$\theta_{r(n+1)} = Z_r' - \frac{\sum_{i=r+1}^{M} a_{ri}'\,\theta_{i(n+1)}}{a_{rr}'}$$

where, r=M-1, M-2, M-3 . . . . until all nodal temperatures are established. The value of node 1, 7, 1 the collector fluid node, is transferred to matrix I. Back-substitution in matrix I yields the temperature of each internal surface of the collector. For each construction in turn, the internal surface temperature is transferred to the appropriate C matrix and back-substitution gives the temperature of every node in the construction.

Using the modified Gaussian elimination technique the number of zero-value

$$\begin{bmatrix} R' & -R_1 & -R_2 & -R_3 & -R_4 & -R_5 & -R_7 \\ -R_1 & R' & -R_2 & -R_3 & -R_4 & -R_5 & -R_7 \\ -R_1 & -R_2 & R' & -R_3 & -R_4 & -R_5 & -R_7 \\ -R_1 & -R_2 & -R_3 & R' & -R_4 & -R_5 & -R_7 \\ -R_1 & -R_2 & -R_3 & -R_4 & R' & -R_5 & -R_7 \\ -R_1 & -R_2 & -R_3 & -R_4 & -R_5 & R' & -R_7 \\ -J_1 & -J_2 & -J_3 & -J_4 & -J_5 & -J_6 & J \end{bmatrix} \times \begin{bmatrix} \Theta_{1,1,5} \\ \Theta_{1,2,5} \\ \Theta_{1,3,5} \\ \Theta_{1,4,5} \\ \Theta_{1,5,3} \\ \Theta_{1,6,7} \\ \Theta_{1,7,1} \end{bmatrix} = \begin{bmatrix} Z'_{1,1,5} \\ Z'_{1,2,5} \\ Z'_{1,3,5} \\ Z'_{1,4,5} \\ Z'_{1,5,3} \\ Z'_{1,6,7} \\ Z_{1,7,1} \end{bmatrix}$$

Figure 6.15: The $\underline{I}$ matrix obtained from the $\underline{C}$ matrices (prime denotes modifier coefficients)

$$\begin{bmatrix} J' & & & & & & & -J_7 \\ -U_1 & U & -U_2 & & & & & \\ & \Psi & -\Psi_3 & -\Psi_2 & & & & \\ -\Gamma_1 & -\Gamma_2 & \Gamma & & -\Gamma_1 & & & \\ & -\Psi_1 & & \Psi & -\Psi_3 & -\Psi_2 & & \\ & & -\Gamma_1 & -\Gamma_2 & \Gamma & & -\Gamma_1 & \\ & & & -\Psi_1 & & \Psi & -\Psi_3 & \\ & & & & -\Gamma_1 & -\Gamma_2 & \Gamma & -\Gamma_1 \\ & & & & & & -U_1 & U \\ & & & & & & & -U_1 & U \\ -Y_1 & & & & & & & Y \end{bmatrix} \times \begin{bmatrix} \Theta_{1,7,1} \\ \Theta_2 \\ \Theta_{3,1,R} \\ \Theta_{3,1,F} \\ \Theta_{3,2,R} \\ \Theta_{3,2,F} \\ \Theta_{3,3,R} \\ \Theta_{3,3,F} \\ \Theta_4 \\ \Theta_5 \\ \Theta_6 \end{bmatrix} = \begin{bmatrix} Z'_{1,7,1} \\ Z_2 \\ Z_{3,1,R} \\ Z_{3,1,F} \\ Z_{3,2,R} \\ Z_{3,2,F} \\ Z_{3,3,R} \\ Z_{3,3,F} \\ Z_4 \\ Z_5 \\ Z_6 \end{bmatrix}$$

Figure 6.16: The $\underline{S}$ matrix from Figure (6.12)

A matrix coefficients considered, in the solution of the A matrix shown in Figure 6.12, are reduced to 10% of the number considered using full Gaussian elimination. The reduction in considered zero matrix coefficients is shown by the shaded area of Figure 6.17, in which the X's represent possible non-zero coefficients. It is apparent from Figure 6.17 that a number of zero coefficients will still be considerd. It is a reasonably simple process to consider only non-zero coefficients in the C matrix but it is much more difficult to achieve this for the S matrix, as mentioned earlier.

If there is more than one duct in the collector, more than one fluid node or a two or three dimensional analysis of the absorber plate is conducted, it will be slightly more difficult to ensure that only non-zero coefficients are considered in each C matrix. However, the solution technique will be exactly as described above irrespective of whether or not the zero coefficients in matrices C, R and S are considered. It is important to note that there can be occasions when the C, R or S matrix will not change, therefore these matrices will as a consequence be solved only when one of the matrices coefficients change.

6.1.1 Operation Control of System Components

The modelling of the control operation of system components can be conducted implicitly or alternatively control decisions can be taken at the end of each time increment.

To implicitly model the operation of the system would require iteration of the S and possibly the I and C matrices. When modelling complex systems and their control, the iterative calculation required may be considerable particularly if several nodes are used as control points. To employ this technique, the ability to carry more than one term between the C, I and S matrices must be available to allow control nodes to be solved.

In this model, control decisions will be taken based on the results of

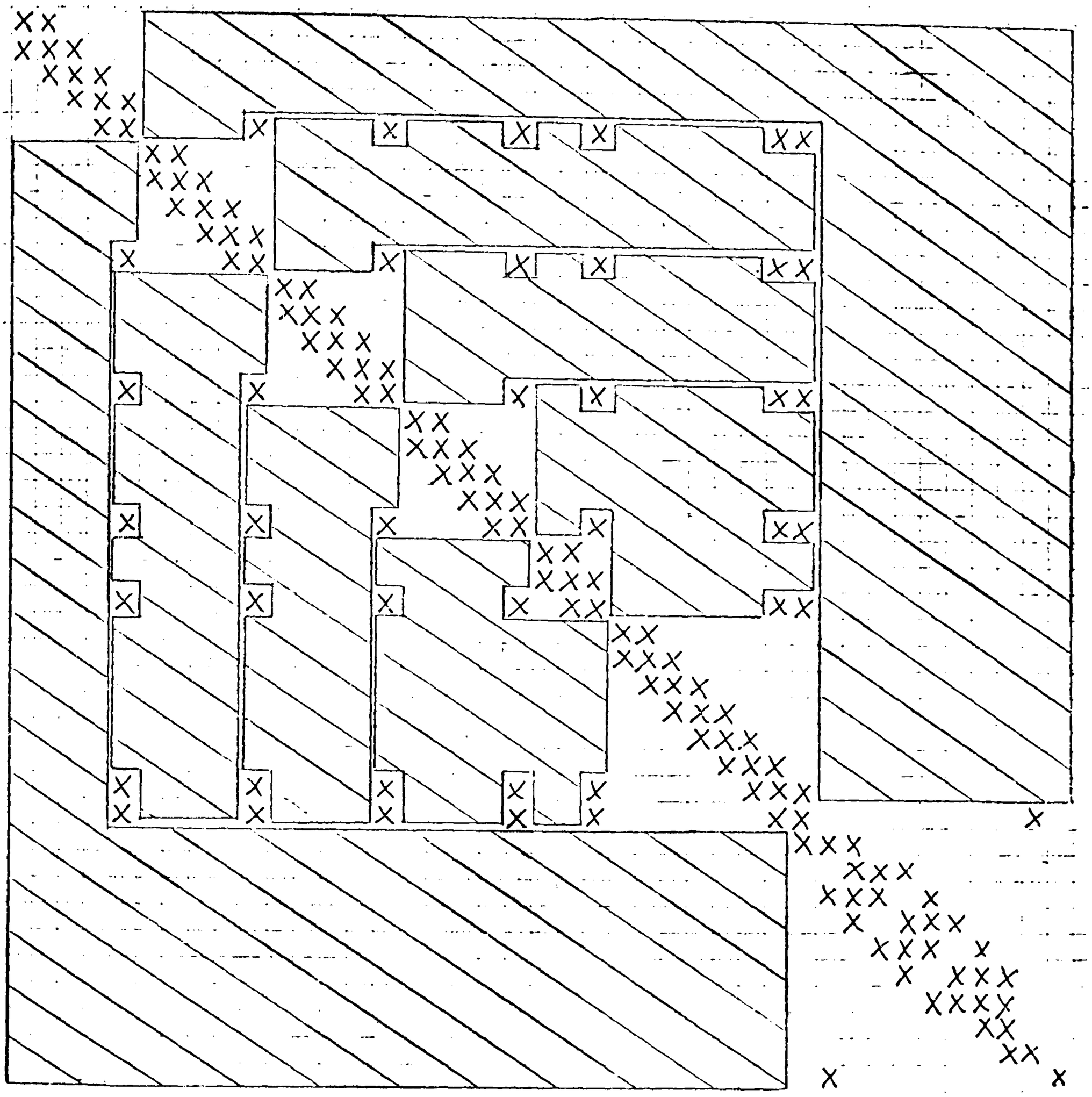

Figure 6.17 Shaded area of the $\underline{A}$ matrix represents zero-value coefficients not considered by the modified Gaussian elimination technique.

the solution of the A matrix at each simulation time increment. Although not as exact as implicit control this method will not require iteration and it allows any node in the system to be the control node. Depending upon the temperature of the control nodes, fans or pumps are switched on or off and valves and dampers are open or closed, etc. The system operates at its new status for one time increment, the new solution of the A matrix will allow the system status to be reappraised in terms of its control philosophy. This procedure is repeated at the end of each time increment. Obviously modelling the system operation by this method will become more accurate as the simulation time increment is reduced.

6.1.2 The Simulation Time Step

The implicit formulation of the thermal model allows the simulation time step to be set at any value without incurring instability problems. However, the length of the time increment should be linked to the requirements of the simulation, for example, if longterm performance of a system is to be estimated then larger time increments can be used than if a shortterm analysis was required. The maximum time increment is one hour, this is compatible with the frequency of recorded climatic data. The minimum time increment is 30 seconds but this is easily modified if a shorter time increment is required. Climatic interpolation routines are employed for more than one time step per hour.

Simulations can also be conducted based on events rather than fixed time increments which may be more suitable to systems simulation. This variable simulation time step can be performed by the aforementioned implicit mathematical model, however, it will probably require more computation time than small fixed time step simulations if every event is to be modelled.

6.2 Application of Solution to More Complex Systems

The application of the basic collector equations (Table 5.8) to a simple solar collector system was shown in the previous section. To show the range of systems which may be modelled several examples will be shown and the appropriate A matrix given. In the A matrix of these examples, all coefficients associated with the difference equations of each node will be designated X. The solution method of A is described in the previous section.

Example 1

Figure (6.18) shows the schematic of the system to be modelled. A number of identical liquid collectors operate in parallel, therefore, only one collector requires to be modelled. The liquid flowing through the collector is a water anti-freeze mixture and a heat exchanger is employed to transfer the energy to a domestic direct hot water storage tank which is designed to meet a particular domestic hot water demand. An automatic draindown facility is available if the liquid approaches boiling or freezing temperature.

The collector has four sides each of single element construction, a single glass cover and an absorber plate with a double bend serpentine tube bonded onto the internal surface, both the absorber surface and the liquid tube are analysed by 9 nodes (see Figure 6.19). Insulation and the casing make up the collector base. In order to eliminate convective losses from the absorber the space above the absorber plate is in vacuum. Nodes required to model the collector are:

Wall 1	-	3 nodes	;	nos. 1-3
Wall 2	-	3 nodes	;	nos. 4-6
Wall 3	-	3 nodes	;	nos. 7-9
Wall 4	-	3 nodes	;	nos.10.12
Cover	-	3 nodes	;	nos.13-15
Base	-	32 nodes	;	nos.16-47
Liquid Tube	-	9 nodes	;	nos.48-56

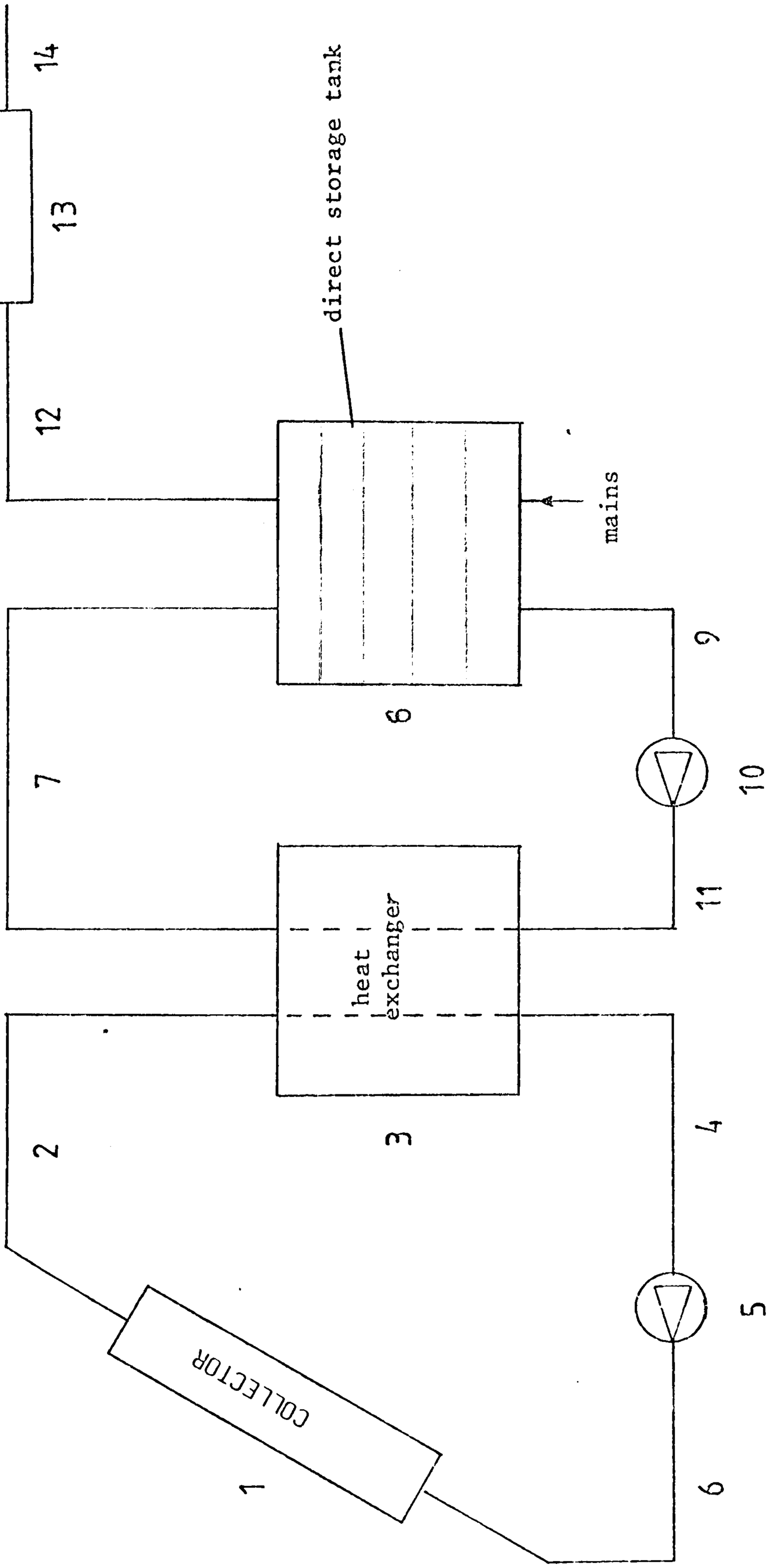

Figure 6.18 Schematic representation of liquid system as described in example 1.

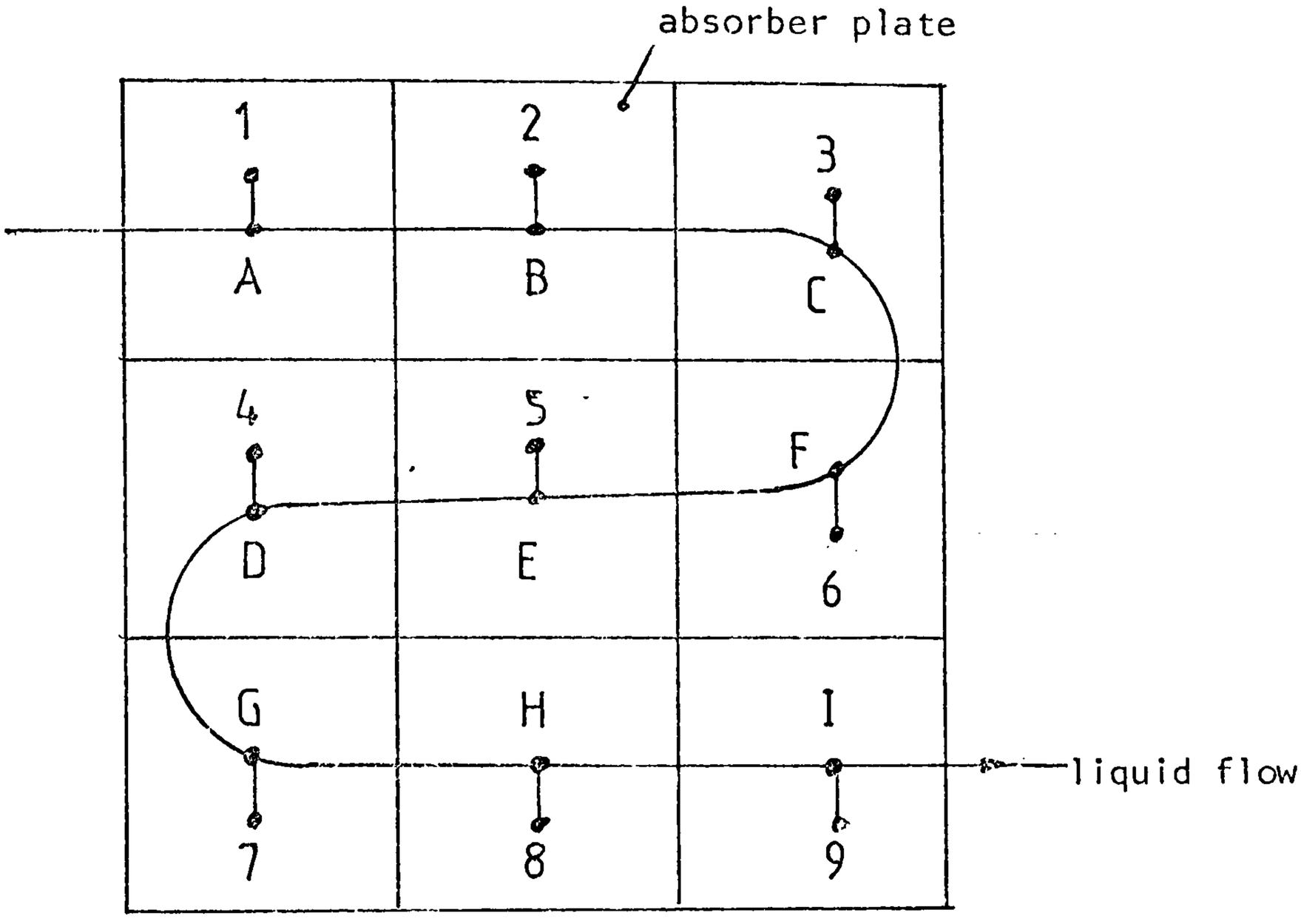

Figure 6.19: Nodal equivalent structure of tube carrying liquid in contact with absorber plate

The remaining system components are modelled using the following nodes:

Conduits - eight nodes representing components 2, 4, 6, 7, 9, 11, 12 and 14. These are given node numbers 51, 60, 62, 63, 69, 71, 72 and 74 respectively.

Pumps - two nodes representing components 5 and 10. These are given nodal numbers 61 and 70.

Heat Exchanger - one two node heat exchanger model is employed. Node number 58 and 59 are used.

Hot Water Storage Tank - component 8 is modelled by 5 nodes, numbers 64 to 68.

Auxiliary Unit - component 13, modelled by node 73.

Figure 6.20 shows the resulting $\underline{A}$ matrix required to model the system, X's are used to represent the self and cross-coupling terms of the difference equations. The solution of this matrix is the same as described in the previous section, however, the portioned matrices are slightly more complex, for example, Figure 6.21 shows the $\underline{C}_6$ matrix for the collector base and Figures 6.22 and 6.23 show the $\underline{I}$ and $\underline{S}$ matrices respectively.

Example 2

Consider the air collector system shown in Figure 6.24. A number of identical solar collectors are connected in parallel and are designed to meet a particular space heating load. Excess energy is transferred to a rock bed storage which is modelled using five rock/air pair nodes. Mains water supply to a domestic hot water tank is pre-heated by passing it through conduits within the first three segments of the storage unit. A total of 19 components are modelled in this system.

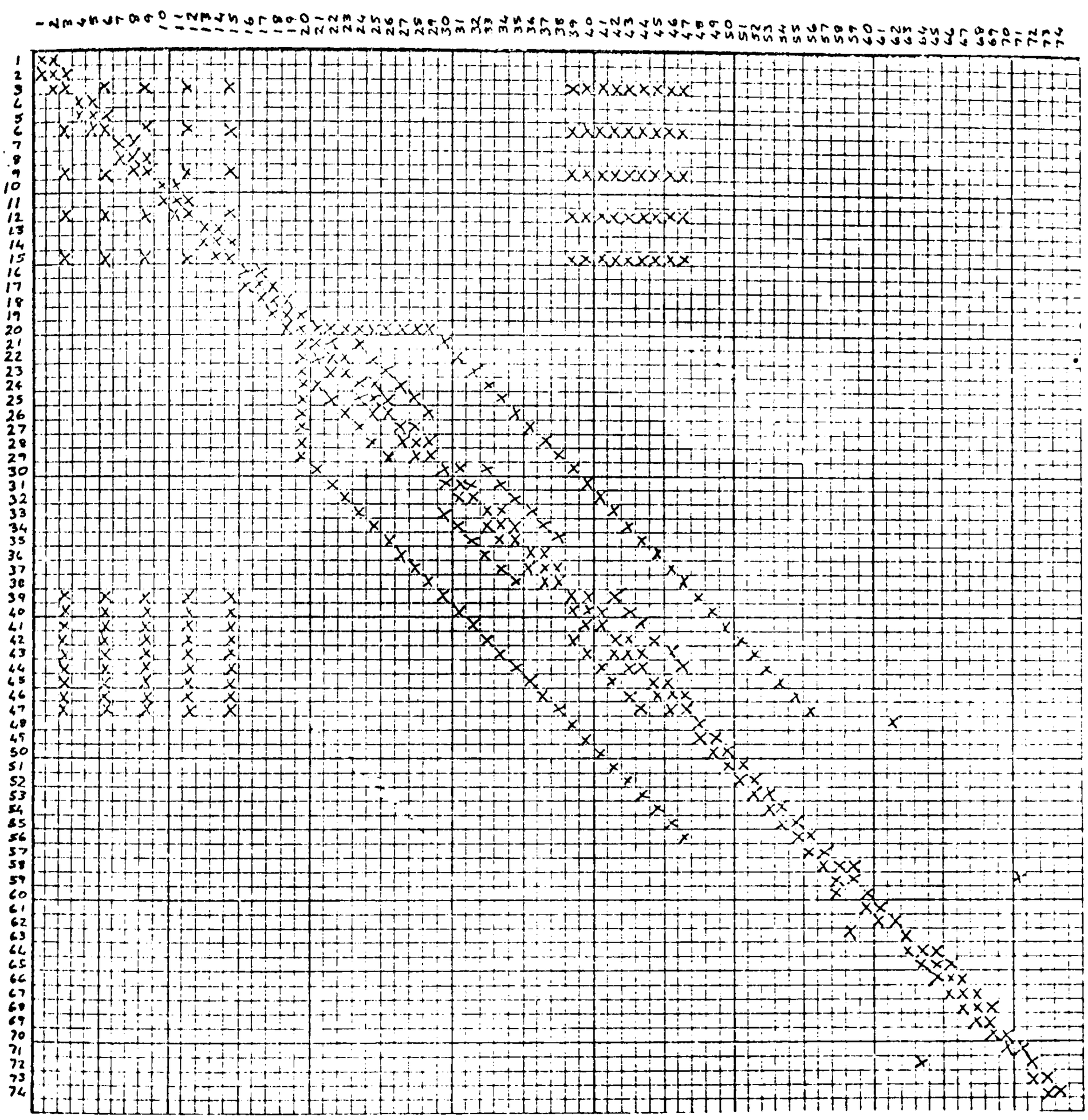

Figure 6.20 $\underline{A}$ matrix for system given in Figure 6.18.
(X's represent temperature coefficients).

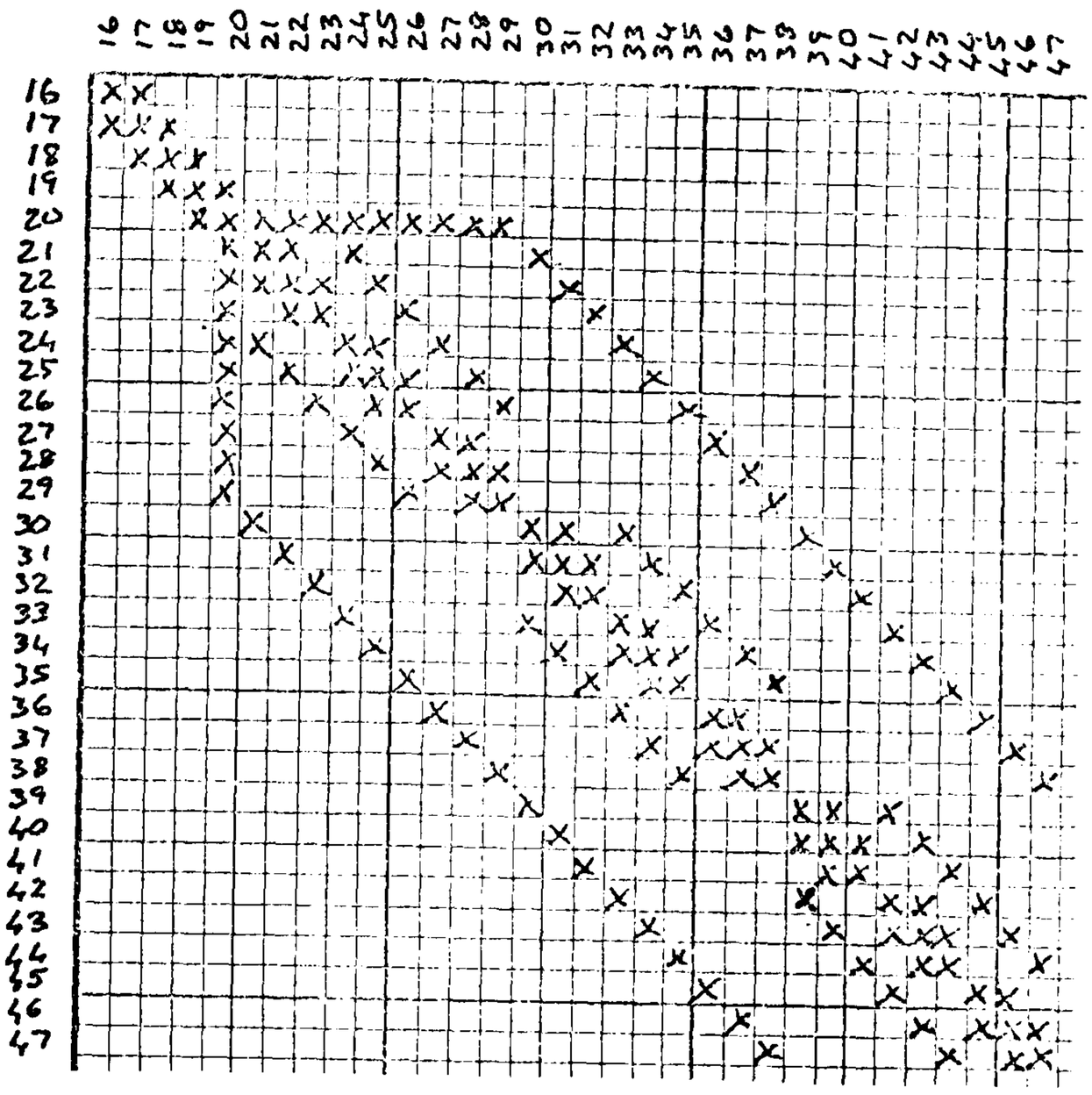

Figure 6.21 The $\underline{C_c}$ matrix - collector base.

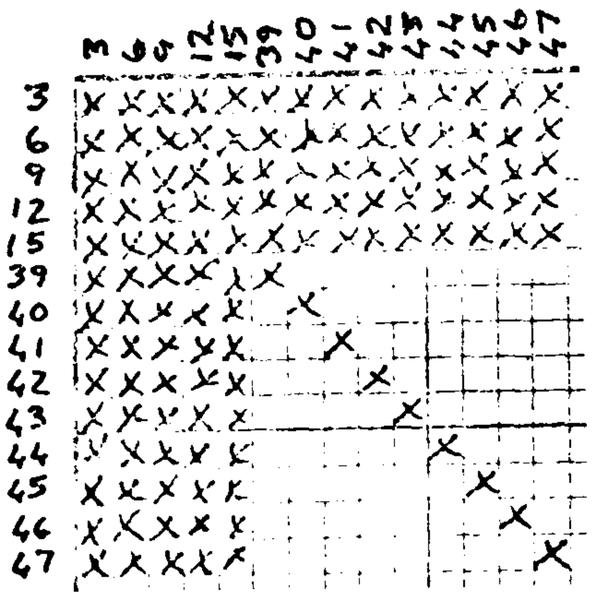

Figure 6.22 The $\underline{1}$ matrix.

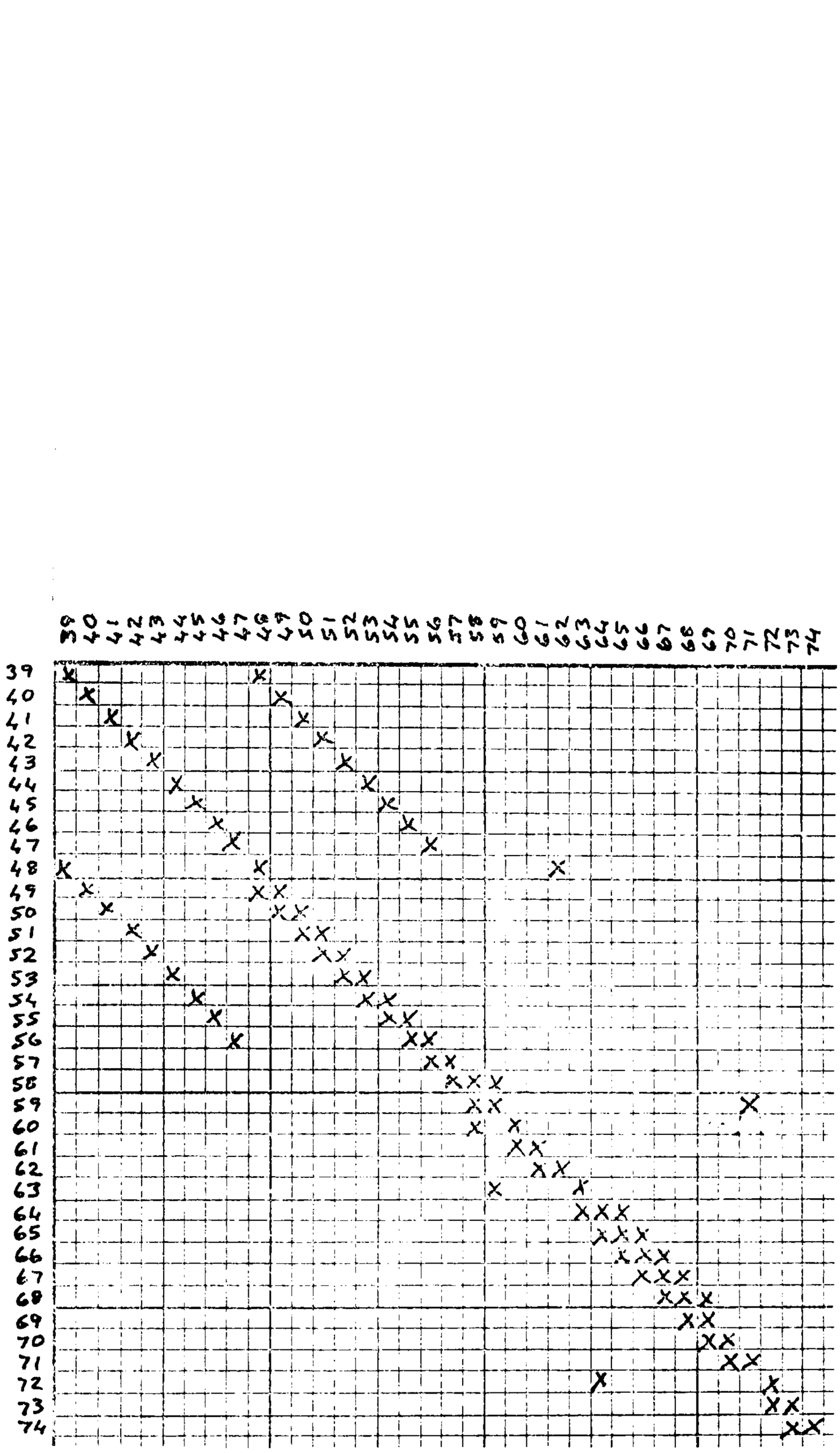

Figure 6.23: The $\underline{S}$ matrix

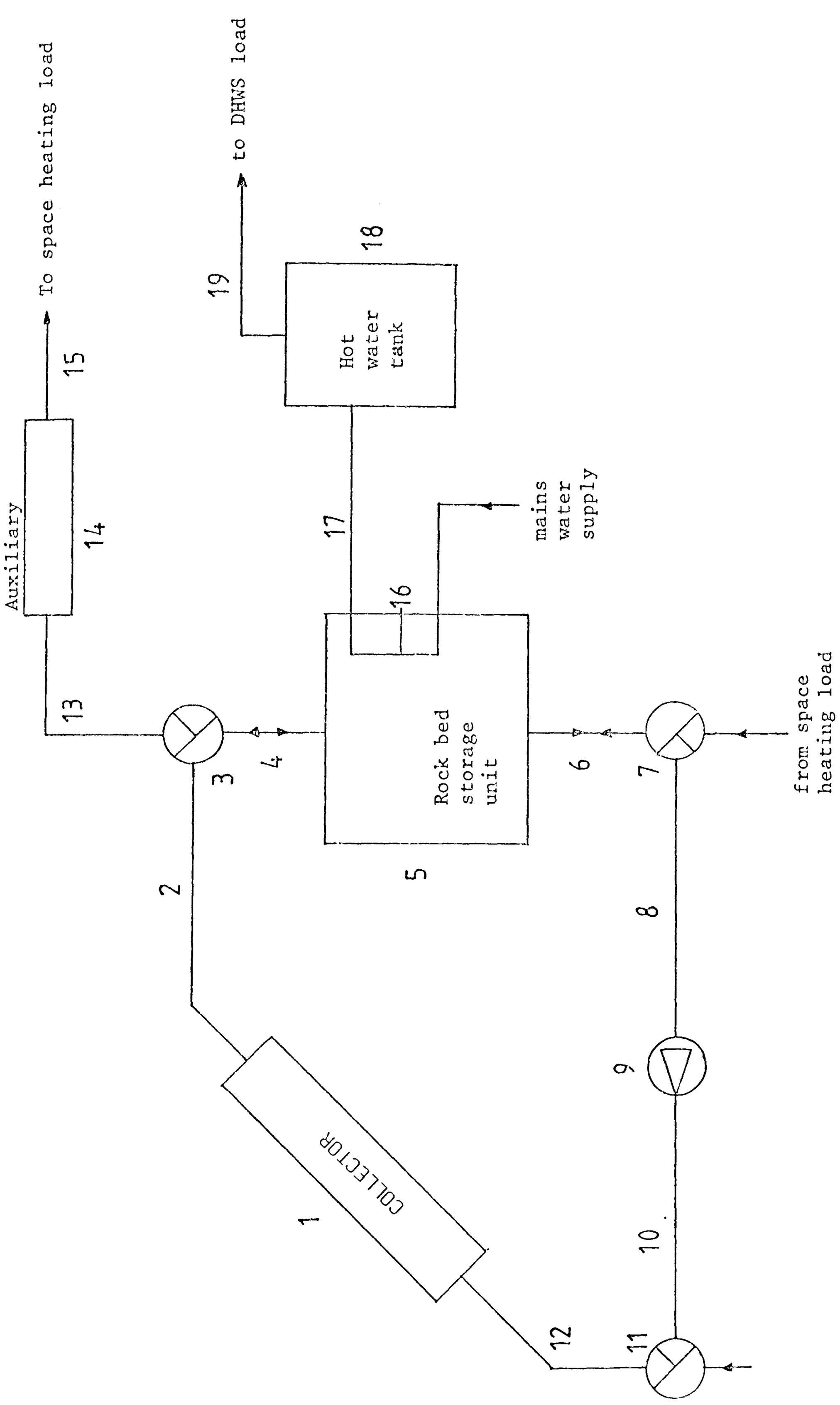

Figure 6.24 Air collector system with domestic hot water supply pre-heat

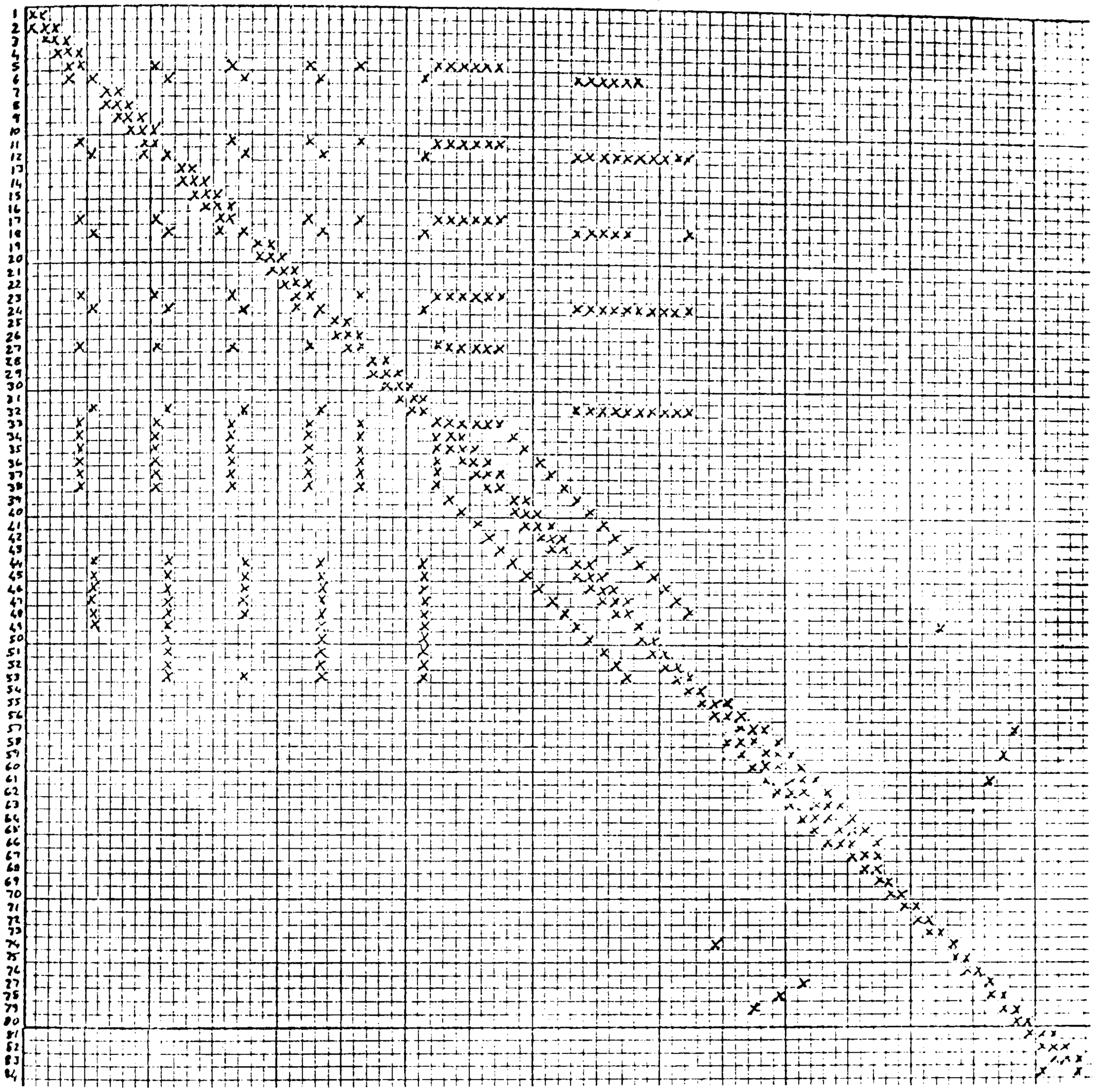

Figure 6.25 The A matrix of system shown in Figure 6.24

The solar collector is a rear duct air collector which is modelled using one fluid node in the upper duct and five fluid nodes in the lower duct in the flow dimension. The absorber plate dividing both ducts is modelled using 5 nodes on each surface and five nodes at its centre. The collector walls and base have two elements and the single glass cover is coated with a magnesium fluoride film to promote solar radiation through the collector cover. Consequently a total of 53 nodes are required to model this collector where the upper duct fluid node is number 32 in Figure 6.25 and the lower duct fluid nodes are numbered 48 to 53.

The five segment rock bed storage unit is modelled by nodes 57 to 66 and the conduit which passes through the storage unit is subdivided into three sections, one for each segment of the storage unit with which the conduit is in thermal contact.

The domestic hot water storage tank has three stratification levels and an electric resistance heater in the uppermost segment, to maintain the required supply temperature for the domestic hot water services.

The $\underline{A}$ matrix of this system is shown in Figure 6.25.

Example 3

This model is not restricted to analysing only identical solar collectors operating in parallel. Any number of solar collectors can be considered if they operate in series, or, if several different solar collectors supply the same system. For this example consider the latter case, where two solar collectors supply the same system, the first collector is an air collector, the second is a photovoltaic/photothermal collector with air as the fluid medium, see Figure 6.26.

The air collector is a fixed position, single duct collector. The PV/air collector is a fully tracking single duct collector using a thin plastic cover. The collector is essentially a photovoltaic collector designed to supply the electrical requirements of all fans and dampers in the system as well as supplying electricity to the collector tracking

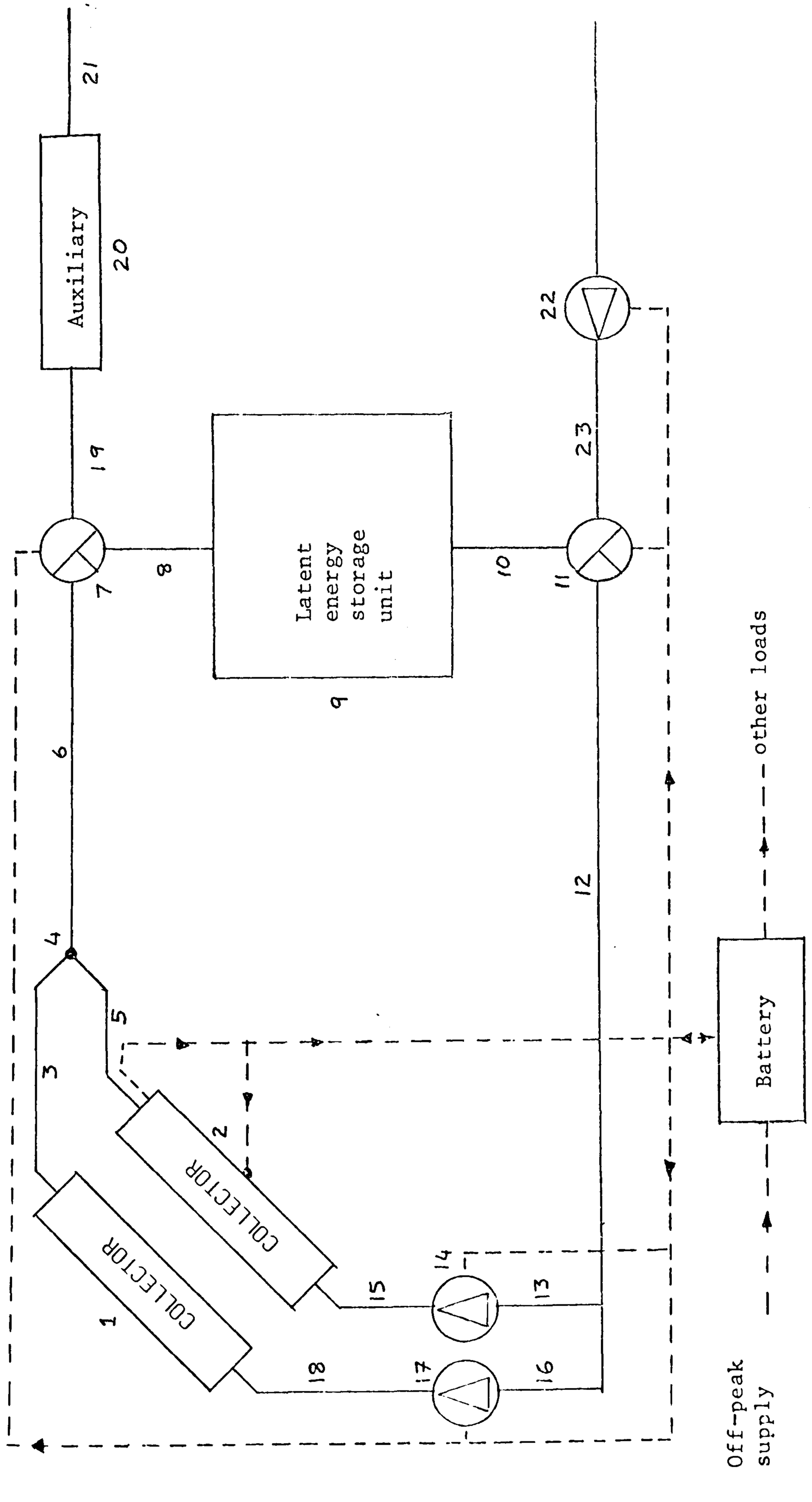

Figure 6.26 Combined air and PV/air collector system.

mechanism. Consequently, the system operation is independent of the electricity grid, however, off peak electricity can be stored in the battery system if the storage at the end of each day is below a desired level. To avoid solar cell efficiency drop due to temperature increases, air is passed over the solar cells to lower cell temperatures and simultaneously collect thermal energy. The thermal energy from both collectors is used for space heating purposes and when in excess is stored in a latent energy storage unit. Each fan in the system is a variable pitch fan.

Both collectors are modelled by 31 nodes, the air collector by nodes 1-31 and nodes 32-62 represent the PV/air collector. The remaining system components are modelled by single nodes, for example, the latent storage unit - component 9 - is represented by node 69. The $\underline{A}$ matrix required to model this system is shown in Figure 6.27.

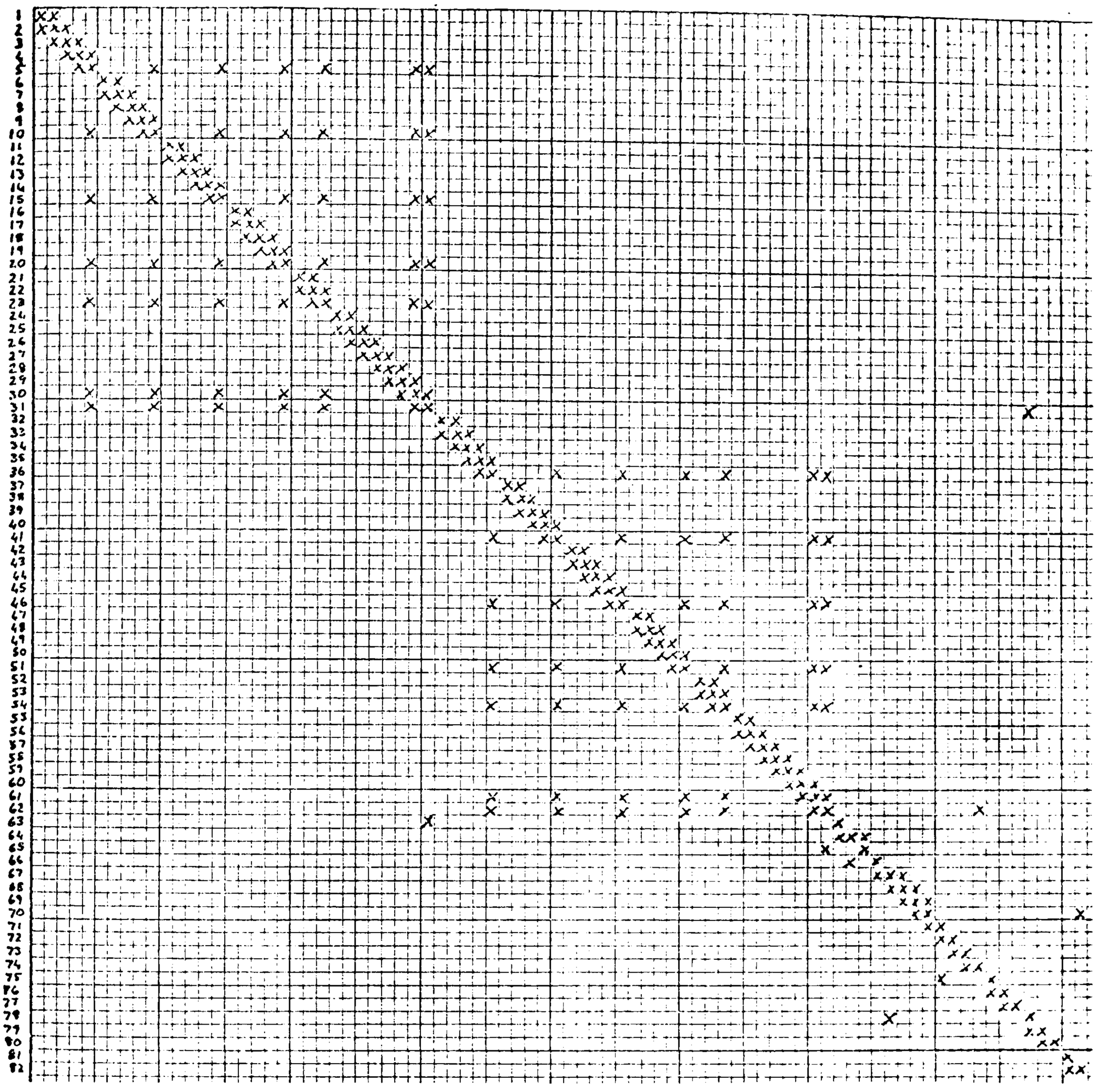

Figure 6.27 The A matrix of system shown in Figure 6.26

6.3 Alternative Applications

Although the mathematical model has been applied to a solar collector and its system there are, however, many alternative applications to which the mathematical model (Chapter 5) can be applied. Different empirical equations may be required to predict the convective heat transfer coefficients in different applications, nevertheless, a brief description of several examples of alternative applications of the model will be given.

1. Trombe Wall

A Trombe wall can be modelled very easily as it is essentially a vertical solar collector. The effects of different glazing configurations can be investigated as well as the use of motorised blinds or shutters. Fans transporting energy away from the wall can be modelled.

2. Solar Ponds

The principal tool for modelling a solar pond will be the theory described in Section 5.3.1 for solar transmission through transparent materials which has been incorporated into the WINDOW program (Appendix 8). Solar absorption at any depth in the pond can be analysed.

3. Extraterrestrial Photovoltaic Performance

At present terrestrial solar cell arrays can be analysed. It is a simple process to model the vacuum surrounding solar cells on a satellite outside the earth's atmosphere and use the extraterrestrial solar spectrum instead of the terrestrial spectrum.

4. Trans-Walls

A trans-wall is a system where a fluid is contained between two panes of glass. This can be modelled by the same method as a solar pond.

5. Concentrator Collectors

These can be modelled using a conduit node - Category 4. If the concentration factor is calculated then a simple concentrating solar collector can be analysed.

CHAPTER 7 The FLARE System

The FLARE system is a group of interrelating computer programs or modules which are used to simulate a solar energy system. The structure of the FLARE system is shown in Figure 7.1, it is analogous to the ESP system - Figure 1.4 of Chapter 1. Each FLARE module, in interactive mode, is controlled (by the user) by means of a dynamic 'menu' interaction graphics technique (77). The system has been developed to be compatible with data generated by existing software, in particular, some of the optional software for the ESP system which performs tasks required by the FLARE solar collector component model. This software includes ESPSHD - an external surface shading prediction program, ESPINS - an internal surface insolation prediction program and ESPVWF which predicts the black body view factor between internal surfaces of an enclosure. These programs, along with other software, are optional input aids that are generally invoked to improve the accuracy of data held in particular files.

The FLARE system is at an early stage of development, however, most modules are available. The structure of the FLARE system is discussed further in Section 7.1.

The FLARE simulation module is a protype program based on the mathematical model described in Chapters 5 and 6. The principal purpose of this program is to test the validity of the mathematical model. At present, the module is based upon the first five difference equations given in Table 5.8 of Chapter 5. Subsequently, it is capable of conducting a rigorous appraisal of the performance of an air (A), liquid (L) or photovoltaic (PV) collector, plus any combination of these energy collection modes, that is, A/L, A/PV, L/PV or A/L/PV. The solar collector can be one of three physical configurations: a no duct, one duct or a two duct collector (Figure 7.2). A maximum of two transparent substrates can be modelled spectrally and any number of thin films can be considered on each substrate. The module allows the user to consider collector ducts in vacuum or, if a double duct air collector, a two pass system can be utilised.

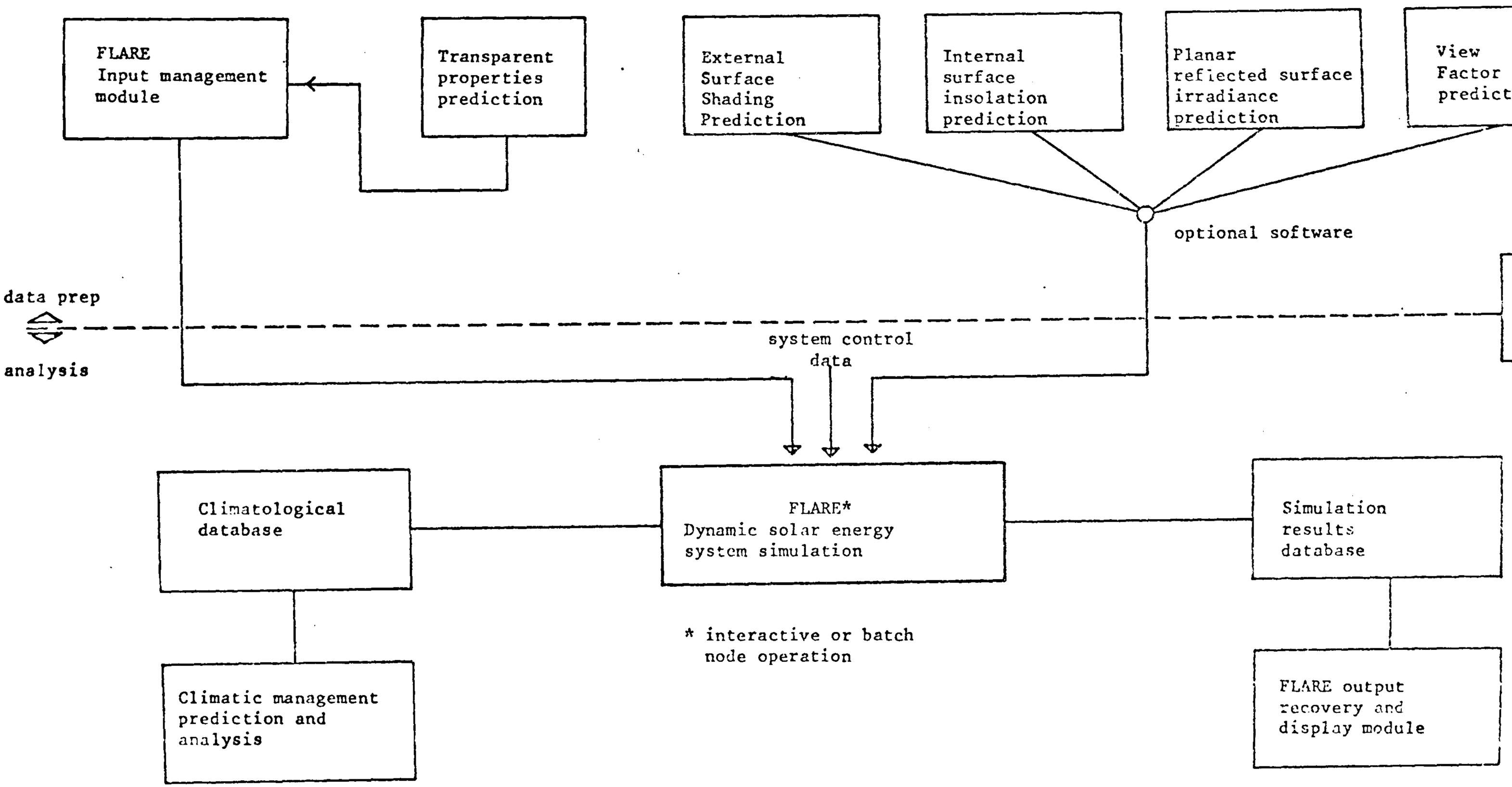

Figure 7.1 The FLARE System

a) No duct

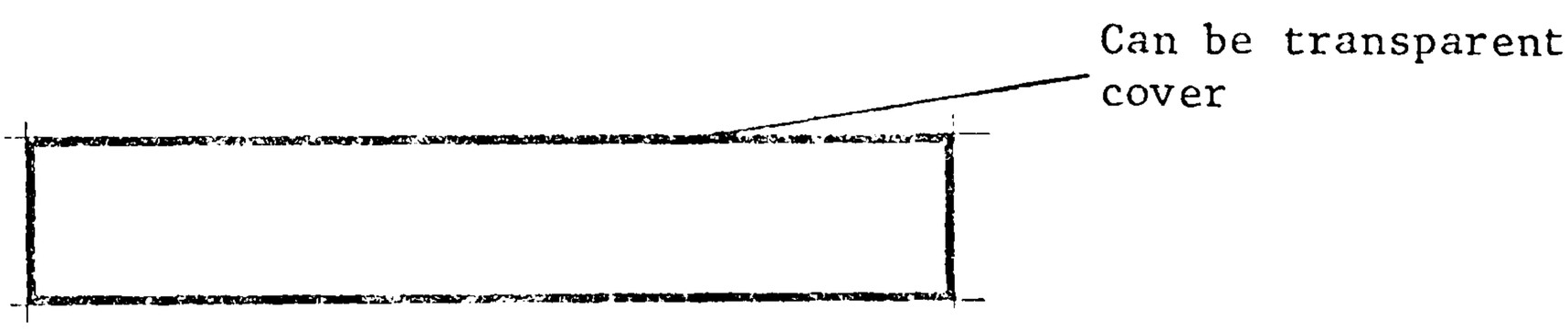

b) One duct

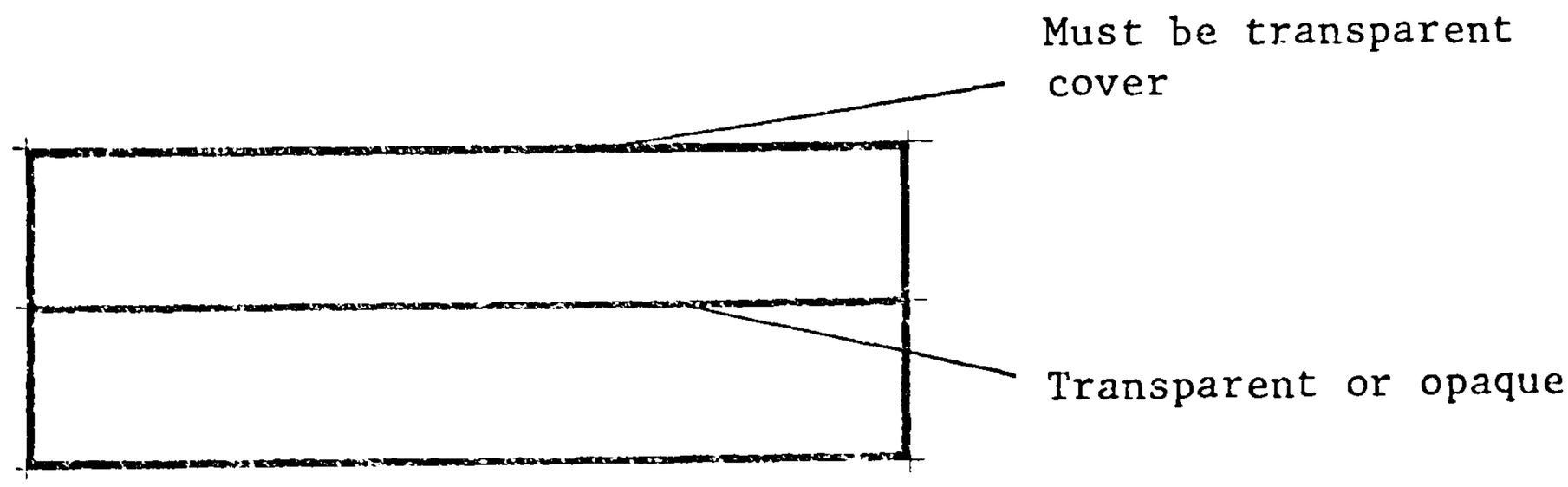

c) two duct

Figure 7.2 Solar collector geometric configuration

Although only a prototype, the FLARE simulation module can be used to investigate and rigorously interrogate the performance of a solar collector and aspects of the design, for example:

- what is the maximum output from a collector and when does it occur?
- how many similar collectors operating in parallel are required to meet a particular load?
- what is the maximum temperature of absorber plate and transparent cover to check for thermal stress?
- does condensation occur?
- what are the effects of leaks to or from the collector?
- what is the net effect of a tracking collector compared to a fixed position collector?
- does freezing or boiling occur in the collector and would an automatic draindown facility or a blind system alleviate the problem?
- what is the effect of different control strategies?
- etc.

Results from the FLARE simulation module are compared with another program and measured data in Section 7.2. The cost of operating this module is discussed in Section 7.3.

The next stage of the development of the FLARE system involves adding the remaining difference equations identified in Table 5.8. This is underway at present and should be completed before the end of 1982. Fortunately, due to the matrix solution technique described in Chapter 6, the system or $\underline{S}$ matrix can be developed independent of the solar collector. The future version of FLARE will operate in the present mode, that is, any number of identical collectors operating in parallel and it will be extended to include two collectors operating in series and two different collectors operating in parallel. The future version of FLARE simulation module will allow the solar collector performance to analyse in a system context and allow more complex control strategies to be considered. Furthermore, information on the thermal effects of

each system component will be available and the simultaneous interactions between components analysed.

7.1 Description of the FLARE System

The operation of the FLARE system is considered in three stages as shown in Figure 7.3. Stage one is concerned with the preparation of the input data via the FLARE Input Management Program and optional software. The second stage is concerned with the operation of the FLARE simulation module and the transfer of all computer results, depending upon a particular control strategy, to a solution file. The third and final stage involves the interrogation of the solution file by means of the FLARE output program. These three stages are described in Sections 7.1.1, 7.1.2 and 7.1.3 respectively.

7.1.1 The FLARE Data Preparation Program

The ease with which data is entered into a program largely determines its acceptability and frequency of use. A free-standing FLARE Input Management Program - FLRIMP - has been developed which allows the interactive construction of data files describing the solar energy system to be subjected to a particular weather condition and simulated over time. All items, at input, are processed through legality and 'within acceptable range' checks before being located in the data file for transfer to the simulation program.

FLRIMP can be used to create all data files, however, a number of optional programs are available which allow a more detailed analysis of a solar collector to be conducted. There are up to 11 different data files that can be constructed via FLRIMP, some of these are specific to the solar collector. Figure 7.4 shows the main menu available to users of FLRIMP. There are several files essential to a simulation, these are the PROJECT, GEOMETRY, THERMAL, SYSTEM, VIEW FACTOR (not required by a solar collector with no ducts), INSOLATION/SHADING and CONTROL FILE. The CONTROL file need not be created by FLRIMP as the same create facility is available in the FLARE simulation program (see Section 7.1.2). There are four other files which are optional: they are the INSOLATION/PLANAR REFLECTOR, LOAD, ADJACENCY and BLIND files. A brief description of the contents of each file follows:

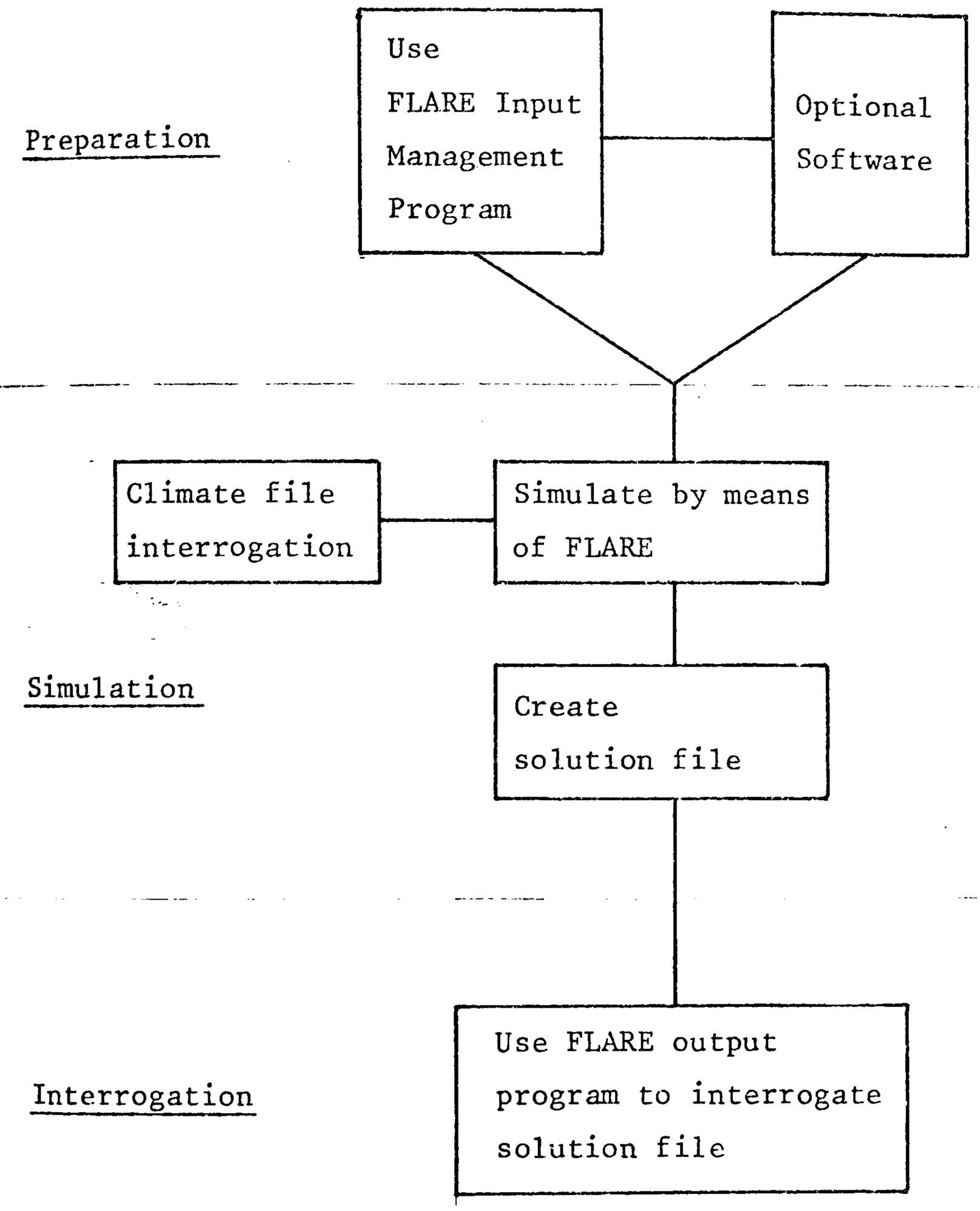

Figure 7.3 Operation of the FLARE System

FLRIMP

1PROJD	————————	PROJECT
2GEOMD	————————	GEOMETRY
3THRMD	————————	THERMAL
4SYSTM	————————	SYSTEM
5VFCNF	————————	VIEW FACTOR
6SHDNG	————————	INSOLATION/SHADING
. . . . .		
7CNTRL	————————	CONTROL
8PREFL	————————	INSOLATION/PLANAR REFLECTOR
9LOADP	————————	LOAD
ØADJFD	————————	ADJACENCY
BLINDD	————————	BLIND

Figure 7.4 Main Menu for the FLARE Input Management Program. Each menu pick allows the user to create, view or modify the approximate file.

- The PROJECT file must be the first file created in order to specify a new system. This file will contain data concerning the site plus general system information.

- The GEOMETRY file contains the geometry data associated with a solar collector and the position of the principal system components relative to a site origin point.

- The THERMAL file can only be created if the GEOMETRY file exists. This file contains all the thermophysical properties of the solar collector and the system. If transparent covers are used in the collector then a WINDOW file can be specified for these elements (see Appendix 8), otherwise a detailed description of the cover's optical properties is required.

- The SYSTEM file contains appropriate data on each system component plus the description of inter-connections between components.

- The VIEW FACTOR file contains the black body view factor relationships between internal surfaces of each duct in a solar collector. A simple algorithm can be employed to predict these relationships based on the GEOMETRY file data or a default case is used where the collector duct is assumed to be two infinite parallel plates.

- The INSOLATION/SHADING file contains the data concerning the effects upon a solar collector of objects external to the collector causing external surface shading and the resulting internal surface insolation. The user can enter a time-series of external surface shading or assume no external surface shading by site objects. A time-series of internal surface insolation values can be entered, or a default case can be invoked where all insolation is injected at the absorber plate node.

- The CONTROL file contains details of the control strategy of the system. This file will be discussed in more detail in Section 7.1.2.

- The INSOLATION/REFLECTOR file contains data concerning the effects of solar radiation reflected from a planar reflector onto a solar collector. This file is similar in construction to the INSOLATION/SHADING file. The default case assumes the reflected beam is incident over all the collector cover surface.

- The LOAD file contains the time-series values of a load which the collector system attempts to meet. FLRIMP can be used to enter the time-series manually, or in order to provide a link with the ESP building energy model, the load can be evaluated by ESP if possible. The ESP solution file is read by FLRIMP and the appropriate load values are automatically written to the FLARE LOAD file. This simple link allows interaction between FLARE and ESP.

- The ADJACENCY file contains the time-series values of the boundary conditions of components that are not exposed to climatic parameters, for example, any component positioned within a building or a solar collector fitted to a roof. Alternatively, the file can be used to describe the condition of re-circulated air from a room, etc. Consequently the file will contain two parameters, the first is temperature and the second depends upon the application: if used as an environmental description then the parameter is radiation; if used to describe a recirculation process, then if the fluid is liquid no variable is required but if the fluid is air then the relative humidity must be recorded. Constant values can be specified instead of time-series values. These ADJACENCY files can be created manually or they can be generated from the ESP solution file in the same way as the LOAD file.

- the BLIND file details the operation of an opaque cover for a solar collector for use when extreme temperatures are liable to occur in the collector.

To enhance the design process of a solar collector, five optional programs can be invoked to increase the accuracy of the data held in the various

files.

(1) A transparent element property prediction program is available which allows the user to interrogate different solar collector cover materials. The properties of the selected design can be written to file to be entered directly into the THERMAL file.

(2) A view factor prediction program is available to predict the black body view factors between internal surfaces of a solar collector. The results are written to a VIEW FACTOR file.

(3) An external surface shading prediction program can be invoked for a detailed thermal analysis of the solar collector. However, it has a secondary role to play in the positioning of a solar collector at a site to minimise shading effects.

(4) A planar reflected beam prediction program is available to analyse the proportion of reflected beam incident upon the collector. This data is useful for a thermal assessment of the effectiveness of a planar reflector. The program also is an aid for the design of the reflector.

(5) An internal surface insolation prediction program can be invoked to operate by itself to analyse the effects of internal shading due to collector walls or it can operate in conjunction with the resulting solution file from both the shading and the planar reflection programs. If this program is used by itself or with the shading data, then the INSOLATION/SHADING file can be created, alternatively, if the planar reflector data is used then the INSOLATION/REFLECTOR file is created.

The technique used in the shading, the planar reflector and the insolation programs is similar and described in Appendix 7.

The structure and procedure required to operate the FLARE Input Management Program is in its final form, however, not all the facilities

described above are currently available, although they shall be in the near future. Some files are in their final form while others will be under continual review as different components are added to the simulation model.

A user-manual describing the current operational procedure and data requirements of the FLARE system is in preparation (78). This will contain a full description of the contents of each data file.

After creating the appropriate data files the user enters the next phase which is to simulate the design data using the FLARE simulation program.

7.1.2 The FLARE Simulation Program

The FLARE simulation program will automatically conduct the placement of nodes throughout the system according to a user system specificaiton. This has the advantage of eliminating user error. Furthermore, the matrix manipulation of the resulting difference equations as described in Chapter 6 is also conducted automatically.

At present, the FLARE simulation program allows the user to perform a detailed analysis of a solar collector. The simulation procedure of FLARE will be the same for the future versions of the program which will incorporate other system components.

The FLARE simulation program operates in one of two modes:

- interactive mode in which the user is in full control of the program
- batch node in which a simulation file is constructed which contains a list of commands which would have been entered had the program been operated interactively.

Prior to operating the FLARE program, the user can interrogate climate files by means of the climate analysis program described in Chapter 3. The selected climatic data must be compatible with the simulation requirements, for example, it is pointless using summer data to test

for freezing in a liquid collector.

The menu structure of the FLARE program is shown in Figure 7.5. The operational logic of the prototype version of FLARE associated with the menu structure is given in Figure 7.6. There are a number of distinct sections within the program, these will be described relative to Figure 7.6.

The input section allows the user to enter the appropriate data files, as described in the previous section into the FLARE program. After specifying the system to be modelled, nodes are placed at selected points throughout the system and the program enters the pre-simulation calculation phase where all areas, volumes, etc are calculated. These values are then used to set up each time-independent coefficient or partial coefficient of the difference equations assuming a one hour time interval. This will save considerable computational effort since these coefficients are only calculated once.

By selecting the '2SIMUL' command the user proceeds to the next phase which involves defining the binary random access solution file to which the appropriate simulation results will be written. This file can contain the results of up to 20 different simulations for the same input data with different climatic or control conditons. The simulation period and the number of time increments are also defined, where the number of time increments is a positive integer value the inverse of which gives the ratio of the time step to one hour. The time independent coefficients are then modified accordingly.

To perform the simulation the user selects the 'RSIMUL' command at which stage the user will specify the CONTROL file, if a new CONTROL file is required then the file is created interactively. This facility is particularly useful when re-simulating the same system under a different control strategy. After entering the CONTROL file the simulation commences and at every time increment the following are considered: collector fluid properties, internal and external longwave re-radiation, solar radiation, etc. These time-dependent values are used in conjunction

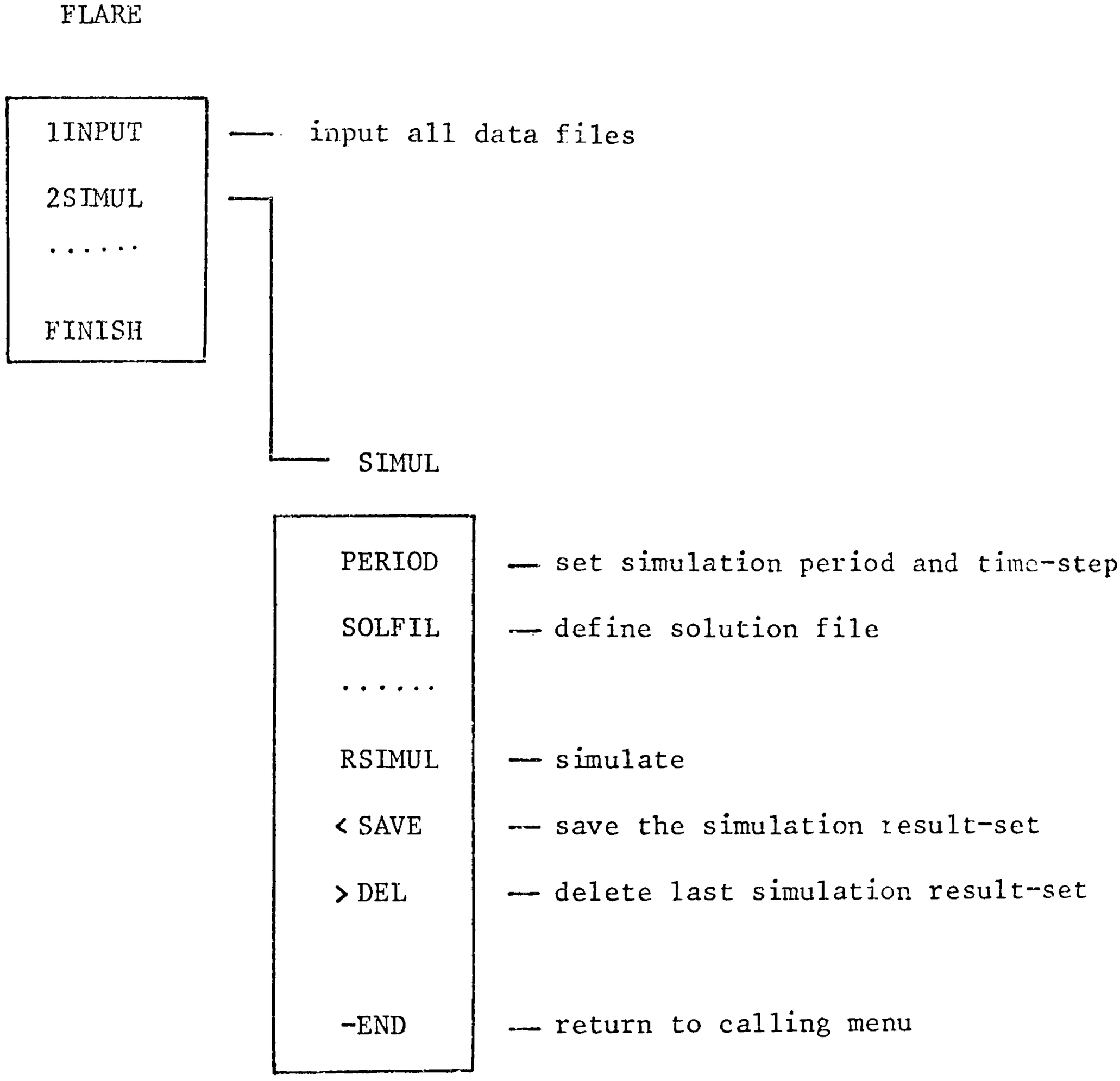

Figure 7.5 Menu structure of the FLARE simulation program

Menu : FLARE

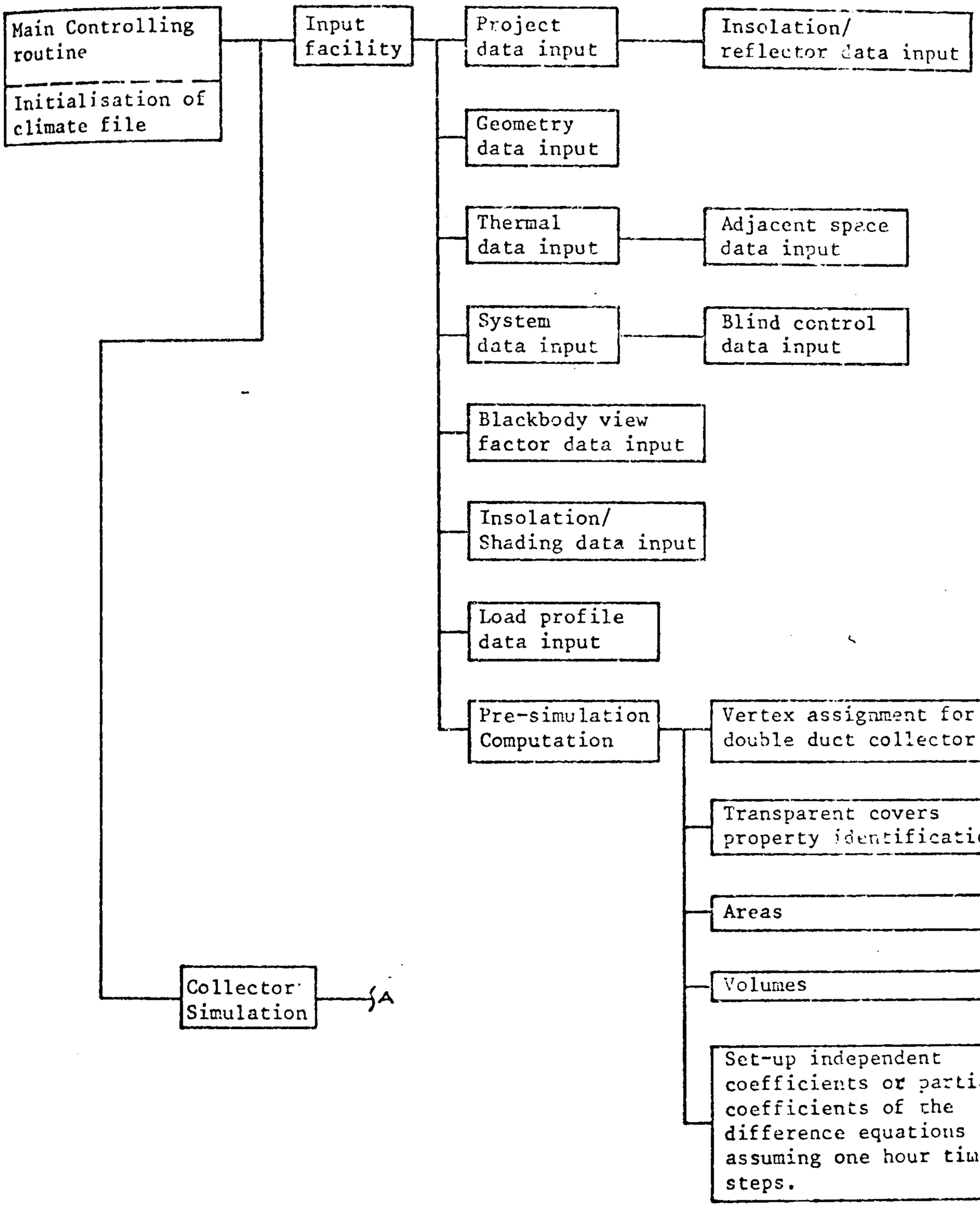

Figure 7.6a FLARE : Logic diagram 1

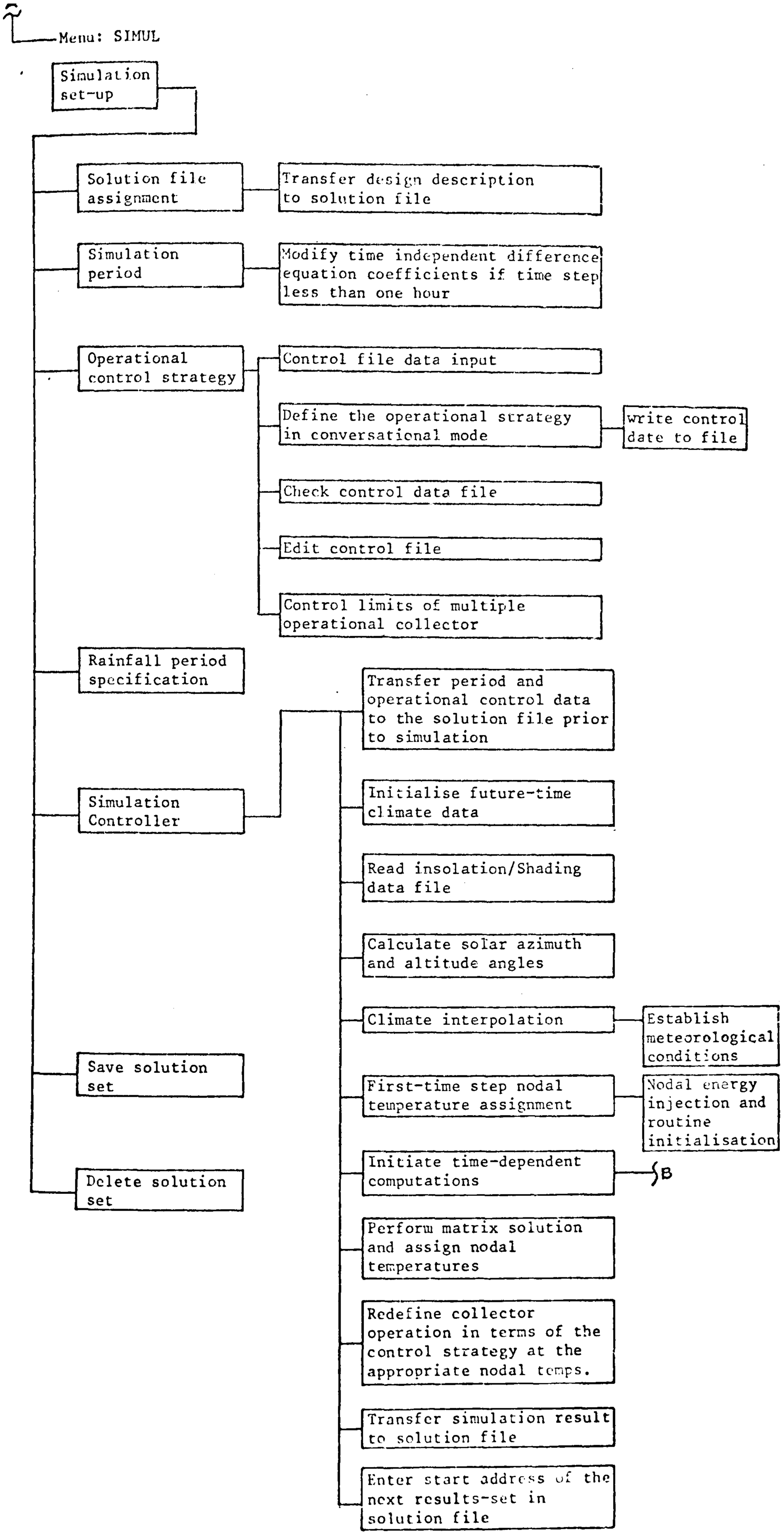

Figure 7.6b FLARE: Logic Diagram 2

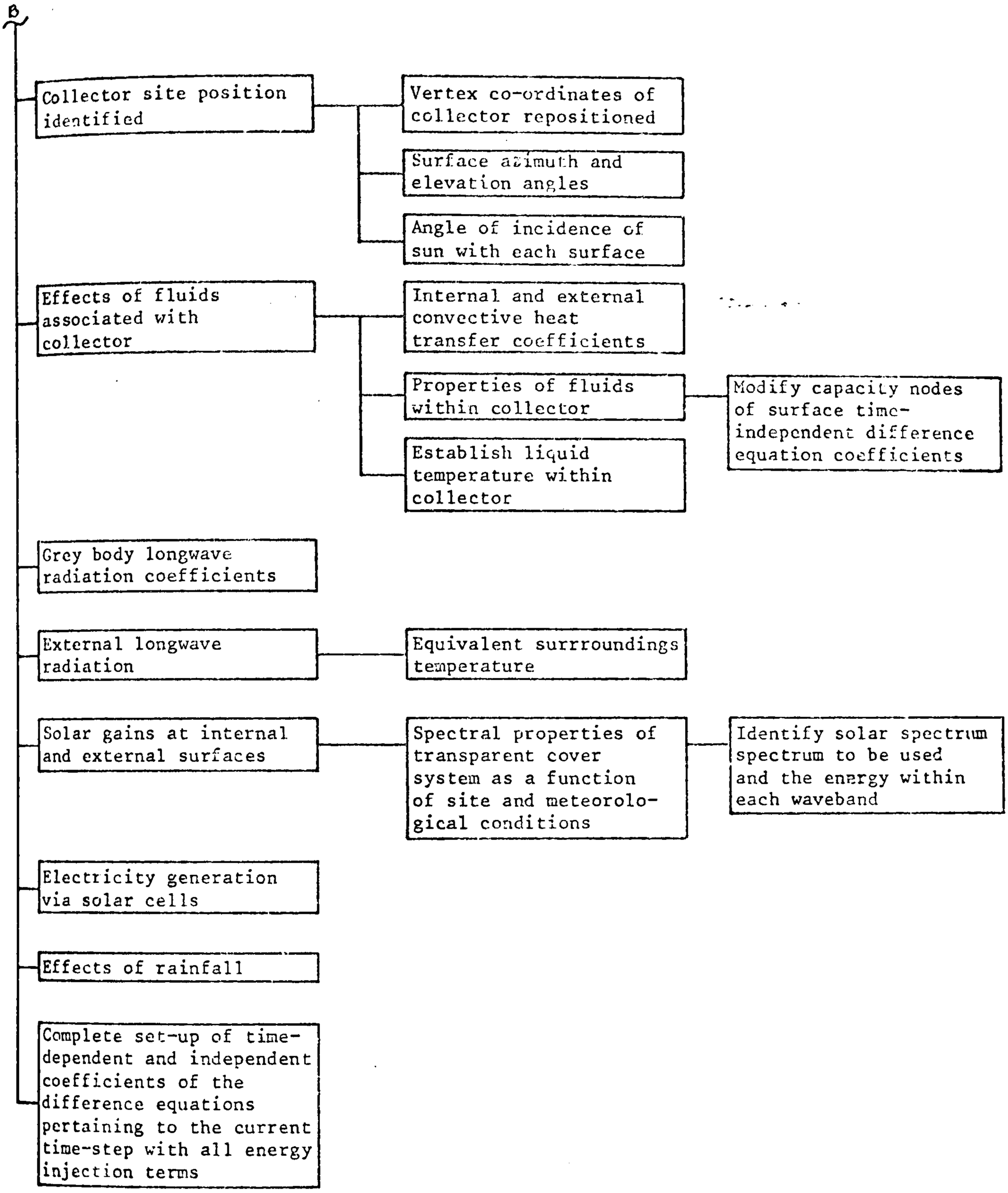

Figure 7.6c FLARE: Logic Diagram 3

with the time-independent coefficients to complete the appropriate difference equations at each time-increment. The difference equations are passed to the matrix handling routines and solved simultaneously. At the end of each time increment selected data are written to the solution file. This process is repeated for subsequent time increments until the end of the simulation period. Upon completion of the simulation the data in the solution file can be saved for subsequent interrogation by means of the FLARE output program.

The operation of the FLARE simulation program is described more fully in the FLARE User Manual (78).

The control facility available with the prototype program involves the user of six sensor positions associated with a solar collector. These may be used for single or dual sensor operational control.

1) Back plate temperature sensor. This sensor can be used in any collector mode, as it is normally one of the hottest spots in the collector and this should be taken into account when it is used because the fluid temperature can be considerably lower than the sensor temperature and not suitable for collection. However, the fan or pump may be switched on regardless.

2) Inlet fluid temperature sensor. This sensor is not applicable to a photovoltaic collector. The principal use of an inlet fluid sensor is in dual sensor control where the inlet temperature is the reference sensor for collector operation.

3) Outlet fluid temperature sensor is also not applicable to PV COLLECTORS. When the fan or pump is off this will assume the temperature value of the next to outlet fluid node. In the present version of FLARE this will be the centre fluid node in an air collector and the mean fluid temperature in a liquid collector.

4) Mean fluid temperature sensor, not applicable to PV collectors.

5) Ambient air temperature sensor. This sensor is used principally

in dual sensor operation similar to the inlet fluid temperature sensor.

6) Solar radiation sensor. This may operate on either the direct normal or the total irradiance.

The function of the sensors is to operate any fans or pumps associated with the collector. If single sensor control is employed the user must define the sensor temperature above which the fan or pump (hereafter termed the fan) will operate. Once the fan is switched on and the sensor drops below the user defined sensor lower set-point temperature the fan or pump will be switched off. To ensure excessive cycling will not occur a controller time lag for the on/off operation is specified. If the simulaiton time increment is less than the time lag for controller operation then no charge in the operational status of the fan will be allowed. (The controller time lag is not in effect if it is of shorter duration than the simulation time increment). A dual sensor controlled fan also employs the time lag philosphy, and a dominant and reference sensor are defined by the user. The temperature difference between the two sensors is compared with the user defined upper set-point and lower set-point values depending upon the fan status, that is, off and on respectively.

Although simple, this method of modelling the system control operation will be used in the future version of FLARE, however many more control points will be allowed. Proportional, differential and integral controllers will be modelled as will micro-processor multi-point controllers.

7.1.3 The FLARE Output Program

The role of the FLARE output program - FLROUT - is to allow interrogation of a simulation solution file. There are three modes by which FLROUT permits the recovery of data from the solution file:

a. synoptic output
b. graphical output
c. total output

Synoptic output is used primarily for an assessment of the collector performance over a defined period. The data given includes the energy collected, the collector efficiency and the maximum and minimum temperatures of the collector.

Graphical output allows the interactive construction of graphs displaying any number of specified parameters simultaneously. Inherent in such graphs are the prevailing cause and effect relationships, on investigation of which will result in effective design modifications.

Total output is simply a daily performance assessment of various aspects of a solar collector, for example, fan or pump operation.

The complete FLROUT menu structure is shown in Figure 7.7.

Synoptic Output

The synoptic output menu is shown in Figure 7.8. For any defined period of a particular simulation solution this menu allows the user to select from two forms of synoptic information:

1. collector data plus ideal storage for the defined period
2. collector data associated with non-ideal storage for the defined period

The first synoptic output selection '1SYNOP' is the method by which the following synoptic information is obtained:

a) the performance of the collector against a particular load. If a load profile is defined then as a consequence of the mismatch between energy supply and the load at each time increment, the auxiliary energy supplied or the solar energy to store is calculated at each increment and the totals for the defined period assessed. It is assumed that there are no losses from the store. These values and the ratio of the solar supply to the load are given for the defined period.

Figure 7.7 Complete output FLROUT menu structure

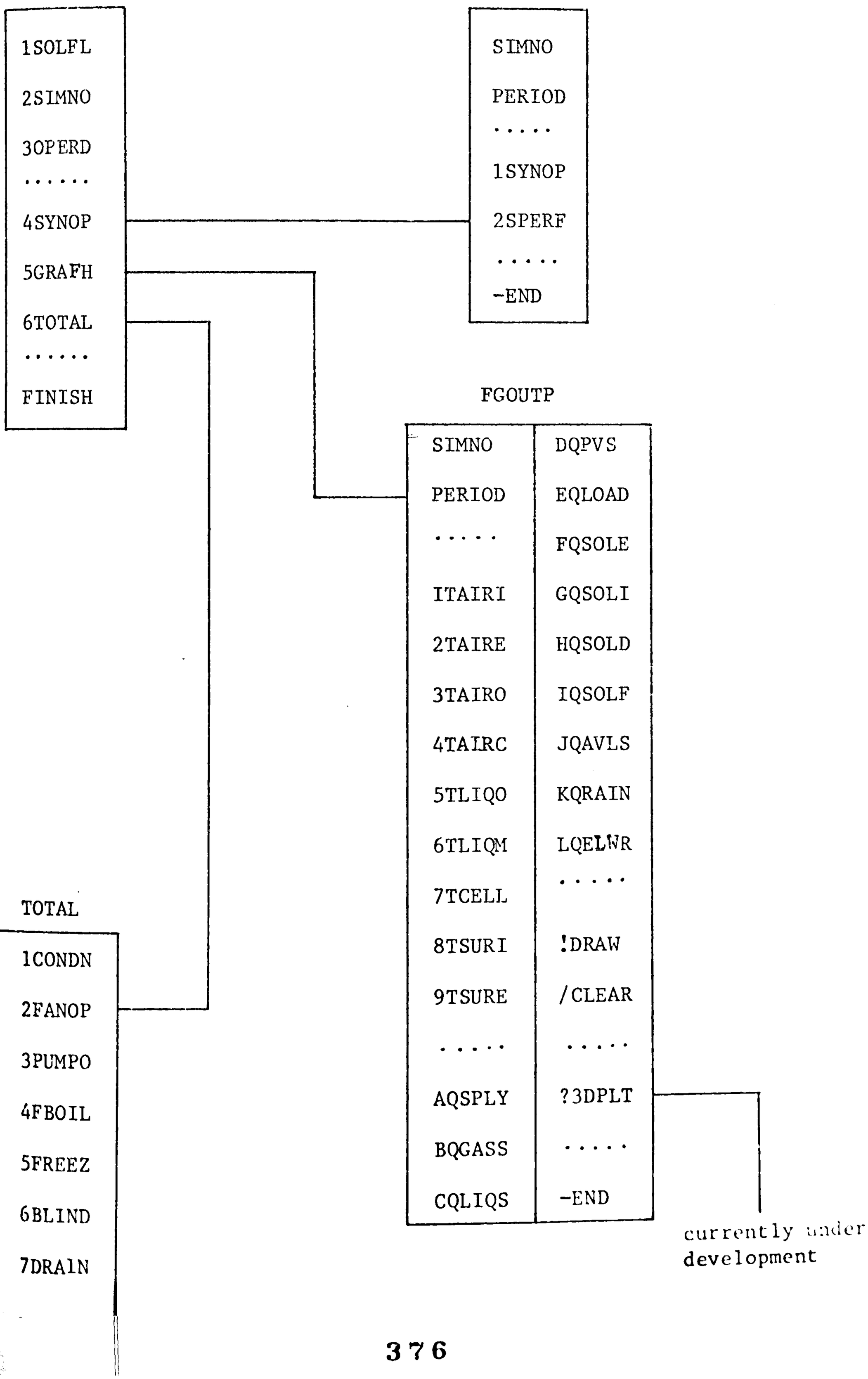

FSOUTP

SIMNO	————	select a simulation from solution file
PERIOD	————	define the output period
.....		
1SYNOP	————	synoptic information
2SPECF	————	synoptic system performance information
.....		
-END	————	return to calling menu.

Figure 7.8 The Synoptic Output Menu

b) the performance of the collector. The quantity of solar energy delivered and the collector efficiency for the defined period are assessed. Also the supplied solar energy is sub-divided into its three collection modes air, liquid and photovoltaic. Obviously the values of the modes not in use will be zero.

c) the maximum and minimum absorber plate temperature and a record of condensation occurrence during the defined period.

An example of this synoptic output facility is shown in Table 7.1

The second synoptic output facility exists at present because FLARE is a prototype model simulating the solar collector and not its associated system. If '2SPERF' is selected the user is required to input data concerning a remote energy store to use in conjunction with the collector. If the quantity of energy in the storage unit at the start of the defined period and the rate of energy loss from the unit are both specified by the user, assuming perfect energy transfer at each time increment between the collector, store and load , a very simple systems model is produced. Although this model is not intended to give accurate results, it will give a crude approximation of the effects of a particular storage system. The synoptic output in addition to the output (a) and (b) above will consist of the energy returned in the store at the end of the defined period, see Table 7.2. Although at present this output facility gives a crude approximation of the collector/storage performance it will have an important role in the development of the FLARE systems model. If the crude model is replaced with the system components identified in Chapter 5 then these can be developed and tested assuming the solar collector data to be a known boundary condition of the system. Consequently, a full implicit solution of the resulting finite difference equations of the system nodal scheme contained in an $\underline{S}$ matrix can be conducted, independent of the solar collector model. Once tested the system component models can be interlinked with the collector model and the full systems simulation can be conducted by FLARE.

```
   SYNOPTIC OUTPUT
   ===============

PERIOD CONSIDERED FROM  1.00 HRS. ON THE 15 TH OF JULY
                  TO 24.00 HRS. ON THE 15 TH OF JULY
PERCENTAGE LOAD SUPPLIED FROM COLLECTORS = 84.08 %

SOLAR ENERGY SUPPLIED          4.793 KWH
ENERGY REQUIRED                5.700 KWH
AUXILIARY SUPPLIED             2.757 KWH
ENERGY TO STORE                1.850 KWH

QUANTITY OF ENERGY DELIVERED =     14.875 KWH
COLLECTOR EFFICIENCY         =     32.219 %

   BREAKDOWN OF SOLAR ENERGY SUPPLIED
-----------------------------------------

ENERGY COLLECTED BY AIR          =      4.793 KWH
ENERGY COLLECTED BY FLUID        =      0.000 KWH
ENERGY COLLECTED BY SOLAR CELLS  =      0.000 KWH
                                        ---------
                                        4.793 KWH

MAX. PLATE TEMPERATURE  =  47.75 DEG. C
MIN. PLATE TEMPERATURE  =  12.69 DEG. C

NO CONDENSATION PROBLEMS DURING THIS PERIOD.
```

Table 7.1 Example output from menu pick '1SYNOP'

```
   SYNOPTIC OUTPUT
   ===============

PERIOD CONSIDERED FROM  1.00 HRS. ON THE 15 TH OF JULY
                  TO 24.00 HRS. ON THE 15 TH OF JULY
ENERGY IN STORE AT START =    2.0000 KWH
ENERGY IN STORE AT FINISH=    1.1682 KWH
RATE OF ENERGY LOSS FROM STORE = 1.0000 %/HR


PERCENTAGE LOAD SUPPLIED FROM COLLECTORS = 84.08 %

SOLAR ENERGY SUPPLIED          4.793 KWH
ENERGY REQUIRED                5.700 KWH
AUXILIARY SUPPLIED             0.000 KWH
ENERGY TO STORE                1.850 KWH

QUANTITY OF ENERGY DELIVERED =     14.875 KWH
COLLECTOR EFFICIENCY         =     32.219 %

   BREAKDOWN OF SOLAR ENERGY SUPPLIED
-----------------------------------------

ENERGY COLLECTED BY AIR          =      4.793 KWH
ENERGY COLLECTED BY FLUID        =      0.000 KWH
ENERGY COLLECTED BY SOLAR CELLS  =      0.000 KWH
                                        ---------
                                        4.793 KWH
```

Table 7.2 Example output from menu pick '2SPERF'.

Upon completion of the FLARE systems model the synoptic output mode may have a more varied synoptic output facility than at present.

Graphical Output

Graphical output from the simulation solution can be constructed via the graphical output menu, shown in Figure 7.7. A description of the graph available from each menu pick is given in Table 7.3. At present the graph point will be drawn for each time increment result. In the near future the user will be allowed to select the output time increment for the results recovery from a specified solution The graph will be drawn for the averaged result over the output interval or only the discrete value at the end of each interval will be recovered.

Upon defining the contents of each graph the user displays the graph by calling the 'DRAW' command. Table 7.4 details the axis drawn, the line plotted and the reference for each graph which may be plotted. Once the graph has been displayed the menu cursor will reappear but not the menu. This allows additional profiles to be added to a graph (the '+ADD'command followed by the required profile), without the menu being redrawn. The menu can be re-displayed at any time by calling the hidden 'M' command. If the graph axis, relating to the distribution to be added, has already been scaled and drawn then in many cases the added distribution may lie outside the bounds of the axis, the '=SCLE' command automatically rescales and redraws the contents of the graph. This is useful for the repeat display of identical graphs but for different simulation result sets. To clear the contents of a graph from memory the '/CLEAR' command is selected allowing a 'fresh' graph to be defined.

If the '?3DPLT' command is selected then a 3 dimensional surface representation of the discrete time step data representing a selected parameter may be drawn. In the display picture the X direction represents the time step division of the day, the Z direction represents the number of days displayed and the Y direction (up) represents the specified parameter. Several days should be selected for this command

Menu Pick	Description
1TAIRI	inlet air temperature.
2TAIRE	ambient air temperature.
3TAIRO	outlet air temperature.
4TAIRC	air temperature in collector ducts
5TLIQO	liquid outlet temperature
6TLIQM	mean liquid temperature in collector
7TCELL	temperature of solar cell
8TSURI	temperature of any specified internal surface temperature.
9TSURE	temperature of any specified external surface temperature.
AQSPLY	total solar energy supplied for N collectors operating in parallel.
BQGASS	solar energy supplied via air
CQLIQS	solar energy supplied via liquid
DQPVS	solar energy supplied via solar cells
EQLOAD	load profile
FQSOLE	solar energy incident upon specified external surface
GQSOLI	solar energy incident upon specified internal surface
HQSOLD	prevailing direct solar radiation
IQSOLF	prevailing diffuse solar radiation
JQAVLS	prevailing global solar irradiation incident upon collector cover
KQDRAW	energy exchange between a specified external surface and prevailing precipitation
LQELWR	net long-wave radiative exchange between a specified external surface and its surrounding envelope.

Table 7.3 List of graphical output options.

Menu Pick	Axis	Line	Line drawn
1TALRI	deg C	Full	
2TAIRE	deg C	Full	
3TAIRO	deg C	Full	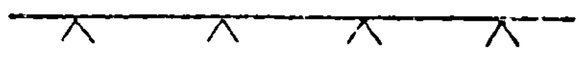
4TAIRC	deg C	Full	
5TLIQO	deg C	Full	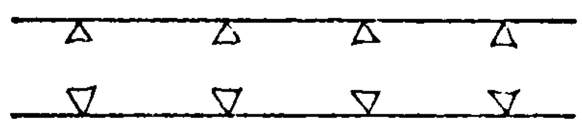
6TLIQM	deg C	Full	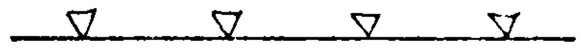
7TCELL	deg C	Full	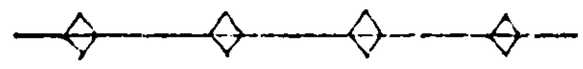
8TSURI	deg C	Full	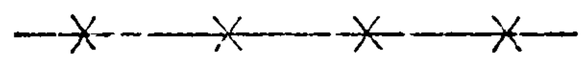
9TSURE	deg C	Full	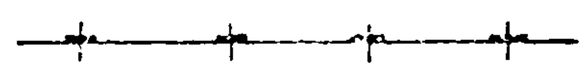
AQSPLY	Watts	broken	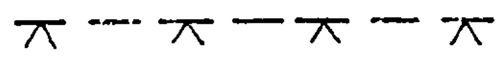
BQGASS	watts	broken	
CQLIQS	watts	broken	
DQPVS	watts	broken	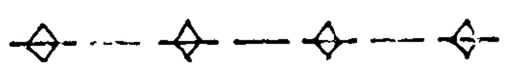
EQLOAD	watts	broken	
FQSOLE	W/M^2	chain	
GQSOLI	W/M^2	chain	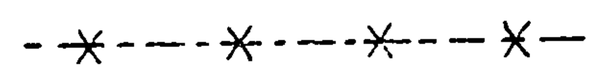
HQSOLD	W/M^2	chain	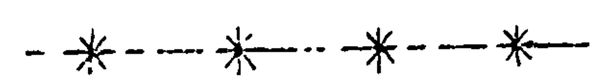
IQSOLF	W/M^2	chain	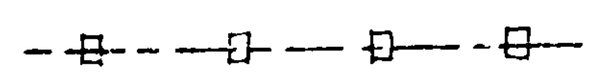
JQAVLS	W/M^2	broken	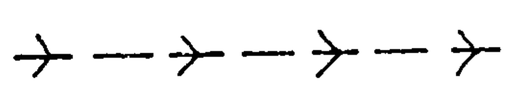
KQRAIN	W/M^2	dot	
LQELWR	W/M^2	dot	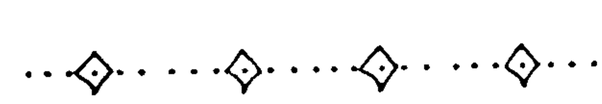

Table 7.4 Details of graphical distributions.

to be effective. This facility is not available to FLARE users as yet and it is currently under development, however, a sample of the potential output is given in Figure 7.9.

The purpose of the following graphs are to illustrate the currently available graphical facilities and for this reason no explanation of the design details to which they relate will be given.

- Figure 7.10 shows the available solar radiaiton and the external longwave radiative exchange at the collector cover
- Figure 7.11 gives the variation of the internal absorber and cover plate temperatures
- Figure 7.12 shows the variation in photovoltaic cell temperature and the quantity of energy supplied by an array of parallel collectors.

Total Output

The total output menu is shown in Figure 7.13. Any selection from this menu will output for a particular day 288 values of the status of the defined parameter in tabular form. For example, if the user wishes to investigate potential fan cycling then by selecting '2FANOP' the status of the fan, i.e. on or off, will be shown. The value given is the status of the fan at the particular time irrespective of the length of the time increment.

This output is a useful aid in the modificaiton of a design, for example,

- the effects on a liquid collector of pump failure and at what stage liquid boiling will occur

- the effect of a particular control strategy on the fan or pump operation

- The occurences of freezing and the use of blinds or automatic drain-down to alleviate the problem

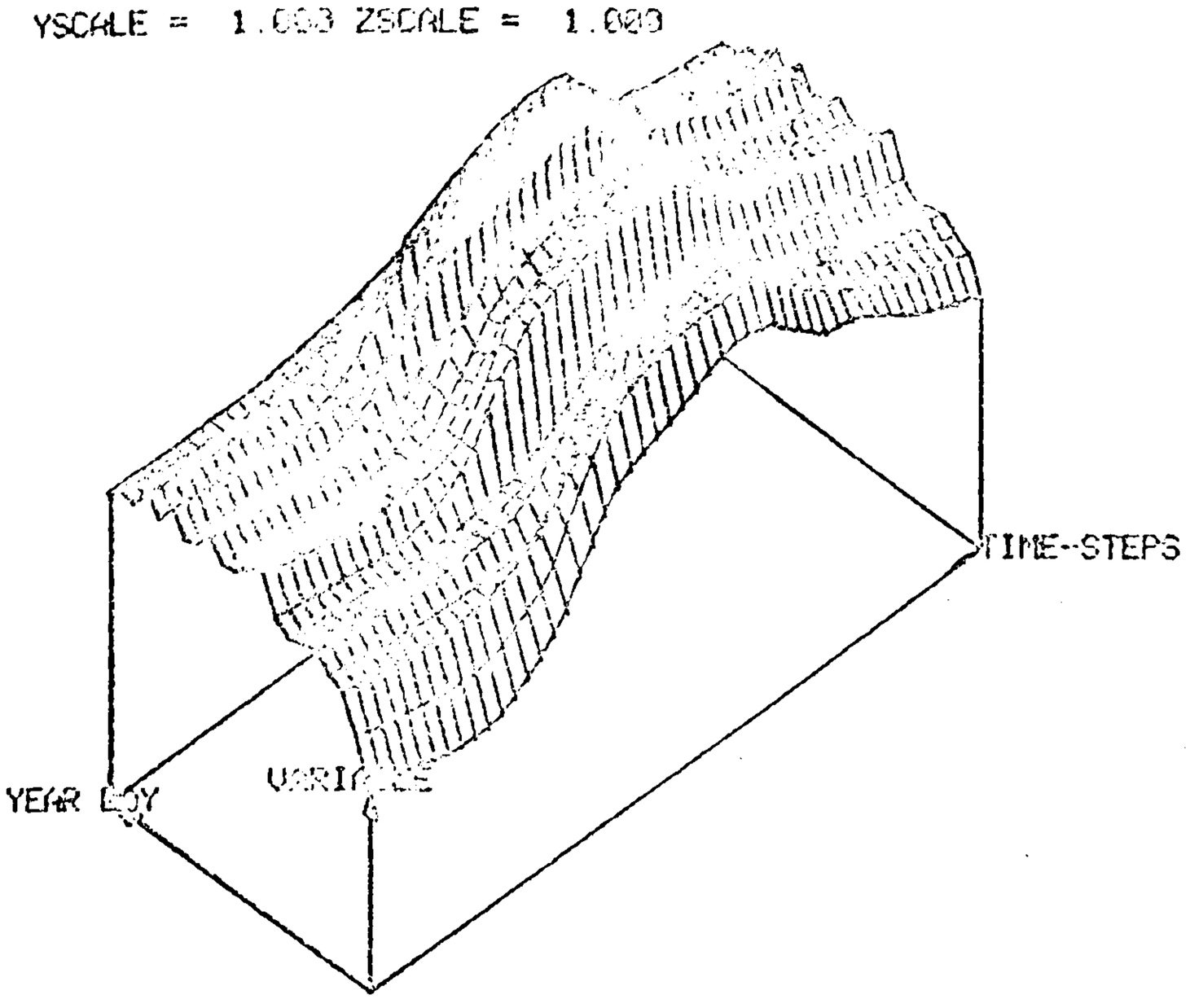

Figure 7.9 Example of 3D plot

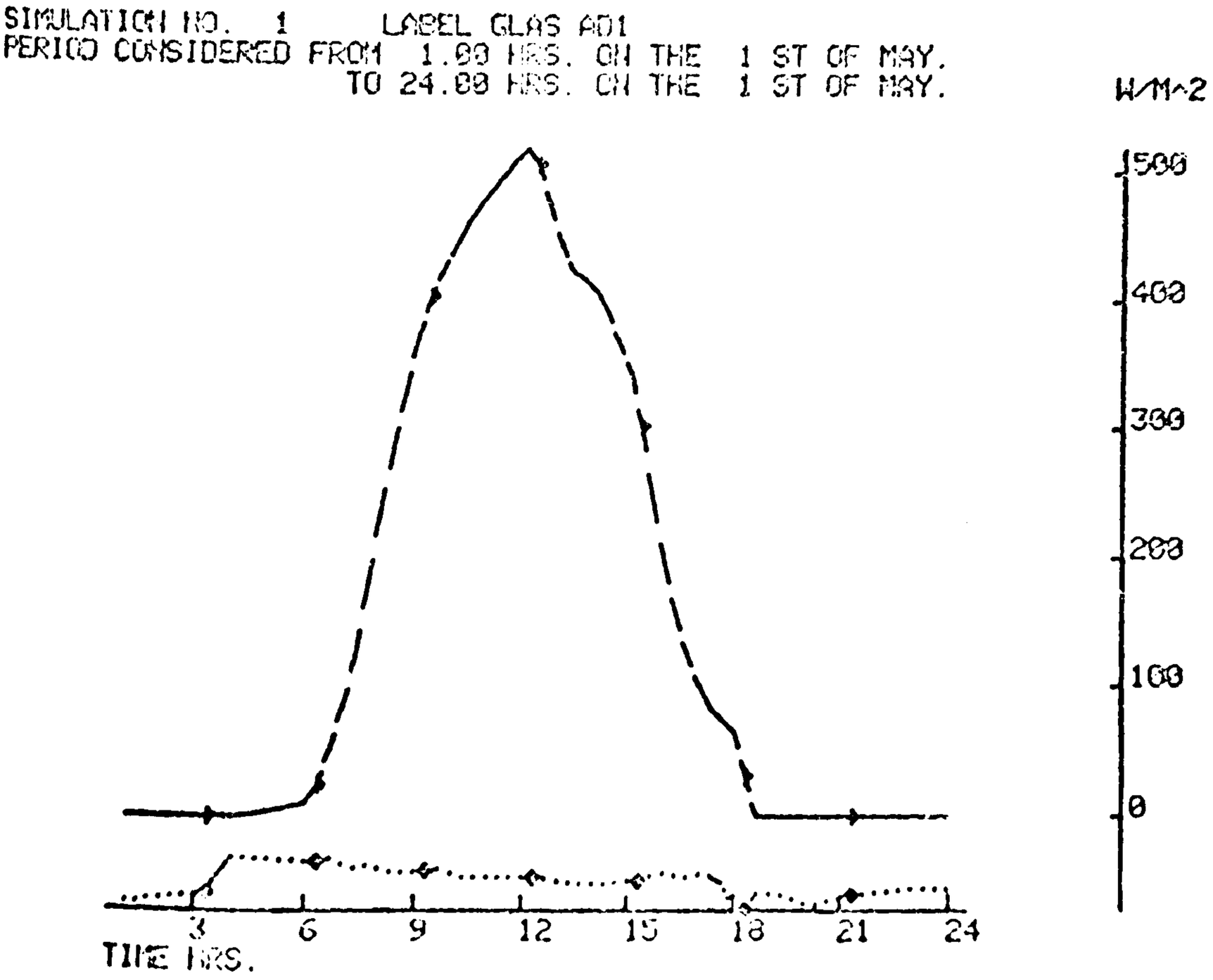

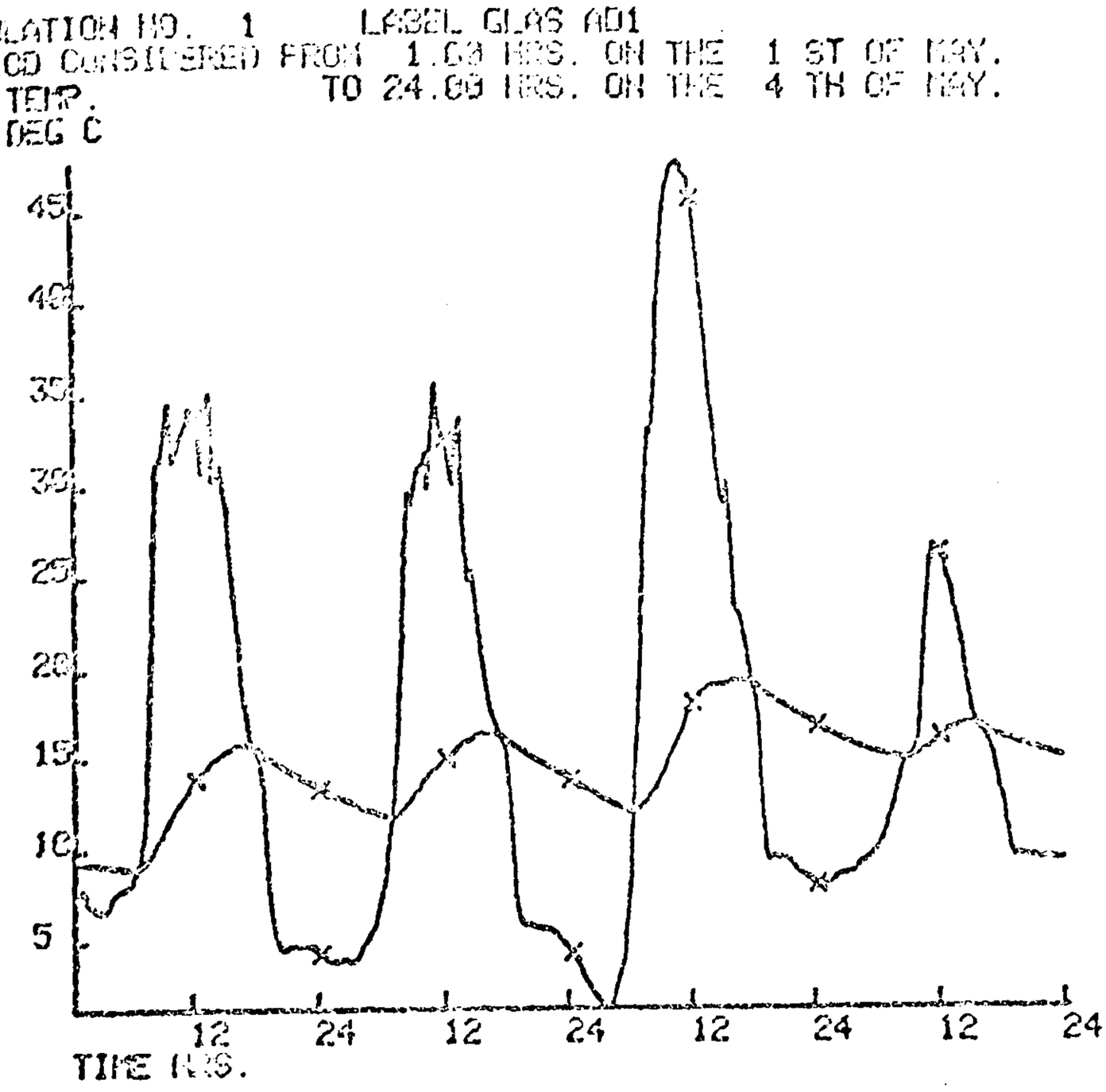

Figure 7.11

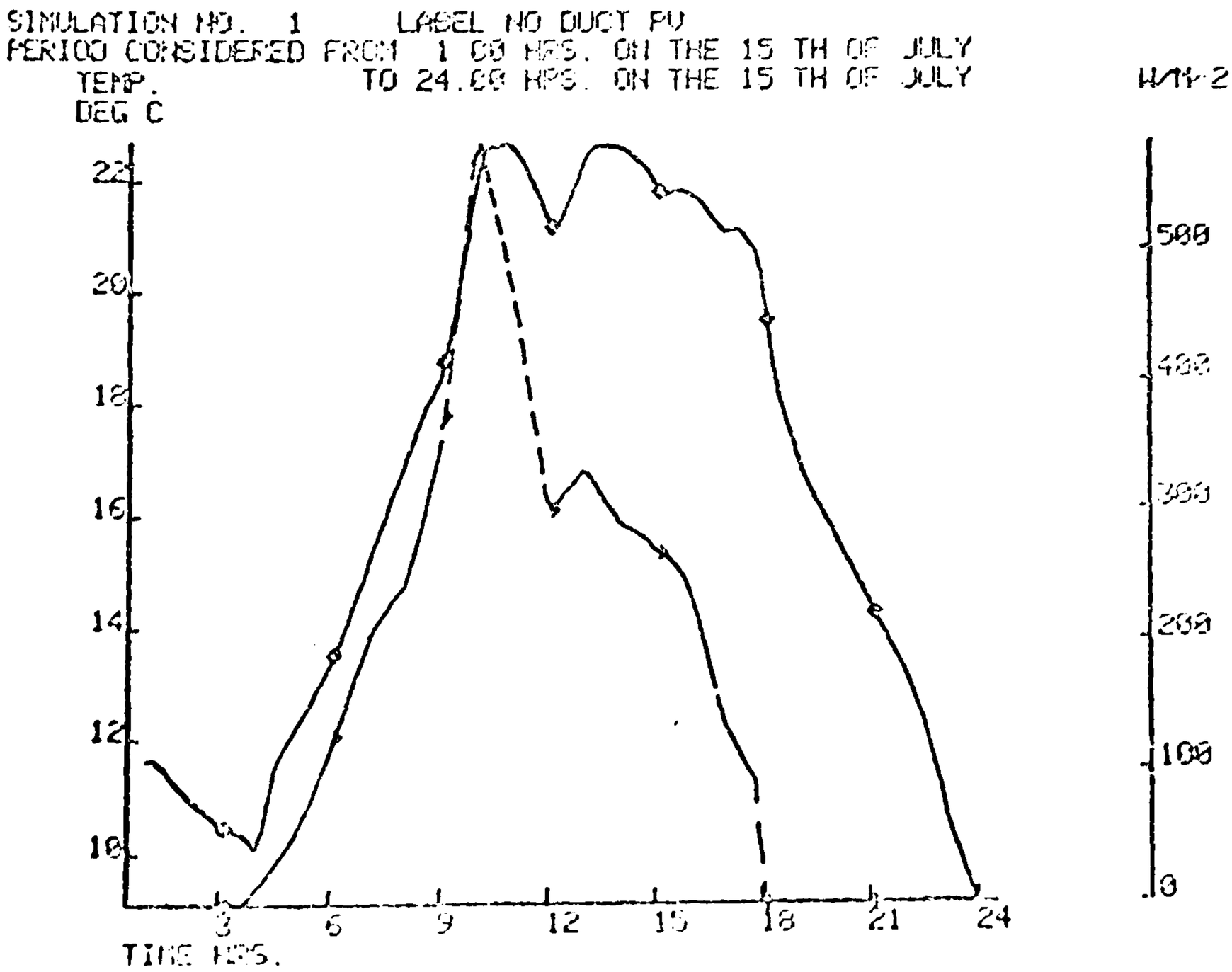

Figure 7.12

TOTAL

1CONDN	———	daily condensation occurances
2FANOP	———	daily fan operation
3PUMPO	———	daily pump operation
4FBOIL	———	daily fluid boiling occurances
5FREEZ	———	daily fluid freezing occurances
6BLIND	———	daily blind operation
7DRAIN	———	daily liquid draindown occurances
-END	———	return to calling menu.

Figure 7.13 The Total Output menu.

- where and when the condensation is liable to occur within the collector.

Figure 7.14 is an example of this output for a fan from which the user can identify on-off periods and determine if cycling is occurring.

As the FLARE simulation model develops then the output program will have to develop in parallel. Consequently, the basic structure of the FLARE output program will remain the same but there will be in increasing number of graphical and total output options and the synoptic output will be made more sophisticated. Regression analysis routines will be employed to allow the user to statistically analyse the results of any simulation.

DAY CONSIDERED IS DAY 15 OF MONTH 7

FAN STATUS :
IF FAN ON THEN VALUE=1, IF FAN OFF VALUE=0

HOUR	MINUTES +5	+10	+15	+20	+25	+30	+35	+40	+45	+50	+55	+60
0	0	0	0	0	0	0	0	0	0	0	0	0
1	0	0	0	0	0	0	0	0	0	0	0	0
2	0	0	0	0	0	0	0	0	0	0	0	0
3	0	0	0	0	0	0	0	0	0	0	0	0
4	0	0	0	0	0	0	0	0	0	0	0	0
5	0	0	0	0	0	0	0	0	0	0	0	0
6	0	0	0	0	0	0	0	0	0	0	0	0
7	0	0	0	0	0	0	0	0	0	0	0	0
8	0	0	0	0	0	0	0	0	0	0	0	0
9	1	1	1	1	1	1	1	1	1	1	1	1
10	1	1	1	1	1	1	1	1	1	1	1	1
11	1	1	1	1	1	1	1	1	1	1	1	1
12	1	1	1	1	1	1	1	1	1	1	1	1
13	1	1	1	1	1	1	1	1	1	1	1	1
14	1	1	0	1	0	1	0	1	0	1	0	1
15	1	1	1	0	1	0	1	0	1	0	1	0
16	1	1	1	1	0	1	0	1	0	1	0	1
17	0	0	0	0	1	0	1	0	1	0	1	0
18	0	0	0	0	0	1	0	1	0	1	0	1
19	0	0	0	0	0	0	1	0	1	0	1	0
20	0	0	0	0	0	0	0	1	0	1	0	1
21	0	0	0	0	0	0	0	0	1	0	1	0
22	0	0	0	0	0	0	0	0	0	1	0	1
23	0	0	0	0	0	0	0	0	0	0	1	0

Figure 7.14 Example of Total Output - menu pick '2FANOP'

7.2 Validation of the FLARE Simulation Model

Increasingly, as a prerequisite of use, designers prefer models to have undergone a validation procedure, consequently, it is very important to validate a model. The FLARE simulation module has been developed primarily to validate the mathematical model described in Chapters 5 and 6. Subsequently, the results of the mathematical model can be compared with measured data via the FLARE simulation model. Despite being at a very early stage of development FLARE will be compared both with measured results and results from another simulation program.

The most satisfactory method of validating a model is by comparison with real data, however due to the cost of physical modelling there are few measured data sets available for solar collectors and their system. Some results are available from steady state testing of rear duct solar collectors at the University of Strathclyde, FLARE was simulated under steady state conditions and compared with the measured results (Section 7.2.2). Due to the lack of measured data models are frequently compared by means of a program-to-program test. FLARE and TRNSYS (see Chapter 4) were used to simulate the same solar collector and the results are given in Section 7.2.1.

Due to the nature of the tests and the fact that FLARE is a prototype program at present only brief explanations of the results will be given.

7.2.1 Comparison between FLARE and TRNSYS

A simple flat plate collector was analysed by both FLARE and TRNSYS and the results compared. The collector was a $4m^2$, fixed position, single duct air collector with a 4mm clear float glass cover. The fan is controlled to operate only when the air inside the collector duct exceeds 35°C. three different tests were conducted, each involved simulating the collector over a single day at 12 minute time intervals. The results from these tests are briefly described.

Test 1

Figure 7.15 gives the direct normal and diffuse horizontal solar irradiance for the test day. The values of the air temperature in the

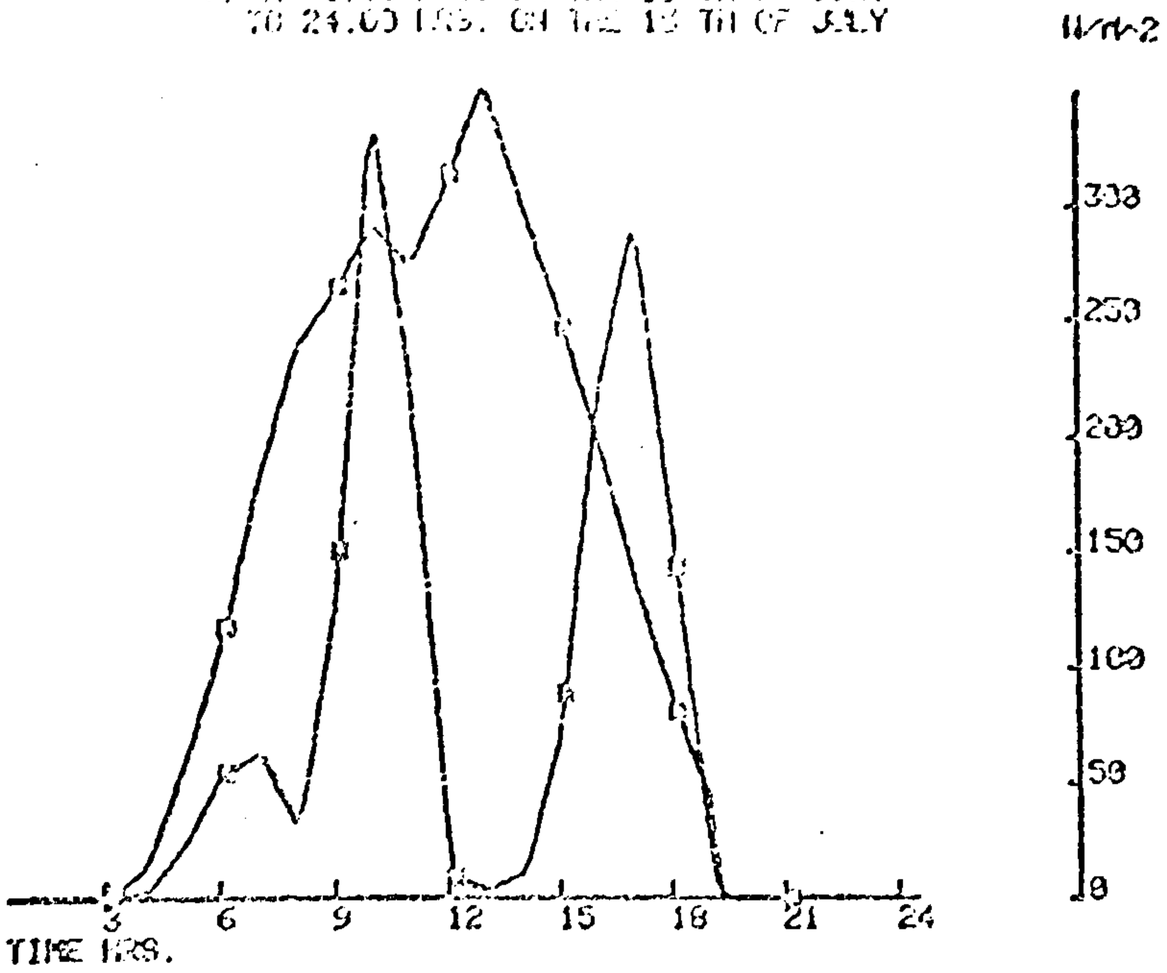

Figure 7.15 Test 1 Solar radiation

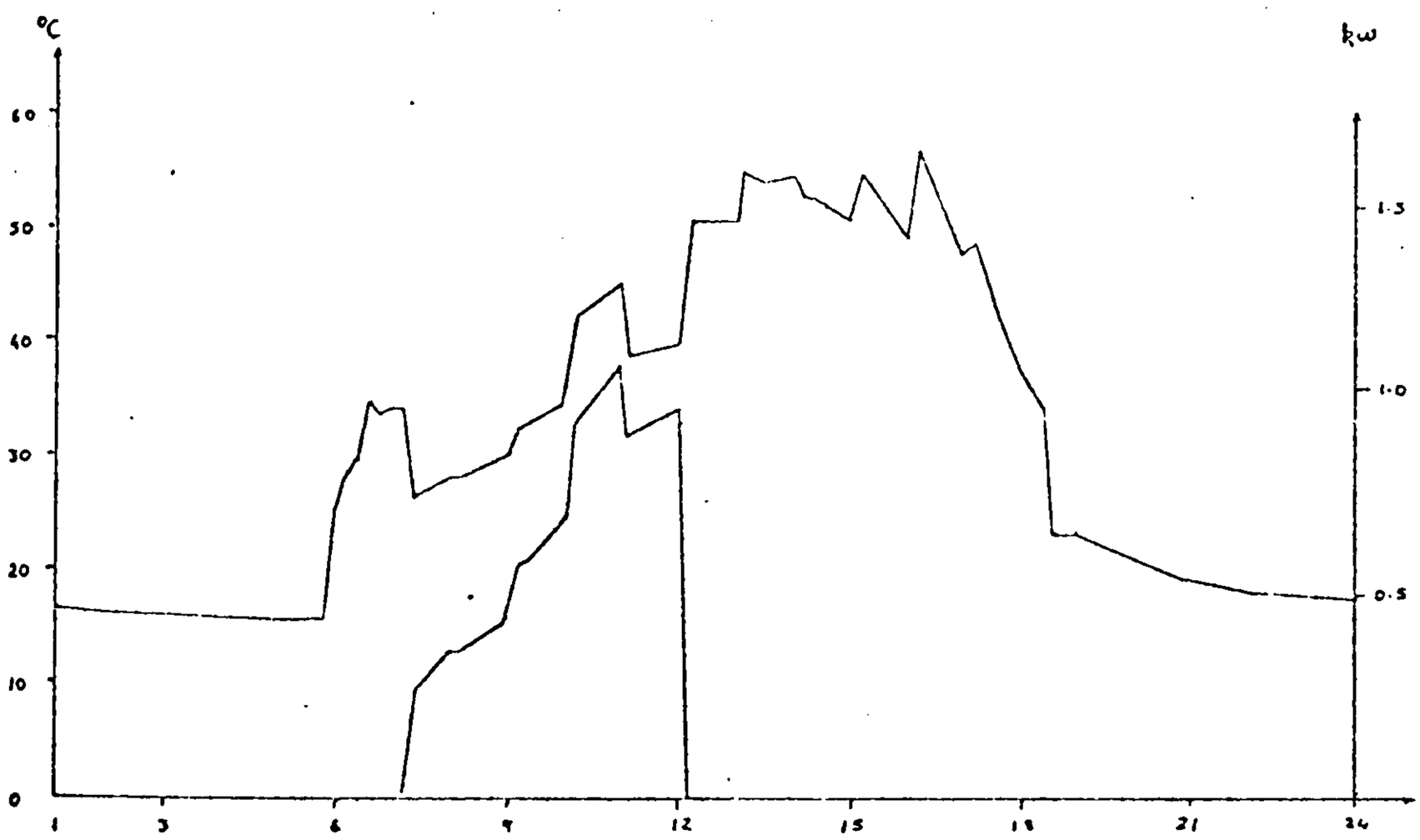

Figure 7.16 Test 1 TRNSYS simulation results

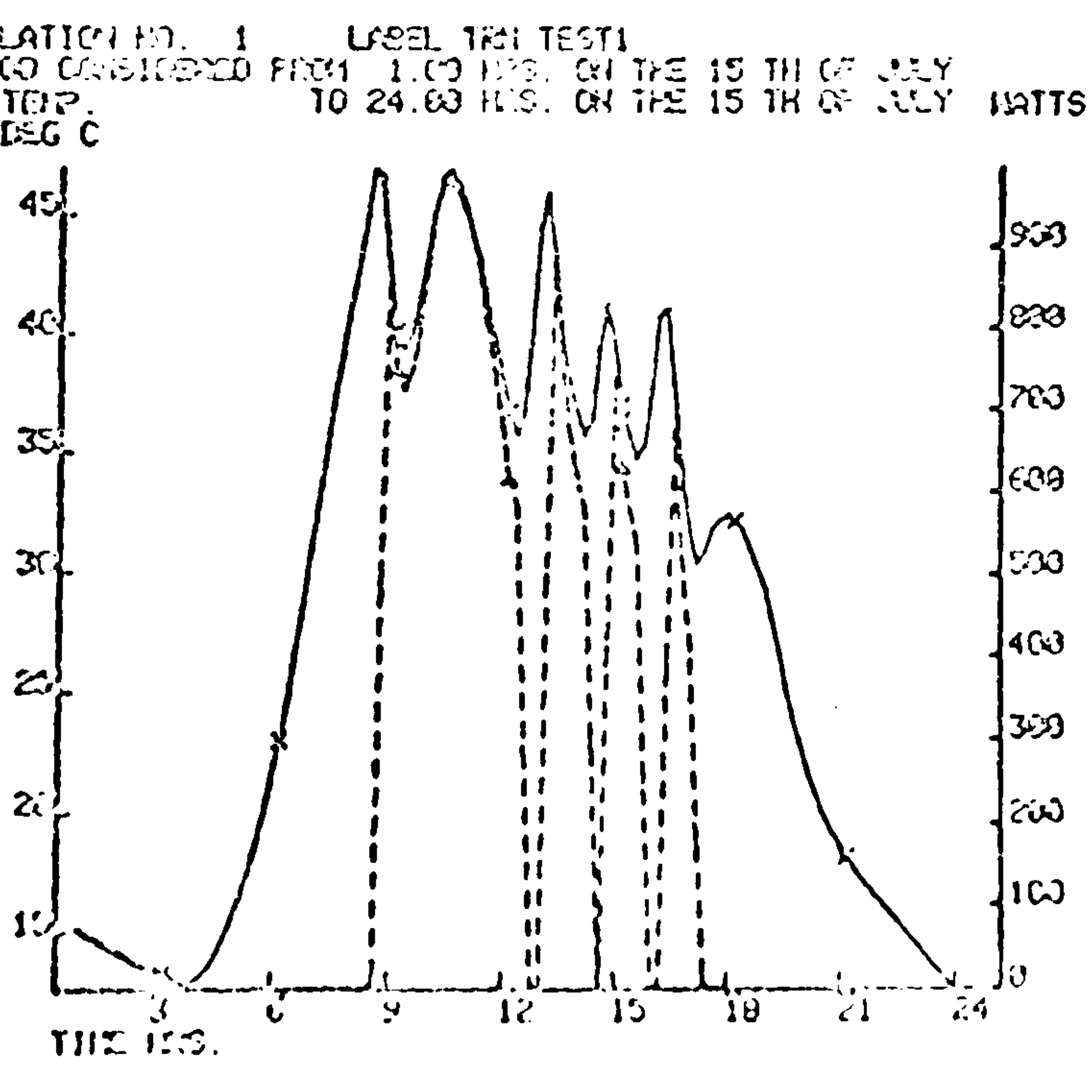

1 FLARE simulation results

collector duct and the quantity of energy supplied by the collector from both TRNSYS and FLARE are shown in Figures 7.16 and 7.17 respectively. The only other data TRNSYS generates relating to the collector is the overall thermal loss coefficient and the $\tau\alpha$ value. FLARE on the other hand gives much more information, selected samples of which follow:

- Figure 7.18 shows the energy supplied from the collector and the quantity of solar irradiance incident upon the collector

- Figure 7.19 compares the variation between the collector duct air temperature and the external air temperature.

- Figure 7.20 shows the temperature at the exposed surface of the collector cover and the longwave radiative exchange between the cover and its surrounds.

- Figure 7.21 gives the synoptic output for the simulation period.

Several points to note are:

1. TRNSYS does not switch on the fan after 12:00 despite the collector air temperature exceeding 35°C. Without further simulation data it is impossible to investigate why the fan will not switch on, but it may be due to a maximum iteration counter in TRNSYS being exceeded.

2. The peak in energy supply from FLARE at 11:00 is smaller than the TRNSYS value but the duct air temperature is approximately the same in both simulations. There are several possible reasons why FLARE predicts lower energy values. A principal reason is the different modelling techniques involved: TRNSYS uses a quasi-steady state model whereas FLARE models the effects of longwave radiaiton exchange, surface absorptivity, surface convective exchange, fluid flow, etc. It is believed that an error may exist in the method FLARE uses to estimate the internal surface heat transfer coefficient

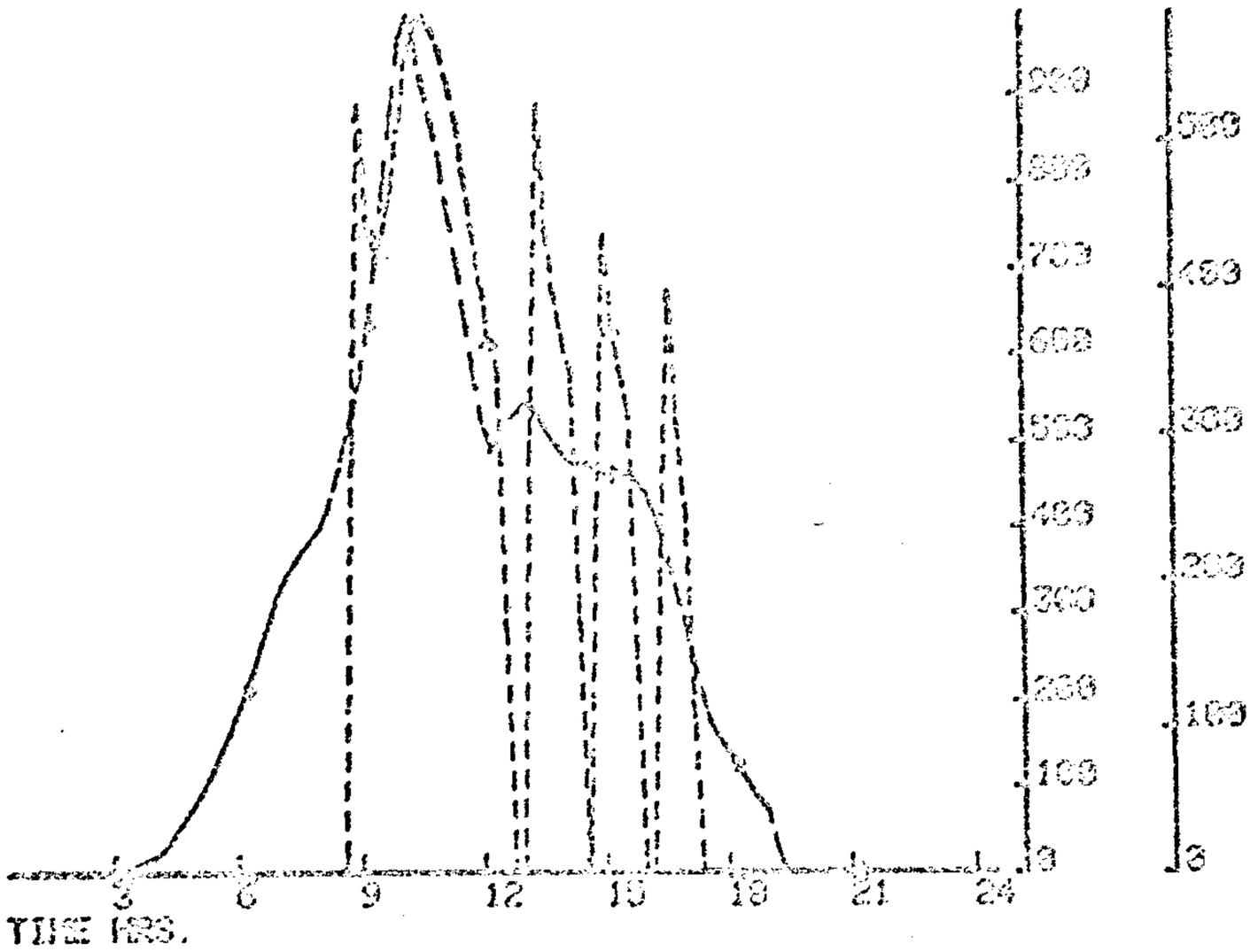

Figure 7.18 Test 1 Collector supply and solar radiation available

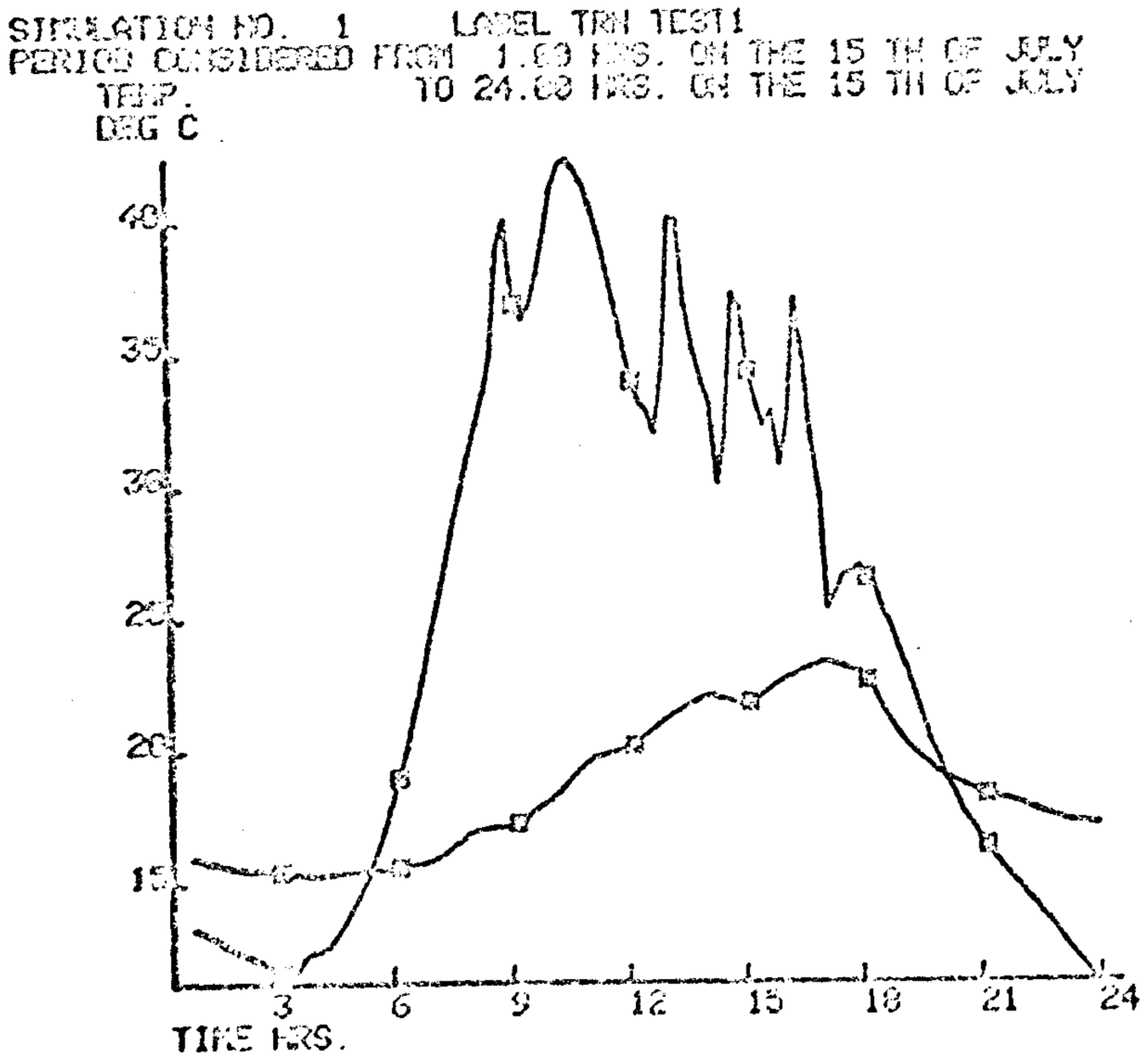

Figure 7.19 Test 1 Collector air duct temperature and external air temperature

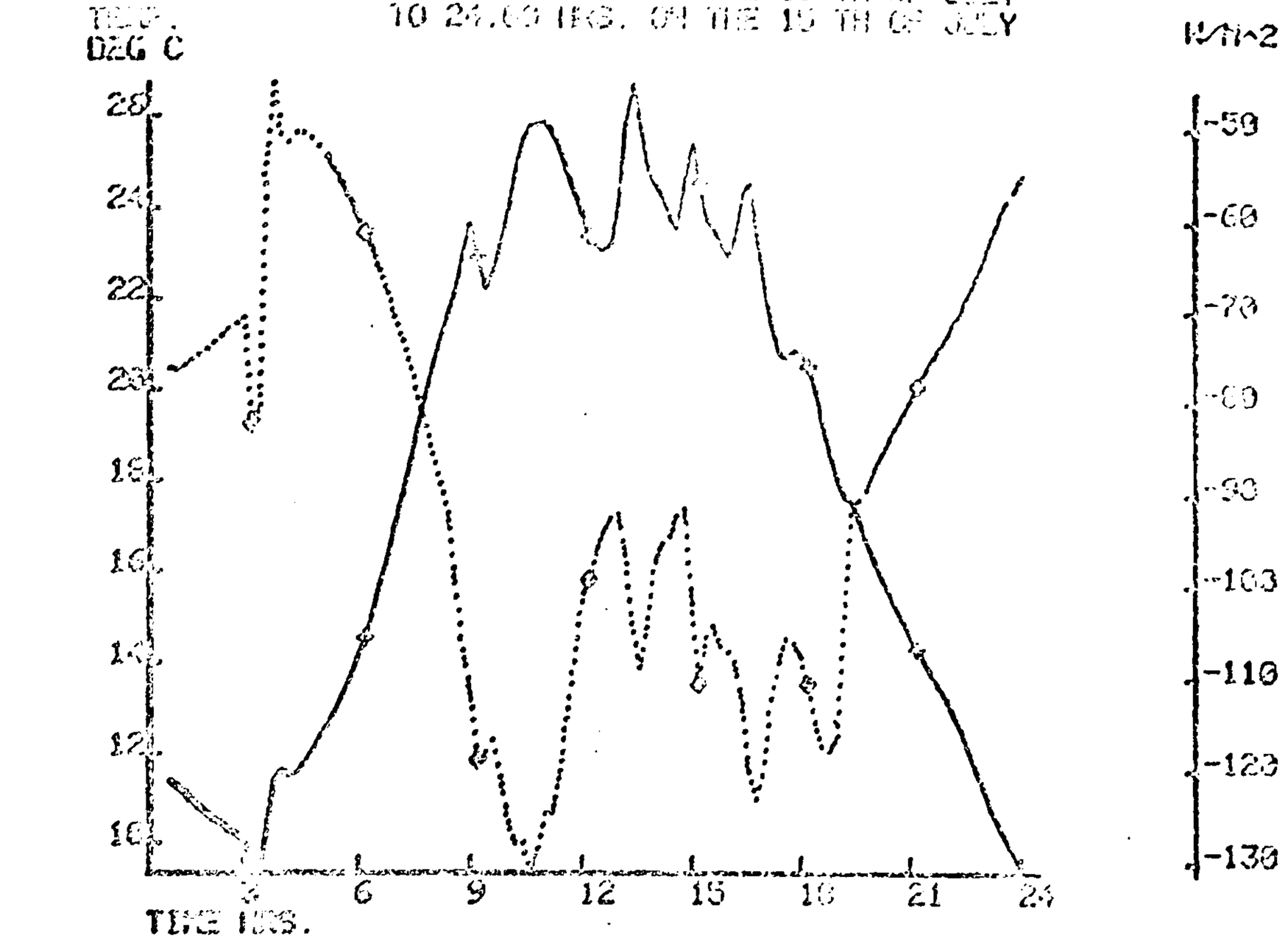

Figure 7.20 Test 1 Temperature of and longwave radiation exchange for collector cover

SYNOPTIC OUTPUT

PERIOD CONSIDERED FROM 1.00 HRS. ON THE 15 TH OF JULY
TO 24.00 HRS. ON THE 15 TH OF JULY
PERCENTAGE LOAD SUPPLIED FROM COLLECTORS = 0.00 %

SOLAR ENERGY SUPPLIED 5.050 KWH
ENERGY REQUIRED 0.000 KWH
AUXILIARY SUPPLIED 0.000 KWH
ENERGY TO STORE 5.050 KWH

QUANTITY OF ENERGY DELIVERED = 14.877 KWH
COLLECTOR EFFICIENCY = 33.945 %

BREAKDOWN OF SOLAR ENERGY SUPPLIED

ENERGY COLLECTED BY AIR = 5.050 KWH
ENERGY COLLECTED BY FLUID = 0.000 KWH
ENERGY COLLECTED BY SOLAR CELLS = 0.000 KWH
5.050 KWH
MAX. PLATE TEMPERATURE = 46.90 DEG. C
MIN. PLATE TEMPERATURE = 12.63 DEG. C

NO CONDENSATION PROBLEMS DURING THIS PERIOD.

Figure 7.21 Test 1 Synoptic output for simulation period

in the turbulent region of fluid flow. This is corroborated by subsequent tests, however, the error does not stop FLARE following the appropriate trends.

3. The effect of fan cycling is clearly seen in the results from FLARE.

Test 2

Figure 7.22 gives the solar irradiance for the simulation period. The comparable results from TRNSYS and FLARE are given in Figures 7.23 and 7.24 respectively. As in the previous test TRNSYS shuts the fan off before it is necessary, however, the results between FLARE and TRNSYS are compatible before this stage. As before FLARE predicts a lower energy supply and a similar duct air temperature.

Test 3

This test was devised to compare the models in winter without the fans operating. Figure 7.25 shows the solar irradiance and Figures 7.26 and 7.27 give the duct air temperatures from TRNSYS and FLARE respectively. Both results are similar expect that the peak temperature from TRNSYS is twice that from FLARE. A possible reason for this is that TRNSYS, being a quasi-steady state model, processes the solar irradiance without due account for other thermal losses.

7.2.2 Comparisons between FLARE and Measured Data

Three steady state tests on flat plate solar collectors were conducted at the University of Strathclyde (109). FLARE operated dynamically against a set of constant climatic to simulate steady state conditions. The results of each test is as follows.

Test 1

A steady state outdoor test was conducted on a rear duct collector, the purpose of which was to generate an instantaneous efficiency expression

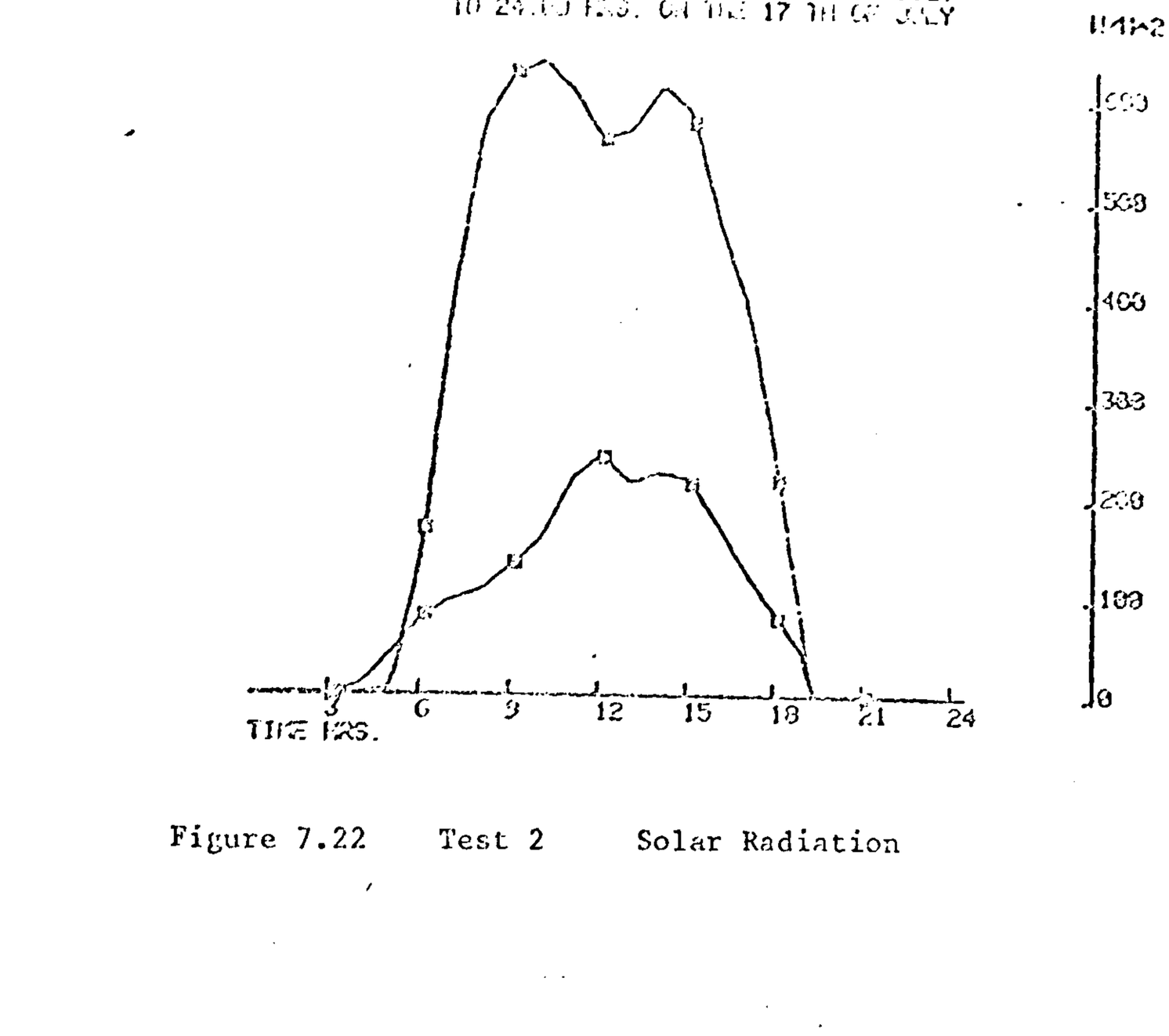

Figure 7.22 Test 2 Solar Radiation

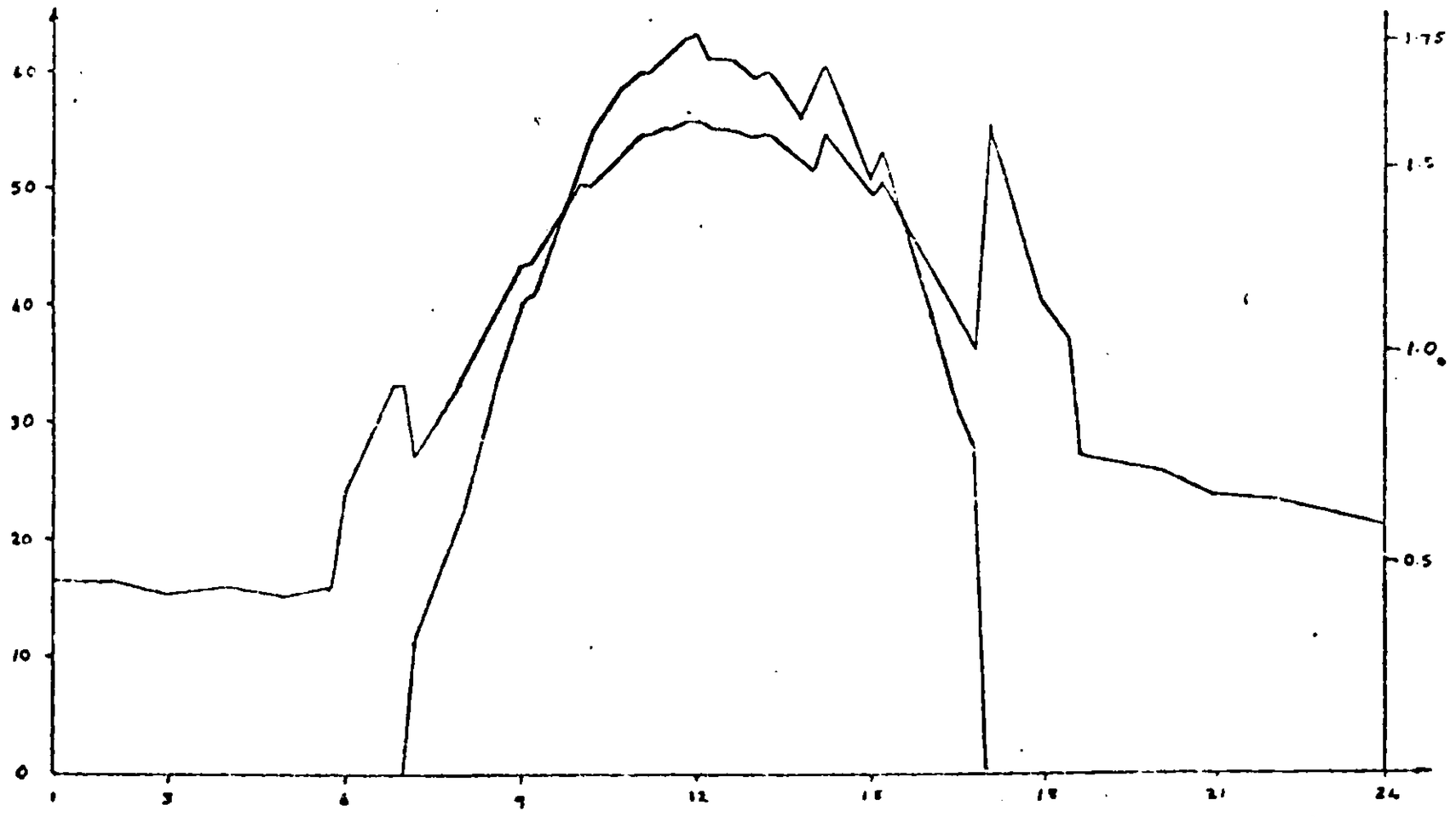

Figure 7.23 Test 2 TRNSYS simulation results

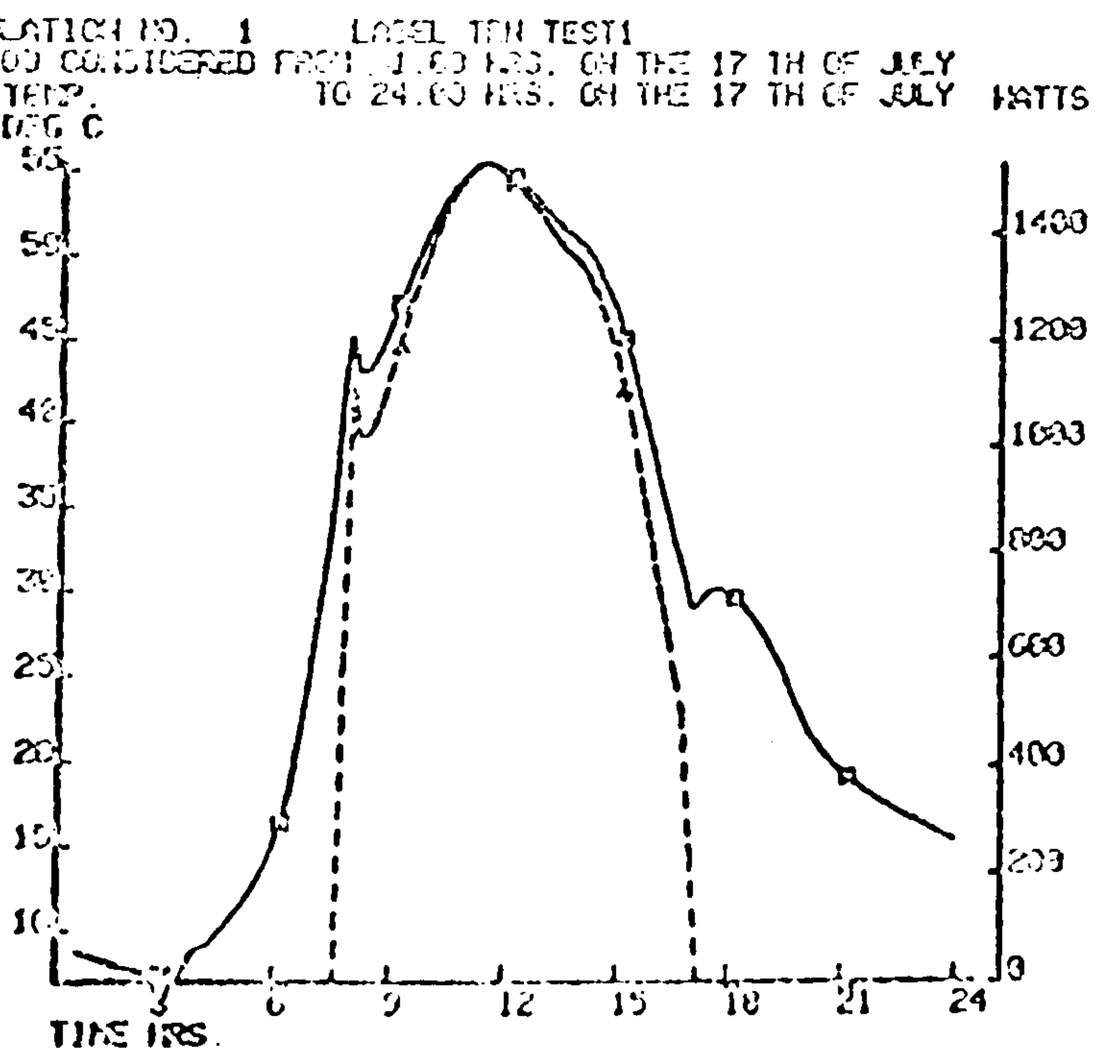

Test 2 FLARE simulation results

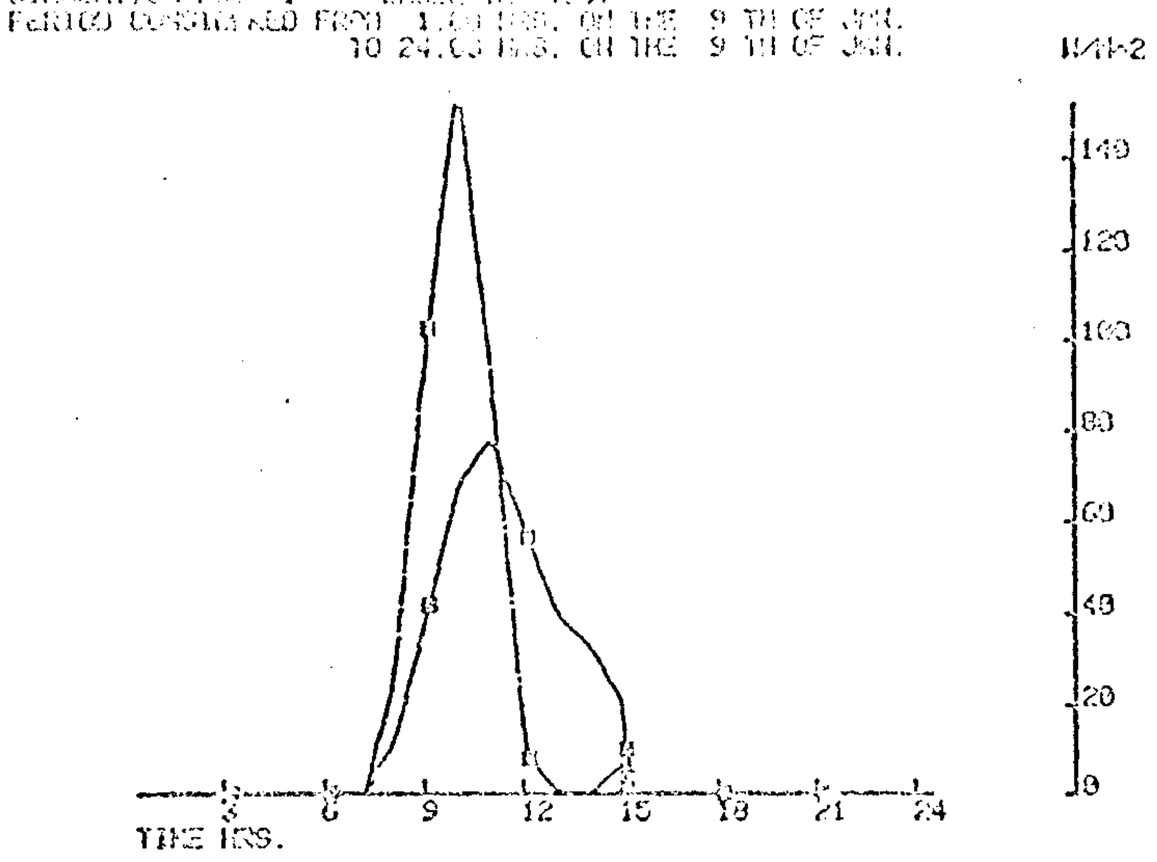

Figure 7.25 Test 3 Solar radiation

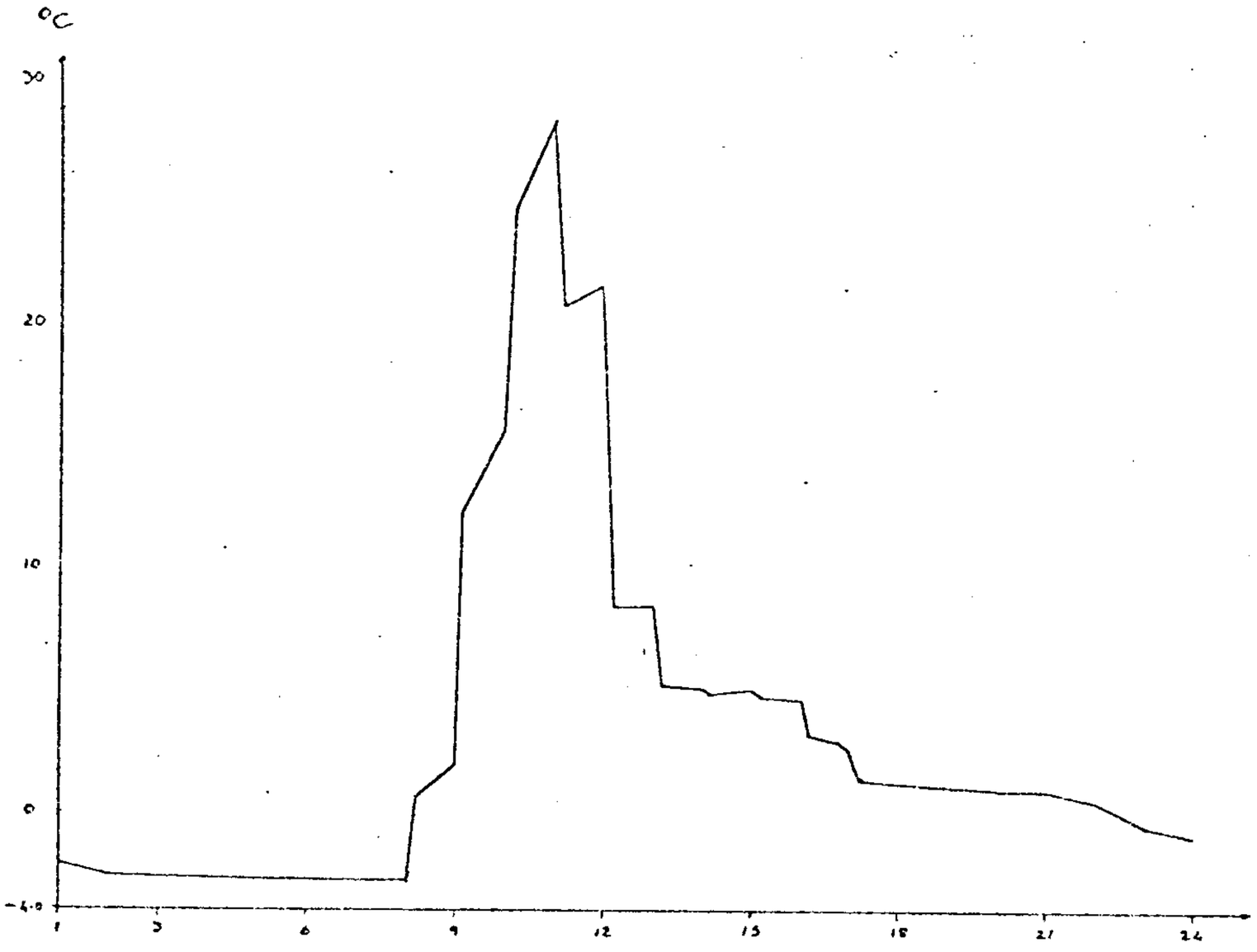

Figure 7.26 Test 3 TRNSYS simulation results

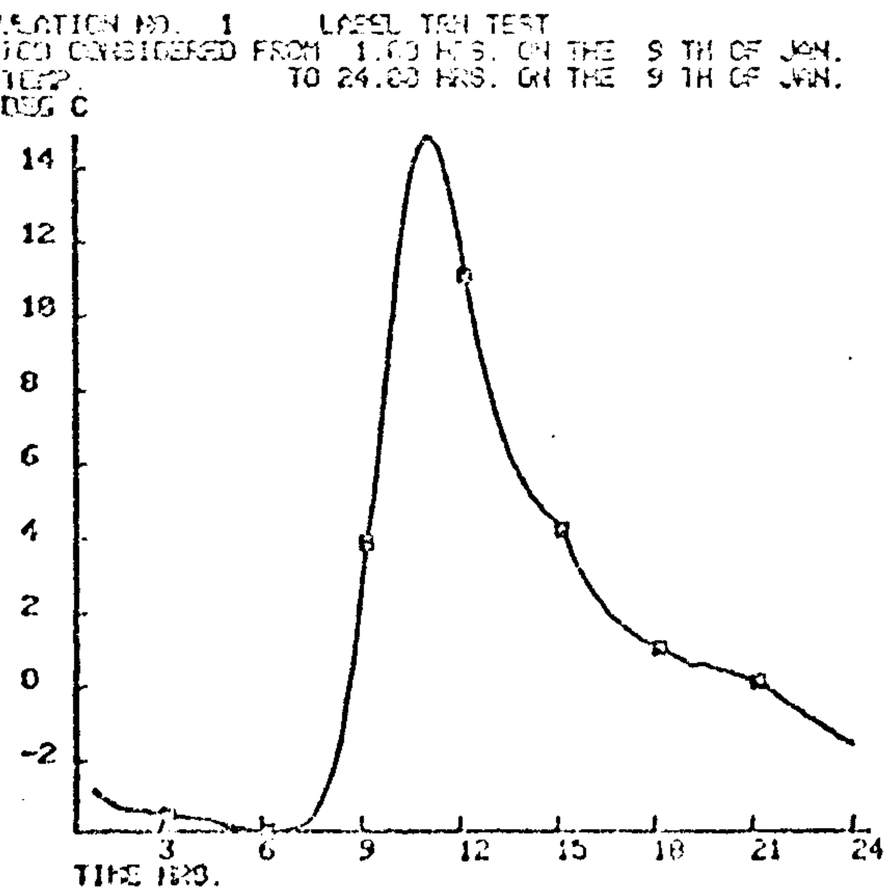

Figure 7.27 Test 3 FLARE simulation results

for the collector, the result of which is given by:

$$\eta_i = 0.425 - \frac{4.43(\theta_{f,i} - \theta_a)}{G_T}$$

where η_i = instantaneous efficiency

$\theta_{f,i}$ = inlet air temperature

θ_a = ambient air temperature

G_T = global irradiance

The expression is drawn and shown in Figure 7.28 along with the results of the FLARE simulations. Comparing the results, it is apparent that FLARE predicts the model to be slightly less efficient and to have a much lower rate of thermal losses to the environment. This result could be due to the method used to model this test as the inlet temperature was progressively increased while all other variables were held constant. However, it is more likely that assumptions for some of the data in the model were incorrect. The lower efficiency is probably due to the surface convective heat transfer coefficient, the lower heat loss could be due to an underestimation in the external long-wave radiation effects.

TEST 2

This test involved conducting a steady state analysis of a rear duct collector indoors under Tungsten lamps while varying the air flow rate. This experiment was conducted for different types of air entrance and exit orifaces. (At present FLARE operates independently of entrance and exit orifaces). The range of results of these experiments for a lower duct 15mm deep and an upper duct 30mm deep are given in Figure 7.29 which also contains the results from the FLARE simulations. Although the FLARE results follow the trend they are considerably lower than the measured results. This could be partially due to the spectrum of the Tungsten lamps not being modelled and the solar spectrum used by default, but again the convective heat transfer coefficients are the likely cause.

Test 3

This test is similar to the previous test, the only difference is that

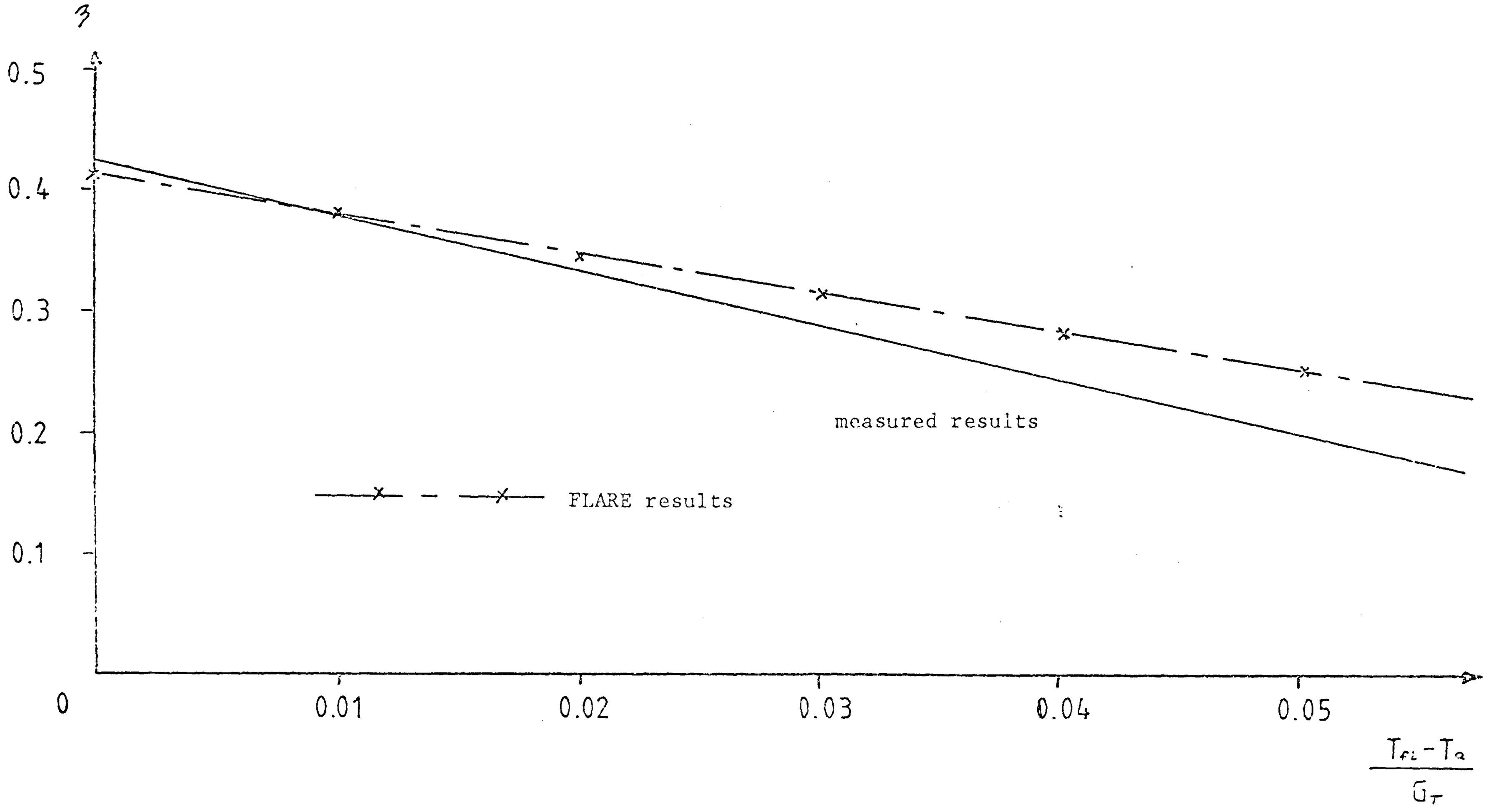

Figure 7.28 Test 1 Results of FLARE against measured data

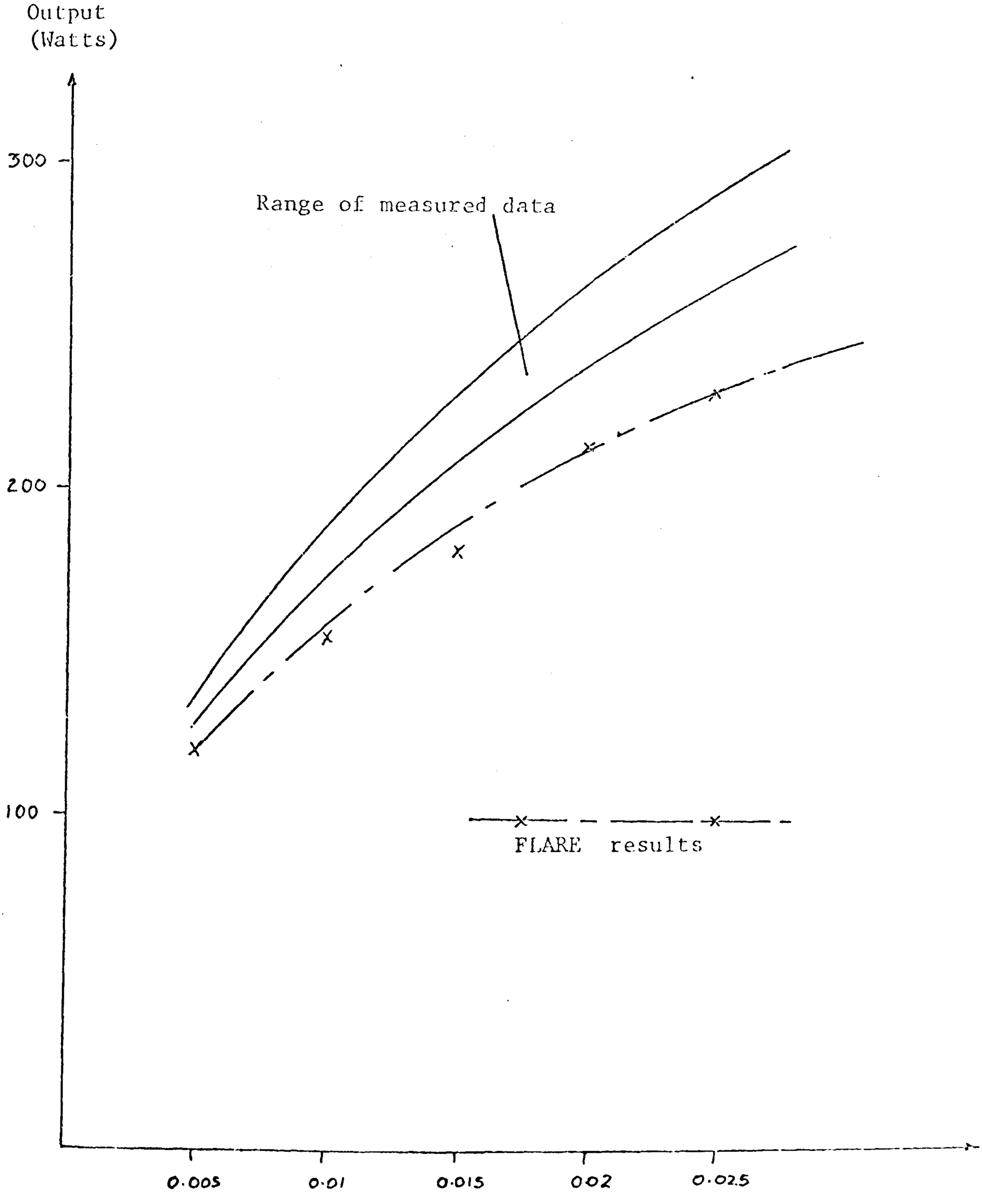

Figure 7.29 Test 2 - FLARE V's measured results

the lower duct is 30mm and the upper duct is 15mm. The measured results and the simulated results are shown in Figure 7.30. This collector is associated with lower velocities in the lower duct (i.e. the duct through which the air passes), therefore, the Reynolds number will be lower and the turbulent effects will be smaller. At the lowest velocities FLARE predicts reasonably close results, however, as the velocity increases the results of FLARE tend to diverge at an increasing rate from the measured results. This indicates that the internal surface convective heat transfer coefficients become less accurate as Reynolds Number increases. Obviously these coefficients require further investigation.

7.2.3 Conclusions of Validation

The comparative tests given above are merely to show the FLARE is generating results that are reasonably acceptable. This does not imply the program is fully valid since the program has still to undergo detailed testing. However, several aspects can be investigated in light of these tests, for example, the effects of entrance and exit orifices in air collectors must be considered and the convective heat transfer coefficients at higher Reynolds numbers must be tested.

Only an air collector was tested because there was no measured data available for liquid or photovoltaic collectors, or any of the hybrid collector designs.

Extensive physical modelling of an air, liquid and photovoltaic system will be required for more complete versions of FLARE. The physical tests should be conducted over a considerable period (a summer and winter season) and readings should be taken throughout the system at points corresponding to nodes in the FLARE model allowing the simulated results to be compared directly. This project would require considerable resources and therefore these tests should be conducted in conjunction with other research establishments. The system may be subsequently compromised to suit all concerned.

As computer programs become more complex, the role of validation will

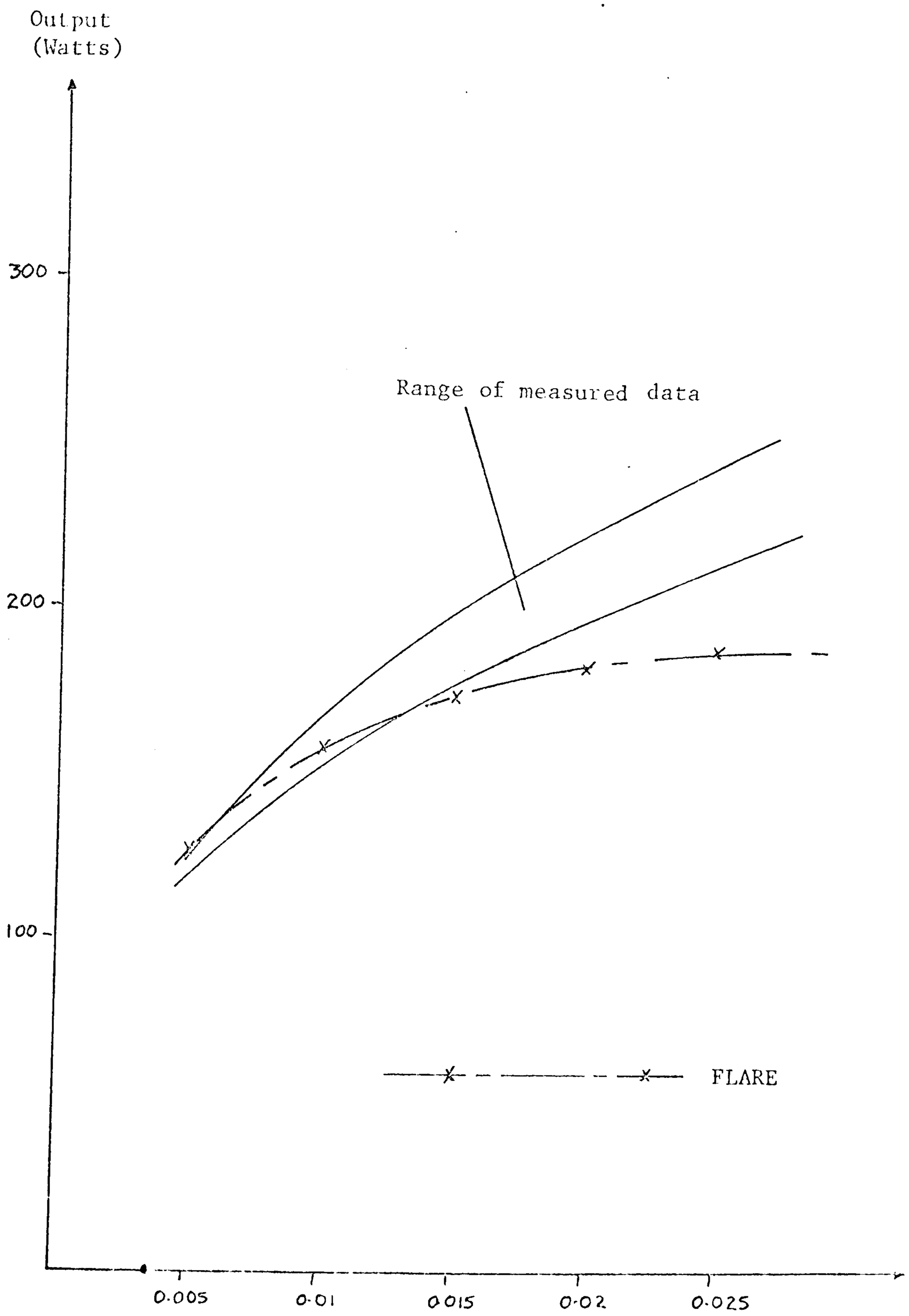

Test 3 - FLARE V's measured results

become increasingly more important because these programs will not be used with confidence unless extensively tested. Therefore a more rational and unified approach to the validation of detailed simulation models such as BLAST, DEROB, DOE3, ESP, FLARE, TRNSYS, etc, is required. The International Energy Agency is currently promoting a number of programmes in which detailed simulation models are tested against measured data: Annex 1 on inter-program comparison (110), (111); Annex 2 a program comparison with real buildings (112); Annex 3 a systems program comparison. Currently the Science and Engineering Research Council's Specially Promoted Programme is encouraging a research effort in the area of dynamic energy model validation. Any funded work will, however, be concerned with underlying theoretical basis and comparisons using existing data rather than large scale building instrumentation as in the IEA Annex 4 project.

7.3 Cost of Operating FLARE

In order to assess the cost of a FLARE simulation a similar exercise has been conducted for TRNSYS so that a comparison can be made. Data preparation is assumed to be completed prior to the simulation. It is believed that by using the FLARE Input Management Program data will be prepared more quickly than data for TRNSYS without the aid of the TRNSYS Input Management Program. Table 7.5 details the cost at full commercial rates of simulating, using either FLARE or TRNSYS, the collector detailed in Section 7.2.1 for one day at time steps of 12 minutes. The connect time for TRNSYS is slightly larger because it does not create solution files but prints out the results, whereas FLARE stores the results in a solution file for subsequent interrogation. A FLARE simulation costs more than double a TRNSYS simulation: however, TRNSYS generates the collector air temperature, energy supplied and overall 'U' value. For double the cost FLARE will generate:

- the collector air temperature
- the collector outlet and inlet temperature
- the temperature of each internal collector surface
- the temperature of each external collector surface
- the energy supplied from collector array
- the energy supplied from individual collector
- the irradiance falling on each internal collector surface
- the irradiance falling on each external collector surface
- the energy exchange due to precipitation on each external surface
- the energy exchange due to longwave radiation at each external surface
- the operational status of the fan

Obviously, the additional data available from FLARE can only serve to aid the designer/user. It is the user's choice as to whether the increased cost is worthwhile. It must be pointed out however that in several years the cost of computing will have reduced considerably and a cost comparison between programs will have much less significance.

	TRNSYS	FLARE
Connect time (min:sec)	03:43	02:15
Runtime (cpu seconds)	0:00:05	0:00:10
Kilocore seconds	206	522
Disc reads (blocks)	753	1660
Disc writes (blocks)	93	942
Computer Resource Units*	0.023	0.052
Approximate cost	£2.50	£5.72

Table 7.5 Interactive simulation on DEC10: details of TRNSYS and FLARE simulating one day's data at a 12 minute time interval.

* A Computer Resource Unit is a weighted sum of the basic resources above

The cost of using FLARE on a consultancy basis would depend on the information required. As an example consider the cost of a detailed comparative design project using FLARE where three collectors are modelled for three different control strategies conducted at 12 minute time intervals for the months January and July. Based on the results of Table 7.5 for a system day simulation at 12 minute time intervals the total simulation cost would be in the region of £2750. Data preparation, output interrogation and labour costs could easily approach a further £2000 for a detailed approach. Considerable savings could be made on simulation expense if a more crude time interval was selected. For example, using one hour time increments the simulation costs for the above simulation are reduced by a factor of 5 to a cost of ~ £600, labour costs etc will also be reduced but not to the same degree.

CHAPTER 8 Conclusions

The world's energy requirements are being met principally by oil and gas, both of which are finite resources that will be exhausted within the next 50 years, at present consumption. The time scale involved to the exhaustion point of oil and gas resources is irrelevant, it is selfish to assume that this is not an immediate problem because inevitably these fuels will be exhausted. Obviously as oil and gas are depleted their cost will soar; as prices increase there will be a changeover to using more coal, nuclear fission power and 'renewable' energy sources. The changeover must be as smooth as possible because if the rate of depletion exceeds the rate of changeover society will suffer due to a rapid reduction in the standard of living.

Energy conservation techniques and passive solar building designs can considerably extend the lifetime of oil and gas by reducing demand, thereby allowing more time to effect the changeover to other energy sources. Recent trends have been for Governments to promote energy conservation techniques by awarding financial inducements for energy conservation techniques to be implemented. Energy conservation will not solve the longterm problem, therefore, major industrialised nations are hoping for a breakthrough in nuclear energy generation. Nuclear energy was once seen as a panacea to the world's energy needs. While this can be said for fusion power, the present method - fission power - has not yet achieved its conceived potential despite massive investment. It takes about 8-10 years to build a nuclear power station and at the present rate of production only 15% of the UK's primary energy requirements will be met by nuclear energy in 2000AD. The disposal of waste from nuclear power stations is a highly controversial issue which must be resolved by the International Atomic Energy Authorities before the problem becomes more serious.

Worldwide coal reserves are large compared to the oil and gas reserves, however, the direct replacement of oil and gas by coal is impractical in many applications. Consequently, oil and gas can be processed from coal but this process reduces energy utilisation because of conversion

inefficiencies (similar to electricity generated by coal). Coal is becoming increasingly more expensive to mine and like all fossil fuels it is both a thermal and an environmental polluter.

Although neither nuclear power or coal cannot be excluded as replacements for oil and gas, until the problems associated with their use have been resolved governments should vigorously promote clean 'renewable' energy sources derived from the sun, such as direct solar energy collection, wind power, biomass, etc. The current trend has been for governments to promote research into the potential for utilisation and methods of solving the numerous technical problems involved in utilising these energy sources. Before the end of the decade most technical problems will have been overcome and renewable energy sources will start to make an impact on the world energy demand.

One area where there is a considerable potential for using a renewable energy source is in the active collection of solar energy to meet the various energy demands in buildings. For example, domestic hot water supply, space heating, electrical power supply and solar cooling. In the UK, by the beginning of the next century, at least 5% of present primary energy requirements could be supplied by solar collectors with the minimum of land usage. In other countries the solar contribution could be much greater. Due to the potential of active solar collection this thesis is concerned with the development of a rigorous and flexible flat plate solar energy collection system simulation model. The model allows a detailed interrogation of each individual system component as well as the interaction between components. At present this model will be used primarily as a research and development tool, or for the design of large solar energy collection installations.

A flat plate collector was selected for modelling because it is the most applicable collector type for the British climate, which has a high diffuse solar radiation content. However, the model is also applicable to concentrating solar collectors and other solar designs (see Chapter7). In Chapter 2 a description of the principles behind both photothermal and photovoltaic flat plate collectors is given. These collectors can be associated with the aforementioned building systems, therefore

the basic components of any solar energy system were identified for subsequent modelling. These were the storage unit, the auxiliary source, the distribution system and the control system.

The mathematical model developed to subsequently analyse a solar energy system comprises most of the principles of solar energy systems outlined in Chapter 2. Because this model analyses the energy flow processes in a solar system in detail, it is at the opposite end of the modelling spectrum to simple models such as the F-Chart (Chapter 4). Simple models offer no real flexibility and can give very inaccurate results if misapplied because of the lack of other cause and effect results as would be available from simulation models. Consequently, due to more rigorous design demands simple models are gradually being replaced as a design tool by simulation models.

Two approaches to systems modelling were identified in Chapter 4 - the module approach and the simultaneous approach. The modular approach is the traditional method of operating a simulation model. Each component in the system is treated as a 'black box' which processes a series of inputs by any method to obtain a number of outputs, which in turn become inputs for subsequent components to be modelled. Although it is possible to assemble a systems model which has detailed component models and is highly informative, by its very nature, the modular approach can only approximate component interaction by means of iteration. This has the secondary effect of making it more difficult to model complex control strategies accurately.

The mathematical model developed in this thesis uses the simultaneous approach allowing the component interactions to be solved simultaneously. As each system component is modelled by means of a rigorous implicit numerical approximation requiring simultaneous solution then the complete system is solved using matrix algebra. Proprietary matrix handling techniques are employed to reduce the computation time requirement. Because the model is based on an implicit technique it is stable for all time increments, although its accuracy will improve with shorter time increments.

A prototype simulation program called FLARE has been developed to test

and validate the mathematical model proposed in Chapters 5 and 6. Validation of any model is a continuous ongoing project. However, the concept of model validity should not be considered as a simple decision on whether the model is absolutely valid or absolutely invalid. A model can be considered valid over a wide range of applications where the user may consider the model's results to indicate a trend rather than the exact result. From comparative tests with simple data (Chapter 7) the FLARE prototype model appears to follow the appropriate trends. The data available was insufficient to perform a full validation and a more detailed study is required.

In the future the simulation model will be expanded to include other solar energy system related components such as heat pumps, solar concentrators etc. To reinforce the connection with ESP a simulation connection will be invoked to allow the dynamics of interaction between the system and the building envelope to be modelled. In addition the model will be connected to hot water or space heating plant models which use the simultaneous approach. This would require radiators, air handling units, etc to be modelled. At present several plant models are under development at ABACUS. The interconnection between these plant models and ESP is a prime objective.

The FLARE simulation program is only a module in a suite of inter-relating computer programs which have been developed to enhance the simulation module. The complete suite of programs are discussed in Chapter 7 and they are know collectively as the FLARE system. Each program module of the FLARE system operates through high level interactive graphic facilities and are controlled by the user.

The FLARE system consists of three distinct areas: data preparation, simulation and interrogation. There are a number of optional modules for data preparation that allow the user to make design decisions prior to simulation. For example, the most suitable collector cover, the best site for the collector, the best position of the planar reflector, etc. Consequently, the number of simulations required may be reduced by this simple design process.

The simulation module is 'driven' by means of any measured or predicted prime climatic data set. The trend has been towards the use of a standard design year or Test Reference Year (TRY) for energy calculations providing a means of comparing different solar energy systems by 'enforcing' simulations to be conducted against the same climatic influences. However, much work remains to be carried out to determine the parameters with which to select the TRY data. The simulation period can be set between a single day and a year, and the time step can be set at any value up to a maximum of one hour. Consequently for very detailed analyses of the solar system very small time steps can be invoked, this will be extremely useful in analysing component interactions and control strategy.

The results of a simulation can be stored for an indefinite period for subsequent interrogation at leisure. The simulation program generates more information then is available from the most sophisticated physical model. Three types of presentation of simulation results are available: synoptic, graphical and total. Synoptic output allows a quick appraisal of the systems performance, graphical output permits the construction of graphs in an attempt to identify the cause and effect relationships and total output indicates the daily status of various system parameters. All outputs are controlled by an interactive menu facility.

The principal advantage of rigorous simulation models such as FLARE is the speed with which a considerable quantity of design information can be obtained compared with physical models. Consequently, FLARE will cost considerably less than a detailed physical model and the results will be obtained in seconds rather than weeks. Therefore, FLARE is an attractive research and design tool for subsequent use by manufacturers, research establishments or by large design practices with their own computing facilities, all of whom may require outright ownership of the model. As computing power increases, FLARE will be mounted onto mini-micros allowing smaller design offices to obtain the model. Due to increasing computer power, the computation cost will reduce subsequently lowering the cost of operating the model.

An alternative to outright ownership of FLARE is to use the model on a consultative basis by a central government funded agency. This agency could provide an information service to the public on methods of promoting energy conservation and 'renewable' energy utilisation. Consequently, design practices and domestic users could operate FLARE through the agency.

To summarise, a period of intensive research is required to identify and correct problems associated with full scale development of solar energy collection devices. To aid this process a detailed dynamic representation of the performance of solar energy systems will be more useful than models based on general assumptions. Systems modelling is a very complex problem due to the interaction of system components, therefore, it is important to accurately model system response to any energy input or load demands. Such a model will lift the dependence on quasi-steady state coefficients to determine solar energy component and system performance, and be less prone to restrictive assumptions which could impair the performance of the system. Although the role of the model is to perform dynamic analysis of the system it can more or less be used for optimising and steady state testing. Interestingly, because this model is an attempt to approximate reality, it is far more suited to the optimisation role or to perform steady state testing than other less detailed models.

The cost of operating simulation models will decrease rapidly over the next few years, whereas the cost of physical modelling will rise sharply. Furthermore, the use of the simple model in the design role will decrease, as more detailed information will be required. Detailed dynamic simulation models will offer the designer, manufacturer and researcher an accurate and informative aid to understand system performance and so, it is to be hoped, encourage more robust and effective design solutions.

PAGE

APPENDICES

APPENDIX 1 Sun Position and Angle of Incidence

At any position on the earth if the sun is above the horizon then its position in the sky is given by the solar altitude, α , and the solar azimuth, γ . The value of the solar altitude and azimuth depend upon the solar declination, the site latitude and the local solar or apparent time.

The solar declination (δ) is the angular displacement of the sun from the plane of the earth's equator. Because the axis of the earth is tilted at an angle of about $23\frac{1}{2}^{o}$ to the axis of the plane in which it orbits the sun, the value of declination will vary throughout the year between $+23\frac{1}{2}^{o}$ to $-23\frac{1}{2}^{o}$. If a section is taken through the earth's orbit around the sun at two positions, one on midwinters day the other on midsummers day in the northern hemisphere, the concept of declination is seen more clearly (Figure 1). The following empirical equation is recommended for calculation of the declination angle, δ , (18).

$$\delta = 23.45 \ \mathrm{Sin}\left[\frac{(N-80)}{370} * 360\right] \qquad (1)$$

where N is the year day number

Local Apparent Time (LAT) is not the same as "clock" time. LAT is based on the principle that the solar altitude is greatest at noon, similar to a sundial. However, it was considered more convenient to create time zones wherein time is uniform. The time within a time zone is called the Local Mean Time (LMT), the UK time zone is known colloquially as Greenwich Mean Time (GMT). LAT can be converted to LMT by using two corrections, one representing the equation of time, the other representing the longitudinal differences between the site and the reference site of the time zone.

$$LMT = LAT - E - (Lst - Ls)/15 \qquad (2)$$

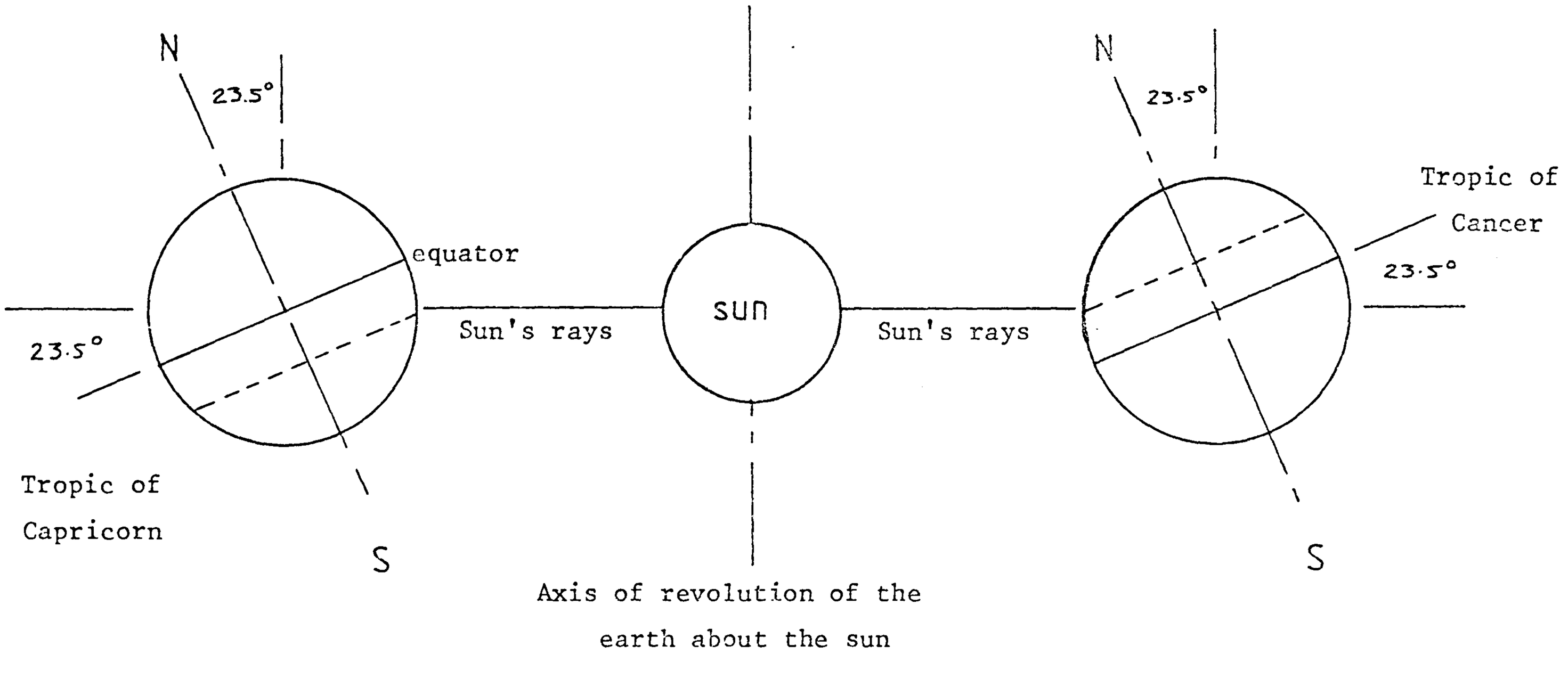

Figure 1 Position of the earth relative to the sun on midwinters and midsummers day (in the northern hemisphere). Declination = $\pm 23\frac{1}{2}$

where, Lst requires the longitude of the reference meridian for the time zone and Ls represents the longitude of the site. The equation of time (E), is the difference between the theoretically day length (24 hours) and the actual day length, which varies slightly with time of year. Rodgers (45) quotes

$$E = \frac{1}{60}\left(0.00037 + \sum_{i=1}^{3}\left(\alpha i \mathrm{COS}(iJ) + bi\ \mathrm{SIN}(iJ)\right)\right) \qquad (3)$$

where J = 360 x N/365.25. The values of αi and bi are given in Table 1.

The solar altitude, α, is the angle between the beam from the sun and the horizontal (Figure 2). It is the complement of the zenith angle, $\not{z}$:

$$\alpha = 90 - \not{z} \qquad (4)$$

An expression solving the value of α can be established by means of trigonometrical relationships (79)

$$\alpha = \mathrm{ARCSIN}\ (\mathrm{SIN}\ \delta\ \mathrm{SIN}\ \phi + \mathrm{COS}\delta\ \mathrm{COS}\omega\ \mathrm{COS}\phi\ ) \qquad (5)$$

where ϕ is the latitude of the site (degrees) and ω is the hour angle, defined as the angular displacement of the sun from solar noon (LAT), i.e.

$$\omega = \frac{360 * T}{15} \qquad (6)$$

consequently, 1 hour corresponds to 15^{o} of angular displacement. The symbol T represents the time in hours from solar noon with mornings positive and afternoons negative.

The Azimuth of the sun, γ, is the angle between the horizontal component of a direct ray from the sun and the true south in the northern hemisphere. It is illustrated in Figure 2. The solar azimuth is measured in degrees of angular displacement and it may be expressed in one of two modes:

i	Ai	bi
1	0.43177	-7.3764
2	-3.1650	-9.3893
3	0.07272	-0.24498

TABLE 1 Coefficients for Equation of Time (Eq 3)

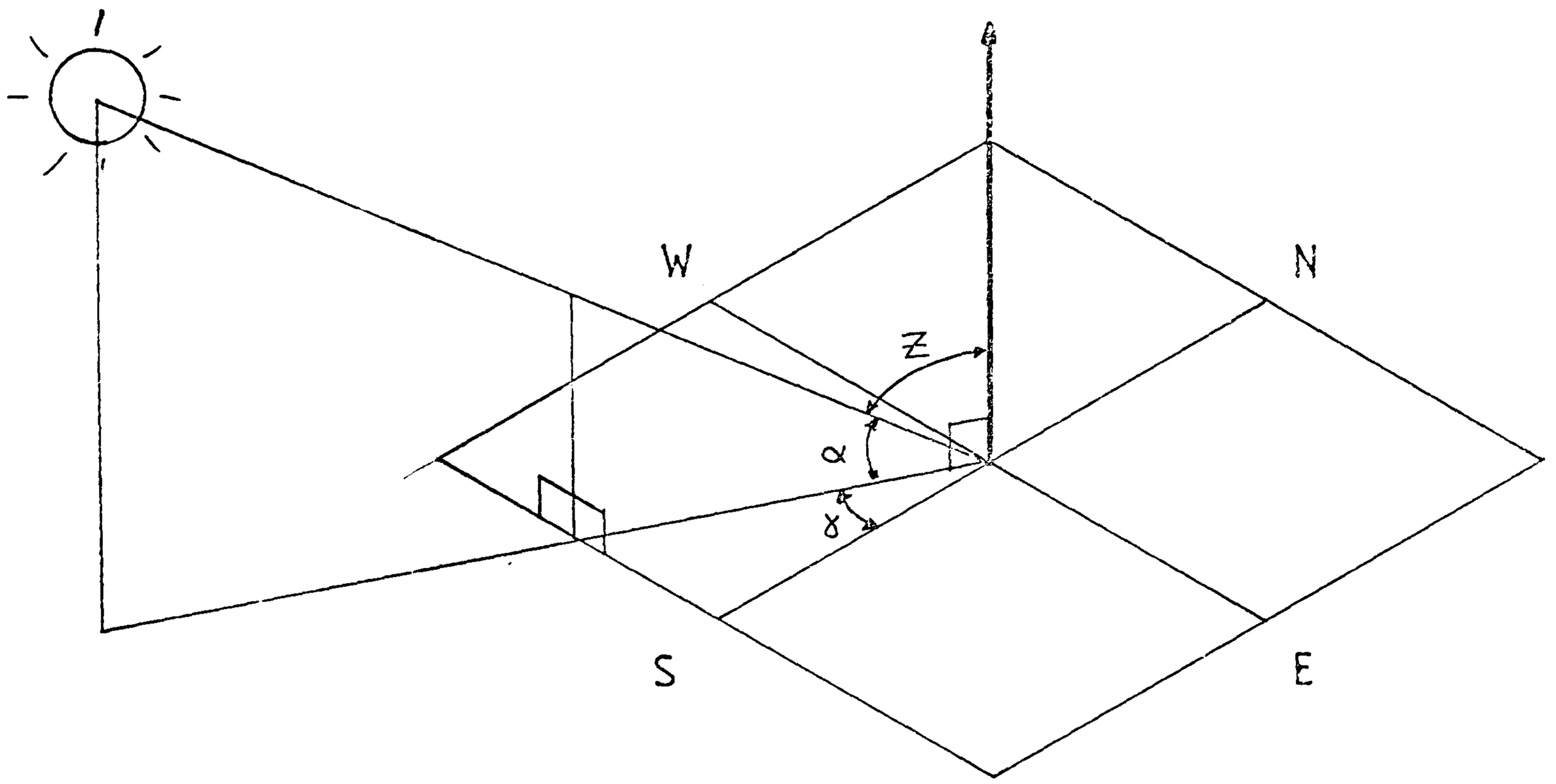

Figure 2 Solar zenith angle Z, altitude α, and azimuth γ shown in their relationship to a horizontal flat surface on the earth's surface

(a) east and west of due south, where south is 0^{o};

(b) a continuous angular displacement through 360^{o} from north.

It has been established using trigonometry (45) that

$$\gamma = \text{ARCTAN}\left(\frac{\text{SIN}\,\omega}{\text{SIN}\,\phi\,\text{COS}\,\omega - \text{COS}\,\phi\,\text{TAN}\,\delta}\right) \qquad (7)$$

an alternative expression is

$$\gamma = -\text{ARCSIN}\left(\frac{\text{SIN}\,\omega\,\text{COS}\,\delta}{\text{COS}\,\alpha}\right) \qquad (8)$$

Both of these expressions are identical with $-90 \leq \gamma \leq +90^{o}$, but it is simple to convert the solar azimuthal angle from one mode of expression to the other.

The times of sunrise and sunset in Local Apparent Time can be obtained by setting the solar altitude in equation (5) to zero. Rearranging gives

$$\text{COS}\,\omega_{sr} = -\frac{\text{SIN}\,\delta\,\text{SIN}\,\phi}{\text{COS}\,\delta\,\text{COS}\,\phi} = -\text{TAN}\,\delta\,\text{TAN}\,\phi \qquad (9)$$

This equation may be solved for ω if $-1 \leq -\text{TAN}\,\delta\,\text{TAN}\,\phi < +1$, then

$$\omega_{sr} = \text{ARCCOS}(-\text{TAN}\,\delta\,\text{TAN}\,\phi) = \omega_{ss} \qquad (10)$$

In LAT the solution for sunrise occurs at

$$T_{sr} = 12 - (\omega_{sr}/15) \quad \text{(hours)} \qquad (11)$$

and sunset at

$$T_{ss} = 12 + (\omega_{ss}/15) \quad \text{(hours)} \qquad (12)$$

If the value of $-\text{TAN}\,\delta\,\text{TAN}\,\phi$ is greater than +1, then Polar Night occurs (i.e. 24 hours of darkness) and if the value is less than -1 then Polar Day occurs with the sun always above the horizon.

The solar daylength, T_D, between the extremes of Polar Day and Polar Night is equal to the time between sunrise and sunset, therefore:

$$T_D = \frac{2}{15}\omega_{sr} \tag{13}$$

The azimuth of the sun at sunrise and sunset can be found by substituting ω_{sr} and ω_{ss} into equation (7) or (8).

The angle of incidence, θ , of beam radiation is the angle measured between the incident beam and the normal to the surface. Using the geometrical relationships between position of the sun and a surface tilted at any angle it has been shown (79) that

$$\cos\theta = \sin\alpha \cos\beta - \sin\beta \cos\alpha \cos(\gamma - \lambda) \tag{14}$$

where β = tilt angle of surface
λ = orientation of surface

Substitution into equation (14) for solar altitude and azimuth, then the expression for the angle of incidence becomes,

$$\cos = f(\delta, \omega, \phi, \lambda, \beta) \tag{15}$$

which can be re-expressed as

$$\cos\phi = C_1 \sin\delta + C_2 \cos\delta\cos\omega + \sin\lambda \sin\beta \cos\delta \sin\omega \tag{16}$$

where $C_1 = \sin\phi \cos\beta - \cos\phi \sin\beta \cos\lambda$
$C_2 = \cos\phi \cos\beta + \sin\phi \sin\beta \cos\lambda$

APPENDIX 2 Psychrometric Properties of Air

If atmospheric air is assumed to behave as an ideal gas mixture, then at standard atmospheric barometric pressure (1.01325 bar), several psychrometric properties can be found if two are known. In FLARE both the dry bulb temperature, θdb, and the absolute or relative humidity, ϕ, are known.

The relative humidity is the ratio of the partial pressure of the water vapour in moist air at a given temperature, θdb, to the partial pressure of the water vapour in saturated air, at the same temperature.

Therefore

$$\phi = \frac{100 p_s}{p_s} \qquad (1)$$

where

p_s = partial vapour pressure (bar)

p_{ss} = saturated vapour pressure (bar)

The saturated vapour pressure may be calculated, the expression used depends upon air temperature.

If θdb $< 0^{\circ}$C use

$$p_{ss} = 0.001 * \text{ALOG}\left(10.5380997 - \frac{2663.91}{273.15 + \theta\,\text{db}}\right) \qquad (2a)$$

and if θdb $\geq 0^{\circ}$C use

$$p_{ss} = \text{ALOG}\Big(28.59051 - 8.2\ \log\ (\theta\,\text{db} + 273.16) + 0.0024804\ (\theta\,\text{db} + 273.16) - \frac{3142.31}{(\theta\,\text{db} + 273.16)}\Big) \qquad (2b)$$

Evaluating p_{ss} and rearranging equation (1) allows the value of the partial vapour pressure to be found.

The dew point temperature, θdew, is defined as the temperature of

saturated air which has the same partial vapour pressure as the moist air under consideration. An empirical formula estimates the dew point temperature from the value of partial vapour pressure is given by ASHRAE (80):

$$\theta_{dew} = 79.047 + 30.579 \ln(p_s) + 1.8893 (\ln(p_s))^2 \qquad (3)$$

where

θ_{dew} is in ^{o}F and p_{ss} is measured in inches mercury.
Converting equation (3) from imperial to metric equates to

$$\theta_{dew} = 95.678 + 24.095 \ln(p_s) + 1.0496 (\ln(p_s))^2 \qquad (4)$$

where

θ_{dew} is in ^{o}C and p_s is in bar.

The mass of water vapour associated with unit mass of dry air is called the moisture content, g. The moisture content can be found from the expression

$$g = 0.622 \frac{p_s}{p_{at} - p_s} \qquad (5)$$

where g is measured in Kg/Kg dry air. Once the moisture content has been established, the specific enthalpy of the moist air can be estimated by adding the enthalpy per unit mass of dry air and the enthalpy of the associated water vapour:

$$h = h_a + g h_g \qquad (6)$$

where

h = specific enthalpy (KJ/Kg)

h_a = enthalpy of dry air (KJ/Kg)

h_g = enthalpy of water vapour (KJ/Kg)

The values of h_a and h_g are best taken from tables, however, approximate equations have been established to evaluate h_a and h_g:

for $0^{\circ}C \leq db \leq 60^{\circ}C$; $h_a = 1.007\,\theta db - 0.026$ (7)

for $-10^{\circ}C \leq db < 0^{\circ}C$; $h_a = 1.005\,\theta db$ (8)

and $h_g = 2500.8 + 1.84 - \theta db$ (9)

These equations can be used to solve equation (6).

The partial vapour pressure can also be estimated if the wet-bulb temperature, θwb, is known.

$$p_s = p_{ss} - p_{at}\, A\, (\theta db - \theta wb) \quad (10)$$

where

p_{ss} = saturation vapour pressure at the wet-bulb temperature

p_{at} = atmospheric pressure (assume 1.01325 bar)

A = a constant which has values as follows depending upon the instrument for measuring wet-bulb temperature

	Wet Bulb $\geq 0^{\circ}C$	Wet Bulb $< 0^{\circ}C$
Screen	$7.99 * 10^{-4}\ {}^{\circ}C^{-1}$	$7.20 * 10^{-4}\ {}^{\circ}C^{-1}$
Sling	$6.66 * 10^{-4}\ {}^{\circ}C^{-1}$	$5.94 * 10^{-4}\ {}^{\circ}C^{-1}$

Conversely, the wet-bulb temperature may be estimated if p_s is known. This requires an iterative process to take place using equations (2) and (10).

The assumption that the atmospheric pressure is constant may result in significant errors in estimating some of the psychrometric properties when the atmospheric pressure is not at 1.01325 bar. However, in the UK the maximum and minimum recorded values of atmospheric pressure are 1.055 bar and 0.925 bar respectively. Fortunately this is not a very large range and consequently the errors involved may not be as large, assuming standard atmospheric pressure.

APPENDIX 3 Predicted and Synthesised Hourly Solar Radiation Values

Clear Sky Solar Radiation Prediction

The method used to predict the direct normal and diffuse solar irradiances, for cloudless sky conditions, is based on work carried out by Rodgers et al (45) at the University of Sheffield. Using values of beam and diffuse irradiance obtained from Unsworth (81) and Parmelee (82) respectively, Rodgers has produced several regression equations which reasonably fit Unsworth's and Parmelee's results.

The direct normal or beam irradiance is influenced by the following (81):

(1) the corrected solar constant, G_{sc}', which is discussed in Chapter 1. The correction factor, C, for the solar constant is found from:

$$C = \frac{G_{sc}'}{G_{sc}} \qquad (1)$$

(2) the path length of the solar beam through the atmosphere, this is also known as the air mass. For stations at or close to sea level, the air mass is related to the solar altitude, α, by:

$$m_{SL} = \frac{1}{\sin \alpha} \qquad (2)$$

where m_{SL} is the air mass at sea level. Equation (2) was found to be more inaccurate the closer the sun was to the horizon. Therefore, for solar altitudes less than 10^{o}, Rodgers has fitted data from the Smithsonion Meteorological Tables by a least squares method for air mass at low solar altitudes,

$$m_{SL} = \exp\left[a_0 + \sum_{i=1}^{6} a_i (\sin h)^i\right] \quad : \quad h < 10^{o} \qquad (2a)$$

where the constants $a_i, i=0,1,\ldots,6$ are given in Table 1. For sites not at sea level a correction factor can be applied to the value of air mass, this correction is the ratio of atmospheric pressure of the site to the standard atmospheric pressure at sea level. Rodgers gives an empirical relationship for this ratio:

$$\frac{p}{p_{at}} = \exp\left(H*\left(-0{\cdot}0017\,H - 0{\cdot}1174\right)\right) \qquad (3)$$

where H is the altitude of the site above sea level in km. The air mass calculated at any site is found from

$$m = \frac{p}{p_{at}} * m_{SL} \qquad (4)$$

(3) the absorption and scattering by atmospheric gases reduce the beam irradiance. Unsworth analysed the effect upon the solar beam of the atmosphere by using an atmospheric model with a fixed concentration of gases, appropriate to the UK and for an irradiance equal to the solar constant. The values of the beam irradiance were then calculated for a range of precipitable water content and air mass values. Rodgers fitted this data by means of the expression

$$G^*_{DN} = G'_{sc} \exp\left[\sum_{i=0}^{3}\left(\sum_{j=0}^{2} b_{ij} W^j\right) m_i^i\right] \qquad (5)$$

where G^*_{DN} is the theoretical direct normal irradiance, W is the precipitable water content and the values of b_{ij} are given in Table 2. The precipitable water content value is the depth of liquid water which would result from the condensation of all the water vapour in a vertical column extended from the earth's surface to the limits of the atmosphere. Over Britain, precipitable water is usually in the range of 5-33mm, with the lower values occurring in winter. Using data supplied by the Meteorological Office on recommended monthly values of precipitable water content, Rodgers has produced the expression,

$$W = 10{\cdot}44 + \sum_{i=1}^{3}\left(a_i \cos(i\omega) + b_i \cos(i\omega)\right) \qquad (6)$$

a_0	=	3.67985
a_1	=	-24.4465
a_2	=	154.017
a_3	=	-742.181
a_4	=	2263.36
a_5	=	-3804.89
a_6	=	2661.05

TABLE 1 Constants associated with equation 2 a

i	0	1	2	3
bi0 $*10^2$	-12.9641	-6.42111	-0.46883	0.0844097
bi1 $*10^2$	0.412828	-0.801046	0.220414	-0.0191442
bi2 $*10^4$	-1.12096	1.53069	-0.429818	0.0374176

TABLE 2 Constants associated with equation 5

where W is measured in mm, values of a_i and b_i are given in Table 3 and ω is found from

$$\omega = 2\pi J/366 \qquad (7)$$

where J is the year day number.

From actual measured results, Unsworth (81) found that the value of beam irradiance was always less than the theoretical value given by equation (5). The additional attenuation of irradiance was attributed to the aerosol in the atmosphere for which Unsworth suggests the use of a turbidity coefficient, τ_a, to describe the attenuation. If the turbidity value of a particular site is known then the direct normal irradiance may be obtained from

$$G_{DN} = G^{*}_{DN} \exp(-\tau_a m) \qquad (8)$$

The main influence on τ_a, is the prevailing airstream. For coastal sites Unsworth recommends $\tau_a = 0{\cdot}05$ in polar airstreams to $0{\cdot}35$ in continental airstreams. These values are modified by natural aerosols produced by vegetation and pollution. Table 4 gives some recommended values.

Parmelee's (82) results indicated that for a fixed solar altitude, α, a linear relationship existed between the diffuse horizontal irradiance and the direct horizontal irradiance. Rodgers (45) checked the suitability of Parmelee's results for this country and expanded the range of validity of the data. The resulting expression used to establish the diffuse irradiance is

$$G_d = C a_o - a_1 G_{DN} \sin\alpha \qquad (9)$$

where G_d = the diffuse irradiance

C = sun-earth distance correction factor (equation (1))

a_0, a_1 = constants for a particular solar altitude, α , they are found from

$$a_o = 2 + \sum_{i=1}^{7} a_{oi} \left(\frac{\alpha}{10}\right)^i \qquad (10)$$

i	a_i	bi
1	-6.468	-3.492
2	1.056	2.049
3	-0.128	0.579

TABLE 3 Constants associated with equation 6

Condition	τ_a
Clear weather in winter	0.09
Clear summer weather in country	0.19
Clear summer weather in town	0.28
Hazy weather	0.37
Heavy warm hazy weather	0.45

TABLE 4 Recommended atmospheric turbidity values

and

$$a_1 = 10^{-3} * \sum_{i=0}^{5} a_{1i} \left(\frac{\alpha}{10}\right)^i \qquad (11)$$

where the values of a_{0i} and a_{1i} are given in Table 5. Hence, if the solar altitude and the beam irradiance are known then the diffuse irradiance incident on the horizontal surface may be estimated.

This model appears to compare favourably with results from other models (45). The diffuse irradiance may vary from site to site by more than the values predicted by equations (9)-(11). In such cases, Rodgers recommends the use of a 'diffuse multiplier' which simply modifies the predicted diffuse irradiance value. In this model the diffuse multiplier will always be equal to one.

Synthesised Solar Radiation Values

There are a number of methods by which solar radiation information can be synthesised from other data. A number of different processes will now be described.

(a) Angstrom Regression Equation

It is possible to use an empirical relationship to estimate the daily global irradiation incident upon a horizontal surface from the total daily hours of sunshine:

$$H_h = H_o (a + b(n/Td)) \qquad (12)$$

where H_h = daily global irradiation upon a horizontal surface

H_o = daily extraterrestrial radiation outside the atmosphere for the same location (see Chapter 1)

n = daily hours of bright sunshine

T_D = solar day length (hours) (see Appendix 1)

a, b = site dependent regression coefficients

i	a_{oi}	a_{1i}
0	0	297.0
1	47.3820	1.8313
2	29.6710	-3.7082
3	-15.8621	4.1233
4	4.3463	$-6.4090 * 10^{-1}$
5	$-5.7764 * 10^{-1}$	$2.8550 * 10^{-2}$
6	$3.4720 * 10^{-2}$	
7	$-7.3620 * 10^{-4}$	

TABLE 5 Constants associated with equations (10) and (11)

The values of constants a and b are derived empirically from several years measured data of both the daily global horizontal irradiation and the daily hours of bright sunlight. Lists are available of coefficients a and b which have been evaluated for a number of sites (34,83).

The accuracy of this model is dependent on the regression coefficients a and b, however, it will be most accurate when predicting the monthly mean daily global irradiation from the monthly mean daily sunshine duration. Care must be taken when predicting the daily global irradiation from the daily sunshine duration. The greater the daily sunshine duration value deviation from the mean daily sunshine duration, the more likelihood of error. Furthermore, on average sunshine duration days considerable errors can be involved, for example, assuming four hours sunshine duration then the effect of four hours early morning sunshine is different from four hours about solar noon, is different from four hours intermittent periods of sunshine.

(b) Estimating Diffuse Radiation from Global Radiation Data

Most of the available solar radiation is global (particularly in the USA) therefore, techniques have been developed to estimate the daily diffuse component of the daily global radiation. Liu and Jordan (84, 85) established that the proportion of diffuse radiation in the monthly global horizontal irradiation was a function of the ratio of the global to extraterrestrial irradiation reaching the site. This ratio is denoted $\overline{K_T}$, and is the month average 'per cent of possible' solar radiaiton, or the 'monthly clearness index'. It is defined by

$$\overline{K_T} = \frac{\overline{H_T}}{\overline{H_o}} \qquad (13)$$

Thus $\overline{K_T}$ represents the average monthly fraction of solar radiation which is transmitted either directly or indirectly through the atmosphere for a given month and location.

Liu and Jordan produced a regression equation for the ratio of monthly average daily diffuse to global radiation against $\overline{K_T}$.

Subsequent work by Collares-Pereira and Rabl (86) established a seasonal dependency on the relationship, unaccounted for by Liu and Jordan. The seasonal dependency is expressed in terms of the sunset hour angle (ω_s) of the mean day of the month (see Appendix 1, equation 10). An equation for $\overline{H_d}/\overline{H_T}$ (with ω_s in degrees) is:

$$\frac{\overline{H_d}}{\overline{H_T}} = 0.775 + 0.00653(\omega_s - 90) - \left[0.505 + 0.00455(\omega_s - 90)\right] \cos\left[115\ \overline{K_T} - 103\right] \qquad (14)$$

Similar to the monthly clearness index a daily clearness index, K_T, can be defined as the ratio of a particular day's radiation to the extraterrestrial radiation for that day, i.e.

$$K_T = \frac{H_T}{H_o} \qquad (15)$$

Liu and Jordan (84) carried out the original work studying the ratio of average daily diffuse to global radiation as a function of K_T. However, more accurate results have been obtained and an equation representing the correlation of the results is (86):

$$\frac{H_d}{H_T} \begin{cases} = 0.99 & \text{for } K_T \leq 0.17 \\ = 1.188 - 2.272\,K_T + 9.473\,K_T^2 - 21.865\,K_T^3 + 14.648 & \text{for } 0.17 < K_T < 0.75 \\ = -0.54\,K_T + 0.632 & \text{for } 0.75 \leq K_T < 0.8 \\ = 0.20 & \text{for } K_T \geqslant 0.8 \end{cases} \qquad (16)$$

(c) Estimating Hourly Global and Diffuse Values

The solar radiation data may be in terms of either daily global and diffuse or hourly global. The values of this data could be measured or in the case of daily global and diffuse estimated by means of equations (14) or (16). When hour by hour data is required for simulation models then either of the two forms of data can be processed to give hourly global and diffuse values.

Statistical studies of the time distribution of diffuse and global horizontal radiation throughout the day conducted by Lui and Jordan (85) led to the development of a technique whereby average hourly

values of diffuse and global irradiation could be establshed from the corresponding daily irradiation values. Two different ratios are defined:

(a) r_d , the ratio of the hourly average diffuse irradiation to the daily diffuse irradiation,

$$r_d = \frac{H_{d\ hourly}}{H_{d\ daily}} \tag{17}$$

(b) r_T , the ratio of the hourly average global irradiation to the daily global irradiation,

$$r_T = \frac{H_{T\ hourly}}{H_{T\ daily}} \tag{18}$$

From measured and theoretical data, a set of curves for both r_d and r_T have been drawn as a function of solar day length and the time interval from solar noon, days are assumed symmetrical about the solar noon.

The curves for r_d, are represented by the following equation,(86):

$$r_d = \frac{\pi}{4} \frac{\cos\omega - \cos\omega_s}{\sin\omega_s - (2\pi\omega_s/360)\cos\omega_s} \tag{19}$$

where ω is the hour angle in degrees for the time in question e.g. the midpoint of the hour for which the calculation is made.

The curves of r_T, are represented by the following equation from Collares-Pereira and Rabl (86)

$$r_T = \frac{\pi}{24}(a + b\cos\omega) \frac{\cos\omega - \cos\omega_s}{\sin\omega_s - (2\pi\omega_s/360)\cos\omega_s} \tag{20}$$

The coefficients a and b are given by

$$\left.\begin{aligned} a &= 0.409 + 0.5016\ \sin(\omega_s - 60) \\ b &= 0.6609 - 0.4767\ \sin(\omega_s - 60) \end{aligned}\right\} \tag{21}$$

When dealing with hourly global radiation values, an hourly clearness index, k_T, has been established. It is the ratio of the global

irradiance to the extraterrestrial irradiance over an hour

$$k_T = \frac{G_T}{G_O} \tag{22}$$

Orgill and Hollands (87) have established an expression which correlates G_d/G_T, the fraction of the hourly diffuse irradiance on a horizontal plane as a function of k_T:

$$\frac{G_d}{G_T} = \begin{cases} 1.0 - 0.249\,k_T & \text{for } k_T < 0.35 \\ 1.557 - 1.84\,k_T & \text{for } 0.35 \leq k_T \leq 0.75 \\ 0.177 & \text{for } k_T > 0.75 \end{cases} \tag{23}$$

Equation (3.1) Chapter 3, and equations (12) through to (23) can be used to generate hourly global, diffuse and direct normal solar radiation values from very primitive data. Obviously, these techniques cannot substitute for raw climatic data but their advantage lies in the ability to use data relative to a site and obtain hourly values. For example, if the daily hours of sunshine duration and the coefficients of equation (12) are known, then for a particular site by using equations (15) to (21) in that order, equation (3.1) Chapter 3, can be used to estimate the hourly direct normal solar radiation values. However, the inaccuracies involved in using these equations may be considerable.

APPENDIX 4 The Fourier Field Equation

Consider an infinitesimally small rectangular parallelepiped as shown in Figure 1, which has a volume $V = \Delta x \Delta y \Delta z$. The parallelepiped is assumed to be of some homogeneous isotropic material which is at temperature, Θ.

An energy balance conducted for the elemental volume may be stated as:

$$\left[\begin{array}{l}\text{I Net rate of heat}\\ \text{entering by con-}\\ \text{duction with}\\ \text{element } \Delta x \Delta y \Delta z\end{array}\right] + \left[\begin{array}{l}\text{II Rate of energy}\\ \text{generated in}\\ \text{element}\\ \Delta x \Delta y \Delta z\end{array}\right] = \left[\begin{array}{l}\text{III Rate of increase}\\ \text{of internal energy}\\ \text{of element}\\ \Delta x \Delta y \Delta z\end{array}\right]$$

The three terms I, II and III in this expression are evaluated below.

(I) Net rate of heat entering by conduction

The net rate of heat entering the elemental volume by conduction is determined by summing up the conductive processes in the x, y and z directions. If q_x is the heat flux in the x-direction at x, the rate of heat flow into the elemental volume in the x-direction through the surface at x is

$$Q_x = q_x \Delta y \Delta z$$

and the rate of heat flow out of the volume element in the x direction through the surface $x + \Delta x$ is

$$Q_{(x+\Delta x)} = Q_x + \frac{\partial Q_x}{\partial x} \Delta x$$

Therefore the net rate of heat flow into the element in the x-direction is

$$\text{Net heat-flow rate entering element in x-direction} = -\frac{\partial Q_x}{\partial x} \Delta x = -\frac{\partial q_x}{\partial x} \Delta x \Delta y \Delta z$$

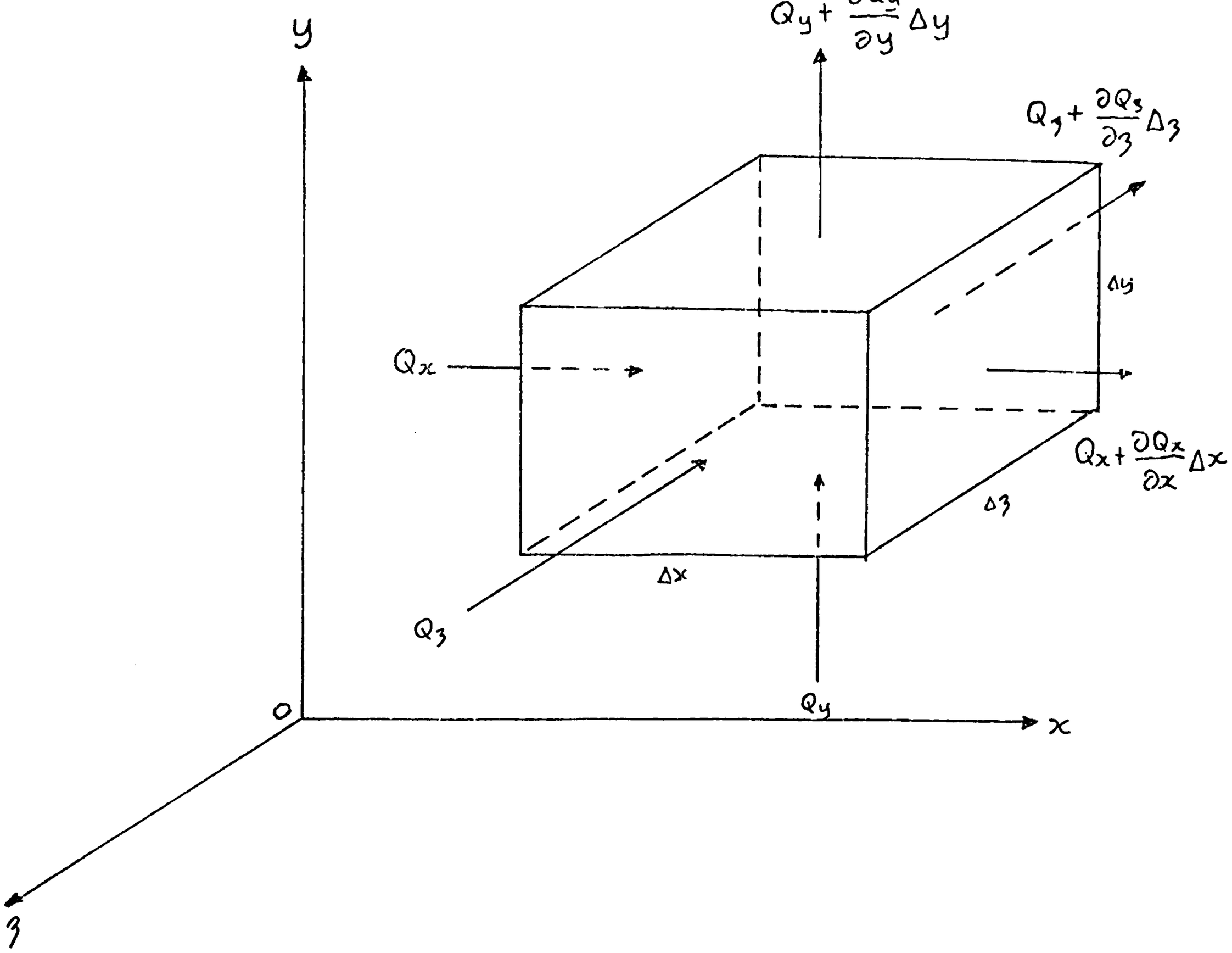

Figure 1 Elemental subvolume for the derivation of the heat conduction equation

Similarly, the net rate of heat entering the elemental volume by conduction in the y and z directions are given, respectively, as

$$-\partial q_y \Delta x \Delta y \Delta z$$
$$-\partial q_z \Delta x \Delta y \Delta z$$

Then, the net rate of heat entering the volume element by conduction is obtained by summing up these three components

$$I \equiv -\left(\frac{\partial q_x}{\partial x} + \frac{\partial q_y}{\partial y} + \frac{\partial q_z}{\partial z}\right) \Delta x \Delta y \Delta z \qquad (1)$$

Fourier's Law states that

$$q_x = -k \frac{\partial \theta}{\partial x}$$

where $\partial\theta/\partial x$ is the temperature gradient in the x-direction . Similar expressions can be derived for the y and z directions. Substituting for q_x, q_y & q_z in equation (1) gives

$$I \equiv k \Delta x \Delta y \Delta z \left(\frac{\partial^2 \theta}{\partial x^2} + \frac{\partial^2 \theta}{\partial y^2} + \frac{\partial^2 \theta}{\partial z^2}\right)$$

this can be rewritten as

$$I \equiv k \Delta x \Delta y \Delta z \nabla^2 \theta \qquad (2)$$

where the Laplacian operator $\nabla^2\theta$ is defined as

$$\nabla^2 \theta = \frac{\partial^2 \theta}{\partial x^2} + \frac{\partial^2 \theta}{\partial y^2} + \frac{\partial^2 \theta}{\partial z^2}$$

II Rate of energy generation

The rate of energy generation in the elemental volume is equal to the strength of the distributed energy sources in the medium, generating heat at a rate of g(x, y, z, τ) per unit time, per unit volume, i.e.

$$II \equiv g \Delta x \Delta y \Delta z \qquad (3)$$

III Rate of change of internal energy

The rate of change of internal energy is reflected in the rate of energy storage in the volume element and assuming constant density, ρ,

and specific heat capacity, C, then

$$III = \rho C \frac{\partial \theta}{\partial \tau} \Delta x \Delta y \Delta z \qquad (4)$$

where τ is time in seconds.

Equating equations (2) and (3) with equation (4) and cancelling out $\Delta x \Delta y \Delta z$ gives:

$$\rho C \frac{\partial \theta}{\partial \tau} = k \nabla^2 \theta + \dot{q} \qquad (5)$$

where

$$\theta = \theta(x, y, z, \tau) \ , \ \dot{q} = g(x, y, z, \tau)$$

Equation (5) can be rearranged to give

$$\frac{\partial \theta}{\partial \tau} = \alpha \nabla^2 \theta + \frac{\dot{q}}{\rho C} \qquad (6)$$

where α is the thermal diffusivity which is a property of the material. The larger its numerical value, the more rapidly is a temperature change propagated through the material.

Equation (6) is known as the Fourier Field equation in three dimensions with heat generation. If there are no heat sources then $\dot{q}=0$ and equation (6) reduces to the diffusion equation,

$$\frac{\partial \theta}{\partial \tau} = \alpha \nabla^2 \theta$$

Considering the steady state form of equation (6) then $\partial\theta/\partial\tau$ is zero. This is known as the Poisson Equation,

$$\nabla^2 \theta + \frac{\dot{q}}{k} = 0$$

and for the case with no heat generation, the resulting relationship is called the Laplace equation,

$$\nabla^2 \theta = 0$$

The Fourier Field equation in one space dimension with heat generation is

$$\frac{\partial \theta}{\partial \tau} = \alpha \frac{\partial^2 \theta}{\partial x^2} + \frac{\dot{q}}{\rho c} \qquad (7)$$

Equation (7) is the basis of most solutions of transient heat conduction. That is, the equation must be solved with the appropriate initial and boundary conditions in all cases of unsteady heat flow. Unfortunately this can be an extremely complex task and in many cases no satisfactory solution exists. However, numerical methods offer a means of solution to most problems.

APPENDIX 5 Finite Difference Approximation to the Fourier Field Equation

The fundamental operation in the difference method is the replacement of each derivative in the partial differential heat conduction equation by an algebraic approximation at each discrete point in the system. Consider the one dimensional Fourier Field equation derived in Appendix 4,

$$\frac{\partial \theta}{\partial \tau} = \alpha \frac{\partial^2 \theta}{\partial x^2} + \frac{\dot{q}}{\rho c} \qquad (1)$$

The replacement of the space and time derivatives by finite differences involves expressing the derivatives in terms of a truncated Taylor's series expansion (88), which besides being both brief and simple, also gives an indication of the error induced due to the truncation of the series expansion. Using the notation given in Figure 1, a Taylor's series expansion is applied to a continuous function of f(x) which is then expanded about a point P in the x-direction only:

$$f_{(x+\Delta x)} = f_{(x)} + \Delta x \frac{\partial f(x)}{\partial x} + \frac{1}{2} \Delta x^2 \frac{\partial^2 f(x)}{\partial x^2} + \frac{1}{6} \Delta x^3 \frac{\partial^3 f(x)}{\partial x^3} + \ldots \qquad (2)$$

and,

$$f_{(x-\Delta x)} = f_{(x)} - \Delta x \frac{\partial f(x)}{\partial x} + \frac{1}{2} \Delta x^2 \frac{\partial^2 f(x)}{\partial x^2} - \frac{1}{6} \Delta x^3 \frac{\partial^3 f(x)}{\partial x^3} + \ldots. \qquad (3)$$

The addition of equations (2) and (3) gives

$$f_{(x+\Delta x)} + f_{(x-\Delta x)} = 2 f_{(x)} + \Delta x^2 \frac{\partial^2 f(x)}{\partial x^2} + \emptyset(\Delta x^4)$$

where $\emptyset(\Delta x^4)$ denotes terms containing fourth and higher powers of Δx. Re-expressing this equation in terms of the second order derivative yields what is more commonly known as the three-point difference formula:

$$\frac{\partial^2 f(x)}{\partial x^2} = \frac{f(x+\Delta x) - 2 f(x) + f(x-\Delta x)}{\Delta x^2} + \emptyset(\Delta x^2) \qquad (4)$$

where $\emptyset(\Delta x^2)$ is the truncation error involved in using a finite difference approximation to represent a second order derivative.

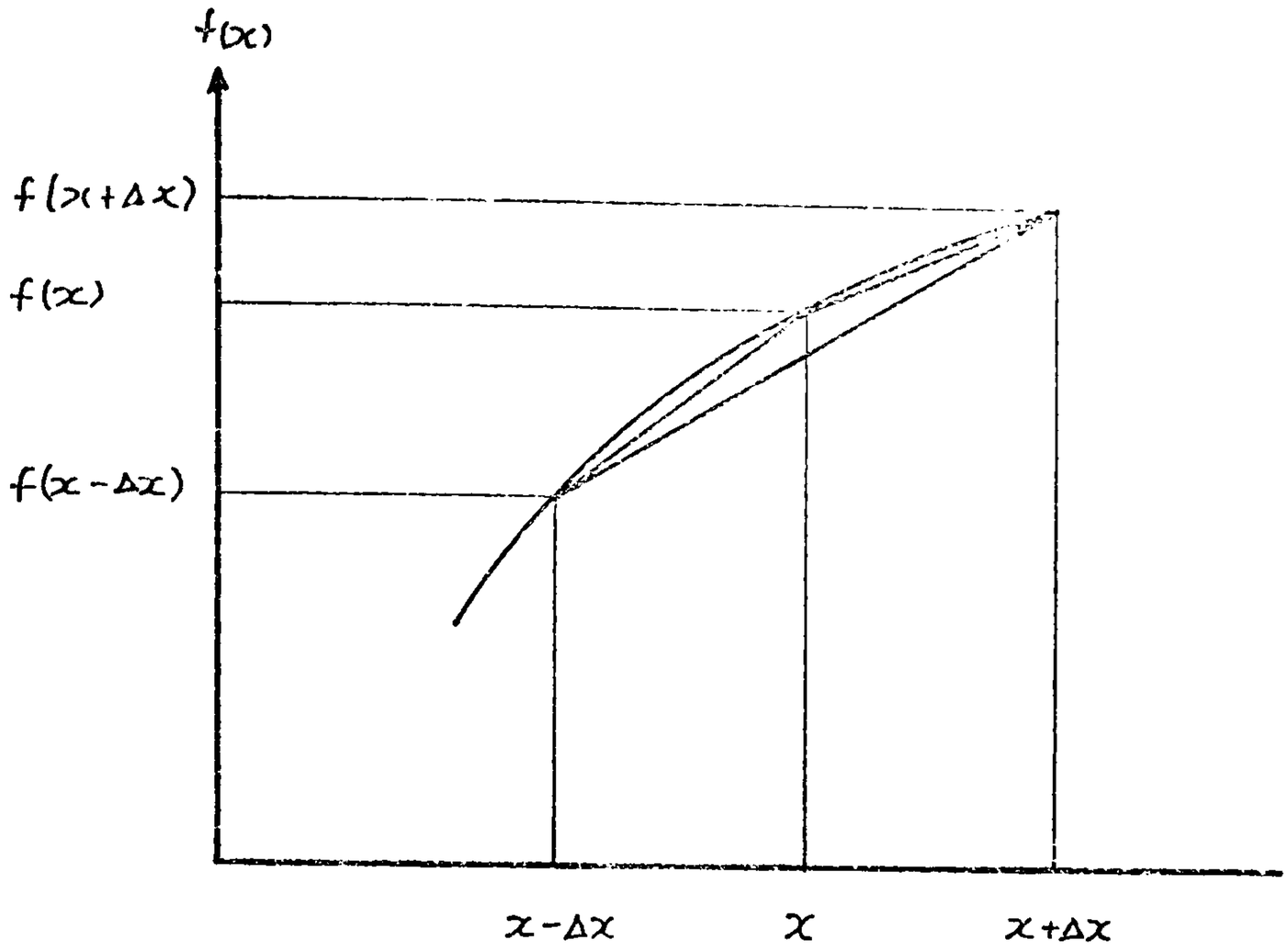

Figure 1 Graphical illustration of finite difference approximation to derivatives

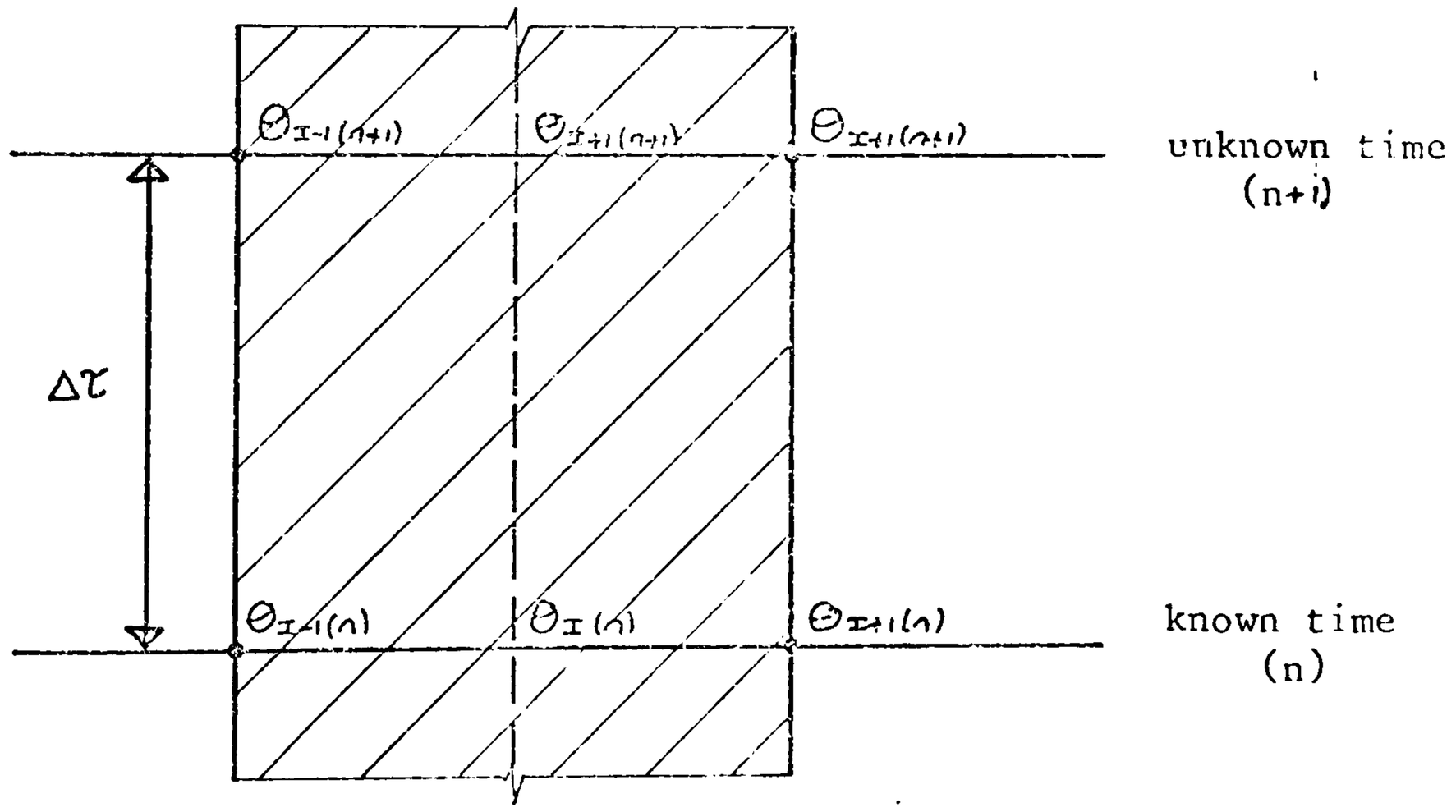

Figure 2 Space and time increments within a homogeneous element

Similarly, by subtracting equation (3) from equation (2) and rearranging the two-point central difference formula is obtained for the first order derivative:

$$\frac{\partial f(x)}{\partial x} = \frac{f(x+\Delta x) - f(x-\Delta x)}{2\Delta x} + \emptyset(\Delta x^2) \qquad (5)$$

There are, however, two other methods of obtaining a difference formula for the first order derivative. The first method involves the truncation of equation (2) after the Δx term, the result is rearranged and is called the first forward difference formula,

$$\frac{\partial f(x)}{\partial x} = \frac{f(x+\Delta x) - f(x)}{\Delta x} + \emptyset(\Delta x) \qquad (6)$$

The first backward difference formula is obtained by applying a similar truncation to equation (3) giving,

$$\frac{\partial f(x)}{\partial x} = \frac{f(x) - f(x-\Delta x)}{\Delta x} + \emptyset(\Delta x) \qquad (7)$$

Equations (4) and (5) have a truncation error of the order of Δx^2 which implies that halving the step length Δx approximately quarters the error, whereas the truncation error in equations (6) and (7) are of the order of Δx, that is, halving the space length only halves the error. In terms of the first order derivative, the two-point central difference formula appears to be more accurate than either the first forward or first backward difference formulae. However, in transient heat conduction problems the two point central difference formula is unstable, the results of which are meaningless. In such circumstances the first forward or first backward difference approximations are both stable.

When confronted with a transient heat conduction problem there are two methods available to transform the Fourier Field equation (given by equation (1)) and its boundary conditions into a set of algebraic equations. The first is called the explicit scheme, the second is the implicit method. Consider Figure 2 which shows a homogeneous element with nodes placed at the centre plane and element boundaries. The temperatures existing at each node at both the present (known) and future (unknown) time rows are also shown. These time rows are

designated by n and n+1 respectively.

The explicit method involves expressing the temperature of the unknown node, $\theta_{x(n+1)}$, in terms of the known nodal temperatures on the previously calculated time row. A straightforward approximation of the equation (1) is to use a first forward difference formula for the first order derivative and the second order derivative is replaced by the three-point central difference formula. Therefore, for a fully explicit scheme, equation (1) is approximated by,

$$\frac{\theta_{I(n+1)} - \theta_{I(n)}}{\Delta\tau} = \alpha \frac{\theta_{I+1(n)} - 2\theta_{I(n)} + \theta_{I-1(n)}}{\Delta x^2} + \frac{\dot{q}}{\rho C} \qquad (8)$$

Rearranging in terms of the unknown nodal temperature gives

$$\theta_{I(n+1)} = \frac{\alpha\Delta\tau}{\Delta x^2}\theta_{I+1(n)} + \left(1 - \frac{2\alpha\Delta\tau}{\Delta x^2}\right)\theta_{I(n)} + \frac{\alpha\Delta\tau}{\Delta x^2}\theta_{I-1(n)} + \frac{\dot{q}\Delta\tau}{\rho C} \qquad (9)$$

Although easy to formulate and solve the explicit solution suffers from instability in certain circumstances and equation (9) is only stable when,

$$R \equiv \frac{\alpha\Delta\tau}{\Delta x^2} \leq 0{\cdot}5$$

This limitation becomes more restrictive as the space dimension Δx is reduced (usually to improve accuracy) then the time step $\Delta\tau$ can become very small so that computation time for even simple problems can become prohibitive.

A fully implicit scheme is more complicated to apply because the expression for the unknown temperature $\theta_{x(n+1)}$ refers to unknown nodal temperatures. The second order derivative in equation (1) is represented in a three-point difference form expressed in terms of the values of temperature at the future time row (i.e. (n+1)th), instead of the present time row (i.e. nth) as used in the explicit scheme. The first order derivative is expressed in the first backward difference form. The fully implicit representation of the Fourier Field equation is,

$$\frac{\theta_{I(n+1)} - \theta_{I(n)}}{\Delta\tau} = \frac{\alpha\left(\theta_{I+1(n+1)} - 2\theta_{I(n+1)} + \theta_{I-1(n+1)}\right)}{\Delta x^2} + \frac{\dot{q}}{\rho C} \qquad (10)$$

rearranging,

$$\theta_{I(n+1)} = \theta_{I(n)} + \frac{\alpha \Delta\tau}{\Delta x^2}\left(\theta_{I+1(n+1)} - 2\theta_{I(n+1)} + \theta_{I-1(n+1)}\right) + \frac{\dot{q}\Delta\tau}{\rho C} \qquad (11)$$

The unknown nodal temperature at the future time row cannot be solved directly from equation (11), subsequently the technique is implicit. The solution is achieved by the simultaneous solution of the resulting set of algebraic equations at the future time step.

The fully explicit and fully implicit methods are both extremes, they can be used in a weighted-average scheme to obtain a solution somewhere between the fully explicit and fully implicit methods. Multiplying equation (10) by some factor F, where F is a value between 0 and 1 and adding equation (8) multiplied by (1-F) gives,

$$\frac{F(\theta_{I(n+1)} - \theta_{I(n)})}{\Delta\tau} + \frac{(1-F)(\theta_{I(n+1)} - \theta_{I(n)})}{\Delta\tau} = \frac{F\alpha(\theta_{I+1(n+1)} - 2\theta_{I(n+1)} + \theta_{I-1(n+1)})}{\Delta x^2}$$

$$+\frac{(1-F)\alpha(\theta_{I+1(n)} - 2\theta_{I(n)} + \theta_{I-1(n)})}{\Delta x^2} + \frac{F\dot{q}}{\rho C} + \frac{(1-F)\dot{q}}{\rho C}$$

$$\Rightarrow \frac{\Delta x^2}{\alpha\Delta\tau}\left(\theta_{I(n+1)} - \theta_{I(n)}\right) = F\left(\theta_{I+1(n+1)} - 2\theta_{I(n+1)} + \theta_{I-1(n+1)}\right)$$

$$+(1-F)\left(\theta_{I+1(n)} - 2\theta_{I(n)} + \theta_{I-1(n)}\right) + \frac{\dot{q}\Delta x^2}{k} \qquad (12)$$

Explicit and implicit schemes are obtained by setting $F < 0.5$ and $F \geqslant 0.5$ respectively. (The fully explicit and fully implicit schemes are obtained for F=0 and F=1 respectively). The Crank-Nicolson formulation is obtained for the arithmetic average of the explicit and implicit schemes which occurs with a value of F=0.5. Equation (12) at F=0.5 is

$$\frac{2\Delta x^2}{\alpha\Delta\tau}\left(\theta_{I(n+1)} - \theta_{I(n)}\right) = \left(\theta_{I+1(n+1)} - 2\theta_{I(n+1)} + \theta_{I-1(n+1)}\right)$$

$$+\left(\theta_{I+1(n)} - 2\theta_{I(n)} + \theta_{I-1(n)}\right) + \frac{\dot{q}\Delta x^2}{k} \qquad (13)$$

The general difference form of equation (12) or (13) can be expanded and applied to two or three dimensional heat conduction (55). However, the difference method is difficult to apply to convective and radiative heat transfer processes and the effects of time and positional dependency of thermal properties and heat generation.

A variational approach called the heat balance method can be used. With this method there is no need to deal with the governing partial differential equation because direct approximations of the laws governing the physical system are applied to the subvolume surrounding each nodal point.

APPENDIX 6 Convective Heat Transfer Coefficient

The convective heat transfer process is a highly complex problem to solve (see Section 5.1.3), therefore, the mathematical model used to analyse a solar energy system relies on empirical or semi-empirical equations to mathematically describe the processes involved. These empirical equations are used to evaluate, $\bar{h}c$, the average convective heat transfer coefficient over the contact area between a solid boundary and a fluid. Thus, the rate of convective heat transfer is given by the expression,

$$Q_{SURFACE-FLUID} = A\ \bar{h}c\ (\bar{T}s - \bar{T}f)$$

where Q_{S-F} = rate of heat transfer between the surface and the fluid (watts)

A = area of contact (m^2)

$\bar{T}s$ = average temperature of the contact surface, (K)

$\bar{T}f$ = the average temperature of the bulk fluid, (K)

The simplicity of this equation is misleading. The numerical value of $\bar{h}c$ is generally non-uniform over the contact area and it is a complex function of the geometry of the system under analysis as well as the fluid flow through the system.

The fluid motion can be induced by either one, or a combination of two different processes. The fluid may be set in motion as a result of density differences due to either temperature variations between the fluid and the surface, or there may be a density gradient within the fluid itself. The buoyancy effects (as it is called) due to these density changes produce a natural circulatory effect causing the fluid to move of its own accord away from a hotter contact surface, to be replaced by fluid which will be similarly affected. This mechanism is called natural convection, a special case of which is known as free convection if the convective process occurs within an enclosure.

The second process by which fluid motion is induced is when an external

agent such as a pump or a fan promotes fluid movement. This motion is called forced convection and it is generally associated with greater velocities and correspondingly higher heat transfer rates than encountered in natural or free convective cases.

Buoyancy effects are always present even in forced convection, but in most cases the effects are negligible and may be disregarded, however, these effects are significant when natural and forced convective effects are of the same magnitude and the convective process is called mixed convection.

The fluid flow within any of the aforementioned convective processes can be described in terms of laminar or turbulent flow. In laminar flow the $\bar{h}c$ values tend to be smaller because the heat is transferred by molecular conduction, as a result the flow can be described as streamlines running side by side so that no mixing between streamlines occurs. On the other hand, turbulent flow is much more vigorous and mixing occurs between streamlines due to eddie currents which are created by the fluctuations of the fluid particles about the mean flow motion, consequently, this mixing between fluid layers results in larger $\bar{h}c$ values. An intermediate zone exists between the laminar and turbulent cases called the transition zone. This zone is poorly understood and it is not easily described empirically.

The condensation of a vapour and the evaporation of a liquid have important implications in a solar energy collection design for a number of reasons, for example, corrosion within a collector and early morning heating and evening cooling of a collector. A vapour will condense on contact with a surface if the temperature of the surface is below the saturation temperature of the vapour. The condensate formed will probably be subcooled due to contact with the surface, consequently, more vapour will condense on the exposed surface, that is the subcooled condensate layer. Condensation cannot occur if the surface temperature exceeds the vapour saturation temperature, if the surface is wet under these conditions then evaporation will take place.

A6.1 Convection

The purpose of this Appendix is to identify the technique and equations used to determine the effects of the various convective heat transfer processes associated with a solar energy collection system. These expressions are normally solved for a dimensionless term called the Nusselt number, which is written

$$Nu = \frac{hc\ L}{k}$$

where L is the characteristic dimension and k is the thermal conductivity of the fluid. The Nusselt number is defined as the ratio of convective heat transfer to conductive heat transfer in a fluid. From dimensional analysis (8 8) it has been shown that for forced convection the Nusselt number is a function of Reynold's and Prandtl's number

$$Nu = f\ (Re, Pr)$$

and for natural or free convection the Grashof number replaces the Reynolds number, thus

$$Nu = f\ (Gr, Pr)$$

Consequently, by establishing the relationships between the Nusselt number and its dependent variables, the convective heat transfer coefficient can be calculated.

The mathematical model of a flat plate solar collector, detailed in Chapter 5 , allows partitioning of the absorber plate and fluid into a number of segments for which a local convective heat transfer coefficient will have to be estimated. Although analytical models are available to evaluate localised heat transfer coefficients, they are normally too specific, for example, a flat plate exposed to a free stream, and there are a few of these models available. Consequently, empirical equations calculating the average convective

heat transfer coefficient will be used to model localised values from the local fluid properties.

A6.1.1 Forced Convective Heat Transfer

Forced convection in a photothermal flat plate solar collector is the principal mechanism for extracting absorbed solar energy and transferring it to where it is required. This flow can be laminar or turbulent and to identify which flow region prevails a dimensionless term called the Reynolds number is used. The Reynolds number (Re) is the ratio of the inertial to the viscous forces in a fluid due to forced convection, thus,

$$Re = \frac{\rho v^2}{\mu v/d} = \frac{\rho v d}{\mu}$$

where, ρ = density of the fluid (KgM^{-3})

v = velocity of the fluid (MS^{-1})

d = hydraulic diameter (M)

μ = dynamic viscosity of the fluid ($MSKg^{-1}$)

In a long conduit where flow is fully developed if $Re < 2300$ laminar flow exists and for $Re > 10^4$ the flow is turbulent. The region between fully developed laminar and turbulent flow is called the transition zone. For Reynolds numbers in excess of 2300, fully developed laminar flow cannot exist and the flow is of such a random nature it is difficult to describe mathematically. The breakdown of laminar flow is more commonly known as the critical zone and it occurs up to a Reynolds number of approximately 4000. After the critical zone, as Re is increased the flow becomes more turbulent in nature so that the probability of fully developed turbulent flow is increased, however, the range of the critical and transition zones depend upon the roughness of the conduit and the nature of the breakdown of the fully developed laminar flow pattern.

Irrespective of flow, be it fully developed laminar or turbulent or transition, as it enters a new geometric region, for example a conduit, then a new flow pattern will be developed until, after a

certain distance in the new region, the flow can be described as fully developed. This region in which flow is still developing is called the Thermal Entrance Region. The length of conduit associated with the developing region is defined by a dimensionless number, L/d, where L is the entrance length and d is the hydraulic diameter of the conduit. This dimensionless number is sometimes called the ratio of equivalent diameters, and the entrance length is normally in the region of 60 equivalent diameters in length before fully developed flow is achieved. In asymmetrically heated air solar collectors this value is closer to 70 in turbulent flow (31).

In laminar flow the entrance length has been correlated to Reynolds number,

$$\frac{L}{d} = \frac{Re}{20}$$

This equation shows that the laminar flow process may require a larger thermal entrance region (>100 equivalent diameters) because of the slower development.

The increase in the local heat transfer coefficient in short circular tubes or in the entrance region with abrupt entrances has been shown by Kreith (89) for gases and liquids in the turbulent region to be,

$$\frac{h_m}{h_\infty} = 1 + (d/L)^n \qquad (1)$$

is valid for L/d less than 20. The exponential value n varies between 0.69 and 0.72 depending upon the entry geometry when air is the heating fluid, otherwise n = 0.7. In this equation h_m and h_∞ represent the local and the fully developed heat transfer coefficients respectively. For $20 \leq L/d < 60$, Kreith quotes

$$\frac{h_m}{h_\infty} = 1 + K\left(\frac{d}{L}\right) \qquad (2)$$

where K = 6. The value of K has also been correlated with the Reynolds number,

$$K = 0.067Re^{0.25}$$

Yaneske and Wiles (31) quote a different value for K based upon experimental data obtained from solar air collectors (90, 91),

$$K = 14.3 \log (L/d) - 7.9$$

where K is constant at L/d = 60 for equivalent diameter values exceeding 60.

Recent experiments have shown the effect of the thermal exit region of a conduit to be more significant than was first thought (31), however, there are no mathematical expressions available to account for this phenomena.

The friction factor or friction coefficient, f, is used to evaluate both the convective heat transfer coefficient, hc, and the pressure drop, Δp, associated with fluid flow in a conduit. The friction factor is both a complex function of both the Reynolds number and the relative roughness of the internal walls of the conduit. The relative roughness is defined as the ratio of the mean height, e, of protrusions above the conduit wall, to that of the internal diameter of the conduit, d. In most solar collector applications the materials used for pipes and conduits are normally copper, glass and mild steel, these materials are considered to be smoothe and not rough, therefore, the empirical equations are less complicated. Drew et al (92) correlated various data into the following expression describing the friction factor for fully developed turbulent flow in a conduit for the range of Reynolds number of $3000 < Re < 3x10^6$,

$$f = 0.0056 + 0.5\ Re^{-0.32} \qquad (3)$$

This equation gives slightly higher values of f than those for perfectly smooth conduits, this is considered to be acceptable.

Equation (3) was compared with other empirical equations for the friction factor, it was found that for the range of 3.25×10^4 to 5×10^5 a more accurate expression was given by MacAdams (93),

$$f = 0.184\ Re^{-0.2} \qquad (4)$$

Therefore, by using equations (3) and (4) the friction factor within relatively smooth conduits for values of Re exceeding 3000 can be calculated.

For fully developed laminar flow a linear expression is sufficient to describe the relationship between the friction factor and the Reynolds number,

$$f = 64/Re \qquad (5)$$

This expression is valid for Reynolds numbers up to 2100.

The critical and transition zones are somewhat truncated compared to those outlined above because there are no protrusions in smoothe tubes which aid the perpetuation of the critical or transition zones so that the value of f can be calculated at Reynolds numbers as low as 3000. From investigation of the experimental results of Drew et al (92), it appears valid to assume that for the critical region ($2100 < Re < 3000$) a linear interpolation between equations (5) and (3) is sufficient to describe the relationship between the friction factor and Re in this region.

Table 1 summarises the formulations which describe the friction factor as a function of Reynolds number for smooth conduits.

The friction factor is also required to calculate the pressure drop through a length of conduit is proportional to the conduit length, dimensional analysis (94) has shown that the pressure drop per unit length for a smooth pipe is

$$\frac{\Delta p}{L} = \phi \frac{f \rho v^2}{2d} \qquad (6)$$

Re Range	Expression	Equation No.
$Re < 2100$	$f = 64/Re$	(5)
$2100 \leq Re < 3000$	linear interpolation	(3) and (5)
$3000 \leq Re \leq 3.25 \times 10^4$	$f = 0.0056 + 0.5\ Re^{-0.32}$	(3)
$3.25 \times 10^4 < Re < 5 \times 10^5$	$f = 0.184\ Re^{-0.2}$	(4)
$Re \geq 5 \times 10^5$	$f = 0.0056 + 0.5\ Re^{-0.32}$	(3)

Table 1. Empirial relationships used to predict the friction factor in smooth conduits.

where $\Delta p/L$= pressure frop per unit length (pa/M)

$\phi = f_{fitting}/f$, for smoothe pipe $\phi = 1$

$f_{fitting}$ = friction factor for any non-smoothe tube or fitting

The function ϕ modifies the pressure drop depending upon the tube roughness or the effect of a system fitting (e.g. valve).

In liquid solar collectors pipes may be serpentined over the surface of the absorber plate, and in the system bends are commonplace, therefore, some account must be taken of the increased resistance to fluid flow encountered in the curved parts of the pipes. Kays (95) proposes two empirical expressions which evaluate ϕ for pipe curvature, one expression is for fully developed laminar flow, the other for turbulent flow. Figure 1 shows the application for Kays expressions where r is the radius of the pipe and Rc is the radius of curvature of the centreline of pipe; for laminar flow

$$\phi = \left[1 - \left\{1 - \left(\frac{11.6}{Re\sqrt{r/Rc}}\right)^{0.45}\right\}^{2.22}\right]^{-1}$$

which is valid for the range $11.6 < Re\sqrt{r/Rc} < 2000$. The equation related to turbulent flow in curved circular tubes is

$$\phi = (Re(r/Rc)^2)^{0.05}$$

for $\quad Re(r/Rc)^2 > 6$

For most fittings the function ϕ is usually a constant. However, using equation (6) it is possible to estimate the pressure drop associated with a complete system in order estimate the size of the fan or pump required. This calculation is more critical in air collector systems (see Chapter 2).

To correct for the variation of properties in a fluid due to the temperature gradient between the average bulk fluid and the fluid at its contact surface, the corrected Nusselt number, Nu_c is found from,

$$\overline{Nu}_c = \overline{Nu}\,\gamma$$

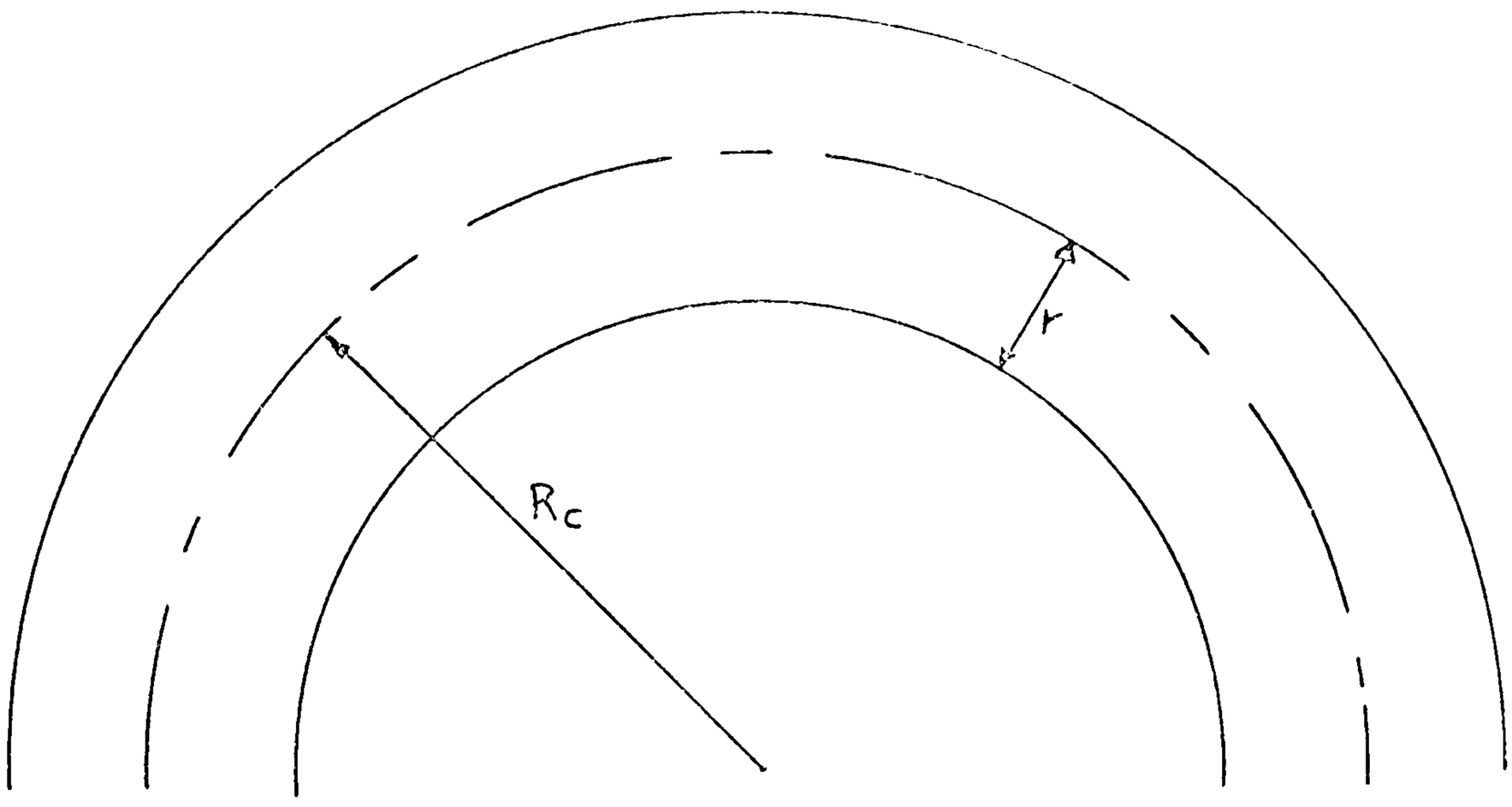

Figure 1 Description of pipe curvature

where γ is the correction applied to the average Nusselt number if all fluid properties are evaluated at the average bulk temperature. For liquids

$$\gamma = \left(\frac{\mu_b}{\mu_w}\right)^{0.14}$$

and for gases

$$\gamma = \left(\frac{T_b}{T_w}\right)^{0.14}$$

where μ_w = viscosity of the fluid at the wall surface
μ_b = viscosity of the free stream fluid
T_w = temperature of the fluid at the wall surface
T_b = temperature of the free stream fluid

This modification can be applied to any forced convection Nusselt value based on average bulk fluid or free stream temperatures.

(a) Laminar Forced Convection in Conduits

Analytical models are available for fully developed laminar forced convective flow in conduits under the strict condition that all fluid properties are constant (96). In a circular tube characterised by uniform surface heat flux the Nusselt number is constant at 4.36 and is independent of the Reynolds number and Prandtl number. For fully developed conditions with a constant surface temperature, the Nusselt number is constant at 3.66. Alternatively, exact mathematical solutions of the boundary layer equation for laminar flow over a flat plane surface the local heat transfer coefficient can be conducted but cannot be applied to convective heat transfer coefficients in conduits. As both of these methods are unsuitable then an alternative means of calculating the Nusselt number is required. An empirical equation that takes account of the entrance length was proposed by Seider and Tate (97),

$$\overline{Nu}_{D_H} = 1.86\,\gamma \left(\frac{Re_{D_H}\,Pr}{(L/D_H)}\right)^{1/3} \qquad (7)$$

where D_H is the hydraulic diameter of the conduit. This expression can be used to determine $\overline{Nu_{DH}}$ for $(Re_{DH}Pr\ D_H/L) > 10$. For small conduit lengths then the following expression can be used for the range $100 < Re_{DH}Pr\ D_H/L < 1500$

$$\overline{Nu_{DH}} = \frac{Re_{DH}\,Pr\,D_H}{4L}\ln\left[\frac{1}{1-\frac{2.654}{Pr^{0.167}(Re_{DH}\,Pr\,D_H/L)^{0.5}}}\right] \quad (8)$$

Therefore, equation (7) should be applied where possible and equation (8) used within its specific range.

The fluid properties in equations (7) and (8) are evaluated at the mean temperature of the fluid in the duct, defined by

$$T_{mean} = \frac{T_{bi} + T_{wi} + T_{bo} + T_{wo}}{4}$$

where T_{bi} = inlet bulk temperature
T_{wi} = wall temperature at inlet
T_{bo} = outlet bulk temperature
T_{wo} = wall temperature at outlet

(b) Turbulent Forced Convection in Conduits

Due to the complexity of the fluid mechanics involved in the analysis of turbulent flow no straightforward mathematical solution is applicable, the only suitable means of analysing this phenomena is by analogy between heat and momentum transfers. The classical technique for predicting the convective heat transfer coefficient is to use the Colburn analogy. Colburn expanded the Reynolds analogy to include values of Pr other than unity (98). The result of the Reynolds analogy was

$$St = \frac{Cf}{2} = \frac{f}{8}$$

where,

St = Stanton Number = $\frac{h_c}{\rho C_p v} = \frac{Nu}{RePr}$

Cf = drag coefficient

f = friction factor

Colburn's modification to this expression in order to correlate with experimental data is

$$St\ Pr^{2/3} = \frac{f}{8} \tag{9}$$

This expression may be rewritten in terms of the Nusselt number by substituting for the Stanton Number, thus

$$Nu = \frac{f}{8} Re\ Pr^{1/3} \tag{10}$$

The traditional method of solving equation (10) is to substitute MacAdams correlation for the friction factor - equation (4) - which gives,

$$Nu = 0.023\ Re^{0.8}\ Pr^{1/3} \tag{11}$$

MacAdams (93) recommends this equation and suggests it be used for symmetrically heated pipes in the range $10^4 < Re < 1.2 \times 10^5$ which have an equivalent diameters ratio greater than 60. MacAdams also introduced the coefficient γ to take account of the temperature gradient within the fluid so that,

$$Nu = 0.023\ \gamma\ Re^{0.8}\ Pr^{1/3} \tag{12}$$

where the fluid properties are evaluated at the average mean temperature. The Prandtl number range for this expression is 0.5 to 17,000.

Equations (11) and (12) are valid for only a small range of Reynolds numbers, however, many authors infer that these equations are suitable for all turbulent flow conditions which is an unfortunate assumption

due to the errors that may be induced at high Reynolds numbers. The range of Reynolds number for which equation (10) is applicable can be extended to all turbulent flow by using the appropriate friction factors identified in Table 1. A second point is that the Colburn Analogy has been used traditionally because of the simplicity of its solution, making it practical for manual calculation. Due to modern computer facilities this is no longer a constraint and a more rigorous analogy can be used called the Von Karmán analogy.

Von Karmán extended the Prandtl analogy by separating the turbulent flow field into three distinct layers: a viscous sublayer, a buffer layer and a turbulent core (98). The Von Karmán's analogy gives,

$$St = \frac{f}{8} \quad \frac{1}{1 + 5\sqrt{f/8}\,[(Pr-1) + \ln\{(5Pr+1)/6\}]} \qquad (13)$$

Re-expressing this equation in terms of the Nusselt number yields

$$Nu = \frac{0.125f\ Re\ Pr}{1 + 1.767767\ \sqrt{f}\,[(Pr-1) + \ln((5Pr+1)/6)]} \qquad (14)$$

It is the author's belief that using the friction factors from Table 1 for turbulent flow to solve equation (14), (for any Reynolds number), will result in a more accurate evaluation of the Nusselt number than using equation (11), based on the Colburn analogy. The Von Karman's analogy, however, is valid for Prandtl numbers in the range $0.5 < Pr < 30$, therefore, by using the fluid temperature gradient modifier, γ, the resulting expression is valid over a much larger range of Prandtl numbers.

$$Nu = \frac{0.125f\ Re\ Pr\ \gamma}{1 + 1.767767\ \sqrt{f}\,[(Pr-1) + \ln((5Pr+1)/6)]} \qquad (15)$$

Equation (15) is applicable only in the regions of flow where both the velocity and temperature profiles are considered fully developed, therefore, the expressions for the entrance length for turbulent flow are applicable. Furthermore, equation (15) assumes that the conduits are symmetrically heated, however, for turbulent air flow

between two parallel asymmetrically heated flat plates - as would occur in an air collector - the Nusselt numbers have been shown to be in the order of 20% less than the values calculated by equation (11), (31, 90, 91). In asymmetrically heated conduits a 20% reduction in the calculated Nusselt value will be assumed.

A 6.1.2 Natural and Free Convection

There are no suitable analytical techniques or analogies to describe the natural convection process, therefore, dimensional analysis methods are employed to identify the dimensional parameters required to correlate experimental data. The Nusselt value for natural convection from dimensional analysis was shown to be a function of the Grashof and Prandtl numbers,

$$Nu = f(Gr, Pr)$$

The Grashof number is defined as the ratio of the buoyancy to the viscous forces in the fluid and it is written as,

$$Gr = \frac{g \beta L^3 (T_1 - T_2)}{\nu^2}$$

where, g = gravitational constant (9.81 m/s^2) for surfaces inclined at angle τ to the horizontal; the gravitational force along the surface is described by $g.sin\tau$

β = coefficient of expansion of the fluid (K^{-1}); for ideal gases $\beta = 1/T$

ν^2 = kinematic viscosity

The temperature difference $(T_1 - T_2)$ depends on the system. For a vertical wall, T_1 is the surface temperature and T_2 is the temperature of the undisturbed fluid. For free convection between two parallel surfaces, T_1 and T_2 are taken as the two surface temperatures.

Consider a rectangular enclosure, tilted at angle τ from the horizontal

(Figure 2) and assume T_1 to represent the temperature of the hot surface and let T_2 be the cold surface temperature. For a horizontal enclosure heated from below ($\tau = 0$) Jakob (94) quotes correlated empirical equations for three distinct regions:

$$\overline{Nu_L} = 1 \qquad \text{for } Gr_L < 1700$$

$$\overline{Nu_L} = 0.21(Ra_L)^{\frac{1}{4}} \qquad \text{for } 10^4 \leq Gr_L \leq 3.2*10^5$$

$$\overline{Nu_L} = 0.075(Ra_L)^{1/3} \qquad \text{for } 3.2*10^5 < Gr_L \tag{16}$$

where these represent conduction, laminar flow and turbulent flow respectively. The term Ra_L is the Raleigh number which is the product of the Grashof and Prandtl numbers. An alternative expression to describe pure convection within a horizontal enclosure was proposed by Globe and Dropkin (99),

$$\overline{Nu_L} = 0.067Ra_L^{1/3}Pr^{0.074} \qquad \text{for } 3x10^5 < Ra_L < 7x10^9 \tag{17}$$

In equations (16) and (17) no account is taken of the aspect ratio of the enclosure.

In a vertical enclosure ($\tau = 90^o$), it is the vertical surfaces that are heated and coolled, the following relationships are recommended where appropriate (100)

$$\overline{Nu_L} = 0.22\left(\frac{Pr}{0.2 + Pr}\,Ra_L\right)^{0.28}(H/L)^{-\frac{1}{4}} \tag{18}$$

which is valid for $2 \leq H/L < 10$, $Pr < 10^5$ and $Ra_L < 10^{10}$, and

$$\overline{Nu_L} = 0.18\left(\frac{Pr}{0.2 + Pr}\,Ra_L\right)^{0.29} \tag{19}$$

for $1 < H/L < 2$, $10^{-3} < Pr < 10^5$, $10^3 < (Ra_L Pr)/(0.2 + Pr)$. For large values of the aspect ratio, (H/L), MacGregor and Emery (101)

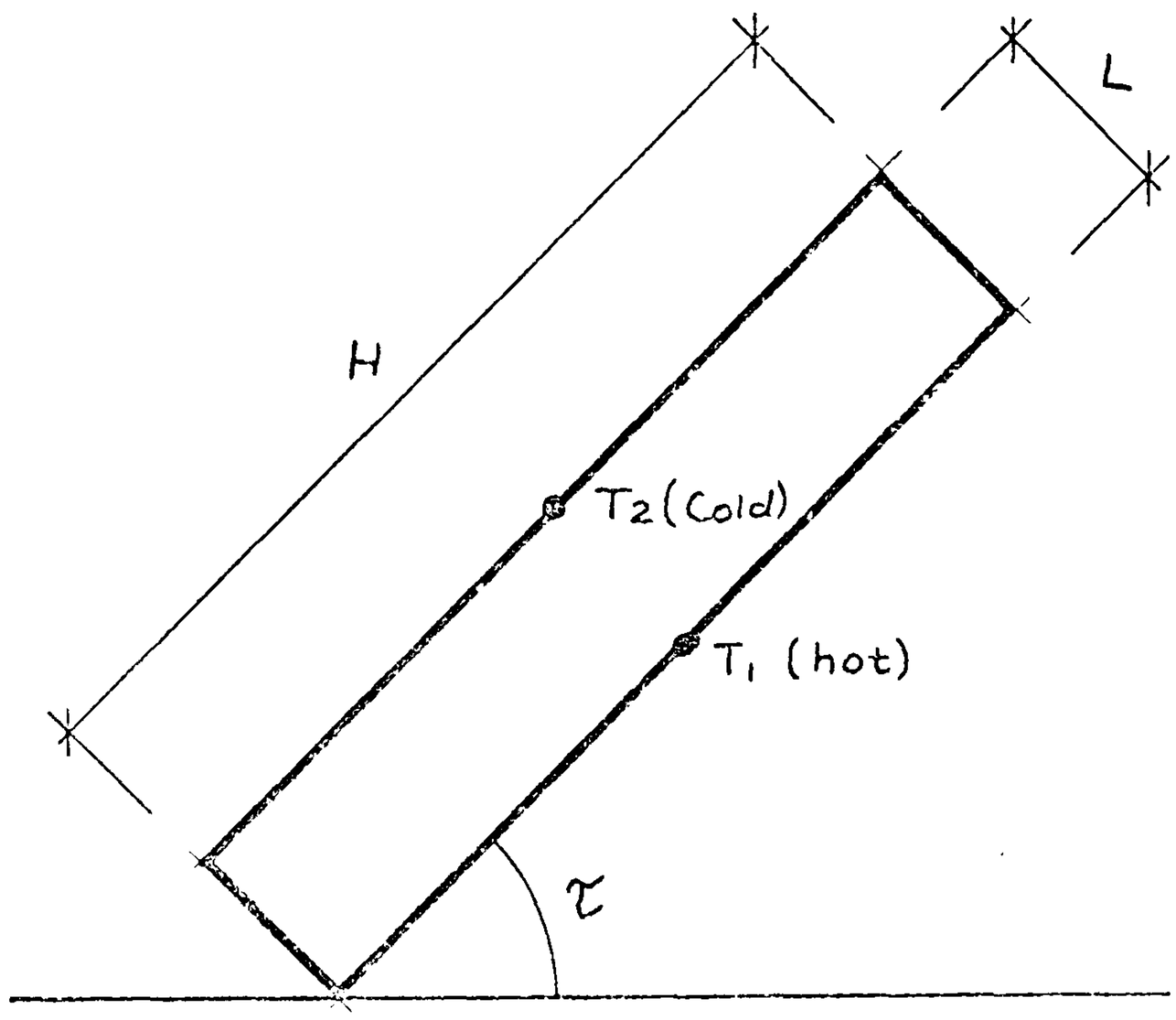

Figure 2: Free convection in a rectangular enclosure

have proposed the following correlations

$$\overline{Nu_L} = 0.42\ Ra_L^{\frac{1}{4}} Pr^{0.012} (H/L)^{-0.3} \tag{20}$$

for $10 < (H/L) < 40$, $1 < Pr < 2*10^4$ and $10^4 < Ra_L < 10^7$, and

$$\overline{Nu_L} = 0.046 Ra_L^{1/3} \tag{21}$$

for $1 < H/L < 40$, $1 < Pr < 20$ and $10^6 < Ra_L < 10^9$.

In flat plate solar collectors the aspect ratios are large, $(H/L) > 12$, and tilt angles are less than the critical value $\tau *$

for such cases the following correlation due to Hollands et al (102) is in excellent agreement with available data,

$$\overline{Nu_L} = 1 + 1.44\left[1 - \frac{1708}{Ra_L \cos\tau}\right]^* \left[1 - \frac{1708(\sin 1.8\tau)^{1.6}}{Ra_L \cos\tau}\right] + \left[\left(\frac{Ra_L \cos\tau}{5830}\right)^{1/3} - 1\right]^* \tag{22}$$

for $(H/L) \geq 12$ and $0 < \tau < \tau *$. The notation $[\ ]^*$ implies that if the quantity in the brackets is negative, then it must be set to zero. For small aspect ratios Catton (100) suggests that reasonable results may be obtained from a correlation of the form

$$\overline{Nu_L} = \overline{Nu_L}_{(\tau=0)} \left[\frac{\overline{Nu_L}_{(\tau=90)}}{\overline{Nu_L}_{(\tau=0)}}\right]^{\tau/\tau^*} (\sin\tau^*)^{(\tau/4\tau^*)} \tag{23}$$

for $(H/L) \leq 12$ and $0 < \tau \leq \tau *$.

Beyond the critical tilt angle the following correlations are recommended for all aspect ratios,

$$\overline{Nu_L} = \overline{Nu_L}_{(\tau=90)} (\sin\tau)^{1/4} \qquad \text{for} \quad \tau^* < \tau < 90^\circ \tag{24}$$

and

$$\overline{Nu_L} = 1 + \left[\overline{Nu_L}_{(\tau=90)} - 1\right] \sin\tau \quad \text{for} \quad 90^\circ < \tau < 180^\circ \tag{25}$$

The mean Nusselt number for vertical and horizontal flat plates were correlated by MacAdams (93) to fit the form

$$\overline{Nu_m} = C\ (Gr_L\ Pr)^m \qquad (26)$$

where L is the length of the plate. Table 2 lists appropriate values of C and m. For surfaces inclined at 45^o Jakob (94) recommends using the average of the vertical and horizontal enclosures to obtain the Nusselt number at 45^o, thus

$$\overline{Nu_{\tau=45}} = 0{\cdot}5\left(\overline{Nu_{(\tau=0)}} + \overline{Nu_{(\tau=90)}}\right) \qquad (27)$$

This equation agreed to within 2% of experimental data. Due to the lack of available information, the following expression based on equation (27) is used to estimate the Nusselt number at any angle of incidence between 0^o and 90^o

$$\overline{Nu_\tau} = \overline{Nu_{(\tau=90)}} + \left(\frac{90-\tau}{90}\right)\left(\overline{Nu_{(\tau=0)}} - \overline{Nu_{(\tau=90)}}\right) \qquad (28)$$

A6.1.3 Mixed Flow

Natural convection is always present in forced convection processes, normally the velocity forces are dominant and the buoyancy forces can be neglected, therefore, the problem may be treated as a pure forced convection case. The converse is true if the velocity forces are insignificant compared to the natural convective process. Ozisik (88) showed that a dimensionless term (Gr/Re^2), can be derived from the momentum equation which provides a measure of the ratio of natural convective to forced convective forces. If $Gr/Re^2 << 1$, then the problem can be treated as forced convection only, if $Gr/Re^2 >> 1$ the problem is a natural convection problem, however, if $Gr/Re^2 \approx 1$ that is, the effects of forced and natural convection are of the same order and neither can be neglected, the flow regime is called Mixed Flow.

Mixed flow remains a poorly investigated field of work, there are however some correlated empirical equations for vertical (55, 103)

		C	n
Vertical			
Laminar	$10^4 < Gr_L Pr \leq 10^9$	0.59	1/4
Turbulent	$10^9 < Gr_L Pr \leq 10^{13}$	0.10	1/3
Horizontal			
Laminar[1]	$10^5 < Gr_L Pr \leq 3x10^{10}$	0.54	1/4
Laminar[2]	$3x10^5 < Gr_L Pr \leq 3x10^{10}$	0.14	1/3
Turbulent[1]	$2x10^9 < Gr_L Pr < 3x10^{10}$	0.27	1/4

Table 2. Constants c and n of equation 26 for free convection from a vertical and horizontal plate.

Nb.1. upper surface heated or lower surface cooled

2. lower surface heated or upper surface cooled

and horizontal (104) pipes. These expressions agree well with experiment but they are for special cases and cannot be applied generally. Three methods have been suggested to evaluate the Nusselt number under fixed flow conditions. The first method was suggested by MacAdams (93) which involved calculating the Nusselt number for both pure forced and pure free convection and using the larger of the two. Oostenhuizen and Bassey (105) showed this method to be in error by as much as 20%, they proposed a second technique for calculating the Nusselt number in a mixed flow region,

$$\overline{Nu} = (\overline{Nu}_{free}^{4} + \overline{Nu}_{forced}^{4})^{0.025}$$

The third method involves an empirical expression developed by Jackson and Yen (106)

$$\frac{\overline{Nu}}{\overline{Nu}_{forced}} = \left[1 + \frac{Gr}{Re^2}\right]^{0.25} \qquad (29)$$

This expression agrees well with experimental results consequently it will be used in forced convective flow applications within a solar energy collection system. The procedure for using equation (29) involves calculating the Nusselt value for forced convective flow and the term Gr/Re^2. If the term $Gr/Re^2 < 0.05$ then $\overline{Nu} = \overline{Nu}_{forced}$; equation (29) is used if $0.05 \leq Gr/Re^2 \leq 20$; and if $Gr/Re^2 > 20$ then the Nusselt number for free convection is calculated and used.

A 6.2 Heat Transfer due to Wind Effects

In the model of a flat plate solar collector the exposed external surfaces are subjected to convective and radiative exchange with their surroundings, as the radiative component is calculated by the external longwave radiation term given in Section 5.3.3 the wind heat transfer coefficient must relate to convective heat transfer only. Duffie and Beckman (34) quote the following expression for the wind convection coefficient

$$hw = 2.8 + 3.0v \tag{30}$$

where v is the wind velocity values of which are contained in the climate file. However, a minimum value of 5 w/m^2K is recommended for still air conditions, therefore, the heat transfer coefficient for the convective component at an exposed external surface can be expressed as

$$hw = \max\left[5,\ 2.8 + 3.0v\right] \tag{31}$$

This does not take account of wind direction which may have a considerable effect on hw. At present there are no suitable algorithms to modify hw for wind direction, therefore, using equation (31) for each surface irrespective of wind direction may result in an overestimation of the effects of hw. However, it is assumed that because a solar collector is a relatively small object the turbulance effects around the collector will result in a value of hw approximately to that calculated by equation (31).

A6.3 Condensation and Evaporation

Condensation of water occurs whenever moist air comes into contact with a surface whose temperature is below the dew-point temperature of the air, it cannot occur if the surface temperature is above the dew-point temperature, however, if the surface under such conditions is wet, evaporation will take place from the surface into the air.

In a solar collector the occurrence of condensation is important as it may promote corrosion of the absorber plate if a metal, consequently the periods of condensation occurrence will be noted in the simulation model.

The thermal effect of condensation and evaporation are so small in a solar collector they can be neglected. For example, if an air collector 2m x 2m x 0.1m is switched off and the retained air in the

collector duct is at 35°C and 70% R.H. and it is assumed that in one hour the internal surfaces of the collector drop to 0°C, then 0.01kg of water vapour will have condensed on the collector internal surfaces representing a loss of energy from these surfaces of ~1w/m^2.

A 6.4 Heat Transfer Coefficient in Packed Beds

In solar air heating systems the usual energy storage media is a packed bed of small rocks or crushed ground. The physical characteristics of pebbles vary widely, however, the convective heat transfer coefficient has been evaluated empirically assuming the pebbles are approximately spherical (20):

$$hv = 650\ (Go/Ds)^{0.7}$$

where hv = the volumetric heat transfer coefficient in w/m^{3}K
Go = mass velocity in Kg/sm^2
Ds = equivalent spherical diameter of the particles in m.

Ds is given by

$$Ds = \frac{6}{\pi r} \times \left(\frac{\text{net volume of particles}}{\text{number of particles}}\right)^{1/3}$$

The relationship between the volumetric heat transfer coefficient, hv, and the area heat transfer coefficient, hc, is

$$hv = 6hc(1 - \varepsilon)\ \frac{\alpha}{Ds}$$

where, ε is the void fraction and α is the surface area shape factor. It is an extremely arduous process to evaluate α, therefore, the volumetric heat transfer coefficient is the preferred term.

APPENDIX 7 Translation, Rotation and Projection Equations

The effect of surrounding obstructions, which cause shading on a solar collector, is to reduce the available incident solar energy, thereby reducing the collection potential of the collector. Similarly, in a ducted collector the absorber plate will receive less energy due to internal shading caused by the opaque side walls of the collector, this will be more critical at high incidence angles. To model these effects requires the ability to project points from one object to another, irrespective of the position of the surface onto which the points are being projected. This problem has already been solved by Clarke (5) for the ESP building energy model. Two programs are available to the users of this model:ESPSHD, which predicts the percentage of external surface shaded due to external obstructions and self-shading and ESPINS which predicts the percentage of an internal surface insolated due to solar transmission through windows (107). These programs can be used immediately with FLARE for fixed position solar collectors. These programs will be extended to analyse tracking solar collectors, to differentiate between these programs and the ESP programs they shall be called FLRSHD and FLRINS.

A planar reflector can be positioned next to a solar collector to increase the solar radiation incident, also, the collector may have some sun tracking mechanism to maximise the solar potential. In either case, the mathematical model established by Clarke can be used to model planar reflectors and tracking collectors. This Appendix will outline Clarke's mathematical model and describe its application to external surface shading, internal surface insolation, planar reflectors and sun tracking collectors. The objective of the model is to allow all points to be expressed in terms of a new local co-ordinate system located at the surface in question and the subsequent projection of points onto the plane of this face.

The general axes transformation and projection equations are as follows:

a) translation - move the coordinate system origin to the first vertex in the face under consideration - see Figure 1. This gives a new coordinate system in which any point (XYZ) translates to a new point $(X_1\ Y_1\ Z_1)$

$$(X_1 Y_1 Z_1) = (X\ Y\ Z\ 1) \begin{bmatrix} 1 & 0 & 0 \\ 0 & 0 & 1 \\ 0 & 0 & 1 \\ -X_o & -Y_o & -Z_o \end{bmatrix} \qquad (1)$$

and $(X_o\ Y_o\ Z_o)$ is the new origin in old coordinates; that is the components of translation in the X, Y and Z directions.

b) rotation - the translated axes must now be subjected to a X_1 Y_1 and Z_1 axis rotation as a function of angles α, β and γ, where

α = the local face orientation angle
β = the surface elevation angle
γ = the local X-axis tilt angle

The three axis rotations will result in the new coordinate system in the plane of the face under consideration. Any point $(X_1\ Y_1\ Z_1)$ therefore transforms to the point $(X_2\ Y_2\ Z_2)$ according to the relationship

$$[X_2\ Y_2\ Z_2] = [X_1\ Y_1\ Z_1] \begin{vmatrix} 1 & 0 & 0 \\ 0 & \cos\beta & -\sin\beta \\ 0 & \sin\beta & \cos\beta \end{vmatrix} \begin{vmatrix} \cos\gamma & 0 & \sin\gamma \\ 0 & 1 & 0 \\ -\sin\gamma & 0 & \cos\gamma \end{vmatrix} \begin{vmatrix} \cos\alpha & -\sin\alpha & 0 \\ \sin\alpha & \cos\alpha & 0 \\ 0 & 0 & 1 \end{vmatrix} \qquad (2)$$

where clockwise axes rotations (looking to the +ve side of the origin) are positive.

Substituting equation (1) in (2) gives the final axes transformation equation set

$$[X_2\ Y_2\ Z_2] = [X\ Y\ Z\ 1] \begin{vmatrix} 1 & 0 & 0 \\ 0 & 0 & 1 \\ 0 & 0 & 1 \\ -X_o & -Y_o & -Z_o \end{vmatrix} \begin{vmatrix} 1 & 0 & 0 \\ 0 & \cos\beta & -\sin\beta \\ 0 & \sin\beta & \cos\beta \end{vmatrix} \begin{vmatrix} \cos\gamma & 0 & \sin\gamma \\ 0 & 1 & 0 \\ -\sin\gamma & 0 & \cos\gamma \end{vmatrix} \begin{vmatrix} \cos\alpha & -\sin\alpha & 0 \\ \sin\alpha & \cos\alpha & 0 \\ 0 & 0 & 1 \end{vmatrix}$$

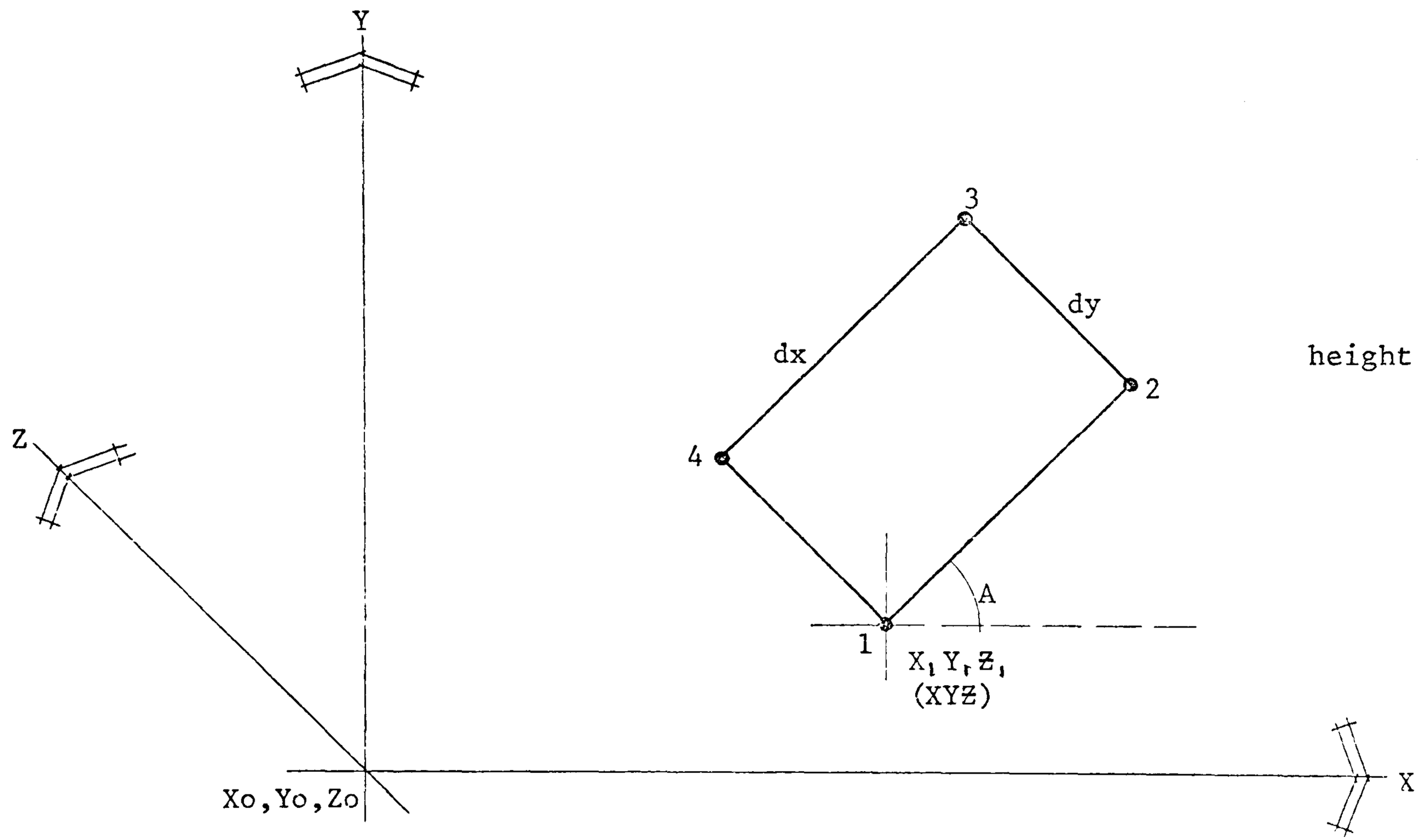

Figure 1 Axis translation

c) Projection - the vertices of the object to be projected can now by projected onto the plane of the X_2 Z_2 axes and the coordinates of the projected point relative to the local face coordinate system retained.

The equation for these projected points in terms of the transformed new local face coordinate system is given in matrix form by

$$\left|X_p \; Y_2 \; Z_p\right| = \left| X_2 \; Y_2 \; Z_2\right| \begin{vmatrix} 1 & 0 & 0 \\ \frac{-\sin\xi}{\cos\phi} & 1 & \frac{-\tan\omega}{\cos\xi} \\ 0 & 0 & 1 \end{vmatrix} \qquad (4)$$

where,

ω is the solar altitude expressed relative to the local face coordinate system

ξ is the solar azimuth expressed relative to the local face coordinate system.

The complete transformation and rotation equation is found by combining equations (3) and (4).

The method of calculating the percentage shading on each external surface is as follows:

1. Determine whether the surface is self-shaded or not. If self-shaded, consider the next surface.
2. Use equation (3) to produce a new local coordinate system for the surface so that an orthogonol view of the surface under consideration is obtained in the XZ axis.
3. Use equation (4) to project each point of a particular obstruction parallel to the sun's rays onto the new coordinate system. This will form a shadow polygon and the intersection of the surface and the shadow polygon represents that part of the surface which is shaded, see Figure 2.

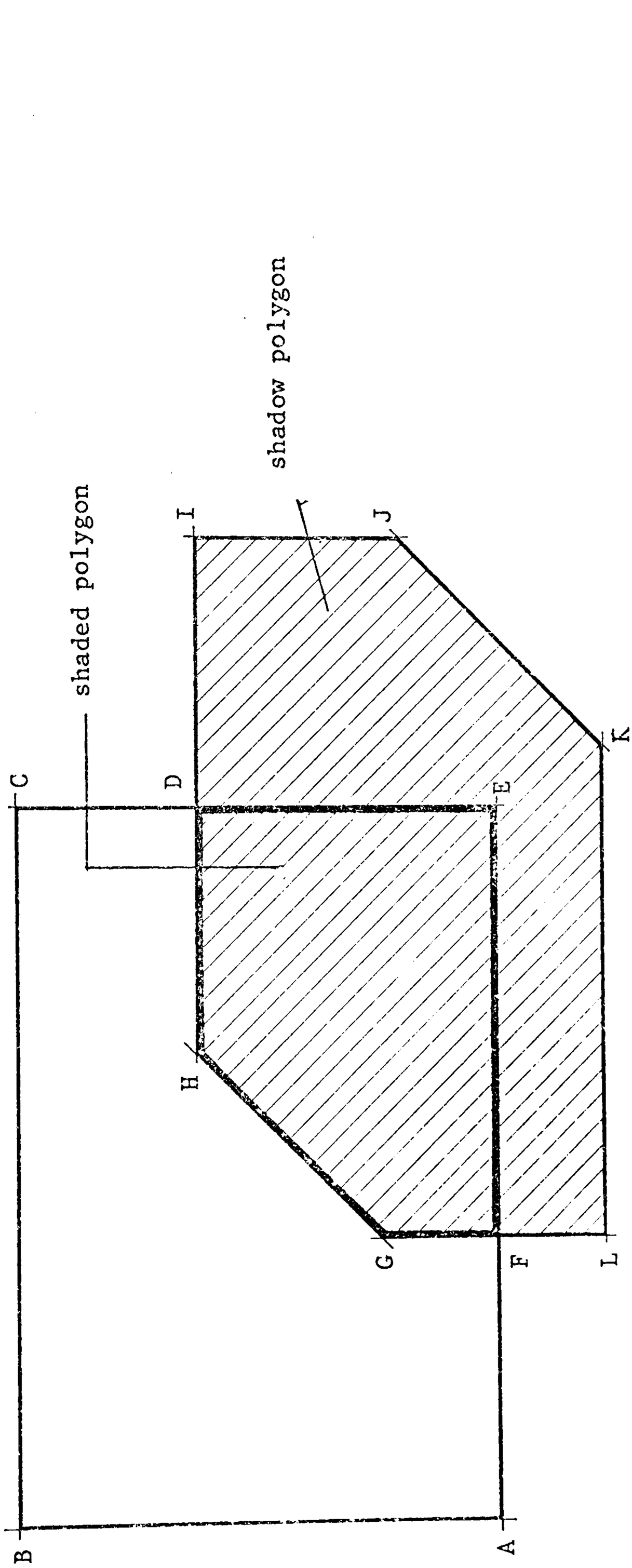

Figure 2: Example of surface shading (Polygon DEFGH)

4. The ratio of the shaded part of the surface to the whole surface is calculated. This is the value S_o required to solve equation (5.100). In a building there are normally several transparent elements and S_T can be calculated for each, where S_T is the ratio of the shaded part of the glazing to the total glazing area for each window. However, in a solar collector the uppermost surface is usually completely glass, therefore, $S_T = S_o$.

5. Return to step 1 unless each surface of the object body is analysed.

The values of S_o and S_T will vary between zero for unshaded and 1 for fully shaded.

ESPSHD will predict the hourly time-series shading of external opaque and transparent surfaces the results of which are transferred to an INSOLATION/SHADING file.

If there are no site obstructions, then a shading analysis is unnecessary however, a insolation analysis may be important for collectors with large side walls and receiving high incidence angles for most of the period under consideration. The procedure for conducting an insolation analysis is similar to that for a shading program. Each internal surface in turn, which is not self shaded relative to the sun, is used to establish a new local coordinate system, the vertices of the unshaded polygon on the window are each projected onto the plane of the surface. The resulting intersection of surface and insolation polygons represents that part of the surface which is insolated. This can be used to determine the value I which represents the ratio of the surface insolated by solar beam radiation. The value varies between zero for not insolated to 1 for fully insolated.

The hourly time series insolation values are transferred to the INSOLATION/SHADING file by the ESPINS program.

The default situation in ESPSHD is that all surfaces are unshaded by external objects and ESPINS assumes all direct solar radiation is input at the absorber plate as a default case.

A planar reflector is a device external to a solar collector as described in Section 5.3.1. It is used to increase the solar irradiation of the collector. Normally a planar reflector is designed to cover all the surface area of the collector - Figure 3 - however, the angle between the reflector and the collector is critical because it dictates the angle of incidence of the solar beam reflected onto the collector. If the angle of incidence is high, then the planar reflector will not be efficient although its reflections may cover the collector. Consequently, it may be necessary to reposition the planar reflector to lower the incidence angle of the reflected beam. A situation could arise where more radiation is obtained at the collector for a planar reflector positioned so that only part of its reflection is incident upon the collector (Figure 4). This situation will arise at other times of the day due to sun position and the finite size of the planar reflector. Therefore, it is important when using a planar reflector to predict the ratio of collector surface receiving the reflected beam - the ratio is denoted R and is required for equation (5.101) in Chapter 5.

A double projection method is used to evaluate the ratio R. Consider a source point projected parallel to the sun's rays onto the plane of an object which in this case is the planar reflector. If the projection is incident on the object plane then the planar reflector will reflect and absorb solar radiation. At this stage the model can take account of surface aberations to establish the reflected beam which can be considered to be the new path of the sun's rays. This problem can now be treated by a similar procedure to the shading procedure given above except that in this case the modified sun's ray after reflection is used to project the vertices of the planar reflector onto the plane of the collector, defined in its local coordinate system.

The maximum value of R is one which corresponds to a fully covered

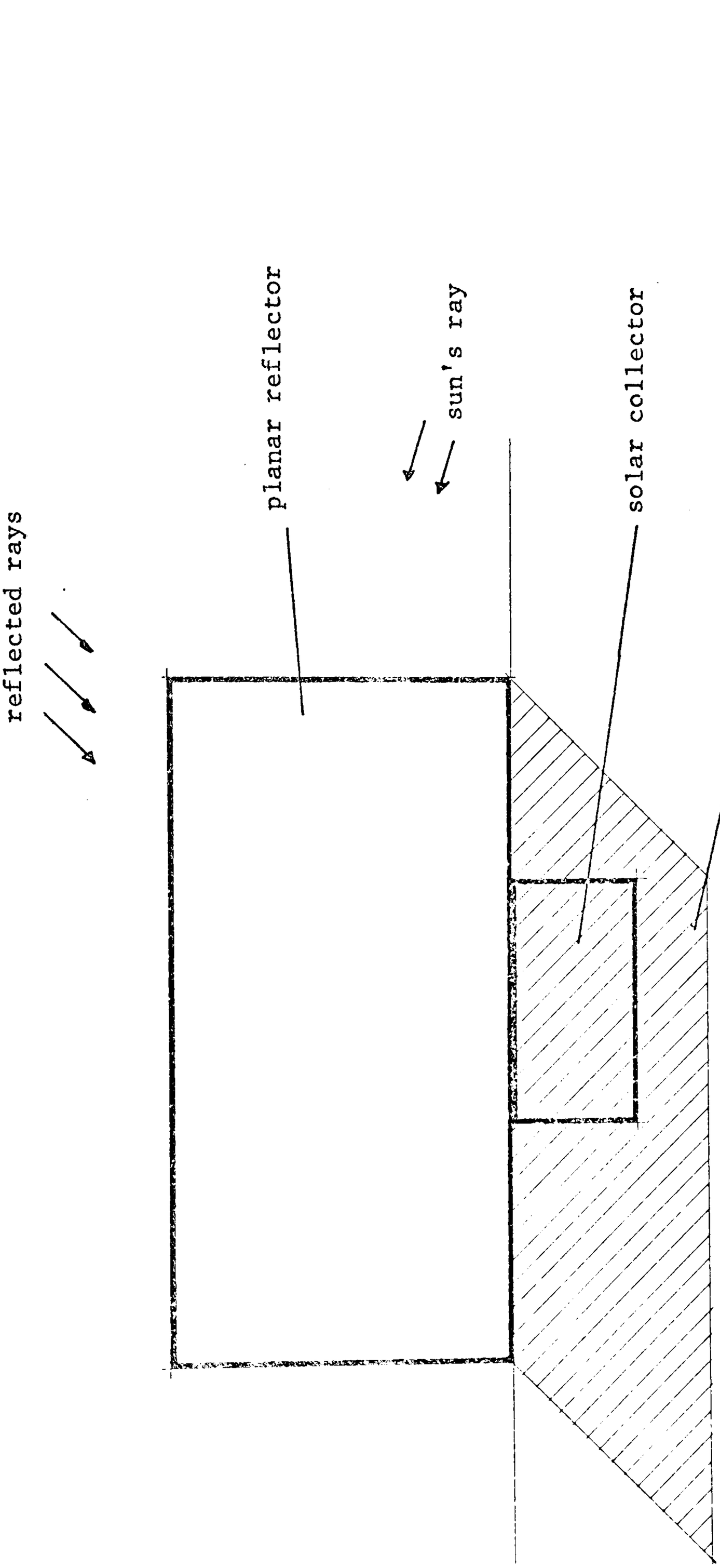

Figure 3: Reflected beam for a planar reflector associated with a solar collector

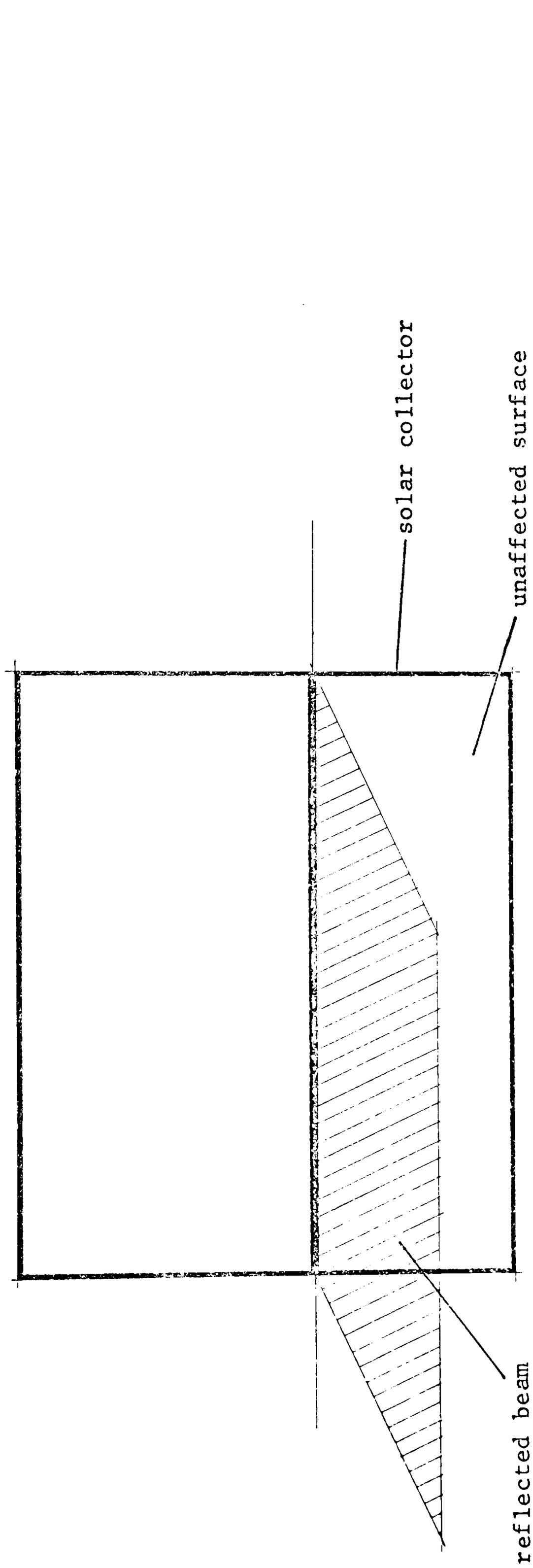

Figure 4: Example of solar reflector which does not fully cover the solar collector

collector surface and a minimum value of zero where there is no incident reflected beam on the surface or no planar reflector.

At present a program called FLRRFL is under development to produce a time series set of R values for a particular collector and planar reflector system. The default value, if a planar reflector is available is set to 1, that is the collector is fully covered by the reflection. Having established the R values it may be necessary to use ESPINS to evaluate which internal surfaces are insolated by the reflected beam from the planar reflector after transmission through the collector cover. An INSOLATION/REFLECTION file can be created in the exact manner of the INSOLATION/SHADING file.

Tracking devices are modelled in FLARE by using only the transformation expression - equation (3). If the rate of angular movement is known in any direction then the angular displacement during a particular time interval can be evaluated and used in equation (3) to predict the new position of the collector. This need only be done for one plane of the collector as the remaining planes are easily calculated because the geometry of the collector has been defined.

APPENDIX 8 The WINDOW Program

The theory required to analyse any transparent cover of a solar collector, where the surfaces are plane and parallel through which an undistorted view is obtained, is detailed in Section 3.3.1. As an aid to the design of the appropriate cover system for a collector a separate computer program called WINDOW has been developed based on the aforementioned theory. The program allows the user to analyse any combination of glass and/or plastic sheets which can have any number of thin films applied to their surfaces. The model will accurately predict the transmitted, reflected and absorbed components of incident radiation spectrally by a series of monochromatic wavebands represented by the mean waveband energy wavelength. This wavelength will vary depending upon the incident spectrum. The thermal properties of the transparent system are predicted at 25 different angles of incidence so that the system performance can be assessed as a function of angle of incidence.

This appendix describes the operation of the WINDOW program and identifies the facilities available to interrogate a particular collector cover design. The overall structure of the WINDOW program is described in Figure 1.

Prior to the prediction of a collector cover system, the user must define the system to be analysed. This data may be entered via menu pick 'INPUT'. The user can select from three different nodes of input (Figure 2), the mode selected depends on available information:

1) The user may have the physical properties of the system, that is, the refractive index, extinction coefficient and thickness of each transparent element for every waveband under consideration. If this is the case, then this facility allows the user to specify the system to be analysed.

2) This facility is the minimum input facility and is suitable only for single or double glazing glass or plastic sheets which have

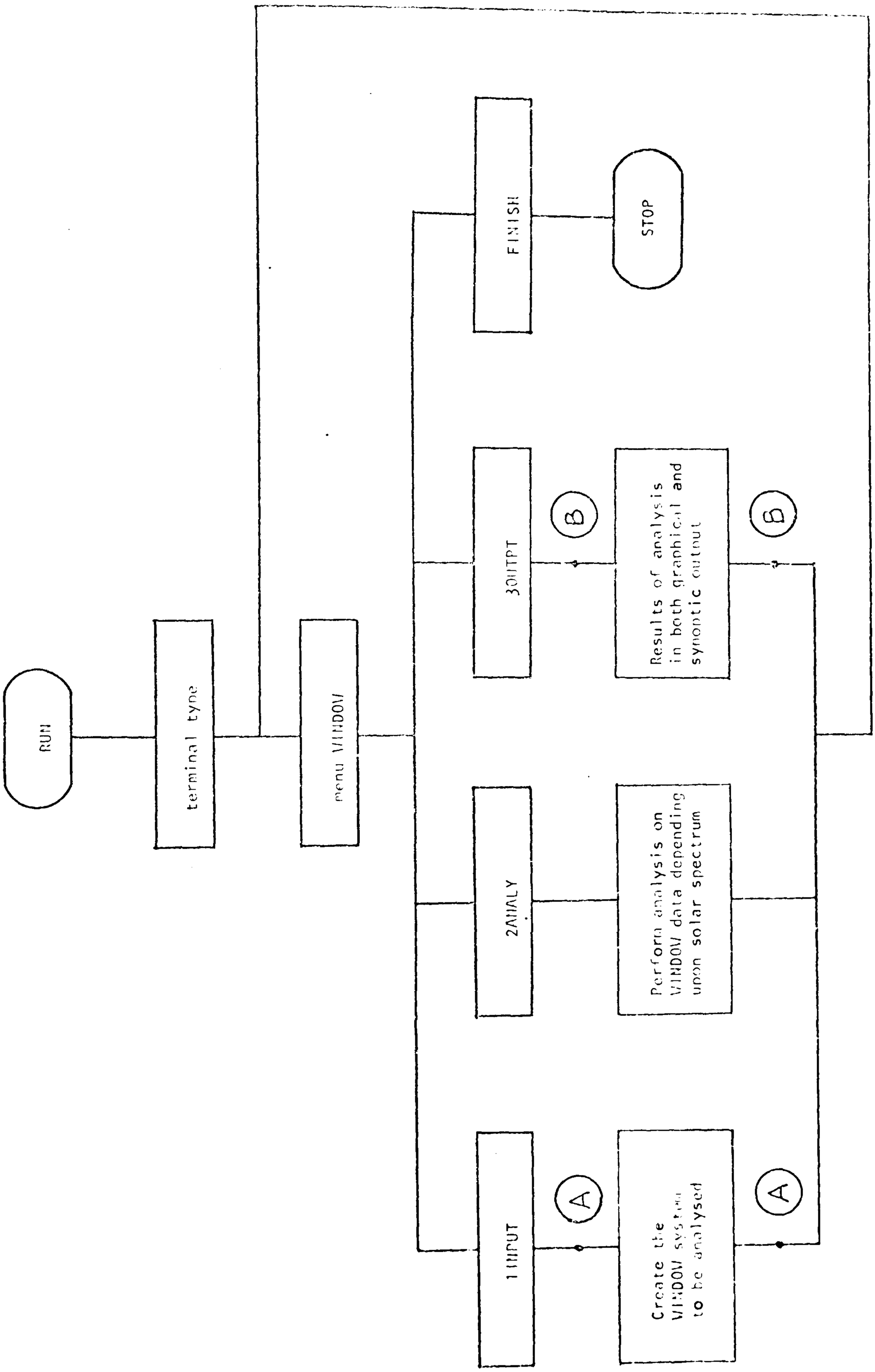

Figure 1 The WINDOW Program

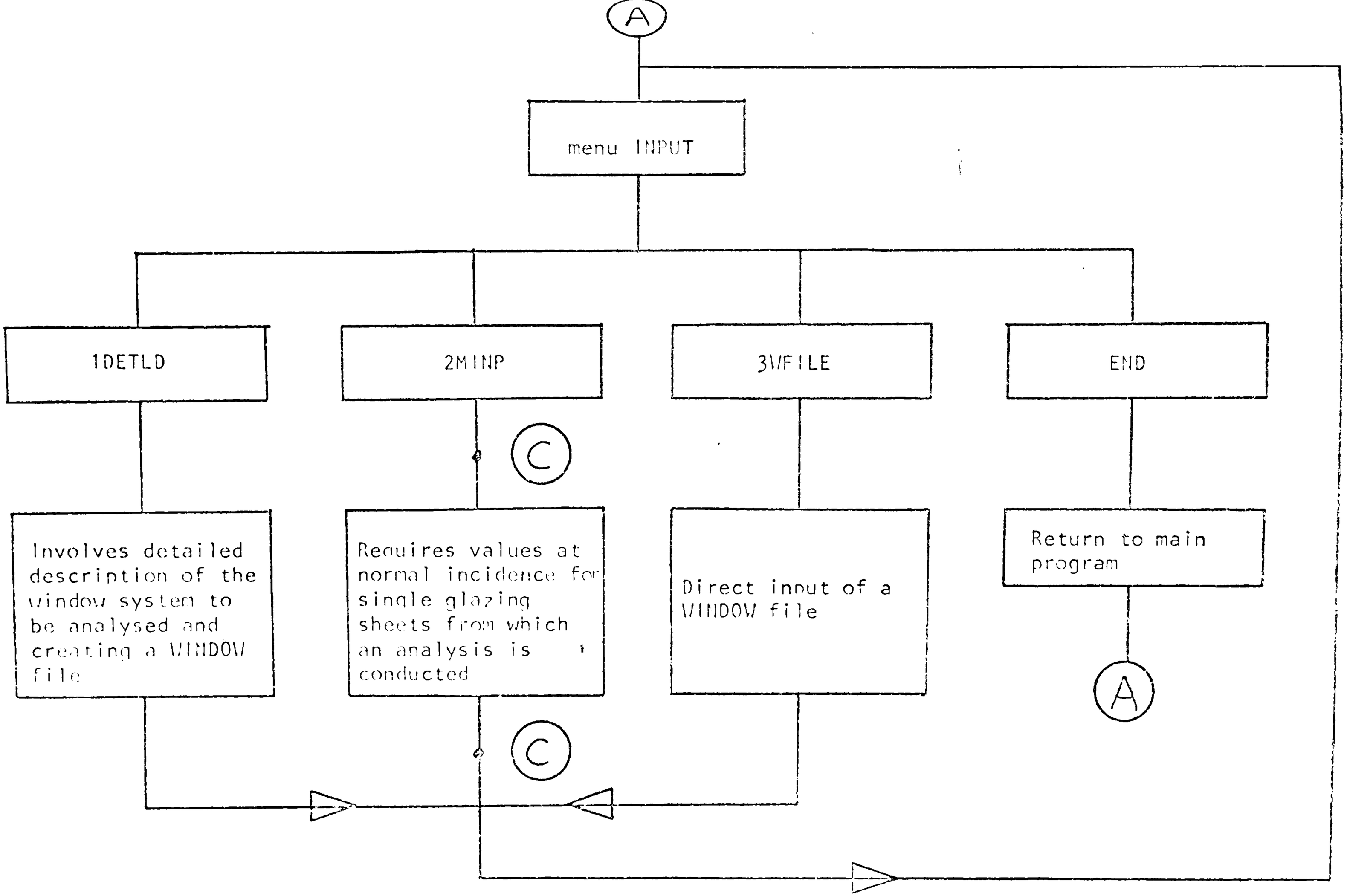

Figure 2 WINDOW : the input facilities

no thin films applied. The user need only know the values of solar transmission at normal incidence for ordinary glass or plastics and solar and light transmission values at normal incidence for heat absorbing glasses. WINDOW uses these values to predict the thermal properties of the system at all angles of incidence (108). If the user wishes to consider more than two sheets or thick films, then their properties should be obtained from this method and used to specify the system via mode 1 above.

3) This allows the direct input of a WINDOW file created manually or by one of the two previous modes.

To aid the detailed specification of a system - mode 1 - an optical properties database is currently under development which will contain the physical properties of a number of different elements. Each element will have a code number and the user will simply enter this number and its thickness to specify its physical properties thereby increasing the system permutations available to the user. The optical code for each element should be set to -1 indicating that this material is not available in the optical code.

The method of analysis of the transparent system depends upon the input mode. If modes 1 or 3 are selected then the user will return to the main menu (Figure 1) to conduct the analysis. The user may select the solar spectrum under which the analysis is conducted. The range of the solar spectrum considered is 0.3 μm to 5.0 μm and it is a function of:

a) the site : rural or urban
b) the sky clarity : clear or overcast
c) the zenith angle of the sun

Manufacturers glazing properties are normally given for the solar spectrum at Air Mass 2 and is equivalent to a solar zenith angle of 60^{o} on a clear day at a rural site. On conducting the analysis the user may view the results graphically or synoptically by means of five different output options, Figure 3.

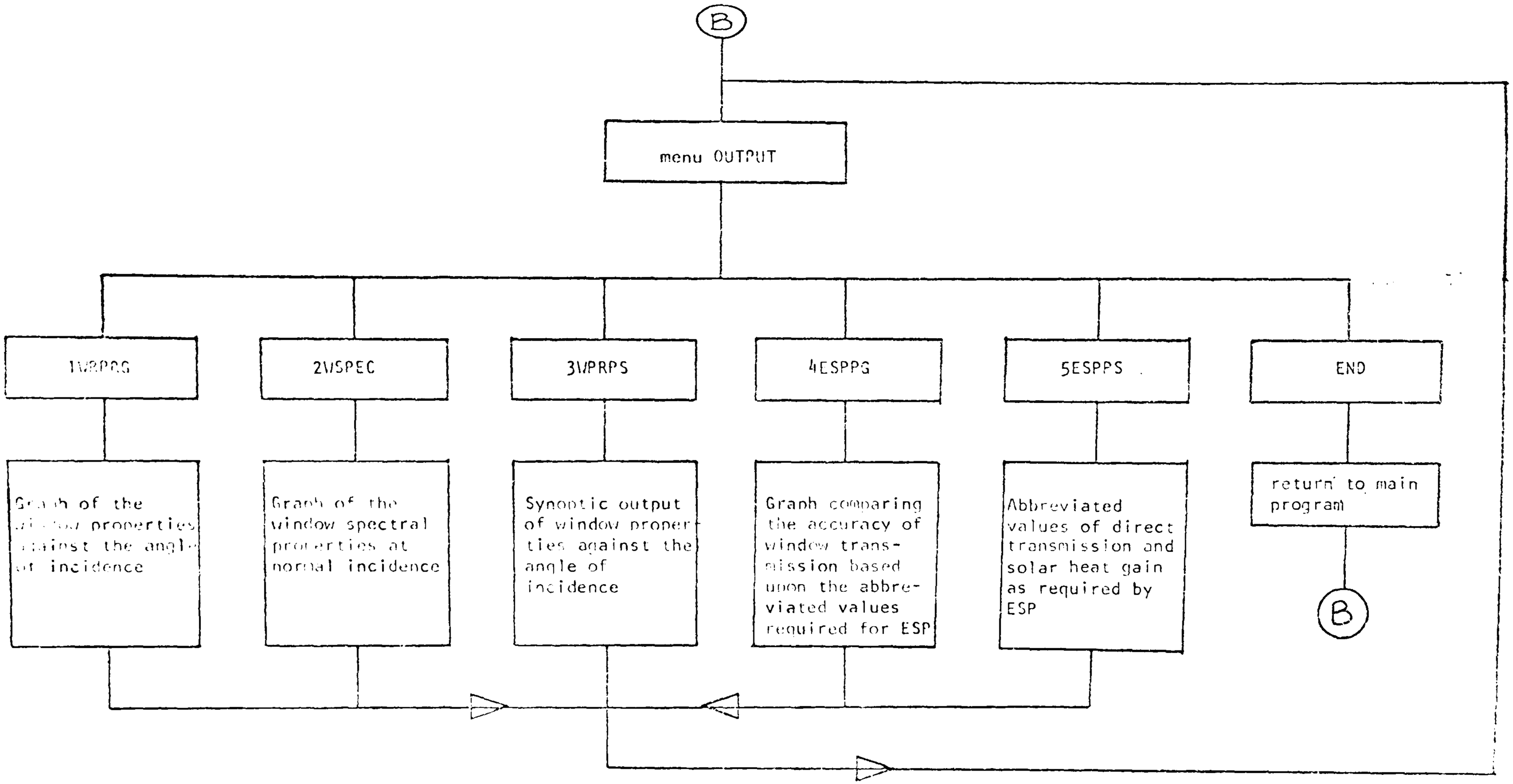

Figure 3: Output options for input modes 1 and 3

If the input mode 2 is employed then the analysis is conducted automatically using the Air Mass 2 spectrum. Upon completion of the analysis the user is presented with menu 'WROUTP', see Figure 4. This menu contains the same output options as obtained for the other input modes, additionally there is a facility to create a WINDOW file of the predicted optical properties and a facility to view the data to be written to such a WINDOW file.

Of the five output facilities available to each input mode, the two principal facilities is a graph of the system's thermal properties - menu pick '1WRPRG'- or a table of thermal properties at selected angles of incidence - menu pick '3WPRPS'. Examples are shown in Figures 5 and 6 respectively. If the system is analysed by a series of wavebands then the spectral performance of the system at normal incidence can be assessed selecting '2WSPEC' - Figure 7.

As WINDOW can analyse any transparent configuration it is also very useful to analyse windows for buildings, therefore, users of the ESP building energy model are currently using WINDOW to obtain the appropriate solar transmission and solar heat gain values as required by ESP (107). Two facilities are specifically for these users: '4ESPPG' and '5ESPPS' as shown in Figures 8 and 9.

The program has been extensively tested against the results of Mitalas and Stephenson (62) and against manufacturer's data. The results from the WINDOW program agreed well with the test data and it can be concluded that the WINDOW program is valid (60).

The ability of the program to analyse thin films makes it a powerful tool in the decision making process in solar collectors, for example, Figure 5 shows the thermal properties for a thin film deposited on 0.4 mm of clear float glass. If the clear float is analysed without the thin film and the results superimposed onto the graph of the glass plus thin film, it can be shown that there is a significant increase in the solar transmission, see Figure 10.

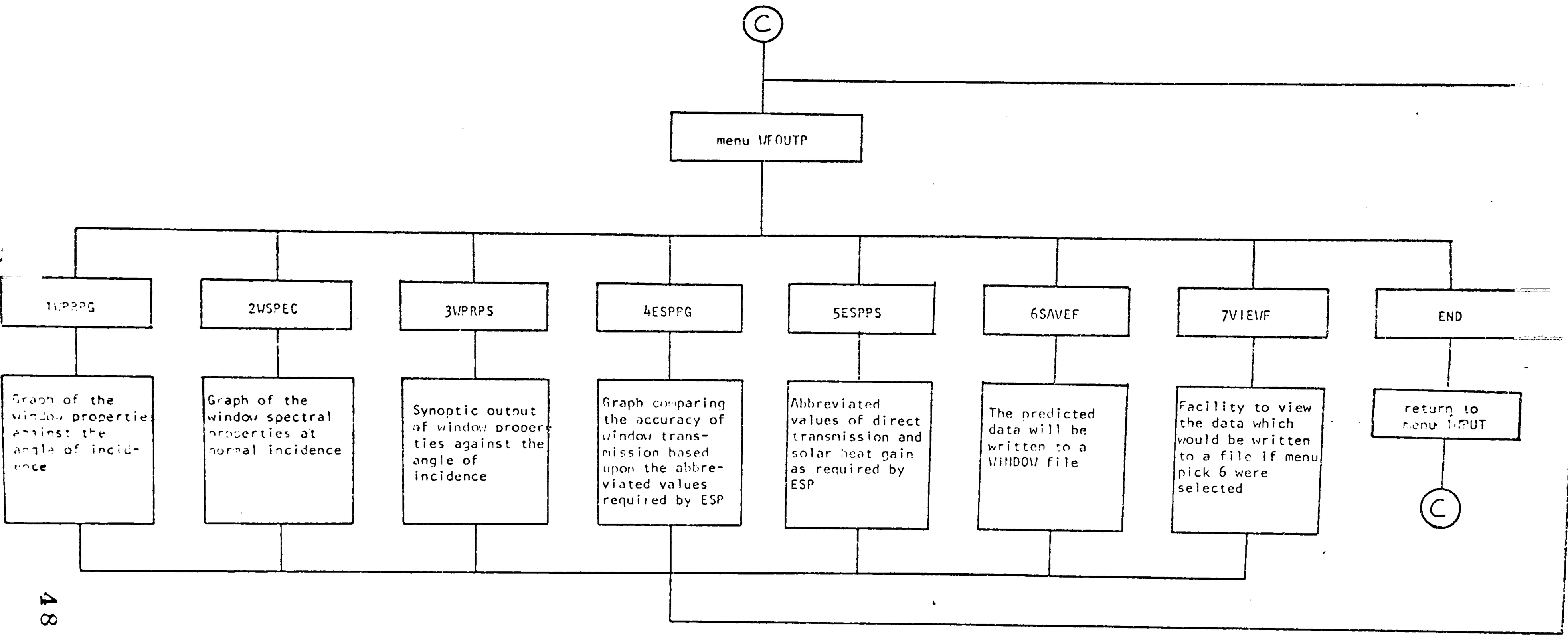

Figure 4 Output facilities for input mode 2

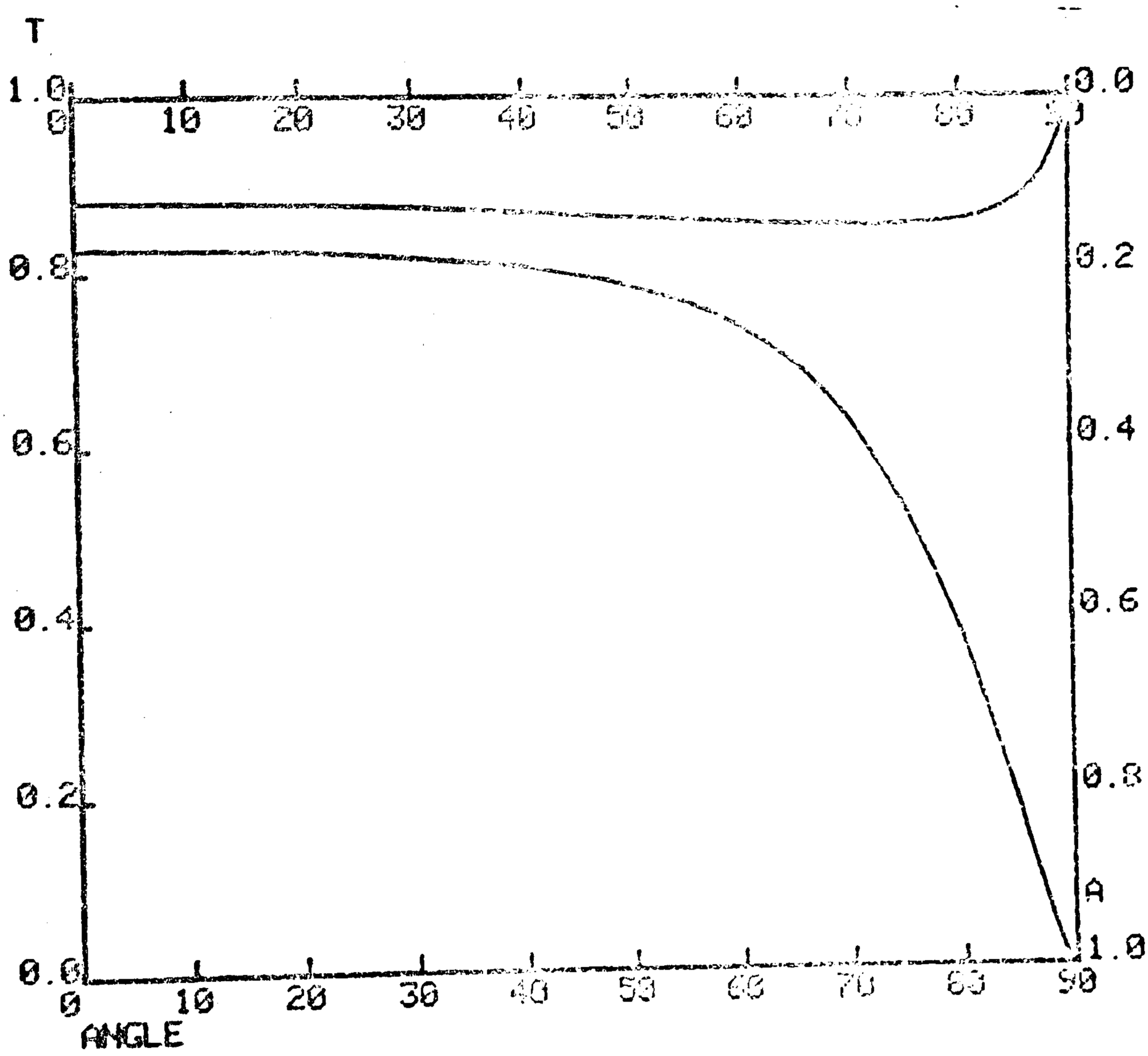

Figure 5 WINDOW graphical output (Menu pick '1WPRPG').

SYSTEM PROPERTIES
TRANSMISSIVITY, REFLECTIVITY & ABSORPTIVITY OF
THE SYSTEM AGAINST THE ANGLE OF INCIDENCE

ANGLE	TRANSM	REFLECT	ABSORB
0.00	.8284	.0537	.1180
20.00	.8250	.0541	.1209
30.00	.8197	.0559	.1244
40.00	.8090	.0618	.1292
48.00	.7920	.0733	.1358
55.00	.7679	.0948	.1373
57.00	.7578	.1034	.1392
60.00	.7391	.1259	.1410
63.00	.7150	.1525	.1425
65.00	.6940	.1721	.1439
68.00	.6635	.1970	.1445
70.00	.6284	.2356	.1460
72.50	.5931	.2718	.1450
75.00	.5279	.3277	.1444
77.50	.4614	.3961	.1425
80.00	.3820	.4788	.1393
82.00	.2897	.5516	.1586
83.50	.2001	.6224	.1775
85.00	.1037	.6904	.1179
86.00	.1423	.7496	.1080
87.00	.0934	.8963	.0953
88.00	.0552	.8550	.0798
89.00	.0179	.9359	.0461
89.50	.0051	.9693	.0255
89.99	0.0009	.9994	.0096

Figure 6 WINDOW tabular synoptic output (Menu pick '3WPRPS')

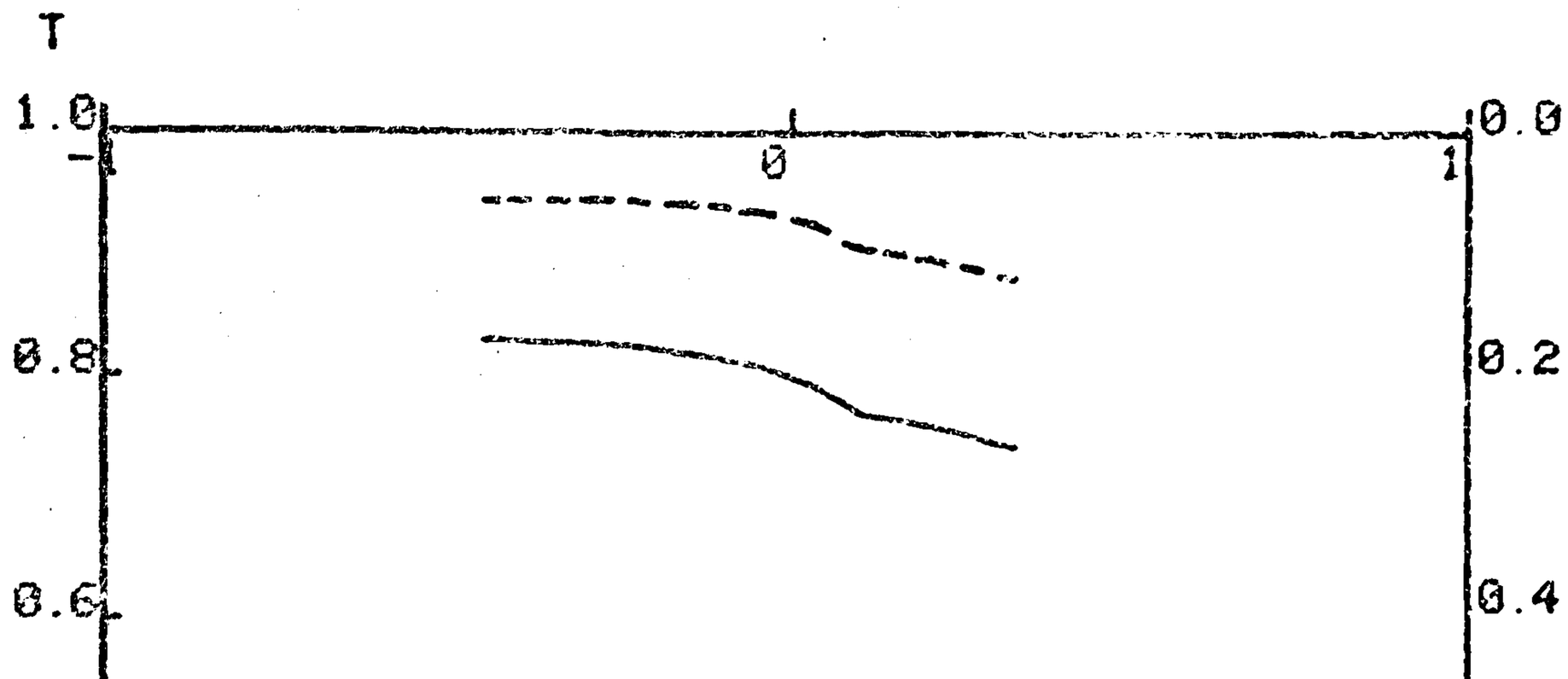

Figure 7 Spectral data at normal incidence (Menu pick '2WSPEC')

MINIMUM INFORMATION

INCIDENT ANGLE	DIRECT TRANS.	SOLAR HEAT GAIN
0.00	.8284	.8638
40.00	.8090	.8478
55.00	.7673	.8084
70.00	.6284	.6719
80.00	.3823	.4239

Figure 8 ESP window input data (Menu pick '4ESPPG')

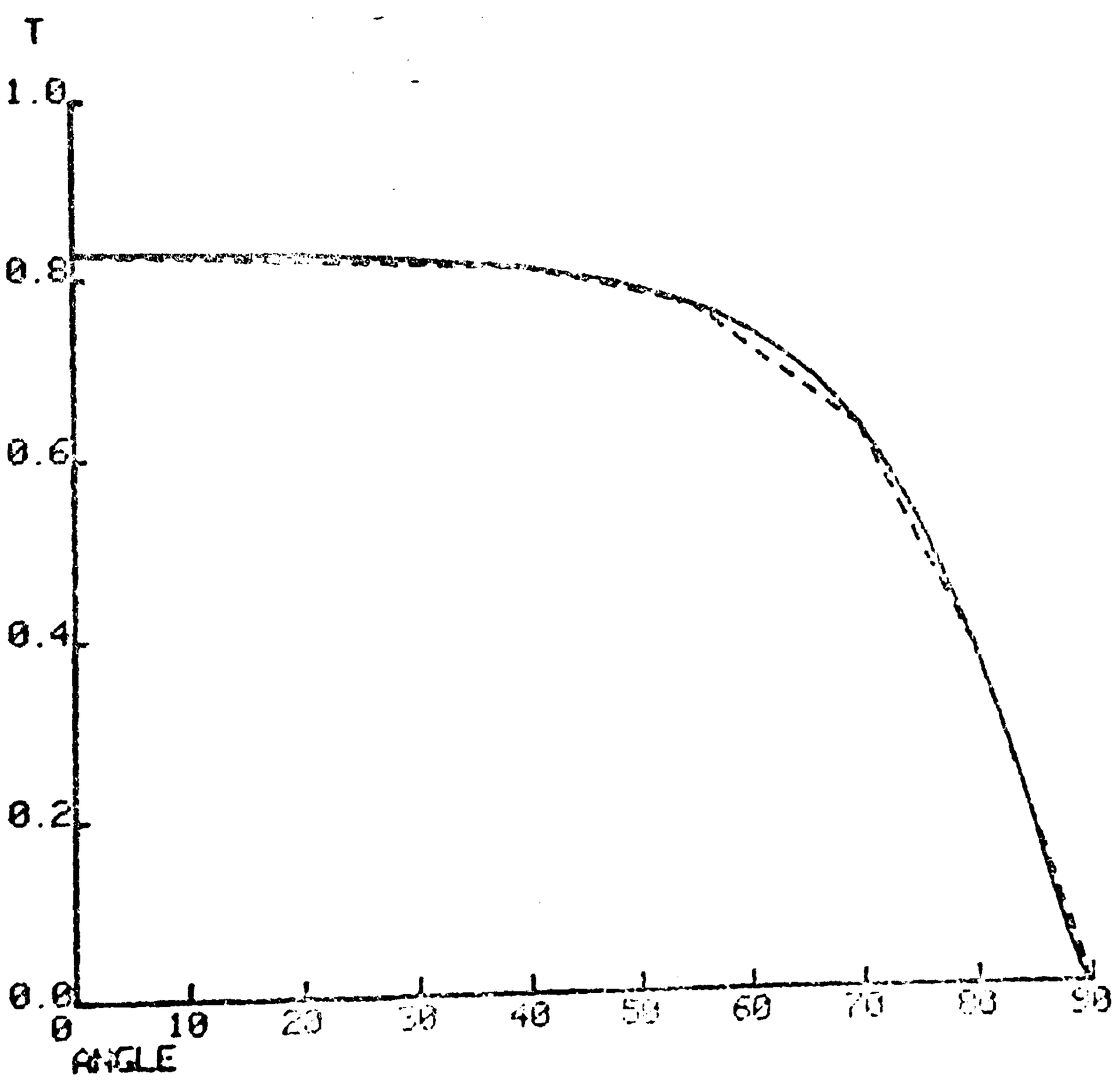

Figure 9 ESP analysis (_ _ _) compared with WINDOW (Menu pick '5ESPPS')

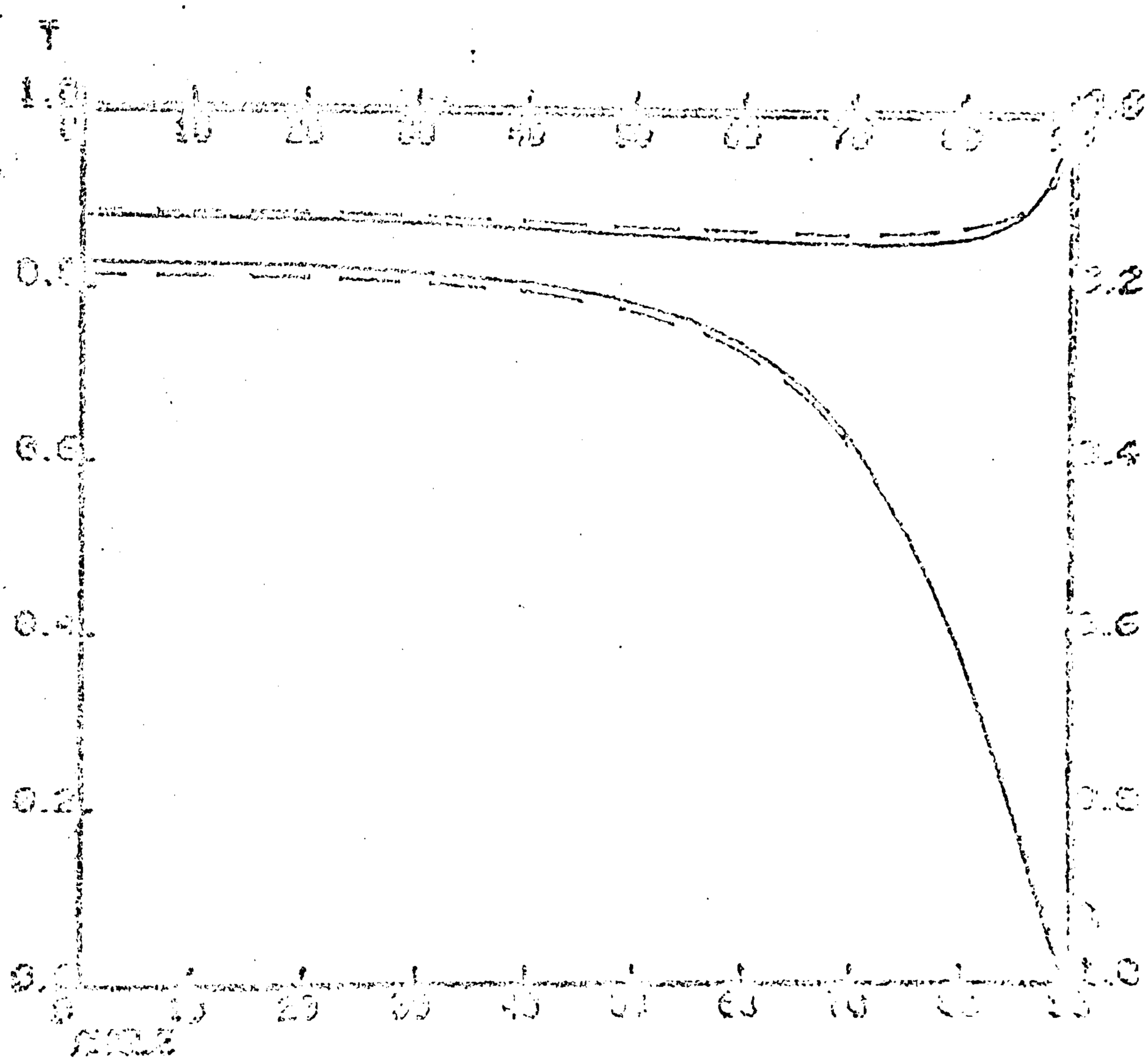

Figure 10 Comparison between glass with film and glass without film. The glass only curve is drawn dashed.

APPENDIX 9 Geometric Relationship between External Surface and Environment

In order to solve the net long-wave radiative exchange between a surface and its surrounding envelope it is necessary to calculate the geometric relationships or view factors of sky, ground and surrounding buildings in the envelope surrounding the 'viewing' surface. Three factors A, B and C have been identified in Section 5.3.3 to represent the view factors of sky, ground and buildings respectively. These factors depend upon:

1. Site application, i.e. the site may be classed as city centre, urban or rural,
2. Inclination of the surface from the horizontal.

Consider a rural site with no surrounding buildings, i.e. C=0, this is shown in Figure 1. The surface-sky and surface-ground view factors described by A and B respectively are,

$$A = (1 + \text{Cos}\ \phi) \ / \ 2 \qquad (1)$$

and

$$B = (1 - \text{Cos}\ \phi) \ / \ 2 \qquad (2)$$

where ϕ represents the angle of inclination of the surface from the horizontal.

If the site is not rural and surrounding buildings are included then the ratio C is involved and equations (1) and (2) are no longer valid as solutions for A and B, nevertheless, these equations are useful for indicating the ratio of the sky vault to ground as viewed by the surface under consideration.

The random nature of the effect of surrounding buildings in the surface's envelope increases the difficulty in calculating view factor C. If assumptions are made concerning the relationship between the viewing surface and its surrounding buildings, it is possible to

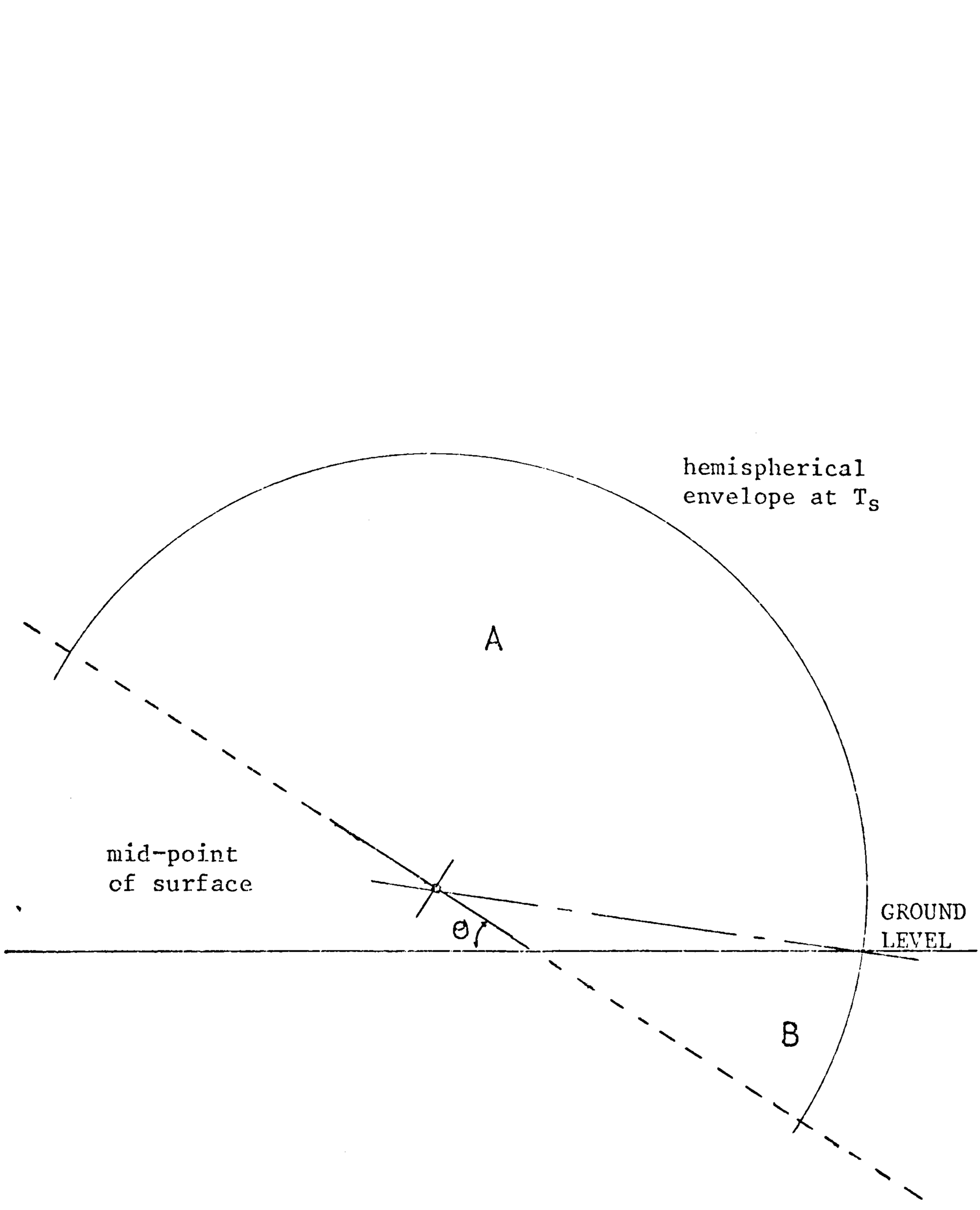

Figure 1 The effect of a tilted surface assuming no surrounding buildings. A and B represent the quantity of the envelope that is sky and ground respectively

establish the value of C. First consider a vertical viewing surface and assume surrounding buildings to be vertical and parallel to the viewing surface, if the form of the surrounding buildings and the distance between them and the surface are assumed then the view factor between the surfaces is denoted Cv, which is the vertical value of C.

The evaluation of Cv is more clearly understood by example. If a vertical surface is within a city centre the surrounding buildings are assumed parallel and at the same height but twice the length of the viewer surface (i.e. the side of a building). The distance between the two vertical planes equals half the height of the viewing surface (Figure 2). The view factor between these two planes was found to be 0.28, this is the value of Cv. Equation (5.122) gives

$$A + B + C = 1$$

therefore, it is possible to write,

$$(1 - Cv) = Av + Bv \qquad (3)$$

and the ratio of A to B from equations 1 and 2 can be used to evaluate the values of Av and Bv in equation (3). Table 1 gives values of Av, Bv and Cv for different applications within different sites, calculated by the technqiue described above. This table is only a guide to the values of Av, Bv and Cv and the user may select any values which are appropriate.

In most solar collector applications the collector will be tilted from the horizontal and the values of Av, Bv and Cv will require modification depending upon the angle of inclination of the surface.

The value of C is a maximum for the vertical case, as the surface deviates from the vertical position then either more ground or more sky will be seen and the value of C diminished. The value of C for any angle of inclination of a viewing surface can be expressed in the form,

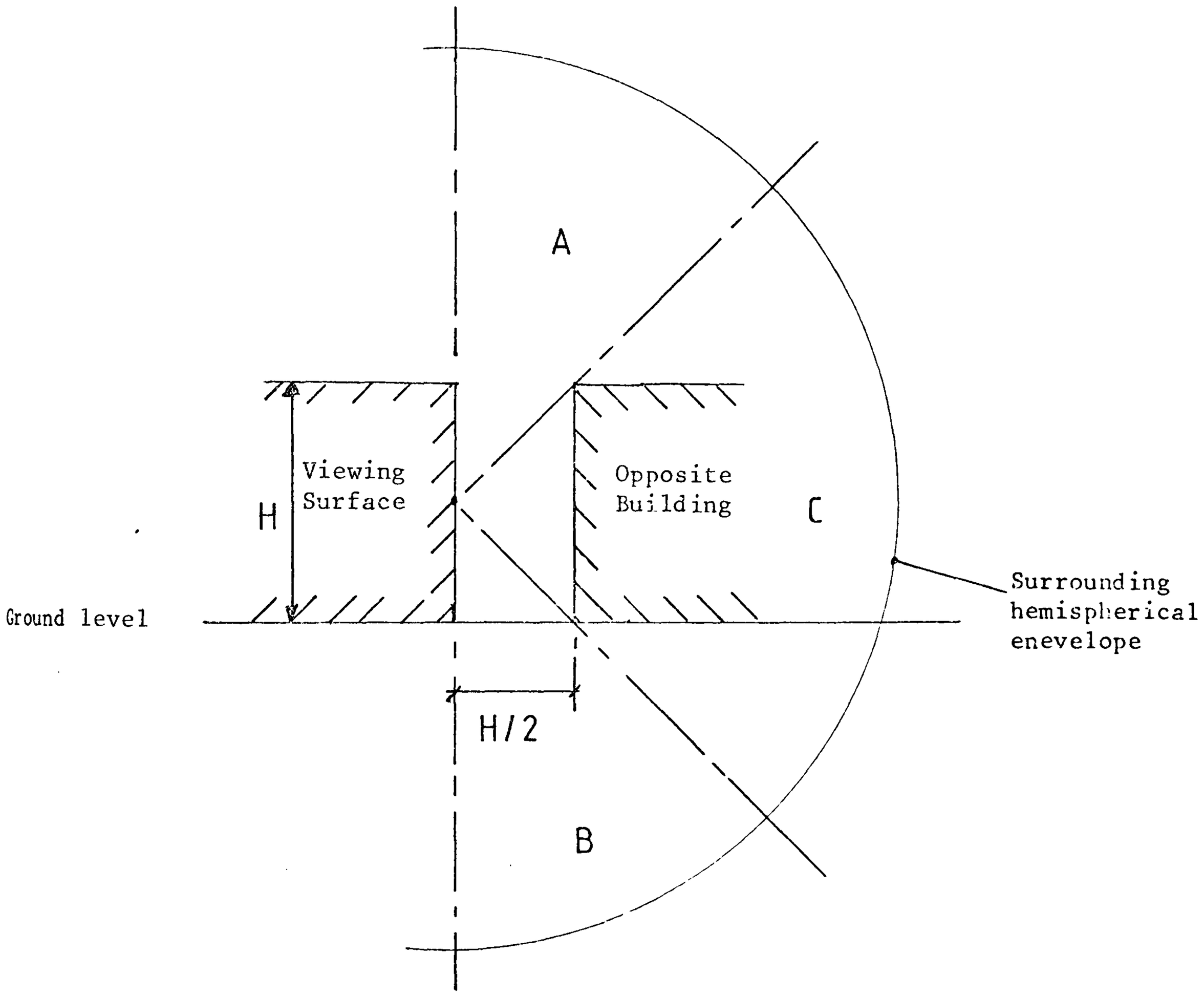

Figure 2 Relationship between the viewing surface and its envelope as detailed in Section 1 of Table 1

TABLE 1 View factors of the sky vault (Av), ground (Bv) and surrounding buildings (Cv), that are in the surrounding envelope of a vertical surface, depending upon the nature of the site under analysis.

	Av	Bv	CV
1. City centre site : surrounding building at same height, twice as long and half the height away from the surface, i.e. normal	0.36	0.36	0.28
2. Urban site : Normal case	0.41	0.41	0.18
3. Rural site : Normal case	0.45	0.45	0.10
4. City centre site : equally weighted proportions	0.33	0.33	0.34
5. City centre site : surface well below the mean height of the surrounding buildings	0.15	0.33	0.52
6. City centre site : surface at same height as surrounding buildings, i.e. sloping roof	0.50	0.20	0.30
7. Urban site : surface at same height as surrounding buildings, i.e. sloping roof	0.50	0.30	0.20
8. Rural site : isolated	0.50	0.50	0.00
9. Total enclosed surface : i.e. if solar collector is tested indoors, surfaces will be surrounded by 'building'	0.00	0.00	1.00

$$C = (1 - |\cos \phi|) * Cv \qquad (4)$$

where $|\cos\phi|$ is the modulus of the cosine of the angle of inclination of the viewing surface. Let the difference in the surface-building view factor between the vertical case and the non-vertical case be ΔC. For non-vertical cases ΔC must be accredited to either view factors A or B. If the surface is tilted towards the sky ($\phi < 90^{o}$) then ΔC is added to A because the surface has been tilted away from both the building and the ground. Similarly if $\phi > 90^{o}$, ΔC is added to view factor B.

In non-vertical cases the dominant view factor A or B includes ΔC and as inferred by equations (1) and (2) it also includes that amount of sky vault or ground that cannot be viewed because of the inclination. When $\phi < 90^{o}$ there is a portion of the vertical ground component, Bv, which cannot see the ground. The surface-ground view factor becomes,

$$B = Bv(1 - \cos \phi) \qquad (5)$$

The difference between Bv and the actual surface-ground view factor B is also added to the surface-sky view factor, thus

$$A = Av + (Bv - B) + (Cv - C) \qquad (6)$$

Alternatively, if $\phi > 90^{o}$, the surface is tilted towards the ground, then

$$A = Av(1 + \cos \phi) \qquad (7)$$

and

$$B = Bv + (Av - A) + (Cv - C) \qquad (8)$$

As view factors A, B and C can be estimated if the mean sky vault, ground and surrounding buildings temperatures are known, then the net radiative exchange between a surface and its surrounds can be calculated.

APPENDIX 10 Evaluation of Sky, Building and Ground Temperatures

1. Sky Vault Temperature, Tsky

The earth emits radiation at infra-red wavelengths greater than 4 μm. If the atmospheric air was completely dry and free of carbon dioxide the mean radiant night-time sky temperature would be very close to the absolute zero temperature of extraterrestrial space, equating to a temperature 280K below the typical ground level air temperature. Fortunately, the presence of water vapour and CO_2 in the atmosphere results in the earth's longwave radiation being partially absorbed and re-emitted back to earth, ensuring the effective clear sky night temperature is usually only 10 to 25K lower than the prevailing ground air temperature. This section is concerned with estimating the mean or effective sky vault temperature at any time, day or night.

The effective sky vault temperature, θ sky, can have a significant effect on the mean hemispherical envelope temperature because it is usually much lower than either the ground or the surrounding buildings temperatures. Due to the dominant effect of the sky temperature particularly during clear sky conditions a number of models often neglect the effects of the ground and surrounding buildings. In this model their effects are included.

In Section 5.3.3 it was assumed that the sky behaved as a black body, therefore, the energy emitted by the sky falling on a surface is,

$$q_{sky} = A\sigma T_{sky}^4$$

where A is the proportion of a surface's hemispherical envelope that is sky vault. If a horizontal surface is considered then A=1 and the maximum available sky radiation, Rs, would be incident upon the surface, therefore,

$$Rs = \sigma T_{sky}^4 \qquad (1)$$

Cole (72) has summarised the available relationships which estimate Rs. The sky radiation value is normally calculated as a function of the screen air temperature, Tsc. Using any one of the relationships given by Cole to calculate Rs allows equation (1) to be solved in terms of the sky vault temperature.

Swinbank (73) has tested an expression for clear sky long-wave radiation against data from different parts of the world and it was found to be very accurate,

$$Rs = 5.31 * 10^{-13} T_{sc}^{\prime 6} \qquad (2)$$

Substituting this expression for Rs into equation (1) and rearranging in terms of the clear sky temperature, as discussed above,

$$Tsky = 0.05532 T_{sc}^{\prime 1.5} \qquad (3)$$

When clouds are present the mean effective sky vault temperature increases because clouds tend to emit more radiation than the clear sky. The amount of cloud in the sky is indicated by the Cloud Cover Factor, CC, which has a numerical value between zero and one. The basic relationship for calculating the available sky radiation, Rs for cloudy skies is

$$Rs = (1-CC)Rs_{sky} + CC * \varepsilon_c \sigma T_c^4 \qquad (4)$$

where, CC = cloud cover factor

Rs_{sky} = clear sky radiation value (watts)

ε_c = emissivity of the cloud base

T_c = temperature of the cloud base (K)

The apparent emissivity of the cloud base, as given by Cole (72) is,

$$\varepsilon_c = (1 - 0.84CC)\,\varepsilon_A + 0.84CC$$

where,

$$\varepsilon_A = 0.527 + 0.161 \exp(8.45\ (1 - 273/T'_{sc}))$$

and the temperature of the cloud base is set equal to the screen air temperature,

$$Tc = T'_{sc}$$

Once equation (4) has been solved, the sky temperature for any cloud cover conditions is found from equation (1) as described earlier, thus

$$Tsky = \left[9.365574*10^{-6}(1-CC)T'^{6}_{sc} + CC\cdot\varepsilon_c T'^{4}_{sc}\right]^{0.25} \qquad (5)$$

2. Mean Surrounding Buildings Temperature, T_{Bld}

It is assumed that the temperatures associated with every building in a surface's surrounding envelope can be related to a mean surrounding building temperature. When estimating the temperature of surrounding buildings, it is advantageous to use the sol-air temperature. Consider any external surface exposed to ambient air temperature, solar radiation and a net longwave radiation exchange, see Figure 1(i). These processes have been combined into a sol-air temperature which results in the same surface temperature and heat flow, Figure 1(ii). The sol-air temperature, θ_{SA}, is given by

$$\theta_{SA} = \theta_A + (\alpha_S G_{T,S} - q_{Lw})/R_{SO}$$

where, θ_{SA} = sol-air temperature (degC)

θ_A = ambient air temperature (degC)

α_S = absorbtivity of the surrounding building surfaces

$G_{T,S}$ = total solar radiation incident upon surfaces (watts)

q_{Lw} = net lonwave radiation exchange per unit area (w/m^{-2})

R_{SO} = the resistance of the outside air film ($m^2.K.w^{-1}$)

The heat flux, q , from the inside of the building structure to the external surface equals the heat flux through the air film resistance,

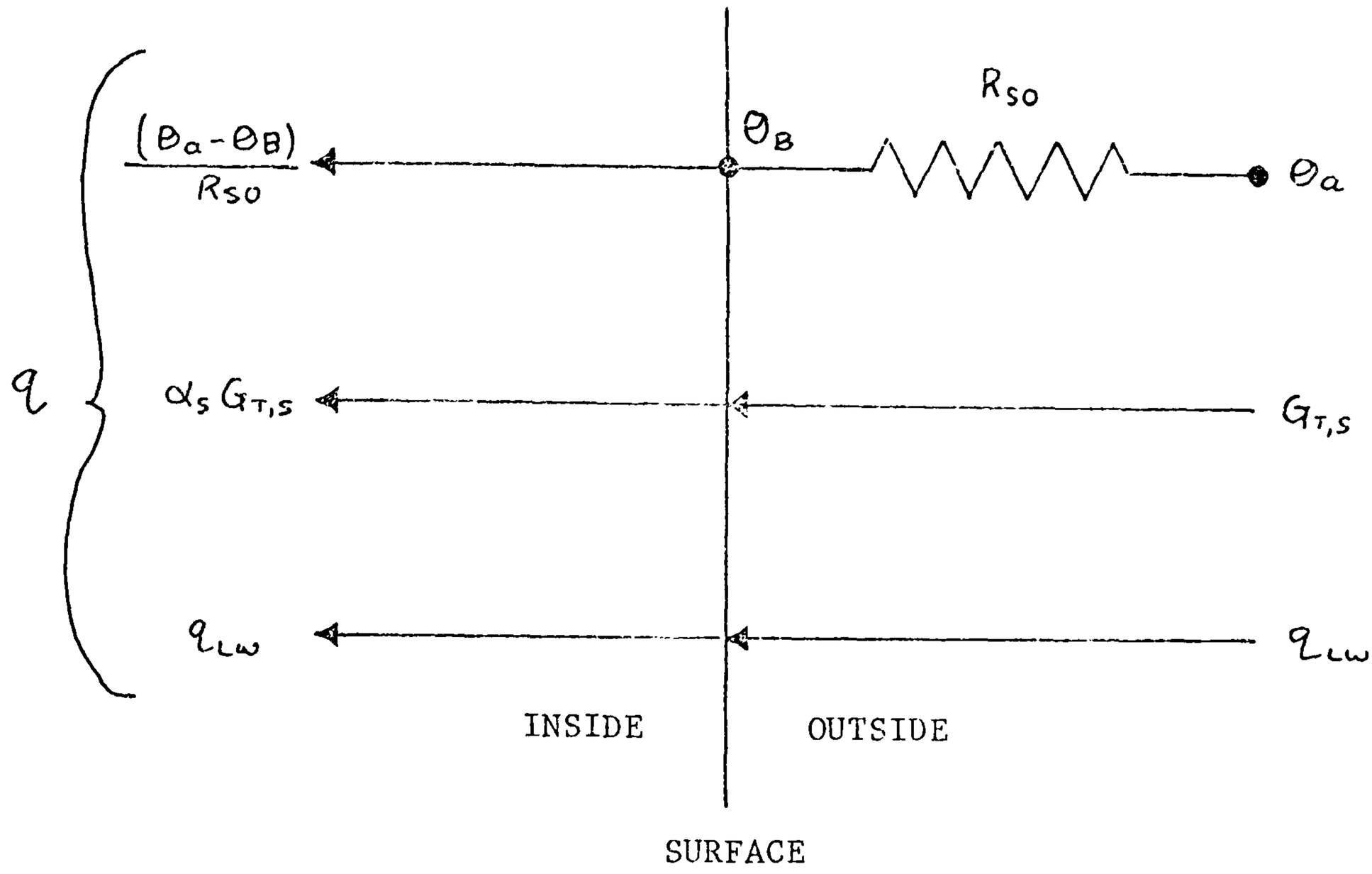

Figure 1(i) Surface with Radiation Exchange

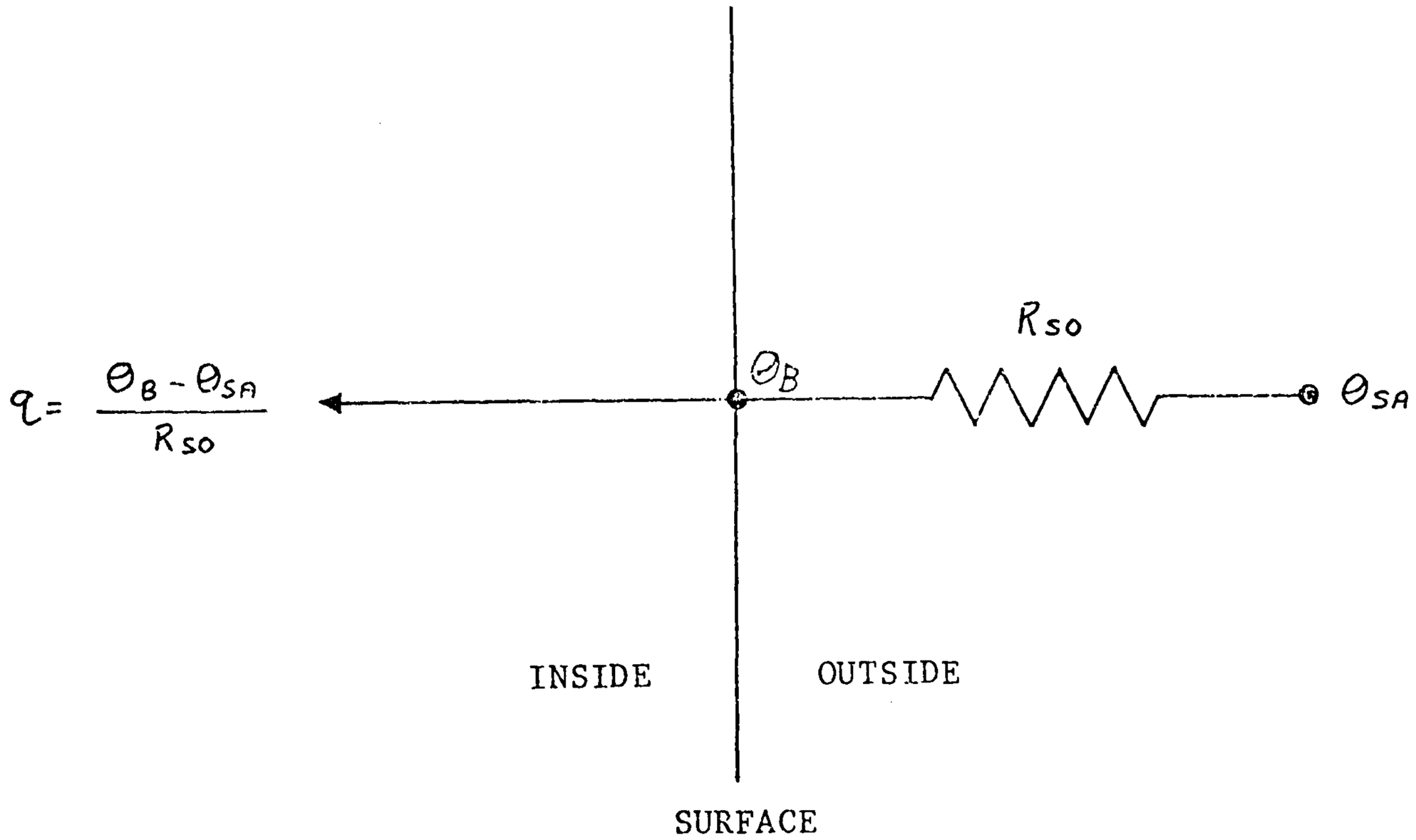

Figure 1(ii) Sol-Air Equivalent

thus

$$U'(\theta_R - \theta_B) = \frac{1}{R_{so}} (\theta_B - \theta_{SA}) \qquad (6)$$

where U' = the heat resistance through the structure, $(w.m^{-2}.K^{-1})$,

θ_R = room temperature, (degC),

θ_B = temperature of the building surface which is in radiative contact with the surface under analysis (degC)

Equation (6) can be rearranged to give,

$$\theta_B = \frac{U'R_{so}\theta_R + \theta_{SA}}{1 + U'R_{so}}$$

The absolute temperature of θ_B is equal to T_{Bld}, therefore,

$$T_{Bld} = \theta_B + 273.15$$

The longwave radiation exchange q_{LW} is given by

$$q_{LW} = \varepsilon_{B_s} \sigma (T_{B_E}^4 - T_{Bld}^4)$$

where ε_{B_s} = emissivity of the surrounding buildings surfaces

T_{B_E} = the hemispherical envelope temperature of the building surfaces (K)

The assumptions required in order to estimate T_{Bld} include:

- surrounding building surfaces parallel to surface under consideration and they have the same physical properties of absorptivity and emissivity

- room temperature can be set at any value, e.g. in a city set to $12^{o}C$, except between 7.00 and 19.00 hours when $\theta_R = 19^{o}C$.

3. Ground Temperature, T_{grd}

Any surface inclined from the horizontal will have some portion of the

ground contained in its surrounding envelope. Ground temperature measurements are seldom taken except for grass temperature readings. The ground temperature around a surface may vary considerably, however, an estimation of the mean ground temperature is required to solve the surfaces' envelope temperature.

The diurnal variation of temperature below the earth surface decreases rapidly with depth. At a depth of 0.3 m the diurnal range of temperature rarely exceeds 2.5°C, and is less than 0.01°C at 1.2 m. Seasonal changes in temperature can be detected at greater depths to more than 10 m. while at 30 m the temperature below open country is practically constant, the only changes occurring due to long term affects. Below 30 m there is a gradual rise in temperature because of earth core heat generation, the average increase in temperature with depth is about 1°C per 30 m.

Using the sol-air temperature concept to estimate the value of the ground temperature yields

$$\theta_g = \theta_A + (\alpha_g G_h - G_{g,LW}) / R_{so,g}$$

where θ_g = ground temperature (degC)

θ_A = air temperature (degC)

α_g = absorbtivity of the ground (see Table 1)

G_h = total solar irradiance incident upon ground (wm^{-2})

$G_{g,LW}$ = long-wave radiation exchange between the ground and its surrounding hemispherical envelope (wm^{-2})

$R_{so,g}$ = the resistance of the ground air film ($m^2K\ w^{-1}$)

The net longwave radiation exchange between the ground and its surrounding envelope is evaluated by a similar technique to that for the viewing surface under consideration (Section 5.3.3), thus

$$G_{g,LW} = \varepsilon_g \sigma (Tg^4 - Te_g^4)$$

where ε_g = the emissivity of the ground (see Table 1), dependent upon site

SITE	NATURE OF GROUND	εg	αg
1 City Centre	All tarmac	0.85	0.85
2 Urban	0.5 grass + 0.5 tarmac	0.875	0.825
3 Rural	All grass	0.9	0.8
4 Enclosed	All concrete	0.85	0.85

TABLE 1 Emissivity and absorptivity of the ground for each site

SITE	Ag	Bg	Cg
1 City Centre	0.34	0.33	0.33
2 Urban	0.60	0.20	0.20
3 Rural	0.95	0.05	0.00
4 Enclosed	0.00	0.00	1.00

TABLE 2 Proportions of the sky vault (Ag), viewing surface (Bg) and surrounding buildings (Cg) with reference to the ground, dependent upon site

Tg = absolute temperature of ground (K), i.e. θ_g + 273.15

Te_g = the absolute temperature of the surrounding hemispherical envelope of the ground (K)

The value of Te_g may be found from solving

$$\sigma Te,g^4 = Ag'\sigma Ts^4 + Bg'\sigma Tv^4 + Cg'\sigma Ta^4 \qquad (7)$$

This equation has a similar format to equation (5.142) although in this equation Tv represents the absolute temperature of the viewing surface. The equation used to solve Ag, Bg and Cg are different from those employed to solve A, B and C in Appendix 9, in this case,

$$Ag' = Ag$$
$$Bg' = Bg * (1 - \cos\theta)$$
$$Cg' = Cg + (Bg' - Bg)$$

where the values of Ag, Bg and Cg are given for various sites in Table 2. Calculating the values of Ag', Bg' and Cg' allows equation (7) to be calculated.

REFERENCES

1. GREELAY, R S. Energy use and climate. National Science Foundation. NSF-RA-N-75-052.

2. DEBS, A S (1981). Solar energy implementation in the Arab world. ISES Conference, Brighton, Pergamon Press.

3. HAMMARSTEN, S and SVENSSON, A (1982). Energy conservation in Swedish buildings 1973-1980. Proceedings CIB W67. Third International Energy Symposium, Dublin.

4. PEZZEY, J (1982). Energy consumption and conservation in buildings 1973-1980. Proceedings CIB W67. Third International Energy Symposium, Dublin.

5. CLARKE, J A (1977). Environmental Systems Performance, PhD Thesis, Glasgow, University of Strathclyde.

6. 1980 International Energy Annual. US Department of Energy, Energy Information Administration.

7. CARROLL, D (1982). Energy consumption and conservation in buildings; an international comparison. Proceedings CIB W67. Third International Energy Symposium, Dublin.

8. HERWIG, O (1981). Overview of Technical and Commercial Solar Energy Developments in the US in 1981. ISES Conference, Brighton, Pergamon Press.

9. LEVERENZ, D J (1982). Energy consumption and conservation in buildings in the US. Proceedings CIB W67. Third International Energy Symposium, Dublin.

10. Department of Energy (1981). Digest of UK Energy Statistics 1981. HMSO, London, UK.

11. B.R.E. Working Party (1975). Energy Conservation, Building Research Establishment, CP 56/75.

12. Department of Energy (1975). EP no. 16. Solar Energy: its potential contribution within the UK. HMSO, London.

13. Journal of CIBS (September 1981), Vol. 3, no. 9, pp. 19.

14. HARDACRE, A C (1981). The UK DEn solar heating R & D programme. ISES Conference, Brighton, Pergamon Press, pp. 3179-3184.

15. GLASER, P E (1981). Progress in the development of Solar Power Satellites. ISES Conference, Brighton, Pergamon Press.

16. RAYMENT, R (1976). Wind Energy in the UK. Building Research Establishment, CP 59/76.

17. WILSON, J I B (1979). Solar Energy, Wykeman Publications (London).

18. LUNDE, P J (1980). Solar Thermal Engineering: space heating and hot water services. Wiley, USA.

19. THEKAEKARA, M P (1973). Solar Energy outside the earth's atmosphere. Solar Energy, Vol. 14, pp. 109-127, Pergamon Press.

20. KREIDER, J F and KREITH, F (1981). Solar Energy Handbook. McGraw-Hill, USA.

21. WIEBELT, J A and HENDERSON, J B (1979). Selected ordinates for total solar radiant property evaluation from spectoral data. Trans. ASME, Ser. Journal of Heat Transfer, Vol. 101, pp.101-107.

22. TABOR, H (1982). Farrington Daniel's Address. ISES Conference, Brighton 1981, Pergamon Press.

23. LINDBERG, R G and TURNER, F B (1982). Environmental considerations in siting solar thermal power systems in deserts of southwestern USA. ISES Conference, Brighton 1981, Pergamon Press.

24. LEBENS, R M (1980). Passive Solar Heating Design, Allied Science Publishers (UK).

25. CLARKE, J A (1982). Computer applications in the design of energy conscious building. C.A.D., Vol. 14, no. 1, pp. 3-9 (editor: J A Clarke).

26. LITTLER, J G F (1982). Overview of some available models for passive solar design. C.A.D., Vol. 14, no. 1, pp. 15-18 (editor: J A Clarke).

27. DUPONGNE, A and HAUGLUSRAINE, J M (1982). Passive Solar Modelling Sub-Group Solar Energy Applications to Dwellings, Vol. 1. Proceedings of the E C Contractors' Meeting, held in Athens 11th-13th November 1981. D Reidel Publication (Holland).

28. TRNSYS User Manual, solar energy laboratory, University of Wisconsin.

29. DUTRÉ, W L (1981). Concerted action European modelling group for space heating systems and domestic hot water systems. Solar Energy applications to dwellings, Vol. 1. Proceedings of the E C Contractors' Meeting, held in Athens 11th-13th November 1981. D Reidel Publication (Holland).

30. LA FONTAINE, L (1981). Active solar energy systems: introduction to the Faber solar simulation program, Faber computing operations.

31. YANESKE, P P and WILES, I C (1980). Physical modelling of air heating collectors. UK ISES, C24, October 1980, pp. 73-83.

32. SOLAREX CORPORATION (1979). Making and using electricity from the sun. TAB Books, USA.

33. JESCH, L F (1981). Solar Energy Today, UK - ISES.

34. DUFFIE, J A and BECKMAN, W A (1980). Solar Engineering of Thermal Processes, Wiley, USA.

35. British Standards Institution (1980). BS 5918: 1980. Code of practice for solar heating systems for domestic hot water.

36. MAYCOCK, P D (1982). Results of the US Residential Photovoltaics Program. ISES Conference, Brighton 1981. Pergamon Press, pp. 2695-2704.

37. PACE, J K and THOMPSON, J L (1982). Planned further development of an integrated climatological data system for building energy modelling. C.A.D., Vol. 14, no. 1, pp. 11-14 (guest editor: J A Clarke).

38. HOLMES, M J and HITCHIN, E R (1978). An "Example Year" for the calculation of energy demand in buildings. Building Services Engineer, January 1981.

39. STAMPER, E (1977). 'Weather Data', ASHRAE Journal, February 1977, p. 47.

40. ANDERSON, B et al. (1974). Meteorological data for design of building and installation: a reference year. Danish Building Research Institute Report No. 89.

41. LUND, H (1976). Requirement and recommendations for the test reference year. CIB Symposium, Vienna.

42. SAITA, H and MATSUO, Y (1974). Standard weather data for SHASE computer program of annual energy requirements and example results of hourly load for ten years in Tokyo. Second symposium on the use of computers for environmental engineering related to buildings, Paris, June 1974.

43. PAGE, J K and FLYNN, R J (1981). The development of a meteorologically validated model for the production of inclined surface irradition for the EEC area. ISES Conference, Brighton, Pergamon Press, pp. 2386-2390.

44. RODGERS, PAGE and SOUSTER (1979). Mathematical models for estimating the irradiance falling on inclined surfaces for clear day, overcast and average conditions. UK - ISES c18.

45. RODGERS, G G, SOUSTER, G G and PAGE, J K. The development of an interactive computer programe SUN 1 for the calculation of solar irradiances and daily irradiations on horizontal surfaces on cloudless days for given conditions of τ and W.C. IRN BS28, University of Sheffield.

46. SOUSTER, PAGE and COLQUHOUN (1979). Climatological values of the turbidity coefficient in the UK for different classes of radiation day.. UK - ISES c18.

47. JONES, W P (1973). Air Conditioning Engineering, Arnold Publishers.

48. PAGE, SOUSTER and SHARPLESS (1979). Mathematical modelling of hourly variations in temperature, wind speed and long wave radiation for different classes of radiation day in the UK. UK - ISES c18.

49. S.E.R.C. (1980). Report on a workshop on meteorological data for modelling. University of Sheffield.

50. BECKMAN, W A, KLEIN, S A and DUFFIE, J A (1977). Solar heating design by the F-Chart method. Wiley and Sons.

51. KLEIN, S A, BECKMAN, W A and DUFFIE, J A (1976). A design procedure for solar heating system, Solar Energy, Vol. 18, p.113.

52. KLEIN, S A, BECKMAN, W A and DUFFIE, J A (1977). A design procedure for solar air heating systems. Solar Energy, Vol. 19, p.509.

53. McLEAN, D J (1980). TIMP: the TRNSYS Input Management Program. Abacus Occasional Paper No. 82.

54. CROFT, D R and LILLEY, D G (1977). Heat transfer calculations using finite difference techniques. Applied Science Publishers Ltd (London).

55. BAYLEY, OWEN and TURNER (1972). Heat Transfer, Nelson.

56. PATANKAR, S.V. (1980) Numerical Heat Transfer and Fluid Flow. Hemisphere Publishing Corporation, USA.

57. STEWART, R, SPENCER, D and HEALEY, J. (1982) An evaluation of models estimating insolation incident upon slopes of different orientations. ISES Conference, Brighton, Pergamon Press.

58. BRANDEMUEHL, M J and BECKMAN, W A (1980). Transmission of diffuse radiation through CPC and flat plate collector glazings. Solar Energy, Vol. 24, pp. 511-513.

59. Optical Society of America. Editor, Driscoll, W G (1978). Handbook of Optics, McGraw-Hill.

60. McLEAN, D J (1981). Window: a computer program for the analysis of architectural glazing configurations. Abacus Occasional Paper No. 84.

61. VASICEK, A (1960). Optics of thin films. North-Holland Publishing Co. (Amsterdam).

62. MITALAS, G P and STEPHENSON, D G (1962). Absorption and transmission of thermal radiation by single and double glazed windows. Research Paper 173, Division of Building Research, National Research Council, Ottowa, Canada.

63. HEAVENS, D S (1955). Optical properties of thin solid films. Butterworth Scientific Publications (London).

64. BORN, M and WOLF, E (1965). Principles of Optics (3rd ed.) Pergamon Press (London).

65. ROUSSEAU and MATHIEU (1973). Problems in Optics, Pergamon Press (London).

66. WRANGHAM, D A (1961). The elements of heat flow, Chatter and Windus, London.

67. HOTTEL, H C and SARAFIM, A F (1967). Radiative Transfer, McGraw-Hill (USA)

68. ASHRAE (1975). 'Procedure for determining heating and cooling loads for computerising energy calculations, compiled by the Task Group on Energy Requirements for Heating and Cooling, New York.

69. CLARKE, J A (1982). The program ESPVWF, user manual, ABACUS, University of Strathclyde.

70. LACY, R E (1977). Climate and building in Britain, B.R.E., HMSO.

71. COLE, R J (1979). The longwave radiation incident upon inclined surfaces. Solar Energy, Vol. 22, pp. 459-462.

72. COLE, R J (1976). The longwave radiation incident upon the external surface of buildings. Building Services Engineer, Vol. 44, December 1976, pp. 195-206.

73. SWINBANK, W C (1963). Longwave radiation from clear skies. Quarterly Journal of the Royal Meteorological Society, Vol. 89, pp. 339-348.

74. KLEIN, S A (1977). Calculation of monthly average insolation on tilted surfaces. Solar Energy, Vol. 19, pp. 325-329. Pergamon Press.

75. GREEN, M A (1982). Solar Cells. Prentice-Hall (USA).

76. EVANS, D L (1981). Simplified method for predicting photovoltaic array output. Solar Energy, Vol. 27, no. 6, pp. 555-560.

77. PARKINS, R (1976). Internal ABACUS note. ABACUS, University of Strathclyde.

78. McLEAN, D J (1982). FLARE, user manual.

79. MEINEL and MEINEL (1977). Applied Solar Energy, Addison-Wesley, USA.

80. ASHRAE (1972). Handbook of fundamentals, ASHRAE.

81. UNSWORTH, M H (1975). Longwave radiation at the ground: II Geometry of interception by slopes, solids and obstructed planes. Quarterly Journal of Royal Meteorological Society, Vol. 101, pp. 25-34.

82. PARMELEE, G V (1945). The transmission of solar radiation through flat glass under summer conditions. Trans ASHVE, Vol. 51, pp. 317-344.

83. PAGE, J K. The estimation of monthly mean values of daily shortwave irradiation on vertical and inclined surfaces from sunshine records for latitudes 60°N to 40°S. I.R.N. BS32 Uni Sheffield

84. LIU, B Y H and JORDAN, R C (1960). The interrelation - ships and characteristic distribution of direct, diffuse and Total solar radiation. Solar Energy 4 (3), pp. 1-19.

85. LIU, B Y H and JORDAN, R C (1963). The long term average performance of flat plate solar energy collectors. Solar Energy, Vol. 7, pt. 2, pp.53-74.

86. COLLARES - PAREIRA, M and RABL, P (1979). The average distribution of solar radiation correlations between diffuse and hemispherical and between daily and hourly insolation values. Solar Energy, Vol. 22, pp. 155-164.

87. ORGILL, J F and HOLLANDS, K G T (1977). Correlation equation for hourly diffuse radiation on a horizontal surface. Solar Energy, Vol. 19, pp. 357-359.

88. OZISIK, M N (1977). Basic Heat Transfer, McGraw-Hill, USA.

89. KREITH, F (1976). Principles of heat transfer (3rd ed.) Harper and Row, New York.

90. TAN, H M and CHARTERS, W W S (1969). Effect of thermal entrance region on turbulent forced-convection heat transfer for an asymmetrically heated rectangular duct with uniform heat flux. Solar Energy, Vol. 12, pp. 513-566.

91. TAN, H M and CHARTERS, W W S (1970). An experimental investigation of forced-convective heat transfer for fully developed turbulent flow in rectangular duct with asymmetric heating. Solar Energy, Vol. 13, pp. 121-125.

92. DREW, T B, KOO, E C and MacADAMS, W H (1932). The friction factor for clear round pipes. IChemE, Vol. 28, pp.56-72.

93. MacADAMS, W H (1954). Heat Transmission, McGraw-Hill (New York).

94. JAKOB, M (1949). Heat Transfer, Vols. 1, 2. J Wiley and Sons, New York.

95. KAYS, W M (1966). Convective heat and mass transfer. McGraw-Hill, USA.

96. KAYS, W M (1955). Numerical solution for laminar flow heat transfer in circular tubes. Trans ASME, Vol. 77, pp. 1265-1274.

97. SEIDER, E N and TATE, C E (1936). Heat transfer and pressure drop of liquid in tubes. Industrial Engineering Chemistry, Vol. 28, p. 1429.

98. GESHART, B (1971). Heat Transfer, McGraw-Hill.

99. GLOBE, S and DROPKIN, D (1959). Natural convection heat transfer in liquids confined by two horizontal plates and heated from below. Journal of Heat Transfer 81c, pp. 24-28.

100. COTTON, I (1978). Natural convection in enclosures. Proc. 6 International Heat Transfer Conference, 1978, Toronto, Canada.

101. MacGREGOR, R K and EMERY, A P (1969). Free convection through vertical plane layers; moderate and high Prandtl number fluids. Journal of Heat Transfer, Vol. 91, p.391.

102. HOLLANDS, K G T, et al. (1975). Free convective heat transfer across inclined air layers. A.S.M.E. 75-HT-55.

103. JACKSON, T W, HARRISON, W B and BOTELER, W C (1978). Combined free and forced convection in a constant temperature vertical tube. Trans ASME. Journal of Heat Transfer, April 1978, pp. 739-745.

104. DEPEW, C A and AUGUST, S E (1971). Heat transfer due to combined free and forced convection in a horizontal and isothermal tube. Trans. ASME. Journal of Heat Transfer, November 1971, pp. 380-384.

105. OOOSTHUIZEN, P H and BASSEY, M (1973). An experimental study of combined forced and free convection heat transfer from flat plates to air at low Reynolds numbers. Journal of Heat Transfer, February 1973, pp.120-121.

106. JACKSON, T W and YEN, H H (1971). Combining forced and free convection equations to represent combined heat-transfer coefficients for a horizontal cylinder. Journal of Heat Transfer, May 1971, pp. 247-248.

107. CLARKE, J A (1982). The ESP system documentation. ABACUS, University of Strathclyde.

108. PETHERBRIDGE, P (1967). Transmission Characteristics of window glasses and sun-controls. B.R.S. Research note no. 72.

109. WILES, I. University of Strathclyde, Personal Communications

110. US Department of Environment (1981). IEA Report Annex 1 - Establishment of methodoligies for load/energy. Determination of Buildings.

111. Oscar Faber and Partners (1980). IEA Report Annex 1 - Results and Analysis of Avonbank Building simulation.

112. COCKROFT, J P (1982). 'Validation of buildings and systems energy prediction using real measurements'. Computer-Aided Design, Vol. 14, no. 1, (guest editor: J A Clarke).